Functional Analysis of Subcortical Maternal Complex Associated Gene, *PADI6*, in Bovine Oocytes and Embryos

Christina Helen Coll

Submitted in accordance with the requirements for the degree of Doctor of Philosophy

The University of Leeds
School of Medicine

January 2020

I confirm that the work submitted is my own and that appropriate credit has been given where reference has been made to the work of others.

Acknowledgements

I would like to express my sincere appreciation to Professor Helen Picton and Dr John Huntriss for their guidance and support throughout my PhD. Thank you for giving me direction and encouragement when I needed it and allowing me to grow as a research scientist and as a person.

My work couldn't have been completed without the help of several people. Special thanks to Dr Erika Bereyni for training me in every aspect of the lab; to Dr Paul McKeegan for all his help in and out of the lab and in setting up and running my amino acid profiling; Phil Warburton who was always there when I needed him and indispensable to the running of the lab and Jade Critchley for persevering with microinjection optimisation during her Master's project. I would also like to thank all my colleagues for their help and support over the past 3 years.

Finally, this thesis is dedicated to my family and friends. Thank you to my parents for your unconditional love, support and encouragement throughout my life. Words cannot describe how grateful I am to you. Thank you to my boyfriend, Joe, for always making me laugh and supporting me when I needed it the most. Thank you to Rachel for completing this PhD journey with me and to my incredible friends for believing in me.

Abstract

PADI6 is a maternal effect gene (MEG) that is expressed throughout oocyte maturation and appears to be critical for early embryo development and embryonic genome activation (EGA). It is described as the fifth member of the oocyte-specific subcortical maternal complex (SCMC), which is involved in transcription, epigenetic regulation and cytoskeletal organisation. PADI6 is also essential for the maintenance of critical structures in the oocyte called cytoplasmic lattices that are believed to function as storage sites for maternal transcripts and proteins. It is hypothesised that *PADI6* is involved in translational regulation in the oocyte in preparation for EGA. Experiments were conducted on bovine oocytes as a physiologically relevant model for functional investigations of the role of *PADI6* and its interaction with the SCMC during human oocyte maturation and embryo development.

Initial studies characterising the expression of *PADI* family genes in different bovine somatic tissues showed that *PADI6* expression was restricted to the oocyte and early embryo. *PADI6* expression patterns were mapped across bovine oocyte meiotic maturation following the *in vitro* maturation (IVM) of oocytes and during preimplantation embryogenesis in embryos derived following *in vitro* fertilisation and embryo culture to the blastocyst stage. Quantitative PCR analysis of Smart-seq2 cDNA libraries from individual oocytes and embryos indicated that *PADI6* was highly expressed in the germinal vesicle (GV) and metaphase II (MII) oocytes and embryos prior to EGA (8-16 cell stage in bovine) and thereafter was significantly reduced by the blastocyst stages. This expression pattern was in marked contrast to the tissue distribution of other members of the *PADI* family *PADI1-4* which showed no expression in oocytes and early embryo development in the bovine model. The expression patterns of the other members of the SCMC – namely *KHDC3L, NLRP5, OOEP* and *TLE6* were also mapped across oocyte maturation and preimplantation embryo development.

Functional analysis of the role of *PADI6* during bovine oocyte maturation was conducted using a validated system for the microinjection of double-stranded short-interfering RNAs (dsiRNAs) into cumulus-enclosed GV oocytes (n=17) relative to duplex buffer injected (n=22) and scrambled siRNA (n=19) controls. Gene knockdown (KD) was assessed following 24 hr of IVM and was found to reduce the expression of *PADI6* by an average of 74±3.6% ($p<0.05$). KD of *PADI6* did not affect oocyte meiotic progression to metaphase II or cumulus expansion after IVM. However, targeted real-

time PCR highlighted 7 transcripts (*DNMT3A, DPPA3, PLAGL1, PRDX1, TRIM28, ZP1* and *ZFP57*) associated with oocyte and embryo developmental competence and epigenetic regulation that were significantly dysregulated in *PADI6*^{KD} oocytes. Full transcriptome analysis by RNA sequencing was conducted on 6 individual *PADI6*^{KD} MII oocytes and 12 controls. Bioinformatic analysis identified 452 differentially expressed genes (DEGs): 165 genes were downregulated and 287 genes were upregulated following *PADI6* KD. Network analysis revealed that 61 DEGs were directly or indirectly linked to *PADI6.* A diverse number of transcripts were involved in RNA processing and translation. Genes from 7 downstream networks and 10 downstream networks were associated with infertility and organisation of the cytoskeleton, respectively. Finally, KD of *PADI6* appeared to impact oocyte metabolism as the regulation of 5 amino acids was altered in *PADI6*^{KD} oocytes compared to controls.

Overall, the results of this thesis suggest a role for *PADI6* in translational control of maternal transcripts which may impact on oocyte developmental competence in the bovine.

Presentations of work

Fertility 2018 SRF PhD student short paper prize session

British Fertility Society, Society for Reproduction and Fertility and Association of Clinical Embryologists.

Christina Coll, Erika Berenyi, John Huntriss and Helen Picton (2018) Characterisation of the SCMC associated gene PADI6 in bovine oocyte and preimplantation embryo development.

University of Leeds Early Career Science Day 2018 Poster presentation

Faculty of Biology, Medicine and Health and Faculty of Biological Sciences.

Christina Coll, Erika Berenyi, John Huntriss and Helen Picton (2018) Functional analysis of subcortical maternal complex associated gene, PADI6, in bovine oocyte and preimplantation development.

Fertility 2019 Poster presentation

British Fertility Society, Society for Reproduction and Fertility and Association of Clinical Embryologists.

Christina Coll, Erika Berenyi, John Huntriss and Helen Picton (2019) Effects of PADI6 siRNAi knockdown in bovine GV oocytes on gene expression and preimplantation embryo development.

Table of Contents

List of Tables

List of Figures

List of Abbreviations

5meC: 5-methylcytosine
A: Adenine
AA: Amino acid
AAP: Amino acid profiling
AKT: Protein kinase B
AGO: Argonaute
ALCAM: activated leukocyte cell adhesion molecule
ANOVA: Analysis of variance
AMH: Anti-Müllerian hormone
APC: Anaphase promoting complex
AR: Acrosome reaction
AURKA: Aurora kinase A
ASCL2: Achaete-Scute Family BHLH Transcription Factor 2
B: Blastocyst
ATP: Adenosine triphosphate
BLAST: Basic local alignment search tool
AU-rich: Adenylate-uridylate rich
BLIMP1: B lymphocyte-induced maturation protein 1
B2M: Beta-2-microglobulin
BMP: Bone morphogenetic proteins
BDNF: brain derived neurotrophic factor
BRG1: Brahma-related gene 1
bFGF: Basic fibroblast growth factor
BSA: Bovine serum albumin
BSA FAF: Bovine serum albumin, fatty acid free
Ca^{2+}: Calcium ions
BSA FrV: Bovine serum albumin, fraction V
CaMKII: Calmodulin-dependent protein kinase II
BWS: Beckwith-Wiedermann syndrome
cAMP: Cyclic adenosine 3',5'-monophosphate
CATERPILLER: caspase activation and recruitment domains, transcription enhancer, R [purine]-binding, pyrin, lots of leucine repeats
CDC20: Cell division cycle 20c
CDK: Cyclin-dependent kinase
cDNA: complementary deoxyribonucleic acid
CDKN1B/P27: Cyclin-dependent kinase inhibitor 1B
CDX2: Caudal type homeobox 2
CDKN1C: Cyclin-dependent kinase inhibitor 1C
CENPM: centromere protein M
cGMP: Cyclic guanosine 3′,5′-monophosphate
CGBP: CpG binding protein
CNV: Copy number variation
CL: Corpus luteum
CPE: Cytoplasmic polyadenylation element
COC: Cumulus oocyte complex
CPEB: Cytoplasmic polyadenylation element binding proteins
CpG: Cytosine-phosphate-guanine residues
CPLs: Cytoplasmic lattices
CTCF: CCCTC-binding factor
CSF: Cytostatic factor
CXCR4: C-X-C chemokine receptor type 4
DABA: 2,4-diaminobutyric acid
DMR: Differentially methylated region
DB: Duplex buffer
DNMT: DNA methyltransferases
DNA: Deoxyribonucleic acid
dNTP: Deoxynucleoside trisphosphate
EBSS: Earle's balanced salt solution
DPBS: Dulbecco's phosphate buffered saline
EGF: Epidermal growth factor
DPPA3: Developmental pluripotency associated
EHMT2: Euchromatic Histone Lysine Methyltransferase 2
dsDNA: Double-stranded deoxyribonucleic acid
eIF-4E: Eukaryotic initiation factor 4E
dsiRNA: Double-stranded short interfering ribonucleic acid
ELP3: Elongator Acetyltransferase Complex Subunit 3
DTT: 1,4-dithiothreitol
ET: Embryo-tested
EAA: Essential amino acid
FASN: Fatty acid synthase
EB: Expanded blastocyst
FBHM: Familial biparental hydatidiform mole
EDTA: Ethylenediaminetetraacetic acid
FF-MAS: Follicular fluid-derived meiosis-activating sterol
EGA: Embryonic genome activation
FIM: Follicle isolation media
EGA: Embryonic genome activation
FLOPED: Factor located in oocytes permitting embryo development
EMI: Early meiotic inhibitor

FOSL1 Fos-related AP-1 transcription factor
F-TALP: Fertilisation Tyrode's medium base, albumin, lactate and pyruvate
FOXL2: Forkhead box L2
FOXO3A: Forkhead box O3A
GAPDH: Glyceraldehyde 3-Phosphate Dehydrogenase
GVBD: Germinal vesicle break down
H-SOF: Hepes synthetic oviduct fluid
H-TALP: Hepes Tyrode's medium base, albumin, lactate and pyruvate
H2A: Histone H2A
HA: Hyaluronic acid
HAT1: Histone acetyltransferase 1
hESCs: Human embryonic stem cells
HLA: human leukocyte antigen
HM: Hydatidiform mole
HOXD1: Homeobox D1
HPLC: High performance liquid chromatography
HPRT1: hypoxanthine phosphoribosyltransferase 1
ICAM4: Intercellular adhesion molecule 4
IGF: Insulin growth factor
IGFR: Insulin-like growth factor receptor 1
ING2: Inhibitor of growth family member 2
IL: Interleukin
IVM: *In vitro* maturation
IUGD: Intrauterine growth defects
KAT5: Lysine acetyltransferase 5
KD: Knockdown
KDM1B: Lysine specific histone demethylase 1B
KRT5: Keratin 5
KRT8: Keratin 8
LB: Luria-Bertani
LIF: Leukemia inhibitory factor
LRR: Leucine rich repeat
MAPK: Mitogen-activated protein kinase
MEM: Minimum eagle's medium
MEST: Mesoderm Specific Transcript
MIMT1: MER1 Repeat Containing Imprinted Transcript 1
MLID: Multilocus imprinting disorder
MPF: Maturation promoting factor
mRNA: Messenger ribonucleic acid
MSY2: Y-box binding protein 2
NAPL5: Nucleosome Assembly Protein 1
NGF: Nerve growth factor
NLRP: Nucleotide-binding, leucine-rich repeat and pyrin domain-containing protein
NNAT: Neuronatin
NF- ƙB: nuclear factor kappa-light-chain-enhancer of activated B cells
NPPC: Natriuretic peptide precursor type C
NPR: Natriuretic peptide receptor

ER: Endoplasmic reticulum
FGSC: Female germline stem cell
FIGLA: Factor in the germline alpha
FSH: Follicle stimulating hormone
GDF9: Growth differentiation factor 9
GC skew: Guanine-cytosine skew
GC: Granulosa cell
GM130: Golgin subfamily A member 2
GST: glutathione S-transferase
GV: Germinal vesicle
HFEA: Human Fertilisation and Embryology Authority
HSF: Heat shock factor
HSP: Heat shock protein
HRP: Horseradish peroxidase
HSF: Heat shock factor
ICM: Inner cell mass
ICR: Imprinting control region
ICSI: Intracytoplasmic sperm injection
IP_3: 1,4,5-inositol triphosphate
IPTG: Isopropyl β-D-1-thiogalactopyranoside
IVF: *In vitro* fertilisation
JUN: Jun proto-oncogene
KHDC3L: KH domain containing 3 like
KL: Kit ligand
KLD: Kinase, ligase, *Dpn* reaction
KGF: Keratinocyte growth factor
LH: Luteinising hormone
LHX8: LIM-homeobox protein 8
LNA: Locked nucleic acids
MAD2: Mitotic arrest deficient 2
MATER: Maternal antigen that embryos require
MBD: Methyl-binding domain
MCS: Multiple cloning site
MEG: Maternal effect gene
MEK1: Mitogen-activated protein kinase kinase 1
MET: Maternal-zygotic transition
MI: Metaphase I
MII: Metaphase II
mtDNA: Mitochondrial deoxyribonucleic acid
NANOG: Nanog homeobox
NANOS3: Nanos C2HC-type zinc finger 3
NCBI: National Center for Biotechnology Information
ncRNA: Non-coding ribonucleic acid
NEAA: Non-essential amino acid
NENF: neudesin neurotrophic factor
NLS: Nuclear localisation signal
NOBOX: Newborn ovary homeobox

NSN: Non-surrounded nucleolus

OD600: Optical density 600
OPA: o-phthaldialdehyde
ORF: Opening reading frame
P13K: Phosphoinositide 3 kinase/
PARN: PolyA-specific ribonuclease

PBL: Peripheral blood leukocyte
PCR: Polymerase chain reaction
PDE: Phosphodiesterase
PGK1: phosphoglycerate kinase 1
PHLDA2: Pleckstrin Homology Like Domain Family A Member 2
PKA: Protein kinase A
PLAGL1: Pleomorphic adenoma gene-like 1

PLC: Phospholipase C
PolyA: Polyadenine
PRDX1: Peroxiredoxin 1

PRMT: Protein arginine methyltransferase
PTEN: Phosphatase and tensin homolog
PVDF: Polyvinylidene fluoride
PVDF: polyvinylidene difluoride
RAB-12: ras-related protein Rab-12
RAB-32: ras-related protein Rab-32
RIPA: Radio-immunoprecipitation assay
rRNA: Ribosomal ribonucleic acid
RT: Room temperature

SDS-PAGE: sodium dodecyl sulfate-polyacrylamide gel
SETDB1: SET Domain Bifurcated Histone Lysine Methyltransferase 1
SN: Surrounded nucleolus
SNRPN: Small Nuclear Ribonucleoprotein Polypeptide N
SNS: Single nucleotide substitution

SOFaaBSA: Synthetic oviduct fluid supplemented with amino acids and bovine serum albumin
SPAM1: Sperm adhesion molecule 1
TBS-T: Tris-buffered saline with Tween 20
TGF: Transforming growth factor
TNF: Tumour necrosis factor
TSC-1: Tuberous sclerosis 1
USP29: Ubiquitin Specific Peptidase 29
UTR: Untranslated region
UNCX: UNC homeobox
XIST: X-inactive specific transcript
YWHA: Tyrosine 3-Monooxygenase/Tryptophan 5-Monooxygenase Activation Protein
YY1: Yin-yang 1
ZAR1: Zygote arrest 1
ZP: Zona pellucida
ZNF705B : zinc finger protein 705B

NSF: *N*-ethylmaleimide sensitive fusion protein
OC: Ovarian cortex
OCT4: Octamer binding transcription factor 4
OOEP: Oocyte expressed protein
PADI6: Peptidylarginine deiminase 6
PAWP: Post-acrosomal sheath WW domain-binding protein

PBS: Phosphate buffered saline
PEG: Paternally expressed gene
PGC: Primordial germ cell
PLK1: Polo-like kinase 1

PRDM: PR domain zinc finger protein
PRAGL1: PEAK1 related, kinase-activating pseudokinase 1
RHOA: Ras homology family member A
RISC: RNA-induced silencing complex
RGL1: ral guanine nucleotide dissociation stimulator like-1
RNA: Ribonucleic acid
RNAi: Ribonucleic acid interference
RNP: Ribonucleoprotein
ROS: Reactive oxygen species
RPS6KA1: Ribosomal Protein S6 Kinase A1
RSK: Ribosomal s6 kinase
SAC: Spindle assembly checkpoint
SCMC: Subcortical maternal complex
SCR: Scrambled double-stranded short interfering ribonucleic acid
SDF1: Stromal cell-derived factor 1

SEM: Standard error of the mean

siRNA: Short interfering ribonucleic acid
SNARE: Soluble NSF-attachment receptor

SOHLH: Spermatogenesis and oogenesis-specific basic helix-loop-helix transcription factor
SOX2: Sex determining region Y-box 2

STRA8: Stimulated by retinoic acid 8
TBE: Tris borate EDTA
TE: Trophectoderm
TET: Ten eleven translocation
TIF: Transcription intermediary factor
TLE6: Transducin like enhancer of split 6
TRC: Transcription requiring complex
TRIM: Tripartite motif family
TRH: Thyrotrophin releasing hormone
TSO: Template-switching oligonucleotide
UCSC: University of California, Santa Cruz

WNT3: Wnt family member 3
ZFP: Zinc finger protein
ZGA: Zygotic genome activation
ZNF382: zinc finger protein 382

Chapter 1 Introduction

For females, the path to procreation begins many years prior to puberty during the specialisation of oocytes (female gametes) in the foetal ovary. Development of the oocyte (oogenesis) requires paracrine signalling from follicular somatic cells in a highly specialised unit of the ovary known as the follicle. Simultaneously, the oocyte and follicle grow and mature in response to intraovarian factors and endocrine signalling (Sanchez and Smitz, 2012). Oogenesis begins with the development of oogonia from pluripotent primordial germ cells (PGCs). Oogonia enter meiosis to become diploid primary oocytes and immediately arrest at the dictyate stage of prophase I, forming a germinal vesicle (GV) (Figure 1.1) (Virant-Klun, 2015). GV oocytes become enveloped by somatic precursor cells giving rise to primordial follicles. Although meiosis has stopped, GV oocytes are transcriptionally active and continue to grow within follicles. In cows, there are 4 GV chromatin configurations, GV0 to GV3. At GV0, uncondensed chromosomes are dispersed in the nucleoplasm. The transition of chromatin configurations through GV1 and GV2 is characterised by condensation of chromosomes until by GV3, there is a distinct focus of chromatin occupying a small region of the nucleus (Lodde et al., 2007). The GV chromatin state changes with follicle development as small antral follicles primarily have GV0 configuration whereas medium antral follicles have a mixture of GV1-GV3 configuration (Luciano and Sirard, 2018a). In the GV oocyte, maternal mRNAs are transcribed but many are translationally repressed for storage (Winata and Korzh, 2018). The transition from GV0 to GV3 is associated with transcriptional silencing, changes to the epigenetic signature and acquisition of developmental competence (Luciano and Sirard, 2018a). At appropriate developmental time points, stored mRNAs are activated and translated into proteins for processes such as meiotic maturation or early embryo development. Primary oocytes are maintained in the ovary for many years until puberty begins. At puberty, cyclic gonadotrophins stimulate primary oocytes to complete meiosis I and extrude the first polar body giving rise to a secondary oocyte. The secondary oocyte arrests again at metaphase II (MII) meiosis II (Figure 1.1). For monoovular species, such as human and bovine, 15-20 follicles are recruited during each reproductive cycle but only 1 follicle, known as the dominant follicle, matures and is ovulated (Salha et al., 1998). Meiosis is only completed upon sperm entry and a second polar body is extruded.

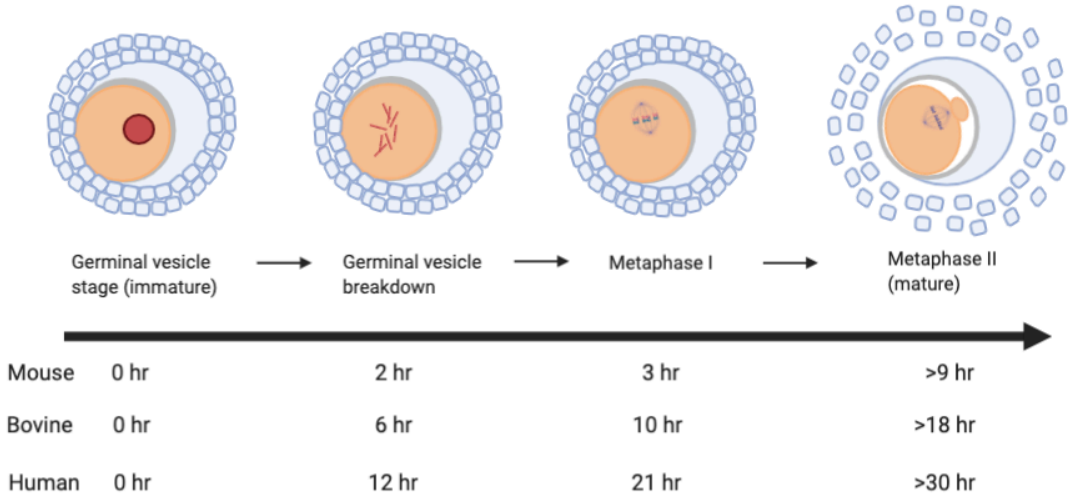

Figure 1.1 Timeline for oocyte meiotic maturation in mouse, bovine and human species. The diploid primary oocyte arrests in dictyate stage of prophase I, forming a germinal vesicle, within a follicle. Cyclic gonadotrophins stimulate primary oocytes to undergo germinal vesicle breakdown and complete meiosis I to extrude the first polar body giving rise to a secondary oocyte. The secondary oocyte arrests again at metaphase II until fertilisation.

Upon fertilisation, the sperm and oocyte pronuclei are processed and epigenetically reprogrammed by factors in the oocyte to produce a totipotent zygote (Biechele et al., 2015). The development of a healthy embryo requires a plethora of male and female genetic, epigenetic and cellular factors that act in concert to enable cell division, epigenetic reprogramming and differentiation. Epigenetic modifications describe dynamic changes to gene expression without changing the DNA sequence. They are responsible for cell differentiation, X-chromosome inactivation and imprinting (Sasaki and Matsui, 2008). The genome must lose pre-existing somatic epigenetic marks, gain gamete-specific marks and subsequently undergo selective reprogramming to produce a successful embryo. To this end, maternal factors that have accumulated during oocyte maturation, known as maternal effect genes (MEGs), coordinate early embryonic processes (Fraser and Lin, 2016). The embryo is said to be under maternal control for the first few cleavage divisions until the embryonic genome is activated (EGA). Mutations in MEGs can have detrimental effects on embryo development and lead to a variety of human pathologies, including female infertility (Li et al., 2010a).

Recently, a maternally derived multi-protein complex called the subcortical maternal complex (SCMC) was identified in the oocytes and embryos of mice and humans that appears to be fundamental to preimplantation embryo development. Individual members of the SCMC, KH domain containing 3 like *(KHDC3L),* transducin like

enhancer of split 6 (*TLE6)* and peptidylarginine deiminase 6 (*PADI6)*, have been linked to female infertility characterised by early embryonic arrest (Alazami et al., 2015; Parry et al., 2011; Xu et al., 2016). The function of the SCMC is currently unclear but research has recently led to the identification of key interactors and networks that will advance our study in this area. Better knowledge of the role of this supra-molecular complex and the biological mechanisms and pathways that it controls within the oocyte/embryo, may facilitate earlier diagnosis after failed *in vitro* fertilisation (IVF) cycles and add to our understanding of early developmental failure.

It is worth noting that there are differences in oogenesis, fertilisation and preimplantation embryo development between the mammalian species. The mouse model is often used for research due to its small size, relatively short life span and ease of genetic manipulation to produce knockout offspring (Quinn and Horstman, 1998; Taft, 2008). Although much research has been conducted in mice and has facilitated the development of assisted reproduction in humans, the mouse is not the most physiologically relevant animal to human oocyte maturation and embryo development (Santos et al., 2014). Firstly, the mouse is polyovulatory meaning that it releases multiple oocytes at each ovulation. There are also differences in gene expression, response to growth factors and timing of developmental stages between mice and humans. For example, activin enhances PGC proliferation in humans but inhibits it in mice (Martins da Silva et al., 2004; Richards et al., 1999). The timing of oogenesis and folliculogenesis also differ between human and mouse (Pepling, 2006). However, the nature of implantation in humans is closely reflected in mouse (Taft, 2008). Alternatively, the bovine is a good model for human oocyte and preimplantation embryo development: it is monovulatory and has a similar gestation time and endocrine signalling (Adams and Pierson, 1995; Malhi et al., 2007). Likewise, the bovine and human oocyte are similar in their size and timings of development, and in the fine regulation of processes such as folliculogenesis, polyadenylation and metabolism (Menezo and Herubel, 2002). This review aims to provide an insight into the regulation of oocyte and follicle development as well as background literature on the SCMC and *PADI6*. Much of the work that is described originates from research in mice but efforts will be made to address human and bovine species throughout.

1.1 Specification of primordial germ cells

PGCs are the germline precursor cells that enter meiosis to produce gametes. Much of the current knowledge about mammalian PGC specification stems from research in mice due to the ethical and logistical challenges that surrounds human embryo research (Nikolic et al., 2016; Tilgner et al., 2008). During gastrulation of the embryo, a small number of cells are set aside to become the germ cell population. Such PGCs display high alkaline phosphatase expression which has facilitated the identification and tracking of these cells through the embryo (Chiquoine, 1954; Ginsburg et al., 1990). PGCs differentiate from the proximal epiblast as a result of signalling from transforming growth factor beta (TGF-β) superfamily ligands, bone morphogenetic proteins (BMP) (Lawson et al., 1999; Lawson and Hage, 1994). Specifically, BMP4 and BMP8b, secreted from the extra-embryonic ectoderm, activate downstream signal mediator Smads that translocate to the nucleus to alter gene expression (Hayashi et al., 2002; Shi and Massague, 2003). BMP8b augments the action of BMP4 by antagonising anterior visceral endoderm development, which would otherwise inhibit PGC differentiation (Ying et al., 2000; Ying et al., 2001). Alongside BMP4, BMP2 signalling from the visceral endoderm has an additive effect on PGC specification (Ying and Zhao, 2001). Further, Wnt family member 3 (WNT3) signalling from the epiblast activates intracellular transcriptional factor T/Brachyury (Aramaki et al., 2013). PGC fate is determined by activation of transcriptional regulators B lymphocyte-induced maturation protein 1 (*Blimp1)* and PR domain zinc finger protein 14 (*Prdm14)* in the epiblast (Ohinata et al., 2009; Saitou et al., 2005). In mouse and humans, BLIMP1 and PRDM14 repress somatic cell programming, such as homeobox genes, and upregulate PGC/pluripotency genes, such as sex determining region Y-box 2 (*Sox2),* Nanog homeobox (*Nanog),* Octamer binding transcription factor 4 *(Oct4),* Nanos C2HC-type zinc finger 3 *(Nanos3)* and Developmental pluripotency associated 3 (*Dppa3) (*also known as *Stella* or *Pgc7)* (Kurimoto et al., 2008a; Ohinata et al., 2005; Sato et al., 2002; Sybirna et al., 2019; Yamaji et al., 2008). PGCs also undergo extensive genome-wide epigenetic reprogramming (Section 1.6.2) (Hackett et al., 2012; Seki et al., 2007).

Proliferating PGCs migrate to the hindgut due to Kit Ligand (KL) signalling, where they occupy the gonadal ridge and differentiate to become male or female gametes (Chiquoine, 1954; Farini et al., 2007; Gu et al., 2009). PGC migration and survival is dependent upon C-X-C chemokine receptor type 4 (CXCR4)-stromal cell-derived

factor 1 (SDF1) signalling whereby PGCs expressing receptor CXCR4 are attracted to high levels of the ligand SDF1 in the gonadal ridge (Molyneaux et al., 2003). Downregulation of phospho-Smad159 was found to decrease the sensitivity of PGCs at the base of the allantois to Bmp signalling to maintain PGC identity in mice (Senft et al., 2019). In female gonads, PGCs become oogonia that undergo many rounds of mitosis before clustering to form a nest, or syncytium, connected to one another via cytoplasmic bridges (Oktem and Urman, 2010; Pepling and Spradling, 1998; Pepling and Spradling, 2001). Oogonia undergo pre-meiotic DNA synthesis, mediated by stimulated by retinoic acid 8 (STRA8), and enter meiosis to become primary oocytes (Baltus et al., 2006). Primary oocytes maintain meiotic arrest at diplotene of prophase I, meiosis I and only resume meiosis upon ovulation (Baker and Franchi, 1967; Picton et al., 1998). At this stage they are known as GV oocytes as the DNA is arranged in decondensed chromosomes packed within a nucleus called the GV. Primary oocytes become surrounded by somatic pre-granulosa cells (GCs) and enter folliculogenesis.

In females, dogma states that there is a finite pool of oocytes that degenerate over time to a threshold level, at which time menopause occurs (Faddy et al., 1992; Lintern-Moore and Moore, 1979; Zuckerman, 1951). It has been suggested that in some species a subset of oocytes selectively die to provide cellular components, such as mitochondria, for other oocytes, similar to nurse cells in *Drosophila* (McNatty et al., 2000; Pepling and Spradling, 2001). Meanwhile, pre-GCs invade the germ cell nest and envelop the remaining diploid primary oocytes to form PGCs (Pepling and Spradling, 2001). Although widely accepted since the work of Zuckerman (1951), the dogma of ovarian programming was challenged by numerous researchers who identified so called “postnatal ovogenesis” or “neo-oogenesis” in the adult ovaries of different species (David et al., 1974; Duke, 1967; Pansky and Mossman, 1953; Porras-Gomez and Moreno-Mendoza, 2017; Vermande-Van Eck, 1956). More recently, Johnson et al. (2004) published their discovery and isolation of female germline stem cells (FGSCs) from adult mice ovaries that formed follicles upon transplantation into the ovaries of adult wild-type mice. Further, Zou et al. (2009) were able to produce healthy offspring from isolated mouse FGSCs following implantation into chemotherapy-sterilised mice. Further proof of concept of the existence of FGSCs has been provided for other mammals, including human as FGSCs have been isolated from ovarian surface epithelium of adult ovaries (Parte et al., 2011; Virant-Klun et al., 2008; White et al., 2012). The research surrounding so called FGSCs or oocyte stem cells has been heavily criticised, but with emerging data to support this

hypothesis, the general consensus may be changing (Clarkson et al., 2018; Johnson et al., 2005; Martin et al., 2019; Telfer et al., 2005).

1.2 Folliculogenesis

Female gametes require the support of somatic cells that envelop immature oocytes in the ovary of the developing foetus to form follicles. Communication between these cell types is essential for correct oocyte maturation and follicle growth (McNatty et al., 2004; Russell et al., 2016). Somatic cell-derived factors act on the oocyte to regulate transcription and translation whilst oocyte-derived factors stimulate proliferation and differentiation of follicular somatic cells (Gilchrist et al., 2006). Previously it was thought that the oocyte developed passively as a result of somatic cell signalling. It is now understood that the oocyte is an active driver of its own development, and this continues after fertilisation as the embryonic genome is not activated until after the first few cleavage divisions (Eppig, 2001; Eppig et al., 2002). The 2 main somatic cell types are GCs and theca cells. They respond to growth factor signalling through a variety of receptors and later in folliculogenesis become gonadotrophin-dependent responding to follicle stimulating hormone (FSH) and luteinising hormone (LH) (Sanchez and Smitz, 2012). GCs are the primary supporting cells of oocyte growth from primordial follicle activation to post-ovulation. In the latter follicles, from secondary stages onwards, both cell types undergo steroidogenesis to produce progesterone, oestrogens and androgens (Channing, 1980; Haney and Schomberg, 1981; McNatty et al., 1979; Rimon-Dahari et al., 2016; Skinner, 2005).

Primordial follicles are considered the “resting pool” from which follicles can develop or be depleted by atresia (Skinner, 2005). They consist of a single primary oocyte surrounded by a layer of flattened GCs enclosed within a thin membrane. GCs differentiate into cuboidal GCs and proliferate to form primary follicles, which are considered the first stage of the “growing follicle pool” (Lintern-Moore and Moore, 1979; Picton, 2001). Subsequently, cuboidal GCs proliferate and the theca interna and zona pellucida form, giving rise to the secondary follicle (Picton et al., 1998). The zona pellucida is a glycoprotein layer that separates the oocyte from GCs. Gap junctions form between GCs and the oolemma permitting communication with the growing oocyte (Anderson and Albertini, 1976; Conti et al., 2012). By the preantral follicle stage, there are 7-8 layers of GCs and a theca layer comprised of the theca internal and theca externa. The thecal cell layers provide an independent blood

supply to the growing follicle and signal transduction between GCs and the oocyte (McLaughlin and McIver, 2009). These early stages of folliculogenesis are not gonadotrophin-dependent. During the early antral and antral stages, fluid-filled spaces appear in the GCs. When follicles reach a diameter of around 200-500µm, the antral cavity forms and is filled with follicular fluid providing the oocyte with oxygen, carbohydrates, amino acids (AAs), growth factors etc. (Picton et al., 1998; Sutton et al., 2003). Furthermore, GCs differentiate into mural GCs and cumulus cells to form the cumulus-oocyte complex (COC). The latter follicle stages from ~8-9mm in diameter in cow and humans become progressively more gonadotrophin-dependent (Rimon-Dahari et al., 2016). For monoovulatory species, a dominant follicle is selected to progress to ovulation in each reproductive cycle from puberty onwards, while other antral follicles undergo atresia (Hsueh et al., 1994). A preovulatory surge of LH triggers nuclear and cytoplasmic maturation of the oocyte and resumption of meiosis to a MII oocyte (Binelli and Murphy, 2010; Hsueh et al., 1994). Furthermore, the increase in LH induces expression of fibronectin in follicular walls and causes secretion of hyaluronic acid which results in granulosa mucification (Chen et al., 1993; Kitasaka et al., 2018). The follicle protrudes from the ovary and ruptures to release a secondary MII oocyte in preparation for fertilisation. After ovulation, the granulosa and theca cells undergo remodelling to become the corpus luteum (CL) which secretes progesterone and oestradiol until the placenta can support the pregnancy (Kwintkiewicz and Giudice, 2009).

1.2.1 Primordial follicle formation

Primordial follicle formation relies on the expression of a number of transcriptional regulators in the ovary: factor in the germ line alpha (*FIGLA*), newborn ovary homeobox (*NOBOX*), LIM-homeobox protein 8 (*LHX8*), spermatogenesis and oogenesis-specific basic helix-loop-helix transcription factor (*SOHLH*) 1 and *SOHLH2* (Choi et al., 2008a; Choi et al., 2008b; Pangas et al., 2006; Rajkovic et al., 2004; Soyal et al., 2000). Knockout studies in mice have shown that ablation of any 1 of these genes precludes primordial follicle formation and maintenance, and disrupts the regulation of additional genes in folliculogenesis (Lim and Choi, 2012). For example, *Figla* knockout female mice display normal PGC differentiation and migration, however, primordial follicles do not form and oocytes rapidly deplete resulting in female sterility (Soyal et al., 2000). FIGLA regulates the transcription of zona pellucida proteins (*Zp1, 2* and *3*), together with other key oocyte genes *Oct4*, *Dppa3, Padi6*

and nucleotide-binding, leucine-rich repeat and pyrin domain-containing protein (*Nlrp)* family (Joshi et al., 2007; Liang et al., 1997). Its expression is also maintained throughout folliculogenesis, suggesting it regulates downstream genes that are necessary for follicle formation (Choi and Rajkovic, 2006b). Similarly, *Nobox* knockout mice have impaired primordial follicle development, post-natal oocyte loss and downregulation of many critical oocyte genes including growth differentiation factor 9 (*Gdf9), Oct4* and *Padi6* (Choi et al., 2010; Choi and Rajkovic, 2006a; Rajkovic et al., 2004). Genetic ablation of *Figla* and *Nobox* shows a sexually dimorphic phenotype with male counterparts displaying normal fecundity.

On the other hand, ovarian progesterone suppresses the formation of primordial follicles in the foetal ovary by inhibiting tumour necrosis factor α (TNF-α), which is responsible for the selective apoptosis of oocytes to allow other oocytes to be packaged into primordial follicles (Allen et al., 2016; Kezele and Skinner, 2003; Marcinkiewicz et al., 2002; McNatty et al., 2000; Nilsson and Skinner, 2009). Inhibitory factors such as tuberous sclerosis 1 (*Tsc-1),* Phosphatase and tensin homolog *(Pten),* Forkhead box O3a *(Foxo3a),* Cyclin-dependent kinase inhibitor 1B *(Cdkn1b/p27)* and Forkhead box L2 (*Foxl2)* prevent the primordial to primary follicle transition thereby maintaining the ovarian reserve (Oktem and Urman, 2010).

1.2.2 Primordial to primary follicle transition

A range of paracrine, autocrine and endocrine factors have been implicated in the transition from primordial to primary follicle. Firstly, GC-derived KL-2 acts on its receptor, c-Kit, expressed in developing oocytes and theca cells (Horie et al., 1993; Horie et al., 1991; Manova et al., 1993; Tuck et al., 2015). Depending on how the mRNA is spliced, KL can be expressed as either a soluble (KL-1) or membrane bound form (KL-2) (Huang et al., 1992). The balance between KL-1 and KL-2 expression is thought to be critical for correct oocyte development (Hutt et al., 2006). KL-2 was found to promote primordial to primary folliculogenesis through activation of the PI3K/AKT pathway and repression of FOXO3, as well as by stimulating stroma and theca cell proliferation and thecal androgen synthesis (Parrott and Skinner, 1999; Reddy et al., 2005; Yoshida et al., 1997). Further, basic fibroblast growth factor (bFGF) in oocytes increases granulosa-derived KL expression and stimulates theca and stroma cell growth (Nilsson et al., 2001; Nilsson and Skinner, 2004; van Wezel et al., 1995). Leukaemia inhibitory factor (LIF), augmented by endocrine-derived

insulin, also promotes primordial to primary follicle transition by inducing KL-2 expression in GCs (Kezele et al., 2002a; Nilsson et al., 2002). Nerve growth factor (NGF) promotes the differentiation of flattened GCs into cuboidal GCs in preantral follicles (Dissen et al., 2001) but can inhibit meiotic maturation of oocytes in antral follicles if present at excessive levels (Zhai et al., 2018). Transcription factor, FOXL2, is expressed in pre-GCs and is believed to be necessary for their proliferation and differentiation (Schmidt et al., 2004; Uda et al., 2004). Many other factors have been identified that contribute to the development of primary follicles: TGF-α, activins, neurotrophins, Keratinocyte growth factor (KGF) and BMP4, 7 and 15, although some functional redundancy may exist (Choi and Rajkovic, 2006b; Ernst et al., 2017; Kezele et al., 2002b; Skinner, 2005). Interestingly, the regulation of the primordial to primary follicle transition also involves an inhibitory factor. Anti-Müllerian hormone (AMH), produced by the GCs of secondary, preantral and antral follicles, reduces primary oocyte apoptosis and inhibits follicle assembly as a form of negative feedback in all species (Durlinger et al., 1999; Gruijters et al., 2003; Nilsson et al., 2011; Visser and Themmen, 2005) (Gigli et al., 2005; Pankhurst, 2017). It is currently the only known negative growth factor involved in primordial follicle progression. It also appears to decrease the sensitivity of preantral follicles to FSH later in folliculogenesis (Durlinger et al., 2001).

1.2.3 Primary to preantral follicle transition

Oocyte-specific expression of TGF-β superfamily members, GDF9 and BMP15, is essential for primary to secondary follicle progression (Aaltonen et al., 1999; Dube et al., 1998; McGrath et al., 1995; Monniaux, 2016). Folliculogenesis does not progress past the primary stage and oocyte degeneration is evident in *Gdf9* null mice, as GCs fail to proliferate and the theca layer does not develop (Dong et al., 1996). Likewise, *in vivo* treatment with GDF9 increases follicle activation (Vitt et al., 2000). BMP15 is also important in this transition, although *Bmp15* null mice remain fertile (Yan et al., 2001). BMP15 stimulates FSH-independent GC proliferation in preantral follicles (Otsuka et al., 2000). Furthermore, BMP15 may be involved a negative feedback loop with KL to regulate GC mitosis (Hutt and Albertini, 2007; Otsuka and Shimasaki, 2002). Interestingly, sheep with heterozygous mutations in *GDF9* and *BMP15* are used in farming as they have an increased ovulation rate and can produce more offspring, however, homozygous mutations in ovine *GDF9* and *BMP15* cause infertility (Hanrahan et al., 2004). In bovine, GDF9 stimulates thecal proliferation but

inhibits steroidogenesis in early stage follicles (Spicer et al., 2008) and prevents cumulus cell apoptosis within the COC (Hussein et al., 2005). Juengel et al. (2009) demonstrated that immunisation of cattle against BMP15 resulted in either infertility or increased prolificacy while immunisation against BMP15 with GDF9 peptides increased ovulation rates. KD of BMP15 in pigs markedly reduced fertility by supressing FSH receptor expression and causing premature luteinisation of GCs (Qin et al., 2019). Moore et al. (2004) suggest that GDF9 and BMP15 determine ovulation quota. It has also been observed that theca-derived androgens, particularly testosterone, act on GCs of preantral follicles to promote follicular growth thereby decreasing the pool of primordial follicles (Steckler et al., 2005; Vendola et al., 1998). This is also true for early follicular development in the bovine species (Yang and Fortune, 2006).

1.2.4 Antral follicle development and dominant follicle selection

Activins and TGF-β appear to promote later stages of folliculogenesis characterised by continual proliferation of surrounding somatic cells and increasing volume of the oocyte (reviewed by Wijayarathna and de Kretser (2016). Granulosa-derived activin A induces antral follicle growth and suppresses early folliculogenesis (Liu et al., 1998b) by promoting FSH and LH receptor expression, oestradiol synthesis, oocyte maturation and aromatase activity (Findlay, 1993). These molecular changes are critical as disruption to activin activity causes arrest of follicle development (Matzuk et al., 1995). TGF-β expressed from granulosa and theca cells in the early antral stages is also thought to increase FSH and LH receptor expression and stimulate progesterone and inhibin production (Chegini and Flanders, 1992; Matzuk et al., 1996). Further, in all species, activin A, TGF-β, theca-derived BMP4 and 7 and oocyte-derived BMP6 induce aromatase activity and inhibit LH-induced androgen production in theca cells (Brankin et al., 2005; Glister et al., 2005; Knight and Glister, 2006). As follicles mature and grow in size, there is a switch in expression in GCs from activin A to inhibin A (Yamoto et al., 1992). Inhibin A increases LH-induced androgen secretion from theca cells which increases oestrogen production during the preovulatory period whilst suppressing FSH secretion (Oktem and Urman, 2010). In addition, activin A has been shown to accelerate oocyte maturation and improve developmental competence whereas inhibin A can act as a meiotic inhibitor (Alak et al., 1998; Silva et al., 1999; Silva and Knight, 1998).

In monovulatory species, dominant follicle selection relies on sensitivity to FSH (Baerwald et al., 2012; Picton and McNeilly, 1991). Early folliculogenesis up to primary stages is not gonadotrophin-dependent and BMP15 inhibits the expression of FSH receptors in developing follicles (Otsuka et al., 2000). Later, follistatin prevents the inhibitory action of BMP15, allowing expression of FSH receptors on the surrounding GCs (Otsuka et al., 2001). High expression of follistatin has been observed in dominant follicles, showing that high granulosa FSH receptor expression alongside granulosa cell LH receptor and FSH-induced aromatase activity, is important in dominant follicle selection (Oktem and Urman, 2010). BMP15 and GDF9 act in synergy to inhibit FSH-induced progesterone synthesis and therefore avoid premature luteinisation (McNatty et al., 2005; Vitt et al., 2000). Theca-derived BMP4 and 7 also prevent early luteinisation by suppressing FSH-dependent progesterone production and enhancing FSH-dependent oestradiol production (Lee et al., 2001). In bovine, 2-3 waves of follicular development consisting of 3-6 antral follicles of >5mm in diameter occur per oestrous cycle in response to high levels of FSH (Ginther et al., 2003; Ginther et al., 1996). A few days later, 1 follicle becomes larger (approximately 8mm in diameter) than the other follicles, which are now called subordinate follicles, and continues to grow at a faster rate (Beg and Ginther, 2006). Large antral follicles shift from requiring FSH to requiring LH (Campbell et al., 1995; Rodgers and Irving-Rodgers, 2010). Under LH stimulation, the dominant follicle produces enough oestradiol to induce the preovulatory LH surge and cause ovulation of the oocyte from the dominant follicle and atresia of the subordinate follicles (Baird and McNeilly, 1981). Figure 1.2 shows the stages of folliculogenesis from germ cell nest breakdown to ovulation of a mature MII oocyte and formation of the CL (Georges et al., 2014).

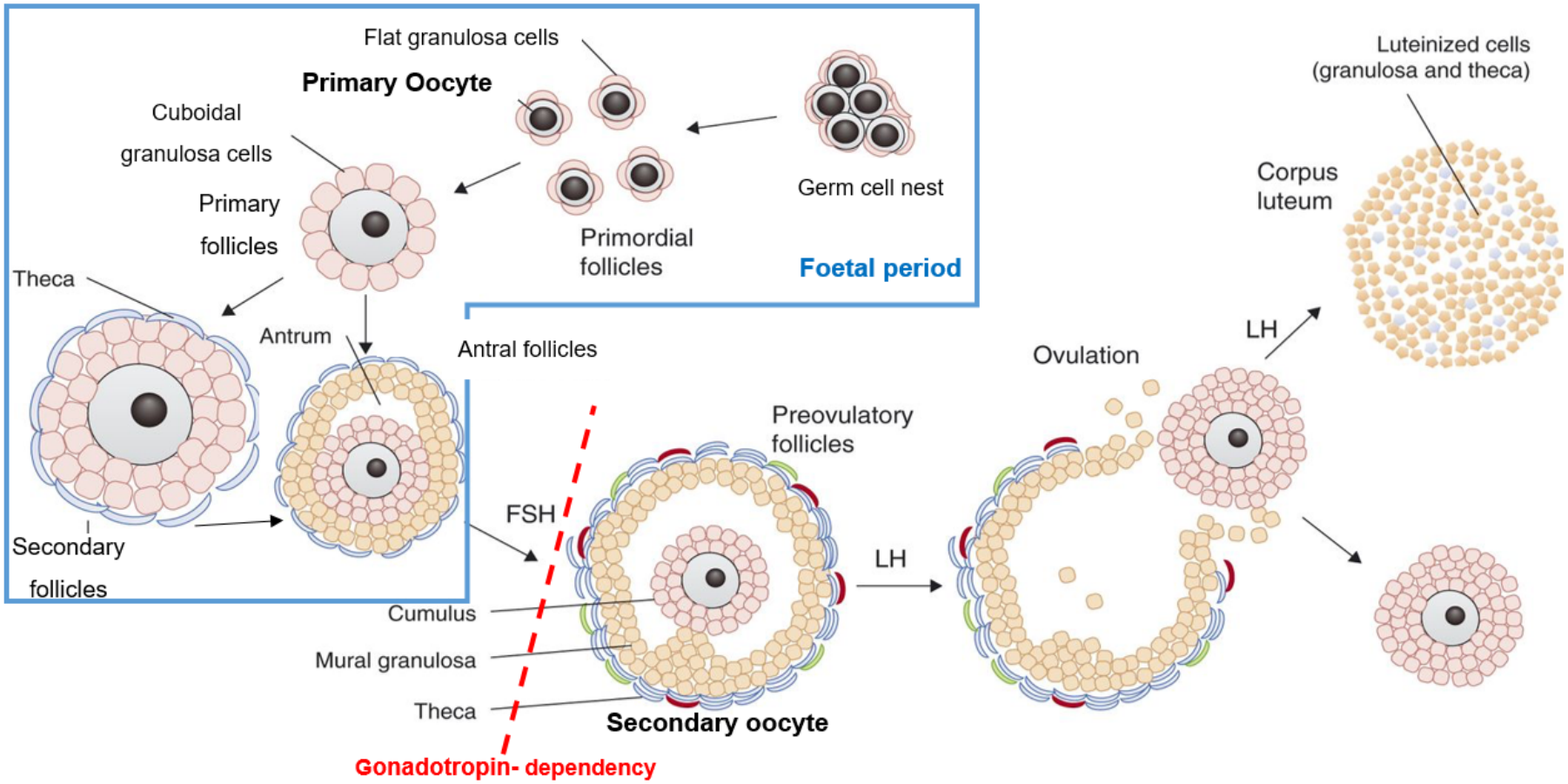

Figure 1.2 The stages of folliculogenesis adapted from Georges et al. (2014). Before birth, germ cell nests breakdown and primary oocytes become surrounded by flat GCs to form primordial follicles. As the follicle develops, the somatic cells differentiate into thecal cells, mural GCs and cumulus cells. At puberty, gonadotrophins stimulate resumption of meiosis, selection of the dominant follicle and ovulation of a mature MII oocyte. The red line shows the switch to gonadotropin-dependency.

1.3 Oogenesis

The complexity of female gamete production is partly demonstrated by the interplay between somatic cells and the oocyte during folliculogenesis (Figure 1.2). The process of oogenesis describes the nuclear and cytoplasmic maturation of an oocyte within a follicle to become developmentally competent. Nuclear, or meiotic, maturation describes the pausing and resumption of meiosis to create a haploid genome. Cytoplasmic maturation involves the production and storage of proteins and transcripts for fertilisation, resumption of meiosis, sperm processing, organelle redistribution, epigenetic reprogramming and early embryonic development. Oogenesis is a complex and tightly coordinated process that has been intensively studied for many years, with particular emphasis on meiosis. It is only more recently that researchers have recognised the importance of cytoplasmic maturation.

1.3.1 Meiotic arrest and nuclear maturation of the oocyte

The mechanisms used to maintain meiotic arrest and the resumption of oocyte nuclear and cytoplasmic maturation are increasingly well understood and generally conserved between mice, humans and bovine (reviewed by Pan and Li (2019). Oogonia undergo leptotene, zygotene and pachytene stages of prophase I before arresting as primary oocytes at diplotene. The DNA has been duplicated (2n, 4C) and genetic recombination/crossing over of parental chromosomes has occurred (Picton et al., 1998). Inhibitory signals must maintain meiotic arrest of oocytes for several years in large mammals (Mehlmann, 2005). One such signal, cyclic adenosine 3',5'-monophosphate (cAMP), is produced in the oocyte by conversion of adenosine triphosphate (ATP) by adenylyl cyclase (AC) in response to activation of G-protein coupled receptors on the plasma membrane (Mehlmann et al., 2002). Also produced in cumulus cells in response to FSH, cAMP is transferred to the oocyte through gap junctions (Byskov et al., 1997). High levels of cAMP in the oocyte prevent the progression of meiosis by activating protein kinase A (PKA) which activates phosphatases Wee1/Myt1. In turn, Wee1/Myt1 inactivate Cyclin-dependent kinase 1 (Cdk1) of Cdk1/Cyclin B complex called maturation promoting factor (MPF), therefore precluding mitogen-activated protein kinase (MAPK) signalling (Duckworth et al., 2002; Vaccari et al., 2008). Degradation of cAMP by phosphodiesterases (PDEs) releases meiotic inhibition (Conti et al., 2002; Masciarelli et al., 2004). Additional inhibitory signals, granulosa-derived hypoxanthine and cyclic guanosine 3′,5′-

monophosphate (cGMP), inhibit PDE3A thereby protecting elevated levels of intraoocyte cAMP (Downs et al., 1985; Eppig and Downs, 1987; Sirard and Bilodeau, 1990; Vaccari et al., 2009). Moreover, a feedback pathway involving natriuretic peptide precursor type C (NPPC) from mural GCs and its receptor natriuretic peptide receptor 2 (NPR2) on cumulus cells has been observed. Binding of NPPC to NPR2 activates guanylyl cyclase activity in cumulus cells to produce cGMP, which enters the oocyte through gap junctions, maintaining meiotic arrest. To this end, oocytes upregulate the expression of NPR2 in cumulus cells, which further sensitises cumulus cells to NPPC (Zhang et al., 2010). Figure 1.3a shows a simplified mechanism for maintaining meiotic arrest of primary oocytes.

Resumption of meiosis occurs due to preovulatory activation of LH receptors on mural GCs (Peng et al., 1991). During germinal vesicle break down (GVBD), the first polar body is extruded, and the chromatin condenses. Prior to GVBD, chromatin exists in an open state allowing maximal transcription for oocyte growth. During maturation, chromatin condenses into heterochromatin around the nucleolus, termed surrounded nucleolus (SN) in mice, and the oocyte becomes transcriptionally inactive in preparation for the resumption of meiosis for the second time (Christians et al., 1999). This is consistent with the observed decrease in transcripts in MII oocytes compared with GV oocytes. Chromatin condensation appears to be required for developmental competence (Lodde et al., 2007). Cumulus-oocyte communication, involving cAMP signalling, is key to chromatin remodelling as denuded oocytes remain transcriptionally active (De la Fuente and Eppig, 2001; Luciano et al., 2011b). In bovine, premature removal of cAMP resulted in immediate condensation of chromosomes into GV2/GV3 configuration and resulted in lower cleavage and blastocyst rates (Luciano et al., 2011a).

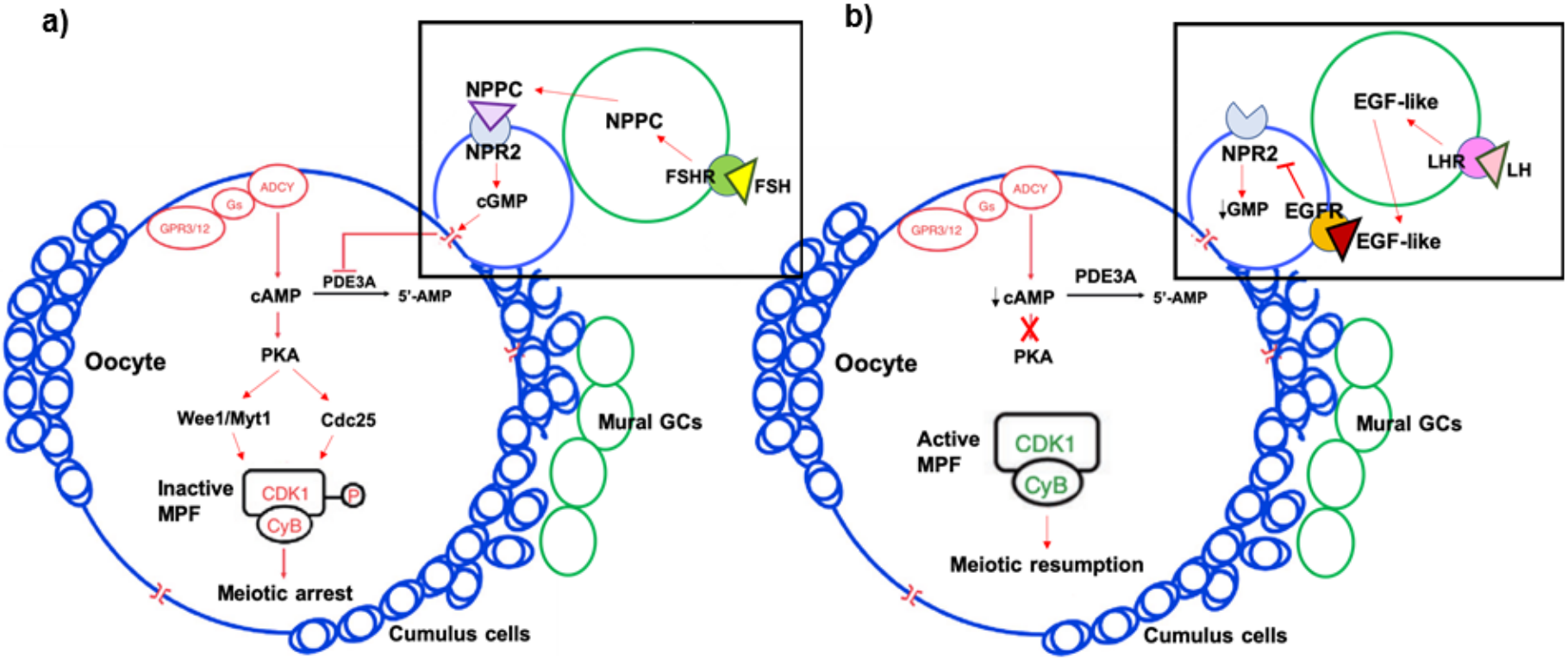

Figure 1.3 **a)** Meiotic arrest of primary oocytes at prophase I of meiosis I. cAMP activates PKA which activates phosphatases Wee1/Myt1 and Cdc25 leading to inactivation of MPF. FSH stimulation of mural GCs causes production of NPPC that acts on NPR2 on cumulus cells. Activation of NPR2 causes production of cGMP in cumulus cells which enters the oocyte through gap junctions. cGMP inhibits PDE3A activity and hydrolysis of cAMP, so cAMP levels remain high. **b)** Resumption of meiosis I by LH stimulation. LH stimulates the production of EGF-like factors in mural GCs which act on cumulus cells to inhibit expression of NPR2. As a result, GMP production decreases and PDE3A hydrolyses cAMP to 5'-AMP thereby releasing the inhibition of MPF and resuming meiosis. Adapted from Liu et al. (2013).

The way in which LH indirectly promotes meiotic maturation is unclear. One mechanism proposes that LH causes expression of epidermal growth factor (EGF)-like proteins from GCs that act on cumulus cells to promote cumulus expansion and oocyte maturation (Downs et al., 1988; Panigone et al., 2008; Park et al., 2004). EGF signalling disrupts cumulus-oocyte gap junctions by MAPK-induced phosphorylation of connexin-43, the principal gap junction protein in oocytes (Kanemitsu and Lau, 1993; Norris et al., 2008). In the absence of gap junctions, the influx of cGMP from cumulus cells stops, PDE3A hydrolyses intraoocyte cAMP and MPF is active (Figure 1.3b) (Norris et al., 2009). In support of this, Cotterill et al. (2012) identified induction of an EGF-like ligand, amphiregulin (*AREG)*, in sheep COCs and mural GCs after gonadotrophin exposure *in vitro*. LH also causes release of paracrine growth factors that may act on cumulus cells to produce steroids and follicular fluid-derived meiosis-activating sterol (FF-MAS) that promote meiotic maturation (Jamnongjit and Hammes, 2005).

Following resumption of meiosis I, oocytes progress to MII (1n, 2C) where they arrest again until fertilisation. MII arrest is dependent upon the action of so-called cytostatic factor (CSF) activity, now known to be that of Mos and early meiotic inhibitor 2 (Emi2) (Masui and Markert, 1971; Reimann et al., 2001; Tung et al., 2005). Interestingly, much of this research was carried out in *Xenopus* oocytes. In a phosphorylation cascade, Mos activates MAPK kinase (MEK1), upstream of MAPK signalling (Posada et al., 1993). In turn, MEK1 activates MAPK, which phosphorylates a ribosomal protein S6 kinase (p90Rsk). p90Rsk increases cyclin B synthesis, thereby stabilising MPF. MAPK signalling is essential for arrest at the spindle assembly checkpoint (SAC) which prevents missegregation of sister chromatids (Minshull et al., 1994). Activation of SAC proteins by p90Rsk inhibits degradation of MPF and of sister chromatid adhesion protein, cohesin, by the anaphase promoting complex (APC) to maintain cell cycle arrest at metaphase (Tunquist and Maller, 2003). It is noteworthy that unlike in *Xenopus* oocytes, p90Rsk is not the downstream CSF of MAPK signalling in the mouse (Dumont et al., 2005).

Emi1 was suggested as a CSF due to its mitotic inhibition of APC-activator, cell division cycle 20 (Cdc20) (Reimann et al., 2001). However, MII arrest by Emi1 does not require MAPK signalling nor is it released by calcium exposure (Ohsumi et al., 2004). Instead, research into family member, Emi2, identified a suitable candidate for CSF activity. Emi2 is phosphorylated by MAPK, inhibits the APC, stabilises MPF and is degraded by polo-like kinase 1 (Plk1) in response to calcium signalling (Tung et al.,

2005). It is suggested that the Mos pathway maintains MPF therefore MII arrest while the Emi2 pathway acts as a switch for completion of meiosis in response to fertilisation (Madgwick and Jones, 2007; Tiwari and Chaube, 2017).

1.3.2 Cytoskeleton dynamics during meiosis

Meiosis in females is asymmetric, yielding 1 viable oocyte and 3 redundant polar bodies (Sun and Kim, 2013). Moreover, oocytes of many species, including humans and bovine, lack centrosomes and instead, rely on microtubule nucleation to coordinate spindle dynamics (Roeles and Tsiavaliaris, 2019; Sathananthan, 1997; Szollosi et al., 1972). In the GV oocyte, microtubules are found in close proximity to the chromosomes and actin filaments occupy the cortical regions (Figure 1.4) (Li et al., 2005). At GVBD, microtubules associate with the meiotic spindle in the centre of the oocyte, forming the metaphase plate (Albertini, 1992). The chromosomes move towards the cortex, a process which defines the so-called animal pole of the oocyte where the polar bodies will be extruded (Marlow, 2018). Meiotic spindle positioning is eccentric to maintain the maximal volume of cytoplasm in the oocyte. GVBD and meiotic spindle formation in meiosis I is microtubule-dependent but eccentric cortical meiotic spindle positioning is mediated by actin filaments (Sun and Schatten, 2006; Verlhac et al., 2000). Mutations in actin-binding proteins such as Formin-2 (Fmn2) and Myosin-2 cause aneuploidy in mouse oocytes due to central spindle positioning (Schuh and Ellenberg, 2008). Spindle migration appears to occur in 2 distinct movements: a slow random initial movement, followed by a fast and directed movement (Yi et al., 2013). The first movement is thought to be mediated by Fmn2-induction of F-actin nucleation as spindle movement in *Fmn2*$^{-/-}$ mouse oocytes is disrupted. Conversely, the second movement coincides with a phenomenon called cytoplasmic streaming whereby the cytoplasm is drawn away from the cortical region to the opposite pole before returning to the centre of the oocyte, which pushes the MI spindle towards the cortex. It has been suggested (Yi et al., 2013) that the slow chromosome movement towards to cortical stimulates localisation and activation of actin-related protein 2/3 complex (Arp2/3) which induces actin nucleation and cytoplasmic streaming. Moreover, Arp2/3 are responsible for the formation of a thicker cortical region called the subcortex (Namgoong and Kim, 2016). Inhibition of Arp2/3 in porcine oocytes prevented meiotic maturation (Wang et al., 2014a).

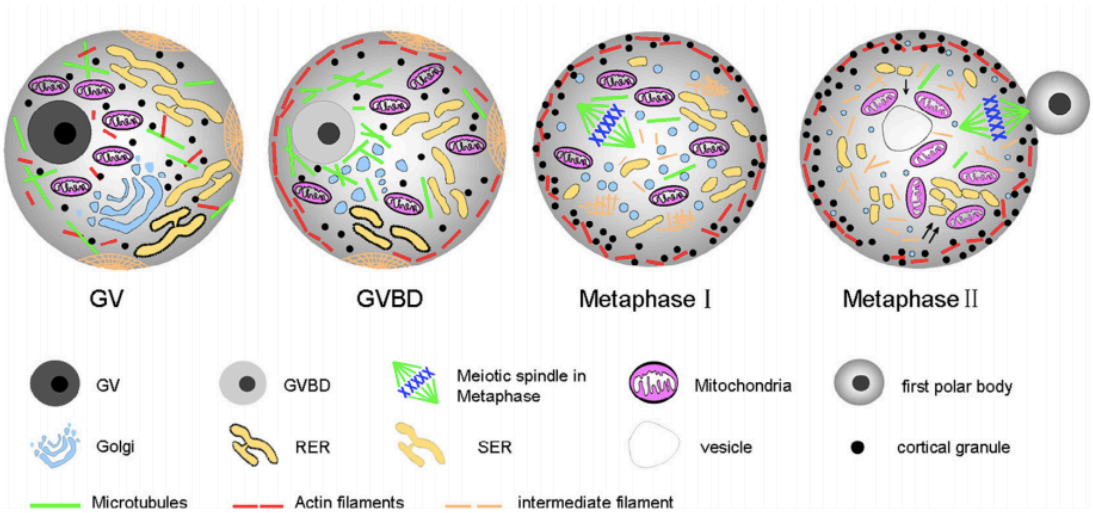

Figure 1.4 Distribution of cytoplasmic organelles and the cytoskeleton during oocyte maturation. In GV oocytes, the ER is a fine network, Golgi fragments are found in stacks and cortical granules and microtubules are diffuse in the cytoplasm. Intermediate filaments accumulate in the subcortex. Following GVBD, mitochondria surround the metaphase I spindle, the ER migrates towards the oocyte cortex and Golgi stacks disperse into smaller clusters. At MI, microtubules form the meiotic spindle and cortical granules translocate to the cortical regions along actin filaments. By MII arrest, the first polar body has been extruded, the meiotic spindle has formed, ER clusters are seen in the cortical regions away from the MII spindle and mitochondria are more diffusely spread in the oocyte. Figure from Mao et al. (2014).

As the chromosomes segregate during anaphase I, both microtubules and actin filaments are observed around the chromosomes. Actin is thought to be necessary for assembly of kinetochore fibres (K-fibres) consisting of microtubule bundles and associated proteins attached to chromosome kinetochores that facilitate chromosome segregation (Mogessie and Schuh, 2017). Furthermore, actin filaments in spindles appears to be conserved between species (Mogessie and Schuh, 2017). Research in *Xenopus* oocytes suggests that the association of actin and K-fibres is mediated by the actin-binding protein, Nabkin (Samwer et al., 2013). It is observed that eccentric positioning of the GV and meiotic spindle coincides with enrichment of gap junctions with cumulus cells (Barrett and Albertini, 2010). Interestingly, an increased number of microtubules and actin filaments associate with the chromosome set that is destined for the polar body (Li et al., 2005). The MII spindle is also maintained at the periphery by cytoplasmic streaming through the action of Arp2/3 complex (Yi et al., 2011). In mouse oocytes, chromosomes at the periphery initiate formation of an actin cap surrounded by a ring of Myosin-2 which facilitates extrusion of the polar bodies (Brunet and Verlhac, 2011; Maro et al., 1986). It is believed that formation of

the actomyosin cap and cytoplasmic streaming by Arp2/3 occurs through a cascade of events mediated by Ras-related nuclear protein (Ran) signalling (Coticchio et al., 2015; Deng et al., 2007). Recently, an abundance of actin was identified near the spindle in the cortex of MII oocytes but not GV oocytes in humans (Coticchio et al., 2014). Interestingly, the same study recognised a reduction in actin abundance and polymerisation with increasing maternal age.

1.3.3 Cytoplasmic maturation of the oocyte

Less well documented are the dynamic processes surrounding cytoplasmic or molecular maturation. These processes facilitate fertilisation, sperm DNA processing, resumption of meiosis, epigenetic reprogramming and early embryo development (Ajduk et al., 2008). Furthermore, cytoplasmic maturation involves stockpiling all the necessary transcripts and proteins for overseeing the oocyte to embryo transition (Picton et al., 1998). A large number of MEGs have been identified whose sole purpose is to facilitate early embryo development (discussed in Section 1.7) (Li et al., 2013). It is critical for the cytoskeleton to be dynamic throughout meiosis and oocyte maturation. The cytoskeleton is not only responsible for correct alignment and segregation of chromosomes but also the reorganisation and trafficking of organelles and proteins within the oocyte (Coticchio et al., 2015). Figure 1.4 shows the changes in distribution of cytoplasmic organelles and cytoskeleton during oocyte maturation.

1.3.3.1 Reorganisation of the endoplasmic reticulum

At fertilisation, sperm entry triggers IP_3-induced oscillations of Ca^{2+} from the smooth endoplasmic reticulum (ER), which in turn causes cortical granule release and resumption of meiosis (Ducibella et al., 2006). In preparation, the ER undergoes drastic reorganisation during oocyte maturation. In mouse GV oocytes the ER is a fine network in the cytoplasm (Figure 1.4) (Coticchio et al., 2015). After GVBD, the ER and Formin-2 (Fmn2) assemble into a dense ring surrounding the chromosomes in the centre of the oocyte (Yi et al., 2013). This co-localisation is critical for spindle migration to the cortex. ER redistribution is mediated by microtubules and its motor protein, dynein (FitzHarris et al., 2007). During maturation, the ER associates with the meiotic spindle apparatus and migrates towards the oocyte cortex. Experimental disruption to ER localisation causes dispersion of Fmn2 around the spindle and inhibits spindle migration in mouse oocytes (Yi et al., 2013). By MII arrest, the ER rings are no longer present and instead, fine ER clusters are seen in the cortical

regions away from the MII spindle (Mehlmann et al., 1995; Shiraishi et al., 1995). Alongside this, IP_3 receptors become enriched in cortical regions and localise in ER clusters (Fujiwara et al., 1993; Mehlmann et al., 1996). In bovine, reorganisation of the ER is slightly different as the ER is predominantly cortical in GV oocytes and becomes dispersed in small clusters in MII oocytes (Payne and Schatten, 2003). Intracellular stores of Ca^{2+} increase during the GV to MII transition (Tombes et al., 1992) (Coticchio et al., 2012). As a result of oocyte maturation, the ER is sensitised and poised for sperm entry. Following resumption of meiosis and polar body extrusion, the ER clusters disassemble and calcium signalling stops (Stricker, 2006). Interestingly, Kim et al. (2014) demonstrated abnormalities in ER redistribution and Ca^{2+} oscillations in mouse oocytes with partial loss of function mutations in *Mater* gene (see Section 1.7.2.1).

1.3.3.2 Redistribution of mitochondria

Oocyte growth demands an increased production of ATP to facilitate maturation processes and ultimately, early embryo development (Stojkovic et al., 2001). Correct mitochondrial functioning, copy number and distribution are required for metabolic pathways to ensue. At fertilisation, ATP is necessary for Ca^{2+} oscillations, which in turn increases mitochondrial production of ATP (Dumollard et al., 2004). In mouse GV oocytes, mitochondria are positioned peripherally but upon GVBD, they surround the metaphase I (MI) spindle (Figure 1.4) (Dalton and Carroll, 2013). At this stage, there is also an increase in mitochondrial membrane potential that is dependent upon meiotic progression (Al-Zubaidi et al., 2019). Mitochondria remain positioned by the meiotic spindle and ER as the chromosomes migrate to the periphery along microtubules (FitzHarris et al., 2007). After extrusion of the first polar body they are found diffusely spread in the cytoplasm and associated with lipid droplets (Fair et al., 1997b). In MII oocytes, mitochondria are more diffusely spread in the oocyte but again, distribute around the pronuclei in the cytoplasm of the zygote to meet the increased energy requirements of spindle apparatus (Van Blerkom et al., 2000). It has been noted that a subpopulation of highly polarised and functionally active mitochondria reside in the subcortical region of the MII oocyte, possibly in preparation for fertilisation (Van Blerkom et al., 2002; Yu et al., 2010). Redistribution of mitochondria in bovine and human oocytes is similar to mouse oocytes (Hyttel et al., 1997; Van Blerkom, 2004).

Large numbers of mitochondria are critical for oocyte competence as it ensures sufficient production of ATP and redistribution of organelles in the oocyte and developing embryo (Zeng et al., 2009). Mitochondrial DNA (mtDNA) copy number in human MII oocytes has been estimated between 20,000 and 800,000 copies (Van Blerkom, 2004). Cotterill et al. (2013) showed that there was an increase in mtDNA copy number of >1000 fold from primordial follicle to antral follicle stage in sheep. An increase in oocyte metabolism coinciding with antrum formation has also been documented in mice (Harris et al., 2007; Harris et al., 2009). Furthermore, oocyte-derived Gdf9 and Bmp15 have been shown to stimulate cumulus metabolism in mouse oocytes at this stage (Sugiura et al., 2007). Mitochondrial distribution and ATP content in bovine oocytes positively correlated with increased blastocyst rate in *in vitro* produced embryos (Hashimoto et al., 2019; Stojkovic et al., 2001). With increasing maternal age, mitochondrial copy number and ATP production is reduced in mice, hamsters, sheep and humans while mitochondrial abnormalities and mutations are increased (Rambags et al., 2014; Rebolledo-Jaramillo et al., 2014; Simsek-Duran et al., 2013).

After fertilisation, mitochondrial activity is said to be intermediate during early embryo development to reduce toxicity by reactive oxygen species (ROS) produced as a by-product of mitochondrial metabolism (Ferreira et al., 2009). In bovine and porcine, mtDNA replication does not take place in the preimplantation embryo until after the morula stage as mtDNA replication factors are not expressed (May-Panloup et al., 2005; Spikings et al., 2007). As a result, the mtDNA copy number in each blastomere decreases with each embryonic cleavage event. At the blastocyst stage, upregulation of mtDNA replication factors such as polymerase gamma A (POLGA) in the trophectoderm causes an increase in both mtDNA copy number and ATP production by oxidative phosphorylation (St John, 2012; St John et al., 2010) while the inner cell mass maintains low levels of mtDNA to support undifferentiated cell division (St John et al., 2017).

1.3.3.3 Redistribution of cortical granules and the Golgi apparatus

In somatic cells, the Golgi apparatus functions in the post-translational modification and packaging of proteins for intracellular trafficking and extracellular secretion. During mitosis, the Golgi associates with the centrosome at interphase and subsequently fragments upon centrosome duplication at S phase to distribute equal

amounts of the organelle into both daughter cells (Huang and Wang, 2017). The distribution of the Golgi complex in meiosis is not clear as the centrosomes are lost during early oogenesis. Likewise, its role in extracellular protein secretion is not required in the oocyte, however it is necessary for the production of cortical granules (Coticchio et al., 2015).

In mouse and bovine GV oocytes, Golgi fragments are found in stacks, known as "mini-Golgis" in the cytoplasm with moderately more stacks residing in the centre than in the periphery (Hyttel et al., 1986; Moreno et al., 2002). At GVBD, the stacks disperse into smaller clusters with homogenous distribution throughout the cytoplasm. In bovine, the distinct clusters associate with ER vesicle export regions, not the meiotic spindle as observed in mitosis (Figure 1.4) (Payne and Schatten, 2003). This is believed to prevent loss of Golgi complex to polar bodies upon cytokinesis. The Golgi structure contains various proteins including cis-Golgi matrix protein, GM130 (Nakamura, 2010). Phosphorylation of GM130 by Cyclin B-CDC2 is believed to cause dispersion of the Golgi into fragments – a necessary step in Golgi redistribution during oocyte maturation (Racedo et al., 2012). The same study found that Golgi localisation and anchoring of the Golgi at GVBD was dependent upon dynein and microtubules, respectively. Moreover, GM130 is thought to play a role in spindle dynamics in the mouse oocyte as gene knockdown (KD) disrupted spindle migration and resulted in extrusion of a large polar body (Zhang et al., 2011).

The function of the Golgi in the oocyte is elusive, however in mouse oocytes, inhibition of trafficking from the ER to the Golgi reverses meiotic maturation (Moreno et al., 2002). This suggests that membrane trafficking and post-translational modification of proteins by the Golgi is necessary for meiotic progression. In support of this, ablation of different glycosyltransferases in the Golgi negatively impacts oogenesis (Akintayo and Stanley, 2019). In addition, the Golgi complex is necessary for the production of cortical granules during oocyte development (Coticchio et al., 2015). Cortical granules release proteolytic enzymes into the perivitelline space that modify zona pellucida protein, ZP2, thereby inhibiting sperm entry (Sun, 2003). In GV oocytes, cortical granules are diffuse in the cytoplasm but translocate to the cortical regions along actin filaments upon maturation (Figure 1.4) (Cran and Cheng, 1985; Wessel et al., 2002). This redistribution is essential in preparation for fertilisation as the cortical reaction is critical to block polyspermy – the fertilisation of an oocyte by >1 sperm which is detrimental to the embryo (Snook et al., 2011). In response to Ca^{2+} signalling by the ER after fertilisation (described in Section 1.4), cortical granules fuse with the plasma

membrane in a vesicle exocytosis mechanism that is believed to be mediated by soluble NSF-attachment receptor (SNARE) proteins (Liu, 2011; Tsai et al., 2011).

1.3.3.4 Accumulation of maternal transcripts and polyadenylation

After resumption of meiosis, gene expression ceases until the embryonic genome is activated. Maternally-derived transcripts that accumulated during prophase I must be carefully stored and temporally translated during oocyte maturation and early embryo development (Lodde et al., 2017). Inactive transcripts are incorporated into ribonucleoprotein (RNP) structures to prevent mRNA from degradation (Davidson, 1976). Translation of dormant maternal mRNAs can be regulated by polyadenylation (Reyes and Ross, 2016). Polyadenylation describes the addition of adenine (A) to the 3' end of the mRNA by polyA polymerase. Long polyA tails are generally found on translationally active mRNAs whereas short polyA tails render transcripts inactive and may precede mRNA degradation (Curtis et al., 1995). Transcripts for storage have a cytoplasmic polyadenylation element (CPE) in the 3' untranslated region (UTR) that is bound by cytoplasmic polyadenylation element binding proteins (CPEB) (Paris and Richter, 1990). CPEB proteins function as both repressors and promoters of polyadenylation depending upon the phosphorylation status. End-to-end communication has been observed between the 3' UTR and 5' regulatory cap of mRNA (Dreyfuss et al., 1996). In the repressive state, 3' CPEB and 5' translation initiation complex eIF-4E become bound by maskin and polyA specific ribonuclease (PARN) which inhibits protein synthesis (Stebbins-Boaz et al., 1999). In contrast, upon re-entry into meiosis, phosphorylation of CPEB releases inhibition and allows polyadenylation of mRNA leading to protein synthesis (Kim and Richter, 2006). This mechanism is responsible for the translational activation of dormant transcripts, *Mos* and *cyclin B1* of MPF, during oocyte maturation (Reyes and Ross, 2016). At GVBD, there is an increase in polyadenylation of transcripts which continues until MII arrest. Consequently, an increase in protein synthesis is observed from GVBD to MI but this ceases by MII stage, suggesting a mechanism of polyA mRNA translational repression (Tomek et al., 2002b). It has been demonstrated that polyadenylation is essential for meiotic progression of bovine oocytes (Traverso et al., 2005). With the advancement of RNA sequencing (RNA-seq) technologies, Reyes et al. (2015) have recognised changes in polyA tail length during bovine oocyte maturation which might have been previously missed or described as changes in gene expression. With this, new information can be gathered about the translational silencing of mRNAs by deadenylation.

Recently, a novel regulatory mechanism involving RNA methylation was recognised in *Xenopus* and mouse oocytes (Ke et al., 2015; Qi et al., 2016). Mapping of N^6-methyladenosine (m^6A) in the mammalian transcriptome showed that it is a prevalent mRNA modification that is enriched at stop codons and within 3' UTRs (Ke et al., 2015; Meyer et al., 2012). In *Xenopus* oocytes, m^6A was identified in >4000 transcripts and after integrating the data with transcriptomic data, m^6A was detected in 1030 mRNAs. During the GV to MII oocyte transition, m^6A decreased in all 1030 transcripts. When combined with proteome data, Qi et al. (2016) found that transcripts with high levels of m^6A had low corresponding protein levels and *vice versa*. Furthermore, m^6A in the coding DNA sequence (CDS) correlated with lower protein levels while m^6A in 3' UTR corresponded to higher protein expression. It was suggested that RNA methylation in CDS regions might suppress mRNA translation during oocyte maturation. In support of this, m^6A writers, *Mettl3* and *Mettl14*, and m^6A eraser, *Alkbh5*, were detected at high levels in growing mouse oocytes (Pan et al., 2005). Moreover, knockout of *Ythdf2*, an m^6A reader that destabilises m^6A-containing transcripts, caused infertility in female mice characterised by embryonic arrest at the 2-cell stage (Ivanova et al., 2017). They found that ~200 additional transcripts were present in *Ythdf2*-/- MII oocytes compared to control MII oocytes and concluded that YTHDF2 is necessary to regulate transcript dosage during oocyte maturation.

Finally, non-coding RNAs (ncRNAs) such as long ncRNAs (Section 1.6 and 1.6.1) and microRNAs (miRNAs) have a significant role in post-transcriptional gene regulation in development. miRNAs bind to target mRNA, reduce translation and cause transcript degradation through an endogenous RNA-induced silencing pathway (Section 4.1). There are now >12000 known miRNA sequences that are believed to regulate approximately 1/3 of protein-coding genes (Krol et al., 2010). miRNAs do not require complete complementarity to repress transcripts however the degree of similarity is thought to determine the mode of silencing (Hayder et al., 2018). To this end, miR-145 was found to regulate multiple key factors, IGF1R, EGFR, IRS1 and ERK, within a pathway involved in trophoblast proliferation (Forbes, 2013). The importance of gene regulation by miRNAs is highlighted by knockout experiments of miRNA-processing factors including *Dicer, Dgcr8, Drosha* and *Ago2* that result in embryonic loss and infertility in mice (Park et al., 2010). miRNAs are critical in regulating every stage of development from folliculogenesis, oocyte maturation, placentation and development *in utero* (Tesfaye et al., 2018). miR-21 was found to have an anti-apoptotic effect in granulosa cells of mouse preovulatory follicles (Carletti et al., 2010) and inhibition of miR-21 reduced the percentage of

porcine oocytes that progressed to the MII oocyte stage and negatively impacted preimplantation embryo development (Wright et al., 2016). It is interesting to note that many of the 3' UTRs enriched in m^6A also contained miRNA binding sites, suggesting there might be a functional link between m^6A and miRNA in transcript regulation (Meyer et al., 2012). In support of this, it is believed that the addition of m^6A to primary miRNAs by METTL3 enables recognition by DiGeorge Critical Region 8 (DGCR8), which enables cleavage into precursor miRNA by DROSHA (Alarcon et al., 2015). Finally, another group of small ncRNAs, piwi-interacting RNAs (piRNAs), have been identified in non-murine mammalian oocytes and preimplantation embryos (Roovers et al., 2015). piRNAs are essential for germ line development (Ketting, 2011) as they mediate silencing of transposable elements and repetitive sequences in the genome (Saito and Siomi, 2010).

1.3.3.5 Redistribution of ribosomes

Oocyte maturation is important for producing and storing all the components necessary for early embryo development. To this end, protein synthesis is critical. In bovine GV oocytes, the nucleolus is granular, and no ribosome or protein synthesis is observed (Ferreira et al., 2009). Following GVBD and in concordance with increased polyadenylation of mRNAs, there is a substantial increase in protein synthesis, characterised by the presence of a fibrillogranular nucleolus (Fair et al., 1997a; Fair et al., 2001). In bovine, this is coupled with phosphorylation of eukaryotic translation initiation factor 4E (EIF4E) which binds to the 5' cap of mRNAs and supports the binding of the small ribosomal subunit to promote translation (Tomek et al., 2002a). By the MII stage, the nucleolus has dissolved, protein synthesis has slowed, and ribosome levels are low (Tomek et al., 2002b). Despite this, EIF4E remains phosphorylated which led to the identification of an EIF4E repressor 4E-BP1 that is believed to suppress EIF4E in both bovine and porcine MII oocytes (Ellederova et al., 2006; Tomek et al., 2002a). The change in abundance of ribosomal components coincides with the changing requirements for growth and protein synthesis throughout oocyte maturation (Jansova et al., 2018). Genome-wide transcriptome analysis has shown that mRNAs for ribosomal components are degraded during maturation and replaced by embryonic transcripts after EGA (Susor and Kubelka, 2017).

During oocyte maturation large cytoskeletal structures known as cytoplasmic lattices (CPLs) accumulate. They are characteristic of growing mammalian oocytes and remain present in the early embryo (Schlafke and Enders, 1967). There are several proposed functions of CPLs but evidence shows that they provide a necessary storage site for ribosomes in the mature oocyte (Bachvarova et al., 1981). The formation of CPLs requires expression of MEG PADI6 (Wright et al., 2003). In mouse oocytes, knockout of *Padi6* and subsequent loss of CPL structures caused an increase in free ribosomes in the cytoplasm (Yurttas et al., 2008). This also resulted in reduced levels and aberrant localisation of ribosomal S6 protein and RNA polymerase II which was accompanied by global decrease in protein synthesis in *Padi6*$^{-/-}$ mouse embryos. The structure and significance of CPLs is discussed in more detail in Section 1.7.3.2.

1.4 Fertilisation and oocyte activation

Once ovulated the secondary oocyte is arrested in MII and will only complete meiosis and become activated upon fertilisation. In order for fertilisation to occur, the sperm must undergo a form of physiological maturation within the female reproductive tract, known as capacitation (Puga Molina et al., 2018). During capacitation, sperm gain greater motility and become able to penetrate the egg via the acrosome reaction (AR) (Ickowicz et al., 2012). Efflux of cholesterol increases the membrane permeability to Ca^{2+} and bicarbonate, which consequently stimulates cAMP production and PKA activation (Visconti et al., 1995; Visconti et al., 1999). Resultant tyrosine phosphorylation causes F-actin polymerisation and PLC is translocated to the plasma membrane (Spungin et al., 1995; Swann and Lai, 2016). PKA activation also causes hyperactivated sperm motility allowing sperm to swim vigorously to the oocyte (Ho and Suarez, 2001). This may be controlled by progesterone signalling from cumulus cells (Lishko et al., 2011). Fertilisation of intact cumulus-oocyte complexes is more efficient than that of oocytes alone (Jin et al., 2011). Cumulus-derived progesterone acts as a chemo-attractant for directing sperm motility (Oren-Benaroya et al., 2008). Furthermore, cumulus cells are enriched in hyaluronic acid (HA) which enables sperm progression to the oocyte due to hyaluronidases, such as SPAM1, on the sperm surface (Kimura et al., 2009). It is also believed that sperm hyaluronidases breakdown cumulus-HA into HA fragments which activate toll-like receptors (TLR2 and TLR4) on cumulus cells. In turn, cumulus cells produce chemokines that facilitate sperm capacitation creating a regulatory feedback loop (Shimada et al., 2008).

Once capacitated the sperm must penetrate the zona pellucida via the AR. The oocyte plasma membrane fuses to the outer acrosomal membrane of the sperm and hydrolytic enzymes, principally acrosin, are released from the sperm head (Hedrick et al., 1989; Rahman et al., 2017). The AR was originally thought to occur as a result of sperm binding to ZP proteins but studies have since shown completion of the AR prior to sperm-zona interactions (Jin et al., 2011). Nevertheless, gamete binding is facilitated by zona pellucida proteins, ZP1-4 in humans, although the precise mechanism is not clear. There are 2 theories: 1) ZP3 glycan release model and 2) ZP2 cleavage model (Avella et al., 2013). The latter is more widely accepted as mutant ZP2 that cannot be cleaved allows binding of more than 1 sperm, even after cortical granule release (Gahlay et al., 2010). Likewise, mammalian sperm-oocyte fusion depends on the interaction of cell surface proteins: *Juno/Izumo1r* on the oocyte

and *Izumo1* on the sperm (Bianchi et al., 2014; Inoue et al., 2005). Genetic ablation of these genes causes female and male infertility, respectively, as gamete fusion is prevented. Further, oocyte cell surface protein, CD9 antigen, is thought to facilitate this interaction by organising Juno expression within the oolemma, thereby regulating sperm adhesion sites on the oocyte (Chalbi et al., 2014).

Upon entry, a sperm oocyte-activating factor, argued to be either phospholipase C zeta 1 (PLCzeta) or post-acrosomal sheath WW domain-binding protein (PAWP), induces 1,4,5-inositol triphosphate (IP3) -dependent waves of Ca^{2+} from the ER (Amdani et al., 2015; Miyazaki et al., 1993; Yoon, 2019). Ca^{2+} signalling causes the release of CSF and activates the APC via calmodulin-dependent protein kinase II (CaMKII) (Lorca et al., 1993; Lorca et al., 1991). The APC triggers degradation of cyclins and cohesin leading to inactivation of MPF and separation of sister chromatids, respectively (Sagata, 1996; Sanders and Swann, 2016). MAPK signalling terminates as Mos protein is degraded and maternal *Mos* mRNA is deadenylated (Tunquist and Maller, 2003). Furthermore, Emi2 is degraded by Plk1. Progression through anaphase and extrusion of a second polar body upon sperm entry completes meiosis. Ca^{2+} signalling also prevents polyspermy as it triggers cytoplasmic release of cortical granules that lead to hardening of the zona pellucida and digestion of ZP proteins (Horner and Wolfner, 2008). Ovastacin from cortical granules causes cleavage of ZP2 to stop further sperm-zona binding (Bleil et al., 1981; Burkart et al., 2012). Premature cleavage of ZP2 by ovastacin is prevented by fetuin-B produced by the liver (Dietzel et al., 2013). Moreover, polyspermy may also be avoided by the vesicular export of Juno from the oocyte following fertilisation to inhibit sperm-oocyte fusion (Bianchi et al., 2014).

Karyogamy describes the fusing of the sperm and oocyte pronuclei after fertilisation to give way to a newly formed zygote. The sperm genome is highly condensed, packaged around protamines and is transcriptionally inactive (Miller, 2015). As the oocyte completes meiosis, the sperm genome is remodelled in a series of phosphorylation events; the nuclear membrane is dissolved by phosphorylation of lamin B, protamines are exchanged for histones, potentially through the action of nucleoplasmins and a new nuclear envelope is produced by the ER to complete the male pronucleus (Imschenetzky et al., 2003; Inoue et al., 2011a; McLay and Clarke, 2003). The paternal DNA undergoes extensive epigenetic remodelling; removal of protamines facilitates chromatin decondensation and incorporation of histone variants that are compatible with the female pronucleus and global DNA demethylation

triggers minor zygotic genome activation (Sections 1.5.1 and 1.6) (Okada and Yamaguchi, 2017). Both the male and female genomes undergo epigenetic reprogramming after fertilisation to create a totipotent zygote (discussed in Section 1.6.3). The sperm-derived centriole associates with maternal proteins to become a centrosome and astral microtubules reach for the female pronucleus (Schatten, 1994). The male and female pronuclei migrate towards one another, and the nuclear membranes dissolve to reveal duplicated chromosomes in prophase (Clift and Schuh, 2013). The first mitotic spindle assembles and mitosis ensues. Numerous studies have reported the importance of delivery of sperm RNA to the oocyte upon fertilisation (Boerke et al., 2007; Guo et al., 2017; Jodar, 2019). Research using sperm from *Dicer*- and *Drosha*-mutant mice revealed that sperm deliver small RNAs into the oocyte that improve developmental potential (Yuan et al., 2016). Further, studies have shown that sperm from fathers that have experienced stress transfer altered phenotypes to their offspring (Jodar, 2019).

1.5 Preimplantation embryo development

Following fertilisation, the 1-cell zygote enters mitosis which marks the start of embryonic cell divisions. Pluripotency of the embryo is maintained during the first cleavage divisions by expression of master transcriptional regulators OCT4, SOX2 and in turn, NANOG (Rodda et al., 2005). Johnson et al. (1995) showed that, unlike in other model animals, the 4 blastomeres of a 4-cell bovine embryo could develop into 4 calves, demonstrating the totipotency of the bovine 4-cell embryo (De Paepe et al., 2014). As detailed in Section 1.3.3, MEGs are transcribed during oocyte maturation and stored alongside translational machinery until after fertilisation. In the zygote, maternal mRNAs are translated to coordinate early embryo development until the embryonic genome is activated. The conventional view of timing of EGA was observed to vary among species: at the 2-cell stage in mice, 4-8 cell stage in humans and 8-16 cell stage in bovine (Telford et al., 1990) (Table 1.1). There are many genes implicated in EGA that will be discussed in Section 1.5.1.

Table 1.1 Developmental time points, including EGA, in mouse, human and bovine species

Species	Developmental time points			
	Oocyte IVM	**1st embryonic cleavage after IVF**	**Cell stage at EGA**	**Blastocyst formation**
Mouse	12-18 hr	24-32 hr	2-4-cell	Day 3-4
Human	24-30 hr	18-24 hr	4-8-cell	Day 5-6
Bovine	24-26 hr	18-24 hr	8-16-cell	Day 7

Around the 8-16 cell stage, the embryo undergoes compaction to form a morula (Clift and Schuh, 2013). Blastomeres flatten and adhere to one another while microvilli and plasma membrane components redistribute away from areas of cell-cell contact (Nikas et al., 1996). In mouse, contact asymmetry in 8-cell embryos has been shown to induce apical-basal polarity, a key determinant of lineage specialisation in the blastocyst stage (Johnson and Ziomek, 1981). Furthermore, correct expression of E-cadherin is thought to be necessary during this stage as knockout of *E-cadherin* affects cell polarity and trophectoderm (TE) formation in mouse embryos (Watson et al., 2004). After compaction, a fluid-filled cavity called a blastocoel appears in the embryo, which is now termed a blastocyst (Fleming et al., 2001). Expression of Na/K-ATPase on the basolateral membrane of the TE mediates fluid movement across the TE to fill the blastocoel cavity (Madan et al., 2007). The embryo differentiates to give rise to the first cell lineages which will become the embryo and extra-embryonic structures: the inner cell mass (ICM) and TE, respectively (Johnson and Ziomek, 1981). In mouse, cell fate appears to be dependent upon the position of the cell in the embryo as peripheral cells become TE while inner cells become the ICM (Tarkowski and Wroblewska, 1967). Movement of cells from the periphery to the centre of the blastocyst causes a switch in cell fate to ICM. This appears to be caused by the apical polarisation of cells at the 8-cell stage (Korotkevich et al., 2017). Random allocation of blastomeres to TE and ICM has also been recognised in bovine (Sepulveda-Rincon et al., 2016).

Early embryo patterning is determined by the differential expression of lineage-specific genes. In mouse, caudal type homeobox 2 (CDX2)-restriction of pluripotency genes, *Oct4* and *Nanog*, in the TE is responsible for lineage segregation from the ICM (Strumpf et al., 2005; Wu and Scholer, 2014), although prolonged colocalisation of OCT4 and CDX2 has been observed in the TE of bovine and human blastocysts but not mouse (Berg et al., 2011). Pluripotency gene *Sox2* is also necessary for TE formation by regulating TE –specific genes such as transcription enhancer factor family 4 (TEAD4) and its coactivator Yes-associated protein 1 (YAP1) which are required for zygotic CDX2 expression (Gasperowicz and Natale, 2011). Single-blastocyst sequencing (Wei et al., 2017) showed that alongside *CDX2,* keratin 8 (*KRT8),* ATPase H+/K+ transporting non-gastric alpha2 subunit *(ATP12A),* msh homeobox 2 *(MSX2),* disabled homolog 2 *(DAB2),* transcription factor AP-2 alpha *(TFAP2A)* were highly expressed in TE while goosecoid homeobox *(GSC)*, platelet derived growth factor receptor alpha (*PDGFRA)*, hepatocyte nuclear factor 4 alpha *(HNF4A)*, signal transducer and activator of transcription 3 (*STAT3*), runt related transcription factor 1 (*RUNX1*), *PRDM14*, *LIFR*, *FGFR4*, and *NANOG* were markers of ICM in bovine. FGF/MAPK signalling influences differentiation of the ICM into the primitive endoderm (PE) and the epiblast (EPI) (Rossant and Tam, 2009) by expression of PE- and EPI-specific transcription factors, *Gata6* and *Nanog*, respectively (Chazaud et al., 2006). SOX17 also causes PE specification by inducing GATA binding protein 6 (*Gata6)* and *Gata4* expression and inhibiting pluripotency-related genes (Gasperowicz and Natale, 2011). Single-embryo sequencing has revealed that developmental heterogeneity of blastomeres is apparent prior to lineage specification (Lavagi et al., 2018; Wei et al., 2017). *NANOG* transcripts were identified in the 8-cell bovine embryo (Graf et al., 2014) and expression of *SOX2* was observed from the 16-cell stage in bovine embryos before becoming restricted to the ICM alongside *OCT4* (Goissis and Cibelli, 2014). The blastocyst continues to expand until the embryo hatches from the zona pellucida and implants into the endometrium (Clift and Schuh, 2013; Forde and Lonergan, 2012).

1.5.1 Embryonic genome activation

Embryonic genome activation (EGA) is necessary for preimplantation embryogenesis. It is characterised by the production of embryonic transcripts and removal of maternal factors, signifying the transition from maternal to embryonic control (Tsukamoto and Tatsumi, 2018). Until this point the competence of the oocyte is pivotal (Zhang and Liu, 2015). EGA was first characterised in mice when the

inhibition of RNA polymerase II and III prevented zygotic genes from being transcribed, leading to arrest of development at the 2-cell stage – known as the '2-cell block' (Goddard and Pratt, 1983; Golbus et al., 1973; Latham and Schultz, 2001).

The developmental stage at which EGA is said to occur describes the major wave of embryonic activation, however EGA is thought to begin after fertilisation (Hamatani et al., 2004; Jukam et al., 2017). In mice, 3 distinct waves of EGA have been recognised: minor EGA after fertilisation, major EGA around the 2-4-cell stage and mid-preimplantation gene activation (MGA) around the 4-8-cell stage (Figure 1.5) (Wang and Dey, 2006). Zygotic transcripts have been recognised as early as the 2-cell embryo stage in humans (Vassena et al., 2011). Minor EGA is required for zygotic genome activation as inhibiting transcription at this stage reduced developmental progression past the 2-cell stage in mice (Abe et al., 2018). High throughput sequencing has shown that minor EGA is genome-wide and consists of low-level transcriptional activation in mouse 1-cell embryos (Abe et al., 2015). It is also believed that H3K4 methylation of the paternal pronucleus is required for minor genome activation (Aoshima et al., 2015). Vassena et al. (2011) demonstrated that each developmental stage was associated with distinct phases of gene expression. For example, the first wave of gene expression (~2-cell stage) was associated with upregulation of protein synthesis machinery while genes involved in transcriptional, translational and post-translational regulation were upregulated during the 4-8-cell stages (Vassena et al., 2011). MGA upregulates intracellular adhesion molecules prior to compaction and blastocyst formation (Hamatani et al., 2004). Global transcriptome assessment of normal versus EGA-inhibited 8-16-cell bovine embryos identified 2459 transcripts of embryonic origin that functioned in embryo patterning and development (Bogliotti et al., 2019). Alternatively, the maternal transcripts related to silencing gene expression and the shared transcripts were involved in epigenetic regulation. Wei et al. (2017) found that *DNMT1* and *DNMT3B* were downregulated during the 8-16 cell transition in bovine which is likely to facilitate EGA. Importantly, 3 embryonic transcription factors (KLF4, KLF5 and KLF9) were identified that targeted ~50% of the embryonic genes to direct reprogramming during bovine EGA (Bogliotti et al., 2019). Finally, differences in alternate splicing of transcripts have been observed at different developmental stages in humans (Yan et al., 2013).

As detailed in Section 1.3.3, the maternal contribution to the embryo is organised during oocyte maturation in preparation for driving early preimplantation embryogenesis prior to EGA. Many maternally-derived factors from the oocyte have

been implicated in the control of the maternal-zygotic transition (MZT) including *Ago2, Ctcf,* oocyte-specific DNA methyltransferase 1 *(Dnmt1o), Dppa3,* Heat shock factor 1 *(Hsf1), Nlrp5, Oct4, Padi6,* Zygote arrest 1 (*Zar1)* and *Zfp36l2* (Table 1.2) (Li et al., 2013; Minami et al., 2007). The functions of such genes vary, from roles in meiosis and transcriptional activation to epigenetic regulation and maternal mRNA degradation (Li et al., 2010a). Disruption to any of these genes prevents embryonic cleavage and results in developmental arrest, often at the time of EGA. For example, *Zar1* appears to function before EGA as most *Zar1*$^{-/-}$ mouse embryos arrest at the 1-cell stage displaying 2 distinct parental nuclei. A small number arrest at the 2-cell stage but no embryos progress past the 4-cell stage (Wu et al., 2003). Defective zygotic transcription in *Zar1*$^{-/-}$ mice was defined by the absence of the transcription requiring complex (TRC), a marker of EGA (Conover et al., 1991).

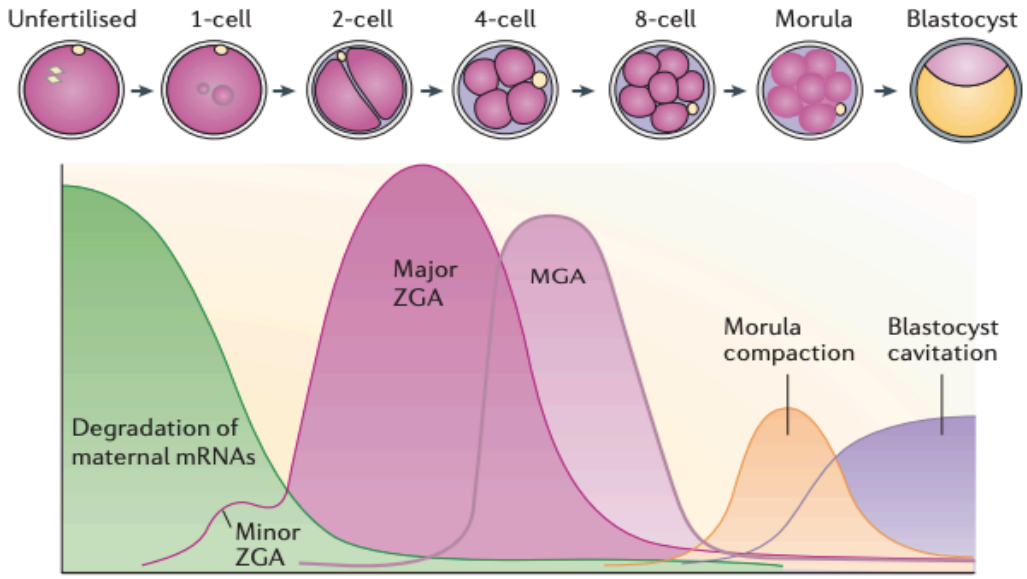

Figure 1.5 Changes in gene expression during mouse preimplantation embryo development. Degradation of maternal mRNAs is necessary for EGA. 3 distinct waves of EGA can be observed: minor EGA, major EGA and mid-preimplantation gene activation (MGA). Figure from Wang and Dey (2006). In bovine, the changes in gene expression are similar to mouse, however the process of EGA is slower as the embryonic genome becomes active at the 8-16-cell stage.

After fertilisation, post-transcriptional regulation of maternal mRNAs coordinates EGA (Section 1.5.1). Degradation of maternal transcripts and proteins is an essential step in the transition to embryonic control (Clegg and Piko, 1983; Schier, 2007). Maternal components and zygotic miRNAs facilitate mRNA degradation while ubiquitin-

dependent pathways and autophagy coordinates the removal of maternal proteins (Giraldez, 2010; Tsukamoto and Tatsumi, 2018). *Argonaute (Ago2)* is involved in mRNA degradation, specifically RNA silencing in response to double-stranded RNA (dsRNA) species (Meister and Tuschl, 2004). Ablation of *Ago2* in mouse embryos results in developmental arrest at the 2-cell stage, stabilisation of a set of maternal transcripts and reduced transcription of specific zygotic mRNAs. Further, embryonic miRNAs have been identified that target specific maternal transcripts, activate AGO2 of the RNA-induced silencing complex (RISC) and result in their degradation (Lykke-Andersen et al., 2008). For example, miRNA-212 represses *FIGLA* mRNA in bovine 4-8-cell embryos (Tripurani et al., 2013). RNA methylation has been implicated in maternal mRNA stability and clearance in the embryo. 5-mC has been recognised in mRNAs and found to regulate mRNA stability alongside 5-mC binding proteins Ybx1 and Pabpc1a in zebrafish (Yang et al., 2019). Loss of Ybx1 decreased maternal mRNA transcript abundance and caused developmental arrest. Inactivation of *ythdf2* in zebrafish resulted in reduced clearance of m^6A-modified maternal mRNAs which disrupted EGA and caused long term developmental delay of the larvae (Zhao et al., 2017). They showed that the removal of transcripts was enhanced by the m^6A mark. Moreover, an enzyme called Wispy was identified in *Drosophila* that adenylates miRNAs, interacts with Ago2 and is believed to facilitate clearance of maternal miRNAs during EGA (Lee et al., 2014b). Similarly, disruption to *Zfp36l2* stabilises a subset of maternal transcripts and inhibits embryonic progression past the 2-cell stage (Ramos et al., 2004). Like transcription, degradation of maternal mRNAs occurs in waves that correspond to zygotic transcription and the metabolic processes of the embryo in humans (Vassena et al., 2011). It is now understood that paternally transcribed RNAs also play a major role in EGA (Jodar et al., 2015). 5 sperm RNAs were identified in mice that are thought to function alongside maternal components to coordinate mRNA and protein clearance (Ntostis et al., 2017).

Table 1.2 Genes involved in MZT and their biological functions (C. – chromosome; SCMC – subcortical maternal complex)

Gene	Location	Function	Source
Ago2 *Argonaute 2*	Mouse C.15 Bovine C. 14	A member of the RNA-induced silencing complex which inhibits gene expression through RNA interference.	*(Lykke-Andersen et al., 2008)*
Ctcf *CCCTC-binding factor*	Mouse C.8 Bovine C. 18	A regulatory factor that functions as both a transcriptional repressor and activator by binding various elements of DNA.	*(Wan et al., 2008)*
Dnmt1o *DNA methyltransferase 1 oocyte-specific*	Mouse C.9 Bovine C. 7	An oocyte-specific, truncated form of DNMT1 responsible for maintaining methylation marks and regulating transcription.	*(Doherty et al., 2002)*
Dppa3 (Pgc7/Stella) *Developmental pluripotency associated 3*	Mouse C.6 Bovine C.5	A multi-functional, essential factor in preimplantation development. Protects the maternal genome and a subset of the paternal genome from demethylation.	*(Nakamura et al., 2007)*
Hsf1 *Heat shock factor 1*	Mouse C.15 Bovine C.14	A transcriptional regulator that binds to heat shock elements on target genes in response to stress, e.g. heat and oxidative damage.	*(Bierkamp et al., 2010)*
Nlrp5 (Nalp5/Mater) *NLR-family pyrin domain 5*	Mouse C.7 Bovine C.18	A member of the SCMC in the oocyte and critical for early embryo development beyond EGA.	*(Tong et al., 2000)*
Oct4 *Octamer-binding transcription factor 4*	Mouse C.17 Bovine C.23	An embryonic stem cell pluripotency transcription and regulatory factor.	*(Foygel et al., 2008)*
Padi6 *Peptidylarginine deiminase 6*	Mouse C.4 Bovine C.2	An enzyme that converts arginine to citrulline in proteins, a member of the SCMC, critical for oocyte CPL formation and embryonic progression past EGA.	*(Yurttas et al., 2008)*
Zar1 *Zygote arrest 1*	Mouse C.5 Bovine C.6	An oocyte-specific, cytoplasmic factor which appears to function in the maternal to zygotic transition.	*(Wu et al., 2003)*
Zfp36l2 *Zinc finger protein 36-like 2*	Mouse C.17 Bovine C.11	RNA-binding protein that binds to AU-rich elements causing deadenylation and destabilisation of transcripts.	*(Ramos et al., 2004)*
Zfp57 *Zinc finger protein 57*	Mouse C.17 Bovine C.23	DNA-binding protein that is responsible for methylation maintenance and transcriptional repression.	*(Li et al., 2008c)*

EGA is regulated in part through reorganisation of the chromatin structure which modulates promoter activity and controls gene expression (Bogliotti and Ross, 2015; Schultz, 2002). Replacement of sperm protamines with maternally-derived histones that are more highly acetylated enhances expression of the paternal genome (Adenot

et al., 1997; Zhou and Dean, 2015). Research in mice suggests that maternal factors initiate the MZT and subsequently, chromatin combines with newly-synthesised somatic histones and condenses into a repressive state to regulate zygotic gene expression (Latham and Schultz, 2001). In support of this, EGA does not occur in the absence of chromatin remodelling factors, Brahma-related gene 1 (BRG1) and Transcription intermediary factor 1 alpha (TIF1α) (Bultman et al., 2006; Torres-Padilla and Zernicka-Goetz, 2006). DNA replication is also crucial for the expression of genes involved in EGA. Prevention of the first round of replication in mouse embryos does not inhibit EGA but results in decreased levels of TRC and eukaryotic initiation factor, eIF-1A (Davis et al., 1996; Wiekowski et al., 1991). Inhibition of the second round of replication suppresses HSP70 expression, in addition to TRC and eIF-1A (Christians et al., 1995). In part, this may be due to disruption of replication-mediated demethylation of parental genomes (Shen et al., 2014).

1.6 Epigenetics

Epigenetics describes chemical modifications of DNA or histones, known as epigenetic marks, or RNA-mediated epigenetic control which alters the way a gene is read by the transcriptional machinery thereby influencing its expression (Handy et al., 2011). As cells possess the same DNA content, epigenetic mechanisms are responsible for determining different somatic cell phenotypes by switching on or off subsets of genes (Rakyan et al., 2008). Epigenetic mechanisms also regulate X chromosome inactivation in female embryos as a form of dosage compensation (Lyon, 1999; Riggs, 1975). Changes in the epigenome can be deleterious, however, for embryo development to occur the epigenome must be erased, reprogrammed and subsequently maintained in a time-dependent manner (Eggermann et al., 2015; Reik et al., 2001). A subset of genes that are epigenetically marked or imprinted in a parent-specific manner escape reprogramming during development (Glaser et al., 2006). These imprinted regions of parental chromosomes are functionally non-equivalent and have specific roles during development (Section 1.6.1) (McGrath and Solter, 1984; Reik and Walter, 2001b). It is worth noting that *in vitro* culture of embryos has been associated with epigenetic changes and imprinting disorders (Lazaraviciute et al., 2014).

There are various modifications which constitute epigenetic marks including DNA methylation and covalent histone modifications, such as methylation, acetylation,

ubiquitination, phosphorylation, citrullination in addition to other modifications (Holliday and Pugh, 1975; Kouzarides, 2007). Epigenetic modifications are stable and heritable, yet also reversible. In different ways, epigenetic marks alter the folding, accessibility and interactions of the DNA with regulatory factors to control gene expression (Table 1.3) (Handy et al., 2011). For example, DNA methylation at promoters silences gene expression whereas histone acetylation promotes gene transcription (Canovas and Ross, 2016; Keshet et al., 1986; Kuo and Allis, 1998). DNA methylation, specifically 5-methylcytosine (5-mC), is the most studied epigenetic modification (Tomizawa et al., 2012). There are specific groups of enzymes that control the establishment and removal of epigenetic marks. DNA methyltransferases (DNMTs) are the primary DNA methylating enzymes that commonly methylate cytosines of cytosine-guanine dinucleotides (CpGs) at stretches of the genome known as differentially methylated regions (DMRs) within imprinting control regions (ICRs) (Goll and Bestor, 2005). This family of enzymes regulate dynamic changes in the DNA methylome during gametogenesis and preimplantation embryogenesis. During development, 5-mC can be readily converted into 5-hmC by ten eleven translocation (TET) enzymes which leads to demethylation of the DNA (Rasmussen and Helin, 2016). Expression of a number of different proteins is necessary to protect methylation marks at parent-of-origin imprinted loci (Messerschmidt, 2012). This will be discussed further in the following sections.

Histone modifications are regulated by many different proteins and can have different effects based on their location on the histone as detailed in Table 1.3 (Bannister and Kouzarides, 2011). Moreover, epigenetic factors often recruit DNMTs to chromatin locations to promote further methylation (Canovas and Ross, 2016). For example, ZFP57 binds to a specific sequence of the DNA and recruits TRIM28 which facilitates binding of a heterochromatin-inducing complex containing H3K9me3 histone methyltransferase, SET Domain Bifurcated Histone Lysine Methyltransferase 1 (SETDB1), heterochromatin protein 1 (HP1) and DNMTs (Messerschmidt, 2012). This mechanism is crucial for maintaining genomic imprints during development (Section 1.6.3.1). Finally, epigenetic gene regulation also occurs through post-transcriptional RNA-associated gene silencing by short non-coding RNAs (ncRNAs) such as miRNAs, as described in Section 1.3.3.4 (Holoch and Moazed, 2015). miRNAs that target pericentromeric DNA repeat regions are known to promote heterochromatin formation and H3K9 methylation (Volpe et al., 2002; Yu et al., 2014a). Similarly, long ncRNAs that are transcribed from the genome coat the complementary chromosomal location and recruit silencing factors like polycomb

repressive complex 2 (PRC2) H3K27 methyltransferase (Kung et al., 2013). The most characterised long ncRNA is the X-inactivation transcript, *Xist*, that is transcribed from the X chromosome that will become inactive (Holoch and Moazed, 2015). Moreover, many imprinted clusters contain protein-coding genes and antisense long ncRNAs.

Table 1.3 Types of epigenetic marks and their effects on gene expression. (DNMT-DNA methyltransferase; HAT-Histone acetyltransferase; KAT-Lysine acetyltransferase; HDAC-Histone deacetylase; HMT-Histone methyltransferases; PRMT-arginine methyltransferase; K-Lysine; S-Serine).

Epigenetic mark	***Effectors***	***Main target sites***	***Effect on gene expression***
DNA methylation	DNMTs	CpG dinucleotides	Promoter = silencing; Intragenic region = activation
Histone acetylation	HATs KATs HDACs	H3 K5,8,12,16 H4 K9,14	Gene activation
Histone methylation	HMTs Histone demethylases	H3 K4me2/3; K36me3; K79me2	Gene activation
		H3 K9me3; K27me3 H4 K20me3	Gene silencing
	PRMT5 PRMT1	H4 Rme2	Gene silencing
Histone phosphorylation	Aurora B	H3 S10,28	Gene activation
Long ncRNA	RNA polymerase II	Complementary transcript	Transcription repression
Small ncRNA	RNA polymerase II Dicer AGO2	Complementary transcript	Transcription repression

1.6.1 Parent-of-origin imprinting

Genomic imprinting is the phenomenon in which 1 parental allele of an imprinted gene is expressed in the offspring while the other is silenced, as a form of gene expression control (Monk et al., 2019; Reik and Walter, 2001b). Research has shown that embryos that are experimentally produced with either 2 maternal pronuclei or 2 paternal pronuclei do not develop to term (Surani and Barton, 1983). This is not due to aberrant genetic contribution but functional non-equivalence between parental chromosomes – now known to be the result of genomic imprinting (McGrath and Solter, 1984). Genes that are paternally expressed are often involved in the growth and development of extra-embryonic structures while genes that are maternally

expressed coordinate early preimplantation embryo development (Barton et al., 1984). There are over 200 known imprinted genes in humans that are often clustered together in ~1 megabase DNA regions (Huntriss et al., 2018). They are controlled by CpG-rich cis-acting sequences called ICRs (Bartolomei and Ferguson-Smith, 2011). The majority of imprinted genes receive epigenetic marking upon passing through the female germline (Wilkins et al., 2016). In 1991, one of the first imprinted genes identified was the maternally methylated *Igf2r* cluster (Barlow et al., 1991). Unlike paternally methylated ICRs which reside in intergenic regions, maternally methylated ICRs are located in promoters (Bartolomei and Ferguson-Smith, 2011). Within the second intron of *Igf2r* lies the *Airn* promoter (Figure 1.6a) (Braidotti et al., 2004). At the maternal locus, the CpG island in the *Airn* promoter is methylated which allows maternal expression of *Igf2r* (Stoger et al., 1993; Wutz et al., 1997). On the paternal chromosome, it is unmethylated and the *Airn* promoter is activated. *Airn* is a non-coding RNA (ncRNA) that is transcribed in the anti-sense direction to *Igf2r* to repress its expression (Lyle et al., 2000; Zwart et al., 2001). 2 genes downstream of *Igf2r, Slc22a2 and Slc22a3,* are also repressed on the paternal chromosome as a result of *Airn* – a mechanism known as *cis* spreading (Nagano et al., 2008). *Cis* spreading describes the silencing of distant genes through interaction with their promoter and recruitment of histone modifying factors (Marcho et al., 2015). Other examples of *cis* spreading include: *Kcnq1, Snrpn* and *Gnas* clusters (Bartolomei and Ferguson-Smith, 2011).

Another mechanism of genomic imprinting regulation is described at the *Igf2-H19* gene locus, which regulates a variety of genes in embryogenesis, primarily those involved in placental development (Figure 1.6b) (Constancia et al., 2002). The locus is under the control of an intergenic ICR upstream of *H19* and shares enhancer sequences downstream of *H19* (Nordin et al., 2014; Tremblay et al., 1997). The parent-specific methylation status of the ICR determines the expression of either *Igf2* or *H19*. On the maternal chromosome, the DMR is unmethylated and transcriptional regulator, CCCTC-binding factor (CTCF), can bind (Kim et al., 2015b). CTCF blocks the binding of enhancers to the *Igf2* promoter and inhibits its expression (Bell and Felsenfeld, 2000; Gabory et al., 2009). As a result, enhancers bind to the *H19* ncRNA promoter downstream and *H19* is expressed. Interestingly, miR-675 was identified within the first exon of *H19* ncRNA whose function is to suppress placental growth (Keniry et al., 2012). On the paternal chromosome, the DMR is imprinted so CTCF cannot bind. Subsequently, enhancers activate *Igf2* promoter and *Igf2* is expressed

(Bartolomei and Ferguson-Smith, 2011). This mechanism of imprinting regulation is known as CTCF-dependent chromatin insulation (Ishihara et al., 2006).

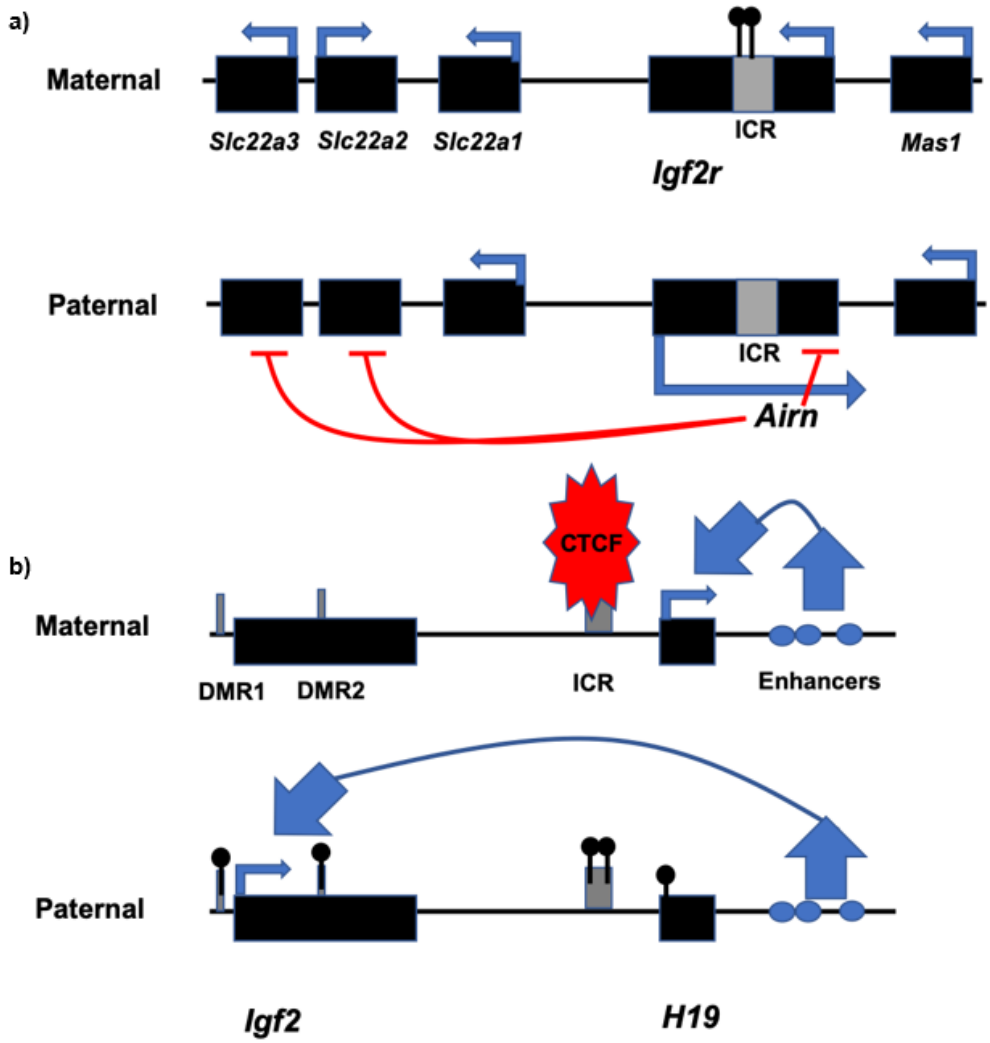

Figure 1.6 Mechanisms for differential gene expression from imprinted loci. **a)** Cis-spreading at *Airn-Igf2r* locus: At the maternal locus, the *Airn* ICR is methylated so *Airn* is silenced allowing *Igf2r* to be expressed. The paternal locus is unmethylated so *Airn* is expressed which represses *Igf2r* expression (red lines). **b)** CTCF-dependent chromatin insulation at the *Igf2-H19* locus: At the paternal locus, the *H19* ICR is methylated so *H19* is silenced and *Igf2* is expressed. At the maternal locus, the *H19* ICR is unmethylated so CTCF can bind and *H19* is expressed. black circles and blue arrows show methyl marks and gene activation, respectively. Figures redrawn from **a)** Abramowitz and Bartolomei (2012) and **b)** Gabory et al. (2009).

1.6.2 Epigenetic reprogramming of the germ line

Epigenetic reprogramming of the germ line is necessary for gamete production and succeeding embryo development (Hill et al., 2018). PGCs undergo active global DNA demethylation and chromatin remodelling, followed by precise re-methylation in a parent-specific manner during gametogenesis (Allegrucci et al., 2005; Li et al., 2004; Reik et al., 2001). Upon migration of PGCs to the gonadal ridge, the methylome is similar to that of the parental somatic cells (Hajkova et al., 2002). Once at the gonadal ridge, the chromatin landscape changes dramatically: DNA is largely demethylated and many histone modifications are lost. Initially, DNA demethylation is thought to occur by replication-dependent dilution (Ohno et al., 2013). During replication, UHRF1 recognises hemi-methylated DNA and recruits DNMT1 to methylate CpGs on the newly replicated DNA strand (Bostick et al., 2007). However, downregulation of *Uhrf1* during early PGC specification prevents methylation maintenance by DNMT1 and leads to dilution of DNA methylation with each replication event (Kurimoto et al., 2008b). The second stage of DNA demethylation is coordinated by TET enzymes which catalyse the oxidation of 5-mC to 5-hmC (Monk et al., 2019). *Tet1* and *Tet2* expression increases during PGC specification reaching peak levels around day E10.5-11.5 in mouse while *Tet3* is not detected (Hackett et al., 2013). As DNMTs cannot recognise 5-hmC, DNA methylation is lost during DNA replication (Figure 1.7a) (Inoue et al., 2011b). With this, an overall upregulation of gene expression was observed following global demethylation of DNA (Yamaguchi et al., 2013). This shows the biological importance of epigenetic changes in the germline for reprogramming PGCs prior to meiosis. Furthermore, Yamaguchi and colleagues recognised the presence of stable pericentric 5-hmC marks in both male and female PGCs that were catalysed by TET1 (Yamaguchi et al., 2013; Yamaguchi et al., 2012). Loss of *Tet1* in mouse PGCs increased the expression of major satellite repeats that are usually silenced in the germ line (Magaraki et al., 2017; Yamaguchi et al., 2013).

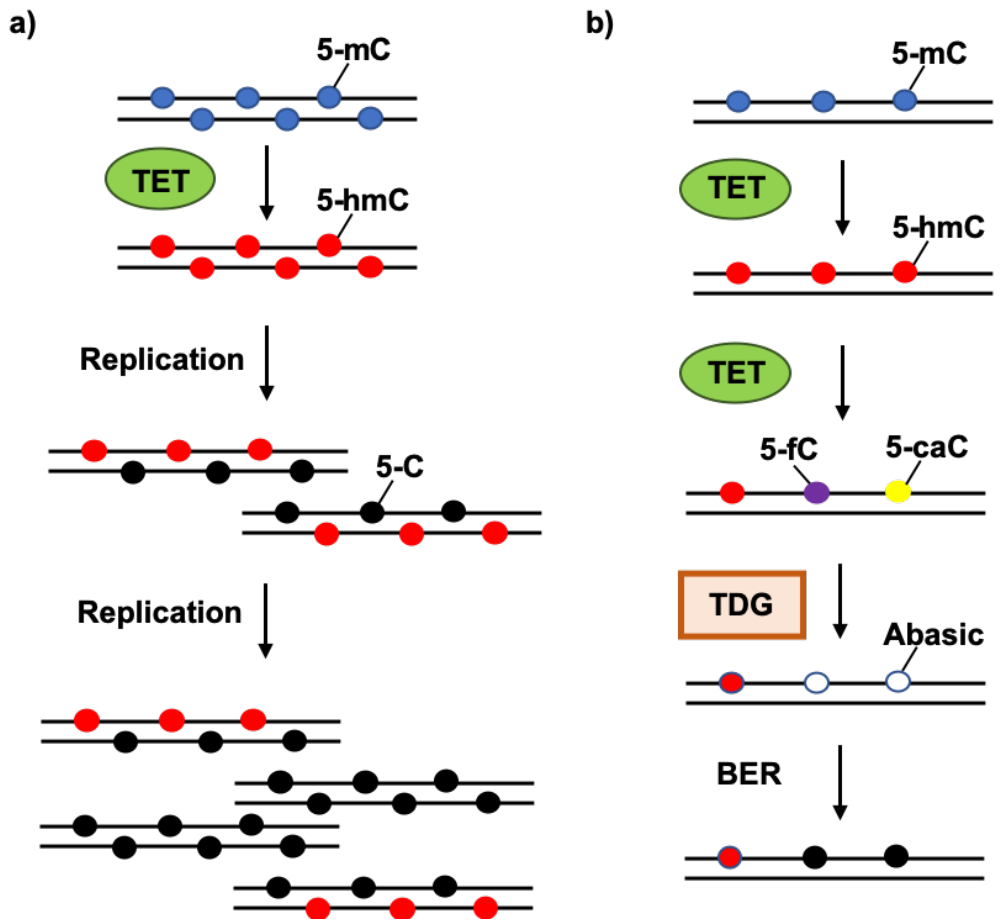

Figure 1.7 TET-mediated DNA demethylation followed by **a)** passive replication-dependent dilution: 5-mC is converted to 5-hmC by TET enzymes. As 5-hmC is not recognised by DNMT1, DNA methylation is gradually lost during each DNA replication event; and **b)** thymine DNA glycosylation (TDG) and base excision repair (BER): 5-mC is converted to 5-hmC and subsequently, 5-formylcytosine (5-fC) and 5-carboxylcytosine (5-caC) by TET enzymes. TDG excises 5-fC and 5-caC from the DNA to leave an abasic site which is repaired by BER enzymes. Figure redrawn from Kohli and Zhang (2013).

Hajkova and colleagues observed extensive chromatin decondensation in germ cells, which might enable demethylases to access and erase methylation marks (Hajkova et al., 2008; Hill et al., 2014). For instance, they observed a permanent loss of the early PGC repressive chromatin mark, dimethylation of arginine 3 on histone H2A and H4 tails, which they speculate could be due to citrullination by peptidylarginine deiminase 4 (PADI4) (Ancelin et al., 2006; Wang et al., 2004). This was dismissed for various reasons, including lack of PADI4 expression in their single-cell PGC data. This mechanism may now be worth re-visiting in light of the fifth PADI family member, PADI6, which is expressed primarily in the oocyte and is essential for embryonic

genome activation (Section 1.7.3.1) (Wright et al., 2003; Yurttas et al., 2008). Instead, Hajkova et al. (2008) suggests that there is an active mechanism of histone replacement that is not facilitated by replication. This model may relate to a DNA repair imprinting mechanism co-ordinated by DNA glycosylase *Demeter* that was previously reported in plants (Choi et al., 2002). It suggests that a DNA repair protein with the ability to remove 5-mC recognises modified bases and induces chromatin structural changes and histone replacement (Gehring et al., 2006; Gong et al., 2002). Interestingly, thymine DNA glycosylase (TDG) in mammals has been implicated in chromatin remodelling (Tini et al., 2002). Oxidation of 5-mC to 5-hmC by TET enzymes also produces 5-formylcytosine (5-fC) and 5-carboxylcytosine (5-caC) (Ito et al., 2011). It is thought that 5-fC and 5-caC are substrates for TDG which excises the modified cytosines from the DNA (He et al., 2011; Maiti and Drohat, 2011) and the resultant abasic site is repaired by the endogenous base excision repair (BER) pathway in a tightly coordinated mechanism (Figure 1.7b) (Weber et al., 2016). In support of this, disruption to *Tdg* in mouse embryos results in lethality and failure to establish proper DNA methylation (Cortellino et al., 2011).

Re-methylation of the paternal genome occurs prior to birth whereas re-methylation of the maternal genome occurs during oocyte maturation and is fully established by MII stage (Lucifero et al., 2002; Pan et al., 2012). Imprinting establishment in the oocyte is progressive and stage-specific for each imprinted gene, for example: *Snrpn* is imprinted during the primordial to primary follicle transition; *Peg3* in the secondary follicle; *Mest* during the tertiary to early antral follicle transition; and *Impact* in the antral oocyte in mice (Obata and Kono, 2002). It is thought that there is a switch in transcription start sites of many imprinted genes between germ cells and growing oocytes and that this may correspond with the expression of specific transcription factors and transcription events that traverse germline DMRs (gDMRs) (Tomizawa et al., 2012). This would explain the asynchronous establishment of methylation at imprinted gene loci. In bovine, increased methylation of imprinted genes, *SNRPN, PEG10* and *PLAGL1,* coincided with expression of DNMT3 proteins during oocyte growth (O'Doherty et al., 2012). DNMT3A and DNMT3B are the *de novo* methyltransferases responsible for laying down imprints in oocytes and preimplantation embryos (Kaneda et al., 2010; Okano et al., 1999). Human *DNMT3A* and *DNMT3B* are expressed throughout folliculogenesis, oocyte maturation and preimplantation development to the blastocyst stage (Huntriss et al., 2004). Knockout of either *Dnmt3a* or its cofactor *Dnmt3l* in the mouse embryo results in cell death whereas ablation of *Dnmt3b* yields viable offspring (Kaneda et al., 2004). It is

therefore proposed that DNMT3A and DNMT3L are essential for methylation of gDMRs of imprinted loci in germ cells.

Imprinting establishment by *de novo* DNMTs is thought to depend upon CpG sequences, histone modifications and transcription (Bartolomei and Ferguson-Smith, 2011). gDMRs are comprised of CpG repeats, known as CpG island-like elements, that cover up to a few kilobases of DNA (Tomizawa et al., 2011). Jia and colleagues resolved the crystal structure of the DNMT3A-DNMT3L complex to find that optimal methyltransferase activity required regular spacing of 8-10 CpGs along the DMR (Jia et al., 2007). They observed this CpG spacing in twelve maternally imprinted gDMRs but not in 3 paternally imprinted gDMRs or 10 control CpG islands. Despite this, the DNMT3A-DNMT3L complex is likely to function by recognising modified histones (Messerschmidt et al., 2014). For example, DNMT3L interacts with the N terminus of histone H3 to methylate DMRs (Ooi et al., 2007). It is suggested that histone H3 lysine 4 (H3K4) methylation and histone H3 acetylation disrupts this interaction and can therefore protects DMRs from methylation (Figure 1.8) (Delaval et al., 2007; Fournier et al., 2002). At the *U2af1-rs1* locus, it appears that methyl-CpG-binding-domain (MBD) proteins recruit chromatin remodelling factors to the maternally methylated gDMR resulting gene silencing (Fournier et al., 2002). The paternal allele, however, is protected from silencing as a result of H3K4 methylation and H3 acetylation (Farhadova et al., 2019). This has also been observed at the *Igf2r* locus (Vu et al., 2004). In support of this, gDMRs of certain imprinted genes do not become methylated in oocytes lacking H3K4 demethylase *Kdm1* (Ciccone et al., 2009).

Finally, epigenetics can be regulated through transcription. In some promoter regions, CpG islands remain unmethylated due to high GC skew, which enables R loops to form during transcription (Ginno et al., 2012). These DNA:RNA structures exclude DNMTs, specifically DNMT3B1, from methylating promoter regions and silencing gene expression (Ginno et al., 2012). This method of protection from methylation relies on transcriptional activity and therefore, occurs in the promoters of actively transcribed genes such as regulatory and housekeeping genes (Bird, 2002; Saadeh and Schulz, 2014). On the other hand, at some gDMRs, transcription is necessary to maintain an open chromatin state to allow DNMTs to lay down *de novo* epigenetic marks (Chotalia et al., 2009). For example, in growing oocytes, the *NESP55* promoter, which is upstream of 2 gDMRs of the CpG island promoter for imprinted gene *GNAS*, is actively transcribed and transcription continues through the *GNAS*

gDMRs (Frohlich et al., 2010). When *NESP55* promoter regions are deleted or transcription is ablated, the gDMRs fail to become methylated (Bastepe et al., 2005).

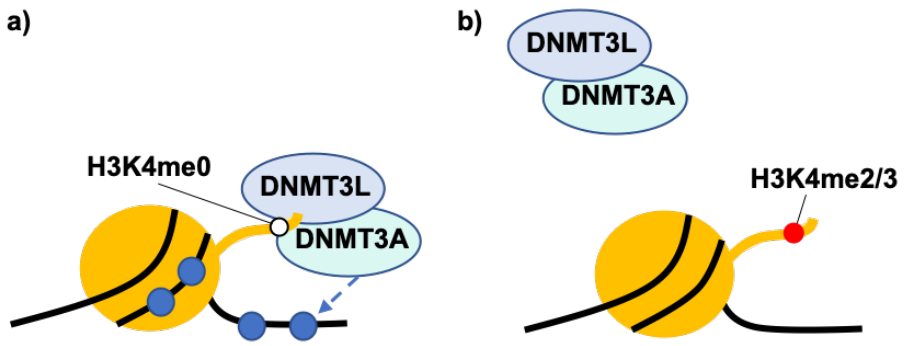

Figure 1.8 *De novo* DNA methylation by DNMT3A-DNMT3L complex is dependent upon the methylation status of histone H3 lysine 4 (H3K4). **a)** H3K9 is unmethylated so DNMT3A-DNMT3L can methylate (blue circles) the DNA (black line). **b)** H3K9 is di- or tri-methylated so DNMT3A-DNMT3L cannot methylate the DNA. Histone H3 is represented by a large yellow circle. Figure redrawn from (Tomizawa et al., 2012).

1.6.3 Epigenetic reprogramming of the preimplantation embryo

Following fertilisation, the zygotic genome undergoes extensive reprogramming and activation to pluripotency (Clift and Schuh, 2013; Morgan et al., 2005). As the haploid paternal genome is tightly packaged around protamines, in place of histones, the paternal genome undergoes sperm chromatin remodelling while the maternal genome completes meiosis (Miller, 2015; Santos et al., 2002). By the blastocyst stage, embryos are devoid of almost all DNA methylation. However, through the chromatin reorganisation and global DNA demethylation, parent-specific imprinted loci are maintained (Monk et al., 1987; Reik et al., 2001).

In the mammalian zygote, demethylation of parental genomes is asynchronous (Inoue and Zhang, 2011). The paternal DNA is actively and rapidly demethylated through TET3-mediated conversion of 5-mC to 5-hmC before the first mitotic division followed by replication-dependent passive dilution (Figure 1.9) (Iqbal et al., 2011). The role of TET3 was discovered as oxidative derivatives of 5-mC were asymmetrically enriched on the paternal chromosomes (Wossidlo et al., 2011). In mice, maternal *Tet3* mRNA accumulated during oocyte growth and subsequently, the protein was localised at the paternal pronucleus in the zygote (Gu et al., 2011;

Sakashita et al., 2014). Furthermore, oxidation of 5-mC in the paternal genome was not observed following KD of *Tet3* in mouse zygotes (Gu et al., 2011; Sakashita et al., 2014). DNA demethylation is biologically important for the transcriptional activation of zygotic genes from the paternal genome (Aoki, 1997; Reik and Walter, 2001a). In support of this, ablation of *Tet3* disturbed the demethylation and therefore transcription of paternal pluripotency genes, *Oct4* and *Nanog,* and markedly reduced embryo development in both mice and bovine species (Cheng et al., 2019; Gu et al., 2011). It was believed that the maternal genome was mostly demethylated in a replication-dependent manner as methylation maintenance protein DNMT1 is prevented from entering the nucleus until the 8-cell stage (Figure 1.9) (Branco et al., 2008; Carlson et al., 1992). However, recent methylation profiling has shown that 5-hmC is present in the mammalian maternal pronucleus which suggests that there is active demethylation of the maternal genome by TET3-mediated oxidation, albeit at a lesser extent than that of the paternal genome (Guo et al., 2014; Wossidlo et al., 2011). Both maternally-derived, oocyte-specific DNMT1o and zygotic somatic DNMT1 (DNMT1s) are necessary to maintain methylation marks by recognising and binding hemi-methylated DNA (Figure 1.10c) (Hirasawa et al., 2008; Howell et al., 2001; Kurihara et al., 2008). Methylation maintenance at imprinted loci is essential for correct development as disruption to *Dnmt1o* cannot be tolerated and results in embryonic failure (Howell et al., 2001; Li et al., 1992; Petrussa et al., 2014).

Whole genome bisulphite sequencing (WGBS) has facilitated further investigation into methylation patterns during embryonic reprogramming in bovine (Duan et al., 2019; Jiang et al., 2018; Salilew-Wondim et al., 2018). After fertilisation, global demethylation caused CpG methylation to decrease from ~73% in sperm and ~30% in oocytes to ~27% in 4-cell bovine embryos (Duan et al., 2019). Methylation was at its lowest level (~15%) in 8-cell embryos and subsequently doubled (~32%) in 16-cell embryos – concordant with major EGA in bovine. It is suggested that changes to the methylome reflect changes in the expression of epigenetic regulators such as DNMTs (Duan et al., 2019). On the other hand, non-CpG methylation showed the inverse effect with highest methylation observed at the 8-cell stage, suggestive of a regulatory role in pluripotency (Jiang et al., 2014). Finally, it is important to note that differences in DMRs were observed between *in vitro* and *in vivo* matured oocytes which confirms the association between imprinting abnormalities and *in vitro* derived embryos (Hattori et al., 2019; Jiang et al., 2018).

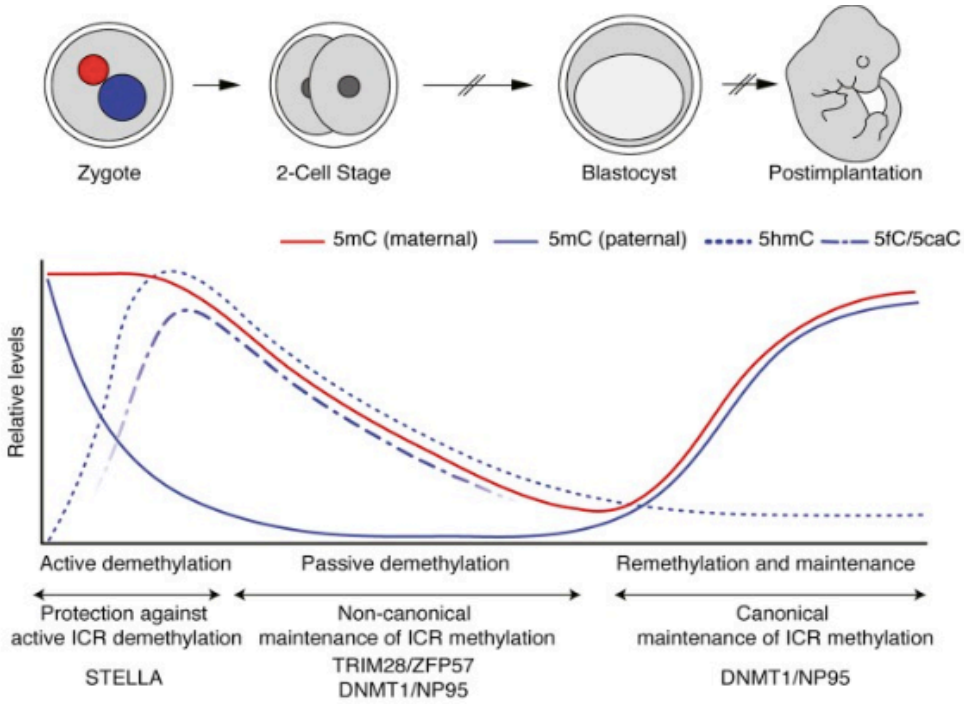

Figure 1.9 Changes in methylation during preimplantation embryo development and postimplantation from Messerschmidt et al. (2014). After fertilisation, the paternal genome is actively demethylated (blue line), however DPPA3 binds to H3K9me2 sites to protect imprinted loci from TET-mediated demethylation. With each embryonic cleavage event the maternal genome is passively demethylated (red line) but both parental imprints are maintained. To this end, ZFP57 recruits TRIM28, SETDB1 and DNMT1 to the DNA at H3K9me2 sites which causes further methylation of the histone and prevents demethylation of imprinted loci in the reprogramming embryo. The dotted blue lines show the increase in intermediate products, 5-hmC and 5-fC/5-caC, formed by oxidation of 5-mC.

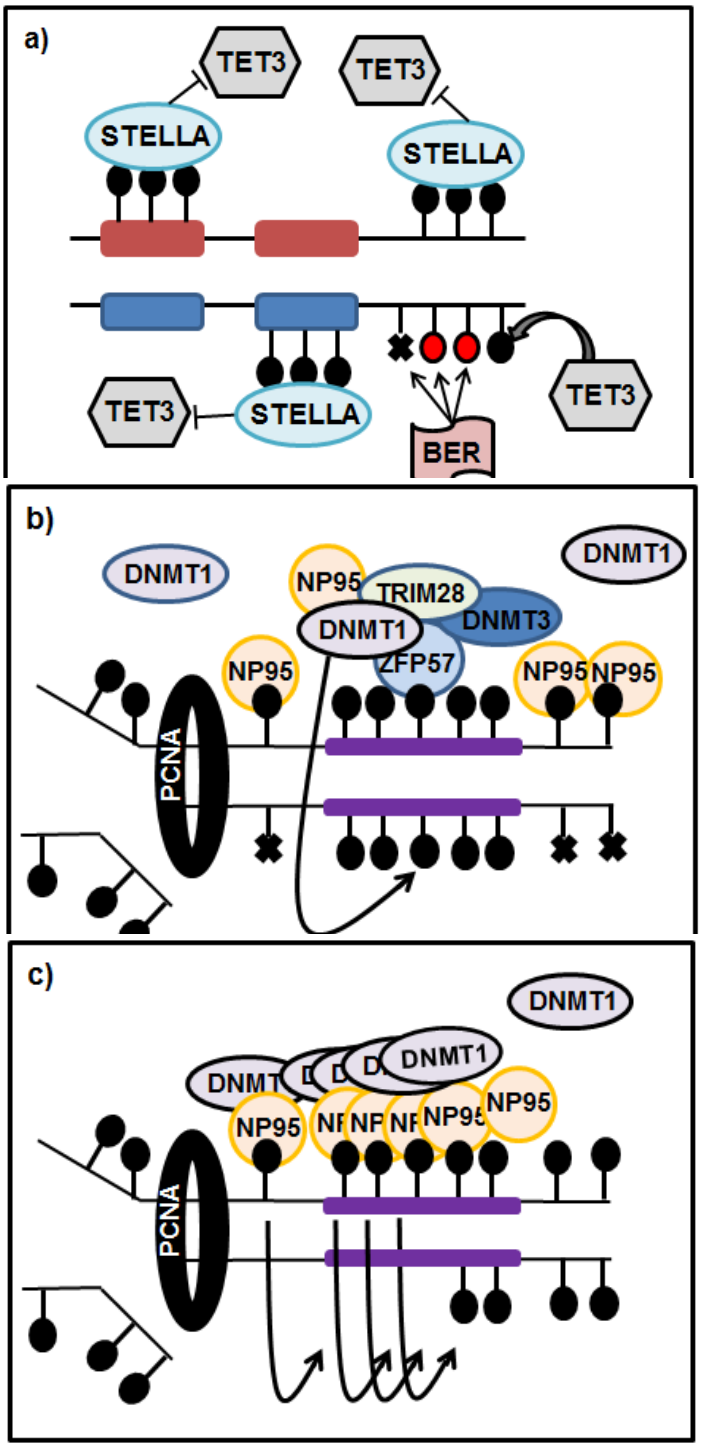

Figure 1.10 a) Protection of imprinted loci by STELLA/DPPA3. DPPA3 binds to DMRs to prevent TET3-mediated demethylation. In the absence of DPPA3, TET3 converts 5-mC to 5-hmC which is repaired by BER leading to loss of methylation. **b)** Protection of imprinted loci by TRIM28, ZFP57, DNMT1 and NP95/UHRF1. ZFP57 binds to DMRs and recruits TRIM28, NP95 and DNMTs which maintains methylation at these loci. c) DNA methylation maintenance by NP95/UHRF1 and DNMT1. NP95 binds to hemimethylated DNA and recruits DNMT1 to maintains methylation at imprinted loci. Figure redrawn from Messerschmidt et al. (2014).

1.6.3.1 Protecting imprinted loci from demethylation

Despite demethylation of the parental genomes, imprinted genes DMRs remain methylated (Clift and Schuh, 2013; Morgan et al., 2005). WGBS confirmed that 5 maternally and 3 paternally imprinted genes were protected from global demethylation during embryonic reprogramming (Jiang et al., 2018). Trans-acting factors have been identified that prevent demethylation of imprinted loci during essential reprogramming events. DPPA3 protects many maternal imprints and a subset of paternal imprints from demethylation in the zygote by inhibiting TET3-mediated 5-mC oxidation and consequent DNA demethylation (Figure 1.10a) (Bian and Yu, 2014; Gu et al., 2011; Nakamura et al., 2007). DPPA3 functions by binding to a consensus sequence on the DNA and H3K9me2, a histone mark that is enriched in the maternal genome, which alters the chromatin structure and prevents TET3 activity (Bian and Yu, 2014; Nakamura et al., 2012; Santos et al., 2005). Loss of *Dppa3* activity in mouse zygotes causes loss of 5-mC from both pronuclei and increased 5-hmC staining in the maternal genome (Wossidlo et al., 2011). As well as protecting imprinted loci from demethylation, DPPA3 also prevents hypermethylation of the DNA at inappropriate loci by DNMT1 (Li et al., 2018). DPPA3 regulates the subcellular localisation of UHRF1 in mouse oocytes, thereby controlling methylation by DNMT1. Loss of *Dppa3* results in aberrant localisation of UHRF1 in the nucleus and hypermethylation of the oocyte methylome which markedly impaired embryonic development.

Similarly, zinc finger protein 57 (ZFP57) maintains methylation at a subset of both maternally and paternally imprinted genes in the mouse preimplantation embryo (Figure 1.10b) (Li et al., 2008c; Riso et al., 2016). ZFP57 binds to the DNA in a sequence- and methylation-dependent manner and recruits TRIM28 to the methylated allele of ICRs where it acts as a scaffold for chromatin-modifying proteins such as nucleosome remodelling and deacetylase (NuRD) complex, SETDB1 and DNMTs to induce a heterochromatic state such as H3K9me3 (Quenneville et al., 2011; Zuo et al., 2012). Loss of both maternal and zygotic *Zfp57* displays a maternal-zygotic lethal effect due to disruption of multiple imprinted loci (Li et al., 2008c). Mutations in *ZFP57* result in human imprinting disorders including transient neonatal diabetes mellitus caused by aberrant imprinting of *PLAGL1* (Mackay et al., 2008). Similarly, in mouse embryos, loss of maternal *Trim28* is lethal and there is high variability in embryonic phenotypes due to the mosaicism of imprinting abnormalities

that arise (Messerschmidt et al., 2012). In contrast, CXXC-type zinc finger protein 1 (CXXC1), a CpG binding protein of unmethylated CGs, is proposed to maintain the hypomethylation status of CpG islands in order to sustain the activation of genes that are essential in peri-implantation development (Carlone and Skalnik, 2001; van de Lagemaat et al., 2018).

1.7 Maternal effect genes involved in epigenetic regulation of the oocyte and preimplantation embryo

Genes that are transcribed from the maternal genome and are critical to the functioning of the oocyte and early embryo prior to EGA are termed MEGs (Li et al., 2010a). *Mater/NLRP5* was one of the first MEGs to be identified in mice, and later found to be an essential component of the subcortical maternal complex (SCMC) alongside *KHDC3L, OOEP, TLE6, PADI6, NLRP2* and *NLRP7* (Li et al., 2008a; Tong et al., 2000; Zhu et al., 2015).

1.7.1 *NLRP*- gene family

The *NLRP*- gene family are known for their roles in inflammasome assembly during the innate immune response (Martinon et al., 2007). However, the discovery that *NLRP*- genes were highly expressed in the oocyte and early embryo suggested a novel role for *NLRPs* in embryonic development (Amoushahi et al., 2019; Zhang et al., 2008).

1.7.1.1 NLRP7

Mutations in *NLRP7/NALP7* were identified in a congenital imprinting disorder called familial biparental hydatidiform mole (FBHM) (Table 1.4) (Hayward et al., 2009). FBHM is a maternal-effect, autosomal recessive condition caused by defective maternal imprinting of the oocyte thereby mirroring the presence of paternal DNA only (Van den Veyver and Al- Hussaini, 2006). It is characterised by embryonic failure and the presence of masses of hyper-proliferated, extra-embryonic trophoblastic tissue clinically known as moles. Mutations in *NLRP7/NALP7* were first discovered using linkage analysis in affected families and individuals with recurrent hydatidiform mole (HM) (Moglabey et al., 1999; Murdoch et al., 2006). Since then, approximately 60 homozygous and compound heterozygous mutations have been identified in *NLRP7*

(Reddy et al., 2016). *NLRP7* belongs to the *NLRP* family of CATERPILLER proteins, which play a role in inflammation, establishment of the trophoblast and preimplantation development (Mahadevan et al., 2014; Messaed et al., 2011; Zhang et al., 2008). Investigation into the structure and function of NLRP7 did not reveal DNA binding or methyltransferase activity, making it unlikely to be directly involved in imprinting (Murdoch et al., 2006). However, the presence of the evolutionary conserved leucine-rich repeat (LRR) region indicates that NLRP7 is involved in protein binding. Considering this, several deleterious mutations in NLRP7 reside in the LRR region, suggesting that protein-protein interactions are essential for its function (Kou et al., 2008). Mahadevan and colleagues searched for NLRP7 interactors and succeeded in pulling down a protein, Yin-yang 1 (YY1), that binds to the DMRs of imprinted genes, depending on their methylation status (Kim, 2008; Mahadevan et al., 2014). They continued to knock down *NLRP7* transcripts in human embryonic stem cells (hESCs), and subsequently stimulate their differentiation to trophoblastic lineages to model FBHM (Schulz et al., 2008). They discovered that *NLRP7*^{KD} cells had significantly higher expression of trophoblastic markers and increased secretion of human chorionic gonadotrophin – histopathological characteristics of FBHM. Moreover, they observed changes in the CpG island methylation status of over 200 genes, 15 of which are targets of YY1 (Mahadevan et al., 2014). It must be noted that there is no mouse orthologue of *NLRP7* so although hESCs do not maintain the same imprints as embryos they can provide useful tools for looking at MEGs (Rugg-Gunn et al., 2007).

Analysis of *NLRP7*-defective FBHM moles by Nguyen et al. (2014) showed that the completeness of the mole was positively correlated with the severity of the *NLRP7* mutation and the expression of maternally-expressed *CDKN1C* (Hatada and Mukai, 1995). It seems that moles with missense mutations in *NLRP7* had low expression of CDKN1C which resulted in a partial mole phenotype, containing embryonic tissue of ICM origin and minor trophoblastic proliferation. Alternatively, moles with truncated NLRP7 had no expression of CDKN1C which resulted in complete moles with no remnants of embryonic tissue. Here, they suggest that NLRP7 is involved in controlling the switch from trophoblastic proliferation to differentiation therefore, loss of function of NLRP7 results in hyperproliferation of the trophoblast – distinctive of HM (Nguyen et al., 2014). Furthermore, it appears that NLRP7 is involved in the process of implantation of the blastocyst in the uterus. During peri-implantation development, interleukin 1-beta (IL-1β) is responsible for modulating the protease network that facilitates correct invasion of the embryo into the endometrium

(Karmakar and Das, 2002). NLRP7 negatively regulates IL-1β to control the extent to which the trophoblast can invade (Murdoch et al., 2006). Deregulation of this process by *NLRP7* mutants may explain the varying phenotypic consequences on development, as described in Table 1.4 (Slim and Mehio, 2007). It is also postulated that deregulation of inflammatory pathways in the zygote and early embryo may interrupt the factors responsible for epigenetic reprogramming (Deb et al., 2004; Messaed et al., 2011; Reddy et al., 2013). Nevertheless, mutations in *NLRP7* do not account for all cases of FBHM, signifying heterogeneity in the condition.

1.7.1.2 NLRP2

Another NLRP family member, *NLRP2*, has been linked to an imprinting congenital disorder in humans called Beckwith-Wiedemann Syndrome (BWS) (Table 1.4) (Meyer et al., 2009). Interestingly, it is believed that *NLRP7* evolved from *NLRP2* as a result of duplication events in primates and some livestock animals (Duenez-Guzman and Haig, 2014; Tian et al., 2009b). Similarly to *NLRP7*, mutations in *NLRP2* affect the LRR region and protein binding but have a milder effect on reproductive outcome as they can produce viable offspring (Meyer et al., 2009). KD of *Nlrp2* in mice inhibits embryonic progression past the 2-cell stage, proving it to be essential for the MZT (Peng et al., 2012). Studies suggest that NLRP2 localises to the subcortical regions of the oocyte but has the ability to be chaperoned into the nucleus through nuclear pores, which is concordant with a possible role in imprinting establishment or maintenance (Mahadevan et al., 2017; Peng et al., 2012). This differs to the observed cytoplasmic localisation of other NLRP family members (Sanchez-Delgado et al., 2015; Tong et al., 2004). Interestingly, NLRP2 interacts with SCMC proteins at the subcortex and *Nlrp2*$^{-/-}$ oocytes exhibit abnormal localisation of TLE6 – a member of the essential, multifaceted SCMC of the oocyte (Section 1.7.2) (Mahadevan et al., 2017). KD of *Nlrp2* in mice also affects the localisation of methylation maintenance enzyme, DNMT1, further suggesting its involvement in epigenetic regulation. Overexpression of *Nlrp2* has no effect on EGA or trophoblast lineage differentiation but increases apoptosis in the blastocyst (Peng et al., 2012). This may be due to the presence of the pyrin domain, which is now a recognised member of the death-domain superfamily involved in apoptosis signaling (Kohl and Grutter, 2004). Furthermore, it is proposed that NLRP2 plays a role in preventing rejection of the embryo by the maternal immune system through the regulation of

human leukocyte antigen C (HLA-C) expression and nuclear factor kappa-light-chain-enhancer of activated B cells (NF-κB) activation (Tilburgs et al., 2017).

Table 1.4 Mutations in SCMC associated factors that result in human female infertility characterised by imprinting defects of the embryo. The developmental consequence of knockout in mouse is also shown. SNS – single nucleotide substitution; MLID – Multilocus Imprinting Disorder; IUGD – intrauterine growth defects; EA – early embryonic arrest.

Gene	***Gene Location***	***No. of mut.***	***Types of mut.***	***Pathogenic phenotype***	***Mouse knockout phenotype***	***Source***
KHDC3L	6q13	6	SNS Deletion	FBHM	Arrest of 50% of embryos by morula stage	*(Parry et al., 2011; Rezaei et al., 2016)*
NLRP2	19q13.42	1	Deletion	BWS MLID	No knockout Knockdown causes early embryonic arrest	*(Meyer et al., 2009)*
NLRP5	19q13.43	8	SNS Deletion Duplication CNV	MLID Infertility Molar pregnancy	Embryonic arrest at 2-cell stage	*(Docherty et al., 2015)*
NLRP7	19q13.42	60	SNS Deletion	FBHM Miscarriage Still birth IUGD	No mouse ortholog	*(Murdoch et al., 2006; Reddy et al., 2016; Soellner et al., 2017)*
PADI6	1p36.13	14	SNS	EA Infertility	Embryonic arrest at 2-cell stage	*(Maddirevula et al., 2017; Qian et al., 2018; Wang et al., 2018a; Xu et al., 2016; Zheng et al., 2019)*
TLE6	19p13.3	1	SNS	EA Infertility	Embryonic arrest at 2-cell stage	*(Alazami et al., 2015)*

1.7.2 Subcortical maternal complex

In 2008, a critical oocyte complex named the SCMC was identified in mice, and later, in humans (Figure 1.11) (Li et al., 2008a; Zhu et al., 2015). The SCMC is composed of Maternal antigen that embryos require (*Mater)/NLRP5*, *Filia/KHDC3L*, Factor located in oocytes permitting embryo development (*Floped)/*Oocyte expressed

protein (*OOEP)* and *Tle6/TLE6* in mice and humans, respectively, although the complex is predicted to be larger than 4 proteins, with *Nlrp2/NLRP2, Nlrp7/NLRP7* and *Padi6/PADI6* as suggested members (Li et al., 2010a; Mahadevan et al., 2017). Loss of any of these proteins leads to premature embryonic arrest, primarily at the stage of EGA (Li et al., 2008a; Zhu et al., 2015). As its name suggests, the SCMC appears to be localised to the subcortex of the oocyte and becomes excluded from areas of cell-to-cell contact in the embryo of mice and humans (Li et al., 2008a; Zhu et al., 2015). It may play a role in embryo cleavage by interacting with F-actin and regulate translation of the embryonic genome via co-ordination of oocyte CPLs (Wright et al., 2003; Yu et al., 2014b).

1.7.2.1 Mater/NLRP5

Mater was one of the first MEGs to be characterised and subsequently, identified as a member of the SCMC in mice (Tong et al., 2000). Initially, it was recognised as an antigen in a mouse model of autoimmune premature ovarian failure (Tong and Nelson, 1999). Since then, mutations in *NLRP5* have been associated with multilocus imprinting disorders and reproductive losses in humans (Table 1.4) (Docherty et al., 2015). Like NLRP2, NLRP5 is thought to regulate NF-ƙB via its pyrin domain. In 1999, an *in vitro* study in mice using NF-ƙB inhibitors showed that its activation was required for early embryonic cleavage events but had no effect after the 2-cell stage (Nishikimi et al., 1999). This is concordant with the expression and function of NLRP5 during EGA. Further research in female mice revealed that *Mater/NLRP5* is not necessary for folliculogenesis, oocyte maturation, ovulation or fertilisation (Tong et al., 2004). Instead, it was shown to have a predominantly cytoplasmic localisation which adds confusion to its potential role in EGA.

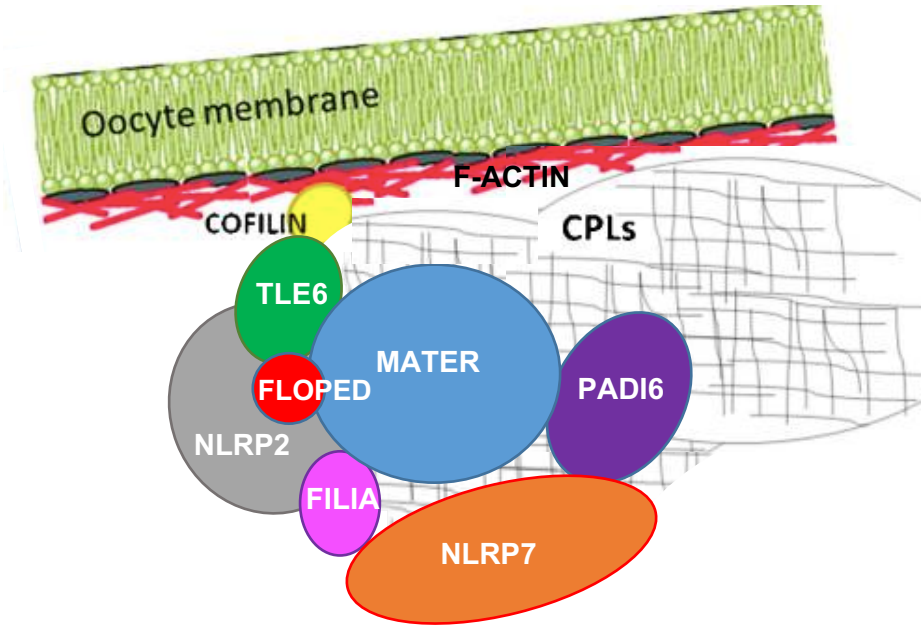

Figure 1.11 Schematic representation of the hypothesised structure of the SCMC and localisation within the MII oocyte based on experimental protein interaction studies. This figure has been adapted from Bebbere et al. (2016) to include NLRP2 and NLRP7 (Akoury et al., 2015; Mahadevan et al., 2017; Qian et al., 2018). Located at the subcortex of the oocyte, the complex binds to both the F-actin network via cofilin and CPLs via PADI6.

1.7.2.2 Filia/KHDC3L

Investigations into *Mater* led to the discovery of an interaction partner, *Filia*, whose protein expression relies on the presence of MATER (Ohsugi et al., 2008). FILIA-MATER co-localise with F-actin at the subcortical region of the mouse oocyte but after embryonic cleavage, are excluded from regions of cell-to-cell contact. Removal of calcium from the media was able to disrupt E-cadherin blastomere adhesion and reverse FILIA-MATER localisation to the subcortical regions (Ohsugi et al., 2008). Moreover, FILIA-MATER was found only in the TE and not the ICM at the blastocyst stage. This suggests it may either play a role in maintaining totipotency or driving polarisation of the embryo. Unlike other SCMC members, loss of *Filia* does not cause sterility but slows blastomere cleavage and has been associated with increased aneuploid embryos, suggesting a role in mitotic events such as spindle morphogenesis (Zheng and Dean, 2009). Indeed, removal of *Filia* disrupted the localisation of AURKA, RhoA, PLK1 and MAD2.

Besides *NLRP7* mutations, the second predisposing gene for FBHM is *KHDC3L*, the human orthologue of *Filia* (Table 1.4) (Parry et al., 2011). It belongs to a cluster of

genes on chromosome 6 that are only found in eutherian mammals; *Khdc31, Dppa5, Khdc3l* and *Ooep,* respectively (Pierre et al., 2007). This is not surprising given that reproductive genes are known to be under immense evolutionary pressure (Tian et al., 2009a). *Khdc3l* contains an atypical K homology domain which is associated with RNA binding, however some changes to the AA sequence suggest that this is no longer the case for *Khdc3l* (Pierre et al., 2007). Like defects in *NLRP7*, FBHM with *KHDC3L* mutations display aberrant expression of maternally expressed imprinted transcripts including CDKN1C (Fallahian et al., 2013). Hayward et al. (2009) suggested the effect was not widespread across the embryo as normal methylation of maternal imprints, such as those that regulate the *PEG10* gene, was been observed. However, Demond et al. (2019) observed genome wide methylation loss after bisulphite sequencing of oocytes from a patient with an inactivating *KHDC3L* mutation. Akoury et al. (2015) and colleagues recognised co-localisation of KHDC3L and NLRP7 at the cytoskeleton and cortical regions in growing human oocytes. To add to this, co-localisation of KHDC3L and NLRP7 was also observed in transfected haematopoietic cells, further supporting their overlapping function (Reddy et al., 2013).

1.7.2.3 Floped/OOEP

A *KHDC3L*-related MEG and SCMC member, *Floped/OOEP,* was identified in mice in 2008 (Li et al., 2008a). As suggested by the name, FLOPED is required for progression of embryo development past the 2-cell stage and, like MATER, is necessary for the formation of the SCMC (Tashiro et al., 2010). Co-immunoprecipitation using anti-FLOPED antibodies confirmed the presence of the supramolecular complex and identified TLE6 as another member of the SCMC (Li et al., 2008a). Mouse knockout of *Tle6* mirrors that of other MEGs and disrupts the formation of the SCMC, demonstrating that it is necessary for the complex disposition (Yu et al., 2014). Recently, a causative mutation in *TLE6* was identified in cases of human infertility (Table 1.4) (Alazami et al., 2015). The serine to tyrosine substitution interrupts a phosphorylation site that facilitates the binding of TLE6 to the SCMC. This supports the notion that a complete and stable SCMC is required during EGA. To add to this, *Tle6*$^{-/-}$ embryos display spindle abnormalities which leads to asymmetrical embryonic cleavage (Yu et al., 2014b). F-actin supports spindle dynamics therefore the relationship between F-actin and the SCMC was explored (Chew et al., 2012). It was found that there was no change in F-actin abundance in *Tle6*$^{-/-}$ oocytes but

significant disruption in zygotes. Investigation into the known regulators of actin revealed abnormal localisation and decreased phosphorylation of cofilin in *Tle6*$^{-/-}$ oocytes and embryos (Bernstein and Bamburg, 2010). A similar result was also observed in *Mater*$^{-/-}$ and *Floped*$^{-/-}$ embryos (Li et al., 2008a; Yu et al., 2014b). Further study showed that cofilin localises at the subcortex and interacts with SCMC members, MATER and TLE6 (Ma et al., 2009). This indicates that the SCMC regulates F-actin embryonic cleavage via interaction with cofilin at the early stages of development.

1.7.3 *PADI-* gene family

The PADI family of enzymes convert arginine residues to citrulline in the presence of Ca^{2+} (Rogers et al., 1977). This post-translational modification (PTM) alters the charge of the residue, resulting in a change in protein folding (Vossenaar et al., 2003). The family consists of 5 proteins, PADI1-4 and PADI6, that each has different tissue-specific expression patterns, therefore distinct substrates and functions (Mechin et al., 2007). *Padi6* was first identified through investigations into the downstream targets of *Figla* and subsequently, found to interact with FLOPED in co-immunoprecipitation experiments (Joshi et al., 2007; Li et al., 2008a). PADI6 is primarily expressed in the oocyte and peripheral blood leukocytes (PBLs) (Chavanas et al., 2004; Zhang et al., 2008). PADI1, 3 and 4 are mainly expressed in the epidermis, hair follicles and immune cells (neutrophils and eosinophils), respectively (Vossenaar et al., 2003). PADI2 is more ubiquitously expressed with observed detection in skeletal muscle, secretory glands, brain and spleen. The PADI family is highly conserved, both in terms of sequence similarity between PADIs and between mammalian species (Chavanas et al., 2004). Interestingly, multiple PADI family members have been associated with disease phenotypes; PADI1 is involved in psoriasis, PADI2 has been linked to multiple sclerosis and both PADI2 and PADI4 have been implicated in rheumatoid arthritis and a variety of cancers (Gyorgy et al., 2006; Lange et al., 2017).

PADI4 has been well studied and is understood to catalyse the conversion of histone arginine to citrulline to decondense chromatin (Wang et al., 2009; Zhai et al., 2017). It is the only PADI gene known to have a nuclear localisation signal (Nakashima et al., 2002). It can also citrullinate methylarginines found on histone tails, further implying a role in gene regulation (Di Lorenzo and Bedford, 2011; Wang et al., 2004).

Further, PADI4 has been shown to citrullinate DNMT3A, which specifically increases its activity (Deplus et al., 2014).

1.7.3.1 PADI6

So far, the link between the SCMC and epigenetic regulation is unsolved; however, it may be that PADI6 can bridge the gap. Firstly, the citrullinating activity of PADI6 is under debate. Enzymatic assays comparing the activities of PADI4 and PADI6 *in vitro* revealed that PADI6 did not citrullinate the substrates in question (Raijmakers et al., 2007). Choi et al. (2010) suggests that PADI6, regulated by the oocyte-specific transcription factor newborn ovary homeobox (NOBOX), has its own substrates that are critical for folliculogenesis (Choi et al., 2010). They also showed that KD of NOBOX impacts *Padi6* expression, which is consistent with the known role of NOBOX as a master regulator of MEGs in the oocyte. Further, fertilisation mediates an influx of Ca^{2+} which would align well with the activation of PADI6, decondensation of chromatin and EGA in theory (Whitaker, 2006). However, comparative analysis of *Padi* genes suggests that the calcium binding region of PADI6 is missing but the catalysis side chain is still present (Arita et al., 2004; Raijmakers et al., 2007). *PADI6* is said to be under positive selection so favourable AA changes will be selected for, while other *PADIs* are under purifying selection so changes are removed from the population (Chavanas et al., 2004). Snow and colleagues suggest that the loss of *Padi6* calcium binding is necessary to prevent widespread epigenetic changes following fertilisation (Snow et al., 2008).

Like other SCMC genes, knockout of *Padi6* in mice does not affect oocyte development, maturation or fertilisation (Esposito et al., 2007). *Padi6*-null mice are phenotypically normal and male mice are fertile. Female *Padi6*-null mice have normal hormone levels and menstruation cycles but cannot produce offspring. Instead, embryo development arrests at the 2-cell stage, suggesting a role for *Padi6* in EGA. Since 2016, mutations in human *PADI6* have been identified in females experiencing recurrent embryonic arrest and infertility (Table 1.4) (Maddirevula et al., 2017; Wang et al., 2018a; Xu et al., 2016; Zheng et al., 2019). *Padi6* expression is observed from the primordial follicle stage and during oocyte maturation in mouse (Wright et al., 2003). Cytoskeletal structures such as the CPLs accumulate during oocyte growth and are maintained in the preimplantation embryo. PADI6 attracts interest as it co-localises to CPLs and appears to be necessary for their formation (Esposito et al.,

2007; Wright et al., 2003). Fellow SCMC members, FLOPED/OOEP and MATER/NLRP5 also localise to CPLs and are required for their precise formation (Kim et al., 2010; Tashiro et al., 2010). This indicates that there is a much wider role for the SCMC in the preimplantation embryo.

1.7.3.2 Oocyte cytoplasmic lattices

First described in 1971, the conserved cytoskeletal structures in the oocyte have long been recognised as a critical component for oocyte competence (Burkholder et al., 1971; Gallicano et al., 1992). CPLs are a network of intermediate filaments, namely keratin, with a proteinaceous and RNA component. They are found only in the oocyte and embryo (Capco et al., 1993). It is thought that they support the storage of ribosomal components and RNAs in anticipation of protein synthesis following EGA (Bachvarova et al., 1981; Sternlicht and Schultz, 1981). They undergo reorganisation at specific time points in the presumptive zygote and embryo, such as fertilisation, compaction and blastocyst formation (Capco and McGaughey, 1986). The discovery that PADI6 localises to CPLs and is necessary for their presence is intriguing (Wright et al., 2003). Cytokeratin is a proposed substrate of PADI activity, which suggests that citrullination of keratin may be necessary to hold the lattice in formation (Senshu et al., 1999). Snow and colleagues suggest that PADI6 activity is dependent upon its phosphorylation status (Snow et al., 2008). This was suggested after they showed that PADI6 was phosphorylated during oocyte maturation, which specifically enabled interaction with Tyrosine 3-Monooxygenase/Tryptophan 5-Monooxygenase Activation (YWHA) proteins in MII oocytes but not GV oocytes. YWHA proteins modulate the subcellular localisation, stability and interactions of bound proteins in a phosphorylation-dependent manner (Morrison, 2009). This finding could unveil a potential mechanism for activation of PADI6 activity. There are many kinases expressed throughout oocyte maturation that could phosphorylate PADI6. Protein kinase C is both localised to CPLs and able to phosphorylate PADI6, supporting this as a possible form of regulation of PADI6 (Wright et al., 2003).

Around 50 years ago, researchers discovered that a sudden decrease in ribosomes coincided with the formation of CPLs in mature oocytes (Garcia et al., 1979). Since then, it is understood that CPLs provide a storage site for ribosomes in the oocyte. More recent studies confirmed this after knockout of *Padi6* and loss of CPL structures caused an increase in free ribosomes in the cytoplasm (Yurttas et al., 2008). *Padi6*$^{-/-}$ embryos also had reduced levels and aberrant localisation of ribosomal S6 protein

and RNA polymerase II which was accompanied by a global reduction in protein synthesis. It has previously been discussed that EGA requires protein synthesis (Wang and Latham, 1997). Concurrently, not only does ablation of the SCMC cause embryonic arrest at EGA, it also results in a decrease in mRNA and protein synthesis measured by lower levels of the TRC (Tong et al., 2000; Yurttas et al., 2008). Furthermore, SCMC members, NLRP5 and OOEP, are thought to be essential for the formation of CPLs and it is suggested that the SCMC is involved in RNA metabolism and transcription due to the known RNA binding abilities of KHDC3L and OOEP and aberrant localisation of RNA polymerase II in *Padi6*$^{-/-}$ oocytes (Kim et al., 2010; Pierre et al., 2007; Tashiro et al., 2010; Wang et al., 2012a; Yurttas et al., 2008). Bebbere et al. (2016) proposed that the SCMC, localised at CPLs, compartmentalises translation as a form of post-transcriptional regulation. In the oocyte, the SCMC localises to the subcortex and following embryonic cleavage, is restricted from areas of cell-cell contact (Li et al., 2008a). It is subsequently excluded from inner cells after a few cleavage events. Furthermore, blastomeres destined for TE lineage specification have lower H3R26me levels and increased *Cdx2* transcripts (Jedrusik et al., 2008; Torres-Padilla et al., 2007). It is suggested that the SCMC may therefore play a role in sequestering transcripts in the outer cells (Johnson and McConnell, 2004). This might elucidate the mechanism behind the first cell lineage specialisation into the ICM and TE and explain the characteristic TE hyperproliferation that is observed in FBHM. Another protein, Y-box binding protein 2 (MSY2), is believed to localise to CPLs and protect maternal transcripts from degradation by RNA masking (Liu et al., 2017). Interestingly, its activity is dependent upon its phosphorylation status and may be regulated in parallel to PADI6 to regulate translation of maternal mRNA prior to EGA (Yu et al., 2001). Rong et al. (2019) found that KO of *Zar1* also caused a reduction in maternal mRNAs, protein synthesis and EGA. They concluded that ZAR1 bound mRNAs and interacted with MSY2 and CPLs to regulate translation in the oocyte. Further, they showed that ZAR1 bound PADI6 and MATER when co-expressed in HeLa cells which proposes a new role for ZAR1 in the oocyte.

It is also suggested that CPLs may be responsible for reorganisation of organelles such as the ER and mitochondria in the oocyte. Organelle transport and redistribution relies upon the action of motor proteins and tubulin acetylation (Friedman et al., 2010; Hirokawa et al., 1998). PADI6 has been shown to co-localise with alpha-tubulin in cytoplasmic microtubules at CPLs of both mouse and human oocytes (Kan et al., 2011). Cytoplasmic alpha-tubulin acetylation is reduced in *Padi6* knockout oocytes, but spindle alpha-tubulin is unaffected. Further, loss of PADI6 causes aberrant

organelle positioning during oocyte maturation. In wild-type oocytes, mitochondria and ER move with the dynamic meiotic spindle whereas in *Padi6*$^{-/-}$ oocytes, organelles reside in the cortical regions or diffusely spread in the cytoplasm (Kan et al., 2011; Mehlmann et al., 1995). As a result, it is proposed that CPLs provide a site for formation of stable microtubules or act as a scaffold for their post translational modification.

1.8 Summary

This literature review has highlighted the complexity and importance of oocyte maturation for developmental competence of the embryo. Furthermore, it has shown the variety of MEGs and epigenetic regulators that are necessary for embryonic development prior to EGA. Of these, the SCMC and PADI6 are critical in coordinating processes in the oocyte and early embryo; however, their functions are still not clear. Considering the involvement of such genes in human imprinting pathologies, a relationship between the SCMC and epigenetic mechanisms has not yet been defined. PADI6 poses an interesting candidate for this role: it is an oocyte- and embryo-specific gene; it interacts with the SCMC; it is necessary for the formation of CPLs that sequester maternal transcripts and ribosomes; it has been implicated in transcriptional and translational regulation; it is required for embryonic development past EGA; it coordinates distribution of organelles in the oocyte; and it has potential citrullinating activity. The question remains: through which role(s) is PADI6 functioning in the oocyte? On the basis of the published literature it is hypothesised that *PADI6* functions in regulating maternal transcripts in the oocyte in preparation for early embryo development prior to EGA. Further, this role may include the regulation of transcripts involved in epigenetic mechanisms.

1.9 Aims and objectives

Much of the research into the SCMC and *PADI6* has been conducted in mouse oocytes and preimplantation embryos but less is known about these factors in the development of monovulatory species such as human and bovine. It is understood that correct expression of the SCMC is a critical determinant of oocyte developmental competence as dysregulation to complex members is associated with a variety of imprinting disorders. *PADI6* is an oocyte and embryo-specific gene that is necessary for embryonic development past EGA, however, evaluation of *PADI6* gene function during oocyte maturation and preimplantation embryo development in monovulatory species such as the cow and human has not yet been investigated. With the hypothesis of this thesis stating that *PADI6* functions in regulating maternal transcripts in the oocyte, the objectives of this research were as follows:

1. To characterise the tissue distribution and expression patterns of *PADI6* and associated *MEGs* across all stages of bovine oocyte maturation and preimplantation embryo development using real-time PCR analysis
2. To evaluate the function of *PADI6* during bovine oocyte maturation *in vitro* by studying the impact of targeted *PADI6* gene KD by microinjection of dsiRNA on parameters such as: i) meiotic maturation, ii) cumulus mucification and expansion and iii) gene expression pathways.
3. To evaluate the impact of *PADI6* KD in GV oocytes on the transcriptome of bovine MII oocytes.
4. To evaluate the impact of *PADI6* KD on a number of functional indices including: i) PADI6 protein expression, ii) amino acid metabolism and iii) bovine preimplantation embryo development *in vitro.*

Chapter 2 Materials and methods

2.1 *In vitro* production of mature bovine oocytes

Medias were prepared from the stock solutions detailed in Appendix I. All culture media and additives were made as appropriate in sterile, tissue culture grade, embryo tested H_2O.

2.1.1 Bovine ovary collection

Female bovine reproductive tracts were collected from the abattoir (J.C. Penny and sons, Rawdon, Leeds, UK) and placed in an insulated carrier at room temperature (RT) before being transported to the laboratory. The methods for ovine tissue collection and IVM of ovine oocytes have been described previously (Cotterill, 2008; Cotterill et al., 2012; Danfour, 2001). On arrival to the laboratory, ovaries were cut from the reproductive tracts and placed in pre-warmed ovary wash medium (Table 2.1) in an autoclaved glass beaker (Scientific Laboratory Supplies (SLS), Yorkshire, UK). The ovary wash medium was composed of phosphate buffered saline (PBS), which was made by dissolving 1 PBS tablet (18912014, Gibco™ Life Technologies, Netherlands) in 1L dH_2O. PBS was autoclaved at 180°C before penicillin, streptomycin and fungazone were added in sterile conditions according to Table 2.1a. Before use, it was incubated overnight in a non-gassed, 39°C incubator (Stuart hybridisation oven, Staffordshire, UK).

The isolated ovaries were washed twice in pre-warmed ovary wash medium and briefly washed twice in 70% (v/v) ethanol before being held at 39°C in follicle isolation medium (FIM) until the cumulus-oocyte complexes (COCs) were aspirated. The composition of FIM is shown in Table 2.1b. The solution was sterilised using a 0.2 µM cellulose acetate rapid vacuum filtration system (Techno Plastic Products (TPP), Switzerland) and left to equilibrate overnight in a non-gassed, 39°C incubator prior to use. Excess medium was stored at 4°C for up to 1 week.

Table 2.1 Composition of **a)** ovary wash medium and **b)** follicle isolation medium (FIM). *BSA: Bovine serum albumin, fraction V cell culture grade.

a)

Components	Stock	Volume	Final concentration
PBS GIBCO 18912-014		1000 ml	1x
Penicillin/Streptomycin SIGMA P4333	Pen: 10000 IU/ml Strep: 10 mg/ml	5 ml	Pen: 100 IU/ml Strep: 0.1 mg/ml
Fungazone GIBCO 15209-026	250 µg/ml	1 ml	0.25 µg/ml

b)

Components	Stock	Volume	Final concentration
HEPES Minimal Essential Media (MEM) SIGMA M7278		470 ml	
Penicillin/Streptomycin SIGMA P4333	Pen: 10000 IU/ml Strep: 10 mg/ml	5 ml	Pen: 100 IU/ml Strep: 0.1 mg/ml
***BSA** SIGMA A9418	80 mg/ml	25 ml	4 mg/ml

2.1.2 Isolation of oocytes

Cumulus oocyte complexes (COCs) were aspirated from antral follicles of approximately 2-5 mm in diameter on the washed ovaries using a 19 gauge needle (Terumo UK Ltd, Surrey, UK) and 10 ml syringe (BD Plastipak^{TM}, Drogheda, Ireland), which was pre-filled with 1 ml oocyte holding medium (H199+). The composition of H199+ is detailed in Table 2.2. Before adding heparin and stock BSA, the osmolality of the medium was measured by inputting a sample into the osmometer (Model 3320, Advanced Instruments Inc., USA). The osmolality was adjusted to ~285 mOsm/kg by adding either dH_2O or 10 X PBS if the osmolality was too high or low, respectively. To finish, the solution was sterilised using a 0.2 µM cellulose acetate rapid vacuum filtration system and left to equilibrate overnight in a non-gassed, 39°C incubator prior to use. Excess medium was stored at 4°C for up to 1 week.

Each follicle in the ovary cortex was punctured and the follicular fluid removed by aspiration. The contents of the syringe were emptied into a sterile 30 ml universal and placed in a non-gassed, 39°C incubator for 15 min to allow the oocytes to sediment. The supernatant was removed using a Pasteur pipette until there was a volume of approximately 5 ml remaining. This was transferred into a sterile 90 mm plastic Petri dish (Thermo Scientific Ltd, Newport, South Wales) with a scored base allowing the COCs to be visualised easily under the stereomicroscope (Olympus Ltd, Middlesex, UK) fitted with a heated stage that was held at 39°C (Tokai Hit Co. Ltd, Japan). COCs

were collected using a 20 µl pipette and transferred to a 35 mm embryo tested NUNC™ IVF Petri dish (150255, Thermo Scientific Ltd) containing fresh H199+ medium. Ovaries and oocytes were held in their respective pre-warmed media on a hotplate at 39°C throughout the isolation process.

Table 2.2 Composition of oocyte holding medium (H199+). The composition of each stock solution can be found in Appendix I. *BSA: Bovine serum albumin, fraction V cell culture grade.

Components	Stock	Volume	Final concentration
Embryo tested (ET) water SIGMA W3500		192.5 ml	-
M199 10x GIBCO 21180-021		25 ml	1x
Bicarbonate stock	250 mM	4 ml	4 mM
HEPES stock	250 mM	21 ml	4 mM
Penicillin/Streptomycin SIGMA P4333	Pen: 10000 IU/ml Strep: 10 mg/ml	2.5 ml	Pen: 100 IU/ml Strep: 0.1 mg/ml
Check osmolality:	~ 285 mOsm/kg		
Heparin	5000U/ml	152 µl	0.02mg/ml
***BSA** SIGMA A9418	20x	5ml	4mg/ml

2.1.3 *In vitro* maturation of COCs in group culture

50 COCs were transferred into sterile 4-well dishes (176740, NUNCLON Surface, NUNC) containing 500 µl of serum-free *in vitro* maturation (IVM) medium prepared according to Table 2.3 (Danfour, 2001). The osmolality was measured and adjusted to 285 mOsm/kg. Media was sterile filtered through a 0.2 µM cellulose acetate syringe filter (GVS Filter Technology, USA) and stored at 4°C for up to 1 week. IVM plates were made the previous day and placed in a 39°C, 5% CO_2 incubator to equilibrate overnight. Following aspiration, groups of 50 COCs were washed 3 times in 500 µl of serum-free IVM media before being placed into a well containing fresh media. COCs were cultured for 24 hours in a 5% CO_2 humidified incubator at 39°C. The methodology for IVM of bovine oocytes has been extensively validated by (Hemmings et al., 2012).

Table 2.3 Composition of serum-free IVM medium. The composition of each stock can be found in the Appendix I.

Components	Stock	Volume	Final concentration
αMEM SIGMA M4526		9ml	-
L-Glutamine SIGMA G7513	200 mM	100 µl	2 mM
Pyruvate Stock SIGMA P4562	47 mM	100 µl	0.47 mM
Bovine Holo-transferrin SIGMA T1283	5 mg/ml	10 µl	5 µg/ml
Na-selenite SIGMA S9133	50 µg/ml	1 µl	5 ng/ml
Bovine Insulin SIGMA I1882	10 mg/ml	10 µl	10 ng/ml
Ovine FSH SIGMA F8174	2 IU/ml	3 µl	0.0006 IU/ml
Ovine LH SIGMA L5269	2 IU/ml	1.5 µl	0.0003 IU/ml
Penicillin/Streptomycin SIGMA P4333	Pen: 10000 IU/ml Strep: 10 mg/ml	15 µl	Pen: 15 IU/ml Strep: 15 µg/ml
Long-R3 IGF-1 SIGMA I1271	100 µg/ml	1 µl	10 ng/ml
BSA FAF stock SIGMA A6003	200 mg/ml	200 µl	4 mg/ml

2.2 *In vitro* fertilisation of bovine oocytes

2.2.1 Preparation of fertilisation medium

Fertilisation and washing plates were prepared the day before IVF by adding 250 µl/well of fertilisation Tyrode's medium base, albumin, lactate and pyruvate (F-TALP) (Table 2.5) to a 4-well NUNC dish. The dishes were placed in a 5% CO_2 humidified incubator at 39°C to equilibrate overnight before use.

2.2.2 Preparation of Percoll® Gradient

In order to separate the spermatozoa from other elements of the semen, a discontinuous gradient of 45% and 90% Percoll® (Amersham plc, UK) was established. 90% Percoll® was made in a 50 ml conical centrifuge tube (Corning®, USA) according to Table 2.4. The pH was adjusted to pH 7.3 using 5M NaOH and the osmolality to 285-295 mOsm/kg (Parrish et al., 1995). 45% Percoll® was made by mixing 1ml of 90% Percoll® with 1ml of sperm washing medium HEPES Tyrode's medium base, albumin, lactate and pyruvate (H-TALP) (Table 2.5) at a ratio of 1:1 in a 2.5 ml universal tube. The gradient was prepared by pipetting 2 ml of 90% Percoll® into a 15 ml conical centrifuge tube (Corning®, USA). Following this, 2ml of 45% Percoll® was slowly pipetted onto the side of the tube to ensure that the 2 layers did

not mix. The gradient was freshly prepared 2 hours before fertilisation and put to 39°C in a non-gassed incubator.

Table 2.4 Composition of 90% Percoll® solution. The composition of stock A and lactate stock can be found in Appendix I.

Components	Stock	Volume	Final concentration
Percoll Amersham, UK		44.5 ml	90%
HEPES (free acid)		126 mg	10.5 mM
HEPES sodium salt SIGMA H3784		137 mg	10.5 mM
Stock A	NaCl 1.07 mM KCl 71.6 mM KH_2PO_4 11.09 mM $MgSO_4.7H_2O$ 7.4 mM Na-Lactate 70 mM	5 ml	0.107M 7.16 mM 1.19 mM 0.74 mM 7 mM
Lactate stock	170 mM	0.5 ml	
$NaHCO_3$ SIGMA S6297		96 mg	22 mM

2.2.3 Sperm preparation

Cryopreserved straws of bull semen were purchased from GENUS Breeding, LTD, Nantwich, UK. Semen from the same bull (Classic) was used for all experiments. Straws were taken from liquid nitrogen and immediately put into warm water to thaw. Following plug removal, the semen was layered over the previously prepared Percoll® gradient and centrifuged at 2100 rpm at RT for 30 min. The supernatant was discarded and 4 ml of pre-warmed H-TALP medium (Table 2.5) was added to wash the sperm pellet. The sperm were centrifuged at 1200 rpm at RT for 10 min. Again, the supernatant was discarded and the sperm were resuspended in 200 µl of pre-warmed fertilisation medium (F-TALP) (Table 2.5) and held at 39°C in a non-gassed incubator until fertilisation.

Table 2.5 Composition of H-TALP and F-TALP. The composition of each stock can be found in Appendix I. BSA FrV: Bovine serum albumin, fraction V; BSA FAF: Bovine serum albumin, fatty acid free; Pen/Hyp: Penicillamine and hypotaurine stock.

H-TALP	
Components	**Volume**
ET water	18.8 ml
10x TL stock	2.55 ml
Bicarbonate stock	200 µl
Pyruvate stock (32.7 mM)	200 µl
Calcium chloride stock	300 µl
HEPES stock	1.5 ml
Lactate stock	750 µl
Magnesium chloride stock	250 µl
Check osmolality	~285mOsm/kg
BSA FrV stock	500 µl

F-TALP	
Components	**Volume**
ET water	14.32 ml
10x TL stock	2 ml
Bicarbonate stock	2 ml
Pyruvate stock (32.7 mM)	160 µl
Calcium chloride stock	240 µl
Lactate stock	600 µl
Magnesium chloride stock	200 µl
Check osmolality	~285mOsm/kg
BSA FAF stock	400 µl
Heparin	100 µl
Pen/Hyp	200 µl

2.2.4 Sperm counting

Sperm were diluted 20-fold in dH_2O to immobilise the cells for counting. An undiluted sample was also analysed to assess sperm motility. Sperm were counted using a haemocytometer whereby 1 set of 16 corner squares represents 1 x 10^4 cells/ml. 5 squares of the haemocytometer were counted and the average sperm count was calculated to a final concentration of $1x10^6$/ml. The 20-fold dilution and haemocytometer grid were factored into the total sperm/ml in the following equation:

Total sperm count/ml = Average sperm count x dilution factor x 10^4

2.2.5 Fertilisation of COCs in group culture

Groups of 50 COCs were washed 3 times in sterile 4-well dishes containing 500 µl F-TALP. Following this, COCs were transferred in a 50 µl volume to a previously prepared 4-well NUNC dish containing 250 µl F-TALP/well. 1 x 10^6 sperm/ml F-TALP were added to the 50 COCs and the total volume was made up to 500 µl using F-TALP. The dish was then incubated at 39ºC, 5% CO_2 for 18 hours

2.3 Bovine embryo culture

2.3.1 Preparation of embryo culture media

Embryo culture media, HEPES synthetic oviductal fluid (H-SOF) and synthetic oviductal fluid supplemented with AAs and bovine serum albumin (SOFaaBSA), were made a day prior to embryo culture according to Table 2.6. H-SOF was placed in a non-gassed, 39ºC incubator overnight**.** 40 µl wash drops and 20 µl culture drops of SOFaaBSA (Table 2.6) were pipetted onto a 35 mm embryo tested NUNC™ IVF Petri dish before covering with prewashed, embryo tested, mineral oil (M5310, Sigma, Dorset, UK). Dishes were incubated in MINC™ benchtop incubators (MINC-1000, COOK Medical, Brisbane, Australia) at 39ºC, 6% CO_2, 5% O_2 and 89% N_2 overnight.

2.3.2 Zygote denudation and embryo culture

~18 hours after IVF incubation, all embryos were transferred to a sterile 5 ml round bottom Falcon™ tube (Corning®, USA) containing 1 ml of pre-warmed H-SOF (Table 2.6). The tube was vortexed for 2 min at 35 Hz to mechanically remove the cumulus cells. Embryos were then transferred in H-SOF to a 35 mm embryo tested NUNC™ IVF Petri dish and the remaining cumulus cells removed using a 130 µm EZ-Tip and EZ-Grip denudation and handling pipettor (RI, Denmark). Denuded embryos were washed 3 times in SOFaaBSA before being put into the culture drops. Embryos were first washed through the 40 µl wash drops before being transferred in a minimal volume to the 20 µl culture drops. 20 embryos were cultured per 20 µl drop. Culture dishes were incubated for up to 9 days at 39ºC, 6% CO_2, 5% O_2 and 89% N_2 in a MINC incubator. Embryos were imaged at different stages of development using a Nikon Eclipse Ti inverted microscope (Nikon Instruments, Amstelveen, Netherlands) fitted with a heated stage at 39°C and a Watec WAT-221S camera (Camtronics BV,

Eindhoven, Netherlands). Research Instruments (RI) viewer software was used to examine the images on the computer. Figure 2.1 shows the experimental workflow of bovine oocyte collection, IVM, IVF and embryo culture.

Table 2.6 Composition of H-SOF and SOFaaBSA. The composition of each stock can be found in Appendix I. NEAA: Non-essential amino acid; EAA: Essential amino acid; BSA FrV: Bovine serum albumin, fraction V; BSA FAF: Bovine serum albumin, fatty acid free.

H-SOF	
Component	**Volume**
ET water	13 ml
Na/K stock	2 ml
Bicarbonate stock	400 µl
Pyruvate stock (32.7 mM)	200 µl
Calcium chloride stock	200 µl
Glucose stock	500 µl
HEPES stock	1.6 ml
Lactate stock	200 µl
Magnesium chloride stock	200 µl
Check osmolality	~285 mOsm/kg
BSA FrV stock	400 µl
Pen/Strep	200 µl

SOFaaBSA	
Component	**Volume**
ET water	6.55 ml
Na/K stock	1 ml
Bicarbonate stock	1 ml
Pyruvate stock (32.7 mM)	100 µl
Calcium chloride stock	100 µl
Glucose stock	250 µl
Glutamine stock	5 µl
Lactate stock	100 µl
Magnesium chloride stock	100 µl
100x NEAA	100 µl
50x EAA	200 µl
Check osmolality	~285 mOsm/kg
BSA FAF stock	400 µl
Pen/Strep	100 µl

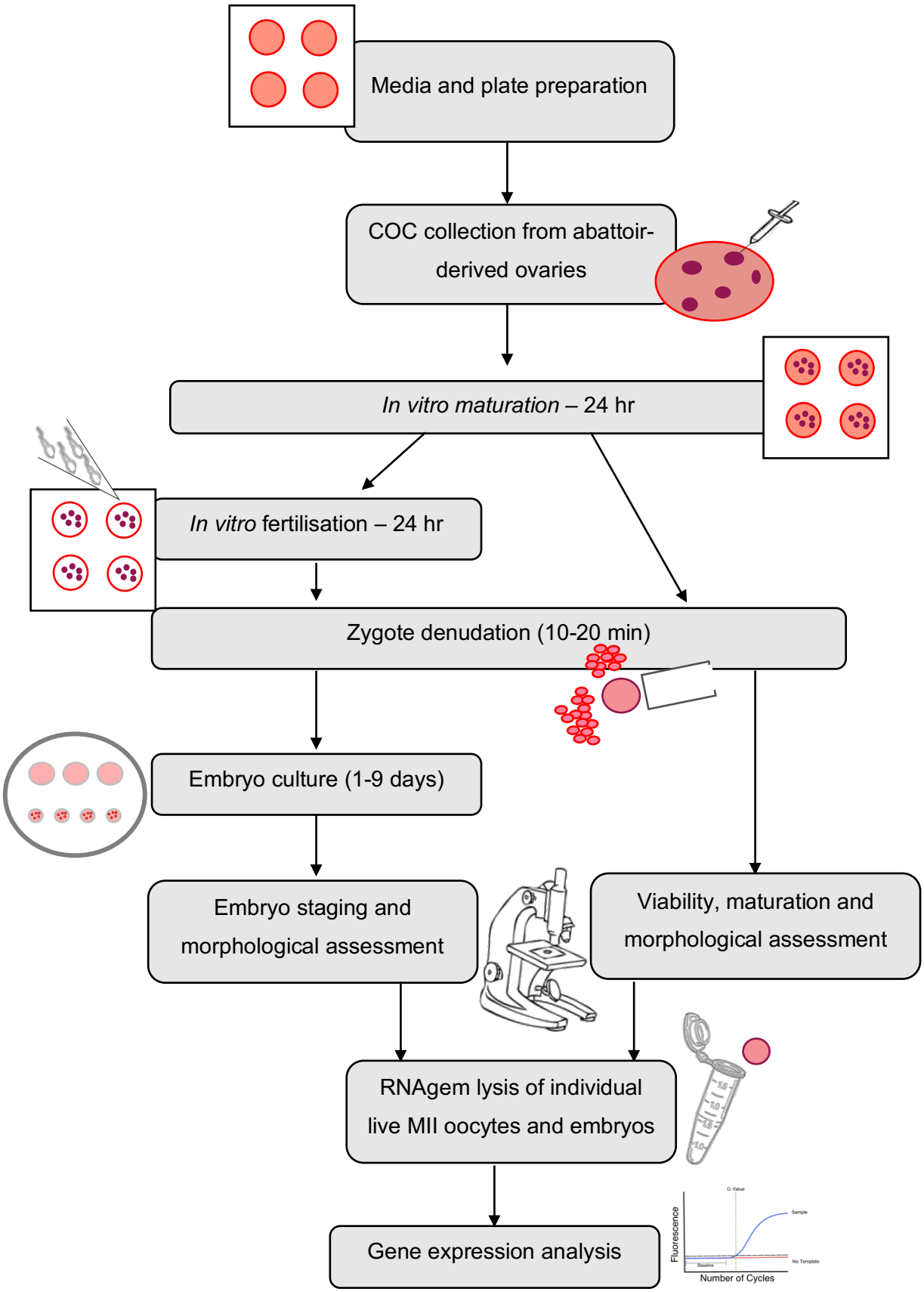

Figure 2.1. Experimental workflow of bovine oocyte collection, IVM, IVF and embryo culture.

2.4 cDNA synthesis

2.4.1 Cell lysis

Prior to cDNA synthesis, oocytes/embryos were washed 3 times in Dulbecco's calcium (Ca^{2+}) and magnesium (Mg^{2+}) free PBS (DPBS, 14190, Gibco™, UK). Single oocytes/embryos were placed into sterile 0.5 ml PCR tubes (STARLAB International, Germany) containing 2 µl of RNAGEM™ lysis solution (RNAGEM™ Tissue PLUS, RTP0100, ZyGEM, Southampton, UK) (Table 2.7a) and immediately put on ice. Oocytes/embryos were stored in RNAGEM™ lysis solution at -80°C until further use.

Table 2.7 Composition of **a)** RNAGEM™ lysis solution; **b)** DNase solution (1x).

a)

Component	Volume (µl)
H_2O	44
10x Buffer	5
RNAGEM™ (ZyGEM RTP0100)	1

b)

Component	Volume (µl)
10x DNase Buffer	0.3
RNase-free DNase 1 (ZyGEM RTP0100)	0.2
Total volume	0.5

2.4.2 Removal of DNA contamination

Oocytes/embryos in RNAGEM™ lysis solution were taken from the -80°C freezer and heated to 75°C for 10 min to lyse the cells. The thermal cycler was cooled to 37°C and 0.5 µl of DNase solution (RNAGEM™ Tissue PLUS, RTP0100, ZyGEM) (Table 2.7b) was added. Samples were incubated at 37°C for 5 min to permit DNA degradation. The temperature was then increased to 75°C for 5 min to denature the DNase 1 enzyme (Table 2.8). On completion, the samples were put to ice.

Table 2.8 Thermal program for DNA degradation.

Step	Temperature (°C)	Time (min)
Lysis	75	10
DNA degradation	37	5
DNase1 degradation	75	5
Hold	4	∞

2.4.3 Smart-seq2 reverse transcription

The Smart-seq2 cDNA synthesis protocol was taken from Picelli et al. (2014). Reagents and samples were kept on ice throughout the process. After DNA degradation, a 1:1 master mix of oligo-dT primer and dNTP mix was made and 2 µl was added to each sample (Table 2.9). The tubes were vortexed and centrifuged briefly. Samples were incubated at 72°C for 3 min to allow the primer to bind to the mRNA polyA tail. A reverse transcriptase (RT) master mix was prepared according to Table 2.10. 5.7 µl of the RT mix was added to each sample and mixed by pipetting. The samples were centrifuged again and put to the thermal program shown in Table 2.11.

Table 2.9 Oligo-dT primer and dNTP mix (1x). *Biomers.net, Ulm, Germany.

Component	Volume (µl)
Oligo-dT$_{30}$VN primer (10 µM) Biomers.net* 5'-AAGCAGTGGTATCAACGCAGAGTACT$_{30}$VN-3'	1
dNTP mix (10 µM each) Thermo Scientific™ R0192	1
Total volume	**2**

Table 2.10 Smart-seq2 reverse transcriptase master mix (1x). *Invitrogen Ltd.

Cycles	Step	Temperature (°C)	Time (min)
1	Reverse transcription and template-switching	42	90
2-11	Unfolding of RNA secondary structures Continuation of reverse transcription and template-switching	50 42	2 2
12	Enzyme inactivation	70	15
13	Hold	4	∞

Table 2.11 Thermal program for Smart-seq2 reverse transcription

Component	Volume (µl)	Final concentration
SuperScript II reverse transcriptase (200 U µl^{-1}) Invitrogen* 18064-014	0.50	100 U
RNase inhibitor (40 U µl^{-1}) Invitrogen 15518-012	0.25	10 U
SuperScript II first-strand buffer (5x) Invitrogen 18064-014	2.00	1x
DTT (100 mM) Invitrogen 18064-014	0.50	5 mM
Betaine (5 M) Sigma B0300	2.00	1 M
$MgCl_2$ (1 M) Sigma M1028	0.06	6 mM
LNA-containing TSO (100 µM) 5'-AAGCAGTGGTATCAACGCAGAGTACATrGrG+G-3' Exiqon, Qiagen, West Sussex, UK.	0.10	1 µM
Nuclease-free water	0.29	-
Total volume	**5.70**	**-**

2.4.4 Smart-seq2 cDNA amplification

Following reverse transcription, the cDNA was amplified by polymerase chain reaction (PCR). A master mix was made according to Table 2.12a and of this, 15 µl was added to the first-strand reaction. The tubes were vortexed and centrifuged briefly before putting to the Veriti® 96 well thermal cycler (Applied Biosystems, Foster City, USA). The thermal program is detailed in Table 2.12b. After cycling, the amplified cDNA concentration was measured using a spectrophotometer (ND-1000, NanoDrop Technologies, USA) and subsequently stored at -20°C until further use. Before PCR experiments, cDNA was diluted 1:1000 using nuclease-free water to a concentration of approximately 1 ng/µl. Figure 2.2 shows the flowchart for Smart-seq2 cDNA synthesis and verification of cDNA libraries by PCR for housekeeping genes adapted from Picelli et al. (2014).

Table 2.12 Smart-seq2 cDNA amplification **a)** master mix (1x). *KAPA Biosystems, Cape Town, South Africa and **b)** thermal cycling program.

a)

Component	Volume (µl)	Final concentration
KAPA HiFi HotStart ReadyMix (2x) KAPA Biosystems KK2601	12.50	1x
ISPCR primers (10 µM) Biomers.net 5'-AAGCAGTGGTATCAACGCAGAGT-3'	0.25	0.1 µM
Nuclease-free water	2.25	-
Total volume	**15**	-

b)

Cycles	Step	Temperature (°C)	Time
1	Denaturing	98	3 min
2-19	Denaturing Annealing Extension	98 67 72	20 s 15 s 6 min
20	Extension	72	5 min
21	Hold	4	∞

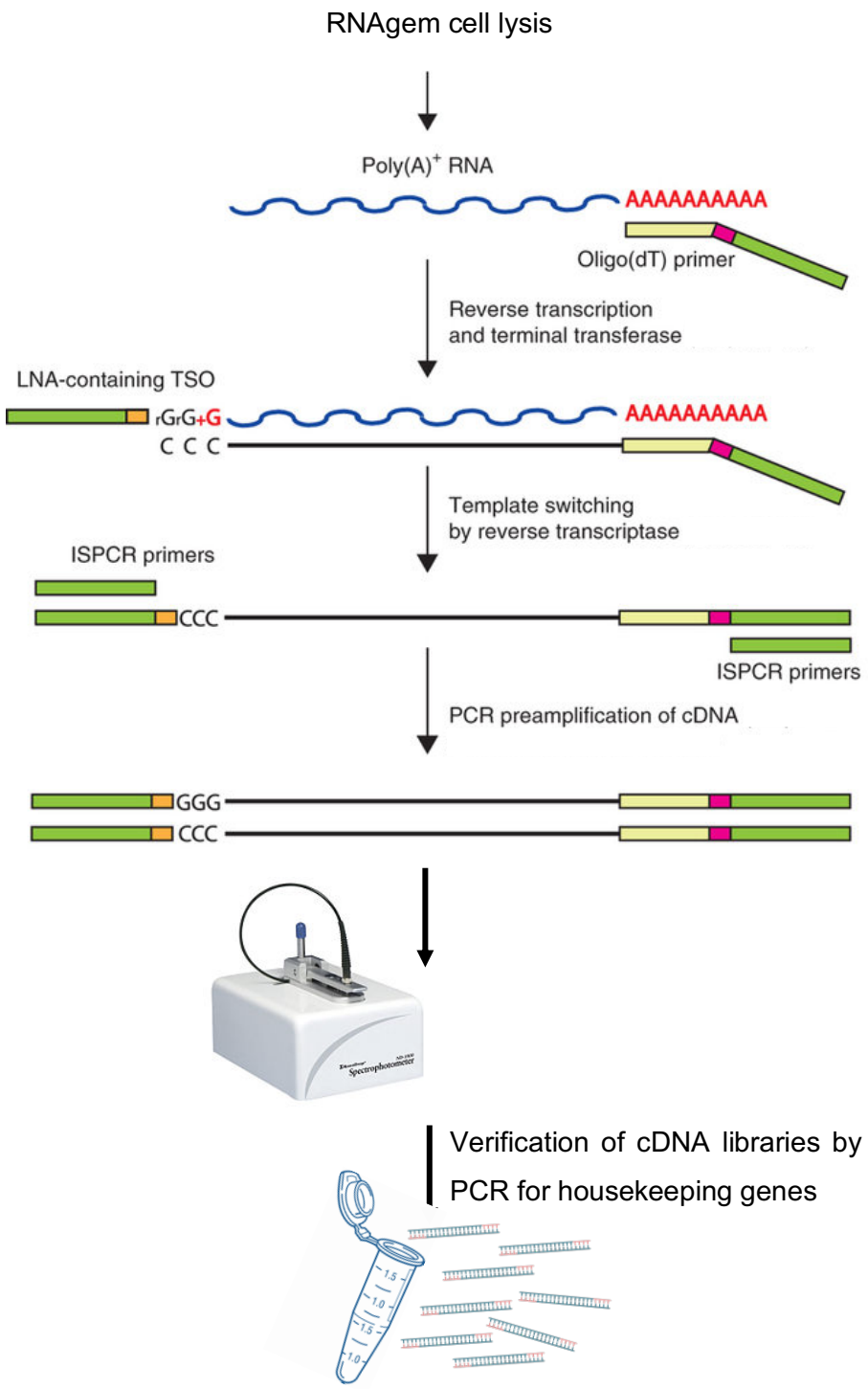

Figure 2.2. Flowchart of Smart-seq2 cDNA synthesis and verification of cDNA libraries by PCR for housekeeping genes. Figure was adapted from Picelli et al. (2014).

2.5 Polymerase chain reaction

The successful construction of each cDNA library was verified using specific housekeeping primers. For primer design, the sequences of bovine genes of interest were obtained from either the Ensembl database (https://www.ensembl.org/Bos_taurus/Info/Index) or National Centre for Biotechnology Information (NCBI) (https://www.ncbi.nlm.nih.gov/). The obtained sequences were inserted into the PrimerQuest primer design tool on Integrated DNA Technologies (IDT, USA) website to produce different sets of primers. Widely expressed housekeeping genes with stable expression in both somatic and gametic cells at the relevant stages of oocyte and embryo development were used for the experiments detailed in the thesis. These included *Glyceraldehyde 3-Phosphate Dehydrogenase* (*GAPDH*), *Histone H2A* (*H2A*) and *Tyrosine 3-Monooxygenase/Tryptophan 5-Monooxygenase Activation Protein Zeta* (*YWHAZ*). Primarily, *GAPDH* is an enzyme that catalyses the oxidative phosphorylation of glyceraldehyde-3-phosphate during glycolysis (Ercolani et al., 1988). It has commonly been used as a housekeeping gene because it is highly expressed in all cell types due to its vital function, and readily produces a single, sharp band after PCR amplification (Suzuki et al., 2000). Histones are also used as reference genes as they are necessary for the formation of chromatin and are therefore abundant in most cell types. *H2A* has been demonstrated as the most stable of housekeeping genes across a variety of cell types, including bovine preimplantation development (Jeong et al., 2005; Robert et al., 2002; Yan et al., 2014). Finally, *YWHAZ* gene encodes a 14-3-3 adapter protein that recognises phosphoserine- or phosphothreonine-containing proteins to mediate a variety of cellular activities such as signal transduction, metabolism, apoptosis and cell cycle regulation (Morrison, 2009). Alongside *GAPDH*, another study found that *YWHAZ* was among the most stable reference genes across bovine preimplantation embryo stages (Goossens et al., 2005).

The primer sequences are detailed in Table 2.13. All primers were diluted to a working concentration of 10 µM with dH_2O. Figure 2.3 shows the expression levels of housekeeping genes, *GAPDH* and *YWHAZ*, in a range of bovine somatic tissues (lung, liver, brain, heart, kidney, muscle prepared in-house by Hemmings et al. (2012)) and ovary, ovarian cortex (OC), oviduct, uterus and CL prepared according to Section 3.2.3. This figure highlights the consistent expression of *GAPDH* and

YWHAZ across different cell types in the bovine and verifies their use in the evaluation of the expression of candidate genes.

Table 2.13 Primer sequences of bovine housekeeping genes for PCR and real-time PCR verification of cDNA library generation (F: forward primer; R: reverse primer).

Gene	Primer sequences (5'→3')	Product size (bp)	Reference
GAPDH Bovine	F: GAAACCTGCCAAGTATGATGAG R: CAGCATCGAAGGTAGAAGAGTG	143	ENSBTAT00000037753
H2A Bovine	F: GAGGAGCTGAACAAGCTGTTG R: TTGTGGTGGCTCTCAGTCTTC	104	XM_002686087.4
YWHAZ Bovine	F: GAGAAAGCCTGCTCTCTTGC R: CAGCTTCGTCTCCTTGGGTA	157	XM_025001430.1

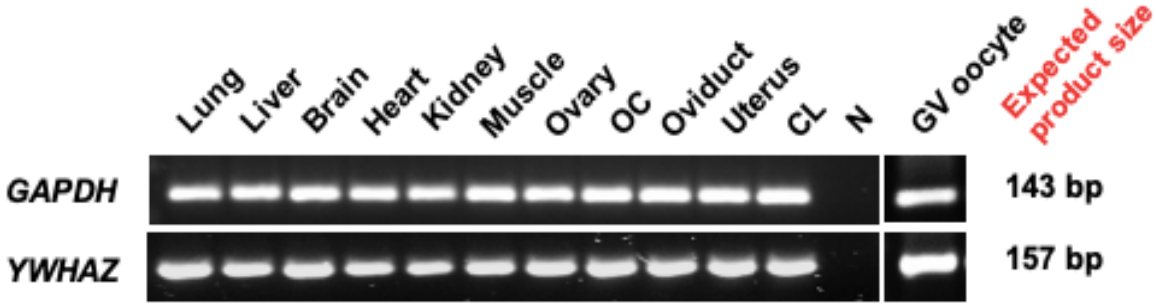

Figure 2.3. Gel electrophoresis of PCR amplification of housekeeping genes, *GAPDH* and *YWHAZ,* in a range of bovine somatic tissues: lung, liver, brain, heart, kidney, muscle, ovary, OC, oviduct, uterus and CL. GV oocyte and negative control (N) are also shown. Expected product sizes are displayed. A 100 bp DNA ladder (not shown) was used to verify the expected product sizes.

The controls set up alongside the test samples included 0.5 µl of dH_2O as a negative control and 0.5 µl of a previously verified GV cDNA library containing a single oocyte as a positive control. PCR was performed according to the *Taq* DNA polymerase manufacturers protocol (Invitrogen) in a final reaction volume of 12.5 µl. To perform the PCR experiment, a master mix was made in a 1.5 ml Eppendorf tube using recombinant *Taq* polymerase (Invitrogen). The cDNA was not included in the master mix and instead, 0.5 µl was added to each tube individually. Table 2.14 shows the PCR master mix and thermal program. The PCR reaction was performed using the Veriti® 96 well thermal cycler.

Table 2.14 **a)** PCR master mix (1x) and **b)** thermal cycling program.

a)

Component	Volume (µl)	Final concentration
***Taq* DNA polymerase** Invitrogen 10342020	0.05	0.02 U
10x PCR buffer Invitrogen 10342020	1.25	1x
dNTP mix (10 µM each) Thermo Scientific™ R0192	0.25	0.2 µM
$MgCl_2$ Invitrogen 10342020	0.38	1.5 mM
Forward primer (10 µM)	0.5	0.4 µM
Reverse primer (10 µM)	0.5	0.4 µM
Nuclease-free water	9.07	-
cDNA	0.5	-
Total volume	**12.5**	-

b)

Cycles	Step	Temperature (°C)	Time
1	Denaturing	94	3 min
2-31	Denaturing Annealing Extension	94 60 72	45 s 30 s 90 s
32	Extension	72	10 min
33	Hold	4	∞

2.6 Agarose gel electrophoresis

On completion of PCR, agarose gel electrophoresis was performed to separate out the resultant PCR products by size. The agarose gel was prepared by adding 100 ml of 1 x tris-borate ethylenediaminetetraacetic acid (TBE) buffer, pH 8.3 (Appendix II) to 1.5 g molecular grade agarose powder (Bio-41025, Bioline Ltd, UK) in a glass beaker, resulting in a final concentration of 1.5% (w/v). The beaker was then heated for 2 min in a 750 V microwave oven until the agarose was dissolved. The beaker was cooled by running it under cold water and subsequently, 5 µl of GelRed (41003, Biotium, USA) was added to allow for visualisation of the DNA. The gel was poured into a gel clamp (Bio-Rad Laboratories Ltd, Hertfordshire, UK) containing a 15 or 20 well comb to allow regular spacing of each test sample and the gel was allowed to set at RT for 30 min. 1x loading buffer (G7654, Sigma) was added to each sample and the samples were mixed by pipetting. Once the gel was set it was placed into a Sub Cell GT Tank with Powerpac 300 (Bio-Rad) covered in 1 x TBE buffer and the comb was removed. The samples were loaded into the wells alongside a 100 bp DNA ladder (N0551S, NEB). Gel electrophoresis was performed at 100 V for 60 min at RT.

Using an ultraviolet transilluminator (Gel Doc XR+ system, Bio-Rad), PCR products were visualised in the form of bands.

2.7 Real-time polymerase chain reaction

Real-time PCR is a sensitive technique that can accurately quantify relative transcript abundance of genes of interest in multiple samples at the same time (Heid et al., 1996). It can provide information about gene expression patterns during preimplantation embryo development. Furthermore, coupled with Smart-seq2 cDNA synthesis, it can be used to analyse mRNA levels in single oocytes and embryos (Kimble et al., 2018; Picelli et al., 2014). Housekeeping genes provide internal endogenous controls to which genes of interest can be normalised. This is based on the assumption that the efficiency of cDNA synthesis is the same for all transcripts and between all samples (Livak and Schmittgen, 2001). Many studies have investigated the expression of common housekeeping genes across embryo development to determine which gene is the most stable for use as an internal control for real-time PCR (Goossens et al., 2005; Jeong et al., 2005; Mamo et al., 2007; Robert et al., 2002). One study showed that expression of *GAPDH* and *YWHAZ* was consistent in all stages of bovine preimplantation development while another showed that *H2A* was the most stable (Goossens et al., 2005; Robert et al., 2002). As a result, *GAPDH, H2A* and *YWHAZ* were chosen as internal references for real-time PCR experiments in this thesis. Calculation of the geometric mean of 3 stable housekeeping genes is optimal as it controls for small expression differences (Goossens et al., 2005). Figure 2.5 shows the real-time PCR expression results of internal reference genes, *GAPDH, H2A* and *YWHAZ,* across bovine preimplantation development. Plotted in panel D of Figure 2.5 are the geometric means of each housekeeping gene across all oocyte and embryo stages. The results show that *GAPDH, H2A* and *YWHAZ* expression fluctuates significantly between the different stages of bovine preimplantation development ($p<0.05$). For *H2A* and *YWHAZ*, there was an increase in Ct values in the later embryo stages whereas *GAPDH* expression fluctuated throughout development. However, the geometric means of the 3 housekeeping genes did not significantly change between developmental stages, except for the 16-cell embryo stage. It is likely that this is caused by the low number of samples here with only 3 individual embryos collected at this stage. This finding demonstrates the importance of using the geometric mean of at least 3 housekeeping genes as an internal reference for normalisation of the expression of genes of interest.

For real-time PCR experiments, SYBR green technology (Applied Biosystems) was used to quantify the total amount of each transcript. SYBR green is an asymmetrical cyanine dye that intercalates between the bases of dsDNA and emits fluorescence that is proportional to the amount of dsDNA present (Zipper et al., 2004). Primers were purchased from IDT as described in Section 2.5 and diluted to a working concentration of 10 μM with dH_2O. Primers were designed with a desired amplicon size of around 100 bp and poly-base runs of ≤3 consecutive, repeat bases. Primer specificity for each gene was verified by the formation of 1 clean product of the correct size on the gel electrophoresis image. The real-time PCR master mix was prepared in a sterile 1.5 ml Eppendorf tube according to Table 2.15. 14 μl of master mix was loaded to a clear 96-well plate (E1403-8200, Starlab) and 1 μl of cDNA (1 ng/μl) was added to each well. The samples were run in triplicate to minimise error and increase the stability of the results. Furthermore, 3 negative controls were included for each real-time PCR to ensure there was no contamination in the reagents or PCR plate. The plate was run according to the thermal program in Table 2.16**.** A dissociation stage was included at the end of every real-time PCR experiment to exclude the formation of non-specific PCR products**.** To this end, the sample is slowly heated to denature the dsDNA and dissociate the SYBR green from the DNA. Upon cooling, the DNA anneals once again and the association of SYBR green to the PCR products is detected. If the primers are highly specific, only 1 PCR product will form and only 1 peak will be present on the dissociation curve (Figure 2.4). The real-time PCR experiments were run on an ABI PRISM 7900HT real-time PCR machine (Applied Biosystems).

In order to obtain accurate relative quantification of a target mRNA, the expression of 3 endogenous control transcripts, *GAPDH*, *H2A* and *YWHAZ,* where also obtained in triplicate. The Ct measurements from triplicate repeats were averaged for both the genes of interest and housekeeping genes. The geometric mean of the housekeeping genes was then calculated for each sample. The ΔCt of the chosen gene compared to the geometric mean of 3 housekeeping genes was calculated for each developmental stage. This was named the relative mRNA levels measured in arbitrary units. The data must be converted into a linear form by taking the log base 2 of ΔCt ($2^{-\Delta Ct}$) (Livak and Schmittgen, 2001). If this was not performed, highly expressed genes would have lower values and less abundant genes would have higher values. The arithmetic mean was then taken for each group and the resultant values were plotted on a histogram. The standard error of the mean (SEM) was displayed as error bars.

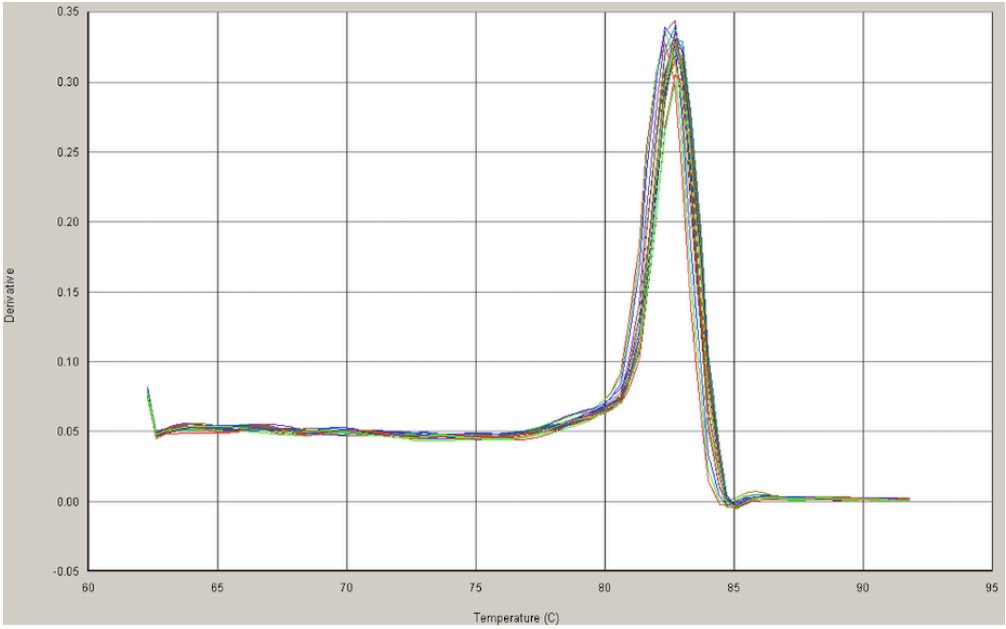

Figure 2.4. Example of a representative dissociation curve following real-time PCR experiment. This dissociation curve shows the amplicon from *GAPDH* housekeeping primers in 6 individual GV oocytes. The presence of only 1 peak demonstrates that the primers are highly specific to the gene as only 1 PCR product has formed.

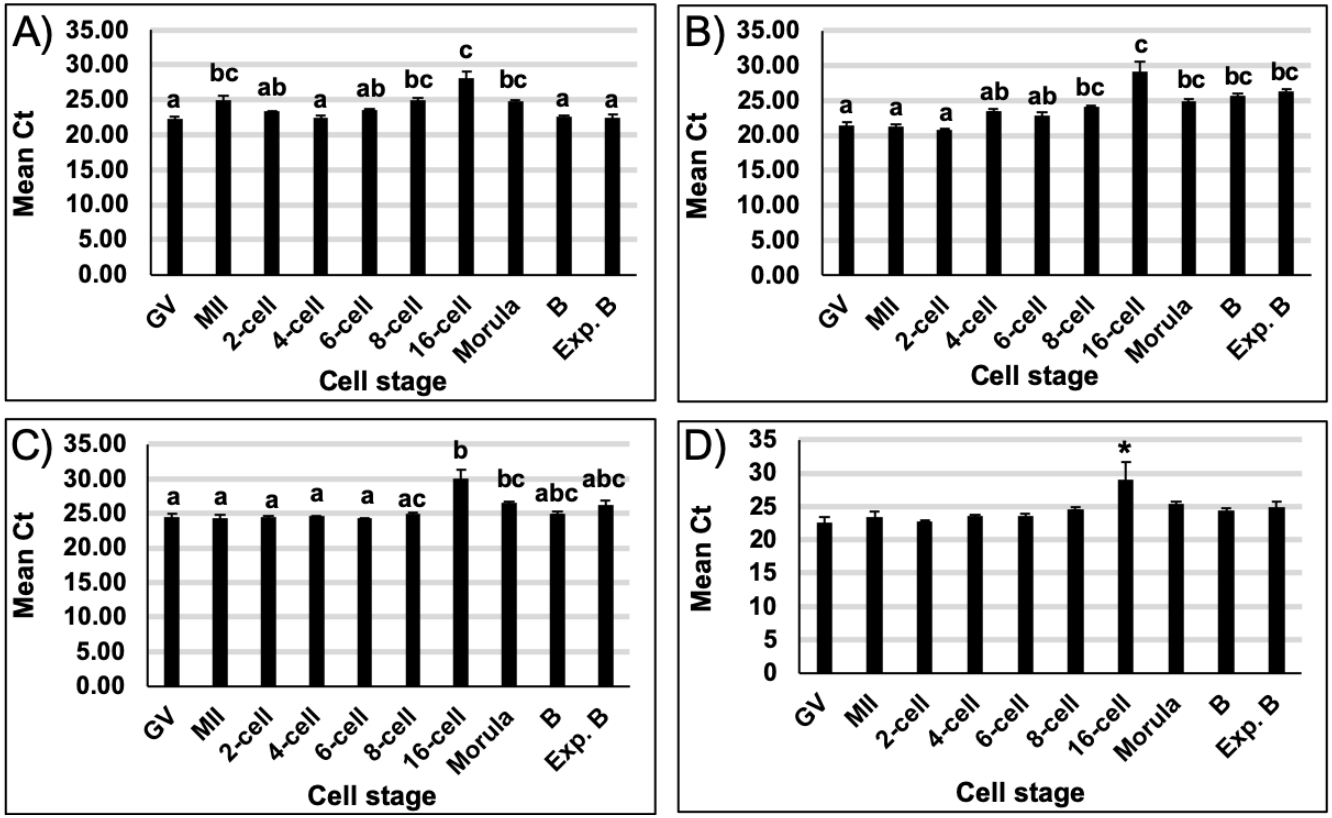

Figure 2.5. Real-time PCR quantification of housekeeping gene expression, A) *GAPDH,* B) *H2A* and C) *YWHAZ*, across oocyte maturation and preimplantation embryo development stages: germinal vesicle (GV) and metaphase II (MII) oocytes, 2-cell, 4-cell, 6-cell, 8-cell, 16-cell, morula, blastocyst (B) and expanded blastocyst (EB) embryos. Individual bars show the mean ±SEM for n = 6 single oocytes/embryos for each developmental stage except 16-cell where n = 3. D) The geometric mean of the 3 housekeeping genes at each stage of preimplantation development. This value was used to calculate the ∆Ct between the internal reference and gene of interest to normalise expression levels. Different letters or * on the bar denote significant differences between means ($p<0.05$) determined by one-way ANOVA.

Table 2.15 Real-time PCR master mix (1x)

Component	Volume (µl)	Final concentration
SYBR green PCR master mix Applied Biosystems 4309155	7.5	1x
Forward primer (10 µM)	0.5	330 nM
Reverse primer (10 µM)	0.5	330 nM
Nuclease-free water	5.5	-
Total volume	**14**	-

Table 2.16 Real-time PCR thermal program

Cycles	Step	Temperature (°C)	Time
1	Denaturing	95	10 min
2-41	Denaturing Annealing Extension	95 60 72	15 s 30 s 1 min
42	Dissociation stage	95 60 95	15 s 15 s 15 s
43	Hold	4	∞

2.8 Statistical analysis

Data generated in the thesis were processed using Microsoft Excel. All statistical analyses were performed by GraphPad Prism 7. The D'Agostino-Pearson test was used to test data for normality. Data containing '0' was transformed by $\sqrt{(x + 0.5)}$. Statistical analyses were performed on transformed data. Culture data and real-time PCR data were analysed using one-way analysis of variance test (ANOVA) or unpaired t-test for normally distributed data. Kruskal-Wallis or Mann-Whitney U tests were performed on data that were not normally distributed. In all analyses, p values of <0.05 were considered to be statistically significant. Untransformed data were plotted. Letters or an asterisk (*) were used to denote significant differences between means where $p<0.05$: if no significant differences between means were observed, bars were annotated with the same letter. Conversely, bars were annotated with different letters or * where significant differences between means were observed. Further information about the statistical tests that were used is detailed in each chapter-specific methods sections.

Chapter 3 Characterisation of *PADI6* and maternal effect genes across bovine oocyte maturation and preimplantation embryo development

3.1 Introduction

In oogenesis, asymmetric meiotic cell divisions unevenly distribute cytoplasm to the oocyte allowing maximal retention of cytoplasmic factors and production of 2 redundant polar bodies (Coticchio et al., 2015). Essential meiotic pauses enable reorganisation and accumulation of cytoplasmic components, protein synthesis and cytoskeletal rearrangements as described in Chapter 1. With specific emphasis on the GV to MII transition, the oocyte undergoes cytoplasmic maturation to gain competence for fertilisation, pronucleus formation and early embryogenesis, prior to EGA. Complex genomic reorganisations and epigenetic changes must occur to open the chromatin state and allow for zygotic transcription (Luciano and Sirard, 2018a). The many factors involved in these processes are transcribed from the maternal genome and are therefore termed MEGs. The majority of MEGs appear to be critical for developmental competency of the embryo and defective expression of these genes may result in female infertility at various stages. Among these MEGs are those that are important within the SCMC including *NLRP* genes. Interest in these genes stemmed from the involvement of *NLRP7* and *KHDC3L* in familial biparental hydatidiform mole (FBHM) (Murdoch et al., 2006; Parry et al., 2011). FBHM is a maternal imprinting disorder that causes recurrent miscarriage of the embryo and hyperproliferation of the trophoblastic tissues (Judson et al., 2002). There are intriguing questions as to how mutations in *NLRP7* and *KHDC3L* cause global imprinting abnormalities in the oocyte as they have no known role in imprinting mechanisms.

Investigation of the functional role of SCMC genes has shed some light on novel regulatory proteins that are essential for early embryogenesis. The SCMC was discovered after an investigation into the downstream targets of oocyte-specific master transcriptional factor, *Figla* (Soyal et al., 2000). The SCMC is believed to function in epigenetic regulation, organelle distribution, translation, EGA and spindle positioning (Bebbere et al., 2016; Yu et al., 2014b). FBHM-associated gene *KHDC3L,* together with *NLRP5, OOEP, PADI6* and *TLE6* constitute the core members of the

SCMC. Ablation of these genes precludes complex formation and embryo development, suggesting that a complete inventory is required for correct functioning of the SCMC (Li et al., 2008a). Mutations in *PADI6* and *TLE6* have been associated with human infertility characterised by early embryonic arrest (Alazami et al., 2015; Xu et al., 2016). Similarly, mutations in *NLRP5* have been associated with MLID (Docherty et al., 2015). The SCMC is proposed to contain more protein components than its 5 known members, adding the possibility that other *NLRP* genes are involved. Considering this, mutations in *NLRP2* and *-7* have been identified in human imprinting pathologies: BWS and MLID, and FBHM, respectively (Meyer et al., 2009; Murdoch et al., 2006).

SCMC proteins are abundant in the mammalian oocyte and early embryo but begin to diminish once the embryonic genome is activated. The SCMC has been primarily studied in the mouse model so much of the literature that will be discussed in this thesis was discovered in mice. The SCMC is localised to the subcortex of the oocyte but is excluded from regions of cell-to-cell contact in the embryo and absent from the ICM of the blastocyst (Li et al., 2008a). Similarly, mouse NLRP2 and NLRP7 are also cortically distributed in the oocyte and restricted from cell-to-cell contact in the embryo (Akoury et al., 2015; Mahadevan et al., 2017). Protein interaction studies showed that NLRP5 binds OOEP, TLE6 and PADI6 and interacts independently with KHDC3L (Li et al., 2008a; Ohsugi et al., 2008). Moreover, it has been observed that NLRP7 interacts with KHDC3L and PADI6 while NLRP2 interacts with KHDC3L, NLRP5, OOEP and TLE6 (Akoury et al., 2015; Mahadevan et al., 2017; Qian et al., 2018). Consequently, it is therefore likely that *Nlrp2* and *-7* are members of the SCMC. To add to this, it is understood that SCMC proteins NLRP5, OOEP and PADI6 are necessary for the formation of CPLs in the oocyte and early embryo (Kim et al., 2010; Tashiro et al., 2010; Wright et al., 2003). Studies have also observed localisation of NLRP7 and KHDC3L to CPLs (Akoury et al., 2015). Figure 1.11 shows a schematic representation of the hypothesised structure of the SCMC according to the aforementioned physical interactions that have been described for individual SCMC proteins. This figure was adapted from Bebbere et al. (2016) to include likely SCMC members, NLRP2 and NLRP7. Collectively, this strongly suggests a tight relationship between the SCMC and CPLs.

Still, the question of how the SCMC regulates imprinting establishment or maintenance remains. The cytoplasmic localisation of the SCMC negates a direct role for the complex in genomic imprinting. It could be that the SCMC coordinates the spatial and temporal localisation of epigenetic regulators (Monk et al., 2017). The expression and function of *Dnmt1, Dnmt3a, Dnmt3b, Dppa3, Trim28* and *Zfp57* has been interrogated in mouse preimplantation embryo development. *Dppa3, Trim28* and *Zfp57* are essential for maintaining imprints in the embryo (Section 1.6.2 and 1.6.3). DPPA3 prevents demethylation of specific maternal imprints after fertilisation by binding to an enriched maternal histone mark, H3K9me2, to block TET3-mediated 5-mC oxidation (Figure 1.9) (Nakamura et al., 2007; Nakamura et al., 2012). Similarly, ZFP57 is required for establishment of some maternal imprints in the oocyte and for maintenance of both maternal and paternal imprints during reprogramming of the embryo (Li et al., 2008c). ZFP57 recruits TRIM28 to the methylated allele of ICRs where it acts as a scaffold for chromatin-modifying proteins to induce a heterochromatic state (Quenneville et al., 2011; Zuo et al., 2012). Specifically, TRIM28 recruits methylation maintenance protein, DNMT1, to ICRs and disruption to this process results in loss of germline methylation (Figure 1.9) (Alexander et al., 2015). Both maternal and zygotic DNMT1 are required for maintaining parental imprints (Hirasawa et al., 2008). Interestingly, knockout of *Nlrp2* in mice resulted in abnormal localisation of DNMT1, suggesting a potential role for the SCMC in subcellular localisation of epigenetic factors (Mahadevan et al., 2017). DNMT3A and -3B display distinct expression patterns in the mouse oocyte and embryo. It seems that DNMT3A is maternally expressed in the oocyte and early embryo whereas DNMT3B is not expressed until after EGA (Hirasawa et al., 2008). In mouse, DNMT1 appears to be essential for maintaining methylation in the embryo while DNMT3A is required for establishment of maternal and paternal imprints in the oocyte and spermatozoa, respectively (Kaneda et al., 2004). In humans, high levels of *DNMT3A* were also observed in the oocyte from the early primary follicle stage, throughout oocyte maturation and in preimplantation embryo development to the blastocyst stage (Huntriss et al., 2004). High expression of *DNMT3B* was observed in the maturing oocyte and preimplantation embryo while *DNMT1* was highly expressed in the mature oocyte and early embryo but reduced in the blastocyst stage.

Most of the research into SCMC gene expression has been conducted in mice or humans but recently, the presence and developmental importance of the SCMC was confirmed in the ovine species (Bebbere et al., 2014). The SCMC appears to be highly conserved between mammalian species, which facilitates cross-species investigations (Lu et al., 2017). Characterisation of all SCMC genes across bovine oocyte maturation and preimplantation development has not yet been performed, though Pennetier et al. (2004) have characterised expression of *NLRP5* in cattle. Finally, knowledge of how MEGs are expressed in normal development will enable researchers to observe changes in expression that occur as a result of genetic manipulation.

3.1.1 Aims and objectives

The aim of this study was to characterise the expression and tissue distribution of *PADI6* in the cow and during human folliculogenesis. This study represents the first step towards investigating the expression pattern and the function of this gene in a monovulatory animal model that is physiologically relevant to human. The cow is considered a good model of oogenesis and preimplantation embryo development because it shares many similarities to human in terms of ovarian function and follicular physiology (Adams and Pierson, 1995; Adams et al., 2012; Baerwald et al., 2003a; Baerwald et al., 2003b; Ginther et al., 2001; Rovani et al., 2017). Both cows and humans are monovulatory, carry their young for approximately 9 months and have similar length reproductive cycles i.e. 28 days (Adams and Pierson, 1995). As an experimental model, IVM, IVF and embryo culture is widely used in the bovine embryo transfer industry and for research (Menezo and Herubel, 2002). Bovine oocytes and embryos are a similar size and have a similar developmental time frame to humans. They also express key oocyte genes and have enabled the study of mRNA and protein profiles during oocyte maturation and early embryogenesis (Bonnet et al., 2008; Vallee et al., 2005).

The primary aim of the current experiments was to map the expression pattern of *PADI6* in bovine oocytes during the final stages of Graafian follicle development and maturation *in vitro* and in IVF-derived preimplantation embryo stages by interrogating cDNA libraries from all stages of development by real-time PCR. The work also aimed to characterise the tissue distribution pattern of *PADI6* and other *PADI* family members (*PADI1-4*) across a range of bovine somatic tissue cDNA libraries by PCR.

Finally, associated MEGs, SCMC members and epigenetic regulators were characterised across bovine oocyte and embryo development by real-time PCR, with the objective of comprehensively mapping linked gene expression patterns across bovine and human oocyte maturation and preimplantation development.

3.2 Materials and methods

3.2.1 Oocyte and embryo isolation

The methods used for bovine oocyte isolation and *in vitro* embryo culture have been described and validated previously (Hemmings et al., 2012). As detailed in Chapter 2, bovine ovaries were isolated from reproductive tracts and GV oocytes were obtained following aspiration of COCs from 2-5 mm follicles. A subset of GV oocytes were denuded from the surrounding cumulus cells using hyaluronidase immediately following oocyte harvest. Sterile 4-well dishes were prepared by pipetting 500 µl of 300 µg/ml hyaluronidase into the first well and 500 µl of H199+ (Table 2.2) into the other 3 wells. In groups of 10, oocytes were transferred into the hyaluronidase well for 30 sec using an EZ-Grip denudation and handling pipettor attached to a 170 µm pipette tip. Oocytes were then transferred to a fresh H199+ well and mechanically denuded. To ensure that all the cumulus cells were removed, the pipette tip was changed to a 140 µm diameter pipette tip and gentle pipetting was continued. For generation of MII oocytes, 50 COCs were subjected to IVM for 24 hours in serum-free IVM medium (Table 2.3) at 39°C in a 5% CO_2 humidified incubator (Hemmings et al., 2012) as described in Section 2.1. After maturation, subsets of 10 COCs were denuded in hyaluronidase as described above, and oocyte meiotic status was confirmed by detection of the presence of the first polar body using an inverted microscope. Oocytes were washed twice in a sterile 4-well dish containing 500 µl of DPBS. Oocytes were individually placed into 0.5 ml Eppendorf tubes containing 2 µl of RNAGEM lysis buffer and frozen at -80°C (Section 2.4.1). For generation of preimplantation embryos, 50 COCs were fertilised following 24 hours in serum-free IVM medium and cultured in groups of 20 in 20 µl SOFaaBSA media as described in Section 2.2 and 2.3 (Hemmings et al., 2012). Embryo developmental stage was assessed using an inverted microscope. Embryos were washed twice in a sterile 4-well dish containing 500 µl of DPBS. Oocytes were individually placed into 0.5 ml Eppendorf tubes containing 2 µl of RNAGEM lysis buffer and frozen at -80°C (Section 2.4.1). Oocytes and embryos were imaged using a Nikon Eclipse Ti inverted microscope (Nikon Instruments, Amstelveen, Netherlands) fitted with a heated stage at 39°C and a Watec WAT-221S camera (Camtronics BV, Eindhoven, Netherlands). Research Instruments (RI) viewer software was used to examine the images on the computer.

To assess the rates of oocyte maturation, embryo cleavage and blastocyst formation *in vitro,* 3 discrete cultures were conducted. For each culture, aspirated COCs were placed into a 4-well dish containing 500 µl of IVM media in groups of 50 for 24 hours as detailed in Section 2.1.3. After IVM a representative subset of 10-15 COCs was removed from each culture and oocytes were denuded in hyaluronidase as described above. Oocyte viability was measured by incubation with NR dye. NR dye is a widely used viability stain as it can be applied to living cells without killing them and be visualised using standard light microscopy (Borenfreund and Borrero, 1984; Repetto et al., 2008). NR dye diffuses through the plasma membrane and is taken up by lysosomes in living cells (Triglia et al., 1991). The uptake and retention of NR by a cell depends on the cell's ability to maintain pH gradients (Repetto et al., 2008). When a cell dies or becomes damaged, the cell loses this ability and cannot uptake NR dye. As a result, live oocytes stain red while dead oocytes remain unstained so distinct oocyte populations can be counted. This staining method was validated previously for use on ovarian tissue and GCs (Campbell et al., 1996; Chambers et al., 2010). Moreover, 1 µl of 50 µg/ml of neutral red (NR) dye was added to each 20 µl microdrop of oocytes and allowed to incubate for 15-20 min. The numbers of live and dead oocytes were recorded. Oocyte maturation was determined by the extrusion of a polar body after 24 hours in IVM media using an inverted microscope. Next, COCs were fertilised and cultured in groups of 20 in drops of SOFaaBSA medium as detailed in Sections 2.2 and 2.3. Embryonic cleavage was recorded by the presence of 2-cell embryos 24-36 hours after sperm were added (Day 1-2). From Day 2-4, 4-16 cell embryos were recorded, and around Day 5, embryos started to compact and form the morula. Finally, blastocyst rates were documented on Day 7 or 8 (Figure 3.1).

Finally, the aim of this isolation was to generate 6-12 cDNA libraries of individual oocytes or embryos for each developmental stage: GV and MII oocytes, 2-cell, 4-cell, 6-cell, 8-cell, 16-cell, morula, blastocyst and expanded blastocyst embryos. For GV and MII stages, oocytes were generated over 2 discrete cultures. 6 individual oocytes were frozen per culture to give a total of 12 oocytes per stage for cDNA synthesis. For the generation of embryos at each developmental stage, 5 discrete cultures were performed, and individual embryos were frozen based on their developmental stage until 6-12 individual embryos were collected for each developmental stage (Figure 3.1).

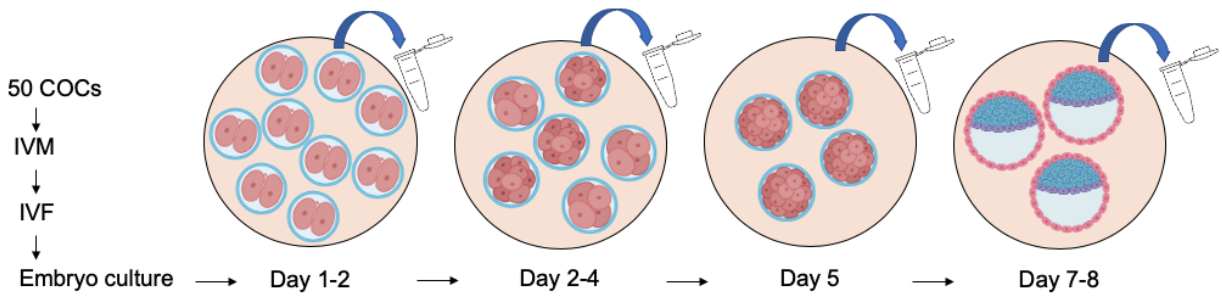

Figure 3.1 Generation of embryos at each developmental stage. 50 COCs were subject to IVM, IVF and embryo culture as described in Chapter 2. At the appropriate developmental time point, a subset of embryos was removed from the culture dish and embryos were individually frozen for cDNA synthesis. This was repeated over 5 discrete cultures until 6-12 embryos were collected for each developmental stage.

3.2.2 cDNA synthesis

Before cDNA synthesis, samples were subject to a DNA degradation protocol to remove contaminating DNA, as detailed in Section 2.4.1. In brief, the samples were heated to 75°C for 10 min to lyse the cells. The thermal cycler was cooled to 37°C and 0.5 µl of DNase solution (Table 2.7b) was added. Samples were incubated at 37°C for 5 min to permit DNA degradation. The temperature was then increased to 75°C for 5 min to denature the DNase 1 enzyme. Following DNA degradation, full-length cDNA synthesis was performed for individual oocytes and embryos according to Smart-seq2 cDNA synthesis protocol described in Picelli et al. (2014) as described in Section 2.4. A 1:1 oligo-dT primer and dNTP mix was added to each sample (Table 2.9) and samples were incubated at 72°C for 3 min to allow the primer to bind to the mRNA polyA tail. 5.7 µl of the RT mix (Table 2.10) was added to each sample and samples were put to the thermal program shown in Table 2.11. Following reverse transcription, the cDNA was amplified by polymerase chain reaction (PCR) as detailed in Section Table 2.11. Finally, cDNA was diluted 1:1000 using nuclease-free water to a concentration of approximately 1 ng/µl and stored at -20°C until further use.

3.2.3 RNA extraction from fresh bovine tissues

RNA extraction and cDNA synthesis were performed on fresh bovine abattoir-derived tissue (J.C. Penny and sons, Rawdon, Leeds, UK). Bovine reproductive tracts were received from the abattoir and 0.1-0.15 g cross-sections were cut through the ovary, oviduct, uterus and corpus luteum. The tissue was placed into 2 ml Safe-Lock

microcentrifuge tubes (0030120094, Eppendorf®, Germany) alongside 5mm stainless steel beads (69989, Qiagen Ltd) and 1 ml of TRIzol™ (15596026, Invitrogen™ Ltd). The tissue was homogenised in a TissueLyser system (Qiagen Ltd). Once the majority of tissue was homogenised, the supernatant was transferred by pipetting into sterile 1.5 ml Eppendorf tube.

RNA extraction was performed in accordance with the TRIzol™ manufacturer recommendations (Invitrogen™ Ltd). 0.5 ml of isopropanol was added to each sample and allowed to incubate for 10 min. The samples were then centrifuged at 12,000 x g for 10 min at 4°C. The supernatant was removed by pipetting and discarded. The RNA pellet was resuspended by pipetting in 1 ml of 75% ethanol. The samples were vortexed briefly before centrifuging at 7500 x g for 5 min at 4°C. Again, the supernatant was removed by pipetting and discarded. The RNA pellet was left to air-dry for 10 min. Finally, RNA was resuspended by pipetting in 50 µl of RNase-free water. RNA was quantified using a spectrophotometer (ND-1000, NanoDrop Technologies, USA). The spectrophotometer was washed 3 times with 1 µl dH_2O before calibrating a blank measurement using 1 µl dH_2O. Each RNA sample was measured by adding 1 µl of sample to the spectrophotometer. The results were recorded and approximately 1 µg of RNA was used as starting material for cDNA synthesis.

cDNA synthesis from the range of fresh bovine tissue RNA was performed according to Smart-seq2 cDNA synthesis protocol described in Picelli et al. (2014) (Section 2.4). Additionally, cDNA synthesis was performed on archived RNA preparations of bovine somatic abattoir-derived tissues (J.C. Penny and sons, Rawdon, Leeds, UK) prepared by Dr Karen Hemmings (Leeds Institute of Cardiovascular and Metabolic Medicine, University of Leeds). These included bovine lung, liver, brain, heart, kidney and muscle RNA. Only 1 RNA sample was available for each tissue and Smart-seq2 cDNA synthesis was repeated twice.

3.2.4 Molecular evaluation of the bovine developmental series

Real-time PCR was used to quantify the changes in *PADI6* expression over bovine development (GV, MII, 2-cell, 4-cell, 6-cell, 8-cell, 16-cell, morula, blastocyst and expanded blastocyst) compared to housekeeping genes *GAPDH, H2A* and *YWHAZ* (Table 2.13). 6 samples were analysed per developmental stage and each sample was performed in triplicate. The *PADI6* primer sequences are shown in Table 3.1. The real-time PCR experiments were conducted as detailed in Section 2.7. Figure 3.2 shows the experimental workflow from oocyte isolation and *in vitro* embryo culture to Smart-seq2 cDNA synthesis and real-time PCR analysis. Bovine somatic libraries were also analysed for expression of *PADI* genes including *PADI6* by PCR to evaluate the bovine tissue distribution patterns of members of the *PADI* family. PCR was performed as detailed in Section 2.5 and the *PADI* primer sequences are shown in Table 3.1. Following the PCR analysis, 12 µl of each sample was run alongside a 100 bp DNA ladder on a 1.5% (w/v) agarose gel at 100 V for 1 hour as described in Section 2.6.

Table 3.1 PCR primer sequences for bovine *PADI* family genes

Gene	Primer sequences (5'→3')	Product size	Reference
PADI1	F: CCCTCTTTCCTTTACCAGCTAC R: CCGAGTTTCCTTGTCCTGATT	108 bp	ENSBTAT00000015977.6
PADI2	F: CTACAGCAAGGAAGACCTGAAG R: AGTCCGACATGGAGATGTAGA	110 bp	ENSBTAT00000004411.6
PADI3	F: GAACTGCGACAGAGACAGTATG R: CCGCAGAATCATCACAGACA	103 bp	ENSBTAT00000015978.6
PADI4	F: TGACTGACCTTGACTCCTTTG R: GTAACCGCTGTCTCCAATGA	104 bp	ENSBTAT00000015991.6
PADI6	F: AAAAAGGACTTCCGGCTGCT R: GAGCTGGTCCTTCCTAAGCC	120 bp	XM_002685797.5

The cDNA libraries representing developmental stages from the GV oocyte to the blastocyst embryo were also interrogated against multiple MEGs including *KHDC3L, OOEP, TLE6, NLRP2, NLRP5, NLRP7, FIGLA, DNMT1, DNMT3A, DNMT3B, DPPA3, TRIM28* and *ZFP57* by real-time PCR. The primer sequences for MEGs are shown in Table 3.2. For each developmental stage, 6-12 independent oocyte or embryo cDNAs were analysed by real-time PCR (Section 2.7). It is worth noting that differences in oocyte/embryo numbers (n) may exist as analyses of gene expression for individual samples were excluded from the final analyses if the real-time PCR

experiment failed. dH_2O was used as a negative control in each real-time PCR reaction to check for contamination. Ct measurements from triplicate repeats were averaged for both the genes of interest and housekeeping genes as detailed in Section 2.7. The geometric mean of the housekeeping genes was then calculated for each sample. The ΔCt of the chosen gene compared to the geometric mean of 3 housekeeping genes was calculated for each developmental stage. The arithmetic mean was taken for each group and presented as a histogram displaying the mean ±SEM for the number of observations shown.

Table 3.2 RT-PCR primer sequences for bovine MEGs

Gene	Primer sequence (5'→3')	Product size	Reference
DPPA3	F: GAGCCTACAGCATCACCTTC R: GGTCCAGGTTGGGTTATCTTC	104 bp	NM_001111108.2
DNMT1	F: ACCGTATTGGCCGCATAAA R: GGGTAGACTTGTGTGTGTTCTC	123 bp	NM_182651.2
DNMT3A	F: CGAGGTAGTGACACAAGGTTAAA R: CTTCTGGGTGCTGATACTTCTC	98 bp	NM_001206502.2
DNMT3B	F: CTCCGAGATTCCAGCAGATAAG R: GTACATGGCCTTCCTGTAAGAG	103 bp	NM_181813.2
FIGLA	F: ACGAGACCCCGATCATCAGA R: GGGGAATCTATCCACTGCCA	161 bp	NM_001281920.1
KHDC3L	F: GACTACAGCATGGCCTCTCCC R: GATGAACGTGAAGCAGGGTC	241 bp	ENSBTAT00000081682.1
NLRP2	F: GTGCGAGGCTTTGAAGAAAC R: TTACTCCACTGGACCCCAAG	164 bp	ENSBTAT00000074039.1
NLRP5	F: AAATAAGGTGGCGGACCAGG R: GTCCTCGCACAGAAGGTTCA	385 bp	NM_001007814.2
NLRP7	F: GATCTCACTGCAGGTAGGAAAG R: CCCAGAGTTGGAGAGAATGATG	110 bp	ENSBTAT00000062990.2
OOEP	F: GTCGAAGTCACCGTTTTCGC R: CTCACGCTCCTGACAACACT	196 bp	ENSBTAT00000077348.1
PADI6	F: TGCTCTTTGAAGGGCTTAGG R: TCATTCTGCTTCCTCATCTTCTC	103 bp	XM_002685797.5
TLE6	F: ATCCTCTGTCATGTGCTGTG R: CTCAGTATGTGAGCTGGTACAC	95 bp	XM_010807029.3
TRIM28	F: GCTCTCCAAGAAGCTGATCTAC R: CGTTGAGGTCCCACTGAAAT	104 bp	ENSBTAT00000008424.6
ZFP57	F: CTCAGTTGCTGGAAGGTAGATAG R: CTTCTCTTCCATGCTGTCTCTT	102 bp	XM_010818393.3

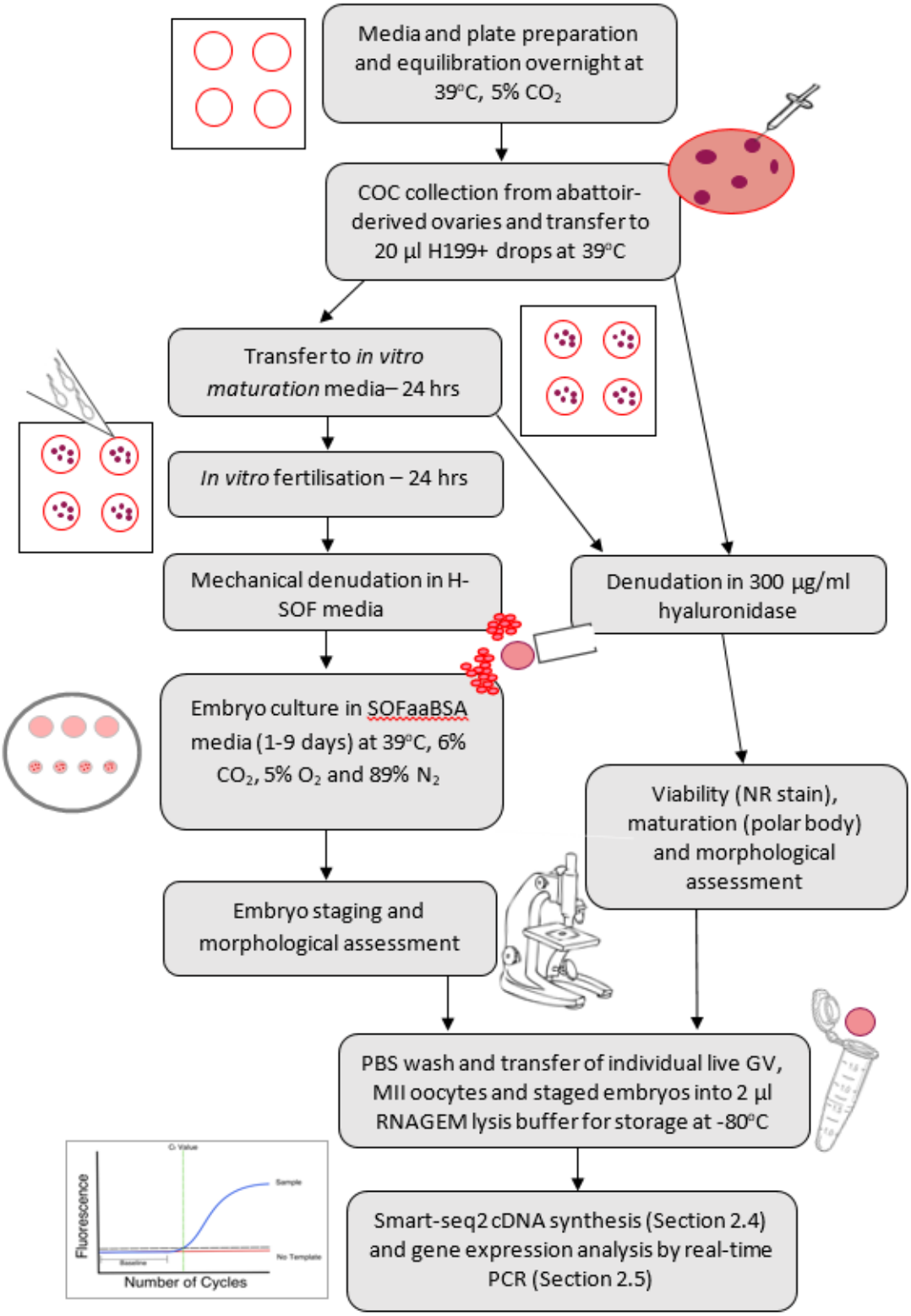

Figure 3.2 Experimental workflow of bovine oocyte maturation and embryo culture *in vitro* followed by Smart-seq2 cDNA synthesis and real-time PCR analysis.

3.2.5 Molecular evaluation of the human developmental series

Primers were also designed against human *PADI6* gene for analysis of *PADI6* in previously verified, human archived cDNA samples from Dr John Huntriss (Huntriss et al., 2006). The samples included 1 x pool of 10 primordial follicles, 1 x individual samples of GV and MII oocytes, 4-cell, morula and 2 x individual blastocyst embryos that were donated by patients under ethically approved protocols licensed by the Human Fertilisation and Embryology Authority (HFEA). Human *PADI6* and housekeeping gene *GAPDH* primer sequences are shown in Table 3.3. *PADI6* primer sequences were previously used in Chavanas et al. (2004). PCR was performed in accordance with the manufacturer's recommendations for GoTaq® Hot Start Polymerase (Promega, USA). The reaction was made in a 20 µl volume consisting of 1 x buffer, 0.2 mM each dNTP, 2.5 mM $MgCl_2$, 0.5 µM each primer, 1.25 units polymerase, <500 ng template DNA and dH_2O. 12 µl of each sample was run on a 1.5% (w/v) agarose gel at 100 V for 1 hour as described in Section 2.6.

Table 3.3 Primer sequences for human *PADI6* and *GAPDH* for PCR.

Gene	Primer sequence (5'→3')	Product size	Reference
PADI6 Human	F: GGCAAGAACCTGGGGATCC R: GGTGACAGTGGGCCATCCA	270 bp	Chavanas et al. (2004)
GAPDH Human	F: ACAACAGCCTCAAGATCATCAG R: GGTCCACCACTGACACGTTG	312 bp	ENST00000396856

3.2.6 Statistical analysis

Real-time PCR results were analysed by calculating the ΔCt of the chosen gene compared to the geometric mean Ct value of 3 housekeeping genes, *GAPDH*, *H2A* and *YWHAZ* for each developmental stage. The arithmetic mean was taken for each group and presented as a histogram displaying the mean ±SEM. For oocyte maturation, fertilisation and blastocyst rates, the arithmetic mean was calculated across replicate cultures and presented as a histogram displaying the mean ±SEM. Data were tested for normality using the D'Agostino-Pearson test. Data containing '0' was transformed by $\sqrt{(x + 0.5)}$ and one-way analysis of variance tests (ANOVA) or unpaired t-test were used for data that was normally distributed data and Kruskal-Wallis or Mann-Whitney U tests were performed on data that was not normally

distributed. p values of <0.05 were considered to be statistically significant. Untransformed data were plotted.

3.3 Results

3.3.1 *In vitro* production of mature bovine oocytes and embryos

Mature bovine oocytes and embryos were produced *in vitro* using the IVM, IVF and embryo culture system previously validated by Hemmings et al. (2012) . Figure 3.3 shows representative images of the different stages of bovine preimplantation development. Oocyte maturation, embryonic cleavage and blastocyst rates were recorded at appropriate time points to validate the methods for IVM and embryo culture (Figure 3.4). Maturation rates were calculated based on the subset of oocytes that were denuded for each culture replicate. Cleavage rates were expressed as the percentage of COCs that were inseminated and blastocyst rates as the percentage of cleaved embryos that progressed to the blastocyst stage. The table shows the raw data across 3 discrete culture weeks (Figure 3.4a) and the mean ±SEM was calculated for each developmental rate (Figure 3.4b). The results showed that 83% (n = 201/242) of GV oocytes matured to MII stage *in vitro* (Figure 3.4 – maturation rate). Of 150 oocytes that were fertilised *in vitro* and transferred to embryo culture, 69% (n = 104/150) cleaved into 2-cell embryos (Figure 3.4 – cleavage rate) and 31% (n = 46.5/150) developed into blastocysts (Figure 3.4 – blastocyst rate).

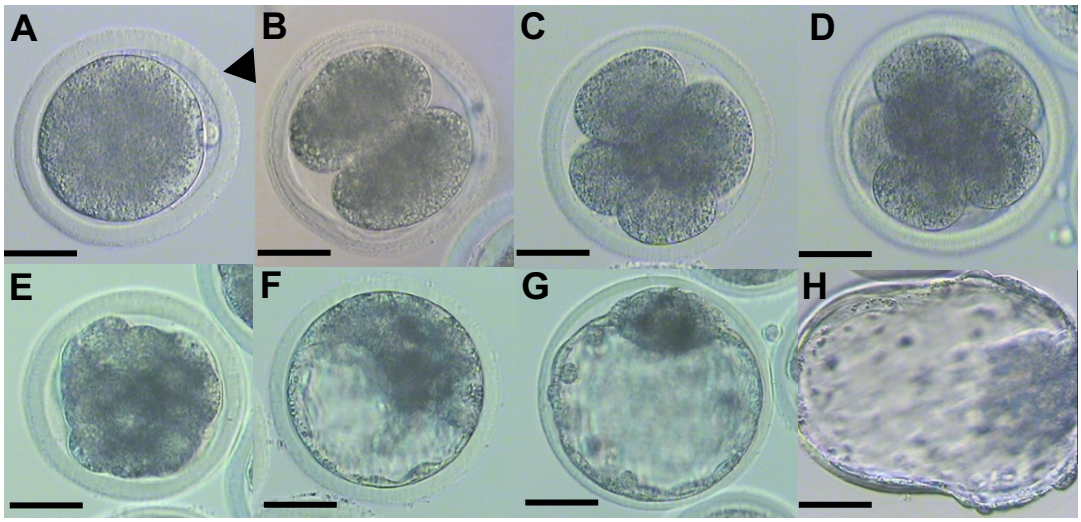

Figure 3.3 Representative images of the different stages of bovine preimplantation embryo development: (A) MII oocyte showing 1 polar body (arrow head); (B) 2-cell embryo; (C) 4-cell embryo; (D) 8-cell embryo; (E) compacting morula; (F) blastocyst; (G) expanding blastocyst; (H); hatching blastocyst. The scale bar represents 40 µm (200X magnification).

a)

Repeat	No. COCs for IVM	Maturation rate (%)	No. COCs for IVF	No. COCs for embryo culture	Cleavage rate (%)	Blastocyst rate (%)
1	75	81	60	52	54	32
2	120	90	100	78	82	30
3	47	78	38	20	70	30
Mean ±SEM		**83% ±3.6%**			**69% ±8.1%**	**31% ±0.7%**

b)

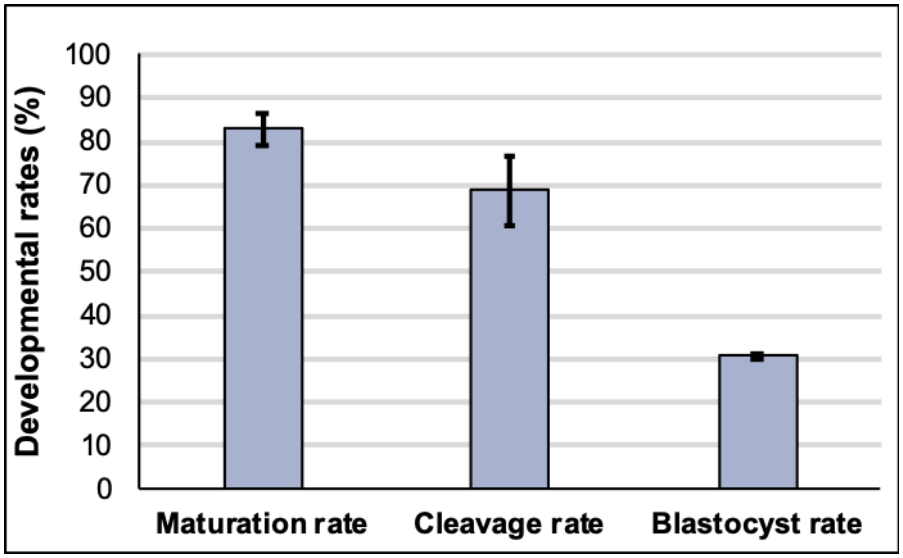

Figure 3.4 **a)** Raw data of the developmental rates of bovine oocytes and embryos over 3 discrete repeats. Maturation rate was calculated for a representative sample from each culture. **b)** Developmental rates of bovine oocytes and embryos. The mean oocyte maturation, embryo cleavage and blastocyst rates are plotted ±SEM for 3 discrete cultures. n = 242 oocytes for maturation rate of which 150 embryos were inseminated for cleavage and blastocyst rates.

3.3.2 Characterisation of the *PADI* family gene expressions in bovine somatic tissues

The profile of *PADI6* expression was analysed in 11 bovine somatic tissues: lung, liver, brain, kidney, muscle, heart, oviduct, OC, uterus, ovary and CL. A single GV oocyte was analysed alongside somatic tissues as a positive control and housekeeping gene, *GAPDH,* was used as an internal control. PCR and gel electrophoresis were repeated 3 times, obtaining the same result each time. *PADI6* gene expression was not detected in bovine lung, liver, brain, kidney, muscle, heart, oviduct, uterus, ovary and CL samples (Figure 3.5a). *PADI6* was, however, expressed in the bovine OC, albeit at a lower level than in the GV oocyte positive control. These consistencies verify that *PADI6* gene expression is restricted to the oocyte so confirming that *PADI6* is an oocyte-specific gene in the bovine. *GAPDH* expression was constant across bovine somatic tissues.

Following the confirmation of the oocyte-specific expression pattern of bovine *PADI6*, the expression of other *PADI* family members was characterised across bovine somatic tissues (lung, liver, brain, kidney, muscle, heart, oviduct, OC, uterus, ovary and CL) and GV oocyte by PCR. The PCR was repeated twice, obtaining the same result each time. Housekeeping genes, *GAPDH* and *YWHAZ,* were used to ensure that the cDNA libraries were of sufficient quality for the determination of gene expression. The results are shown in Figure 3.5b. *PADI1* was barely detected in any bovine somatic tissue, although very low expression may have been present in lung and brain samples. *PADI2* was highly expressed in both lung and brain tissues and moderate gene expression was detected in the liver. In addition, low expression of *PADI2* gene was present in muscle. *PADI3* appeared to be the most ubiquitously expressed with expression detected in lung, liver, brain, heart, oviduct and uterus tissues, albeit at low levels. *PADI4* was highly expressed in the liver, and low expression was detected in the heart and muscle samples. cDNA smears were observed in *PADI4* lung and uterus samples. In comparison to *PADI6*, low expression of *PADI3* and *4* was detected in the GV oocyte sample and no expression of *PADI1* and *2* was observed. These results strongly suggest that *PADI6* is the most readily detectable *PADI* family member in the bovine oocyte using these methods.

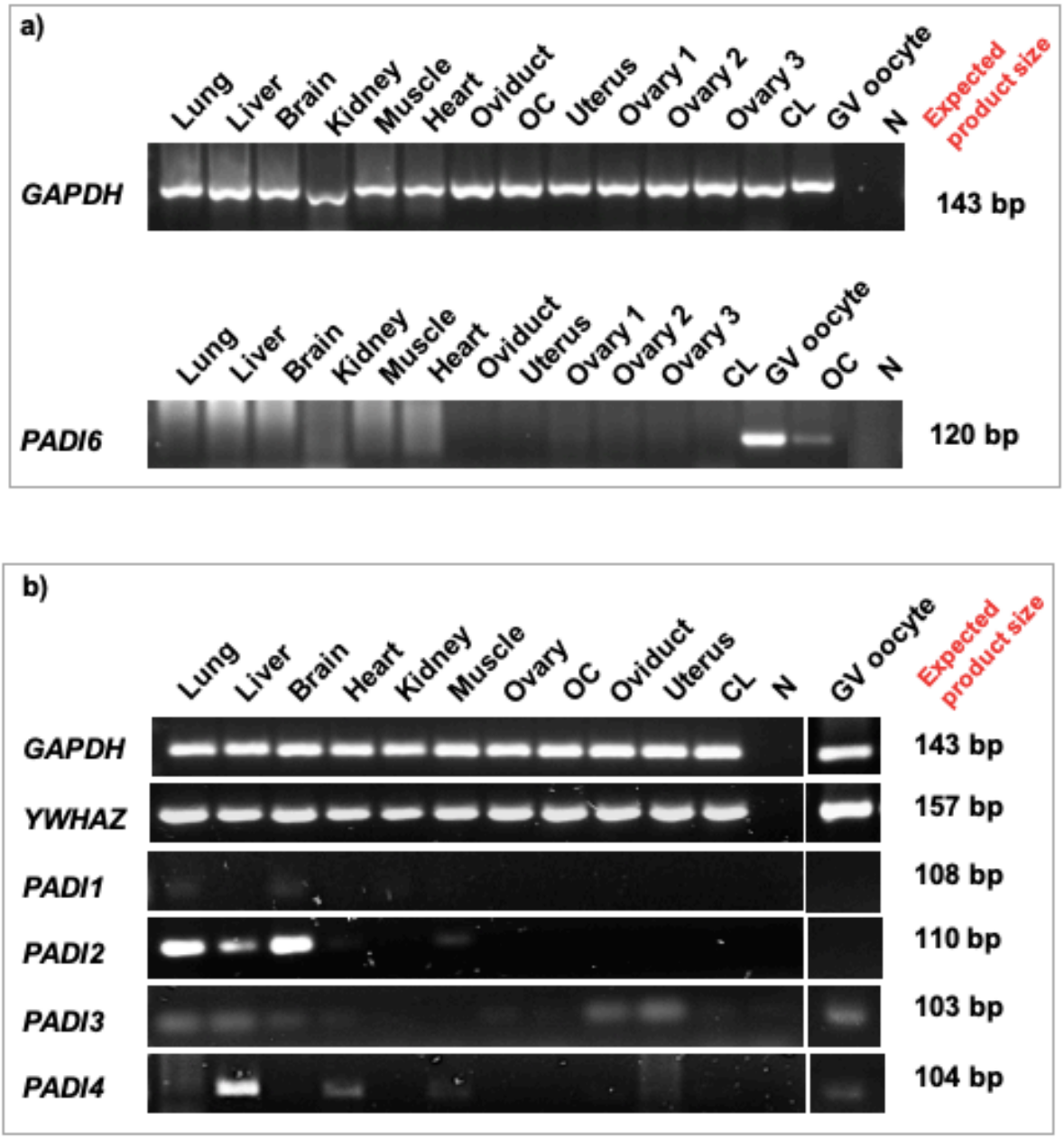

Figure 3.5 Representative gel showing **a)** *PADI6* gene expression and **b)** other PADI family members, *PADI1, 2, 3* and *4*, across bovine somatic tissues: lung, liver, brain, kidney, muscle, heart, oviduct, OC, uterus, ovary and CL. A GV oocyte sample served as a positive *PADI6* control and *GAPDH* was used as a loading control. Expected product sizes are displayed. A 100 bp DNA ladder (not shown) was used to verify the expected product sizes.

3.3.3 Characterisation of *PADI6* expression across bovine oocyte maturation and preimplantation embryo development

In light of the observed oocyte-restricted *PADI6* expression shown in Figure 3.5a, the expression profiles of bovine *PADI6* in the maturing oocyte and preimplantation embryo were analysed by real-time PCR (Figure 3.6). 6-12 independent oocyte or embryo cDNA libraries were analysed in triplicate for each developmental stage. *PADI6* expression was at its highest in GV oocytes but sharply decreased by almost 10-fold from GV to MII oocyte transition ($p<0.05$). *PADI6* mRNA persisted at moderate levels in the early embryo until the 8-16 cell stage (EGA in the bovine), after which little to no expression was observed in the morula and blastocyst stages. Figure 3.10 shows a corresponding gel electrophoresis image that corroborates the presence of *PADI6* prior to EGA and subsequent lack of *PADI6* in the blastocyst stage. Overall, *PADI6* gene expression appears to exist at moderate levels in the bovine oocyte in comparison to the other MEGs that were assessed. Considering this, PCR was performed on archived human preimplantation samples: primordial follicle, GV and MII oocyte and 4-cell, morula and blastocyst embryos (Figure 3.7). The results showed that human *PADI6* is highly expressed in the GV and MII oocyte and early embryo but absent from blastocyst stages of development, as observed in bovine. Unfortunately, there was no further human cDNA available for real-time PCR.

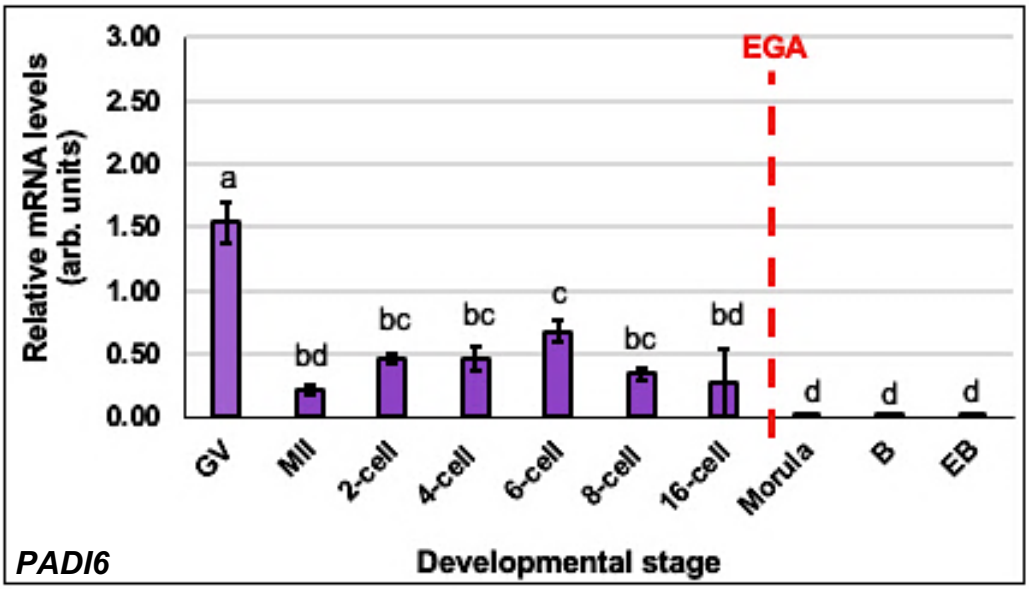

Figure 3.6 Real-time PCR quantification of *PADI6* expression across bovine oocyte maturation and preimplantation embryo development stages: GV (n=12) and MII oocytes (n=12), 2-cell (n=12), 4-cell (n=12), 6-cell (n=6), 8-cell (n=10), 16-cell (n=6), morula (n=11), blastocyst (B) (n=12) and expanded blastocyst (EB) (n=10) embryos. Data were standardised against *GAPDH, H2A* and *YWHAZ* housekeeping mRNA levels to give the relative mRNA level in arbitrary units. Individual bars show the mean ±SEM. Different letters on the graph were used to denote significant differences between means ($p<0.05$). EGA is shown by the red dotted line.

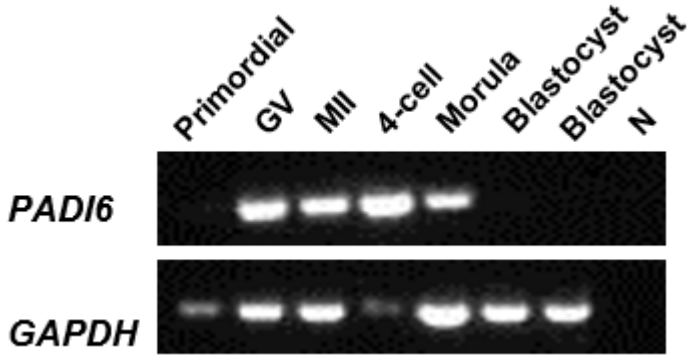

Figure 3.7 *PADI6* gene expression in human oocyte and preimplantation development: primordial follicle, germinal vesicle (GV) and MII oocyte, 4-cell, morula and blastocyst embryos after PCR and DNA fragment separation by gel electrophoresis.

3.3.4 Characterisation of SCMC and *NLRP* gene expression across bovine oocyte maturation and preimplantation embryo development

Although the focus of this research was on *PADI6*, the oocyte is a highly dynamic cell that relies on the coordinated functions of multiple genes. Specifically, *PADI6* interacts with the SCMC and possibly with epigenetic regulators to carry out its function. Therefore, in this study, the expression profiles of a number of MEGs were analysed across bovine oocyte and preimplantation development. Like *PADI6*, SCMC and *NLRP* genes demonstrated the characteristic expression pattern that is typical of a MEG. For each of these transcripts, expression was at the highest level in the oocyte and early embryo but little to no expression was detectable after EGA. For *KHDC3L,* transcript abundance doubled from GV to MII oocyte stages, although this was not significant ($p>0.05$) (Figure 3.8b). Further, *KHDC3L* expression increased further to peak around the 2-cell stage, after which it started to decline until it was barely detected after embryonic compaction (morula stage). Overall, *KHDC3L* was detected at levels that were 10-fold lower than that of *PADI6* (Figure 3.6), suggesting that it is a less prominent transcript in the oocyte.

OOEP gene expression was high in both GV and MII oocytes and no distinct changes in transcript abundance were observed during oocyte maturation ($p>0.05$) (Figure 3.8c). There was a significant decrease in *OOEP* expression post-fertilisation in the 2-cell embryo ($p<0.05$). *OOEP* was constantly expressed at higher levels than *PADI6* (Figure 3.6) in the early embryo until EGA. Little to no *OOEP* expression was observed in morula and blastocyst stages. Relatively, *TLE6* transcript abundance was lower than that of *OOEP* and comparable to that of *NLRP5* and -7 (Figure 3.9b and c). *TLE6* gene expression was also unchanged during the GV to MII transition and present throughout early embryo development ($p>0.05$). After the 16-cell stage there was a sharp decline in *TLE6* expression and transcripts were barely detected in the blastocyst stage embryo ($p<0.05$). Figure 3.10 shows that *OOEP* and *TLE6* transcripts in the blastocyst were visible on a DNA agarose gel, despite low detection in real-time PCR.

Similarly, *FIGLA* expression was highest in GV oocytes ($p<0.05$) and decreased by almost 10-fold from the GV to MII oocyte transition (Figure 3.8a). From MII to 16-cell embryo, *FIGLA* expression remained very low and no detection was observed after

EGA. Figure 3.10 shows a decline in *FIGLA* expression from GV oocyte to 8-cell embryos and complete absence of *FIGLA* detection in blastocysts.

NLRP2, -5 and *-7* exhibited very similar expression patterns across oocyte maturation and preimplantation embryo development (Figure 3.9a-c). Although there were no significant differences in *NLRP5* expression between the developmental stages, the pattern of expression was similar to that of *NLRP2* and *NLRP7*. *NLRP2, -5* and *-7* were all detected at their highest levels in GV oocytes. Likewise, they all exhibited a sharp decrease in transcript abundance from GV to MII oocyte transition ($p<0.05$ for *NLRP2* and *NLRP7*). Further, low gene expression was observed in the early embryo and little to no gene expression was detectable after EGA. Overall, *NLRP2* (Figure 3.9a) was the most abundant of the *NLRP* family members that were assessed in the GV oocyte. However, in the early embryo, all *NLRPs* were expressed at similarly low levels. The expression patterns observed across the developmental series do not reflect RNA degradation as development progresses as the quality of all samples were checked against housekeeper gene expression levels using gel electrophoresis as illustrated in Figure 3.10.

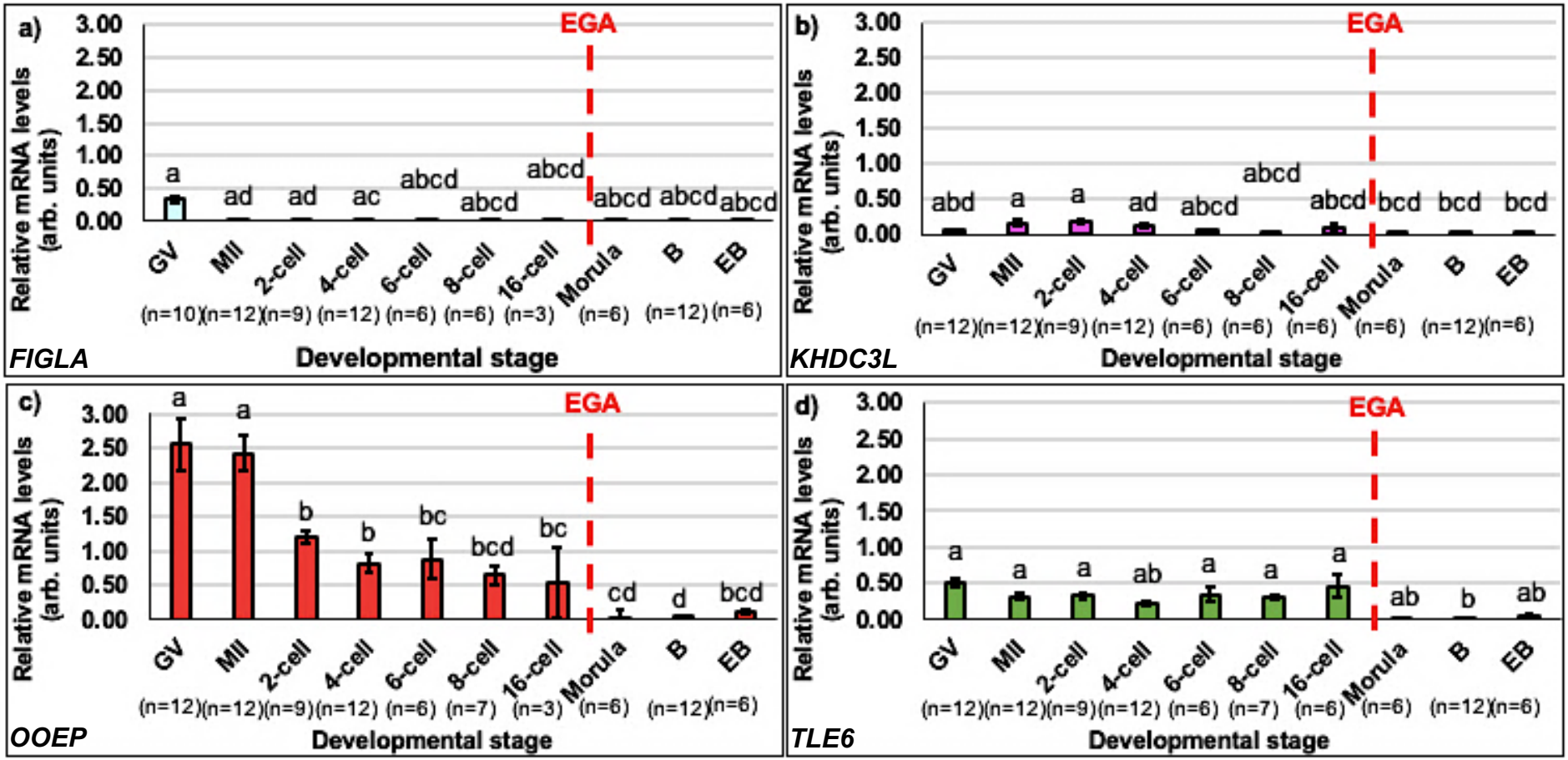

Figure 3.8 Real-time PCR quantification of **a)** *FIGLA*, **b)** *KHDC3L,* **c)** *OOEP* and **d)** *TLE6* expression across bovine oocyte maturation and preimplantation embryo development stages: GV and MII oocytes, 2-cell, 4-cell, 6-cell, 8-cell, 16-cell, morula, blastocyst (B) and expanded blastocyst (EB) embryos. Data were standardised against *GAPDH, H2A* and *YWHAZ* mRNA levels to give the relative mRNA level in arbitrary units. Individual bars show the mean ±SEM. Different letters or * denote significant differences between means or relative to other stages analysed, respectively ($p<0.05$). EGA is shown by the red dotted line.

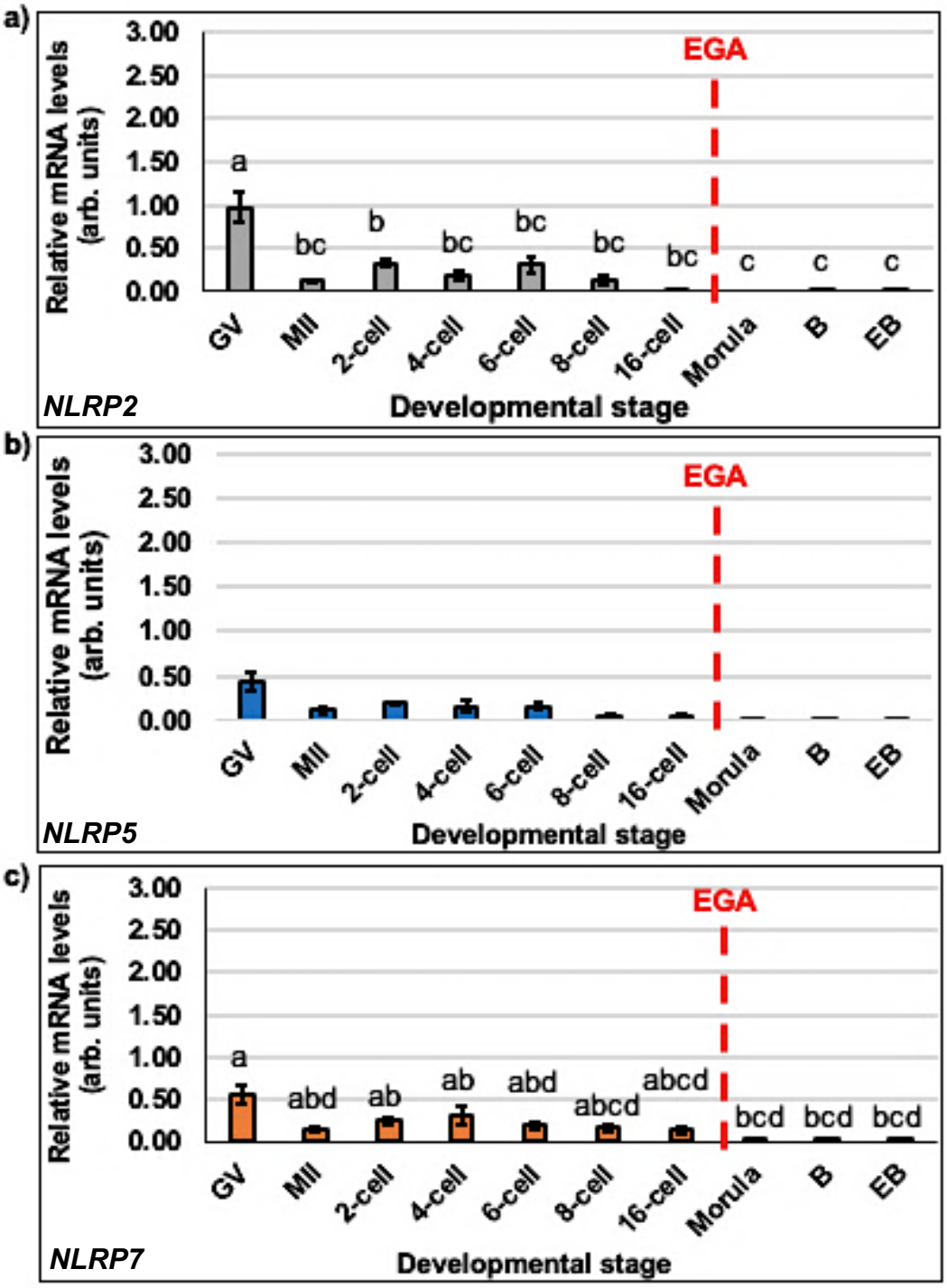

Figure 3.9 Real-time PCR quantification of **a)** *NLRP2,* b) *NLRP5* and c) *NLRP7* expression across oocyte maturation and preimplantation embryo development stages: GV (n=12) and MII (n=12) oocytes, 2-cell (n=9), 4-cell (n=12), 6-cell (n=6), 8-cell (n=6), 16-cell (n=3), morula (n=6), blastocyst (B) (n=12) and expanded blastocyst (EB) (n=12) embryos. Data were standardised against *GAPDH, H2A* and *YWHAZ* mRNA levels to give the relative mRNA level in arbitrary units. Individual bars show the mean ±SEM. Different letters or * were used denote significant differences between means or relative to other stages analysed, respectively ($p<0.05$). EGA is shown by the red dotted line.

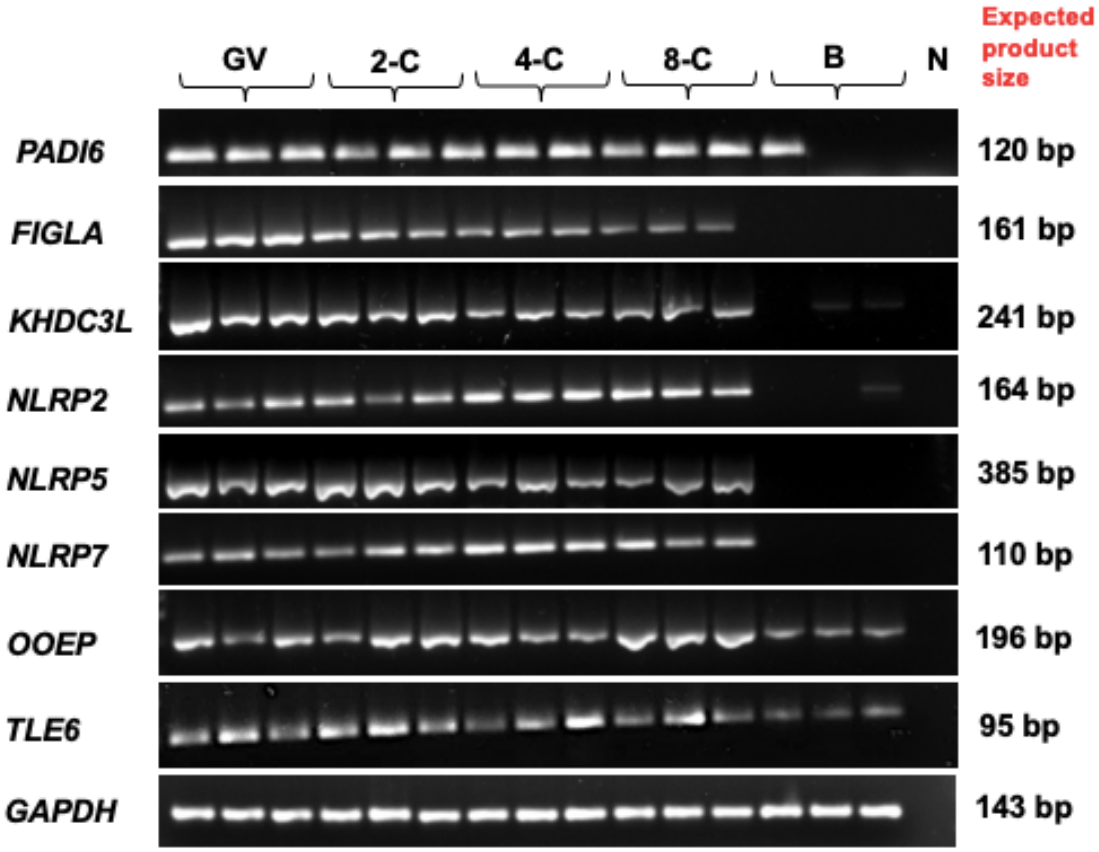

Figure 3.10 Expression of *PADI6*, *FIGLA, KHDC3L, NLRP2, NLRP5, NLRP7, OOEP* and *TLE6* in the germinal vesicle (GV) oocyte and preimplantation embryos: 2-cell, 4-cell, 8-cell and blastocyst (B) embryos after real-time PCR and DNA fragment separation by gel electrophoresis. MII, 6-cell and EB stages were omitted for convenience. Negative control (N) and expected PCR product sizes are displayed.

3.3.5 Characterisation of the expression of epigenetic regulators across bovine oocyte maturation and preimplantation embryo development

Epigenetic regulators, *DNMT1, DNMT3A, DNMT3B, DPPA3, TRIM28* and *ZFP57*, were characterised across bovine oocyte maturation and preimplantation embryo development by real-time PCR. Firstly, the expression of DNA methyltransferases was investigated. *DNMT1* was detected at low levels in the oocyte and early embryo (Figure 3.11a). There were no significant changes in expression during oocyte maturation and embryo development to the 8-cell stage. However, there was a significant decrease ($p<0.05$) in expression from the 8-cell embryo to the blastocyst embryo, coinciding with EGA. Conversely, *DNMT3A* and *DNMT3B* displayed low expression in the oocyte and early embryo and higher expression after EGA (Figure 3.11b and c). For both genes, there was a peak in expression at the onset of EGA at the 16-cell embryo stage relative to expression in the GV oocyte. This was significant for *DNMT3A* ($p<0.05$) but not significant for *DNMT3B*. After EGA, expression of *DNMT3B* significantly decreased ($p<0.05$) in the morula stage relative to the 2-cell, 6-cell and 8-cell embryo stages. On the other hand, *DNMT3A* expression increased to reach its highest level in the expanded blastocyst embryo ($p<0.05$).

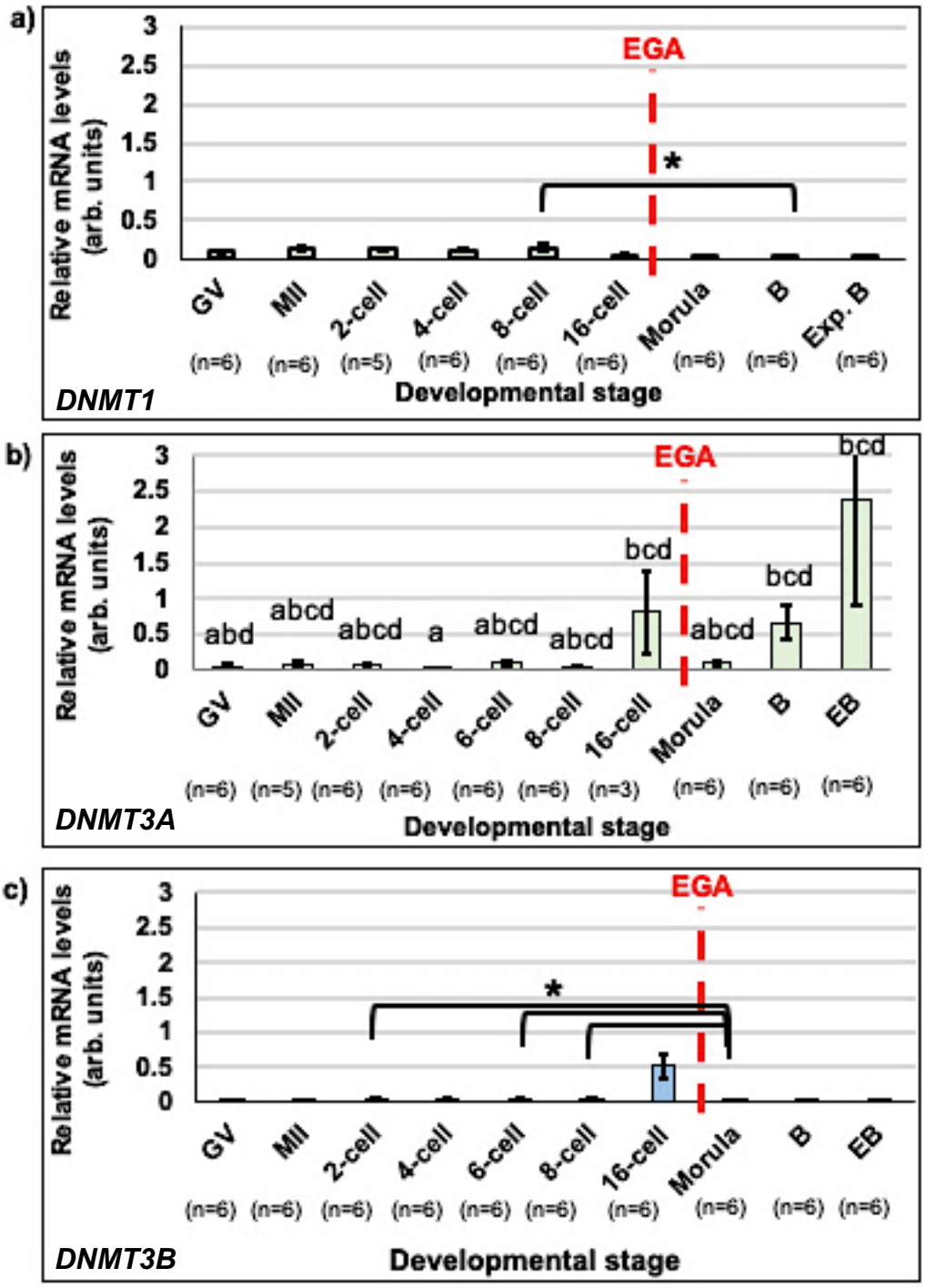

Figure 3.11 Real-time PCR quantification of **a)** *DNMT1*, **b)** *DNMT3A* and **c)** *DNMT3B* expression across oocyte maturation and preimplantation embryo development stages: GV and MII oocytes, 2-cell, 4-cell, 6-cell, 8-cell, 16-cell, morula, blastocyst (B) and expanded blastocyst (EB) embryos. Data were standardised against *GAPDH, H2A* and *YWHAZ* mRNA levels to give the relative mRNA level in arbitrary units. Individual bars show the mean ±SEM. Different letters or * were used denote significant differences between means or relative to other stages analysed, respectively ($p<0.05$). EGA is shown by the red dotted line.

Additional epigenetic regulators that are known to be important in the process of maintaining embryonic imprints, *DPPA3, TRIM28* and *ZFP57* were investigated (Figure 3.12a-c). *DPPA3* expression was very high in the oocyte and there was no change in transcript abundance during the GV to MII transition ($p>0.05$) (Figure 3.12a). From the 2-cell to 8-cell embryo stages, *DPPA3* expression slowly increased but after EGA, expression drastically declined ($p<0.05$). On the other hand, *TRIM28* was expressed in all stages of preimplantation development (Figure 3.12b). From GV to MII oocyte, there was no change in *TRIM28* expression ($p>0.05$) and expression remained consistent until the 8-cell stage. At the morula stage, *TRIM28* expression increased significantly, relative to the 8-cell stage, to its highest level in the preimplantation embryo ($p<0.05$). However, by the blastocyst stages *TRIM28* expression had returned to its previous level.

Unlike *DPPA3* and *TRIM28, ZFP57* expression was barely detected in the oocyte and early embryo, before EGA (Figure 3.12c). At the 16-cell stage, a sharp peak in *ZFP57* expression was observed but this was not significant. After EGA, *ZFP57* transcript abundance was significantly increased ($p<0.05$) in morula and blastocyst stages compared to the MII oocyte and 2-cell embryo stages. Overall, expression of *DPPA3* was very high in comparison to other MEGs analysed, with approximately 10 times more transcripts detected by real-time PCR, relative to housekeeping genes. Figure 3.13 shows a composite figure of *DNMT3A, DNMT3B, TRIM28* and *ZFP57* expression across preimplantation development to enable comparisons between genes. A distinct peak in expression of all 4 genes was observed at the 16-cell stage around the time of EGA. Furthermore, at this stage, the standard error of the mean was greater than at other stages, indicative of more variation in gene expression between embryos.

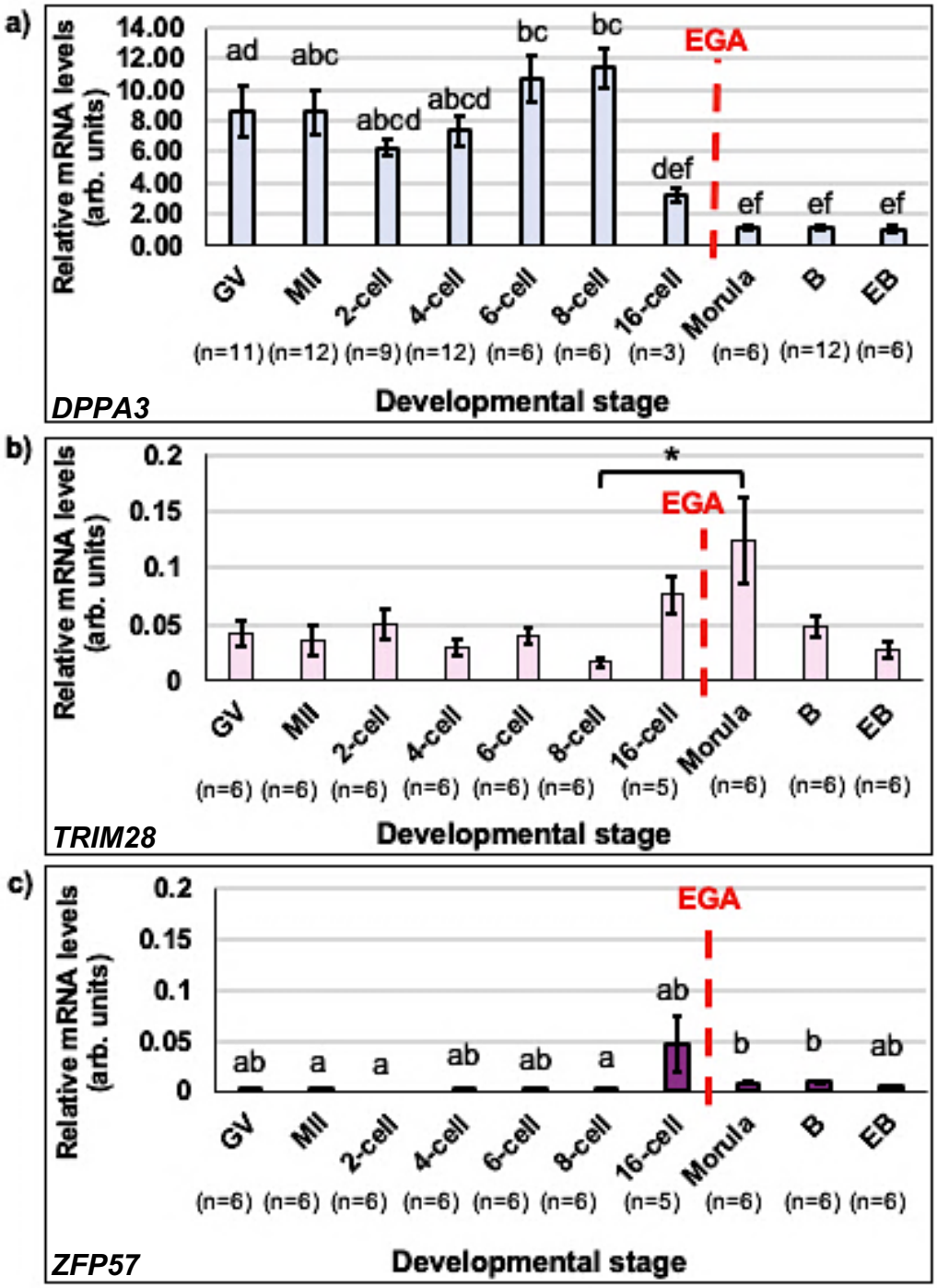

Figure 3.12 Real-time PCR quantification of **a)** *DPPA3*, **b)** *TRIM28* and **c)** *ZFP57* expression across oocyte maturation and preimplantation embryo development stages: GV and MII oocytes, 2-cell, 4-cell, 6-cell, 8-cell, 16-cell, morula, blastocyst (B) and expanded blastocyst (EB) embryos. Data were standardised against *GAPDH, H2A* and *YWHAZ* mRNA levels to give the relative mRNA level in arbitrary units. Individual bars show the mean ±SEM. Different letters or * were used denote significant differences between means or relative to other stages analysed, respectively ($p<0.05$). EGA is shown by the red dotted line. Please note the different scale for *DPPA3.*

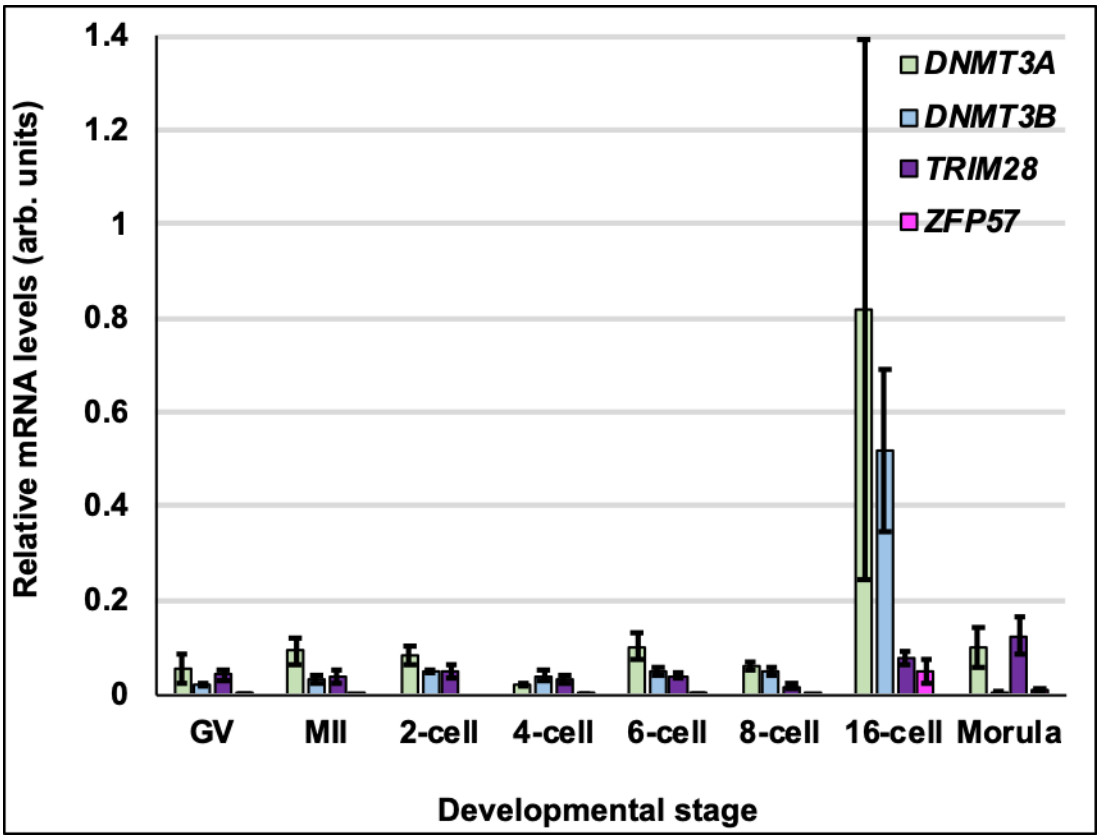

Figure 3.13 Composite figure showing expression of bovine *DNMT3A, DNMT3B, TRIM28* and *ZFP57* in GV and MII oocyte and 2-cell, 4-cell, 6-cell, 8-cell, 16-cell and morula embryo stages. Data were standardised against *GAPDH, H2A* and *YWHAZ* mRNA levels to give the relative mRNA level in arbitrary units. Individual bars show the mean ±SEM.

3.4 Discussion

3.4.1 *In vitro* production of mature bovine oocytes and embryos

Mature bovine oocytes and embryos were successfully produced *in vitro* using the culture system that was previously validated by Hemmings et al. (2012). In this thesis, the average oocyte maturation rate was comparable to that of Hemmings et al. (2012) with 83% and 85% of oocytes progressing to MII, respectively. The embryo cleavage rate that was observed here was around 10% lower than that of Hemmings et al. (2012) (69% vs 80%, respectively). This may be caused by the sperm that were used as sperm from different bulls have different capacities to fertilise the oocyte. Furthermore, Hemmings et al. (2012) used a different approach and culture medium for sperm preparation as well as a procedure for immobilising and separating presumptive zygotes. Finally, the rate of blastocyst formation (31%±0.7%) that was achieved in this thesis was similar to other studies that report bovine blastocyst rates of 26.67±1.05% (Wang et al., 2014b) and 37.9±4.9% (Cagnone et al., 2012). Bovine blastocyst rates of 20-40% have been reported in the literature (Lonergan et al., 1997; Sirard, 2018; Sirard et al., 1988; Sturmey et al., 2009) but it is worth noting that differences in oocyte maturation, IVF and culture media greatly affect development of the embryo to the blastocyst stage.

3.4.2 Bovine *PADI6* expression

Bovine *PADI6* gene expression was not detected in the majority of somatic tissues that were analysed in this study by PCR (Figure 3.5a). It is worth noting that the archived RNA samples that were used for cDNA synthesis were relatively old and might have been subjected to repeated freeze-thaw cycles which could cause RNA degradation. There was also only 1 RNA sample available for each tissue type so it is possible that a problem with the sample could preclude our findings. However, the expression of *GAPDH* indicated that cDNA synthesis was successful, and that the integrity of the RNA was satisfactory in all samples, except the kidney sample where the PCR product for *GAPDH* was slightly smaller. *PADI6* was strongly detected in the bovine GV oocyte, suggesting that bovine *PADI6* expression is restricted to the oocyte and preimplantation embryo before EGA. This is concordant with other studies that have shown that *Padi6* is primarily expressed in the oocyte (Chavanas et al., 2004; Zhang et al., 2004). Likewise, *PADI6* was absent from the corpus luteum

formed from remodelling of the somatic follicle granulosa and theca cells following ovulation, which would be expected if *PADI6* is oocyte and embryo specific as this tissue defines the post-ovulatory state. Furthermore, *PADI6* expression was observed at low levels in the OC. This tissue is likely to contain some very early stage follicles, such as primordial and primary follicles, which would account for the positive result (Newton, 1998). Indeed, studies have detected *Padi6* expression as early as the primordial follicle stage in mice which may therefore explain the detection of *PADI6* expression in this tissue sample (Wright et al., 2003). The absence of *PADI6* expression from the bovine ovary library could be due to a lack of oocytes in the ovarian sections that were taken or due to major dilution of oocyte RNA species such as *PADI6* transcripts relative to more prominently expressed genes in the ovary.

3.4.3 Tissue-specific gene expression patterns of other *PADI* family members in the bovine

It has been well documented that *Padi* family members display distinct tissue-specific expression patterns (Mechin et al., 2007). In light of this, bovine somatic tissues were explored for expression of *PADI1-4* (Figure 3.5b). Bovine *PADI1* was barely detected in the samples tested. This may be expected as *PADI1* is thought to be expressed in the epidermis, prostate, testis, placenta, spleen and thymus, none of which were included in the somatic cell series tested here (Chavanas et al., 2004). *PADI2* is known to be ubiquitously expressed in a variety of tissues. Here, it appeared to be strongly expressed in bovine lung and brain tissues and moderately expressed in liver tissues. The observed localisation of *PADI2* in the brain supports its known pathogenic role in multiple sclerosis and Alzheimer disease (Ishigami and Maruyama, 2010; Musse et al., 2008). Low expression was detected in bovine muscle samples, but no expression was observed in the reproductive tissues or GV oocyte. Bovine *PADI3* displayed faint expression in most of the somatic tissues that were analysed except the OC. However, low expression was detected in the GV oocyte. Finally, bovine *PADI4* was highly expressed in the liver and some detection was observed in the heart. *Padi4* is thought to be primarily expressed in immune cells such as neutrophils (Li et al., 2010b). Neutrophils originate from haemopoietic stem cells in the bone marrow, travel around the body in the blood stream and play a role in the innate inflammatory response (Borregaard, 2010). They are known to accumulate in the liver upon inflammation or injury, possibly explaining the presence of *PADI4* in the bovine liver tissue (Freitas-Lopes et al., 2017). Likewise, *PADI4* expression in the

bovine heart may be a result of neutrophil accumulation in response to ischemic injury (Mehta et al., 1989). Like *PADI3*, low expression of *PADI4* was detected in the GV oocyte. This suggests that there may be some expression of other *PADI* family members in the oocyte, albeit at lower levels than *PADI6*. Research in mice has identified expression of PADI1-4 proteins throughout oocyte maturation and preimplantation development and suggest that PADI1 citrullines histones in the embryo (Zhang et al., 2016). Similarly, PADI4 has been detected in oocytes and embryos of both mice and pigs (Brahmajosyula and Miyake, 2013). RNA-seq analysis (Chapter 5) may elucidate more about the expression of other *PADI* family members in the bovine oocyte and preimplantation embryo.

Although there was negative expression of many of the *PADI* family members in bovine somatic tissues, the results are not definitive. There is the possibility that the chosen primers do not effectively bind and amplify the transcripts, thereby giving a negative or reduced gene expression result. In order to circumvent this issue, many primers need to be tested under different melting temperatures (Tm) to find the most effective pair for amplification. Furthermore, the effectiveness of primer design depends on the integrity of the inputted cDNA sequence and understanding of splice variants. There may be characteristics of target transcripts that are not yet known which preclude their amplification. Conversely, primers could preferentially bind to off-target genes, leading to amplification of the wrong product. For example, the smears observed in *PADI4* lung and uterus samples (Figure 3.5b) could be due to non-specific primer binding leading to multiple PCR products. Finally, protein studies are necessary to investigate the presence of PADI proteins in GV and MII oocytes and the ovary.

3.4.4 Bovine *PADI6,* SCMC and *NLRP* gene expression patterns

The GV oocyte is known to be transcriptionally active and to accumulate mRNA in preparation for oocyte maturation and early embryo development (Fair et al., 1995). At GVBD in mouse, the oocyte nucleus changes from a decondensed state (non-surrounded nucleolus) to a condensed state (surrounded nucleolus) and transcriptional quiescence ensues until EGA (Mattson and Albertini, 1990) (Liu and Aoki, 2002). This is also observed in humans, and similarly, in bovine during transition from GV0 to GV3 chromatin configurations (Luciano and Sirard, 2018b). MEGs are characteristically present at high levels in the oocyte, with expression reduced to moderate levels in the early embryo and degraded after EGA in mouse (Li et al., 2010a). Mapping of *PADI6,* SCMC and *NLRP* genes across bovine oocyte maturation and preimplantation embryo development confirmed that these are maternally-derived genes (Sections 3.3.3 and 3.3.4). *PADI6*, *FIGLA*, *OOEP, TLE6, NLRP2, -5* and *-7* were mostly highly expressed in GV oocytes and were not transcribed again after EGA. Similarly, *KHDC3L* expression was highest in MII oocytes and 2-cell embryo, but was not present after EGA, supporting its maternal origin.

Many of the MEGs analysed here displayed a sharp decrease in relative transcript abundance from GV to MII oocyte transition (Figure 3.6, Figure 3.8 and Figure 3.9). This observation is a recognised phenomenon. In the cow, almost 2000 transcripts have been shown to decrease in abundance from GV to MII stages, compared to 500 transcripts that increase in this time frame (Reyes et al., 2015). In agreement with the present study, Reyes et al. (2015) also observed a reduction in transcript abundance of *NLRP5* during this transition. One explanation for the decrease in transcripts in MII oocytes could be the translation of mRNAs to proteins in order to facilitate the intracellular signalling required to support meiotic maturation (Kim et al., 2011). Another possibility is the degradation of maternal transcripts, although this mainly appears to be true for transcripts that facilitate oocyte maturation, for example, during the GV to MII oocyte transition in mice, there is dramatic degradation of transcripts that are involved in the production of ATP by oxidative phosphorylation (Paynton et al., 1988; Su et al., 2007). It is suggested that the degradation of such transcripts correlates to the decrease in ATP consumption that was required to maintain meiotic arrest at the GV stage (Su et al., 2007). Further, it is also likely explained by deadenylation of transcripts for storage. Both Reyes and the current study used oligo-dT primers to obtain only translationally active mRNA, classified as mRNA with a

polyA tail length of 18 adenines or more. Therefore, the loss of transcript abundance that was observed here may demonstrate mRNA deadenylation and/or our inability to detect transcripts of short polyA tail length using this method. Through the use of random-hexamer priming, Reyes et al. (2015) showed that for most genes transcript abundance did not change in GV to MII oocytes therefore the principal explanation for this change must be transcript deadenylation. It is worth noting that cDNA synthesis using oligo-dT priming may also preclude the detection of active transcripts with short polyA tails, resulting in incomplete cDNA libraries. Unlike other MEGs, *KHDC3L* transcript abundance increased from GV to MII (Figure 3.8b). *KHDC3L* mRNA may be either polyadenylated during the meiotic transition, which would give the appearance of increased expression, or *KHDC3L* may be continually transcribed, although the latter is unlikely given the changes in chromatin state that occur during meiotic progression.

In the early embryo, *PADI6* and the *NLRP* family transcript abundance appeared to increase slightly from MII to 2-cell stage (Figure 3.6 and Figure 3.9), perhaps reflective of mRNA polyadenylation and the necessity for translationally active transcripts for embryo development. *KHDC3L* and *TLE6* transcript abundance were unchanged and *OOEP* expression decreased significantly ($p<0.05$) in the 2-cell embryo (Figure 3.8). Generally, from the 2-4 cell stage, transcript abundance slowly decreased until it was no longer detectable in morula or blastocyst stages. Decreased transcript abundance is likely to be indicative of translation and protein synthesis of maternal mRNAs. Supporting research in sheep showed that protein synthesis was high during the first few embryonic cleavage divisions but decreased at EGA. Further, protein synthesis was not inhibited by α-amanitin showing that proteins were coded for by maternal transcripts (Crosby et al., 1988). Expression of *OOEP* and *TLE6* was observed at the blastocyst stage on the gel electrophoresis (Figure 3.10) despite little to no expression observed by real-time PCR (Figure 3.7). This can be explained as the gene expression on the gel electrophoresis was not normalised to housekeeping genes as in the real-time PCR analysis.

For all of the MEGs analysed here, gene expression was barely detected after the 8-16 cell stage – the time of EGA in the bovine. This data strongly suggests that there is no zygotic expression of such genes and that there is depletion of maternal-effect transcripts. It is well understood that maternal mRNA degradation is necessary for EGA and inhibition of this precludes embryo development (Schier, 2007). Despite

degradation of the mRNA, it is possible that the protein persists in the embryo until blastocyst stages. This has been confirmed for NLRP5, NLRP7 and OOEP proteins in human blastocysts (Poli et al., 2015). Interestingly, the PCR data for human *PADI6* reflects that of bovine *PADI6* expression (Figure 3.7). Analysis of human *PADI6* was included to investigate the differences in *PADI6* expression between species. Human *PADI6* could not be detected in the primordial follicle sample; however, considering the unusually low *GAPDH* expression for this sample, the result is inconclusive, not least as the sample was old, depleted and had been subject to repeated freeze-thawing. Nevertheless, like in bovine, *PADI6* expression in human GV and MII oocytes was high. Expression was retained in the early cleavage embryo (4-cell) and in the morula whereas bovine *PADI6* is not detected after the 8-16 cell stage. This highlights a potential discrepancy between human and bovine *PADI6* expression, suggesting a delayed or accelerated mechanism of maternal mRNA degradation in humans and bovine, respectively. Finally, *PADI6* expression was not detected in blastocyst stage embryos in either human or bovine.

In terms of overall abundance in the oocyte, it appears that *OOEP* is a highly expressed maternal gene (Figure 3.8c). This result is supported by published studies in mice that showed high levels of *Ooep* mRNA expression in primary to antral follicles (Tashiro et al., 2010). *NLRP2* and *PADI6* seem to be moderately expressed relative to *OOEP* whereas *KHDC3L, NLRP5, NLRP7* and *TLE6* appear to be weakly expressed relative to *OOEP*. It may be that transcript abundance of genes like *NLRP5* is higher in early stage follicles and NLRP5 protein is more prominent in the GV oocyte (Tong et al., 2004). Likewise, FIGLA is a principal activator of oocyte genes and genetic ablation of *Figla* in mice inhibits primordial follicle formation, therefore expression of *Figla* mRNA is also likely to be observed earlier in folliculogenesis (Huntriss et al., 2002; Joshi et al., 2007; Soyal et al., 2000). Investigation of MEG protein expression would provide a more comprehensive understanding of the changes in transcript abundance that are observed during oocyte maturation and preimplantation development. Altogether, this data confirms that *PADI6*, SCMC and the *NLRPs* are maternally-derived transcripts with specific roles in the oocyte and early embryo, prior to EGA, after this developmental milestone they are no longer required for embryonic development and destroyed.

3.4.5 Epigenetic regulator expression patterns across bovine preimplantation development

As the role of the SCMC in imprinting remains to be demonstrated, the expression of a number of genes or key epigenetic regulators was investigated across bovine preimplantation development. The importance of the *DNMTs* has been proven across different species by multiple studies that showed their genetic ablation caused embryonic defects or lethality (Hirasawa et al., 2008; Huan et al., 2015; Uysal et al., 2015; Wei et al., 2011; Yamanaka et al., 2011). In this study, *DNMT1* was expressed at relatively low levels in the oocyte and preimplantation embryo prior to EGA (Figure 3.11a). DNMT1 is critical for imprinting maintenance. After fertilisation, the maternal and paternal pronuclei are exposed to reprogramming factors to alter the chromatin state to totipotency (Tsukamoto and Tatsumi, 2018). To avoid reprogramming of parental imprints, specific epigenetic mechanisms involving DNMT1, as well as DPPA3, TRIM28 and ZFP57, protect imprinted loci (Zhang and Smith, 2015). There are 2 forms of *Dnmt1* in mouse oocytes: oocyte-specific *Dnmt1o* and somatic *Dnmt1s* (Howell et al., 2001). It has been observed in mice that most of the DNMT1 protein present in the preimplantation embryo is of maternal origin (Hirasawa et al., 2008). In support of this, it is likely that the low expression of *DNMT1* detected throughout bovine preimplantation development reflects translation of the mRNA to protein to protect maternal imprints from demethylation. Furthermore, *Dnmt1s* is thought to function in methylation maintenance after transcription from the zygotic genome (Hirasawa et al., 2008). EGA occurs around the 8-16-cell stage in bovine. This could explain the significant reduction in *DNMT1* transcript from 8-cell to blastocyst embryo stage in this study.

Despite the understanding that DNMT3A is responsible for establishing maternal imprints in the oocyte, bovine *DNMT3A* mRNA was detected at low levels prior to EGA (Figure 3.11b) (Kaneda et al., 2004). It is possible that maternal *DNMT3A* mRNA was translated into protein earlier in folliculogenesis so leading to the observed lowering of transcript levels. In support of this idea, high DNMT3A protein expression has been observed across preimplantation development in the mouse (Uysal et al., 2017). Furthermore, expression of *DNMT3A* in blastocyst stages in this study suggests that *DNMT3A* was transcribed from the zygotic genome after EGA for establishment of methylation in the embryo. *DNMT3B* was expressed at low levels throughout preimplantation development but a sharp increase was observed at the

16-cell stage only (Figure 3.11c). In cattle, this is the time of EGA. It is known that EGA requires changes to the chromatin state to allow zygotic transcription, followed by chromatin condensation to regulate gene expression (Latham and Schultz, 2001). It may be that *DNMT3B* is highly transcribed in preparation for establishment of zygotic methylation marks. Furthermore, Golding and Westhusin (2003) studied the expression of *DNMT1, -3A and -3B* across bovine preimplantation development by RT-PCR and concluded that all *DNMTs* were expressed from the 2-cell embryo to blastocyst stages.

DPPA3, TRIM28 and *ZFP57* are also recognised as key epigenetic regulators in preimplantation embryo development, since loss of any of these genes is detrimental to the embryo (Cammas et al., 2000; Payer et al., 2003; Zuo et al., 2012). Like *DNMT1*, these genes are essential in maintaining imprinted loci during preimplantation development (Marlow, 2010). From GV oocytes to 16-cell embryos, bovine *DPPA3* expression was consistently high (Figure 3.12a). This is anticipated as DPPA3 is known to protect maternal imprints from TET3-mediated oxidation in the preimplantation embryo (Nakamura et al., 2007). The observed decrease in *DPPA3* transcript abundance after EGA (16-cell stage) is consistent with that of a maternally-derived mRNA but it is probable that DPPA3 protein remains until the blastocyst stage, as observed in mice (Payer et al., 2003). The same results were observed by (Bakhtari and Ross, 2014). *TRIM28* was expressed throughout bovine preimplantation development with highest expression displayed at the morula stage (Figure 3.12b). This observation may be expected as TRIM28 is responsible for recruiting methylation maintenance enzymes to imprinted regions in the preimplantation embryo (Alexander et al., 2015). The increase in expression at the morula stage might represent zygotic transcription of *TRIM28* for continual methylation maintenance after EGA. In agreement, zygotic *Trim28* has been recognised post-EGA in the 4-cell mouse embryo and is required for sustaining imprints in the preimplantation embryo (Alexander et al., 2015; Messerschmidt et al., 2012). Finally, bovine *ZFP57* expression was only detected after EGA at the 16-cell stage in this study (Figure 3.12c). It is documented that both maternal and zygotic *Zfp57* are required to maintain imprints during preimplantation development in the mouse (Li et al., 2008c). It could be that the maternal transcripts of *ZFP57* have been translated into protein and a switch to zygotic control is being observed here. In this study, *DNMT3A, DNMT3B, TRIM28* and *ZFP57* increase in transcript abundance at the 16-cell stage (Figure 3.13). In bovine, EGA occurs around the 8-16 cell stage. It is known that TRIM28 and ZFP57 recruit DNMTs to imprinted loci to maintain DNA

methylation (Figure 3.14) (Zuo et al., 2012). At EGA, dynamic changes in chromatin structure allow transcription from the zygotic genome (Bogliotti and Ross, 2015). It is therefore hypothesised that *DNMT3A, DNMT3B, TRIM28* and *ZFP57* are upregulated around the time of EGA to protect parental imprints from being lost.

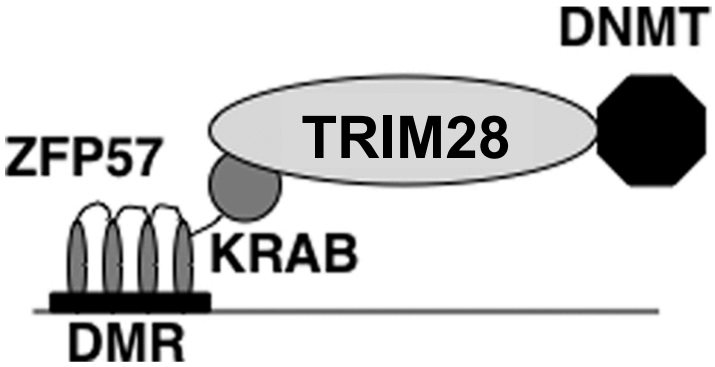

Figure 3.14 Hypothetical model for recruitment of DNMTs to the DMR of imprinted loci by ZFP57 and TRIM28. Figure from Zuo et al. (2012).

Hamatani et al. (2004) analysed global gene expression changes throughout mouse preimplantation development and evidently described some of the genes that were investigated here. In their study (Hamatani et al., 2004), *Zfp57* was identified as transcribed from the zygotic genome. Likewise, *Dppa3* was recognised as an early zygotic gene with peak expression around the time of EGA in the mouse. For *Dnmt1* and *Dnmt3b* genes, their data showed degradation of maternal transcripts followed by zygotic transcription. Finally, *Mater/NLRP5* was identified as an abundant oocyte transcript that was degraded during preimplantation development. This global analysis by Hamatani et al. (2004) confirms many of the expression profiles observed in this study and verifies the importance of the genes that were analysed.

Reflecting on the real-time PCR results, there were some ‘0’ data points that had to be accounted for in the statistical analysis. For the most part, results of ‘0’ were considered undetectable levels of PCR product, therefore little to no expression of the transcript. Although this is likely to be true because cDNA libraries were verified using housekeeping genes, it could be that the primers for the genes of interest were not efficient in amplifying the gene product (Green et al., 2015). Furthermore, some genes such as *ZFP57* were detected at low levels in the oocyte and throughout preimplantation development. This may not be a true result but could be caused by inefficient primer binding and amplification which affects the perceived abundance of transcripts. To further characterise the expression of MEGs in the bovine oocyte and

embryo, it is necessary to look at the protein expression level by western blotting. This would provide information on the abundance of MEGs throughout preimplantation development and the relationship between transcript and protein levels.

3.4.6 Conclusion

This work has for the first time mapped the expression pattern of *PADI6* in bovine oocyte and preimplantation embryo development and confirmed the oocyte-restricted expression of *PADI6* by analysing 11 bovine somatic tissue cDNA libraries. It has also interrogated the tissue distribution of other *PADI* genes in the bovine, which aligns with previously published data on *PADI1-4* expression patterns and suggests that *PADI6* is the predominant *PADI* gene in the bovine oocyte. Finally, the expression profiles of important MEGs have also been mapped across bovine preimplantation development to indicate that the 16-cell stage is likely to be a key phase in bovine preimplantation embryo development with respect to imprinting maintenance/regulation. The data reported here provides a reference for the expression patterns of key transcripts following *PADI6* KD experiments which will be explored in the later chapters of this thesis. With the majority of research into *Padi6* and the SCMC established in mice, the current experimental work documents the initiation of *PADI6* investigations in an animal model than is more physiologically relevant to human oocyte and preimplantation embryo development.

Chapter 4 Validation of *PADI6* gene knockdown by microinjection of siRNA species into bovine GV oocytes undergoing IVM

4.1 Introduction

The importance of the SCMC is highlighted by its role in female infertility and imprinting disorders. *NLRP7* and *KHDC3L* are causative genes in FBHM while *TLE6* mutations cause the earliest human embryo lethality that has been recorded (Alazami et al., 2015; Murdoch et al., 2006; Parry et al., 2011). In addition, a number of different *PADI6* mutations have recently been identified in females experiencing infertility (Maddirevula et al., 2017; Qian et al., 2018; Wang et al., 2018a; Xu et al., 2016; Zheng et al., 2019). Similarly, *Padi6*-null mice cannot bear offspring as their embryos arrest around the time of EGA (Esposito et al., 2007). The significance of *PADI6* has been recognised for some time. First linked to the SCMC in 2008, interest in *Padi6* stemmed from its potentially multi-faceted functionality and its unique oocyte-restricted expression pattern (Li et al., 2008a). Moreover, *Padi6* bridged the gap between the SCMC and CPLs, revealing a new possible function for these supra-molecular structures (Kim et al., 2010; Tashiro et al., 2010; Wright et al., 2003).

Expressed downstream of master oocyte regulators *Figla* and *Nobox, Padi6* is evidently crucial in the oocyte but its function remains enigmatic (Choi et al., 2010; Joshi et al., 2007). Firstly, *PADI6* is part of a family of enzymes that can post-translationally modify proteins by citrullination (Vossenaar et al., 2003). Although its enzymatic activity is under debate, it can potentially alter protein function and interactions by changing the secondary structure of target substrates (Raijmakers et al., 2007). The understanding that histones are substrates for citrullination may explain the role of the SCMC in imprinting disorders. Secondly, *Padi6* is necessary for the formation of CPLs in the oocyte and early embryo (Esposito et al., 2007). CPLs have been implicated in regulating protein synthesis by storing ribosomes and maternal transcripts (Bachvarova et al., 1981; Sternlicht and Schultz, 1981). Moreover, CPLs and PADI6 co-localise with MSY2 – a protein that protects maternal transcripts from degradation (Liu et al., 2017). It is worth noting that keratin is thought to be both a component of CPLs and is therefore a proposed substrate of *Padi6* (Snow

et al., 2008). Overall, *Padi6* may coordinate factors in the oocyte via CPLs in preparation for early embryo development.

For the most part, the functions of novel genes can be determined by observing the consequences of their genetic ablation. This is generally achieved by gene knockout in mice which involves creating chimeras and crossing heterozygotes for the knockout to produce a homozygous knockout (Hall et al., 2009). This is a slow and laborious process that often results in lethality and/or off target effects which masks any effects of gene knockdown (KD). Furthermore, this strategy is not suitable as a means to generate gene knockouts in larger mammals as their life span and gestation periods are too long. In 1997, Fire and colleagues discovered that dsRNA could effectively and specifically disrupt endogenous target mRNA in *C. elegans,* thereby inhibiting gene expression (Fire et al., 1998). A few years later, the finding was replicated in mouse embryos, showing it to be an effective method for gene silencing in mammals (Wianny and Zernicka-Goetz, 2000). RNA interference (RNAi) describes the post-transcriptional, sequence-specific degradation of mRNA through the use of RNA molecules. Its mechanism of action relies on a number of key proteins. Figure 4.1 shows the RNAi pathway that occurs upon the introduction of dsRNA into a cell. Firstly, dsRNA is processed by ribonuclease III, Dicer, into 21-23 nucleotide long fragments with a 2-nucleotide 3' overhang, known as double-stranded short-interfering RNAs (dsiRNA) (Bernstein et al., 2001; Vermeulen et al., 2005; Zamore et al., 2000). The siRNA strand with a less stable 5', known as the guide strand, is integrated into the RNA-induced silencing complex (RISC) while the other strand, the passenger strand, is degraded (Siomi and Siomi, 2009). The guide strand targets the RISC to the homologous mRNA where RISC-member and endonuclease, Argonaute (AGO2), cleaves the mRNA (Hammond et al., 2000). The cleaved mRNA is focussed into cytoplasmic processing bodies (P-bodies), which contain enzymes involved in mRNA turnover and degradation (Sen and Blau, 2005).

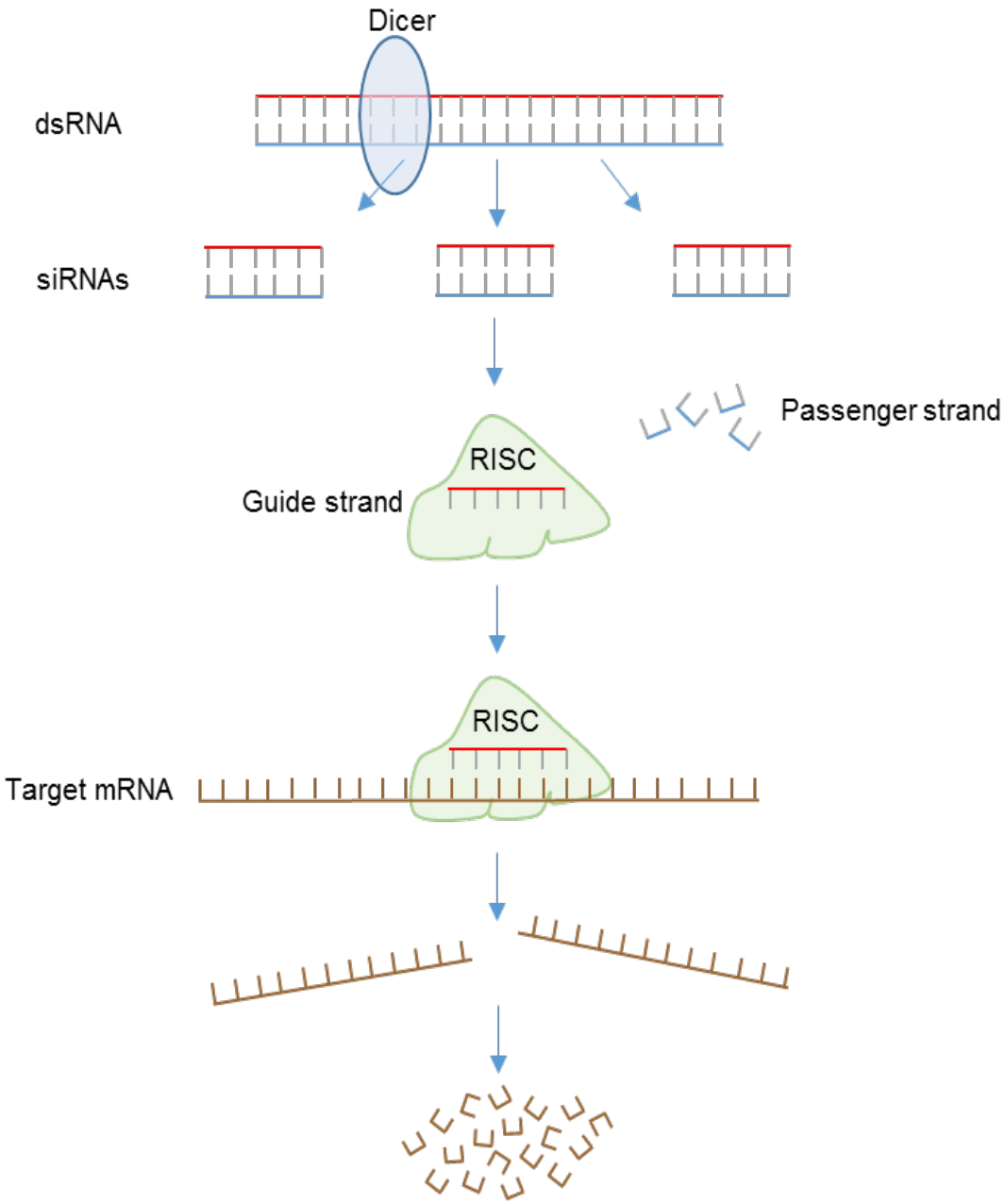

Figure 4.1 The RNAi pathway upon the introduction of dsRNA into a cell. Dicer cleaves the dsRNA into dsiRNAs. The guide strand is incorporated into the RISC complex and targeted to the endogenous mRNA. AGO2 of the RISC cleaves the mRNA at the target site and the mRNA is degraded by additional exonucleases in P bodies.

It is now understood that RNAi evolved for fulfilling various biological functions. First discovered in plants, RNAi was established as a defence mechanism against viral infection (Baulcombe, 1996). Many plant viruses have an RNA genome which is replicated through a dsRNA intermediate (Roth et al., 2004). The RNAi pathway recognises dsRNA and viral replication is halted. Interestingly, RNAi has the ability to spread within the plant, from the initial site of viral infection to neighbouring cells, via the mobile silencing signal, thereby preventing a systemic viral infection from occurring (Mlotshwa et al., 2002; Palauqui et al., 1997). Plant viruses have evolved to inhibit almost every stage of RNAi pathway through the expression of proteins known as viral suppressors of RNAi (VSRs) (Roth et al., 2004). The RNAi immune response is also apparent in *Drosophilia* and *C. elegans* but its role in mammals is debated (Sagan and Sarnow, 2013; Wang et al., 2006; Wilkins et al., 2005).

RNAi may play a role in suppressing mobile elements and transposons within the genome of plants and *C. elegans*. It is proposed that both strands of DNA in a transposable region can be transcribed to produce dsRNA (Plasterk, 2002). This triggers the RNAi pathway to destroy dsRNA and such regions are prevented from moving within the genome. To support this, loss of function mutations in genes involved in RNAi are positively correlated with an increase in active transposable elements in *C. elegans* (Ketting et al., 1999). Furthermore, an RNAi-like mechanism was recognised in eukaryotes that plays a critical role in regulating protein synthesis (Lee et al., 1993). Similar to siRNAs, short endogenous RNAs, named miRNAs (miRNAs), bind homologous mRNA and trigger its degradation or prevent translation to proteins (Carrington and Ambros, 2003). miRNAs are now known to be very important in development (Section 1.3.3.4) and contribute to various disease states, such as cancer (Ardekani and Naeini, 2010).

RNAi is widely used as a tool in research to KD a gene of interest. dsiRNA is chemically synthesised and introduced into a cell where it triggers RNAi and causes degradation of the endogenous mRNA sequences (Elbashir et al., 2001a). RNAi was first used in mouse germinal vesicle (GV) oocytes and embryos to KD maternal mRNAs, *Mos,* and *Plat,* and zygotically expressed, *E-cadherin* (Svoboda et al., 2000; Wianny and Zernicka-Goetz, 2000). Both studies showed that RNAi was specific to the gene of interest, was time- and concentration-dependent and resulted in the same phenotype as a complete gene knockout, thereby establishing it as a suitable technique for exploration of novel gene function in mammals. Since then, RNAi has been widely used for functional gene analysis in different species across

development. With prior knowledge that *Padi6* knockout results in embryonic lethality in mice, RNAi-mediated gene KD was deemed a more suitable choice for this strategic and directed genetic manipulation. Furthermore, bovine oocytes and embryos were used as a model for studying gene function in human oocytes and preimplantation development as the bovine is more physiologically relevant to human than mouse (Adams and Pierson, 1995; Bettegowda et al., 2008; Menezo and Herubel, 2002). KD of *PADI6* using targeted dsRNAi may help to elucidate its roles in oocyte maturation, fertility and preimplantation embryo development, and so shed light on the mechanisms by which it functions in monovulatory species.

4.1.1 Aims and objectives

The aim of this chapter was to identify effective dsiRNAs, develop microinjection methods and expertise therein to bring about effective KD of transcripts of the *PADI6* gene in bovine GV oocytes to determine the function of this gene in the mammalian oocyte. The chosen method for administering dsiRNA into individual oocytes was microinjection. The methodology used was based on the microinjection technique that was previously validated by Cotterill (2008), however cumulus-enclosed GV oocytes were microinjected instead of denuding GV oocytes prior to injection. This strategy improved oocyte health, reduced the oocyte culture time from 2 days to 1 day and removed the need for co-culture of injected oocytes with oocytectomised cumulus cells. The process of dsiRNA injection into bovine COCs have previously been validated in our laboratory by Berenyi (2019). The efficacy of *PADI6* gene KD was determined by real-time PCR following 24 hours of maturation in serum-free IVM medium. Concurrently, data were collected on oocyte viability, meiotic maturation and morphology to study the effects of KD on:

1. Oocyte meiotic progression
2. Cumulus mucification and expansion

Finally, expression of the *PADI1-4* genes was evaluated by real-time PCR to see if *PADI6* dsiRNAs were also capable of targeting KD of other *PADI* gene family members.

4.2 Materials and methods

This experimental system used the serum-free IVM system that was previously developed for bovine oocytes by Hemmings et al. (2012). Tissue was obtained from the abattoir and COCs were harvested as described in Section 2.1. Media was prepared the day before use and culture dishes were prepared a minimum of 3 hours before use and allowed to equilibrate at 39°C under appropriate incubation conditions. Oocyte recovery and micromanipulation was conducted on a microscope fitted with heated stage at 39°C. Only COCs with an intact cytoplasm and more than 3 layers of cumulus cells were selected for microinjection. The micromanipulation system consisted of a Nikon Eclipse Ti inverted microscope (Nikon Instruments, Amstelveen, Netherlands) fitted with a heated stage at 39°C, Integra3 micromanipulator system (Research Instruments Ltd, Cornwall, UK), a Watec WAT-221S camera (Camtronics BV, Eindhoven, Netherlands) and FemtoJet® Microinjector (Eppendorf Ltd, Stevenage, UK).

4.2.1 Experiment 1: Validation of microinjection methodology

Before starting, it was important to consider the best parameters for injection of bovine GV oocytes using the FemtoJet® microinjector system. The objective was to introduce a small but effective volume of dsiRNA without damaging or killing the oocyte. The variable parameters included injection time (Pt), injection pressure (Pi) and compensation pressure (Pc). Compensation pressure ensured that liquid is not lost from the injection pipette into the medium and that medium was not drawn up into the injection pipette from the dish. It was altered by the viscosity and surface tension of the injecting liquid. The optimal compensation pressure allowed small volumes of liquid to flow out of the injection pipette when injection pressure was applied. Injection pressure and time determined the volume of liquid that was administered to the oocyte with each injection. For Femtotip II injection pipettes (930000043, Eppendorf), injection pressures of 50 to 500 hPa for 0.3 to 1.5 sec was recommended by the FemtoJet® operating manual. If the injection pressure was too high or the injection time was too long, it would cause the oocyte to burst. On the other hand, if the injection pressure was too low, liquid would not be forced out of the injection pipette. To this end, COCs were transferred to a 50 mm intracytoplasmic sperm injection (ICSI) dish (353655, Falcon®, UK) containing 20 µl drops of H199+ media under mineral oil. These dishes facilitate microinjection as they have lowered sides which

allows movement of the injection and holding pipette. ICSI-Plus™ Holding 25° pipettes were adjusted to an angle of 25° to hold oocytes in place during injection (7-71-IH 25/20, Research Instruments Ltd). 10 µl of 50 µg/ml neutral red (NR) dye was backloaded using microloader tips (5242956003, Eppendorf) into the Femtotip II injection pipette and adjusted to an angle of 25°. Following adjustment of the tips so the pipettes were at the same level as the injection plate, the pipettes were lowered into the plate. The magnification of the microscope was then increased from low power (40X) to high power magnification (200X) to obtain better visualisation of the oocyte, alignment of the pipettes to the same plane and optimal control of the injection process. Firstly, to determine the correct compensation pressure, the Femtotip II injection pipette containing NR dye was put into a 20 µl drop of H199+ media that did not contain oocytes. Starting with a high compensation pressure, the pressure was gradually decreased until there was no leaking of NR dye out of the injection pipette (Pc = 10 hPa). Next, to determine the injection parameters, the injection pipette was moved into a 20 µl drop of H199+ media that contained 10 oocytes. An injection pressure of 400 hPa for 1 second was chosen as a starting point. Individual oocytes were held by the holding pipette by applying negative pressure by turning the air syringe system. The correct pressure was applied when the oocyte was attached to the holding pipette without distorting the oocyte. Care was taken not to apply too much negative pressure to the oocyte so as not to damage the oocyte. The initial parameters that were chosen caused the oocyte to swell or burst. The parameters were gradually decreased until only a small displacement of cytoplasm could be observed (Pi = 100 hPa; Pt = 0.1s). The exact injection volume was difficult to determine as the volumes were too small to accurately measure using the available equipment. In an attempt to do so, approximately 600 pl of NR dye (50 mg/ml) was pipetted into a drop. The compensation pressure was gradually decreased to allow the NR dye to flow into the injection pipette. Once the drop had been aspirated, the compensation pressure was returned to 10 hPa and the solution was ejected according to the chosen parameters (Pi = 100 hPa; Pt = 0.1s; Pc = 10 hPa). The number of ejections taken to deplete the NR dye from the injection pipette were counted. A total of 30 ejections were recorded, thereby estimating each ejection volume to be around 20 pl. This method of determining injection volume does not consider the internal cell pressure of the oocyte which acts against the injecting pressure. Internal cell pressure has been estimated to reduce the injected volume by up to 30% (Wang et al., 2018b). Furthermore, internal cell pressures differ between cell types so injection parameters must be tailored according to which cells are being manipulated.

To learn and optimise the technique of microinjection without killing oocytes, PBS was used to inject 55 bovine cumulus-enclosed GV oocytes over 3 replicate cultures. Following serum-free IVM for 24 hours according to Section 2.1.3, oocyte viability and meiotic maturation were assessed. Cotterill (2008) and Liperis (2013) used NR dye to confirm viability of ovine oocytes following microinjection. To this end, 1 µl of 50 µg/ml NR dye was added to each 20 µl microdrop of oocytes and allowed to incubate for 15-20 min. The numbers of live and dead oocytes were recorded. Oocyte meiotic maturation was assessed by the presence of a polar body under a stereomicroscope. Oocytes were imaged using a Nikon Eclipse Ti inverted microscope fitted with a heated stage at 39°C and a Watec WAT-221S camera (Camtronics BV, Eindhoven, Netherlands). Research Instruments viewer software was used to examine the images on the computer.

4.2.2 Experiment 2: Optimisation of *PADI6* KD using siRNA and IVM of bovine oocytes

4.2.2.1 Design of dsiRNAs and primers for targeted KD of *PADI6* gene expression in bovine oocytes

DsiRNAs were designed and purchased from IDT. The bovine *PADI6* cDNA sequence from Ensembl database (ENSBTAT00000002772) was inputted as the target template for KD of *PADI6*. Previous work from our lab accrued RNA-seq data in sheep (Lu, J., Iles, D., Huntriss, J. and Picton, H.M., unpublished data) (Figure 4.2). Analysis of ovine *PADI6* in this data suggested that the 3' of *PADI6* transcript was highly represented and therefore may be an effective region to target with dsiRNAs. Although specifically designed so that the dsiRNAs should KD a gene of interest, in practice various limitations can prevail. For example, secondary structures in the mRNA and mismatches between the mRNA and dsiRNA sequences can preclude dsiRNA binding. With this in mind, exons 9 and 13 were chosen as target regions for RNAi and tested for their ability to effectively KD *PADI6* gene expression in bovine oocytes (Table 4.1).

RNAi injection species were resuspended in 20 µl of sterile distilled water (W3500, Sigma) to a stock concentration of 100 µM. 2 µl of stock was diluted in 500 µl of duplex buffer (11-01-03-01, IDT) to a working concentration of 400 nM. A range of concentrations from 10 µM to 375 µM were published for use in bovine oocytes and

embryos (Fu et al., 2017; Lee et al., 2014a; O'Meara et al., 2011; Wang et al., 2012b; Yun et al., 2015) while IDT recommended a concentration of 100 pM to 10 nM. The optimal dsiRNA concentration aims to produce an efficient gene KD without causing concentration-dependent, off-target effects (Persengiev et al., 2004). In this thesis a dsiRNA concentration of 400 nM was used. This dose of dsiRNA was found not to limit oocyte viability or maturation but caused KD of the gene of interest and was therefore deemed suitable for RNAi in bovine oocytes in the current experimental series. A scrambled dsiRNA (Table 4.2) at the same concentration was also microinjected into a group of oocytes to control for any off-target effects that might have occurred from the introduction of exogenous siRNA into the oocyte.

In addition to dsiRNA design, primers were designed to flank the dsiRNA target regions to identify KD of *PADI6* transcripts (Table 4.3). Researchers have shown that primers must be designed in the 5' of the target mRNA or flanking the siRNA cleavage site to detect transcript KD (Holmes et al., 2010; Mainland et al., 2017). Targeting the 3' end of the transcript can often produce a false negative result. This is not an artefact of oligo-dT priming during cDNA synthesis but because the 3' fragment is often not degraded after RNAi cleavage. Therefore, 3 primers pairs were designed to span exons 9-10 to detect *PADI6* KD in exon 9 by dsiRNAs 13.15, 13.23 and 13.28, and 4 primer pairs were designed to span exons 12-14 to detect *PADI6* KD in exon 13 by dsiRNAs 13.1 and 13.3. Figure 4.3 shows the bovine *PADI6* gene and its constituent exons, target sites for RNAi and primer positions for detection of *PADI6* KD.

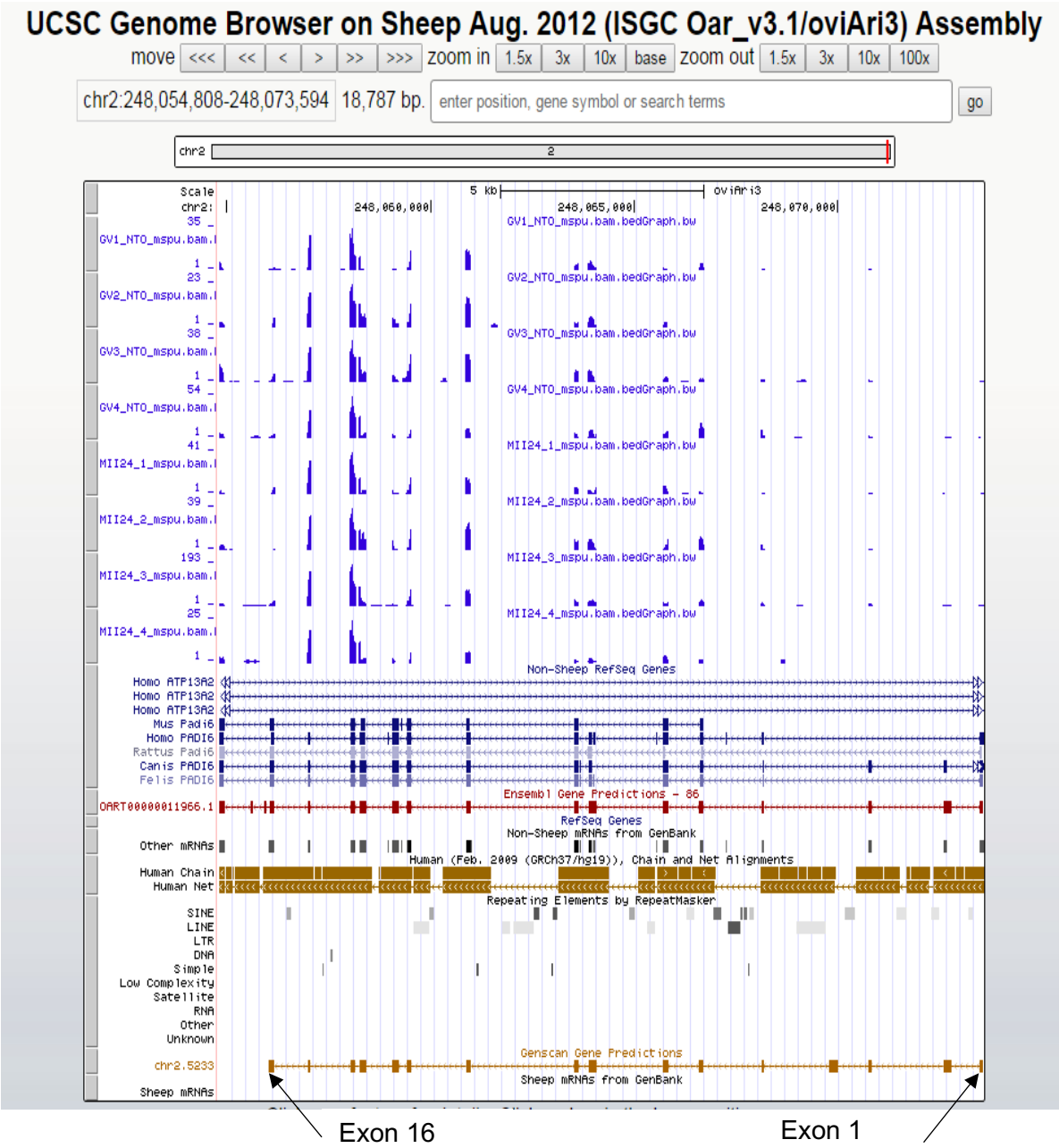

Figure 4.2 Ovine *PADI6* mRNA tracks from RNA-seq data inputted into UCSC genome browser (https://genome.ucsc.edu/) to show exon reads corresponding to the reference ovine *PADI6* genomic landscape (Lu, J., Iles, D., Huntriss, J. and Picton, H.M., unpublished data). Oar_v4.0/oviAri4 assembly was used for genomic building of the ovine RNA-seq data.

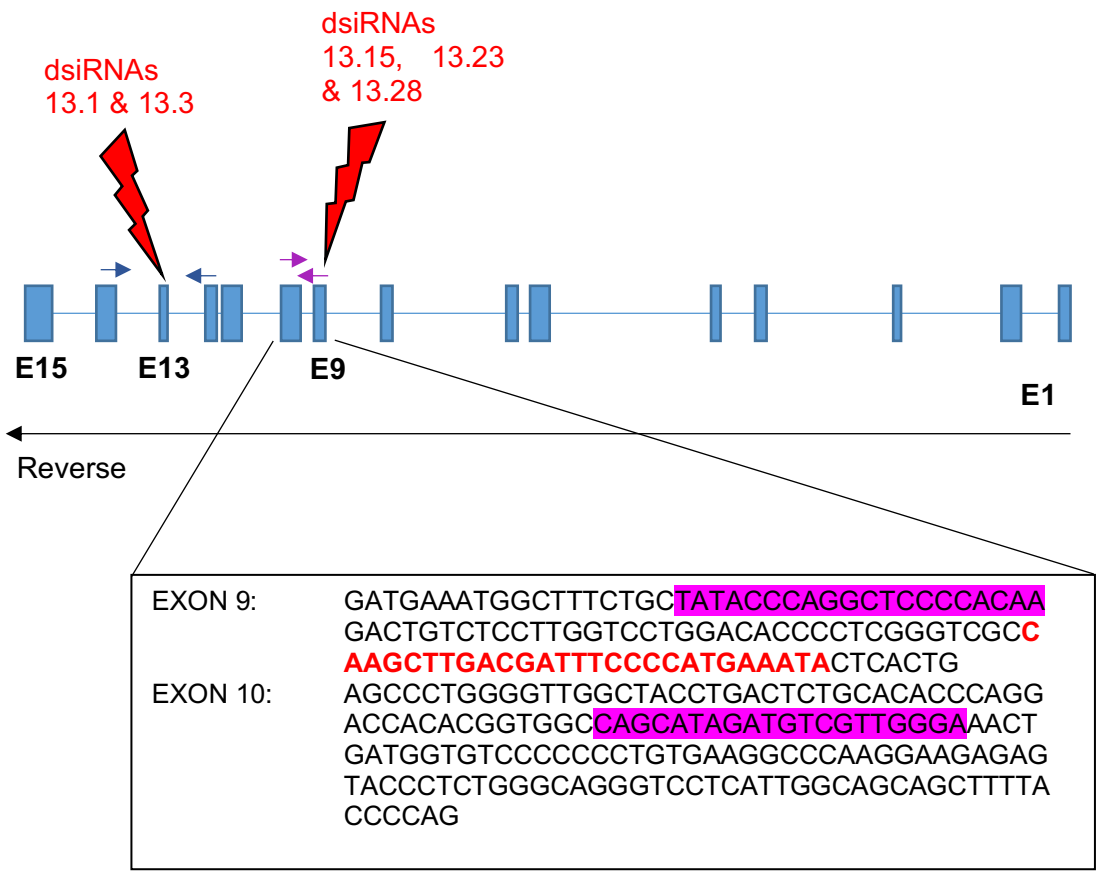

Figure 4.3 Bovine *PADI6* gene structure showing exons (blue rectangles) and target sites (red) for RNAi for KD of *PADI6*. Exon (E) 9 is targeted by dsiRNAs 13.15, 13.23 and 13.28 and E13 by dsiRNAs 13.1 and 13.3 (red). E9 and 10 are expanded in the black box to show the cDNA sequence at the nucleotide level. The dsiRNA target region is highlighted in red while *PADI6* primer set B can be seen flanking the site in pink.

Table 4.1 Sequences of dsiRNAs for KD of *PADI6* gene expression.

DsiRNA number	Sequences (5'→3')	Position (bp) Exon no.
13.1	*Sense*: rGrArCrGrArGrArArGrArUrGrArGrGrArArGrCrArGrArATG *Antisense:* rCrArUrUrCrUrGrCrUrUrCrCrUrCrArUrCrUrUrCrUrCrGrUrCrArG	1636-1661 Exon 13
13.3	*Sense*: rGrArGrArArGrArUrGrArGrGrArArGrCrArGrArArUrGrACT *Antisense:* rArGrUrCrArUrUrCrUrGrCrUrUrCrCrUrCrArUrCrUrUrCrUrCrGrU	1639-1664 Exon 13
13.15	*Sense*: rArGrCrUrUrGrArCrGrArUrUrUrCrCrCrCrArUrGrArArATA *Antisense:* rUrArUrUrUrCrArUrGrGrGrGrGrArArArUrCrGrUrCrArArGrCrUrUrG	1133-1158 Exon 9
13.23	*Sense:* rGrCrUrUrGrArCrGrArUrUrUrCrCrCrCrArUrGrArArArUAC *Antisense:* rGrUrArUrUrUrCrArUrGrGrGrGrArArArUrCrGrUrCrArArGrCrUrU	1134-1159 Exon 9
13.28	*Sense:* rCrArArGrCrUrUrGrArCrGrArUrUrUrCrCrCrCrArUrGrAAA *Antisense:* rUrUrUrCrArUrGrGrGrGrArArArUrCrGrUrCrArArGrCrUrUrGrGrC	1131-1156 Exon 9

Table 4.2 Sequence of scrambled dsiRNA (SCR) used as the siRNA control in *PADI6* KD experiments.

DsiRNA	Sequences (5'→3')
Scrambled dsiRNA	*Sense: CUUCCUCUCUUUCUCUCCCUUGUGA* *Antisense: UCACAAGGGAGAGAAAGAGAGGAAGGA*

Table 4.3 Primer sequences for detection of bovine *PADI6* gene KD

Primer set	Position	Primer sequences (5'→3')	PCR product size (bp)
9A	*PADI6* Exon 9 – 10	F: TTCTGCTATACCCAGGCTCC R: CAACGACATCTATGCTGGCC	163
9B	*PADI6* Exon 9 – 10	F: TATACCCAGGCTCCCCACAA R: TCCCAACGACATCTATGCTG	152
9C	*PADI6* Exon 9 – 10	F: GCTATACCCAGGCTCCCCA R: ATCTATGCTGGCCACCGTG	160
13A	*PADI6* Exon 12 – 14	F: TGCTCTTTGAAGGGCTTAGG R: TCATTCTGCTTCCTCATCTTCTC	103
13B	*PADI6* Exon 12 – 14	F: CGAGAAGATGAGGAAGCAGAATG R: GGGATGATGTCCTCCTCCTG	102
13C	*PADI6* Exon 12 – 14	F: CGAGAAGATGAGGAAGCAGAAT R: CAGGCAGAAGAGCTGTGG	124
13D	*PADI6* Exon 12 – 14	F: GCTCTTTGAAGGGCTTAGGA R: AGTCATTCTGCTTCCTCATCTT	104

The efficacy of dsiRNAs in providing KD of *PADI6* gene expression was assessed in 2 cultures: 1 culture for dsiRNAs targeting exon 9 and the other for dsiRNAs targeting exon 13 of *PADI6*. Freshly aspirated COCs were placed into prepared 50 mm ICSI dishes containing 20 µl drops of H199+ media (Table 2.2) under mineral oil for each injection group. The first culture assessed dsiRNAs in exon 13 by injecting 10 oocytes per group with either dsiRNA 13.1 or 13.3 or an equal mixture of both dsiRNAs, as well as duplex buffer as an injection control (IDT, USA). The equal mixture of dsiRNAs was prepared by adding 10 µl of each 400 nM dsiRNA to a sterile 0.5 ml Eppendorf. The second culture assessed dsiRNAs in exon 9 by injecting 10 oocytes per group with either dsiRNA 13.15, 13.23, 13.28 or an equal mixture of all 3 dsiRNAs, as well as duplex buffer. The injection parameters detailed in Section 4.2.1 were used in the preliminary testing of dsiRNA species. The RNAi system used here was based on an extensively validated 2-day culture system by Cotterill (2008), however Cotterill had previously injected denuded GV oocytes which meant that there was a need for co-culture with freshly harvested cumulus cells on day 1-2 to allow for *in vitro* maturation of oocytes. Cumulus-enclosed GV oocytes were injected here and COCs were put straight into serum-free IVM medium after microinjection, resulting in a 1-day culture system. The following protocol was used:

4.2.2.2 Day 1: Microinjection of cumulus-enclosed GV oocytes

Oocytes were collected from abattoir-derived ovaries as described in Section 2.1. Following aspiration, 10-20 COCs were placed into prepared 50 mm ICSI dishes containing 20 µl drops of H199+ media (Table 2.2) under mineral oil for each injection group. Up to 30 oocytes were transferred to injection dishes for each group per culture, based on the availability of good quality COCs. The final parameters were set as follows: 100 hPa injection pressure, 0.1 second injection time and 10 hPa compensation pressure. Each injection pipette was backloaded with 10 µl of the injection species, either *PADI6* dsiRNA, scrambled siRNA (siRNA control – Table 4.2) (IDT, USA) or duplex buffer (injection control), using microloader tips. A different injection pipette was used for each injection species. Microinjection was conducted as in Section 4.2.1. Multiple dsiRNAs were tested in 2 cultures to determine the most effective species for *PADI6* KD (Table 4.1).

After injecting all 20 COCs in the dish, COCs were transferred to a fresh 35 mm embryo tested NUNC™ IVF Petri dish and washed in 50 µl drops of serum-free IVM media (Table 2.3) under mineral oil. They were then transferred to prepared 35 mm NUNC™ IVF Petri dishes containing 10 µl drops of fresh IVM media/COC under mineral oil and cultured in a humidified atmosphere at 39°C, 5% CO_2 for 24 hours. Figure 4.4 shows the experimental work flow.

4.2.2.3 Day 2: COC assessment and oocyte freezing

After *in vitro* maturation for 24 hours (Section 2.1.3), oocytes were assessed for morphology, viability and meiotic maturation. Morphological indices of cumulus mass (CM) and expansion (CE) were evaluated qualitatively, according to the maturity grading of COCs from 0-2 in Wynn et al. (1998) and Smitz et al. (2007). Table 4.4 and Table 4.5 describe the classifications for cumulus mass and expansion grading. COCs and oocytes were photographed before and after denudation. Oocytes were denuded in 300 µg/ml hyaluronidase using a 130 µm EZ-Tip and EZ-Grip denudation and handling pipettor. Oocyte viability was then measured by incubation with 50 µg/ml NR dye for 15-20 min. Oocytes that did not stain red were unviable and discarded. Oocyte maturation was determined by the presence of a polar body under the stereomicroscope (200X magnification). Live oocytes were washed in 500 µl of DPBS in a 4-well dish before individual oocytes were transferred to a sterile 0.5 ml

microcentrifuge tube containing 2 µl RNAGEM lysis buffer and put to ice (Section 2.4.1). Samples were frozen and stored at -80°C for molecular analysis.

Table 4.4 Cumulus mass (CM) grading (Wynn et al., 1998).

Cumulus mass classification	**Grade**
≤3 layers of cumulus cells	CM 0
<3 but <10 layers of cumulus cells	CM 1
≥10 layers of cumulus cells	CM 2

Table 4.5 Cumulus expansion (CE) grading (Wynn et al., 1998).

Cumulus expansion classification	**Grade**
Tight, dense cumulus cells	CE 0
Moderate expansion of cumulus cells	CE 1
Fully expanded cumulus cells	CE 2

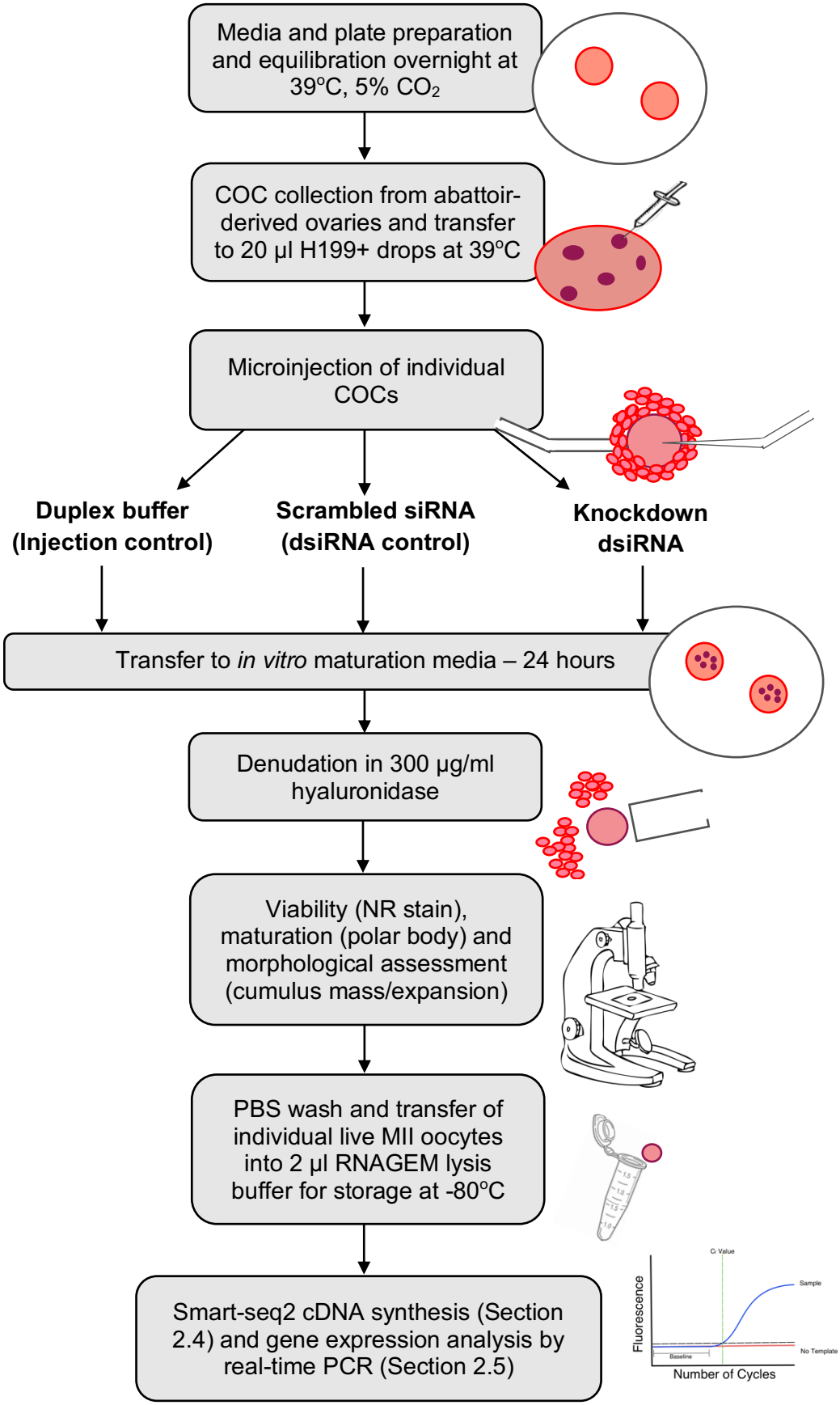

Figure 4.4 Experimental workflow for dsiRNA KD of *PADI6* gene expression.

4.2.2.4 Molecular evaluation of *PADI6* KD

Individual oocytes for each *PADI6* siRNA KD species alongside their respective controls of duplex buffer and scrambled siRNA were thawed on ice and subject to DNase treatment and Smart-seq2 cDNA synthesis as detailed in Section 2.4. Real-time PCR was used to quantify the transcript level of bovine *PADI6* relative to housekeeping genes, *GAPDH, H2A* and *YWHAZ* for each group (Section 2.7). The primer sequences that were used for *PADI6* are detailed in Table 4.3. Real-time PCRs were run in triplicate for each sample. Statistical analyses were performed using GraphPad Prism 7 as in Section 2.8. The siRNA species that provided the highest levels of *PADI6* KD in comparison with the respective controls were selected for subsequent molecular analysis.

4.2.2.5 Molecular evaluation of *PADI1-4* expression after *PADI6* KD

Following KD of *PADI6* gene expression, it was important to assess the expression of other *PADI* genes. The *PADI* genes are conserved (Chavanas et al., 2004; Vossenaar et al., 2003) which poses the question of whether dsiRNAs against *PADI6* may also KD *other PADI* members. To this end, primers for *PADI1-4* were designed and tested using real-time PCR in control-injected (n = 3) and *PADI6* KD MII oocytes (n = 3). Real-time PCR was conducted as detailed in Section 2.7. Multiple primers were tested for each *PADI* gene but only the working primer sequences are shown in Table 4.6. Unsuccessful primer pairs that were tested are detailed in Appendix III - Table III.I.

Table 4.6 Primer sequences for detection of bovine *PADI1-4.*

Gene	Primer sequences (5'→3')	Product size (bp)	Reference
PADI1	F: CCCTCTTTCCTTTACCAGCTAC R: CCGAGTTTCCTTGTCCTGATT	108	ENSBTAT00000015977.6
PADI2	F: CTACAGCAAGGAAGACCTGAAG R: AGTCCGACATGGAGATGTAGA	110	ENSBTAT00000004411.6
PADI3	F: GAACTGCGACAGAGACAGTATG R: CCGCAGAATCATCACAGACA	103	ENSBTAT00000015978.6
PADI4	F: TGACTGACCTTGACTCCTTTG R: GTAACCGCTGTCTCCAATGA	104	ENSBTAT00000015991.6

4.2.3 Statistical analysis

Real-time data for each gene was compared to the geometric mean of 3 housekeeping genes, *GAPDH, H2A* and *YWHAZ,* as detailed in Section 2.7. For oocyte survival and maturation, the arithmetic mean was calculated across replicate cultures and presented as a histogram displaying the mean ±SEM. All data were tested for normality using the D'Agostino-Pearson test. Data containing '0' was transformed by $\sqrt{(x + 0.5)}$. Statistical analyses were performed on transformed data. One-way ANOVA was used for normally distributed data. p values of <0.05 were considered to be statistically significant. Untransformed data were plotted. Values presented for real-time data are arithmetic means ±SEM for the number of observations shown.

4.3 Results

4.3.1 Experiment 1: Pilot evaluation of microinjection methodology

A total of 55 COCs were injected with PBS over 3 repeat cultures during training of the microinjection procedure. The aim of this was to evaluate the user technique of microinjection. Although microinjection can inflict mechanical stress on the oocyte, viability and maturation should not be drastically affected by the procedure. It was therefore important to show the impact of microinjection on COCs to differentiate between the effects of microinjection and the phenotypic consequences of RNAi. Following PBS injections, COCs were allowed to mature for 24 hours before oocytes were denuded and stained with NR dye (50 µg/ml). Table 4.7 shows the resultant viability and maturation of PBS-injected oocytes. On average, 72% (±8.3%) of oocytes survived PBS injections. From culture 1 to 3, oocyte viability improved by around 28%, suggesting that there was an improvement in operator technique during the course of microinjection training. Oocyte maturation was determined by extrusion of the 1st polar body. On average, 81% of oocytes had visible polar bodies and were deemed as mature MII oocytes. Figure 4.5 shows examples of oocytes from PBS injection repeat 2. After validating the methodology and user technique, microinjection was deemed a suitable choice for administering dsiRNA into bovine COCs.

Table 4.7 Oocyte survival and meiotic maturation after injection with PBS for microinjection training. The results are shown in percentage form for 3 discrete cultures and the average oocyte survival and maturation rate to MII was calculated alongside the SEM.

Repeat no.	No. of oocytes injected	**Survival**	**Maturation**
1	15	60%	83%
2	30	69%	89%
3	10	88%	71%
	Average (±SEM)	**72% (±8.3%)**	**81% (±5.3%)**

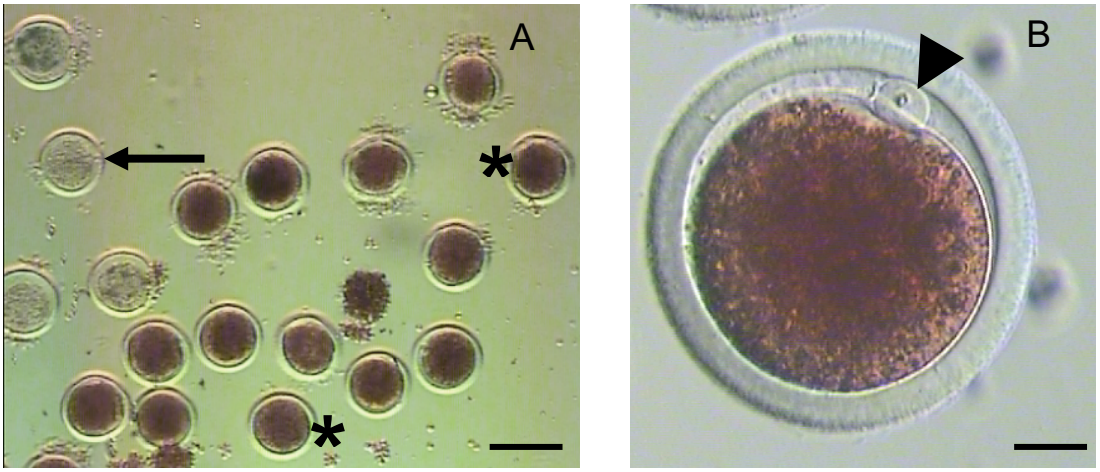

Figure 4.5 Examples of oocytes after microinjection with PBS followed by 24 hours in IVM media. A) NR staining differentiates dead (unstained – denoted with a black arrow) from live (red – denoted with an asterisk) oocytes (40X magnification). B) A NR stained MII oocyte with a polar body shown by the arrow head (200X magnification). The scale bar represents 40 µm.

4.3.2 Experiment 2: Optimisation of *PADI6* KD using dsiRNA and IVM of bovine oocytes

Following validation of the microinjection methodology, dsiRNAs and primers were tested for their ability to KD and detect *PADI6* KD, respectively. In concordance with ovine RNA-seq data, dsiRNAs were designed in exon 9 and 13 in an attempt to achieve effective KD of *PADI6* gene expression in bovine. A concentration of 400 nM was chosen according to the literature as described in Section 4.2.2.1. Preliminary experiments were performed to test 5 dsiRNAs, 3 in exon 9 and 2 in exon 13 (Table 4.1). COCs were injected, matured and lysed for molecular analysis as described in the Sections above. Multiple primers were examined by real-time PCR to ascertain the best pair to detect *PADI6* KD (Table 4.3).

4.3.2.1 Evaluation of *PADI6* dsiRNAs targeting exon 13

The purpose of these preliminary cultures was to select the best dsiRNA species for *PADI6* KD compared to controls. Firstly, dsiRNAs were designed and tested in exon 13. According to ovine *PADI6* RNA-seq data, exon 13 is highly represented and therefore likely to be a good target region for dsiRNA design. In the culture, approximately 40 COCs were injected with either duplex buffer (control), dsiRNA 13.1, 13.3 or a mix of both dsiRNAs (13.1 and 13.3), giving an average of 10 COCs per group. The results are shown in Figure 4.6a. Although the number of oocytes were very low, there was no significant KD of *PADI6* gene expression between the different injection groups ($p>0.05$). Furthermore, multiple primer pairs, 13A, 13B, 13C and 13D, were tested to see if the primer characteristics may have precluded detection of *PADI6* KD (Figure 4.6b). Different primers failed to detect a *PADI6* KD, suggesting that the dsiRNAs designed to target exon 13 were not successful. In the interest of time the culture was not repeated again as dsiRNAs in exon 9 displayed more promising KD results (see Figure 4.7).

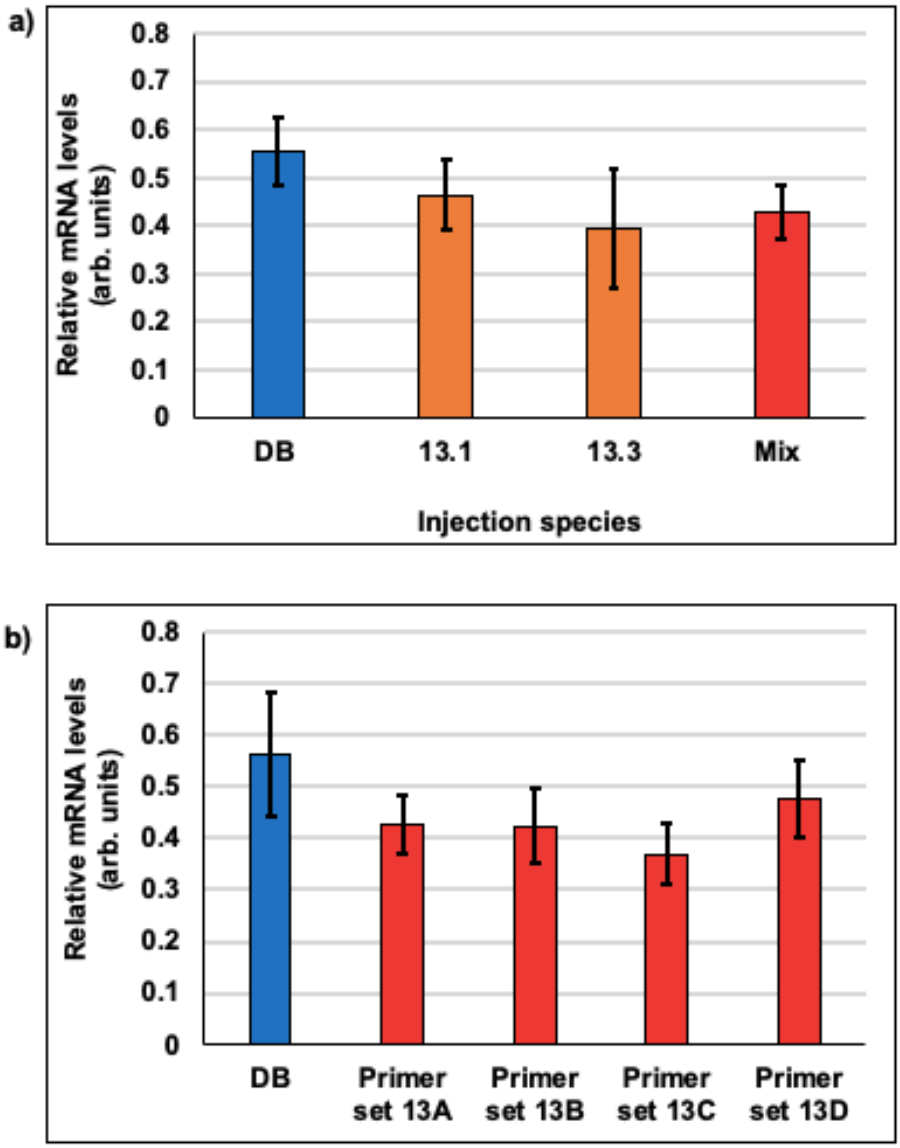

Figure 4.6 Real-time PCR quantification of bovine *PADI6* after injection with **a)** duplex buffer (DB) (n=3) or dsiRNA species, 13.1 (n=6), 13.3 (n=4) or a mixture of both dsiRNAs (mix) (n=5) targeting exon 13 using primer set 13A to detect *PADI6* mRNA levels. **b)** Duplex buffer (DB) or a mix of dsiRNAs (red) using different primer sets (13A-D) to detect *PADI6* mRNA levels. The data were standardised against *GAPDH, H2A* and *YWHAZ* housekeeping mRNA levels. Individual bars show the mean ±SEM. n = 3-6 single oocytes for each injection group as shown. No significant differences were observed (p>0.05).

4.3.2.2 Evaluation of *PADI6* dsiRNAs targeting exon 9

Simultaneously, 3 dsiRNAs in exon 9 were tested for their ability to KD *PADI6* gene expression. In the culture, approximately 50 COCs were injected with either duplex buffer (control), dsiRNA 13.15, 13.23, 13.28 or a mix of dsiRNAs (13.15, 13.23 and 13.28), giving an average of 10 COCs per group. 3 primer pairs, 9A, 9B and 9C, spanning exons 9 and 10 were tested for their ability to detect a reduction in *PADI6* transcript abundance. Figure 4.7a, b and c show *PADI6* transcript abundance in different injection groups using primer pair 9A, 9B and 9C, respectively. Primer set 9A detected no significant changes in *PADI6* gene expression between the different injection species ($p>0.05$) (Figure 4.7a). *PADI6* transcript abundance even appeared to increase in the *PADI6* dsiRNA mix injection group, although this was not significant ($p>0.05$). It is worth noting that high levels of variability in the data as reflected by large standard error bars were obtained with primer set 9A. Overall, there was no apparent change in *PADI6* gene expression between different injection groups using primer set 9A.

Primer set 9B also detected no significant differences in *PADI6* transcript abundance between injection species, but qualitative differences were observed for injection species 13.28 and mixed injection ($p>0.05$) (Figure 4.7b). Both 13.28 and mixed dsiRNA groups showed a decrease in *PADI6* transcript abundance compared to DB control. Moreover, the SEM for the *PADI6* dsiRNA mix injection group was remarkably smaller than the other groups, and other primer sets that were tested. Finally, primer set 9C also failed to detect significant differences in *PADI6* transcript abundance between injection species ($p>0.05$) (Figure 4.7c). Relative expression of *PADI6* in DB control group was much lower than expected from our data in non-injected MII oocytes (Figure 3.6) and other primer sets (Figure 4.7a and b). Further, no qualitative decreases in *PADI6* expression were observed between different dsiRNA groups.

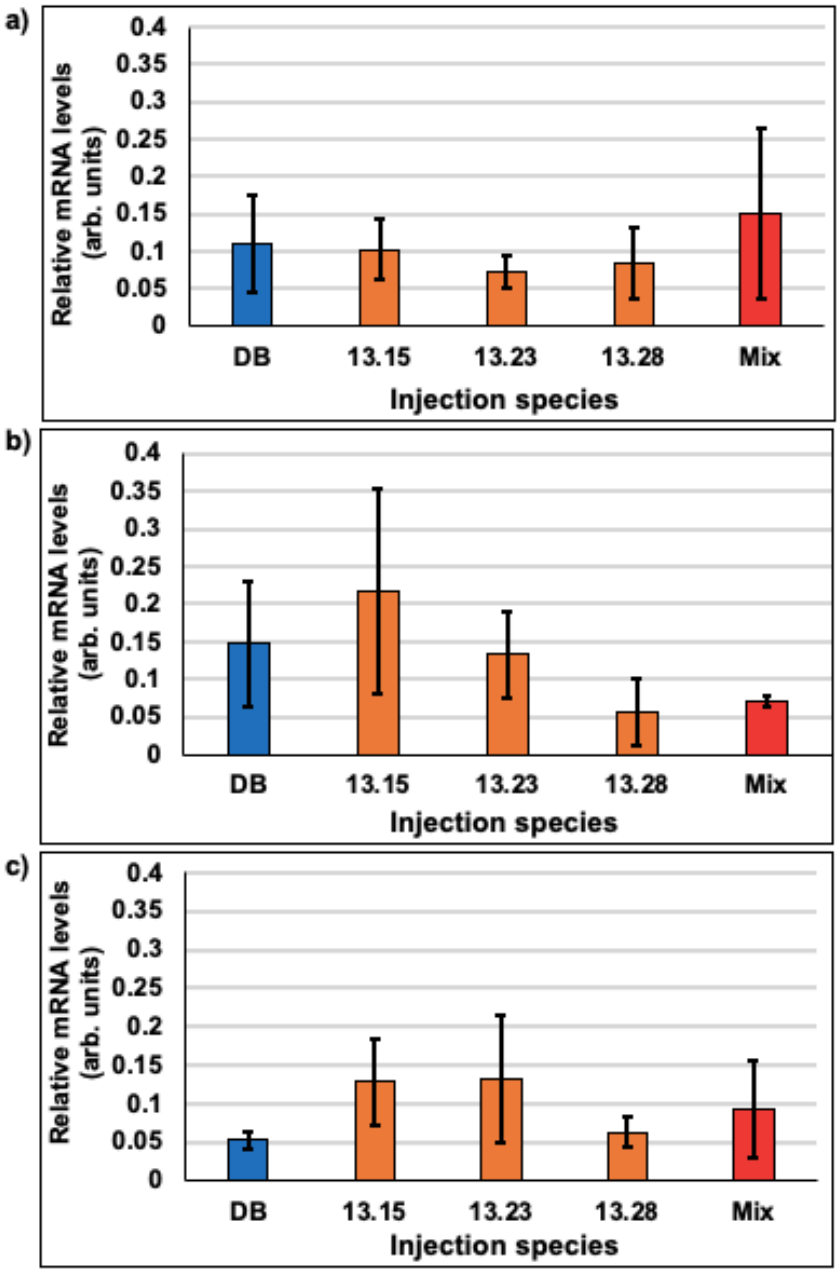

Figure 4.7 Real-time PCR quantification of *PADI6* after injection with duplex buffer (DB) (n=2) or dsiRNA species, 13.15 (n=5), 13.23 (n=4), 13.28 (n=3) or a mixture of all 3 siRNAs (Mix) (n=4) targeting exon 9 using **a)** primer set 9A, **b)** primer set 9B and **c)** primer set 9C. The data were standardised against *GAPDH, H2A* and *YWHAZ* housekeeping mRNA levels. Individual bars show the mean ±SEM. No significant differences were observed (p>0.05).

In conclusion, exon 9 dsiRNAs and primer set 9B were chosen to take forward to the dsiRNA validation stage. Although no significant differences were observed, the decrease in *PADI6* transcript abundance tended to be greater in oocytes injected with dsiRNAs targeting exon 9 than those targeting exon 13. Primer set 9B was chosen as the level of *PADI6* gene expression in DB control oocytes was similar to that of MII oocytes in the developmental series (Figure 3.6), showing a level of consistency in transcript detection. Furthermore, primer set 9B results had smaller standard errors with regard to *PADI6* expression levels and suggested that KD of *PADI6* was achieved after injection with mixture of dsiRNAs, although this was not significant.

4.3.3 Validation of siRNAs for KD of *PADI6* gene expression

The experiments described in Section 4.3.2 identified that targeting exon 9 of *PADI6* appeared to be the most effective means of achieving gene KD and that primer set 9B seemed to be the best means to detect decreases in *PADI6* transcript abundance. From here on, only primer set 9B was used to detect *PADI6* KD. The next aim was to determine which dsiRNA species targeting exon 9 would achieve the highest KD of *PADI6* gene expression. Additional microinjections were performed as follows: for each culture, approximately 10-15 COCs were microinjected with dsiRNA (13.15, 13.23, 13.28 or a combination of all 3, Mix), duplex buffer or scrambled dsiRNA. 3 discrete cultures were performed and the data were pooled. There was no significant difference in *PADI6* gene expression after injection with DB, SCR, 13.15 and 13.28 dsiRNAs ($p>0.05$). 13.23 dsiRNA caused a small decrease in *PADI6* transcript abundance, although this was not significant compared to controls ($p>0.05$). In contrast, injection with a mix of dsiRNAs caused a significant reduction in *PADI6* gene expression compared to both duplex buffer and scrambled dsiRNA injections ($p<0.05$) (Figure 4.8). In conclusion, the combination of 3 dsiRNAs (13.15, 13.23 and 13.28) achieved the highest *PADI6* gene KD and was therefore chosen for use in all future experiments ($p<0.05$).

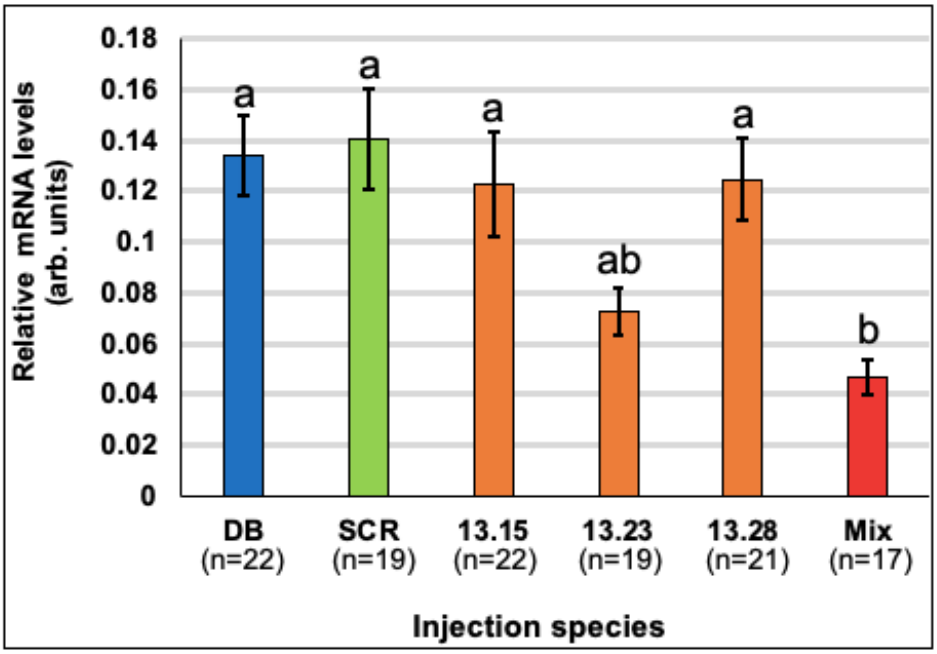

Figure 4.8 Real-time PCR quantification of *PADI6* after injection with duplex buffer (DB), scrambled dsiRNA (SCR), or *PADI6* dsiRNA species, 13.15, 13.23, 13.28 or a mixture of all 3 siRNAs (Mix). The data were standardised against *GAPDH, H2A* and *YWHAZ* housekeeping mRNA levels. Individual bars show the mean ±SEM. n = 17-22 single injected oocytes for each group as shown. Different letters on the bar denote significant differences between means ($p<0.05$).

The 20 oocytes with the highest *PADI6* KD were plotted against control injected oocytes (Figure 4.9). A mean *PADI6* KD of 74±3.6% (0.03 ±0.004 arb. units, n = 20) was achieved in these oocytes using the mix of dsiRNAs compared to the duplex buffer (0.11 ±0.016 arb. units, n = 11) and scrambled dsiRNA (0.12 ±0.014 arb. units, n = 10) control-injected oocytes ($p<0.05$). Molecular real-time PCR analysis in Chapter 5 was performed on all 20 *PADI6* KD samples in Figure 4.9 while RNA sequencing was performed on a subset of 6 of these samples due to the high cost of RNA sequencing.

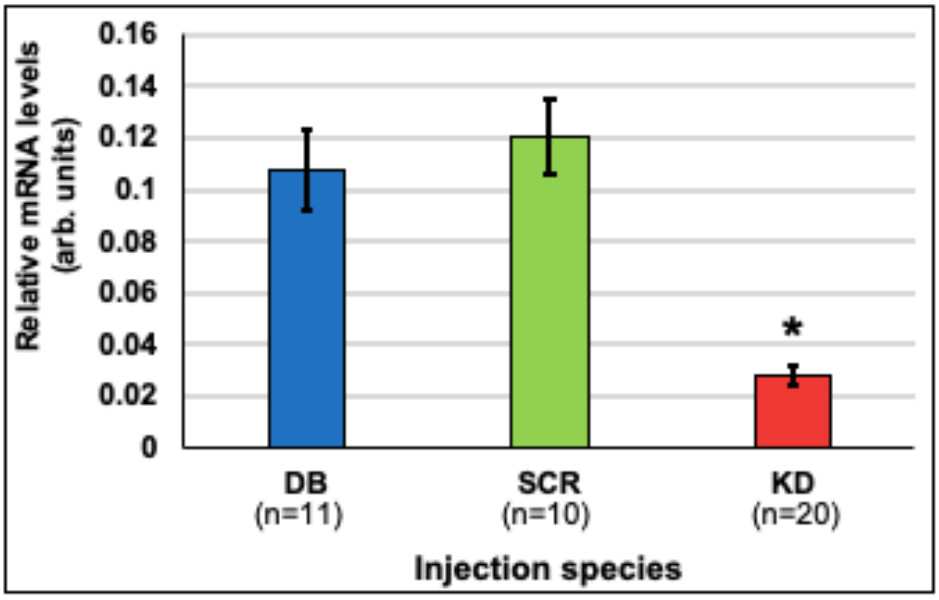

Figure 4.9 Real-time PCR quantification of *PADI6* in oocytes with the greatest *PADI6* gene KD after injection of mix of dsiRNAs (KD). The average relative reduction in bovine *PADI6* gene expression was 74±3.6% compared to control-injected oocytes, duplex buffer (DB) and scrambled dsiRNA (SCR). The data were standardised against *GAPDH, H2A* and *YWHAZ* housekeeping mRNA levels. Individual bars show the mean ±SEM. For *PADI6* KD, 20 repeat cDNA libraries were analysed in triplicate. Each cDNA library contained a single oocyte. The *PADI6* dsiRNA mix injected oocytes exhibited a statistically significant reduction in *PADI6* mRNA levels (* = $p<0.05$) when compared to both groups of control-injected oocytes.

4.3.3.1 Assessment of the impact of *PADI6* KD on bovine oocyte maturation and cumulus expansion *in vitro*

PADI6 gene KD was achieved by targeting exon 9 and appeared to be most effective when dsiRNAs 13.15, 13.23 and 13.28 were used in combination. Consequently, it was important to assess the effects of microinjection of this dsiRNA combination on oocyte survival and maturation. The data were pooled from 3 discrete cultures where approximately 10-15 COCs were microinjected for each group per culture. Oocyte survival was assessed 24 hours following injection and culture in serum-free IVM media by NR staining. Oocyte viability was around 70-80% after microinjection for each group (Figure 4.10a). Therefore, our results indicated that microinjection of dsiRNA had no effect on oocyte viability compared to controls, duplex buffer (DB) and

scrambled dsiRNA (SCR) ($p>0.05$). Furthermore, viability was not significantly different in the efficacious *PADI6* KD group (mix of dsiRNAs – red), suggesting that *PADI6* KD does not cause bovine oocyte death.

Next, the developmental competence of oocytes following microinjection and IVM was assessed by evaluating MII progression of oocytes after 24 hours in serum-free IVM media. Meiotic maturation was assessed by the extrusion of a polar body. The raw counts for each injection group over 3 discrete cultures are shown in Figure 4.10b. Overall, there were no significant differences in meiotic maturation between injection groups ($p>0.05$) (Figure 4.10c). There was more variation in maturation rate after injection with a mixture of *PADI6* dsiRNAs (red) as shown by the large SEM, however the raw counts in Figure 4.10b show that the number of oocytes that progressed to MII in this group in culture 2 was very low compared to other injection groups and culture weeks. This may be due to an unidentified issue with this particular plate. Nevertheless, 59-77% of oocytes matured *in vitro* after microinjection and no significant differences in maturation rates were observed between injected oocytes and non-injected oocytes (yellow) ($p>0.05$). This suggests that the microinjection technique and dsiRNAs used in this study do not disturb meiotic maturation. Finally, maturation was not significantly different in the efficacious *PADI6* KD group, suggesting that *PADI6 per se* does not contribute to oocyte maturation.

a)

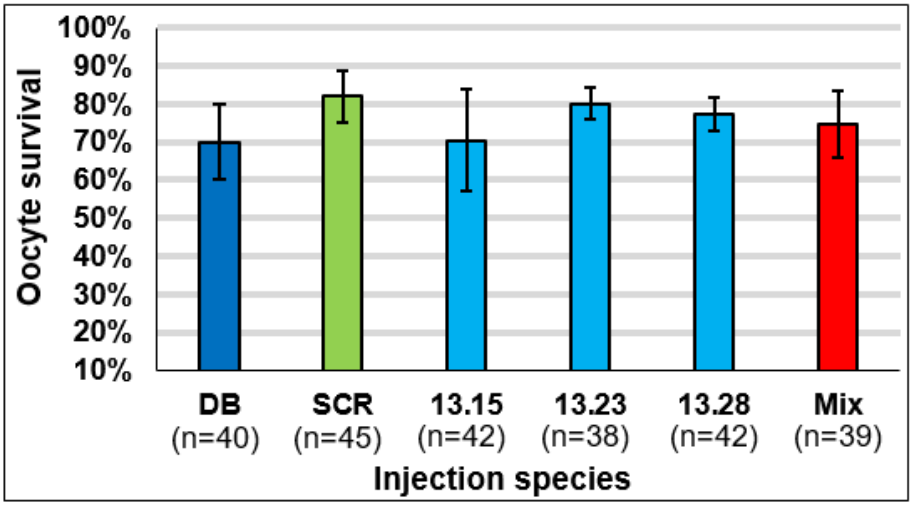

b)

Culture	No. of viable MII oocytes (%)					
	DB	SCR	13.15	13.23	13.28	Mix
1	5/6 (83)	6/9 (67)	7/9 (78)	6/7 (86)	5/6 (83)	6/6 (100)
2	6/6 (100)	5/5 (100)	5/5 (100)	5/6 (83)	5/7 (71)	3/9 (33)
3	12/18 (67)	9/13 (69)	10/15 (67)	6/11 (55)	7/13 (54)	7/12 (58)
Mean ±SEM	23/30 77% ±10%	20/27 74% ±11%	22/29 76% ±10%	17/24 71% ±10%	17/26 65% ±9%	16/27 59% ±19%

c)

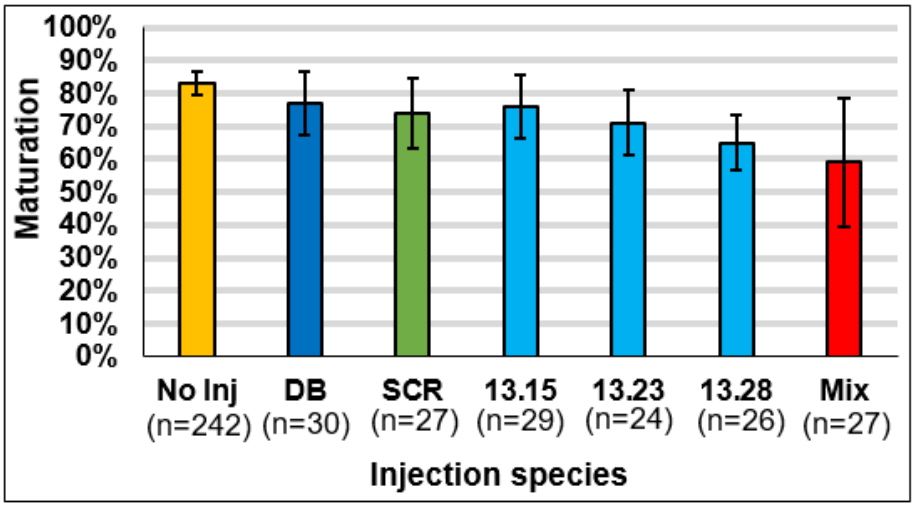

Figure 4.10 Impact of microinjection of GV oocytes on **a)** oocyte survival (%), and b-c) oocyte progression to MII after 24 hours in IVM media: **b)** raw counts of viable MII oocytes and **c)** maturation (%) for each injection group. Injection species included duplex buffer (DB), scrambled siRNA (SCR) or 13.15, 13.23, 13.28 or mixture of all 3 (mix) dsiRNA species. Individual bars show the mean ±SEM from 3 discrete cultures. No significant differences were observed (p>0.05). Oocyte maturation without injection (No Inj.) is displayed on the yellow bar.

COCs from each injection group were photographed before microinjection, after 24 hours in IVM media, after denudation and after NR staining (Figure 4.11). The morphology of cumulus-oocyte complexes (COCs) were qualitatively assessed in terms of cumulus mass and expansion after microinjection and 24 hours IVM, according to Table 4.4 and Table 4.5. The data were pooled from 3 discrete repeats and the mean ±SEM calculated. The results showed that there were no significant differences in cumulus mass after *in vitro* maturation between the 3 injection groups ($p>0.05$) (Figure 4.12a). There was a higher number of oocytes with >3 layers of cumulus cells (CM0) in the KD group compared to control groups, but this was not significant ($p>0.05$). Similarly, there were no significant differences in cumulus expansion between the 3 injection groups ($p>0.05$) (Figure 4.12b). It is noteworthy that no oocytes had fully expanded cumulus cells (CE2) after *in vitro* maturation for 24 hours so this was excluded from the graph. Full expansion to CE2 only occurs in *in vivo* matured COCs. Examples of oocytes with designated cumulus mass and expansion scores are displayed in Figure 4.13 in accordance with Wynn et al. (1998).

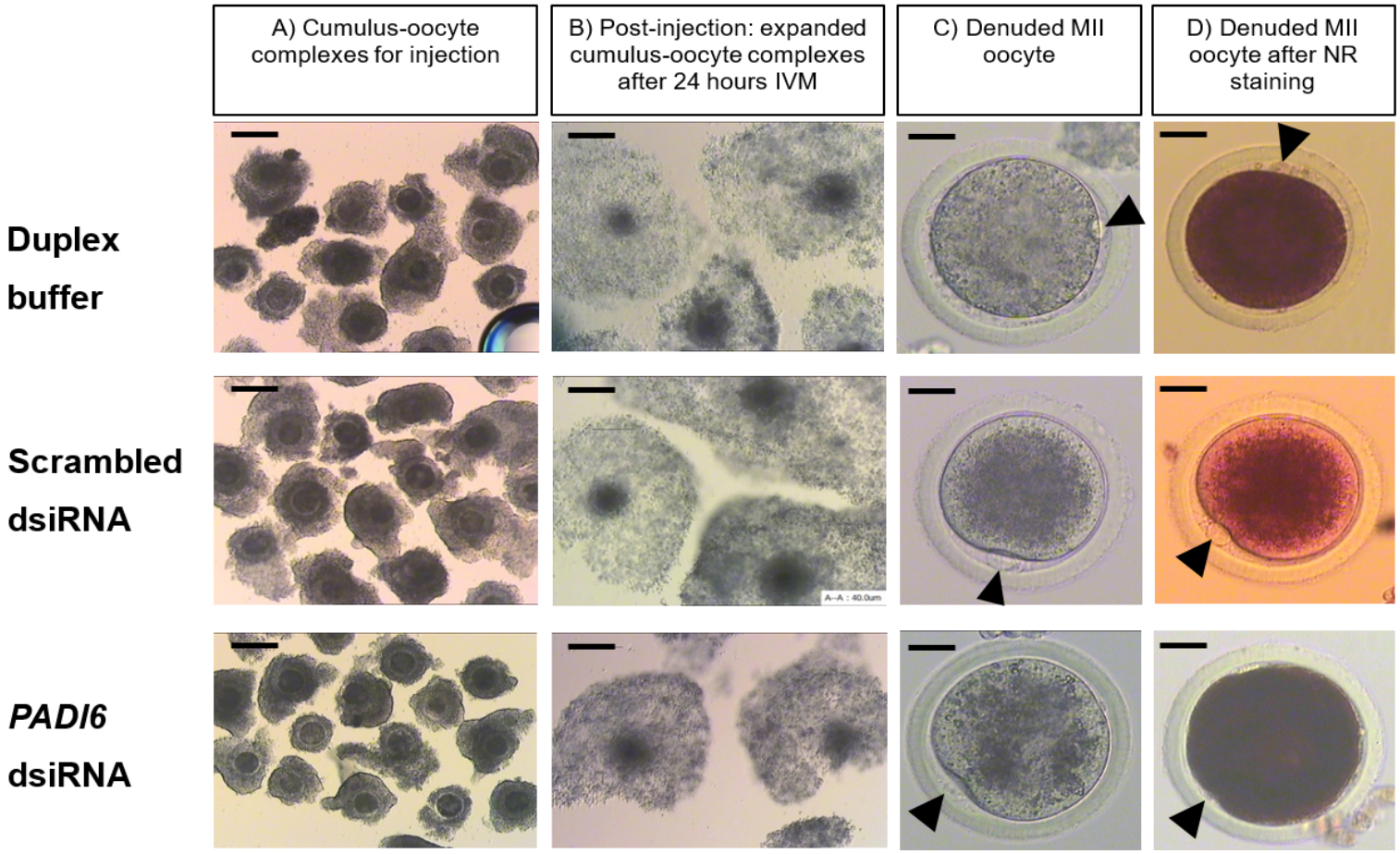

Figure 4.11 Examples of cumulus-oocyte complexes (COCs) microinjected with duplex buffer, scrambled dsiRNA or *PADI6* dsiRNA mix at different stages of the microinjection procedure: A) COCs prior to injection; B) Injected COCs after IVM; C) Denuded MII oocyte; D) NR stained MII oocyte. Oocytes in columns A/B, and C/D were photographed at 40X and 200X magnification, respectively. Polar body is highlighted by an arrowhead. Scale bar = 40 µm.

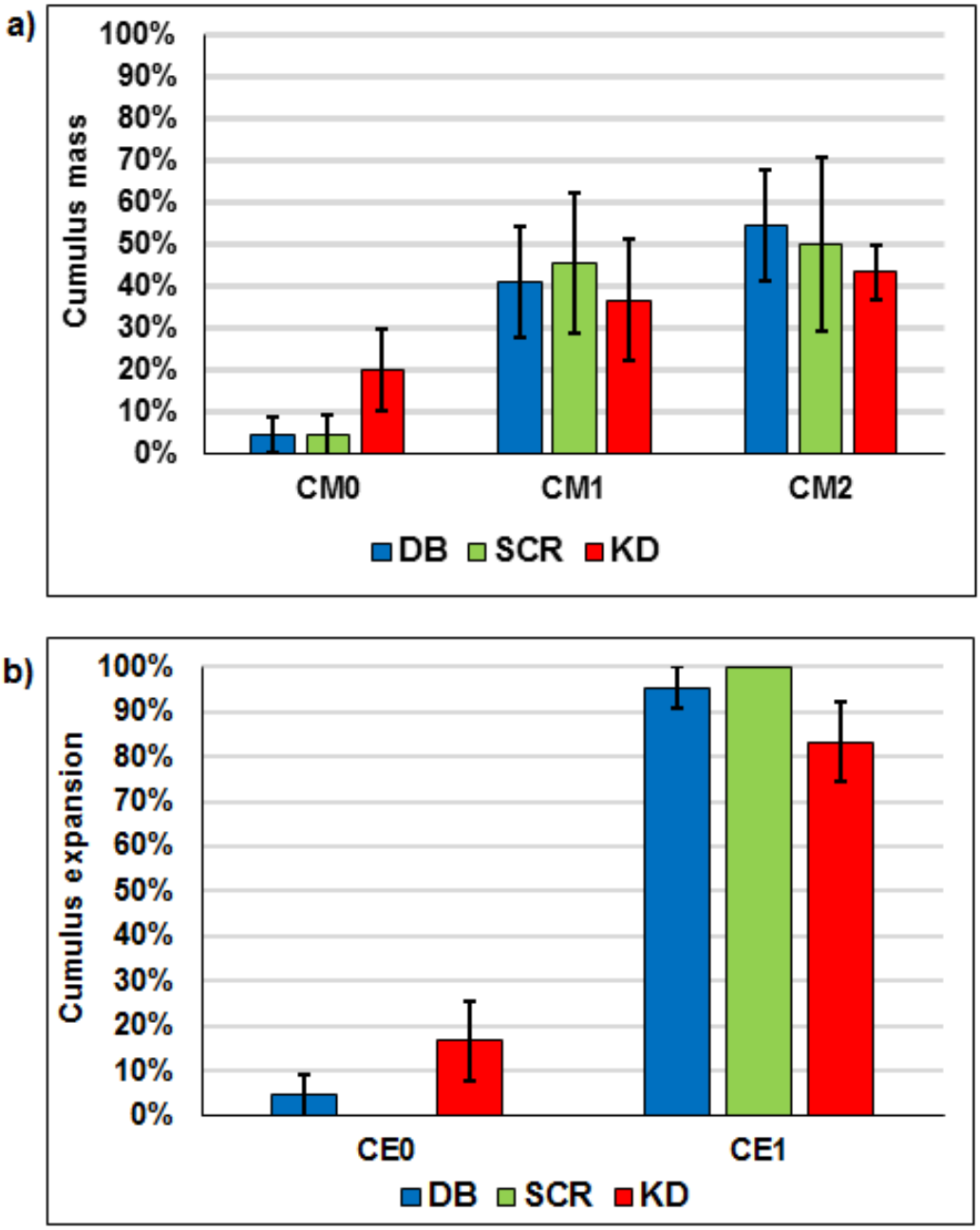

Figure 4.12 Effect of *PADI6* KD on **a)** cumulus coverage score and **b)** cumulus expansion score after IVM for 24 hours (KD), compared to duplex buffer (DB) and scrambled dsiRNA (SCR) control-injected COCs. Individual bars show the mean percentage of oocytes in each category ±SEM from 3 discrete cultures. n = 22-30 single injected oocytes for each group. No significant differences were observed ($p>0.05$).

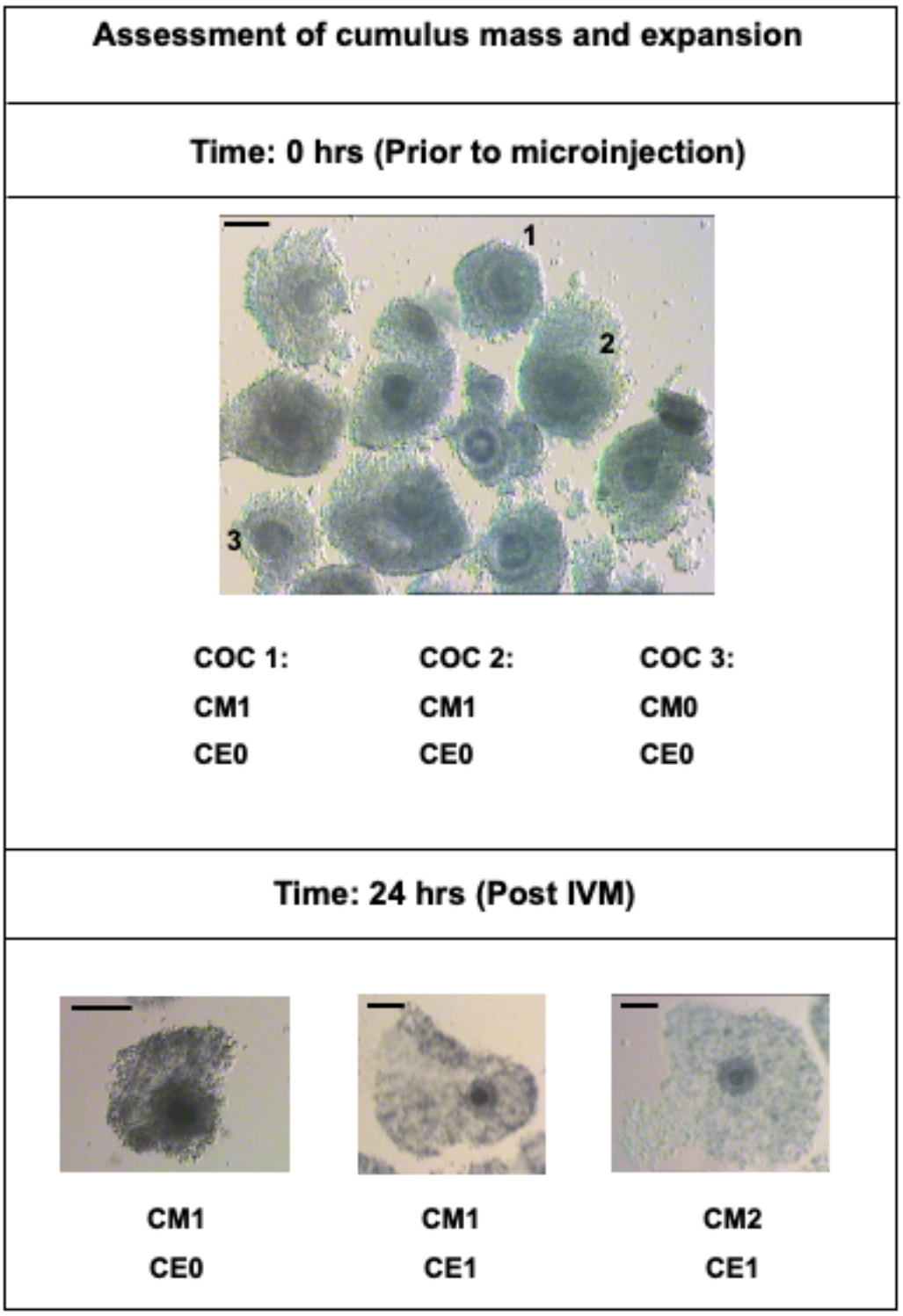

Figure 4.13 Examples of COCs prior to microinjection (Time: 0 hr) and after microinjection and IVM (Time: 24 hr). The designated cumulus mass (CM) and expansion (CE) scores are displayed for each oocyte. Oocytes were photographed at 40X magnification and scale bars represent 40 µm.

4.3.3.2 Evaluation of *PADI1-4* expression after *PADI6* KD

As discussed in Section 3.3.2, expression of other *PADI* family members in the bovine oocyte was very low or not detected. PCR experiments showed that there was faint expression of *PADI3* and *4* in the GV oocyte but could not detect expression of *PADI1* or *2* (Figure 3.5b). Following KD of *PADI6*, expression of *PADI1-4* was investigated to evaluate the effect of *PADI6* dsiRNAs on the expression of other *PADI* genes. To this end, real-time PCR was performed for *PADI1-4* in a subset of duplex buffer control (n=3) and *PADI6* dsiRNA mix KD samples (n=3). Multiple primers were tested for each *PADI* gene, but the majority of primer pairs failed to produce a Ct value in real-time PCR experiments due to the very low levels of expression. The Ct level of *PADI6* expression in control-injected bovine oocytes was 0.10-0.12 relative to housekeeping genes (Figure 3.5). However, data were collected for other *PADI* gene family members and the successful real-time PCR results are shown in Figure 4.14. Due to the high expression of *PADI6*, a split y axis was used in Figure 4.14 to enable visual comparison of *PADI* gene expression.

PADI1 gene expression was detected in both DB and KD MII oocytes at low levels, although *PADI1* was not detected in 1 of the KD MII oocytes so the n value was reduced to 2 oocytes. There was no difference in *PADI1* expression between DB and KD MII oocytes. For *PADI2,* expression was barely detected in MII oocytes with only 1 DB oocyte sample displaying a resultant Ct value from real-time PCR experiments. In concordance with Figure 3.5b, *PADI3* was detected in the bovine oocyte from both DB and KD injection groups. However, there was no difference in *PADI3* expression between DB and KD MII oocytes. Finally, *PADI4* was detected at very low levels in both DB and KD MII oocytes with at least 1 of the triplicate repeats failing to produce a Ct value for each sample. Further, there was no difference in *PADI4* expression between DB and KD MII oocytes. It was not possible to conduct meaningful statistical analyses on this data as a very low number of samples were analysed. However, coupled with the PCR results in Figure 3.5b, these results suggest that *PADI6* is the most highly expressed *PADI* gene in the bovine oocyte and that KD of *PADI6* is unlikely to affect the expression of other *PADI* family members. RNA-seq experiments in Chapter 5 may enable further investigation of *PADI* gene expression in the bovine oocyte.

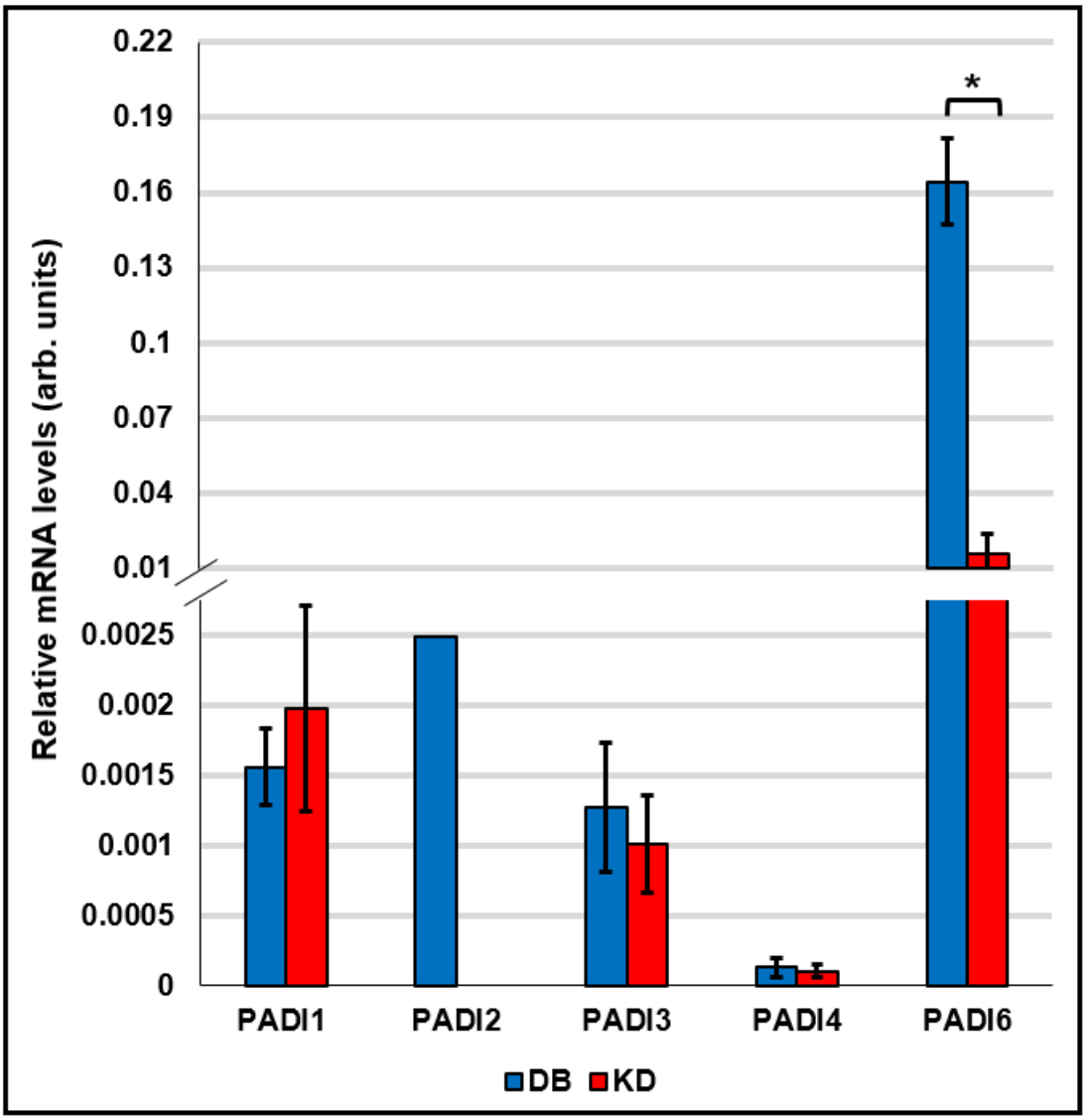

Figure 4.14 Real-time PCR quantification of *PADI1-4* in *PADI6*^{KD} MII oocytes, compared to DB control-injected MII oocytes (n = 3 individual oocytes). Expression of *PADI6* in *PADI6*^{KD} and DB oocytes is also shown for comparison (*$p<0.05$) – please note the split y axis as *PADI6* expression was much higher than the other *PADI* genes. The data were standardised against *GAPDH, H2A* and *YWHAZ* housekeeping mRNA levels. Individual bars show the mean ±SEM.

4.4 Discussion

The experimental work reported here demonstrated that it was possible to conduct targeted KD of *PADI6* gene expression in cumulus-enclosed bovine oocytes by microinjection of dsiRNA. Specifically, different dsiRNA species were evaluated and it was shown that KD of *PADI6* could be detected in individual oocytes relative to control-injected oocytes after 24 hours of IVM. In this thesis, RNAi was most effective when a mixture of 3 dsiRNAs targeting exon 9 of *PADI6* was injected into GV oocytes compared to DB and SCR-injected controls. Furthermore, microinjection of dsiRNAs targeting *PADI6* did not affect oocyte viability or maturation.

4.4.1 Optimisation of RNAi

Theoretically, dsiRNA species that are created using specialised design tools should KD the gene of interest. Meticulous experiments by Elbashir et al. (2001b) showed that certain alterations to siRNA sequences were inhibitory to RNAi whereas others were favourable. For example, a 3' overhang of 4-6 nucleotides was detrimental while 2 was more effective at achieving gene KD. Moreover, mismatches in the centre of target sequences inhibited RNAi-associated mRNA degradation. In contrast, Jackson et al. (2003) observed off-target effects where sequences shared just 11 contiguous nucleotides, equivalent to 50% siRNA sequence similarity. To avoid off-target effects, siRNA sequences were checked against the organism's genome using the BLAST tool (NCBI, USA). DsiRNAs were chosen that were not complimentary to other regions of the bovine genome in an attempt to avoid off-target binding. Nevertheless, understanding that off-target effects can occur with only 50% transcript similarity makes dsiRNA design difficult as short sequences of approximately 20 nucleotides are likely to be common and repeated in the genome. In view of this, an obvious concern is the targeting of other *PADI* family members as *PADI* sequences are conserved within species. The expression of other *PADI* genes was investigated to determine whether *PADI6* alone was ablated. This was also necessary to ensure that the phenotypic effects observed after *PADI6* KD were truly the result of *PADI6* function in the oocyte, and not that of another *PADI* gene. Expression of *PADI1-4* in bovine oocytes is unknown and earlier PCR experiments detected faint expression of *PADI3* and *4* in GV oocytes, but there was no expression of *PADI1* or *2* (Figure 3.5b). Despite this, all *PADI* genes were detected at very low levels in MII oocytes by real-time PCR but there were no significant differences in the expression of other *PADI*

genes between DB and KD MII oocytes as expression was very low. This suggests that *PADI6* dsiRNA KD was specific to *PADI6* gene and did not disrupt or increase the expression of *PADI1-4*. However, these results should be taken with caution. The 'n' values were low with only 3 individual oocytes analysed for each injection group. To ensure that all *PADI* genes are expressed in the bovine oocyte and that *PADI6* dsiRNA is specific to *PADI6*, more samples should be analysed. Furthermore, for *PADI2* and *PADI4* some of the real-time PCR samples or repeats failed to produce a Ct value. It may be beneficial to spend more time testing and optimising different primer pairs to see if a better amplification can be produced. Finally, analysis of oocyte gene expression using other sensitive methods such as RNA-seq (see Chapter 5) may be able to clarify some of the uncertainties surrounding the expression of other *PADI* genes in bovine oocytes and identify other off target effects in genes or associated gene pathways.

Multiple primers were tested to ascertain which pair would successfully identify KD of *PADI6* gene expression. Primers were designed to flank the dsiRNA target region so that if the desired amplicon forms, it shows that the mRNA has not been cleaved. Like siRNA design, many factors can prevent primer binding. The thermodynamic program for real-time PCR is fixed meaning that some primers will be subject to suboptimal conditions. Although primers were checked using the primer-BLAST tool (NCBI, USA), disturbances to melting temperature (Tm) could cause non-specific primer binding and result in false negative KD results. Primer sets A and C displayed large standard errors in the dsiRNA mix samples, perhaps due to the variable specificity of the primers. Further, due to time constraints, microinjection training, siRNA testing and primer optimisation was done simultaneously. As a result, 'n' values were sometimes as low as 2 single oocytes which was less than ideal. Further replicates are needed to aid interpretation.

4.4.2 Microinjection of dsiRNA as a vehicle for gene KD in GV oocytes

Since its discovery, RNAi is often favoured over the creation of genetic knockout animals for numerous reasons. Firstly, the gene of interest can be disturbed in specific cells as opposed to the whole organism. Secondly, if a gene is switched on and off numerous times in a cell, the effects of siRNA KD can be explored at different time points (Wianny and Zernicka-Goetz, 2000). As MEGs are transcribed primarily in the oocyte, RNAi can be used to KD the maternal influence on the embryo. Likewise, RNAi is transient so KD of genes can be observed for short durations and cells are often able to recover from gene KD. It was a concern to researchers that dsiRNA can trigger the interferon response in mammalian cells, which causes non-specific degradation of mRNA and widespread translational repression (Sledz et al., 2003). Fortunately, it is thought that oocytes do not possess this mechanism making RNAi a useful tool in oocytes (Stein et al., 2005).

Gene knockout is time-consuming and expensive compared to RNAi. It results in definite genetic ablation of the target gene, and protein, whereas dsiRNA KD is variable (Wu et al., 2004). This can be both favourable and disadvantageous. Variable gene KDs cause incomplete genetic ablation, creating a spectrum of severity of phenotypic effects. This is advantageous in development as gene knockout of MEGs often causes embryonic arrest, which obscures investigations into gene function. Conversely, the variability of RNAi means that when single oocytes are pooled together for data analysis, KD effects can be masked or do not show significance due to large standard errors of the mean. Gene KD may also show variability as it is possible that oocytes are at different stages of development at the time of injection. As described in Chapter 3, transcript abundances change profoundly throughout oocyte maturation, therefore targeted gene KD of different staged oocytes or embryos may have variable effects. It is known that more highly abundant transcripts are more efficiently targeted by RNAi so for bovine *PADI6,* GV oocytes pose a better target than oocytes transitioning to MII (Hu et al., 2004). Variability from microinjection of siRNA has been observed by other researchers. O'Meara et al. (2011) stated that ablation of their target gene was observed in the range of 0% to 97% KD. Furthermore, RNAi does not necessarily cause a reduction in the target protein so gene function may be unnoticed as a result. In this study, KD of PADI6 protein could not be confirmed as commercially available antibodies could not detect bovine PADI6 (Chapter 6, Experiment 1).

There are multiple methods for administering dsiRNA into a cell but of those most commonly used is microinjection. Microinjection is technically challenging and requires operator training to become proficiently capable at using the equipment. It is, however, repeatable and more consistent in terms of dose administration to each cell than techniques such as transfection. Liposome transfection requires enzymatic removal of the zona pellucida (Carballada et al., 2000) and peptide nanoparticle-mediated transfection requires denudation of oocytes (Jin et al., 2016), both of which are damaging to the developmental potential of the embryo and time consuming. As described in Section 4.3.1, the actual microinjected volume cannot be accurately measured and varies due to the resistance of each oocyte membrane to injection. Further, it is not possible to determine and standardise the exact amount of dsiRNA administered to each cell by transfection. In this study, COCs were microinjected with dsiRNA as opposed to denuded GV oocytes as has been used in earlier studies. COCs consist of 2 cell types, cumulus cells and the oocyte, therefore microinjection ensures that dsiRNA is administered directly to the oocyte and not to cumulus cells. PADI6 expression has been identified in the cumulus cells of bovine GV oocytes, albeit at a significantly lower level than in the oocyte (Peddinti et al., 2010), which suggests that *PADI6* dsiRNA would impact cumulus cell function and oocyte maturation.

Microinjection of COCs is more arduous but has many benefits over injecting denuded oocytes. Cumulus cells conceal the oocyte making it difficult to hold the complex in place and to ensure effective injection of dsiRNA into the oocyte. However, cumulus-intact oocytes have better developmental potential after microinjection (Thomas and Seidel, 1993). Denuded oocytes undergo premature spontaneous maturation as meiotic inhibition caused by cGMP from cumulus cells to the oocyte is removed and MPF becomes active (Norris et al., 2009). Also, spontaneous meiotic progression frequently has to be inhibited by the use of chemicals such as PDE inhibitors to effect gene KD. Further, to facilitate IVM and fertilisation following maturation, denuded oocytes are often co-cultured with cumulus cells to enable more efficient meiotic progression and to support sperm binding and entry into the oocyte (Fatehi et al., 2002). To this end, freshly harvested oocytes must be obtained again from abattoir-derived ovaries on the day following microinjection and the culture time extended by 24 hours. This is time consuming and costly. Finally, denudation of cumulus-enclosed GV oocytes leads to oolemma damage which has a significant negative impact on the oocyte's ability to survive in culture (Fatehi et al., 2002). It also disrupts the

exchange of regulatory factors between oocytes and cumulus cells via gap junctional communication resulting in suboptimal or premature oocyte maturation (FitzHarris and Baltz, 2006; Sela-Abramovich et al., 2006).

4.4.3 *PADI6* gene KD by microinjection of dsiRNA in bovine oocytes

After optimisation of the experimental parameters, an effective *PADI6* gene KD of 74±3.6% was achieved compared to control injected oocytes. As shown in Chapter 4, *PADI6* transcript abundance naturally decreases from GV to MII (Figure 3.6) – an expression pattern that may have disrupted detection of *PADI6* KD. Nevertheless, compared to control injected MII oocytes over the same time period, *PADI6* transcript abundance was considerably lower after microinjection with *PADI6* dsiRNA, confirming KD of gene expression (Figure 4.9). Oocyte viability after IVM was 70-80% across microinjection groups with no significant differences between control and KD injected oocytes ($p>0.05$). Viability staining was performed after microinjection and IVM therefore it may be that few GV oocytes were arrested prior to injection. Moreover, some cell death is expected from the GV to MII oocyte transition as oocytes that are not competent to resume meiosis will degenerate (Wu et al., 2000). Finally, it is most likely that the microinjection technique resulted in apoptosis as it inflicts mechanical stress on the oocyte and can involve prolonged exposure of oocytes to suboptimal temperatures and conditions. This is concordant with the literature where 20-22% cell death was observed after microinjection of bovine zygotes (Nganvongpanit et al., 2006; O'Meara et al., 2011).

Only MII oocytes that were viable after 24 hours of IVM were analysed for expression of *PADI6*. However, it could be that GV oocytes that remained viable but did not progress to MII had the highest *PADI6* gene KD. Although this was not measured, it is unlikely to be true as the rate of meiotic maturation was comparable to non-injected control oocytes ($p>0.05$), as shown in Figure 4.10c. This shows that our microinjection technique and KD of *PADI6* do not disrupt oocyte maturation *in vitro* to MII which validates the protocols developed here for use in further functional studies to test the impact of PADI6 on fertilisation and embryo development. There was no qualitative change in cumulus mass and expansion between different microinjection species, indicating that oocyte maturation was not affected by *PADI6* KD. These results are consistent with the literature that shows *Padi6* knockout mice display normal ovary and oocyte development, ovulation and fertilisation (Esposito et al., 2007).

4.4.4 Conclusion

This work has confirmed that it is possible to generate *PADI6* KD in bovine oocytes by targeted microinjection of gene-specific dsiRNAs. It has provided insight into the efficacy of dsiRNA and use of microinjection as a vehicle for RNAi in bovine cumulus-enclosed oocytes. This experimental series explored the use of different dsiRNA target sites within the same gene and different primer pairs for detection of gene KD. Furthermore, it evaluated the effect of *PADI6* KD on bovine oocyte meiotic maturation and cumulus morphology. In this study, it appears that *PADI6* KD over 24 hours does not affect the maturation potential of bovine oocytes *in vitro*. More extensive investigations of the function of *PADI6* KD on the maturation potential and transcriptome of the MII oocytes and their subsequent developmental competence are necessary to gain further insight into the contribution of *PADI6* to oocyte quality and embryo development in monovulatory species (Chapter 5 and Chapter 6).

Chapter 5 Impact of *PADI6* KD on the transcriptome of bovine oocytes during maturation *in vitro*

5.1 Introduction

It is understood that *Padi6* is necessary for the formation of CPLs in the oocyte and that CPLs provide a storage site for ribosomes and maternal transcripts until EGA (Bachvarova et al., 1981; Sternlicht and Schultz, 1981; Wright et al., 2003). The evidence for this comes from research in mice that showed that knockout of *Padi6* results in the production of oocytes lacking CPLs (Yurttas et al., 2008). This was accompanied by an increase in free ribosomes, supporting the notion that CPLs act as storage sites for ribosomal components. Moreover, *Padi6* knockout mouse embryos displayed reduced expression and aberrant localisation of ribosomal S6 protein and RNA polymerase II, which resulted in a global decrease in protein synthesis. Consequently, defective EGA in the Padi6 knockout mouse embryos prohibited embryonic development. This has also been observed in human arrested embryos that possess *PADI6* mutations (Xu et al., 2016). Not only has *Padi6* been implicated in the formation of CPLs but so have other SCMC members, *Nlrp5* and *Ooep* (Kim et al., 2010; Tashiro et al., 2010). Similar to observations with *Padi6*, genetic ablation of *Nlrp5* causes decreased mRNA and protein synthesis, measured by levels of the transcription requiring complex (TRC) (Tong et al., 2000). Together, this suggests that the SCMC is required for correct formation and functioning of CPLs.

SCMC genes have been implicated in a variety of imprinting disorders in which the disease mechanism is unknown (Begemann et al., 2018). Recently, studies have described that ablation of *Nlrp2* in mice causes aberrant localisation of DNMT1 protein, and reduced levels of *Nlrp7* alters DNA methylation via interactions with chromatin-binding factor, YY1 (Mahadevan et al., 2017; Mahadevan et al., 2014). This is the first study to show that experimental ablation of an SCMC member leads to disruption of epigenetic regulators. SCMC proteins are mainly cytoplasmic and are therefore unlikely to be directly involved in imprinting mechanisms. However, it may be that the SCMC prevents the mislocalisation, degradation or depletion of maternal effect transcripts. As the SCMC is associated with CPLs, there is potential for transcriptional regulation of epigenetic regulators that could indirectly affect genomic imprinting. In this regard, KHDC3L and OOEP have RNA-binding abilities that may

enable the SCMC to sequester maternal transcripts at CPLs (Pierre et al., 2007; Wang et al., 2012a). RNA-masking protein, MSY2, also localises to CPLs and may protect maternal mRNAs from degradation during oocyte growth (Liu et al., 2017). Finally, the storage of ribosomes at CPLs could provide a site for subcellular compartmentalisation of post-transcriptional modifications and protein synthesis (Bebbere et al., 2016). The dynamic reorganisations of CPLs at fertilisation, compaction and blastocyst formation and may coordinate the release of sequestered factors at specific time points to allow for correct EGA (Capco and McGaughey, 1986). This theory would support the reduction in transcription, translation, aberrant localisation of proteins and defective EGA that was observed upon disruption of the supra-molecular SCMC complex. Taken together, this research suggests that there is a tight relationship between CPLs, SCMC and maternal transcripts that indirectly impacts the epigenetic status of the oocyte.

Following the KD of bovine *PADI6* gene expression as described in Chapter 4, it was important to look at the impact of *PADI6* depletion on the transcriptome of the MII oocyte. Candidate genes were chosen for analysis by real-time PCR using 2 arrays designed by Huntriss, J. and Picton, H.M. (unpublished): 1) oocyte quality marker array and 2) epigenetic regulator and imprinted gene array. Firstly, so called “oocyte quality markers” were chosen to assess whether KD of *PADI6* gene expression caused widespread disruption to the transcriptome. Such genes were chosen because of their significant functions in the oocyte, with each of the genes on the array being essential for oocyte developmental competence. Hence the expression pattern observed by using the gene array can be utilised as a measure of oocyte competence in experimentally manipulated oocytes by comparison to the expression observed in control oocytes. A comprehensive list and definitions of the genes to be investigated here is detailed in Table 5.2. For example, *Aurka* is responsible for regulating meiotic maturation, while *Bdnf* appears to regulate both meiotic and cytoplasmic maturation (Anderson et al., 2010; Martins da Silva et al., 2005; Saskova et al., 2008). *Bmp15* and *Gdf9* are well described growth factors (see Section 1.2.3) that are secreted from the oocyte to enhance cumulus expansion for progression to and beyond the secondary follicle stage (Su et al., 2004). Both are associated with oocyte quality (Sanfins et al., 2018). *Bmp2* mediates folliculogenesis, prevents premature luteinisation and has been shown to be an indicator of oocyte quality in humans (Demiray et al., 2017). *Figla, Lhx8, Nobox* and *Sohlh2* are master transcriptional regulators that drive folliculogenesis by controlling the expression of oocyte-specific genes such as *Dppa3, Oct4, Padi6* and *Nlrp* family genes (Choi et al.,

2008a; Choi et al., 2008b; Pangas et al., 2006; Rajkovic et al., 2004; Soyal et al., 2000). *Gtsf1* functions in mRNA processing and spindle organisation and is observed to decrease in abundance with maternal age, suggesting it to be a marker of oocyte quality (Huntriss et al., 2017; Trapphoff et al., 2016). Histone *H1foo* is necessary for meiotic maturation and early embryo development by regulating chromatin condensation (McGraw et al., 2006; Yun et al., 2015). *Hsf1* and *Zar1* are both essential for EGA and early embryo development (Metchat et al., 2009; Wu et al., 2003). *Prdx1 and 2* are antioxidant enzymes that function during meiotic maturation where they coordinate the spindle apparatus, chromosomes organisation and polarisation (Jeon et al., 2017). *Izumo1r* is the sperm receptor that is transiently expressed on the surface of mature MII oocytes that is essential for fertilisation (Bianchi et al., 2014). Finally, *Zp1-3* are responsible for establishing the functional zona pellucida which facilitates sperm binding, prevents polyspermy and protects the developing embryo (Conner et al., 2005). In summary, all of these genes were labelled as markers of oocyte quality because disruption to their expression would negatively impact on the developmental competence of the oocyte (i.e. oocyte quality) and embryo quality. Global changes to these genes following gene KD would suggest a role for *PADI6* in oocyte maturation and quality.

Secondly, imprinted genes and epigenetic regulators were examined to look for more specific effects of *PADI6* on epigenetic mechanisms. As with the oocyte quality marker array, genes on the epigenetic array were chosen due to their known imprinting status or involvement in epigenetic mechanisms. A comprehensive list of genes that were analysed is detailed in Table 5.3. Imprinted genes included *ASCL2, H19, IGF2, IGF2R, MEST, MIMT1, NAP1L5, NNAT, PEG3, PEG10, PHLDA2, PLAGL1, SNRPN, USP29* and *XIST*. Similarly, epigenetic regulators that were analysed included DNA methyltransferases, *DNMT1, -3a* and *-3b*; histone modifiers, *EHMT2, ELP3, HAT1, KAT5, KDM1B* and *PRMT5*; methylcytosine dioxygenases, *TET1, 2 and 3*; key imprinting regulators, *TRIM28* and *ZFP57*; and SCMC genes, *KHDC3L, NLRP2 and 5, OOEP, PADI6* and *TLE6.* As described previously, the SCMC is likely to have an indirect involvement in establishing or maintaining epigenetic marks due to the phenotypic imprinting abnormalities in SCMC-related diseases. By dissecting the effects of *PADI6* gene KD on the transcriptome of the oocyte, it may expose candidate transcripts that are regulated, in part, by *PADI6* and provide a link between the SCMC and epigenetic pathways in the oocyte.

5.1.1 Aims and objectives

The aims of this study were to observe the effects of KD of the bovine *PADI6* gene by RNAi in cumulus-enclosed GV oocytes on the transcriptome of denuded MII oocytes. To this end, the oocytes with the highest *PADI6* KD that were generated in Chapter 4 were analysed by 2 methods:

Firstly, a real-time PCR approach was used, comparing *PADI6* KD oocytes to control-injected MII oocytes. The real-time PCR arrays featured 23 key oocyte quality genes and 46 imprinted genes and epigenetic regulators that were used initially to screen a relatively large number of candidate genes for the effects of gene KD relative to controls. Candidate genes that were highlighted as of interest by virtue of expression change occurring in the initial screen were then subject to more in-depth real-time PCR analysis with higher 'n' values to ascertain significant changes in transcripts after *PADI6* KD.

Secondly, RNA-seq was carried out to look at the widespread impact of *PADI6* gene KD across the entire oocyte transcriptome in MII oocytes, compared to control-injected MII oocytes. Microinjection followed by Smart-seq2 cDNA synthesis was performed as described previously, before sending the amplified cDNA for RNA-seq. Bioinformatic analysis was used to characterise differentially expressed genes (DEGs) between injection groups by performing gene ontology analysis and functional annotation of the candidate genes.

5.2 Materials and methods

Work conducted in this chapter analysed the same Smart-seq2 cDNA libraries that were generated in Chapter 4, Section 4.3.3. *PADI6* KD oocytes were analysed extensively by real-time PCR and RNA-seq alongside the DB and SCR-injected control oocytes that were generated in the same experiments as shown in Figure 4.9. In summary cumulus-enclosed GV oocytes were subject to microinjection with duplex buffer (DB), scrambled dsiRNA (SCR) or were injected with a mix of dsiRNAs against *PADI6* (KD) as defined in Section 4.2 – referred to as *PADI6*^{KD} oocytes in this thesis from this point onwards. For each injection species, oocytes were cultured in groups of 10-20 in 35 mm NUNC™ IVF Petri dishes containing 10 µl drops of fresh IVM media/COC under mineral oil at 39ºC, 5% CO_2 for 24 hours. After 24 hours in IVM media, oocytes were processed as detailed in Section 2.4 and analysed by real-time PCR for KD of *PADI6* transcripts. The oocytes with the highest KD of *PADI6* gene expression relative to control-injected oocytes (shown in Figure 4.9) were analysed in this chapter to observe the effects of *PADI6* gene KD by RNAi in cumulus-enclosed GV oocytes on the transcriptome of denuded MII oocytes.

5.2.1 Molecular analysis of bovine *PADI6*^{KD} oocytes

A number of different real-time PCR experiments were conducted to investigate the effects of *PADI6* gene KD on gene expression compared to control-injected oocytes. 2 real-time PCR arrays were designed by Huntriss, J. and Picton, H.M. (unpublished) to screen for changes in the expression of 1) oocyte quality markers (Section 5.2.1.1), and 2) imprinted genes and epigenetic regulators (Section 5.2.1.2). The initial screens that were performed were intended as a first step to identify potential targets from the broad selection of candidate genes that were featured on the arrays. It was not practical to perform triplicate measurements for each sample using such a large number of genes. To overcome these limitations and produce quality data, once potential candidate targets were identified in the initial screens, further real-time PCR experiments were conducted using these targets in triplicate measurements on all of the control and KD samples from Figure 4.9 (Section 5.2.1.3). The real-time experimental designs are detailed in the following sections:

5.2.1.1 Oocyte quality marker real-time PCR array

To assess the effects of *PADI6* KD on the oocyte, a bovine real-time PCR array (RealTimePrimers.com, USA) containing 23 key genes for oocyte function, termed here as oocyte quality markers, as well as housekeeping genes was used (Table 5.2). Primer sequences are listed in Appendix III - Table III.III. The PCR assays for oocyte genes *MSX1, SEBOX* and *SOHLH1* were also included in the array but were not successful in amplifying a gene product. The master mix composition is detailed in Table 5.1. Primer pairs were diluted to a working concentration of 0.4 µM and 5 µl of 0.4 µM primers was added to each well (2 µM) to give a final volume of 15 µl per well. Real-time PCR was performed according to the thermocycler program in Table 2.16. Due to the high number of genes that were screened in the initial screening phase, only 1 real-time PCR measurement was performed per sample.

Table 5.1 Bovine real-time array master mix (1x)

Component	Volume (µl)
SYBR green PCR master mix Applied Biosystems 4309155	7.5
Nuclease-free water	1.5
Smart-seq2 prepared cDNA (Section 2.4)	1
Total volume	**10**

Table 5.2 The Oocyte Quality Array. List of genes included in the bovine real-time PCR array for oocyte quality markers. Primer sequences can be found in Appendix III -Table III.III. Housekeeping genes are highlighted in yellow.

Gene	
AURKA	Aurora kinase A
BDNF	Brain-derived neurotrophic factor
BMP15	Bone morphogenetic protein 15
BMP2	Bone morphogenetic protein 2
FIGLA	Factor in the germline alpha
GAPDH	Glyceraldehyde 3-phosphate dehydrogenase
GDF9	Growth differentiation factor 9
GTSF1	Gametocyte specific factor 1
H1FOO	H1 histone family, member o, oocyte-specific
H2A	Histone H2A
HSF1	Heat shock factor 1
IZUMO1R	IZUMO1 receptor
LHX8	LIM homeobox 8
NOBOX	Newborn ovary homeobox
OCT4	POU class 5 homeobox 1
PRDX1	Peroxiredoxin 1
PRDX2	Peroxiredoxin 2
SOHLH2	Spermatogenesis and oogenesis specific basic helix-loop-helix 2
YWHAZ	Tyrosine 3-monooxygenase/tryptophan 5-monoxygenase activation protein, zeta
ZAR1	Zygote arrest 1
ZP1	Zona pellucida glycoprotein 1
ZP2	Zona pellucida glycoprotein 2
ZP3	Zona pellucida glycoprotein 3

5.2.1.2 Imprinted genes and epigenetic regulators real-time PCR array

The second bovine real-time PCR array designed by Huntriss, J. and Picton, H.M. (unpublished) contained 46 imprinted genes and epigenetic regulators to look at the effects of *PADI6* KD on imprinting mechanisms (Table 5.3). Primer sequences are listed in Appendix III - Table III.IV *DNMT3L, MEG3, MEG9*, *MSK2, SETD7* and *TSSC4* were also included in the array but were not successful in amplifying a gene product. Due to the large number of genes screened in this array, samples were limited to 6-7 individual oocytes from either KD or the control DB injection groups. SCR-injected oocytes were not included in this initial analysis. Duplicate repeats of real-time PCR were performed for each oocyte. Real-time PCR was performed as described for the oocyte quality marker array.

Table 5.3 List of genes included in the bovine real-time PCR array for imprinted genes and epigenetic regulators. Primer sequences can be found in Appendix III - Table III.III. Housekeeping genes are highlighted in yellow.

Gene	
ASCL2	Achaete-scute family bHLH transcription factor
B2M	Beta-2-microglobulin
DNMT1	DNA methyltransferase 1
DNMT3A	DNA methyltransferase 3A
DNMT3B	DNA methyltransferase 3B
EHMT2	Euchromatic histone-lysine N-methyltransferase 2
ELP3	Elongator acetyltransferase complex subunit 3
GAPDH	Glyceraldehyde 3-phosphate dehydrogenase
H19	H19 (imprinted; maternally expressed transcript)
H2A	Histone H2A
HAT1	Histone acetyltransferase 1
HPRT1	Hypoxanthine guanine phosphoribosyl transferase 1
IGF2	Insulin-like growth factor 2
IGF2R	Insulin-like growth factor 2
KAT5	Lysine acetyltransferase 5
KDM1B	Lysine demethylase 1B
KHDC3L	KH domain containing 3-like
MEST	Mesoderm specific transcript
MIMT1	MER1 repeat containing imprinted transcript 1
NAP1L5	Nucleosome assembly protein 1-like 5
NLRP2	NLR family, pyrin domain containing 2
NLRP5	NLR family, pyrin domain containing 5
NNAT	Neuronatin
OOEP	Oocyte expressed protein
PADI6	Peptidylarginine deiminase 6
PEG10	Paternally expressed gene 10
PEG3	Paternally expressed gene 3
PGK1	Phosphoglycerate kinase 1
PHLDA2	Pleckstrin homology domain, family A, member 2
PLAGL1	Pleiomorphic adenoma gene-like 1
PRMT5	Protein arginine methyltransferase 5
SNRPN	Small nuclear ribonucleoprotein polypeptide N
TET1	Tet methylcytosine dioxygenase 1
TET2	Tet methylcytosine dioxygenase 2
TET3	Tet methylcytosine dioxygenase 3
TLE6	Transducer like enhancer of split 6
TRIM28	Tripartite motif containing 28
USP29	Ubiquitin specific peptidase 29
XIST	X (inactive)-specific transcript
YWHAZ	Tyrosine 3-monooxygenase/tryptophan 5-monoxygenase activation protein, zeta
ZFP57	Zinc finger protein 57

5.2.1.3 In-depth real-time PCR experiments

After initial screening using either the i) oocyte quality marker array or ii) the imprinted gene and epigenetic regulator array, a second set of in-depth real-time PCR experiments were conducted to allow properly controlled assessment of the candidate gene transcripts that were identified in the initial screening. For example, the number of samples analysed using the array in the initial screen was limited to 6-7 individual oocytes due to the large number of genes that were screened, SCR-injected oocytes were not included in the screen and triplicate measurements for each sample were not performed. To resolve these limitations, follow-up real-time PCR was conducted as detailed in Section 2.7 compared to 3 housekeeping genes, *GAPDH, H2A* and *YWHAZ*. SCR-injected oocytes were now included in the in-depth analysis so all of the samples from Figure 4.9 (DB: n = 11; SCR: n = 10; KD: n = 20) were analysed by real-time PCR. The samples were analysed in triplicate. The genes that were selected for these in-depth real-time PCR experiments were: *DNMT1, DNMT3A, DNMT3B, DPPA3, FIGLA, GNAS, HAT1, KDM1, KHDC3L, MEST, MTHFR, NLRP2, NLRP5, NLRP7, OOEP, PHLDA2, PLAGL1, PRMT5, SETDB1, STAT3, TET1, TET2, TET3, TLE6, TRIM28* and *ZFP57*. Primer sequences are listed in Appendix III - Table III.II.

5.2.2 Statistical analysis for PCR evaluations

The data were tested for normality before analysis using the D'Agostino-Pearson test. Real-time data for each gene was compared to the geometric mean of housekeeping genes, *GAPDH, H2A* and *YWHAZ* for the oocyte quality marker array and in-depth real-time PCR analysis, and *GAPDH, H2A, HPRT1, PGK1* and *YWHAZ* for the imprinted gene and epigenetic regulator array, as detailed in Section 2.7. Data containing '0' was transformed by $\sqrt{(x + 0.5)}$. Statistical analyses were performed on transformed data. One-way ANOVA or unpaired t-test was used for normally distributed data. p values of <0.05 were considered to be statistically significant. Untransformed data were plotted. Values presented for real-time data are arithmetic means ±SEM for the number of observations shown.

5.2.3 RNA-seq in *PADI6*^{KD} oocytes

Of the 20 oocytes with high *PADI6* KD from Chapter 4, 6 oocytes were chosen for RNA-seq alongside 6 DB and 6 SCR control-injected oocytes. Due to the high cost of RNA-seq, only 6 oocytes with the highest *PADI6* KD were able to be assessed along with the controls. RNA from single oocytes must be converted to cDNA and subsequently amplified to provide enough material for sequencing as detailed in Section 2.4 (Picelli et al., 2014). RNA-seq was conducted by the Leeds Institute of Molecular Medicine Next Generation Sequencing Facility at the University of Leeds. In summary, the RNA-seq methodology was as follows: 15 µl of cDNA was quantified using Quant-iT™ PicoGreenTM dsDNA Assay Kit (ThermoFisher P11496). Sequencing libraries were made from 1 ng of the cDNA by using Nextera XT DNA library Preparation Kit from Illumina (Illumina FC-131-1096). Library performance was checked on Agilent 4200 TapeStation System followed by PicoGreen quantification. Samples were pooled in equimolar ratios to ensure that each library was evenly represented. The final pool was sequenced on a lane on Hiseq® 3000 Sequencing System (SY-401-3001). FastQ conversion was done by bcl2fastq Conversion Software v2.20 by Illumina.

5.2.3.1 RNA-seq data processing

RNA-seq data were processed by Dr David Iles from Omics Ltd, according to the validated in-house bioinformatic pipeline using R. Raw RNA-seq reads were first subject to quality control using FASTQC. The paired-end input files were compared to ensure proper pairing of reads. The reads were filtered by minimum length of 20 bases, trimmed of sequencing adaptors using Cutadapt (Marcel, 2011) and TrimGalore! The data were mapped to the bosTau8 reference genome using hierarchical indexing for spliced alignment of transcripts 2 (HISAT2), allowing only concordant alignments according to the paired-end constraints (Kim et al., 2015a). The sequence alignment map (SAM) file was converted into a binary alignment map (BAM) file and sorted by genomic position using samtools (Li et al., 2009). Picard MarkDuplicates was applied to identify duplicate reads in the dataset. Duplication ranged from 15-40% and all duplicates were excluded from the dataset. featureCounts was used to determine the total read counts for each exon, which was then summarised by gene ID using bovine reference genome bosTau8 annotated with human transcript entries (Liao et al., 2014). To facilitate comparison between

control and *PADI6* KD groups, gene expression in the SCR control group was subtracted from both the DB and *PADI6* KD groups. This was done to remove any off-target effects caused by injection of an oligonucleotide sequence into the oocyte. Subsequently, topTags in edgeR was used to identify differentially expressed tags between DB control and *PADI6* KD groups (Robinson et al., 2010).

The BAM file was converted to a bedGraph format to determine the genome wide coverage of features and scaled by a constant factor for normalising coverage using bedtools (Quinlan, 2014). bedGraphtoBigWig was used to enable visualisation of the data as tracks in the UCSC Genome Browser server (https://genome.ucsc.edu/). Multidimensional scaling (MDS) plots were generated using R. MDS plots arrange the samples according to the pairwise 'distances' that are determined bioinformatically in a 2-dimensional space where each dimension represents similarity/dissimilarity between samples. Therefore, MDS plots enable visualisation of the level of similarity of individual samples of a dataset i.e. samples with high similarity are seen to cluster (Loraine et al., 2015). Figure 5.1 shows an overview of the workflow that was conducted for processing the RNA-seq data. Finally, Ingenuity Pathway Analysis (IPA) was used to analyse and interpret RNA-seq data. IPA provided insight into causal networks, interactions and cellular phenotypes within the dataset and enabled a deeper understanding of the impact of KD of *PADI6* on the MII oocyte.

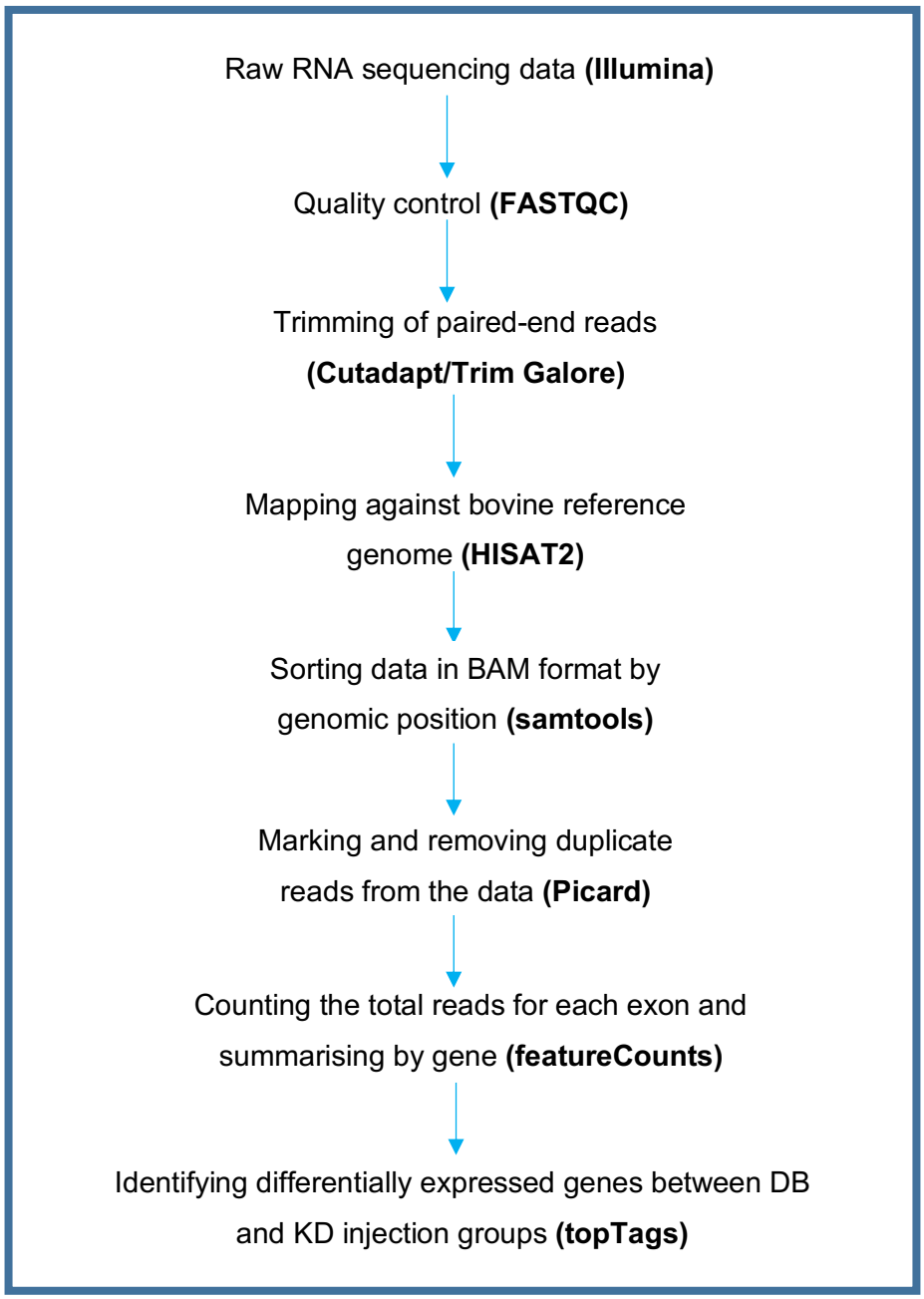

Figure 5.1. Overview of the workflow that was conducted for RNA-seq data analysis.

5.3 Results

5.3.1 Molecular analysis of oocyte quality marker genes in bovine *PADI6*^{KD} oocytes using real-time PCR arrays

Firstly, the real-time PCR array for oocyte quality markers was used to investigate changes to the transcription of key oocyte genes after *PADI6* KD. This was necessary to determine whether KD of *PADI6* causes widespread disruption to the oocyte, displayed by perturbations of multiple quality markers. To this end, DB, SCR and KD samples from Figure 4.9 were analysed. The results are shown in Figure 5.2. It was observed that 2 out of 20 oocyte quality marker genes were significantly different between the 3 injection groups: *PRDX1* and *ZP1* ($p<0.05$). The remaining 18 genes were not significantly different between *PADI6*^{KD} and DB and SCR control MII oocytes. However, *FIGLA* and *IZUMO1R* were increased in *PADI6*^{KD} oocytes ($p=0.086$ and 0.067, respectively) compared to DB-injected oocytes. Moreover, *H1Foo* and *BMP15* were highly abundant transcripts and showed trends towards increased expression in *PADI6*^{KD} oocytes compared to DB-injected oocytes but the results were not significant ($p=0.23$ and 0.14, respectively). Enlarged graphs for *PRDX1* and *ZP1* from Figure 5.2 are shown in Figure 5.3a and b. Relative transcript abundance of *PRDX1* was significantly reduced by 42% in *PADI6*^{KD} MII oocytes compared to SCR injected oocytes ($p<0.05$) but not compared to DB injected oocytes ($p>0.05$) (Figure 5.3a). Moreover, gene expression of *ZP1* was reduced by 41% in *PADI6*^{KD} MII oocytes compared to control oocytes ($p<0.05$) (Figure 5.3b). No significant differences in *ZP1* expression were observed between duplex buffer and SCR dsiRNA injected oocytes ($p>0.05$).

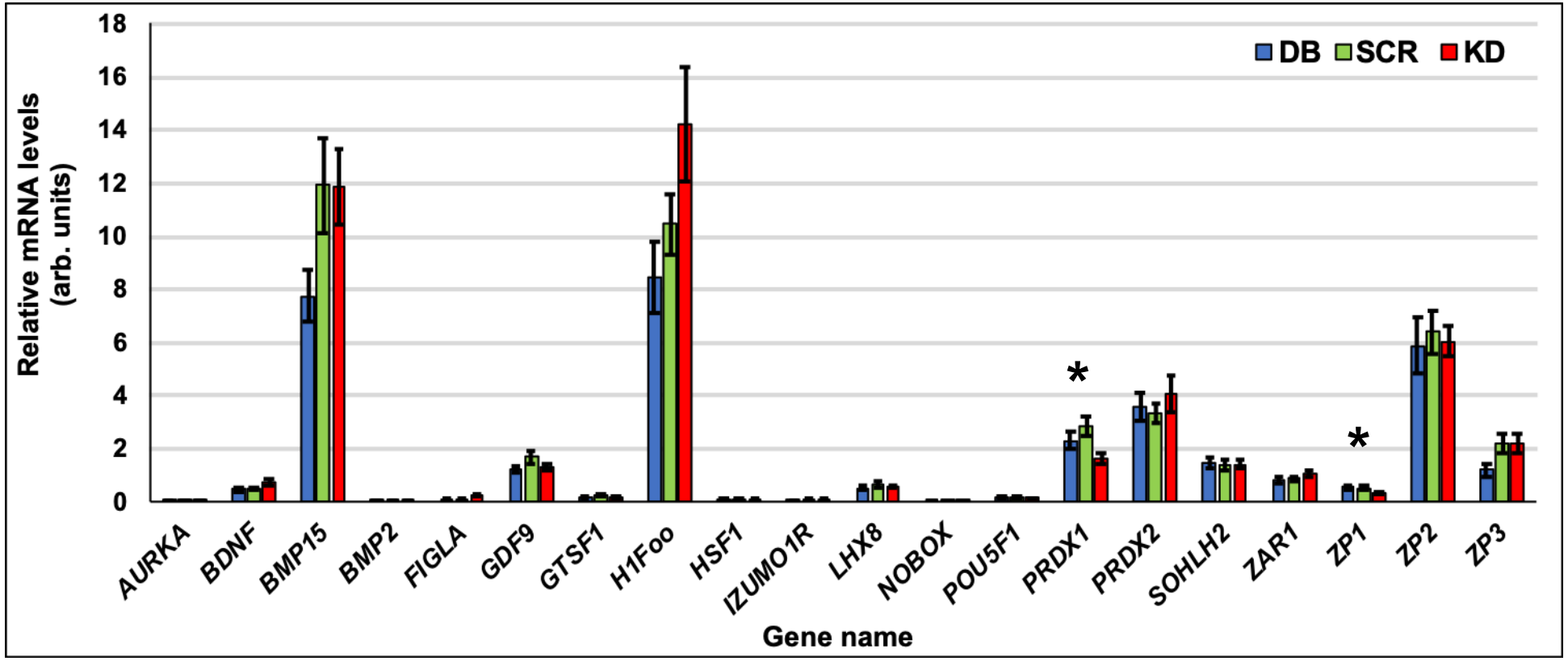

Figure 5.2. Real-time PCR quantification of the effect of *PADI6* KD on the expression of oocyte quality markers in high *PADI6* KD oocytes (KD (red): n = 20), shown together with duplex buffer (DB (blue): n = 11) and scrambled dsiRNA (SCR (green): n = 10) control-injected oocytes. The data were standardised against *GAPDH, H2A* and *YWHAZ* housekeeping mRNA levels. Individual bars show the mean ±SEM. Due to the number of genes screened triplicate repeats were not performed. *PADI6* KD oocytes exhibited a statistically significant difference for *PRDX1* and *ZP1* mRNA levels (* = $p<0.05$) compared to control-injected oocytes. No other significant differences were observed ($p>0.05$).

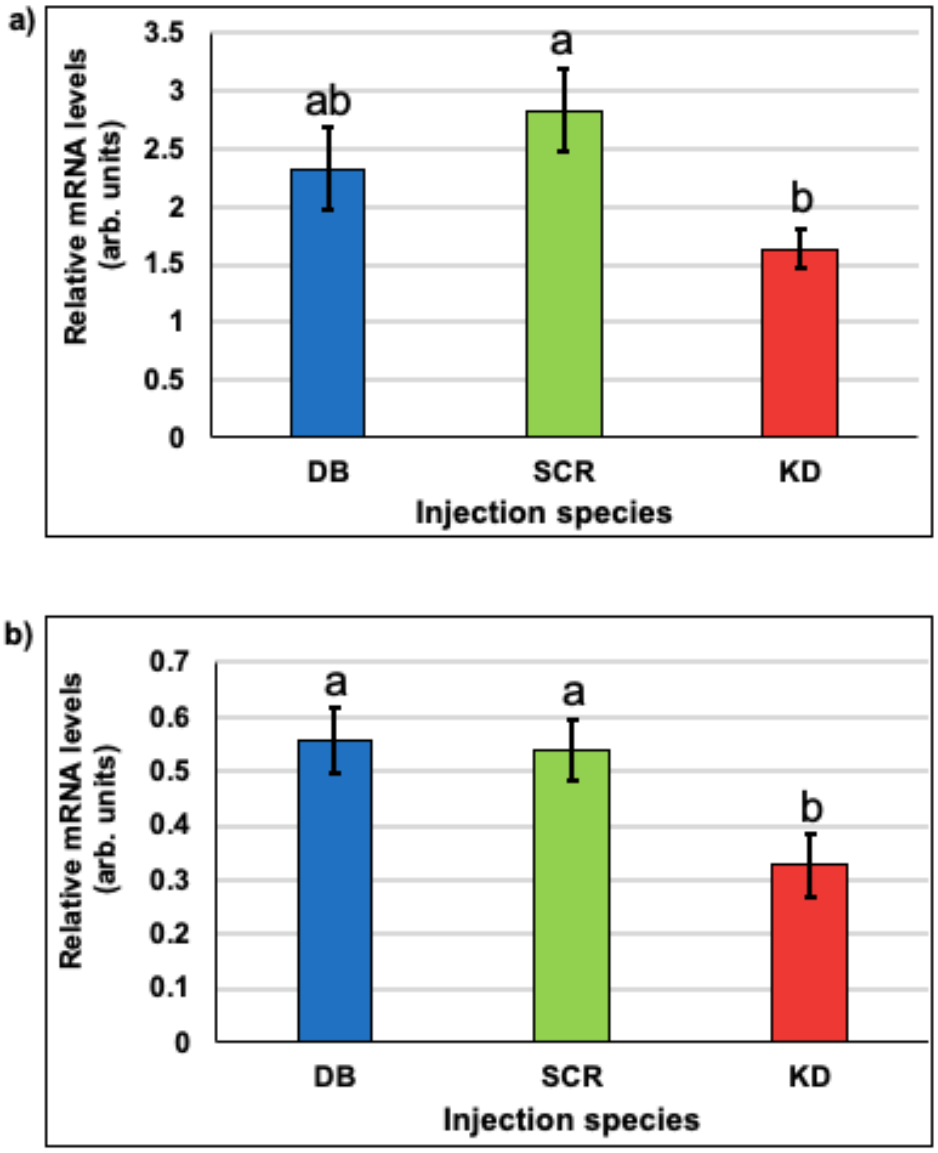

Figure 5.3. Enlarged figures of the initial screen in Figure 5.2 displaying real-time PCR quantification of the effect of *PADI6* KD on the expression of **a)** *PRDX1 and* **b)** *ZP1* in high *PADI6* KD oocytes (KD: n = 20), shown together with duplex buffer (DB: n = 11) and scrambled dsiRNA (SCR: n = 10) control-injected oocytes. The data were standardised against *GAPDH, H2A* and *YWHAZ* housekeeping mRNA levels. Individual bars show the mean ±SEM. Different letters on the graph were used to denote significant differences between means ($p<0.05$). Please note the different scales on the graphs.

5.3.2 Molecular analysis of imprinted genes and epigenetic regulator genes in bovine *PADI6*^{KD} oocytes using real-time PCR arrays

Following this, the real-time PCR array for imprinted genes and epigenetic regulators was used to screen for candidate genes after *PADI6* gene KD (Figure 5.4). Due to the large number of genes that were screened, the number of oocytes analysed for each injection group was low, duplicate repeats were performed rather than triplicate repeats, and SCR-injected samples were not included initially. SCR-injected samples were included in the in-depth real-time PCR analyses in Section 5.3.3. Unpaired t-test was used to determine if the means of the 2 groups were statistically different ($p<0.05$). The results showed that of 35 genes tested, 3 genes were significantly differentially expressed between duplex buffer control and *PADI6*^{KD} MII oocytes: *DNMT3B, OOEP* and *PRMT5*. Enlarged graphs for these genes from Figure 5.4 can be found in Figure 5.5a-c. All 3 genes increased in transcript abundance after *PADI6* KD. *DNMT3B* and *PRMT5* increased by 1.7-fold and *PRMT5* by 1.5-fold in *PADI6*^{KD} MII oocytes compared to DB control oocytes. Other genes did not show significant differences between KD and control oocytes using this array, including *PADI6* ($p=0.27$). However, *DNMT1, KHDC3L* and *NLRP2* showed trends towards increased expression in *PADI6*^{KD} oocytes compared to DB-injected oocytes ($p=0.078$, 0.051 and 0.069, respectively) (Figure 5.4). Moreover, Figure 5.4 showed that *TRIM28* was a highly prominent transcript in the MII oocyte.

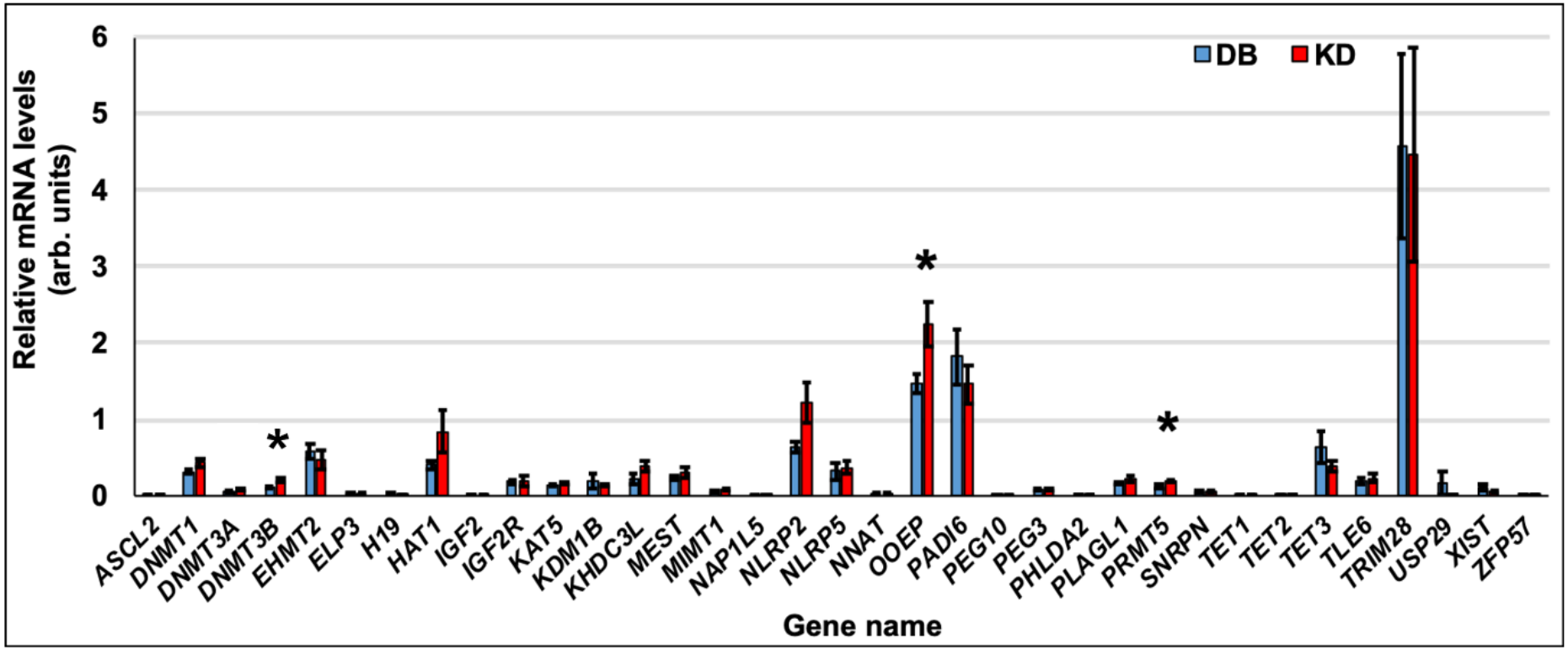

Figure 5.4. Real-time PCR quantification of the effect of *PADI6* KD on the expression of imprinted genes and epigenetic regulators in high *PADI6* KD oocytes (n = 7), shown together with DB (n = 6) control-injected oocytes. The data were standardised against *GAPDH, H2A, HPRT1, PGK1* and *YWHAZ* housekeeping mRNA levels. Individual bars show the mean ±SEM. Duplicate repeats were performed. *PADI6* KD oocytes exhibited a statistically significant difference for *DNMT3A, OOEP* and *PRMT5* mRNA levels (* = $p<0.05$) compared to control-injected oocytes. No other significant differences were observed ($p>0.05$).

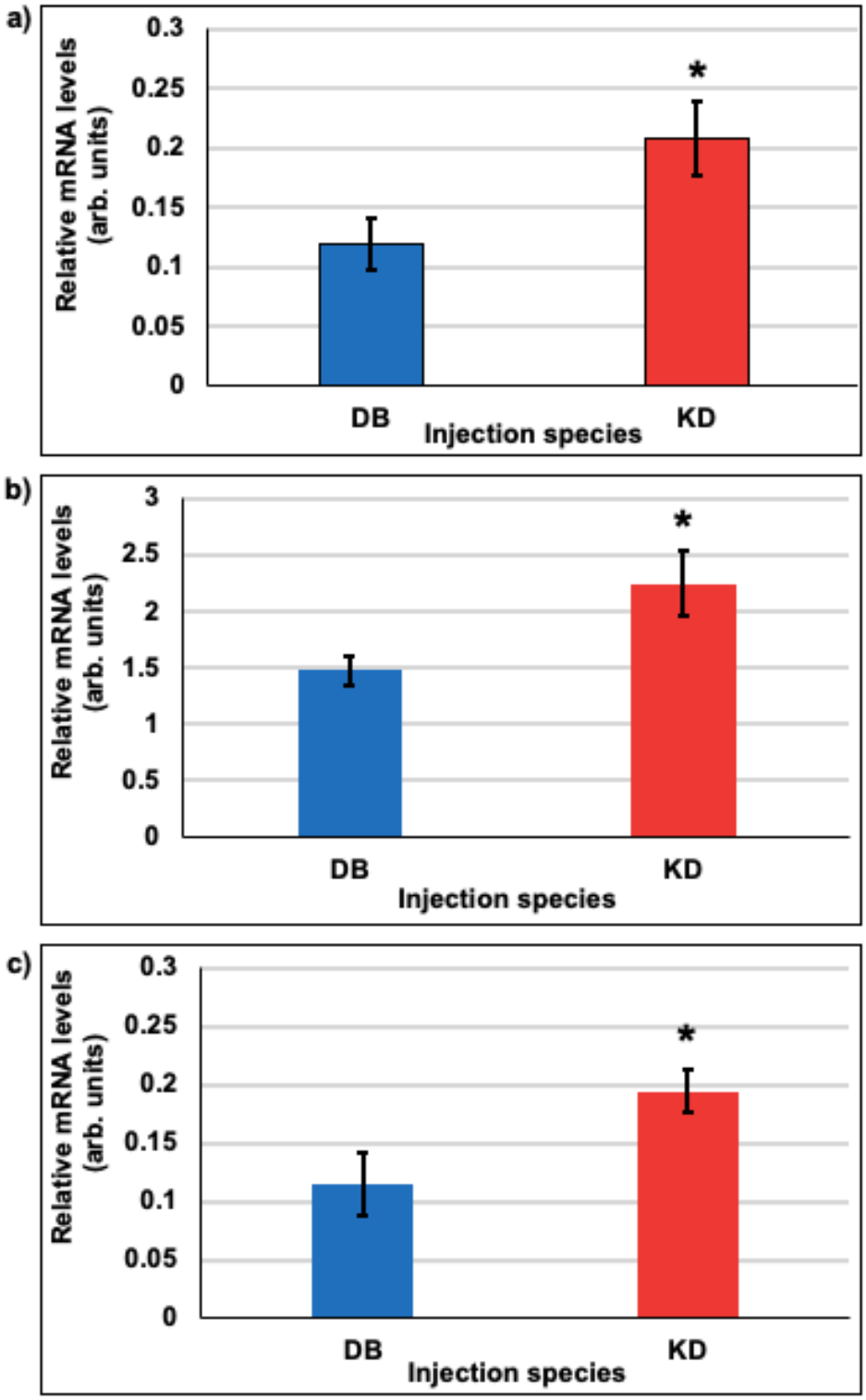

Figure 5.5. Real-time PCR quantification of the effect of *PADI6* gene KD on the expression of **a)** *DNMT3B*, **b)** *OOEP* and **c)** *PRMT5* in high PADI6 KD oocytes (n = 7), shown together with DB-injected oocytes (n = 6). The data were standardised against *GAPDH, H2A, HPRT1, PGK1* and *YWHAZ* housekeeping mRNA levels. Individual bars show the mean ±SEM and duplicate repeats were performed. Statistical significance (*) is indicated where $p<0.05$. Please note the different scale on the graph for *OOEP*.

5.3.3 Identification of differentially expressed genes in *PADI6*^{KD} MII oocytes by real-time PCR

Continuing with this analysis, more in-depth real-time PCR experiments were conducted to quantify resultant changes in gene expression after *PADI6* KD. Instead of using the real-time arrays that were described in Section 5.2.1, genes were selected for thorough real-time PCR testing of all samples from Figure 4.9: DB and SCR-injected control MII oocytes (DB: n = 11; SCR: n = 10) and *PADI6*^{KD} MII oocytes (n = 20). SCR-injected control oocytes were now included in the analysis. Real-time PCR experiments were performed in triplicate for the following genes: *DNMT1, DNMT3A, DNMT3B, DPPA3, FIGLA, GNAS, HAT1, KDM1, KHDC3L, MEST, MTHFR, NLRP2, NLRP5, NLRP7, OOEP, PHLDA2, PLAGL1, PRMT5, SETDB1, STAT3, TET1, TET2, TET3, TLE6, TRIM28* and *ZFP57*. Interestingly, unlike initial screening using the imprinted gene and epigenetic regulator real-time PCR array, in the more in-depth analysis *DNMT3B, OOEP* and *PRMT5* were not significantly different in *PADI6*^{KD} MII oocytes compared to control MII oocytes when more samples were analysed (Figure 5.6a-c). Similarly, most of the genes tested did not change between control and *PADI6*^{KD} MII oocytes due to increased variability in the data (shown in Appendix IV.A).

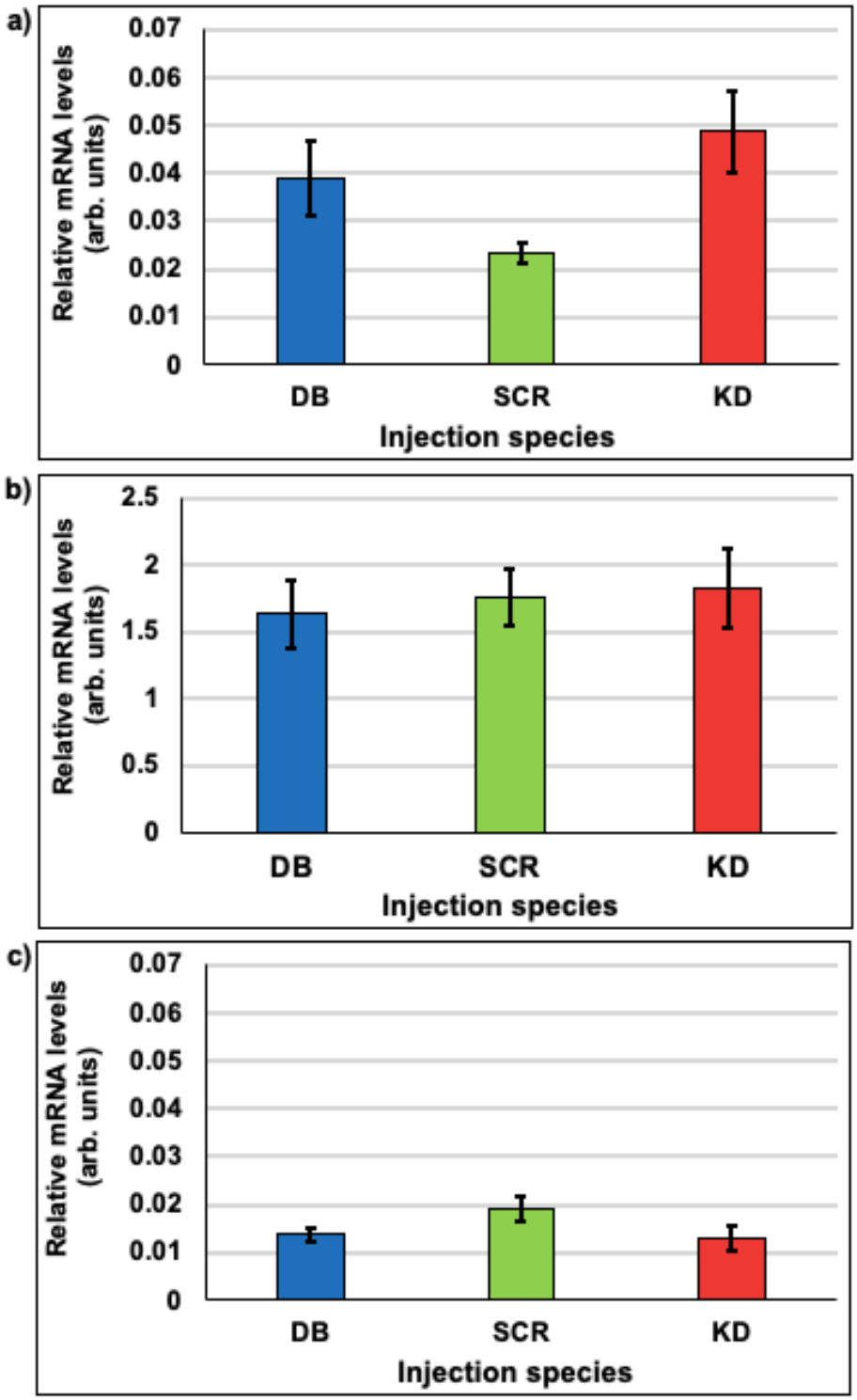

Figure 5.6. Real-time PCR quantification of the effect of *PADI6* gene KD on the expression of **a)** *DNMT3B,* **b)** *OOEP* and **c)** *PRMT5* in high *PADI6* KD oocytes (n = 20), shown together with DB (n = 11) and SCR-injected (n = 10) oocytes (p>0.05). The data were standardised against *GAPDH, H2A* and *YWHAZ* housekeeping mRNA levels. Individual bars show the mean ±SEM. Please note the different scale on the graph for *OOEP*.

However, after analysing a greater numbers of samples by in-depth analysis, 4 other candidate genes from the imprinted genes and epigenetic regulators array, *DNMT3A, TRIM28, ZFP57* and *PLAGL1*, and 1 new gene, *DPPA3*, were found to be differentially expressed between control and *PADI6*^{KD} MII oocytes (Figure 5.7). *DNMT3A* transcript abundance increased by more than 2-fold in *PADI6*^{KD} MII oocytes compared to control oocytes ($p<0.05$) (Figure 5.7a). Similarly, expression of *DPPA3* in *PADI6*^{KD} MII oocytes increased by almost 2-fold ($p<0.05$) compared to control injected oocytes (Figure 5.7b). No significant difference in *DNMT3A* or *DPPA3* expression was detected between duplex buffer and scrambled dsiRNA controls ($p>0.05$). On the other hand, *TRIM28* and *ZFP57* transcript abundance decreased after *PADI6* gene KD. *TRIM28* expression was reduced by around 41% in *PADI6*^{KD} MII oocytes compared to control oocytes (Figure 5.7d). Again, there was no difference in *TRIM28* gene expression between DB and SCR control oocytes ($p<0.05$). *ZFP57* transcript abundance significantly decreased by around 63% in *PADI6*^{KD} compared to DB MII oocytes, but not compared to SCR dsiRNA MII oocytes (Figure 5.7e). No significant differences in *ZFP57* gene expression were observed between *PADI6*^{KD} and SCR MII oocytes ($p>0.05$). Generally bovine *ZFP57* gene expression is relatively low in the oocyte, resulting here in lower 'n' values due to limited amplicon detection by real-time PCR. Furthermore, imprinted gene *PLAGL1* significantly decreased by 43% in *PADI6*^{KD} oocytes compared to DB controls (Figure 5.7c). There were no significant differences in *PLAGL1* expression between *PADI6*^{KD} and SCR injected oocytes due to the large SEM in SCR samples.

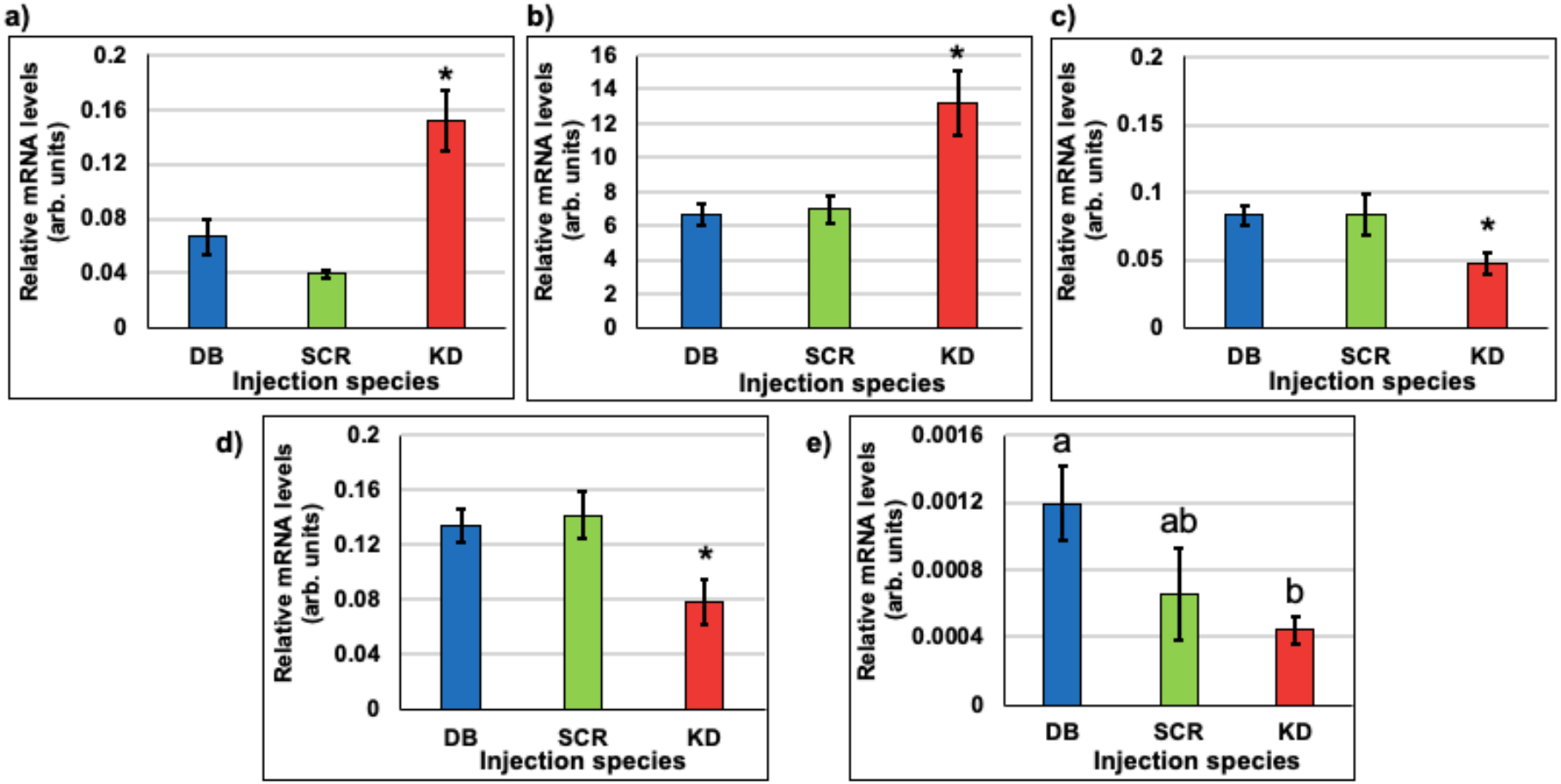

Figure 5.7. Real-time PCR quantification of the effect of *PADI6* gene KD on the expression of **a)** *DNMT3A*, **b)** *DPPA3*, **c)** *PLAGL1*, **d)** *TRIM28* and **e)** *ZFP57* in *PADI6*^{KD} bovine oocytes (n = 20) compared to DB (n = 11) and SCR-injected (n = 10) oocytes. Data were standardised against *GAPDH, H2A* and *YWHAZ*. Individual bars show the mean ±SEM. Statistical significance is indicated with * compared to controls or by different letters where $p<0.05$. Please note the different scales on the graphs for *DPPA3* and *ZFP57*.

5.3.4 RNA-seq analysis in *PADI6*^{KD} oocytes

RNA-seq of Smart-seq2 cDNA libraries (Picelli et al., 2014) successfully generated an average of 81,500 reads per library, of which 70-85% of reads assigned to the bovine reference genome. An MDS plot was generated to look at the similarity of gene expression between the samples. Figure 5.8a shows the MDS plot for all of the samples that were analysed: DB 1-6, SCR 1-6 and *PADI6* KD 1-6. Samples were removed that fell into the top (90th) and bottom (10th) centile using quantile in R. A quantile describes how much of the data lies below a certain value, in this case the 90th or 10th centile. These samples were considered to be outliers as they fell into the two extremes of the dataset. Outliers increase the variability in the data, which decreases statistical power. This led to the exclusion of 4 samples: DB 4 and 5, SCR 3 and KD 2 (Figure 5.8b). Figure 5.8b illustrates that there is no distinct clustering of samples in each group; therefore, there is similarity in the transcriptome between groups.

The RNA-seq results confirmed that KD of *PADI6* was achieved in 5 out of 6 samples. Table 5.4 shows the raw counts of *PADI6* transcripts in individual DB, SCR and KD samples. As described previously, DB 4 and 5, SCR 3 and KD 2 samples were excluded from the analysis as expression of *PADI6* fell into the top (90th) or bottom (10th) centile deeming them outlying samples for the purpose of our comparison. The average raw counts of *PADI6* transcripts in DB, SCR and KD groups were 187.5, 195.2 and 60.2, respectively. *PADI6* expression was reduced by 68% in the KD group compared to DB group but this was not statistically significant with $p=0.07$. However, *PADI6* expression was significantly reduced by 69% in the KD group compared to SCR group ($p<0.05$). To facilitate comparison between control and *PADI6* KD groups, gene expression in the SCR control group was subtracted from both the DB and *PADI6* KD groups in the bioinformatic analyses. This was done to remove any off-target effects caused by injection of an oligonucleotide sequence into the oocyte. Subsequently, topTags in edgeR was used to identify differentially expressed tags between DB control and *PADI6* KD groups. The results from this analysis demonstrated that *PADI6* expression was significantly reduced in KD oocytes compared to DB oocytes ($p<0.01$), confirming successful KD of *PADI6* transcripts.

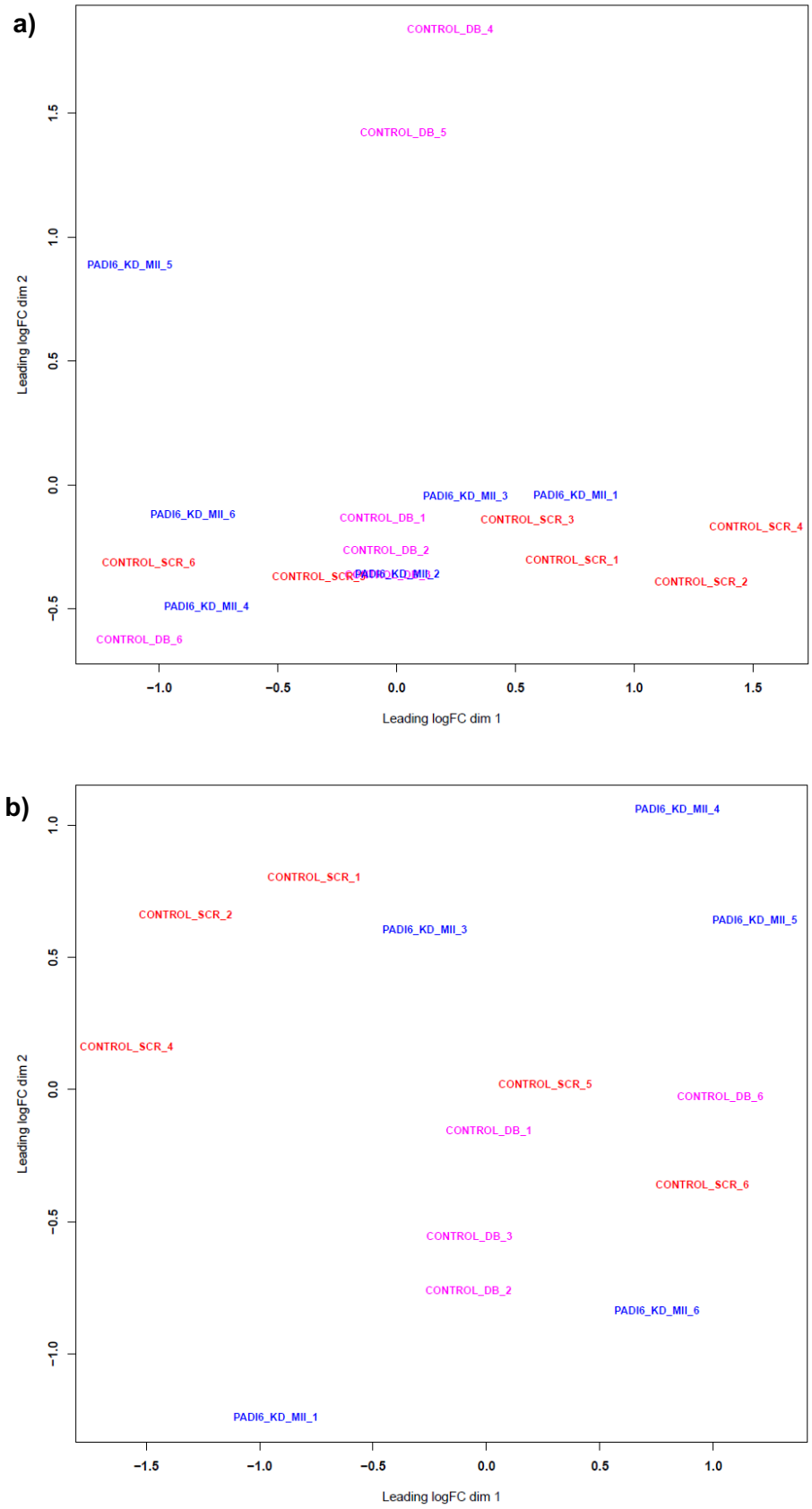

Figure 5.8. MDS plot showing the distribution of **a)** all samples: DB 1-6 (pink), SCR 1-6 (red) and KD 1-6 (blue) and **b)** samples after exclusion of 4 outlying samples: DB 4 and 5, SCR 3 and KD 2.

Table 5.4 Raw counts of *PADI6* reads in bovine MII oocytes from DB (1-6), SCR (1-6) and PADI6 KD (1-6) injection groups. The values in red were excluded as outliers as they fell into the 10th or 90th centile.

Library no.	Injection species		
	DB	**SCR**	***PADI6* KD**
1	196	99	109
2	153	167	188
3	255	66	52
4	35	113	82
5	30	379	37
6	146	218	21
Average counts	187.5	195.2	60.2
***PADI6* expression as a proportion of DB *PADI6* transcripts**	**100%**	**104%**	**32%**

Figure 5.9 shows the RNA tracks from RNA-seq data inputted into UCSC genome browser to show exon reads corresponding to the reference *PADI6* genomic landscape. Each row represents a library derived from an individual oocyte and reads were scaled according to library size to allow direct comparisons between libraries. The RNA-seq results show that there are reads corresponding to the estimated 16 exons of bovine *PADI6*. Throughout the transcript, exons are represented in varying amounts. For example, exons at the 5' are less well represented compared to the exons in the middle of the transcript, a common observation in oligo-dT primed libraries. It also appears that expression of exons at the 3' end is more variable with oocytes showing either high or low 3' exon reads across all groups. Interestingly, there is a read at exon 2 in 17 out of 18 samples that is annotated in *Canis* but not in *Homo sapiens*. This could be a novel exon in the bovine *PADI6* gene or provide an indication of an alternative transcription start site. KD of *PADI6* was achieved by targeting exon 9 of the *PADI6* gene using dsiRNA. Interestingly, exon 9 is not visible on the tracks of KD sample 6, which achieved the lowest KD of *PADI6* transcripts. Nevertheless, for most samples, KD of *PADI6* did not alter the landscape of available *PADI6* transcripts but led to a decrease in the number of transcripts indicative of transcript degradation.

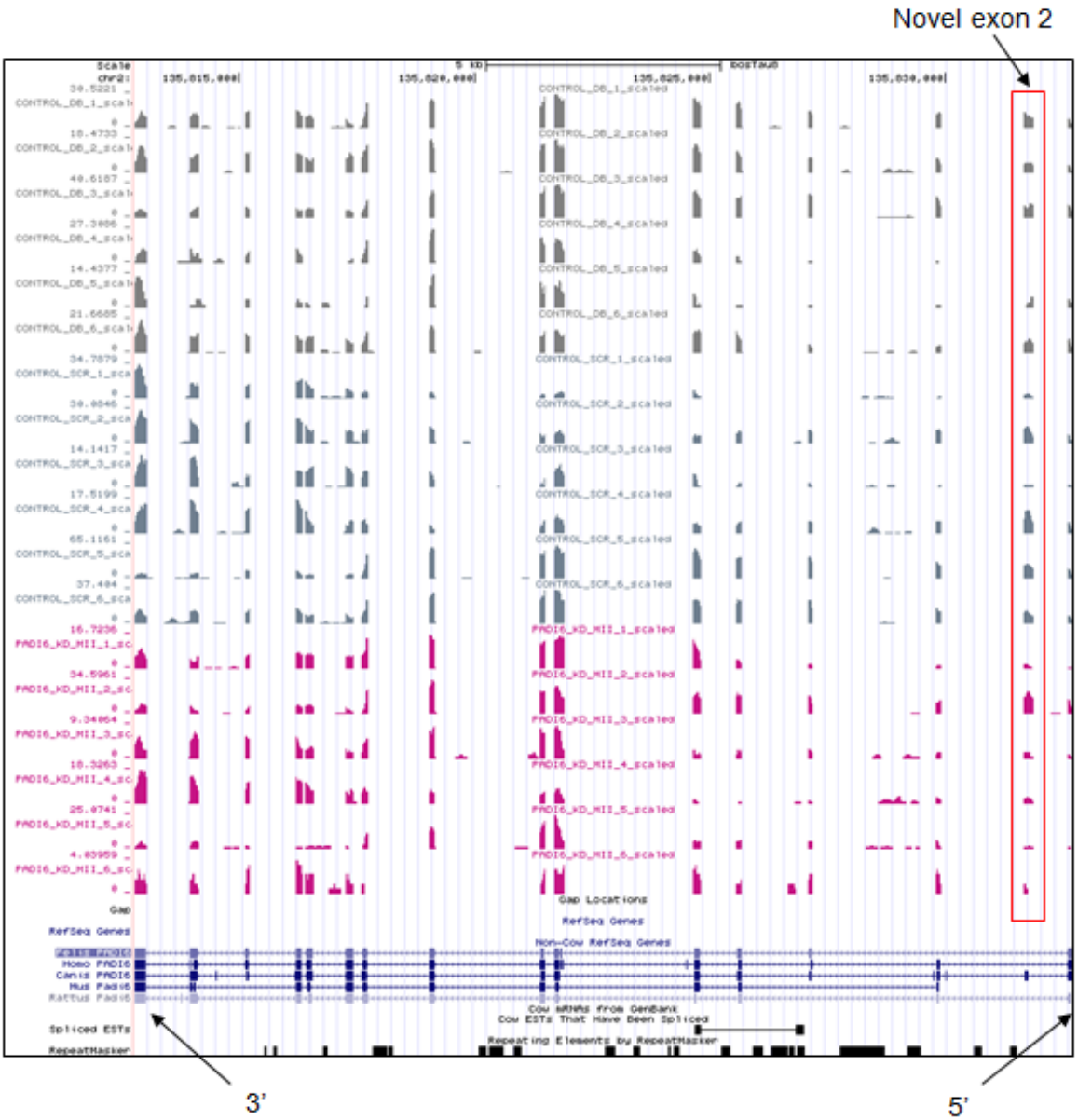

Figure 5.9. Representative mRNA tracks from RNA-seq data inputted into UCSC genome browser (https://genome.ucsc.edu/) to show exon reads corresponding to the reference *PADI6* genomic landscape. Each row represents a single-oocyte library, from top to bottom: controls (grey) DB 1-6 and SCR 1-6, and *PADI6* KD 1-6 (pink). Reads were scaled according to library size to allow direct comparisons between libraries. The numbers above each library label describe the scaled number of reads of *PADI6* per library.

5.3.4.1 Differential expression of genes following KD of *PADI6* in bovine oocytes

RNA-seq demonstrated that *PADI6* expression was reduced in KD oocytes compared to DB oocytes ($p<0.01$), confirming successful KD of *PADI6* transcripts. Following this, a total of 452 genes were found to be differentially expressed ($p<0.05$) in *PADI6*^{KD} oocytes: 165 genes were downregulated and 287 genes were upregulated. A comprehensive list of the 452 DEGs can be found at https://www.dropbox.com/s/qg4b2b4uxskisn8/PADI6_KD_diffgenes.xlsx?dl=0. Due to the large number of genes that were identified, a heatmap was created in R to show most DEGs between individual control and *PADI6* KD oocytes ($p<0.001$) (Figure 5.10). This led to the inclusion of 22 genes into the heatmap: ras-related protein Rab-12 (*RAB12),* inhibitor of growth family member 2 *(ING2),* Jun proto-oncogene *(JUN),* ras-related protein Rab-32 (*RAB32),* activated leukocyte cell adhesion molecule *(ALCAM),* UNC homeobox *(UNCX),* neudesin neurotrophic factor *(NENF),* ral guanine nucleotide dissociation stimulator like-1 *(RGL1),* homeobox D1 *(HOXD1),* thyrotrophin releasing hormone *(TRH)* and *VP233B-DT* were upregulated following *PADI6* KD. On the other hand, fatty acid synthase *(FASN),* zinc finger protein 705B *(ZNF705B),* keratin 5 *(KRT5),* intercellular adhesion molecule 4 *(ICAM4),* PEAK1 related, kinase-activating pseudokinase 1 *(PRAGL1),* zinc finger protein 382 (*ZNF382),* fos-related AP-1 transcription factor *(FOSL1),* centromere protein M *(CENPM),* keratin 8 *(KRT8),* newborn ovary homeobox *(NOBOX)* were downregulated following *PADI6* KD. *NLRP2* and *NLRP7* transcripts were also significantly decreased following *PADI6* KD ($p=0.01$ and 0.006, respectively). Hierarchical clustering at the top of the heatmap groups samples was based on their similarity. Here, this demonstrates that there are 2 distinct groups, DB and KD, which show differing gene expression. Within the DB group there appears to be less variation between samples than KD group as the branches appear more compact and widespread, respectively. Hierarchical clustering at the left-hand side of the heatmap demonstrates similarities between gene expression levels e.g. genes with high or low expression genes are grouped together. It is worth noting that of the genes that were differentially expressed between control and *PADI6* KD samples, the false discovery rate (FDR) was not significant (>0.05). FDR determines the confidence with which the p-value is true e.g. an FDR of <0.05 predicts that <5% of tests will result in a false positive therefore the differential gene expression is likely to be true.

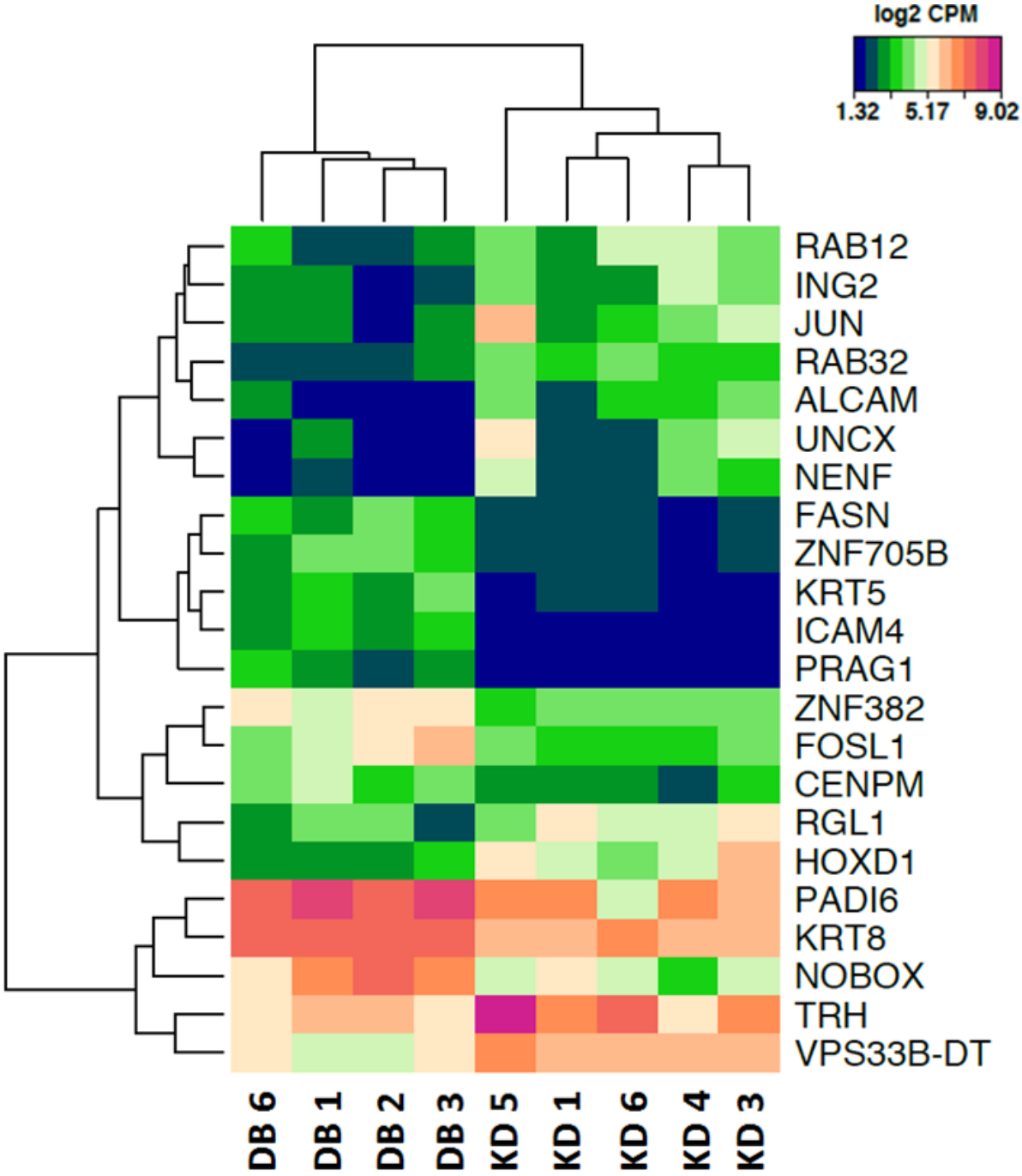

Figure 5.10. Heatmap showing the most statistically significant differential gene expression between DB and KD samples ($p<0.001$). Gene expression is shown as $\log_2$ counts per million counts (cpm) where blue represents low expression and pink represents high expression according to the scale. Hierarchical clustering at the top and left-hand side of the heatmap demonstrates similarities between samples and genes, respectively.

Next, all DEGs were subject to Ingenuity Pathway Analysis (IPA) to evaluate the interactions, causal networks and cellular phenotypes that were altered in *PADI6*^{KD} oocytes. DEGs were involved in many different networks however Figure 5.11a shows the pathways where multiple DEGs were affected. DEGs are displayed as a percentage of the total number of genes in the pathway (shown in bold on the right of the figure) which ranges from 6-14%. Of the canonical pathways that were highlighted, mitochondrial dysfunction, kinase signalling and protein ubiquitination were interesting in the context of *PADI6.* Further, all pathways are significant for oocyte maturation. The roles of DEGs were investigated in the context of disease and function using IPA (Figure 5.11b). DEGs were involved in developmental abnormalities and metabolic disease as well as cellular functions of gene expression, amino acid metabolism and DNA processing.

Finally, pathway analysis was conducted to look at interactions between *PADI6* and DEGs (Figure 5.12). In general, KD of *PADI6* appeared to indirectly impact the expression of downstream genes, for example lysine demethylase 1A *(KDM1A)* expression was unchanged in our dataset (white) but 14 genes downstream of *KDM1A* were upregulated (red) or downregulated (green) following *PADI6* KD This was the same for all 13 gene networks except ubiquitin E3 ligase complex component, F-box, LRR protein 14 (*FBXL14)*. Figure 5.12 shows that 61 DEGs were directly or indirectly linked to *PADI6*. The pathway highlights the variety of genes that were dysregulated following KD of *PADI6* and the figure key shows the diversity proteins that were produced from these gene transcripts. There were a number of ribosomal components and RNA binding proteins that were upregulated following KD of *PADI6.* Further analysis suggested that KD of *PADI6* resulted in an increase in RNA damage pathway which involved mitochondria, ribosomes and transcription (Figure 5.13). Analysis of the role of *PADI6* in disease and functions highlighted links to infertility (red dotted line) and organisation of the cytoskeleton (blue dotted line). Interestingly, genes from 7 downstream networks and 10 downstream networks were involved in infertility and organisation of the cytoskeleton, respectively. Only *PADI6* and inhibin beta A *(INHBA)* were associated with both infertility and cytoskeletal organisation.

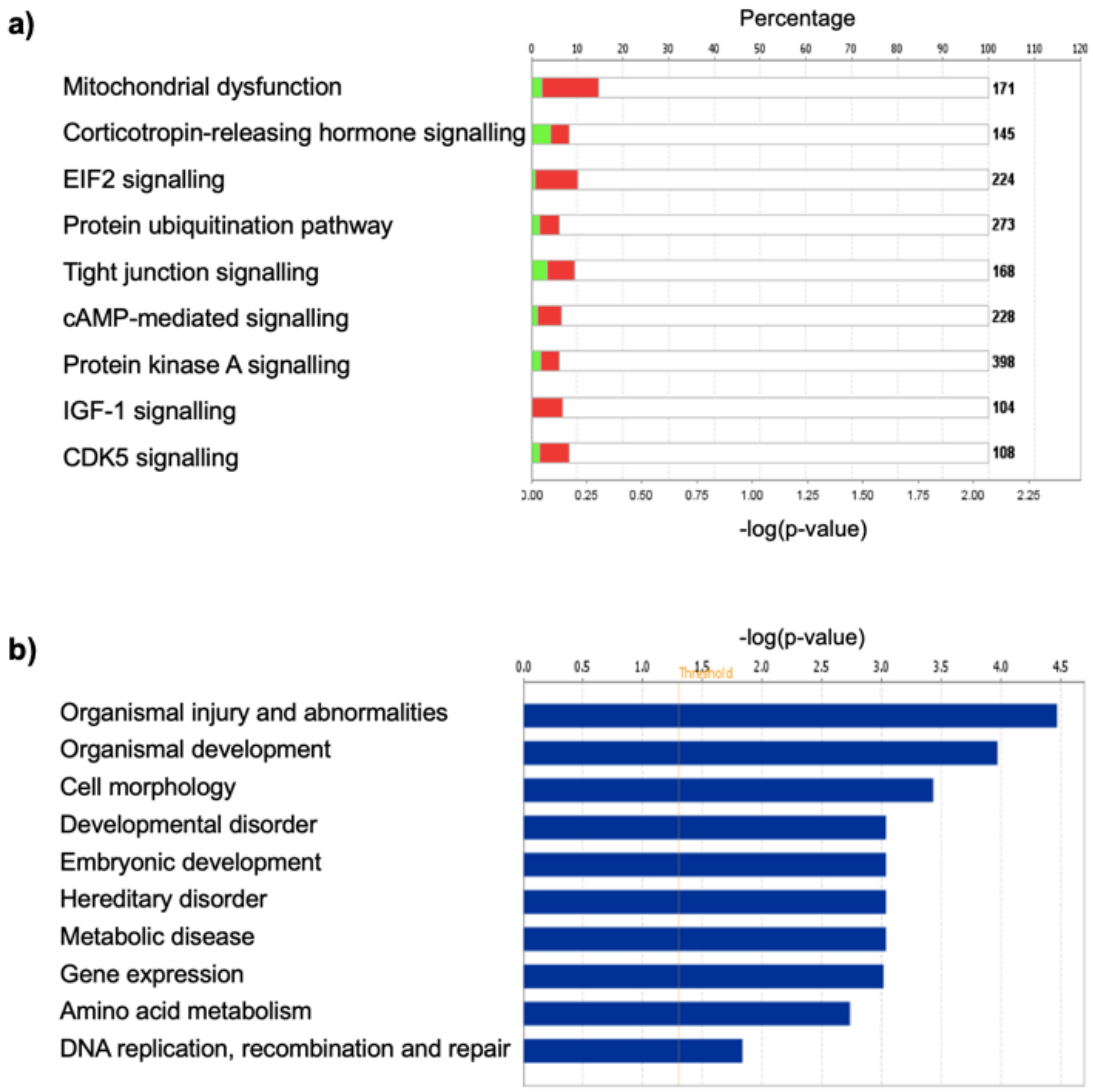

Figure 5.11. **a)** Canonical pathways of DEGs in *PADI6*^{KD} oocytes following IPA. The total number of genes in the pathway are shown in bold on the right and the bars represent the percentage of genes in the pathway that are upregulated (red) and downregulated (green) in *PADI6*^{KD} oocytes. **b)** Disease mechanisms and functional pathways of DEGs following KD of *PADI6* ($p>0.05$) using IPA.

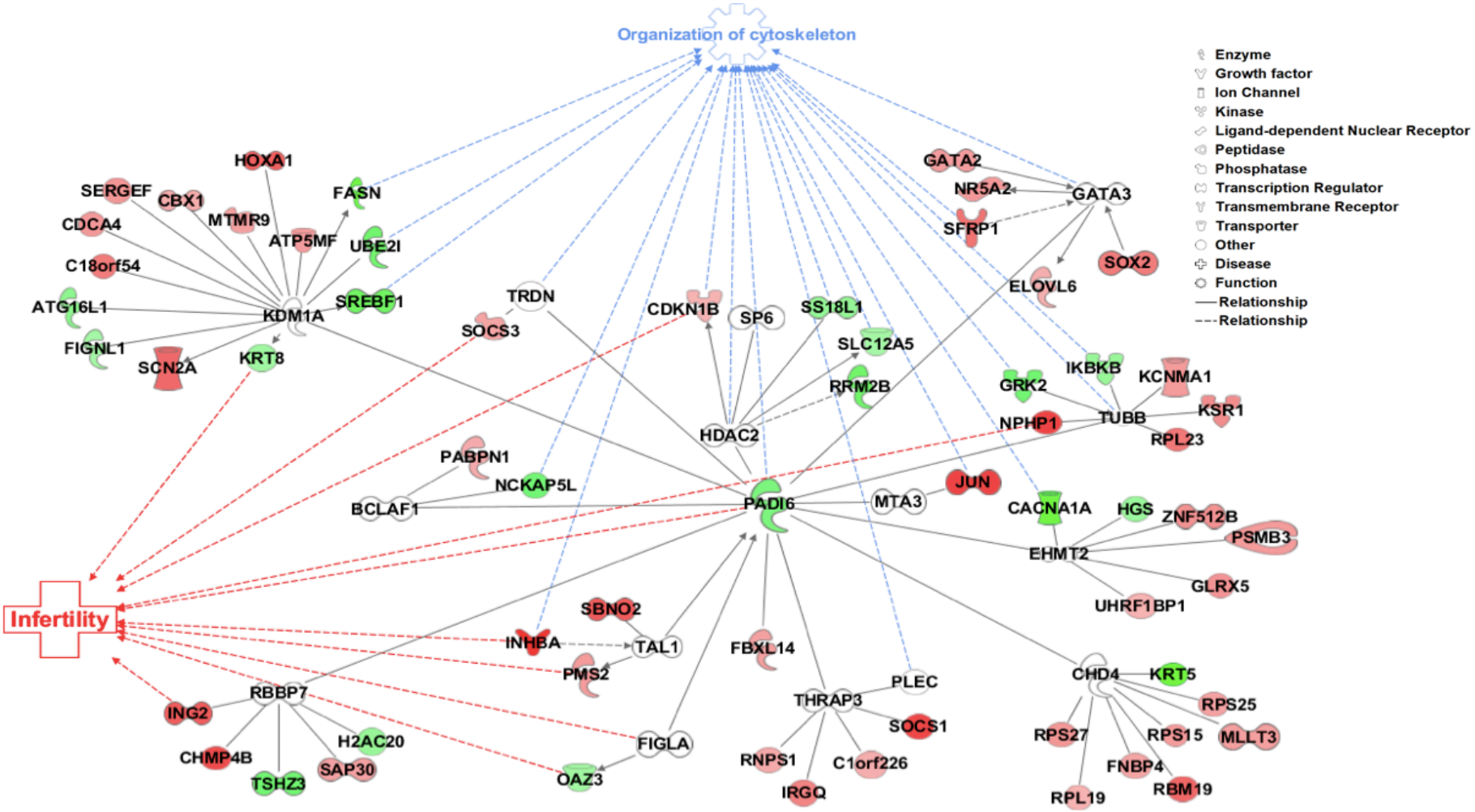

Figure 5.12. Pathway analysis of *PADI6*^{KD} oocytes. The dotted lines represent links to infertility (red) and organisation of the cytoskeleton (blue). Downregulated and upregulated genes following KD of *PADI6* are shown in green and red, respectively. Lines and arrows between nodes represent direct (solid) and indirect (dashed) interactions between molecules as supported by information in the Ingenuity knowledge base.

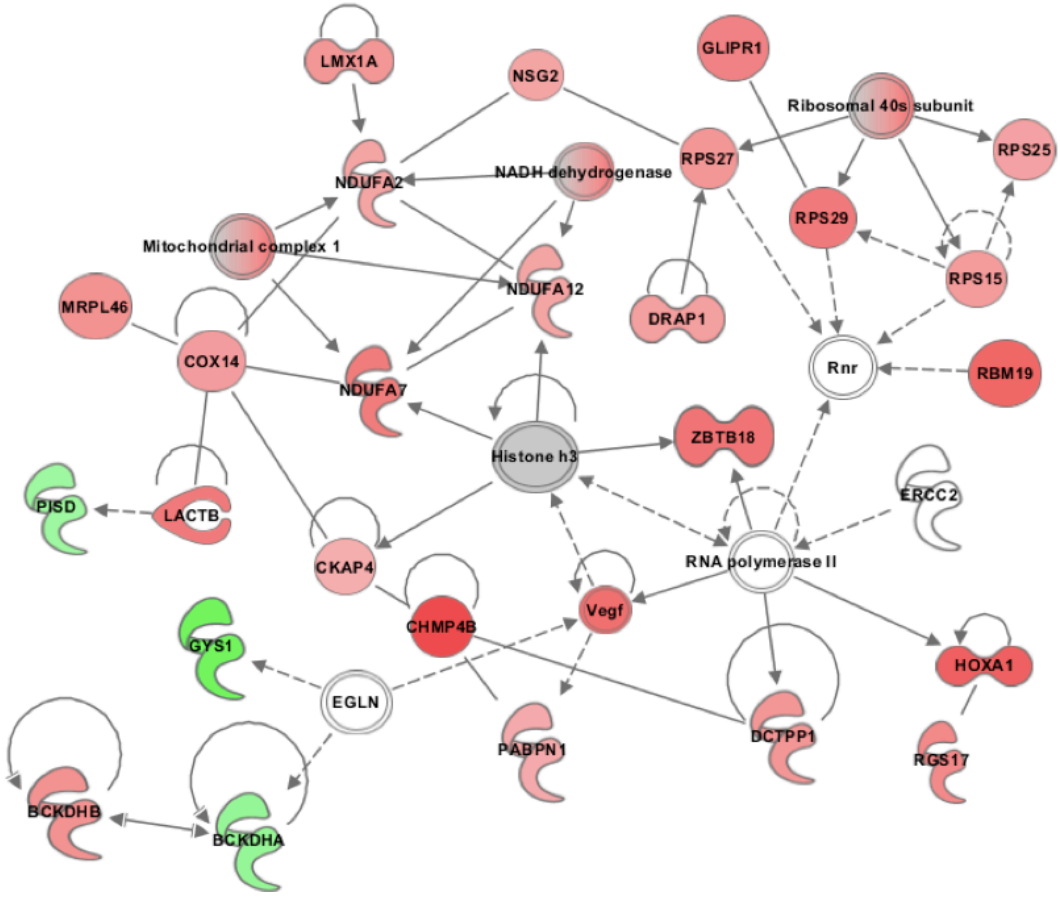

Figure 5.13. Dysregulation of RNA damage pathway following KD of *PADI6*. Downregulated and upregulated genes following KD of *PADI6* are shown in green and red, respectively. Lines and arrows between nodes represent direct (solid) and indirect (dashed) interactions between molecules as supported by information in the Ingenuity knowledge base.

5.3.4.2 Expression of *PADI1-4* in bovine MII oocytes in the RNA-seq data

Researchers suggest that *PADI1-4* are expressed in the mouse oocyte and may account for PADI activity in the oocyte and embryo (Brahmajosyula and Miyake, 2013; Christophorou et al., 2014; Kan et al., 2012; Zhang et al., 2016), therefore it was important to investigate the presence of *PADI1-4* transcripts in the bovine oocyte. Firstly, expression of *PADI1-4* was briefly investigated by real-time PCR in Section 4.3.3.2. Despite testing numerous primers, the Ct values were mostly undetermined and the results were inconclusive (Figure 4.14). However, the RNA-seq results showed that *PADI1-4* were not expressed in any of the MII oocytes that were

analysed (Table 5.5). A maximum of 3 transcripts of *PADI1-4* genes were identified in small number of oocytes compared to a maximum of 379 transcripts of *PADI6*. Furthermore, there were no differences in the expression of *PADI1-4* between DB, SCR and KD groups.

Table 5.5 Raw counts of *PADI* gene reads in bovine MII oocytes from DB (1-6), SCR (1-6) and PADI6 KD (1-6) injection groups.

Gene	DB						SCR						*PADI6* KD					
	1	**2**	**3**	**4**	**5**	**6**	**1**	**2**	**3**	**4**	**5**	**6**	**1**	**2**	**3**	**4**	**5**	**6**
PADI1	0	1	0	0	0	0	0	0	1	0	0	3	0	1	0	0	0	0
PADI2	0	0	0	0	1	0	0	0	1	0	0	0	0	0	0	1	0	0
PADI3	0	1	1	0	0	0	0	0	1	0	2	1	1	2	0	2	0	1
PADI4	0	1	0	0	0	0	0	0	1	0	1	1	0	1	0	2	0	0
PADI6	196	153	255	35	30	146	99	167	66	113	379	218	109	188	52	82	37	21

5.4 Discussion

Targeted analysis of the transcriptome of *PADI6*^{KD} oocytes by real-time PCR revealed changes to the expression of 7 key oocyte genes compared to control-injected oocytes. Of these genes, *PRDX1* and *ZP1* are markers of oocyte quality while *DNMT3A, DPPA3, PLAGL1, TRIM28* and *ZFP57* are factors with known roles in general epigenetic regulation. The RNA-seq results confirmed successful KD of *PADI6* gene expression and identified differential expression of a number of interesting genes following *PADI6* KD*;* however, the FDR was too high to have confidence in these results. RNA-seq also revealed that there was no expression of *PADI1-4* in the bovine MII oocyte, contrary to studies in mice.

5.4.1 Impact of *PADI6* gene KD on oocyte quality markers

The oocyte quality marker real-time PCR array was useful to screen for potential changes in gene expression between control and *PADI6*^{KD} oocytes. It allowed a large number of genes to be analysed in a fairly inexpensive way. Conversely, it was a lengthy process and triplicate measurements could not be performed due to the large number of genes and samples examined. Further, some of the gene assays on the array did not work and had to be excluded from the investigation. Nevertheless, through the use of the array, 2 genes were found to be differentially expressed in *PADI6*^{KD} oocytes.

Firstly, bovine *PRDX1* was identified as significantly reduced in *PADI6*^{KD} oocytes compared to SCR dsiRNA injected oocytes but not DB injected oocytes. *Prdx1* plays a role in redox metabolism which means that it has become known as a biomarker of oxidative stress (Poynton and Hampton, 2014). Peddinti et al. (2010) suggest that cumulus cells induce the upregulation of PRDXs in the oocyte in response to oxidative stress to protect from apoptosis and DNA damage. It is inevitable that the microinjection procedure induces oxidative stress, but this effect should be the same across DB, SCR and KD oocyte groups. To investigate this further, *PRDX1* transcript abundance could be analysed in non-injected MII oocytes to determine a baseline *PRDX1* gene expression level in *in vitro* matured oocytes, prior to micromanipulation. Moreover, different SCR dsiRNA control injection species could be tested to see if this response is specific to the SCR dsiRNA tested in this study or an off-target effect.

Finally, increasing the number of samples should reduce the SEM, potentially creating significance between DB and *PADI6*^{KD} oocytes.

It is interesting to note that *PRDX1* is recognised as a marker of oocyte maturation in the literature as *PRDX1* becomes deadenylated from GV to MII transition (Thelie et al., 2007). It could be that *PADI6* gene KD impacts the storage and polyadenylation of *PRDX1* transcript, resulting in an observed decrease in transcript abundance (Reyes and Ross, 2016). *PRDX1* transcript abundance is also thought to be affected by follicle size, with smaller follicles expressing higher amounts of *PRDX1,* and maternal age, with lower *PRDX1* gene expression observed in oocytes from prepubertal calves compared to adult cows (Romar et al., 2011). The quality of prepubertal oocytes is reduced relative to adult cells. In support of this idea our laboratory has recently shown differential expression of *PRDX1* between young vs. old sheep MII oocytes after IVM (Totipat, C., Lu, J., Huntriss, J. and Picton, H.M., unpublished). Furthermore, PRDX1 localises to spindles in maturing mouse oocytes and its inhibition appears to disturb spindle assembly (Jeon et al., 2017). The SCMC has also been linked to spindle dynamics with *Tle6*-null embryos displaying abnormal spindles and asymmetric cell divisions (Yu et al., 2014b). Knockout of another proposed SCMC member, *Zbed3,* also impairs spindle positioning and F-actin organisation, leading to the production of asymmetric blastomeres in mouse embryos (Gao et al., 2018). Therefore, the data presented here may suggest that *PADI6* links *PRDX1* and the SCMC to spindle formation in the oocyte. This could be investigated using immunofluorescence and co-immunoprecipitation experiments to evaluate the relationships between PADI6, PRDX1, the SCMC and the meiotic spindle.

The second candidate oocyte quality gene to be identified was bovine *ZP1,* which was significantly downregulated in *PADI6*^{KD} oocytes compared to both DB and SCR injected oocytes ($p<0.05$). ZP1 contributes to the formation of the zona pellucida, which surrounds the oocyte, alongside ZP2, 3 and 4 (Lefievre et al., 2004). The zona pellucida is an essential component of the oocyte as it facilitates sperm recognition and entry during fertilisation, prevents polyspermy and protects the early embryo (Conner et al., 2005). Mutations in *ZP1* have been identified in cases of human primary infertility (Huang et al., 2014; Zhou et al., 2019). Oocytes from patients with truncated ZP1 protein completely lack a zona pellucida, which leads to polyspermic fertilisation and failure of the embryo to develop. Ablation of *Zp1* in mice causes abnormal zona pellucida formation and reduced fertility characterised by early embryonic loss (Rankin et al., 1999). At the time of microinjection of the GV oocyte

the zona pellucida is already formed. Microinjection involves penetrating the zona pellucida to administer dsiRNA species into the oocyte. The force of this procedure and disruption to the zona pellucida might lead of dysregulation of *ZP* genes, particularly *ZP1* as it is thought to contribute to the integrity of the zona pellucida by crosslinking other ZP proteins (Rankin et al., 1999). It is important to consider how downregulation of *ZP1* might affect development of the embryo. There are many roles for the zona pellucida in embryo development: it maintains a tight environment for the exchange of autocrine factors between blastomeres, protects the embryo from the maternal immune system as well as harmful pathogens, facilitates passage of the embryo down the oviduct and inhibits ectopic implantation (Familiari et al., 2008). If downregulation of ZP1 perturbs the maintenance of the zona pellucida in the embryo, it is likely to be detrimental to embryo viability and development. In addition to *ZP1*, increased expression of oocyte sperm receptor *IZUMO1R* was also observed in *PADI6*^{KD} oocytes compared to DB injected oocytes (p=0.067) (Figure 5.2). *IZUMO1R* is transiently expressed in mature MII oocytes in preparation for sperm-oocyte fusion (Bianchi et al., 2014). Together with ZP proteins, IZUMO1R facilitates fertilisation of the oocyte (Inoue et al., 2011c). Altered *ZP1* and *IZUMO1R* expression during oocyte maturation are likely to negatively impact developmental competence by impairing fertilisation of *PADI6*^{KD} oocytes.

There was also an increase in *FIGLA* transcript abundance following KD of *PADI6* (p=0.086) (Figure 5.2). It is interesting to note that expression of both *ZP1* and *PADI6* are regulated by FIGLA which may act as a master transcription factor (Joshi et al., 2007). KD of *PADI6* may result in upregulation of *FIGLA* in a feedback mechanism to compensate for ablation of the transcript. The data could also suggest a role for *PADI6* in regulating transcription, or more likely transcriptional storage, in the growing oocyte. KD of *PADI6* could disrupt the storage of maternal mRNAs, exposing them to degradation in the cytoplasm. Furthermore, loss of *PADI6* may lead to changes in polyadenylation and the observed decrease in transcript abundance of both *PRDX1* and *ZP1* could be a false effect of deadenylation. Using random hexamer priming in cDNA synthesis would exclude the idea that changes in transcript abundance are a result of deadenylation. Nevertheless, the effects of *PADI6* gene KD on the oocyte were not widespread but specific to only 2 of the 20 genes analysed. This suggests that the role of *PADI6* is defined to particular genes or developmental time points, in this case the MII oocyte, rather than a global oocyte disruption.

As mentioned previously, the real-time PCR array allowed only for single real-time PCR measurements for each gene, instead of triplicate repeats to increase confidence in the data generated. It would be sensible to repeat this experiment with triplicate measures and higher sample numbers to be certain that the results are true. However, significance was obtained in 20 discrete *PADI6*^{KD} oocytes compared to 21 discrete control oocytes, strongly suggesting a causal relationship. RNA-seq experiments conducted during the course of this chapter were also helpful as a means to confirm and extend the observed real-time PCR results.

5.4.2 Impact of KD of *PADI6* on epigenetic regulators

The focus on epigenetic factors in this experimental series stemmed from the epigenetic abnormalities observed in human pathologies originating from mutations in SCMC genes. Initially, the imprinted gene and epigenetic array was used to rapidly screen for genes of interest (Figure 5.4). Due to the large number of genes that were screened (35 genes), the number of samples that were analysed were limited to 6 or 7 oocytes per group. DB and SCR control oocytes did not show any statistical differences in *PADI6* gene expression (Figure 4.9) therefore SCR injected oocytes were excluded from the initial screen only. Each gene was therefore only analysed in duplicate to save time and reagents. The results showed that 3 of the 35 genes analysed were differentially expressed in *PADI6*^{KD} oocytes compared to DB control injected oocytes: *DNMT3B, OOEP* and *PRMT5* ($p<0.05$). Moreover, all 3 genes were upregulated by similar amounts after *PADI6* KD. Interestingly, the samples analysed on this screen originated from the same oocyte KD and culture replicate. With this in mind, many of the genes tested qualitatively increased in *PADI6*^{KD} oocytes compared to DB controls including *DNMT1* and SCMC members, *KHDC3L* and *NLRP2* ($p=0.078$, 0.051 and 0.069, respectively). Upon further analysis using DB, SCR and *PADI6*^{KD} oocytes from multiple culture weeks, *DNMT3B, OOEP* and *PRMT5* were not differentially expressed between *PADI6*^{KD} and control oocytes ($p>0.05$) (Figure 5.6), posing the question of whether atypical culture conditions in the week of interest could have caused a global alteration in transcript levels relative to other cultures. Analysis of this particular culture using the oocyte quality marker array showed that there were 2 genes out of 20 genes that were significantly increased in *PADI6*^{KD} oocytes compared to DB-injected controls (Appendix IV, Figure IV.IV). These genes, *GTSF1* and *LHX8*, were not significantly altered in the overall analysis (see Figure 5.2) but were significantly altered in the analysis of this culture week. Together, the results

show that in this particular culture week, 5 out of 55 genes that were analysed were significantly increased in *PADI6*^{KD} oocytes compared to DB-injected control oocytes. Although this may be attributed to culture conditions, the results from the addition of samples from multiple culture weeks suggests that this is not a real effect of *PADI6* KD.

When using the imprinted gene and epigenetic regulator array, *PADI6* gene expression was not significantly decreased in *PADI6*^{KD} compared to DB injected oocytes. However, a qualitative reduction in *PADI6* was observed using this array, in which only 7 oocytes were analysed. Analysis of a greater number of oocytes could increase power. As discussed in Chapter 4, primer design for detection of gene KD by real-time PCR is very important. Investigation into the binding position of the array *PADI6* primers revealed that they bind at the very 3' of the transcript in the debated exon 16. The bovine *PADI6* transcript has not yet been experimentally characterised thereby different genomic databases predict different *PADI6* coding regions. Ensembl (ENSBTAT00000002772) predicts there to be 15 exons whereas NCBI (XM_002685797.5) predicts there to be 16 exons. The observed amplicon for exon 16 of *PADI6* in this array alongside the RNA-seq data confirms the presence of the 16th exon.

5.4.3 Impact of *PADI6* KD on the expression of imprinting regulators

Following the initial screen, in-depth real-time PCR analysis was performed using DB, SCR and *PADI6*^{KD} oocyte samples from Figure 4.9 (DB: n = 11; SCR: n = 10; KD: n = 20). 4 candidate genes were recognised: *DNMT3A, DPPA3, TRIM28* and *ZFP57* (Figure 5.7). Firstly, *DNMT3A* gene expression approximately doubled in *PADI6*^{KD} oocytes compared to control injected oocytes ($p<0.05$) (Figure 5.7a). *DNMT3A* expression in DB control oocytes was comparable to that of MII oocytes of the developmental series in Chapter 3 showing that *DNMT3A* expression was unchanged between microinjected and non-injected oocytes (Figure 3.11). *DNMT3A* is a *de novo* methylating enzyme. In bovine, *DNMT3A* mRNA and protein has been observed in preantral and antral oocytes (O'Doherty et al., 2012). This correlates with a critical period in which *de novo* methylation marks are established at imprinted loci. Research has shown that PADI4 can citrullinate DNMT3A which specifically increases its activity (Deplus et al., 2014). The understanding that a related family member to *PADI6* has the ability to interact with and modify DNMT3A could reveal an intriguing function for *PADI6*. One proposal states that KD of *PADI6* gene expression causes a reduction in DNMT3A citrullination, thereby decreasing its activity. As a result, negative feedback promotes transcription of *DNMT3A* to compensate for reduced activity.

Secondly, *DPPA3* was also upregulated by almost 2-fold in *PADI6*^{KD} oocytes compared to control oocytes (Figure 5.7b). Supporting Figure 3.12a, *DPPA3* was again shown to be highly expressed in the oocyte. *Dppa3* is responsible for protecting maternal imprinted loci from active TET-mediated demethylation upon fertilisation and in the preimplantation embryo (Nakamura et al., 2007). Specifically, DPPA3 recognises H3K9me2 histone marks resulting in changes to chromatin state (Nakamura et al., 2012). KD of *DPPA3* in bovine oocytes resulted in increased hydroxymethylation of female pronucleus and reduced developmental competence of the embryo (Bakhtari and Ross, 2014). *Dppa3* is known to protect maternally methylated *Mest, Peg3 and Peg10* and paternally methylated *H19* (Nakamura et al., 2012). Here, analysis of such imprinted genes showed there was no difference in transcript abundance between *PADI6*^{KD} and control injected oocytes, despite upregulation of *DPPA3* (Figure 5.4 and Appendix IV.A). However, if “normal” *DPPA3* expression in MII oocytes is sufficient to maintain methylation at imprinted gene loci, increased *DPPA3* expression should not have an effect on these genes. Instead,

increased *DPPA3* gene expression may impact genomic regions that are enriched in H3K9me2 histone marks or manifest as legacy effects in the embryo during ZGA. To investigate this further, global methylation analysis could be performed to identify differences in H3K9 methylation between *PADI6*^{KD} and control injected oocytes. Finally, like *ZP1*, *DPPA3* expression is also regulated by FIGLA (Joshi et al., 2007), which suggests that the increase in *DPPA3* transcript abundance might occur as a result of *FIGLA* upregulation in *PADI6*^{KD} oocytes (Figure 5.2).

Finally, *TRIM28* and *ZFP57* were downregulated by 41% and 63%, respectively, in *PADI6*^{KD} oocytes compared to control injected oocytes (Figure 5.7d and e). Like DPPA3, TRIM28-ZFP57 play an essential role in protecting imprinted loci from demethylation. ZFP57 binds to methylated DNA at a specific motif in differentially methylated regions (Quenneville et al., 2011). TRIM28 recognises ZFP57 and recruits SETDB1 and DNMT1 to the DNA to promote heterochromatin formation (Denomme and Mann, 2013). It is worth noting that expression of *DNMT1* and *SETDB1* was unchanged between *PADI6*^{KD} and control injected oocytes (Appendix IV.A). This is not surprising for *DNMT1* as the array primer design did not target the predominant oocyte-specific isoform, *DNMT1o* (Cirio et al., 2008). *ZFP57* 'n' values are smaller than other genes tested as detected *ZFP57* expression was very low in this study. *ZFP57* was downregulated in *PADI6*^{KD} oocytes compared to DB injected oocytes but not SCR dsiRNA injected oocytes. The low 'n' values discussed here cause there to be large standard errors of the means and may preclude significance between groups. Greater detection of *ZFP57* transcript could be improved by increasing the starting amount of cDNA in the real-time PCR. *DNMT3A, DPPA3, TRIM28* and *ZFP57* appear to have specific roles in regulating methylation at imprinted gene loci. Our limited study of the oocyte will have missed the legacy effects of gene KD in oocytes that will only become apparent later in development. It is therefore difficult to dissect out how exactly KD of the *PADI6* gene expression results in dysregulation of a specific subset of genes involved in methylation but finding a link between such genes may reveal a novel regulatory role for *PADI6* in the oocyte.

5.4.4 Dysregulation of epigenetic regulators in *PADI6*^{KD} oocytes

Finally, *PLAGL1* gene expression was reduced in *PADI6*^{KD} oocytes compared to control injected oocytes (Figure 5.7c) ($p<0.05$). *PLAGL1* is an imprinted gene that is paternally expressed and methylated on the maternal allele. Methylation of *PLAGL1* has been examined previously in bovine preantral and antral oocytes (O'Doherty et al., 2012). These results showed that *PLAGL1* methylation changed during oocyte growth from 13% in preantral follicles to 86% in antral follicles, progressively silencing the *PLAGL1* gene during oocyte growth. From GV to MII, *PLAGL1* transcript abundance should naturally decrease in all injection groups. However, after *PADI6* KD there was a larger decrease in *PLAGL1* transcript abundance compared to DB and SCR control MII oocytes, suggesting an even greater silencing of the *PLAGL1* gene occurred as a result of *PADI6* KD. The same researchers showed that *DNMT3A* is expressed throughout bovine oocyte growth, therefore it is likely that the enhanced silencing we observed here is a result of increased *DNMT3A* gene expression in *PADI6*^{KD} oocytes. Moreover, excess DNMT3A during oocyte growth has been showed to accelerate the acquisition of *PLAGL1* imprinting in mouse oocytes (Hara et al., 2014). To investigate this further, it would be interesting to examine *PLAGL1* expression in GV oocytes and look to see if there is an observed decrease in transcript abundance from GV to MII oocyte. Finally, it is interesting to note that mice with *Trim28* silencing mutations have reduced *Plagl1* expression (Dalgaard et al., 2016). In the current study, KD of *PADI6* results in downregulation of *TRIM28* and concordantly, downregulation of *PLAGL1* expression. Alongside the study by Dalgaard et al. (2016) the results presented in this thesis suggests a role for *TRIM28* in methylation regulation at *PLAGL1* imprinted gene loci and that this pathway may be modulated by *PADI6*. Finally, *PLAGL1* regulates the expression of a number of imprinted genes involved in placental growth therefore the impact of downregulation of *PLAGL1* will arise later in development as a legacy effect in the trophoblast (Iglesias-Platas et al., 2014).

5.4.5 RNA-seq analysis in *PADI6*^{KD} oocytes

RNA-seq identified 452 DEGs following KD of *PADI6*. The majority of these genes play significant roles in growth, development or epigenetic regulation in the oocyte and early embryo. Of particular interest to *PADI6* was the downregulation of *KRT5* and *8* – keratin components of intermediate filaments of the oocyte and embryo cytoskeleton (Jackson et al., 1980; Mao et al., 2014) (Figure 5.10 and Figure 5.12). Cytokeratins are a suggested component of CPLs as well as possible substrates of PADI6 (Capco et al., 1993; Liu et al., 2017; Senshu et al., 1999; Snow et al., 2008; Wright et al., 2003). *KRT8*-deficient female mice are sterile characterised by mid-gestation embryonic death and failure of proper trophoblast development (Baribault et al., 1993; Jaquemar et al., 2003). Downregulation of keratin genes after KD of *PADI6* may be consistent with failed CPL formation in *Padi6*$^{-/-}$ mouse oocytes (Esposito et al., 2007). The correct organisation and function of the oocyte cytoskeleton is critically important for meiotic spindle formation, chromosome segregation, polar body extrusion and hence production of a fertile gamete.

In this thesis, *NOBOX* was also downregulated by almost 2-fold following KD of *PADI6* in bovine oocytes (Figure 5.10). In support of this observation, a previous study discovered that *Padi6* was downregulated by >5-fold in *Nobox*-KO mouse ovaries (Choi et al., 2007). They showed that Nobox regulated *Padi6* expression by binding to a Nobox binding element within the *Padi6* promoter (Choi et al., 2010). This suggests that there is a dynamic regulatory relationship between *NOBOX* and *PADI6* in the oocyte. Interestingly, another study showed that *Nobox* regulated *Dnmt1o* in mouse ovaries (Rajkovic et al., 2004). The evidence presented in this thesis therefore demonstrates a relationship between master transcriptional regulators, *FIGLA* and *NOBOX*, *PADI6* and key epigenetic regulators in the oocyte.

IPA was used to investigate the relationship between DEGs, disease states, cellular functions and *PADI6* (Figure 5.11 and Figure 5.12). Firstly, the canonical pathways that were highlighted after KD of *PADI6* are known to be critically important for oocyte maturation (Figure 5.11a), particularly PKA and cAMP-mediated signalling in meiotic maturation (Section 1.3). Of interest to *PADI6,* the SCMC and oocyte maturation was the role of DEGs in mitochondrial dysfunction. Further, pathway analysis of DEGs identified increased expression of transcripts involved in an RNA damage pathway (Figure 5.13). This pathway linked mitochondrial activity, translation and transcription.

Mitochondrial and ribosomal components were upregulated following KD of *PADI6*. Genes involved in polyadenylating mRNA (*PABPN1* – polyadenylate-binding nuclear protein 1), anchoring the ER to the cytoskeleton (*CKAP4* – cytoskeleton associated protein 4) and endosome sorting (*CHMP4B* – charged multivesicular body protein 4B) were also upregulated. Previous studies have described dysregulation of ribosomes, RNA Pol II and mitochondria following loss of *Padi6* in mouse oocytes and embryos (Fernandes et al., 2012; Kan et al., 2012; Mehlmann et al., 1995; Yurttas et al., 2008). This finding may be crucial to the understanding of *PADI6* function in the oocyte. Branched chain keto acid dehydrogenase E1, alpha polypeptide (*BCKDHA*) was 1 of 3 genes that were downregulated in the pathway. It is responsible for the breakdown of leucine, isoleucine and valine in mitochondria (Pan et al., 2018), therefore investigations into amino acid metabolism as conducted in Chapter 6 might join these mechanisms together. Evaluation of DEGs in disease states confirmed the crucial role of *PADI6* in development and again suggested there might be a link between *PADI6* and metabolism (Figure 5.11b). As a result, the function of *PADI6* in amino acid metabolism was investigated in Chapter 6. Finally, a role for *PADI6* in gene expression and DNA processing was proposed. It is unlikely that *PADI6* is directly involved with DNA replication given its cytoplasmic localisation (Esposito et al., 2007; Wright et al., 2003; Yurttas et al., 2008), however it may regulate gene expression through a post-transcriptional or translational mechanism (Bebbere et al., 2016). It is necessary to investigate the expression of the above genes of interest by qPCR to validate the findings of RNA-seq.

Of the genes that were differentially expressed between control and *PADI6* KD samples, the FDR was >0.05 suggesting a high likelihood of false positive results. It is probable that the genetic variation of individual oocytes alongside the variable efficiency of *PADI6* dsiRNA KD precludes differential gene expression between injection groups. RNA-seq of individual oocytes was introduced to avoid pooling effects which might have otherwise masked important transcriptomic changes. Here, despite employing single-oocyte RNA-seq, bioinformatic data analysis requires the grouping of samples for statistical comparison of differential gene expression thereby re-introducing the caveat of genetic variation. Furthermore, due to the high cost of RNA-seq, the 'n' for each group was 6 oocytes which was low compared to the numbers used for the epigenetic regulator array (n=20). Increasing the number of oocytes for RNA-seq might have revealed a greater number of DEGs and enabled better comparisons between oocytes with high *PADI6* KD identified through RNA-seq as opposed to qPCR. Moreover, RNA-seq analysis of preimplantation embryos

generated following oocyte *PADI6* KD might have revealed more dramatic signatures associated with the legacy of oocyte *PADI6*.

5.4.6 Conclusion

The creation of individual bovine *PADI6*^{KD} oocytes has facilitated investigation into the functional role of *PADI6.* It appears that KD of *PADI6* gene expression does not have a profound effect on transcription during bovine oocyte maturation as only 2 candidate genes (*PRDX1* and *ZP1*) were identified after assessment of oocyte quality markers while *FIGLA* and *IZUMO1R* showed trends towards significance. Both *PRDX1* and *ZP1* display distinct functions in the oocyte and further investigation is necessary to dissect the interactions with *PADI6*. Alternatively, the imprinted gene and epigenetic regulator array highlighted differential expression of 5 associated genes: *DNMT3A, DPPA3, TRIM28, ZFP57* and *PLAGL1. DNMT1, KHDC3L* and *NLRP2* also showed trends towards significant differentially expression. Such genes are involved in critical epigenetic processes in the oocyte and embryo and pose an interesting link between the SCMC and imprinting abnormalities. The RNA-seq results confirmed that KD of *PADI6* gene expression was successful and showed that a number of genes were differentially expressed between DB and KD groups ($p<0.01$), including *NOBOX* and keratin genes (*KRT5 and 8*). Pathway analysis suggested that KD of *PADI6* altered the expression of genes in an RNA damage network which linked mitochondrial activity, transcription and translation. Finally, the FDRs were not statistically significant, and the candidate epigenetic regulators were not shown to be differentially expressed in the RNA-seq data. This suggests that *PADI6* functions in post-transcriptional or translational regulation in the oocyte in concordance with its documented cytoplasmic localisation. Further studies are needed to confirm the potential role of *PADI6* in post-transcriptional, translational and epigenetic regulation in oocytes.

Chapter 6 Functional analysis of the effects of *PADI6* KD during bovine oocyte maturation *in vitro*

6.1 Introduction

Following investigation into the transcriptome of *PADI6*^{KD} oocytes in the preceding chapters, it was necessary to look at the functional effects of *PADI6* gene KD on MII oocytes and the effect of RNAi on the PADI6 protein itself. Gene knockout guarantees ablation of the protein product but for MEGs this often masks the function of the gene as the phenotype is lethal. Successful KD of a transcript by RNAi is directly identified by real-time PCR. However, KD of the transcript does not always lead to ablation of the protein product (Wu et al., 2004). The half-life and stability of the protein determines how long the protein will persist in the cell. It was therefore critical to investigate protein abundance after siRNA KD by Western blotting. Secondly, considering the potential enzymatic activity of PADI6 and the suggested impact of KD of *PADI6* on amino acid metabolism identified in Chapter 5 (Section 5.3.4.1), experiments were performed to investigate changes to the metabolism of bovine oocytes following *PADI6* KD. Finally, the legacy effect in the bovine preimplantation embryo following KD of *PADI6* in the oocyte during IVM was assessed by generating embryos by IVF in *PADI6*^{KD} oocytes. The function of PADI6 is still unclear therefore it was hoped that these experiments would provide further insight into the role of *PADI6* in the bovine oocyte.

6.1.1 PADI6: the protein

With the exception of the data presented in this thesis, research into PADI6 protein expression and localisation has primarily been investigated using the mouse model. As described in Chapter 1, Section 1.7.3, multiple researchers have shown that PADI6 is localised to the cytoplasm, CPL structures and SCMC in mouse oocytes and embryos (Esposito et al., 2007; Kim et al., 2010; Wright et al., 2003). PADI6 is seen to increase in abundance in the ovaries of 1-day old mice to 7-day old mice as the primary and secondary follicles develop (Xiong et al., 2019). This coincides with a significant oocyte growth phase, secretion of ZP and accumulation of cytoplasmic organelles and transcripts (Section 1.3.3). Furthermore, studies in mice have revealed novel protein interactions and characteristics of PADI6. PADI6 was found to

be phosphorylated during oocyte maturation which facilitated binding to YWHA proteins (Snow et al., 2008). YWHA proteins are ubiquitous adaptor proteins that can modulate protein function, subcellular localisation and interaction (Morrison, 2009). This discovery may indicate that PADI6 function depends upon post-translational phosphorylation. Further, knockout of PADI6 affects the solubility of MSY2 protein, suggesting that PADI6-dependent CPL formation is necessary for anchoring proteins in the oocyte (Liu et al., 2017). Similarly, localisation of ribosomal components, RNA Pol II and organelles were disrupted upon ablation of PADI6 (Kan et al., 2011; Yurttas et al., 2008). Despite its important role in the oocyte, our understanding of PADI6 is incomplete. By co-transfecting CHO and HeLa cell lines, transcription factor SP1 was found to bind to the porcine *PADI6* promoter and regulate *PADI6* mRNA and protein expression (Xia et al., 2016). Further, *in silico* and *in vitro* experiments identified YWHA protein binding sites in human PADI6 peptides and evidence suggests that phosphorylation of PADI6 by RSK-type kinases facilitates this interaction (Rose et al., 2012). Finally, *in vitro* enzyme assays with human PADI6 protein concluded that PADI6 does not function as a deiminase (Raijmakers et al., 2007). *In vitro* and heterologous experiments are useful to discover potential protein interactions and characteristics, but the results must be interpreted with caution as native factors and conditions in the oocyte may confound *in vitro* findings. Thus far, investigation of PADI6 protein in preimplantation development has not been explored. To this end, attempts were made in this chapter to detect bovine PADI6 by Western blotting.

For this project, the commercial antibodies that were available were not raised against bovine PADI6 but rather were against human PADI6 peptides. In order to optimise the PADI6 antibody for bovine use, human PADI6 was used as a positive control. To this end, 2 different cloning methods were explored to produce vectors and proteins with different properties for downstream applications e.g. a specific protein tag for protein purification. Firstly, traditional pET vector cloning was performed to produce a human PADI6 protein possessing a C-terminal histidine tag for protein production in bacteria. The more modern, gateway cloning, was also used to create a versatile entry clone that allows switching of the DNA insert, using bacteriophage site-specific integration, between different destination vectors (Hartley et al., 2000). This method enables the fast and efficient movement of human PADI6 gene into different vectors for use in bacterial or mammalian expression systems. Furthermore, this meant that PADI6 protein could easily express different protein tags depending on which vector it was inserted into. It also could potentially increase the scope for downstream experiments such as expression of PADI6 in different mammalian cell types to look

at protein function. Finally, antibodies and recombinant proteins can be useful tools for assessing protein KD in cells. Antibodies targeting a specific protein can be administered to a cell to bind to its endogenous counterpart. This causes the endogenous protein to be sequestered by the antibody and unable to function, effectively knocking down the protein of interest (Marschall et al., 2015). On the other hand, recombinant proteins can be used to replace a previously ablated protein to see if the KD phenotype can be rescued. If the KD is rescued it ensures that the phenotype was a true effect of KD (Cullen, 2006). Altogether, examining protein abundance after gene KD, followed by the use of antibodies and recombinant proteins to further study protein KD provides a thorough investigation into gene function.

6.1.2 PADI6: the enzyme

As *PADI6* is a member of a family of citrullinating enzymes that convert peptidylarginine to citrulline, the effect of *PADI6*^{KD} on the metabolism of MII oocytes was explored. Citrulline is not a coded AA but is generated by post-translational modification of the protein. This conversion causes a change in protein charge from positive to neutral, which impacts hydrogen bonding therefore protein folding (Vossenaar et al., 2003). Research into other *PADI* family members highlights the importance of citrullination in cells. *PADI4* is the only *PADI* with a recognised nuclear localisation signal (NLS) (Asaga et al., 2001; Nakashima et al., 2002). Coupled to this, it acts on histones to decondense chromatin structures (Neeli et al., 2008; Wang et al., 2009), which may provide interesting information towards how PADI6 is connected to the process of epigenetic regulation. *PADI4*'s major role in immunity involves the formation of neutrophil extracellular traps that consist of decondensed chromatin (Li et al., 2010b). Furthermore, PADI4-mediated citrullination of histones has been implicated in the regulation of multiple genes (Li et al., 2008b; Wang et al., 2004). PADI2 has also been found to catalyse citrullination of histones in numerous cell types, leading to decondensation of chromatin and gene regulation (Cherrington et al., 2010; Zhang et al., 2012). PADI2 does not have a recognised NLS, however in oligodendrocytes, PADI4 nuclear translocation was induced by a stimulus in the form of tumour necrosis factor (Mastronardi et al., 2006). This suggests that there may be a potential mechanism whereby PADI proteins are shuttled into the nucleus by chaperone proteins, without the need for an NLS. PADI2 has also been shown to citrullinate RNA pol II in breast cancer cells (Sharma et al., 2019). Depletion of PADI2 and loss of the citrulline modification caused accumulation of RNA pol II at promoters and reduced gene expression. It is known that loss of *Padi6* also affects RNA pol II,

suggesting a possible overlapping function (Yurttas et al., 2008). Overall, it appears that PADI family members function in various ways to regulate gene expression. The question is how this translates to their function in oocytes and preimplantation embryos.

It is evident that citrullination is a key post-translational modification that is linked to gene regulation but the importance of citrullination in preimplantation development is less clear. Citrullination has been observed in both mammalian oocytes and cumulus cells (Brahmajosyula and Miyake, 2013; Kan et al., 2011). For example, inhibition of all PADI proteins in mouse zygotes using Cl-amidine reduced histone citrullination and resulted in premature embryonic arrest, demonstrating the significance of PADI activity in preimplantation development (Kan et al., 2011). Moreover, treatment with Cl-amidine also reduced histone acetylation, revealing a novel interplay between histone acetylation and citrullination. It is suggested that the citrulline modification provides a platform for interactions with epigenetic regulators and thereby influences transcriptional regulation. Kan et al. (2011) also found that H3Cit26 appeared to localise to lipid droplets in oocyte and embryos, supporting work by Cermelli et al. (2006) that showed that lipid droplets sequester maternal proteins, including histones. Histone H3 is a well-known substrate of PADI4. PADI4 was found to translocate to the nucleus prior to GVBD and localise to the metaphase spindle of mammalian oocytes, suggestive of its role in histone citrullination in the oocyte (Brahmajosyula and Miyake, 2013). Similarly, other PADI family members have been observed in mammalian development. PADI1 appears to be primarily localised to the nucleus of mouse oocytes and embryos (Zhang et al., 2016). Depletion of *Padi1* in mouse embryos markedly reduced histone citrullination and prohibited embryo development. Furthermore, transcription and RNA pol II phosphorylation were also reduced in PADI1-depleted embryos. Finally, Brahmajosyula and Miyake (2013) detected a protein band in oocytes, but not cumulus cells, which was thought to be that of a citrullinated keratin from the oocyte-specific CPL structure. Esposito et al. (2007) also identified loss of CPL formation and loss of citrullination in *Padi6* mutant mouse oocytes. This poses the question of whether PADI6 protein also has citrullinating ability in the oocyte.

As mentioned in Chapter 1, Section 1.7.3, there are many caveats to consider when discussing PADI6 as an enzyme. Firstly, PADI activity requires calcium as a cofactor, however it appears that PADI6 has lost the ability to bind to calcium (Arita et al., 2004; Rogers et al., 1977). Experimentally, *in vitro* enzyme assays have shown that

recombinant PADI6 fails to metabolise known substrates for PADI4 (Raijmakers et al., 2007). Further, studies have shown that PADI6 resides in the cytoplasm of the oocyte, negating a potential role for it in the nucleus (Wright et al., 2003). Yet, there is no definitive proof that PADI6 lacks enzymatic activity. As mentioned previously, *PADI6* has diverged from the other *PADI* family members and displays a restricted, oocyte-specific tissue expression pattern (Chavanas et al., 2004). It is evidently critical for preimplantation embryo development, but its mechanism of action is unknown. *Padi6* is necessary for the establishment of unique oocyte CPLs but it remains unclear as to how it regulates their formation (Wright et al., 2003). Other researchers suggest that *PADI6* has evolved a new regulatory switch, away from calcium regulation, as changes to the gene sequence are said to be under positive selection (Chavanas et al., 2004). This could be feasible as there are many fluctuations in Ca^{2+} throughout oocyte meiotic maturation and preimplantation embryo development, notwithstanding the large influx of calcium upon sperm entry (Whitaker, 2006). There is some evidence that the function of PADI6 may be regulated by phosphorylation. Snow et al. (2008) discovered that PADI6 was phosphorylated during oocyte maturation and PADI6 binds YWHA proteins in a phosphorylation-dependent manner in MII oocytes and embryos but not GV oocytes. YWHA proteins are often involved in protein interactions, stability and localisation thus may serve as a cofactor or scaffold for PADI6 expression. Multiple kinases have been identified that may be suitable candidates for phosphorylation of PADI6: protein kinase B and C and ribosomal S6 kinase, RPS6KA1 (Snow et al., 2008; Wright et al., 2003). Intriguingly, ablation of *Padi6* is associated with reduced phosphorylation of RNA pol II, indicating the potential for a scaffold with which transcripts and proteins are modified to become activated (Yurttas et al., 2008).

Oocyte growth and cytoplasmic maturation requires post-transcriptional regulation of maternal mRNAs as well as synthesis and post-translational modification of proteins (Jansova et al., 2018). Amino acid (AA) metabolism is critical for the generation of precursors for biosynthetic processes such as protein synthesis, cellular signalling, epigenetic regulation and energy metabolism in the oocyte (Collado-Fernandez et al., 2012). Further, AA turnover in oocytes and embryos has been strongly associated with embryo developmental competence, blastocyst formation and pregnancy potential (Hemmings et al., 2012; Hemmings et al., 2013; Houghton et al., 2002; Sturmey et al., 2008). Amino acid profiling (AAP) of oocytes has been extensively validated in bovine oocytes as a non-invasive measure of oocyte health and developmental competence (Hemmings et al., 2012). Using high performance liquid

chromatography (HPLC) it is possible to measure the release and uptake of 19 principal AAs by individual oocytes and embryos analysing the AA content of spent culture media compared to control media. Furthermore, pathway analysis of RNA-seq data in Chapter 5 suggested that KD of *PADI6* affected amino acid metabolism. With this in mind, the effect of *PADI6* gene KD on amino acid metabolism of the oocyte was questioned. To this end, HPLC was used to quantify the AAP of oocytes with/without *PADI6* gene KD. Although this method of AAP cannot detect changes in citrulline *per se*, it was used here to see if *PADI6*^{KD} oocytes displayed fluctuations in AA metabolism, which may be reflective of the role of *PADI6* on the health of the oocyte.

6.1.3 Aims and objectives

The aim of this chapter was to investigate the functional impact of *PADI6* KD during IVM of bovine oocytes. To this end, a series of 3 independent experiments were carried out:

1) Production of recombinant human PADI6 protein using a bacterial expression system for use as a functional protein source to rescue the *PADI6* KD phenotype in bovine oocytes.
2) Characterisation of oocyte metabolism by AAP following *PADI6* KD during bovine oocyte maturation *in vitro.*
3) *In vitro* fertilisation of bovine oocytes following *PADI6* KD during IVM to look at the impact of *PADI6* KD on bovine preimplantation embryos.

The first experiment aimed to investigate the PADI6 protein by creating a human recombinant PADI6 expression vector. With this, a variety of strategies could be explored. Primarily, recombinant PADI6 could be used as a positive control for antibody optimisation in Western blot analysis of PADI6 protein in oocytes and embryos. Furthermore, recombinant protein, if proven to be biologically active, could be used during oocyte culture or KD experiments in other cell types in which PADI6 can be detected to rescue the dsiRNA KD phenotype. However, ultimately recombinant PADI6 could also be used for investigation into PADI6 protein structure and enzymatic activity. To this end, a recombinant human PADI6 protein was produced by cloning a full-length open reading frame of *PADI6* into *E. coli*. 2 different cloning techniques were used to create 2 vectors for use in bacterial and mammalian expression systems, and for expression of proteins with different protein tags. Western blot analysis using a commercially available human PADI6 antibody was used to detect the PADI6 protein in bacterial lysates following induction of protein expression. Alongside this, bovine oocytes were pooled for analysis of PADI6 protein by Western blotting. The final aim was to use the recombinant PADI6 protein and antibody to look at the effects of rescue and KD of PADI6 protein in bovine oocytes, respectively.

The second experiment aimed to characterise the metabolic profile, and specifically AA metabolism of *PADI6*^{KD} bovine MII oocytes compared to DB and SCR dsiRNA injected MII oocytes. To this end, AAP analysis of spent oocyte culture media were conducted. Following microinjection, single oocytes were placed into IVM media for 18 hours, followed by 6 hours in 1 µl drops of AAP-IVM media. After this time, single oocytes were lysed for cDNA synthesis and real-time PCR analysis and the AAP-IVM media drops were frozen for later analysis. AAP was performed on media drops using HPLC (Hemmings et al., 2012). 19 AAs were detected using this method and metabolic profiles of AA uptake and release by individual MII oocytes were created. AA profiles from each injection group were compared for significance using statistical tests.

Finally, the third experiment aimed to investigate the impact of *PADI6* KD on MII oocyte subsequent fertile capacity and embryo developmental competence *in vitro*. Bovine oocytes were subject to microinjection and IVM as detailed in Section 4.2.2. After 24 hours in IVM media, oocytes were fertilised *in vitro* and cultured until the first few embryonic cleavage divisions were completed. Around 2-4 cell stage, embryos were lysed for cDNA synthesis and real-time PCR analysis was conducted to assess the transcript abundance of *PADI6* and hence define the longevity of the effects of gene KD.

6.2 Materials and methods

To investigate the functional effects of *PADI6* KD in bovine oocytes 3 different approaches were explored to assess the impact of targeted KD of *PADI6* on PADI6 protein abundance, oocyte metabolism and developmental competence.

6.2.1 Experiment 1: Production of recombinant human PADI6 protein using a bacterial expression system

Human *PADI6* open reading frame (ORF) in pEnter with C-terminal Flag and His tag (CH824752) was purchased from Vigene Biosciences (Rockville, USA) to be used as a PCR and cloning template (Figure 6.1). 2 different methods of cloning were used: pET vector cloning and gateway cloning. pET vector cloning was used as it was the traditional method for cloning genes into bacterial expression systems for laboratory scale inducible gene expression (Gay et al., 2014). Gateway cloning was also chosen because it creates a flexible vector that can transfer the gene of interest into a range of vectors for both bacteria and mammalian expression systems (Hartley et al., 2000; Marsischky and LaBaer, 2004).

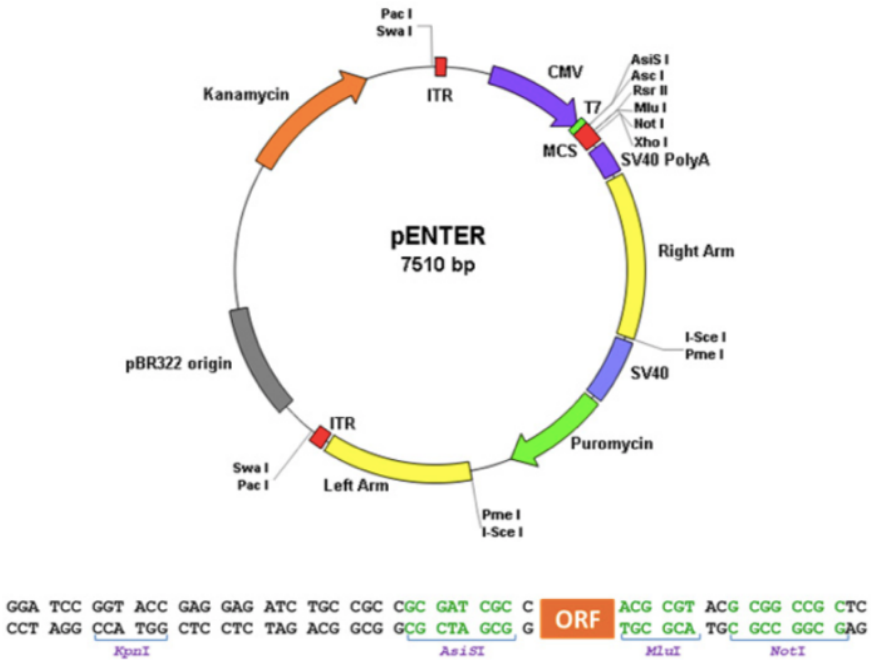

Figure 6.1. Map of pEnter vector that was purchased from Vigene Biosciences (2015). Human *PADI6* gene was inserted into the open reading frame (ORF) site.

6.2.1.1 pET vector cloning

pET-11a was chosen as the pET vector for cloning *PADI6* into a bacterial expression system. pET cloning relies on restriction digestion to cut and move DNA sequences from one vector to another (Tseng, 1999). pET-11a contains various restriction sites including *Nde*I. *Nde*I has the recognition sequence, CATATG, which makes it useful for cutting out genes at their 5' ATG start codon (Watson et al., 1982). The Vigene *PADI6* ORF clone did not possess an *Nde*I site, so site-directed mutagenesis was used to engineer one into the sequence.

6.2.1.1.1 Site-directed mutagenesis

Site-directed mutagenesis was performed according to the Q5 site-directed mutagenesis protocol (E0552S, NEB® Inc) in a 25 µl reaction volume consisting of 1 X Q5 Hot Start High-Fidelity master mix (NEB® Inc), 0.5 µM of each primer, 25 µg human *PADI6* ORF in pENTER DNA template and sterile distilled water (dH_2O). Primer sequences (Table 6.1) were designed using the Q5 site-directed mutagenesis online primer tool (NEB® Inc) to insert 'CAT' before the ATG start codon of *PADI6,* to produce an *Nde*I restriction site (CA^TATG). The PCR thermal cycle is shown in 0. After cycling, 1 µl of product was combined with 1 X Kinase, Ligase and *Dpn*I (KLD) reaction buffer, 1 X KLD enzyme mix and sterile distilled water (dH2O), to produce a circular product, and incubated for 5 min at room temperature. Figure 6.2 shows a schematic representation of site-directed mutagenesis to engineer the *Nde*I sequence into *PADI6* ORF clone. Following this, bacteria were transformed with the *Nde*I-containing *PADI6* ORF clone as detailed in Section 6.2.1.2.

Table 6.1 Primer sequences for site-directed mutagenesis

		Tm
Forward site-directed mutagenesis *PADI6* primer (5'→3')	**CAT**ATGGTCAGCGTGGAGGGCC	72ºC
Reverse site-directed mutagenesis *PADI6* primer (5'→3')	GGCGATCGCGGCGGCAGA	

Table 6.2 Thermal program for site-directed mutagenesis PCR

Cycles	Step	Temperature (ºC)	Time
1	Denaturing	98	30 s
2-26	Denaturing Annealing Extension	98 72 72	10 s 20 s 4 min
27	Extension	72	2 min
28	Hold	4	∞

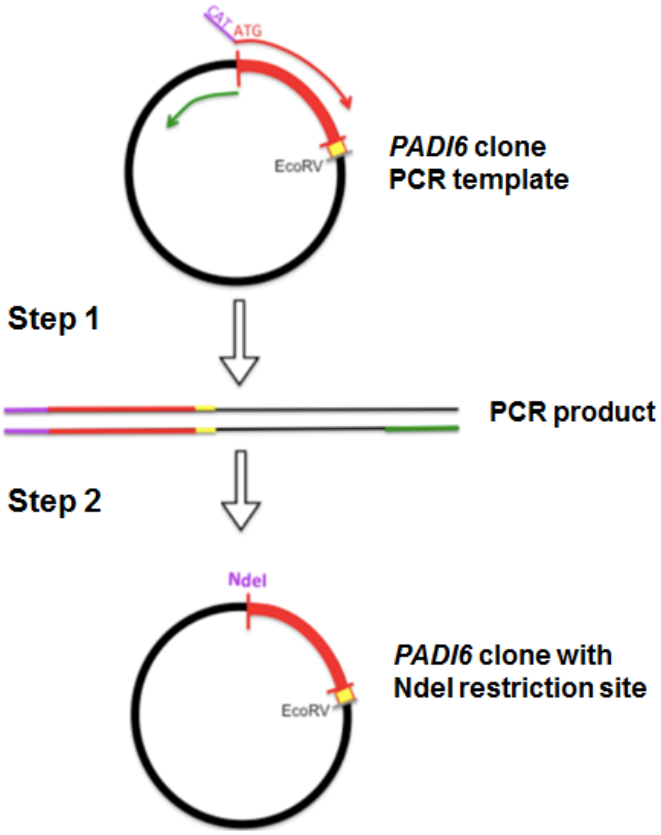

Figure 6.2. Site-directed mutagenesis of *PADI6* clone to introduce a 5' *Nde*I restriction site. **Step 1:** The forward primer (red arrow) with a 5' mismatching 'CAT' (purple) before the ATG start codon was engineered to add an *Nde*I restriction site (CA^TATG) to the start codon of *PADI6* while the reverse primer (green arrow) amplified the vector in the opposite direction. The resultant PCR product was linear and unphosphorylated so it would not re-ligate into a circular piece of DNA. **Step 2:** The kinase, ligase and *Dpn*I (KLD) reaction was performed. The kinase phosphorylated the 5' ends while the ligase joined the 5' and 3' to create a circular plasmid. *Dpn*I degraded the *PADI6* clone PCR template to improve the transformation efficiency. *Dpn*I only degrades methylated adenosines in its GA^TC restriction site, i.e. only degrades parental DNA which originated from methylating bacteria. The histidine tag (yellow) was succeeded by the *Eco*RV restriction site that was used to clone *PADI6* into pET-11a.

6.2.1.2 Bacterial transformation, miniprep and sequencing

50 µl of DH5α chemically competent E. coli (18265017, InvitrogenTM Ltd) were transformed with 1 µl of vector mixture and incubated on ice for 30 min according to the manufacturer's instructions. The cells were heat shocked at 42ºC for 45s. 250 µl of SOC medium was added and cells were incubated at 37oC for 1 hour. Cells were plated onto Luria-Bertani (LB) agar (Appendix II - Table II.IVb) + 50 µg/ml kanamycin plates and left to grow overnight at 37oC. The following day, colonies were picked and grown in LB broth (Appendix II - Table II.IVa) + 50 µg/ml kanamycin at 37oC shaking overnight. On the third day, GenElute Plasmid Miniprep Kit (PLN10, Sigma) was used to isolate the plasmid DNA for sequencing. Plasmids were sequenced according to BigDye® Terminator v3.1 Sequencing Protocol (4337458, Applied Biosystems). An appropriate volume master mix was made equating to 1 µl BigDye® 3.1, 1.5 µl sequencing buffer and 1.5 µl dH2O per well. 4 µl of master mix was combined with 4 µl dH2O, 1 µl plasmid DNA and 1.6 pmol primer. The sequencing thermal cycle is shown in Table 6.3.

Table 6.3 Thermal program for sequencing of plasmid DNA

Cycles	Ramping	Temperature (ºC)	Time
1	Ramp 1ºC /s to:	96	1 min
2-26	Ramp 1ºC /s to:	96 50 60	10 s 5 s 4 min
27	Ramp 1ºC /s to:	4	∞

After cycling, DNA was precipitated by adding 5 µl of 125 mM EDTA and 60 µl of 100% ethanol to each well according to the BigDye® Terminator v3.1 Sequencing Protocol. The plate was centrifuged at 3900 rpm for 30 min at 22°C and then centrifuged inverted at 200 rpm for 1 min. 60 µl of 70% ethanol was added to each well and centrifuged again at 2000 rpm for 15 min at 4°C. As before, the plate was centrifuged inverted at 200 rpm for 1 min and then left to air dry in a dark place Precipitates were re-dissolved in 10 µl Hi-Di Formamide (4311320, Applied Biosystems) and resolved at 60°C using a 36 cm array on an ABI3130xl Genetic Analyzer (Applied Biosystems). POP7 polymer, 3730 sequencing buffer and the FragmentAnalysis36_pop7_1 module was used for all runs. Table 6.4 shows the primer sequences that were used for verification.

Table 6.4 Primer sequences for sequencing of *PADI6* vector clones

Primer name	Primer binding site	Primer sequence (5'→3')
PADI6 1	*PADI6* exon 1- FOR	GAGCCATGTCCTTCCAGAGT
PADI6 2	*PADI6* exon 2- FOR	CGTACGCCACAGTGAAGATG
PADI6 3	*PADI6* exon 3- REV	CCTCGTTGGGCCCATAGTAT
PADI6 4	*PADI6* exon 7- FOR	CTATACCTTGGCCCTCCTCG
PADI6 5	*PADI6* exon 8- FOR	TCACTGAGCCCTGGTATTGG
PADI6 6	*PADI6* exon 11- REV	TCTTTCCCTTGGACCTTGACA
PADI6 7	*PADI6* exon 12- FOR	CAGATTGGCTAATGACTGGCC
PADI6 8	*PADI6* exon 16- FOR	GGCAAGAACCTGGGGATCC
SP6	Vector backbone	TATTTAGGTGACACTATAG
T7	Vector backbone	TAATACGACTCACTATAGGG
pENTER	Vector backbone- FOR	GCACCAAAATCAACGGGACTTTCC
pENTER	Vector backbone- REV	GCTCGACGAATTTATCGTCATCC

Next, the engineered *PADI6* clone was digested with *Nde*I (R0111, NEB® Inc) at the novel 5' CATATG site and *Eco*RV (R0195, NEB® Inc) situated after the histidine (His) tag at the C-terminus. The digested mixture was run on a 1% (w/v) agarose gel containing 1 µl Midori Green Advance (MG04, Nippon Genetics, Germany) in place of ethidium bromide to avoid damaging the DNA. If site-directed mutagenesis was successful, 4 bands of the following sizes were expected: 422 bp, 2194 bp (*PADI6* band), 3440 bp and 3501 bp. The 2194 bp band was cut from the gel and the DNA extracted using the PureLink Quick Gel Extraction Kit according to the manufacturers protocol (K210012, Invitrogen™ Ltd). In brief, a transilluminator was used to visualise the band of interest on the gel. The band was carefully cut from the gel using a clean, sterile scalpel blade (Swann-Morton, UK) taking care not to excise excess agarose surrounding the DNA fragment. The excised band was weighed before placing into a clean 1.5 ml Eppendorf tube. A maximum of 400 mg of gel was allowed per tube. 1.2 ml of gel solubilisation buffer was added per 400 mg of agarose gel and the tube was placed at 50°C on a heat block for 10 min. Every 3 min the tube was inverted by hand to mix the solution. Once the gel had disappeared the tube was incubated at 50°C for a further 5 min. In preparation for DNA purification, 64 ml of >99.8% ethanol (v/v) (51976, Sigma) was added to the wash buffer obtained from the kit. The dissolved gel solution was pipetted onto the centre of a clean Quick Gel Extraction Column

inside a wash tube. A fresh column was used per 400 mg of gel starting material. The tubes were centrifuged at 12,000 x g for 1 min. The flow through was discarded and the column was placed back into the wash tube. 500 µl of wash buffer containing ethanol was added and the tubes were centrifuged at 12,000 x g for 1 min. The flow through was discarded and the column was placed back into the wash tube. The column was centrifuged on maximum speed for 1-2 min to remove residual ethanol. The wash tube was discarded, and a clean 1.5 ml Eppendorf tube was used as the recovery tube. 50 µl of nuclease-free water was added to the column and incubated at RT for 1 min. Following this, the tubes were centrifuged at 12,000 x g for 1 min to elute the DNA. The column was discarded, and the DNA was stored at -20°C until further use.

Concurrently, pET-11a was digested by *Bam*HI (R0136, NEB® Inc) and purified using the PureLink PCR Purification Kit (K310001, Invitrogen™ Ltd). DNA polymerase I large Klenow fragment (M0210, NEB® Inc) was added alongside 1 x NEB buffer 2 containing 33 µM of each dNTP (10297018, Invitrogen™ Ltd) to fill in the 5' overhang leaving a blunt end. 10 mM ethylenediaminetetraacetic acid (EDTA) was added and the mixture heated at 75°C for 20 min to terminate the reaction. The PureLink PCR Purification Kit was used to remove the previous buffers and Klenow fragment. The product was then cut with *Nde*I and purified again using the PureLink PCR Purification Kit.

Finally, the restriction digest products of pET-11a vector and *PADI6* ORF were ligated together by adding a large excess of *PADI6* DNA to digested pET-11a alongside T4 DNA ligase (M0202, NEB® Inc). The mixture was incubated at 4°C overnight before DH5α chemically competent *E. coli* were transformed, miniprepped and sequenced as described in Section 6.2.1.2. Sequence verified bacterial cultures were stored in glycerol at -80°C until further use. Figure 6.3 shows the expected pET-11a vector clone after insertion of *PADI6* ORF.

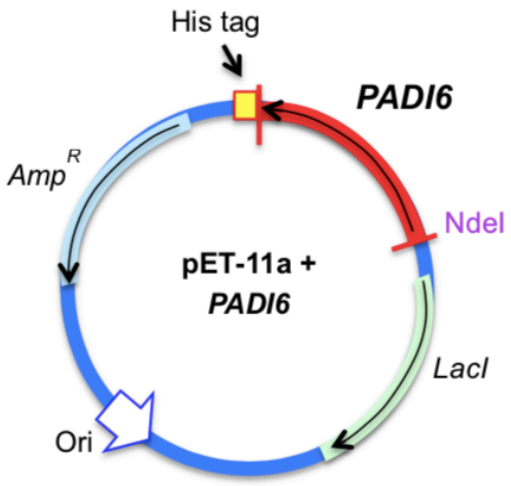

Figure 6.3. Expected *PADI6* pET-11a vector clone. pET-11a has an ampicillin resistance (Amp^R) gene for positive bacterial colony selection and a *LacI* gene, which means it is inducible by the addition of IPTG. Human *PADI6* was cloned with a histidine tag (yellow) into the multiple cloning site (MCS) of pET-11a, between *Nde*I and *Bam*HI, destroying the *Bam*HI site.

6.2.1.3 Gateway cloning

In 2000, Hartley et al. (2000) designed a cloning strategy that was based upon site-specific recombination in bacteria by bacteriophage λ. Now marketed by Invitrogen™, the gateway cloning system consists of the BP and LR recombination reactions performed by BP and LR clonase enzymes, respectively. For recombination to occur, *att* sites must flank the DNA insert and a region of the vector that will be removed – in the gateway system this is the *ccdB* bacterial toxin gene. If recombination is not successful, the *ccdB* toxin is expressed and the bacteria are killed. This is a useful design tool as the colonies that grow should contain the gene of interest. The gateway cloning strategy is summarised in Figure 6.4.

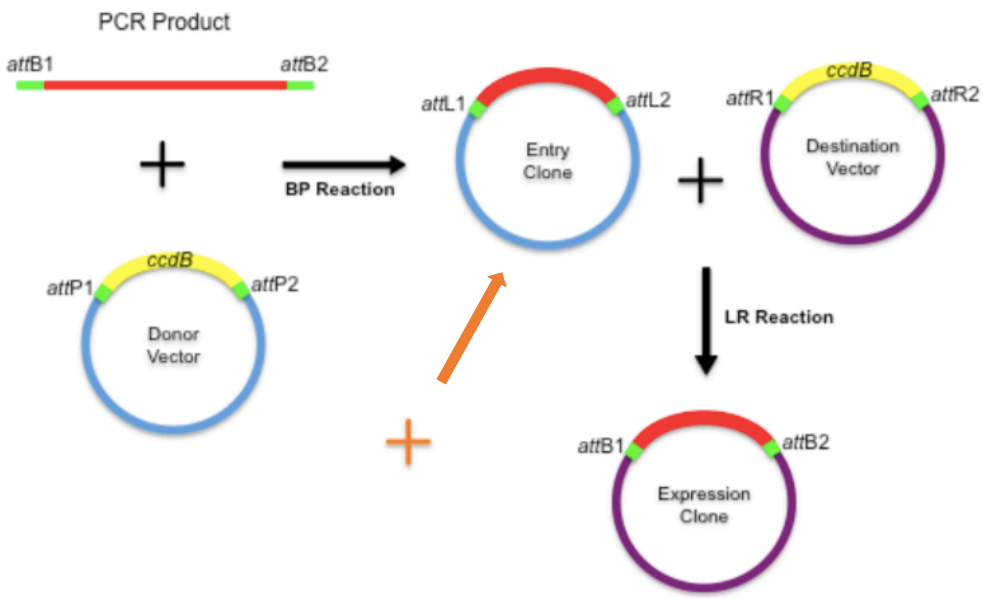

Figure 6.4. Summary of gateway cloning system. PCR is performed to create a DNA insert flanked by *att*B sites. It is subsequently mixed with a donor vector in the BP reaction to produce an entry clone containing the DNA insert. The entry clone is mixed with a destination vector in the LR reaction to produce an expression clone. The system is reversible as the expression clone can be mixed with the donor vector in a BP reaction to create an entry clone again (orange).

6.2.1.3.1 PCR to produce *att*B flanked *PADI6* insert

PCR was performed to produce a full-length ORF of *PADI6* flanked by *att*B sites using the Vigene *PADI6* ORF clone as a DNA template. Platinum *Pfx* DNA polymerase (11708039, Invitrogen™ Ltd) was used according to the manufacturers protocol in a 50 µl reaction volume consisting of 1 X *Pfx* amplification buffer, 1 mM $MgSO_4$, 0.3 mM of each dNTP, 0.3 µM of each primer, <200 ng template DNA, 1 unit Platinum *Pfx* DNA polymerase and dH_2O. Table 6.5 shows *att*B *PADI6* primers designed according to the Gateway Technology Manual (Invitrogen™ Ltd). The PCR thermal cycle is shown in Table 6.6**.** 10 µl of PCR product was ran on a 1.5% (w/v) agarose gel with 0.5 µg/ml ethidium bromide in 1 x tris- acetate-EDTA (TAE) buffer at 90 V for 60 min, to verify the correct product size. The PCR product was subsequently pooled and purified using the PureLink Quick Gel Extraction Kit.

Table 6.5 *att*B *PADI6* primer sequences for gateway cloning (5'→3'). *att*B sequences are in bold.

F-*att*B primer	GGGG**ACAAGTTTGTACAAAAAAGCAGGCT**TCGAAGGA GATAGAACCATGGTCAGCGTGGAGGGCCG	**Product Size** 2161 bp
R-*att*B primer	GGGG**ACCACTTTGTACAAGAAAGCTGGGT**CCTAAGGTA CCATCTTCCACCATTTG	

Table 6.6 Thermal cycle for platinum PCR involving a 3-step and 2-step combined method to produce *att*B flanked *PADI6* insert for gateway cloning.

Cycles	Step	Temperature (°C)	Time
1	Denaturing	94	5 min
2-5	Denaturing Annealing Extension	94 60 68	15 s 30 s 2 min 6 s
6-31	Denaturing Extension	94 68	15 s 2 min 6 s
32	Hold	4	∞

6.2.1.3.2 BP recombination reaction to produce a *PADI6* entry clone

The *att*B flanked *PADI6* fragment was combined with the gateway donor vector, pDONR201, in the BP reaction to produce a *PADI6* entry clone. 150 ng of *att*B *PADI6* PCR product was combined with 150 ng of the donor vector, pDONR201 and 2 µl BP clonase II enzyme mix (11789020, Invitrogen™ Ltd) and incubated at 25°C for 1 hour. 1 µl of proteinase K was added and incubated at 37°C for 10 min to terminate the reaction. DH5α chemically competent *E. coli* were subsequently transformed, miniprepped and sequenced as described in Section 6.2.1.2. Only *PADI6* verified clones were used in the next step of the gateway cloning method. PCR was also performed to verify insertion of PADI6 into pDONR201 vector (Section 6.2.1.4.3).

6.2.1.3.3 PCR to confirm insertion of *PADI6* into pDONR201

A 1051 bp fragment of *PADI6* was amplified to determine whether *PADI6* was present in miniprep DNA from bacterial colonies transformed with pDONR201- *PADI6* vector. PCR amplification was performed according to the GoTaq® Hot Start Polymerase protocol (M5001, Promega) in a 20 µl reaction volume consisting of 1 X buffer, 0.2 mM of each dNTP, 2.5 mM $MgCl_2$, 0.5 µM of each primer, 1.25 units polymerase, <500 ng template DNA and sterile distilled water (dH_2O). In some cases, 0.5% Triton X-100 was added to the PCR mix to reduce secondary DNA structures. The primer sequences and thermal program are detailed in Table 6.7 and Table 6.8, respectively. GeneRuler 100 bp Plus DNA ladder (SM0322, Thermo Scientific™) was used to size the expected products. PCR products were analysed by gel electrophoresis on a 1.5% (w/v) agarose gel with 0.5 µg/ml ethidium bromide in 1 x tris-acetate-EDTA (TAE) buffer at 90 V for 60 min. Gels were visualised under ultraviolet light using Gel Doc™ XR System (BioRad).

Table 6.7 Primer sequences for *PADI6* 1051 bp fragment to check insertion of *PADI6* gene into pDONR201 (5'→3').

		Product Size
PADI6 F-primer	CGTACGCCACAGTGAAGATG	1051 bp
PADI6 R-primer	TCTTTCCCTTGGACCTTGACA	

Table 6.8 Thermal program for GoTaq® Hot Start PCR

Cycles	**Step**	**Temperature (°C)**	**Time**
1	Denaturing	95	5 min
2-36	Denaturing	95	45 s
	Annealing	60	45 s
	Extension	72	1 min 10 s
37	Extension	68	5 min
38	Hold	4	∞

6.2.1.3.4 LR recombination reaction to produce a *PADI6* entry clone

Finally, *the PADI6* entry clone was combined with the gateway destination vector, pDEST15, in the LR reaction to produce a *PADI6* expression clone. 150 ng of *PADI6* entry clone was combined with 150 ng of the destination vector, pDEST15 and 2 µl LR clonase II enzyme mix (11791020, Invitrogen™ Ltd) and incubated at 25°C for 1 hour. 1 µl of proteinase K was added and incubated at 37°C for 10 min to terminate the reaction. DH5α chemically competent *E. coli* were transformed as detailed in Section 6.2.1.2. Colony PCR was performed using a pDEST15 vector T7 primer and a reverse primer in *PADI6* gene to check incorporation of *PADI6* into pDEST15 according to the GoTaq® Hot Start Polymerase protocol as described in Section 2.5. The primer sequences are detailed in Table 6.9. Again, colonies were miniprepped and sequenced as described in Section 6.2.1.2. Sequence verified bacterial cultures were stored in glycerol at -80°C until further use.

Table 6.9 Primer sequences for colony PCR to confirm presence of *PADI6* ORF in pDEST15 following LR reaction

T7 pDEST15 Vector primer (5'→3')	TAATACGACTCACTATAGGG	**Product Size** 1119 bp
PADI6 R-primer (5'→3')	TCTTTCCCTTGGACCTTGACA	

6.2.1.4 Inducing bacterial expression for production of human PADI6 protein

For each clone, *PADI6*-pET-11a and *PADI6*-pDEST15, glycerol bacterial stocks were used to inoculate 2 ml LB + 50 µg/ml ampicillin and 5 ml LB + 100 µg/ml ampicillin, respectively. Bacterial cultures were incubated at 37°C in a shaking incubator overnight. This was then used to inoculate 50 ml LB media + appropriate concentration of ampicillin. After 4 hours, 500 µl was removed from each culture and the optical density was measured at 600 nm (OD_{600}) using a spectrophotometer. Once the cultures had reached an OD_{600} of 0.4 (approx. 7 hours), they were split into 2 cultures and half of each culture was induced to give 1 induced and 1 uninduced culture. *PADI6*-pET-11a was induced by the addition of isopropyl β-D-1-thiogalactopyranoside (IPTG) (I6758, Sigma) at a final concentration of 1mM. *PADI6*-

pDEST15 was induced by the addition of L-arabinose (A3256, Sigma) at a final concentration of 0.2% (w/v). Immediately, 500 µl was removed from each bacterial culture and placed into a clean 1.5 ml Eppendorf tube. The samples were centrifuged at maximum speed for 30 sec and the supernatant discarded. These cell pellets were frozen at -20°C as the zero time points. Cultures were put back to 37°C in a shaking incubator and time points were taken every hour for 4 hours as described for the zero time point samples. Bacterial induction was repeated in 2 distinct experiments.

Prior to Western blotting, bacterial pellets were suspended in 100 µl of protein lysis buffer from the destination vector (pDEST) gateway cloning handbook (Table 6.10) in 1.5 ml Eppendorf tubes and left on ice for 1 hour. Following this, samples were centrifuged at maximum speed (>20,000 x g) at 4°C for 10 min. The supernatant was aspirated into a sterile 0.5 ml microcentrifuge tube and the cell pellet was discarded.

Table 6.10 Protein lysis buffer from pDEST gateway cloning handbook (Invitrogen™). Reagents were measured and dissolved in 90 ml of distilled water (dH_2O). pH was adjusted to 7.8 with HCl and the volume was made up to 100 ml with dH_2O.

Components	**Amount**	**Final concentration**
KH_2PO_4 (1 M)	0.3 ml	50 mM
K_2HPO_4 (1 M)	4.7 ml	
NaCl	2.3 g	400 mM
KCl	0.75 g	100 mM
Glycerol	10 ml	10%
Triton X-100	0.5 ml	0.5%
Imidazole	68 mg	10 mM
dH_2O	90 ml	-
Final volume	**100 ml**	

6.2.1.5 Western blotting

Western blotting was used to examine the expression of PADI6 protein in different protein samples (Section 6.2.1.5.1). The samples were subject to electrophoresis on a sodium dodecyl sulfate (SDS) polyacrylamide gel (PAGE) where the denatured proteins were separated by size and then transferred onto a nitrocellulose membrane. The membrane was exposed to an antibody targeting a protein of interest (PADI6) and the result was visualised by the addition of a conjugated secondary antibody (Towbin et al., 1979).

6.2.1.5.1 Sample preparation

In this study, protein samples for Western blotting consisted of either bacterial lysates, pooled bovine oocytes or human embryo carcinoma cell (ECC) lines, 2102Ep and NTera-2. Oocyte samples were harvested for protein analysis as follows: GV oocytes were aspirated as in Section 2.1.2 and denuded in 300 µg/ml hyaluronidase using an EZ-Grip denudation and handling pipettor, as detailed in Section 3.2.1. Groups of 20 or 50 denuded oocytes were placed directly into 20 µl of radio-immunoprecipitation assay (RIPA) buffer (Appendix II - Table II.Vb). Collection and pooling of GV oocytes for protein analysis was repeated 3 times to give 3 x GV protein samples: 2 x 20 and 1 x 50 pooled GV oocytes.

Embryo carcinoma cell (ECC) lines, 2102Ep and NTera-2, were also tested due to their origin and known expression of a variety of pluripotency genes (Josephson et al., 2007). Ntera-2 originated from a primary embryonal carcinoma of the testis and 2102Ep from a teratocarcinoma, hence were included as cell lines that matched certain transcriptional features of the oocyte/early embryo. ECC lines were a kind gift of Professor Peter W. Andrews, Centre for Stem Cell Biology, University of Sheffield and were grown for our project by Daniele Estoppey (University of Sheffield). ECC cells were cultured (similar to Skotheim et al. (2005)) in their native growth medium DMEM containing 4.5 g/L glucose + 2mM Glutamine + 10% Foetal Bovine Serum (FBS) (41965-039, Life Technologies, UK) at high densities in T75 Corning® Cell culture flasks (Corning Incorporated, Life Sciences) at 37°C under a humidified air atmosphere of 8% CO_2. The cells were passaged every 3-4 days once they were confluent (70-80%), and were split at a ratio of 1:3 or 1:4. 2102Ep cells were passaged by washing with 5 ml DPBS and 1 ml of 0.25% trypsin/ EDTA (similar to Josephson

et al. (2007)), whilst NTera-2 were passaged using scrapers as described by Andrews et al. (1984). Following washing with ice-cold DPBS, protein was extracted by adding 500 µl of RIPA buffer to cells in the T75 flask. The cells were scraped to remove them from the flask and transferred to a clean 1.5 ml Eppendorf on ice using a Gilson p1000 pipette (Gilson Inc, Middleton, USA). The Eppendorf was placed into a falcon tube and allowed to mix on a rotary mixer at 4°C for 30 min. The sample was then centrifuged at 16,900 x g at 4°C for 20 min. The protein supernatant was removed to a fresh 1.5 ml Eppendorf and stored at -80°C until further use.

The human PADI6 antibody that was purchased from Invitrogen (PA5-45758, Invitrogen™ Ltd) was not previously cited in the literature. The peptide sequence that was used to raise the antibody is shown in Table 6.11. As described in the introductory Section of this chapter, bovine antibodies are not often commercially available, therefore it was hoped that the human antibody would be able to detect bovine PADI6. Thus, it was necessary to have a positive control to ensure that the antibody was working. Due to the restricted expression of PADI6 protein, finding a positive protein control cell line would be difficult so a human recombinant PADI6 protein was purchased (Mw 100 kDa) (ab126915, Abcam®). Western blot analysis was repeated 3 times.

Table 6.11 The peptide sequence that was used to raise the human PADI6 antibody in mouse.

Human PADI6 peptide sequence
GAILLVNCNPADVGQQLEDKKTKKVIFSEEITNLSQMTLNVQGPSCILKK

6.2.1.5.2 SDS-PAGE

First described by Laemmli (1970), SDS-PAGE is a widely used biochemical technique for separating proteins by size. SDS is an anionic detergent that denatures the secondary structure of proteins and causes the linear protein to become negatively charged (Waehneldt, 1975). The negative charge facilitates separation of proteins from the anode to the cathode by electrophoresis. For SDS-PAGE, Mini-Protean Tetra Electrophoresis System (Bio-Rad Ltd) containing combs, plates and casting accessories for 10-well, 1 mm thick gels were used. In preparation, the casting plates and combs were washed with 70% (v/v) ethanol and dried using tissue, before securing into the casting cassette. A 12% (v/v) lower separating gel was prepared according to Appendix II - II.IIb in a 50 ml conical centrifuge tube (Corning®, USA). The 12% separating gel was quickly dispensed into the casting cassette using a 10 ml stripette and dH_2O was pipetted on top to allow the gel to set evenly. The gel was left to set for at least 15 min. After this time, the water was removed using a tissue. A 4% (v/v) stacking gel was prepared according to Appendix II - Table II.IIa in a 15 ml conical centrifuge tube and immediately pipetted on top of the 12% separating gel until it reached the top of the casting plates. The comb was carefully inserted, and the gel was left to set for 20-30 min. The SDS running buffer was prepared according to Appendix II - Table II.IIIa.

Protein samples were prepared for loading onto the SDS-PAGE by adding 1x mix of NuPAGE™ sample reducing agent (10x) (NP0009, Invitrogen™ Ltd) and NuPAGE™ LDS sample buffer (4x) (NP0007, Invitrogen™ Ltd) to each 20 µl sample. Samples were boiled at 100°C for 5 min before loading to the prepared SDS-PAGE gel. 7 µl of PageRuler™ Plus Prestained Protein Ladder, 10 to 250 kDa (26619, Thermo Scientific™) was also loaded to the gel as a size reference for protein bands. The prepared SDS-PAGE gel was placed into a clamp and inserted into the tank for electrophoresis. The inner tank that contained the gel was filled with 1 x running buffer and care was taken to ensure that there were no leaks into the rest of the tank. The comb was removed from the gel and any excess acrylamide was removed from the glass using a pipette tip. The outer tank was filled with the remaining running buffer and the samples were carefully loaded into the wells of the gel. The SDS-PAGE gel was run at 30 V until samples reached the separation gel and subsequently, 100 V for 1-1.5 hours at RT. Electrophoresis was conducted with a PowerPac basic power supply (Bio-Rad).

6.2.1.5.3 Protein transfer, blocking and detection

After gel electrophoresis, the gel was immediately transferred onto a PVDF membrane (10600023, Amersham™ Hybond™ P.0.45 µm) (Matsudaira, 1987). This enables separated proteins to be detected using antibodies. For protein transfer, the mini trans-blot cell (Bio-Rad) was used. 1 x transfer buffer was prepared according to Appendix II – Table II.IIIb. A large plastic tray was filled with transfer buffer and within the tray, the transfer clamp was opened, and 2 x black mesh squares were placed on each side of the clamp. This allowed the mesh squares to absorb the transfer buffer for the wet protein transfer method. Whatman filter papers were cut to size and wetted 1 x with transfer buffer. 2 x Whatman filter papers were placed on the black mesh squares on each side of the clamp. Prior to removal of the gel, the PVDF membrane was soaked in 100% methanol for 30 sec. The gel was removed from the clamp and the glass plates were carefully prised apart. Excess acrylamide was removed before the pre-soaked PVDF membrane was placed onto the gel. Care was taken to ensure that there were no air bubbles trapped between the gel and membrane. Together, they were carefully transferred onto the prepared transfer clamp and any air bubbles were removed. The transfer clamp was closed, securing the gel between the mesh on either side. The transfer clamp was placed into the tank and the tank was filled with 1 x transfer buffer. The transfer was run at 100 V for 1 hour at RT.

To avoid non-specific binding of the antibody, membranes were blocked in 5% (w/v) Marvel dried skimmed milk powder in Tris-buffered saline (TBS) (Appendix II – Table II.Va) at RT for 1 hour. The primary PADI6 antibody was diluted 1:500 according to the company's recommendation in 1% (w/v) milk powder in TBS and incubated with the membrane at 4°C, rocking overnight. The following day, the membrane was washed in 3 x 5 min washes using TBS with 0.1% (v/v) Tween 20 (TBS-T) to remove any excess primary antibody. The secondary antibody was diluted 1:5000 in 1% (w/v) milk and incubated with the membrane at RT, rocking for 30 min. The secondary antibody was an anti-mouse HRP-conjugated secondary antibody (61-6520, Invitrogen™ Ltd). This method relies on indirect antibody detection. The secondary antibody binds to the primary antibody at the specific protein of interest. The secondary antibody is conjugated to an enzyme called horseradish peroxidase (HRP) which reacts with an administered substrate to produce a chemiluminescent signal. This signal is then detected at the site of the protein of interest.

After incubation with the secondary antibody, membranes were washed 3x 10 min washes in TBS-T to remove the excess secondary antibody. During the final wash, the HRP substrate for indirect detection of proteins was prepared by mixing 1 ml of SuperSignal™ stable peroxide solution and 1 ml of enhancer solution (34095, SuperSignal™ West Femto Maximum Sensitivity Substrate, Thermo Scientific™). After the final wash, the SuperSignal™ mix was added to the membrane and allowed to incubate for 5 min in the dark. The substrate was blotted off the membrane and the membrane was placed in a plastic sheet. The membrane was developed using a Gel Doc™ XR+ system (Bio-Rad, Hertfordshire, UK).

6.2.2 Experiment 2: Amino acid profiling following *PADI6* KD during bovine oocyte maturation *in vitro*

6.2.2.1 Preparation of oocytes for amino acid profiling

As described in Chapter 4, GV oocytes were subject to microinjection with duplex buffer (DB), scrambled dsiRNA (SCR) or a mix of dsiRNAs against *PADI6* (KD) and placed into normal IVM media (Table 2.3) for 18 hours at 39°C, 5% CO_2. AAP IVM media was made according to Table 6.12. 1 µl of AAP-IVM media was pipetted into drops and then covered with oil in 35 mm embryo tested NUNC™ IVF Petri dish. AAP dishes were prepared the day before use and incubated at 39°C, 5% CO_2 overnight. Dishes were marked with a grid and each oocyte AAP-IVM drop was assigned a number (1-7). Each dish also contained 7 x 1 µl control (c) AAP-IVM drops and 2 x 2 µl wash (w) drops (Figure 6.5). The AAP of individual oocytes was assessed according to the methodology validated in Hemmings (Ph.D thesis) and as detailed in (Hemmings et al., 2012).

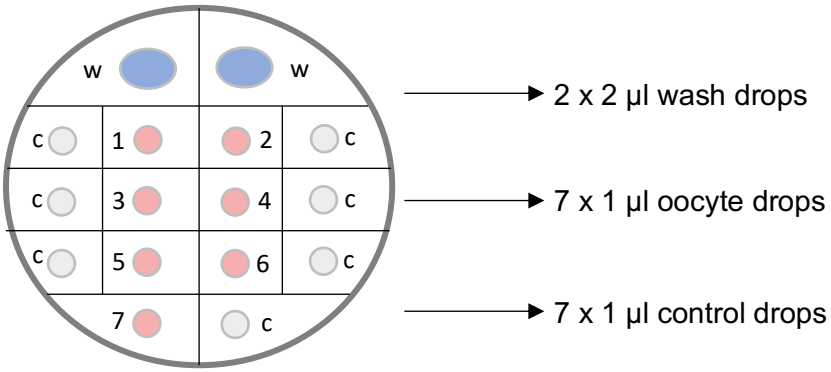

Figure 6.5. AAP *in vitro* maturation media dish layout.

Following 18 hours in normal IVM media, oocytes were denuded of cumulus cells in 300 µg/ml hyaluronidase using an EZ-Grip denudation and handling pipettor. Oocytes were analysed for polar bodies under a stereomicroscope and mature oocytes were noted. Individual denuded oocytes were washed twice in AAP-IVM media wash (w) drops before placing into its respective oocyte drop for 5-6 hours at 39°C, 5% CO_2 (Table 6.12). Oocyte transfer was done in the smallest possible volume to avoid changes to the volume of the drops. Control drops contained AAP-IVM media only.

After 5-6 hours in AAP-IVM media, oocytes were removed from AAP dishes in a minimal volume using a 130 µm EZ-Tip and EZ-Grip denudation and handling pipettor and placed individually into sterile 0.5 ml Eppendorf tubes containing 2 µl RNAGEM lysis buffer for cDNA synthesis and real-time PCR experiments. The EZ-Tip was changed between each oocyte to avoid transfer of RNAGEM lysis buffer into the AAP drops. AAP-IVM dishes were sealed with parafilm and stored at -80°C until later use. Smart-seq2 and real-time PCR for *PADI6* expression were conducted for individual oocytes as described in Section 4.2.2.4 using *PADI6* primers 9B from Table 4.3.

Table 6.12 AAP *in vitro* maturation media composition

Components	Stock	Volume	Final concentration
EBSS SIGMA E2888	5.55 mM Glucose	9.977 ml	5.275 mM Glucose 0.482 mM Pyruvate
α-MEM SIGMA M4526	5.55 mM Glucose 1.25 mM Pyruvate	1.425 ml	
BSA FAF stock SIGMA A6003	20%	60 µl	0.1%
L-Glutamine SIGMA G7513	200 mM	4 µl	62.5 µM
Pyruvate stock SIGMA P4562	47 mM	100 µl	0.47 mM
Penicillin/Streptomycin SIGMA P4333	Pen: 10000 IU/ml Strep: 10 mg/ml	60 µl	Pen: 50 IU/ml Strep: 50 µg/ml
Bovine Holo-transferrin SIGMA T1283	5 mg/ml	12 µl	5 µg/ml
Na-selenite SIGMA S9133	50 µg/ml	12 µl	5 ng/ml
Long-R3 IGF-1 SIGMA I1271	100 µg/ml	12 µl	100 ng/ml
Human Insulin SIGMA 91077C	10 µg/ml	12 µl	10 ng/ml
Human FSH SIGMA F4021	0.16 IU/ml	12 µl	0.016 IU/ml
DABA stock SIGMA 116122	50 mM	15 µl	62.5 µM
Final volume	**11.7 ml**		

6.2.2.2 AAP using high performance liquid chromatography

AAP-IVM media samples were analysed to assess AA release and uptake from oocytes from each experimental group (DB, SCR and KD) using a HPLC method adapted from Hemmings et al. (2012) and Sturmey et al. (2010). ddH_2O was obtained from an ELGA Veolia water purification system. AAP-IVM dishes were allowed to thaw at RT and 9 µl of ddH_2O was added to each 1 µl drop. The whole drop (10 µl) was then aspirated and transferred to brown glass HPLC vials (Chromacol Ltd) containing 15 µl of ddH_2O to give a final volume of 25 µl. O-phthalaldehyde (OPA) was used as the fluorescent adduct to identify 19 AAs (Ala, Arg, Asp , Cys, Glu, Gly, His, Ile, Leu, Lys, Met, Phe, Pro, Ser, Thr, Tyr, Val, Asn, Gln), as well as the synthetic AA, DABA, that acts as an internal reference (Sturmey et al., 2010).

Within the Agilient 1100 HPLC autosampler, 25 µl OPA was added to each sample and mixed. This reaction creates a fluorescent derivative with 450nm excitation and 330nm emission excited at and injected into the mobile phase. The mobile phase was composed of Buffer A (80% 80mM sodium acetate, 19.5% methanol, 0.5% tetrahydrofuran) and Buffer B (80% Methanol, 20% 80mM sodium acetate) in a gradient. All buffers were filtered before use; 0.45µm HVLP filter disc (Millipore) for the aqueous buffer A and 0.45µm HVHP filter disc (Millipore) for the organic buffer B. Chromatography was performed at 25°C with a flow rate of 1.3 ml/min and a total analysis time of 60 min. The parameters for the HPLC machine and injector program for each sample are detailed in Table 6.14. AAs were separated on a Hypoclone ODS c18, 250mm x 4.6 mm, 5µm column (Phenomenex, Macclesfield, UK) fitted with a pre-column guard (KJ04282, Phenomenex), guard cartridges (AJ0-4287, Phenomenex). AAs adhered to the C18 matrix and subsequently, a gradient of hydrophilic to hydrophobic buffers was washed through the column to elute the AAs based on their hydrophobicity. Separated AAs were detected using a Fluorescent Light Detector (Agilent) and identified by comparison to a standard AA mixture (Sigma) containing each of the detectable AAs at 25 µM. The AA standards also provided information about the natural drift in AA output with time. A buffer wash (50:50 Buffer A:B) was also performed half way through each run to clean the column. An example analysis sequence is shown in Table 6.13.

Table 6.13 HPLC sample setup for AAP.

1	AA standards 1	12	Buffer wash 1
2	AA standards 2	13	Oocyte sample 5
3	Oocyte sample 1	14	Control 5
4	Control 1	15	Oocyte sample 6
5	Oocyte sample 2	16	Control 6
6	Control 2	17	Oocyte sample 7
7	Oocyte sample 3	18	Control 7
8	Control 3	19	AA standards 4
9	Oocyte sample 4	20	AA standards 5
10	Control 4	21	Buffer wash 2
11	AA standards 3	22	Buffer wash 3

Table 6.14 HPLC machine **a)** running parameters and **b)** injection program

a)

Wash buffers	Buffer A:	80% (v/v) sodium acetate pH 5.9, 20% (v/v) methanol and 5 ml tetrahydrofuran in 1L
	Buffer B:	80% (v/v) methanol and 20% (v/v) sodium acetate pH 5.9 in 1L
Flow rate	1.30 ml/min	
Pressure	200-350 bar	
Time per sample	55 min	
Temperature	25ºC	
Injection vol. into the column	25 µl	

b)

HPLC injection program (per sample)
Draw 25 µl of OPA from Vial 1
Eject 25 µl of OPA into the sample
Mix sample (25 µl) 5 times
Wait 1:00 min
Needle wash in 50:50 Buffer A: Buffer B 1 times

6.2.2.3 Data analysis

The concentration of AAs in each drop of medium was calculated from the area beneath each peak corresponding to each AA as described previously (Hemmings et al., 2012; Houghton et al., 2002). AAs were always eluted in same order at specific elution times which aided AA identification. The number of pmols of each AA in the culture drops (oocyte and control drops) at the beginning of the culture was calculated using the known concentration of each AA in αMEM. The HPLC system provided the value for the area under the peak of each AA in arbitrary units for each sample analysed. In order to correct for any non-specific dilution, degradation or appearance, the peak area of the internal control DABA was used to calculate the AA corrected peak area in oocyte and control drops. Firstly, the AA peak area was divided by the DABA peak area and then multiplied by 100 for each AA in each control drop. The mean corrected peak area was then taken for each AA in each control drop. Next, the number of pmols of each AA present in the oocyte drops after the 6h incubation could be calculated by using the Rate of Peak Area Variation (increase or decrease in peak area for a given AA before and after 6h oocyte culture) per each oocyte. Values >1

indicate production and values <1 depletion. The Rate of Peak Area Variation of each AA in oocyte drop 1 was calculated as follows:

Firstly, the AA corrected peak area was calculated for each oocyte drop:

AA Corrected Peak area in Oocyte drop 1 = AA Peak Area / DABA Peak Area x 100 (arbitrary units)

Next the Rate of Peak Area Variation was calculated compared to the mean AA corrected peak area in control drops:

Rate of Peak Area Variation (AA, Oocyte 1) = AA Corrected Peak area in Oocyte drop 1 / AA Mean Corrected Control area

Then, the number of pmols of each AA present in the oocyte drops after the 6h incubation was then calculated by multiplying the Rate of Peak Area Variation by the initial number of pmols in the drop (equivalent to pmols in control drops):

AA pmol in oocyte drop 1 after incubation = Rate of Peak Area Variation (AA, Oocyte 1) x AA pmol in a Control drop

Finally, the number of pmols of released or consumed AAs by each oocyte during the 6h incubation period was calculated using:

Number of pmols released during incubation = AA pmol after 6h incubation –AA pmol in Control drops

The release or consumption rate for each AA could then be calculated as the number of pmol of that AA that were produced or depleted per 1 oocyte in 1 hour:

AA consumption rate = pmol of AA consumed / hours of incubation

The sum of consumption and release, known as AA turnover, was also calculated (Hemmings et al., 2012; Houghton et al., 2002). The overall AA release or consumption was calculated by adding up the pmols of all the released or consumed AAs, respectively. The total AA turnover was calculated as the sum of the overall AA consumption and the overall AA release and the net AA turnover was calculated by deducting AA consumption from AA release.

6.2.2.4 Statistical analysis

Statistical analyses were performed as described by Sturmey et al. (2010). Briefly, data were first confirmed as non-parametric by D'Agostino-Pearson test. Significant consumption or release of AAs i.e. changes in concentration from zero was assessed by Wilcoxon signed rank test. Finally, data were compared by Kruskal-Wallis with post-hoc Dunn's test to identify significant differences between experimental groups. Only AAs with significant consumption/release were regarded as having significantly different turnover from other experimental groups. All analyses were performed on GraphPad Prism 8.

6.2.3 Experiment 3: *In vitro* fertilisation of bovine oocytes following *PADI6* KD during IVM

After assessing the impact of *PADI6* KD during the IVM of bovine oocytes in Chapter 5, it was necessary to investigate the developmental competence of oocytes following microinjection with dsiRNA targeted against *PADI6*. Real-time PCR analysis of *PADI6*^{KD} embryos was performed to investigate whether *PADI6* transcript abundance recovered in the embryo, indicative of *PADI6* transcription after the GV oocyte stage. As well as providing information about the regulation of *PADI6* transcription, this may indicate that any affected epigenetic regulators also recover from dysregulation caused by targeted gene KD of *PADI6*. As described in Chapter 4, GV oocytes were subject to microinjection with duplex buffer (DB), scrambled dsiRNA (SCR) or a mix of dsiRNAs against *PADI6* (KD) and placed into IVM media (Table 2.3) for 24 hours at 39°C, 5% CO_2. 20-40 oocytes were microinjected for each group (DB, SCR or KD) and 3 discrete cultures were performed. Table 6.15 shows the number of oocytes that were injected on each culture week and the number of suspected zygotes that were put into embryo culture following IVF. 30-40 GV oocytes were also set aside after aspiration as a non-injected control group for IVM and IVF on weeks 1 and 2. This was included as an important comparison to investigate the impact of microinjection of oocytes on embryo development.

Table 6.15 Number of GV oocytes injected per culture week and the number of zygotes that were cultured to look at the effects of *PADI6* gene KD on fertilisation and preimplantation embryo development.

Culture week	No. of GV oocytes injected				No. of zygotes put into culture			
	DB	SCR	KD	NI	DB	SCR	KD	NI
1	30	30	50	30	26	23	45	22
2	30	30	40	40	29	28	28	40
3	20	20	40	-	20	20	38	-

After 24 hours IVM, oocytes were washed in F-TALP media in sterile 4-well dishes and pre-prepared Classic sperm was added at a concentration of 1 x 10^6 sperm/500 µl F-TALP, as detailed in Section 2.2. After 24 hours IVF, suspected zygotes were denuded of their cumulus cells in H-SOF according to Section 2.3.2. Embryos were put to culture in pre-prepared 35 mm embryo tested NUNC™ IVF Petri dishes of SOFaaBSA, as previously described in Section 2.3. Figure 6.6 shows the modified workflow to combine microinjection during bovine IVM with IVF and embryo culture.

Embryos were cultured in SOFaaBSA for up to 2 days until they reached the 2-8 cell stage. This cut-off was chosen because *PADI6* expression decreases following EGA in bovine (8-16 cell stage). On day 1 or 2, NR dye was added to the culture drops to assess cell viability as detailed in Section 4.2.1. The number of live cells were counted under a stereomicroscope. The number of cleaved embryos were also counted, and the embryonic stages were recorded. Embryos were removed from culture, washed in DPBS and placed into clean Eppendorf tubes containing 2 µl of RNAGEM lysis buffer, as detailed in Section 2.4.1. cDNA synthesis was conducted according to the Smart-seq2 protocol described in Section 2.4. Real-time PCR analysis was performed according to Section 2.7 to analyse the embryonic expression levels of *PADI6* after microinjection with dsiRNA.

6.2.3.1 Statistical analysis

Real-time data for *PADI6* gene expression was compared to the geometric mean of 3 housekeeping genes, *GAPDH, H2A* and *YWHAZ,* as detailed in Section 2.7. Oocyte maturation, viability and fertilisation rates were analysed across all cultures. Values presented for real-time data and developmental progression data are arithmetic means ±SEM for the number of observations shown. All data were tested for normality using the D'Agostino-Pearson test and one-way ANOVA was used for normally distributed data; p values of <0.05 were considered to be statistically significant.

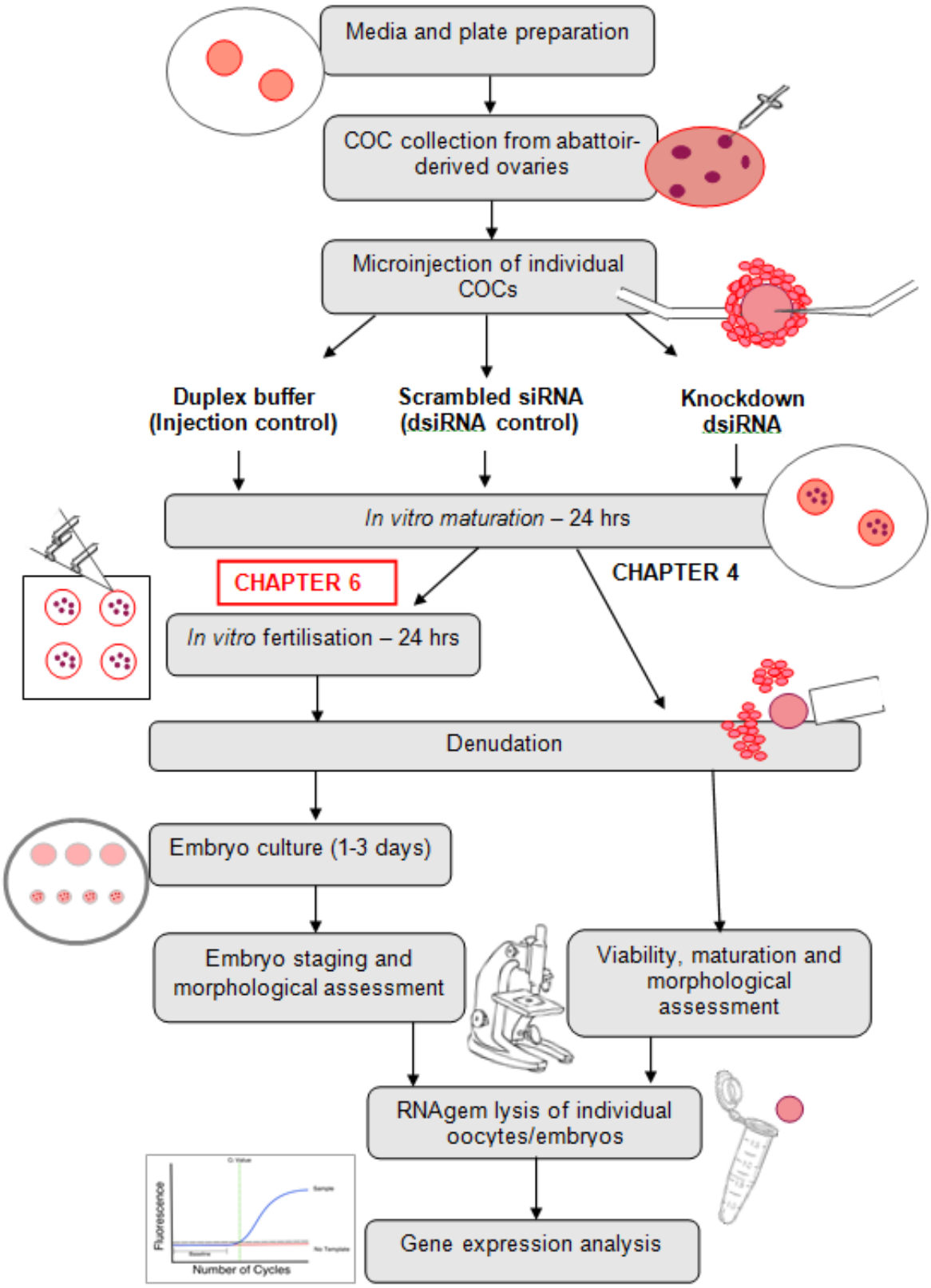

Figure 6.6. Experimental workflow for dsiRNA microinjection during bovine IVM followed by IVF and embryo culture.

6.3 Results

6.3.1 Experiment 1: Cloning of human *PADI6* ORF into bacterial expression vectors

6.3.1.1 pET cloning

Following site-directed mutagenesis to engineer a *Nde*I site into *PADI6* clone, miniprep DNA from colonies 3, 5, 7 and 8 was digested using *Nde*I and EcoRV and ran on an ethidium bromide gel to verify the correct product sizes (Figure 6.7). These colonies were chosen as they yielded >100 ng/µl of DNA following miniprep. If site-directed mutagenesis was successful, 4 bands of the following sizes were expected: 422 bp, 2194 bp (*PADI6* band), 3440 bp and 3501 bp. Figure 6.7 shows a section of this gel containing 2 bands; 1 band just above 2000 bp, expected to be that of *PADI6*, and a stronger band between 3000 and 4000 bp. The latter band might include both 3440 bp and 3501 bp fragments that have not been separated. Sequencing confirmed that DNA from colonies 5 and 7 had incorporated the new *Nde*I site and possessed no base substitutions. The *Nde*I/EcoRV digest of miniprep from these colonies was pooled and run on an agarose gel. The 2194 bp *PADI6* band was extracted from the gel and mixed with pET-11a for bacterial transformation. The sequencing data confirmed the correct incorporation of *PADI6* into pET-11a vector.

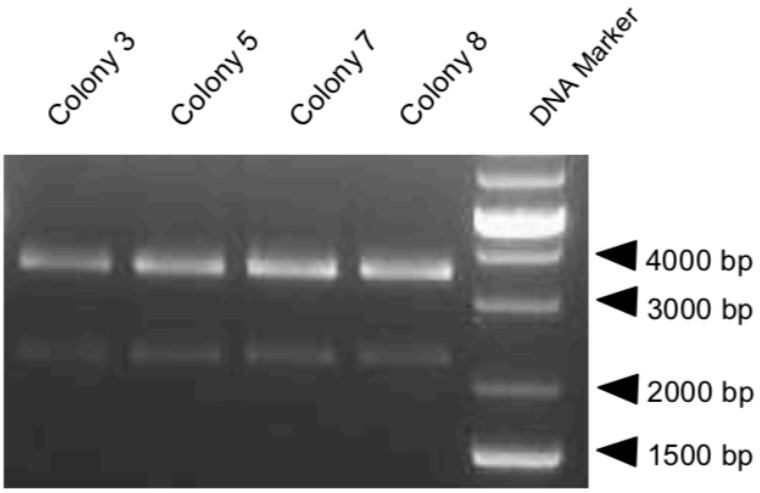

Figure 6.7. Representative gel electrophoresis of *Nde*I and EcoRV restriction digest of *PADI6* clone after site-directed mutagenesis to produce a 5' *Nde*I site. Predicted product sizes are: 422 bp (not shown), 2194 bp (*PADI6* band), 3440 bp and 3501 bp. It is predicted that the latter 2 bands have not separated and can, therefore, be visualised as 1 stronger band. GeneRuler 1 kb Plus DNA ladder is shown to size the expected products.

6.3.1.2 Gateway cloning

PADI6 was amplified from the Vigene *PADI6* ORF clone using primers containing *att*B sites compatible with the gateway system. 10 µl of PCR product was run on an ethidium bromide gel to verify the presence of a band of the correct size. The resultant gel displayed only 1 band, so gel extraction was not required. The remaining PCR product was pooled and purified in preparation for the first recombination reaction. The BP recombination reaction and transformation of *E. coli* was performed and the resultant minipreps from 8 colonies were sequenced**.** PCR was performed using primers for a 1051 bp *PADI6* fragment to identify the insertion of *PADI6*. Figure 6.8 shows the presence of *PADI6* in 8 colonies picked. The sequencing data confirmed *PADI6* insertion into pDONR201 in colonies 2, 3, 6, 7 and 8 and identified any base substitutions. Sequencing of colonies 1, 4 and 5 failed, perhaps due to poor quality minipreps, which is evident in Figure 6.8. Colony 3 was picked to continue to the LR recombination reaction as it contained no substitution mutations.

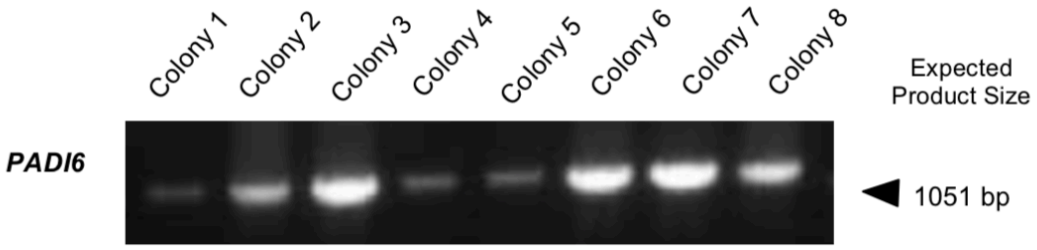

Figure 6.8. Representative gel electrophoresis of PCR for *PADI6* fragment in miniprep DNA from bacterial colonies (1-8) transformed with pDONR201 containing human *PADI6* ORF.

The LR recombination reaction and transformation of *E. coli* was performed as detailed in Section 6.2.1.3.4. 13 resultant colonies were picked for PCR analysis using a T7 vector primer and *PADI6* reverse primer to confirm insertion of *PADI6* ORF into pDEST15 vector. If *PADI6* was correctly inserted into pDEST15, the resultant band would be 1119 bp. Figure 6.9 shows the gel electrophoresis image. All 13 colonies displayed a band just above the 1000 bp DNA marker band, suggesting that all colonies contained the *PADI6* insert. The sequencing results confirmed the correct incorporation of *PADI6* into pDEST15 vector.

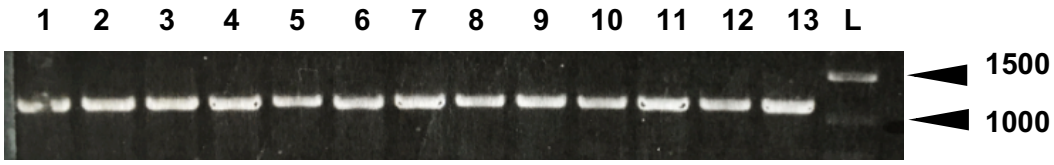

Figure 6.9. Representative gel electrophoresis of PCR in 13 bacterial colonies (1-13) from LR reaction using T7 vector primer and *PADI6* reverse primer to show insertion of *PADI6* ORF into pDEST15 vector. A Section of GeneRuler 1 kb Plus DNA ladder (L) is shown to size the expected products.

6.3.1.3 Detection of cloned PADI6 and bovine oocyte derived PADI6 protein

With both *PADI6* clones sequence verified, efforts were made to induce bacterial PADI6 protein production and verify the presence of PADI6 by Western blotting. The molecular weight of PADI6 protein was expected to be approximately 77 kDa from pET-11a and 100 kDa from pDEST15. PADI6 expression was also investigated in embryo carcinoma cell (ECC) lysates (Section 6.2.1.6.1) following detection of *PADI6* mRNA expression by PCR (Section 2.5 and 2.6) in Figure 6.10. The resultant Western blots are shown in 0. Lane A and B contained untransformed *E. coli* and uninduced *PADI6*-pET-11a, respectively, whereas lane C contained induced *PADI6*-pET-11a. Bands were observed in all bacterial lanes (A, B and C) between 55 and 70 kDa which suggests that the antibody detected bacterial proteins (0a). No bands were present in BSA (E) and ECC lines (F and G). A band was observed in the purchased recombinant PADI6 sample (Lane H) between 100 and 130 kDa. This shows that the commercial PADI6 antibody is effective in detecting human PADI6 protein and would

be useful for further experiments. Finally, no bands were observed for PADI6 in 20 x pooled bovine GV oocytes (Lane I). The same result was also observed when 50 x pooled bovine GV oocytes (Appendix IV.C). 0b shows a Western blot for induced bacterial lysates from both pDEST15 and pET-11a vectors across the different time points (0-3 hr). A gradient of increasing protein abundance would be expected from 0hr to 3hr post-induction. However, a single band of equal abundance and size (between 55 and 70 kDa) was observed in all lanes. These bands appear to be the same as those observed in bacterial samples in 0a.

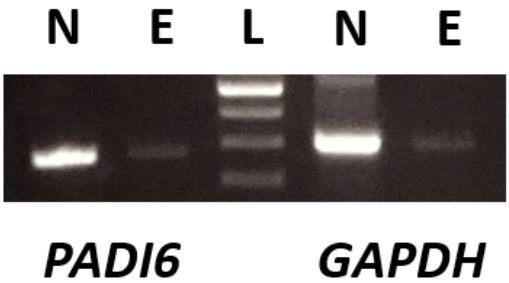

Figure 6.10. PCR for human *PADI6* and *GAPDH* in ECCs NTera-2 (N) and 2101Ep (E). A 100bp DNA ladder (L) was used to size the 270bp *PADI6* and 312bp *GAPDH* bands.

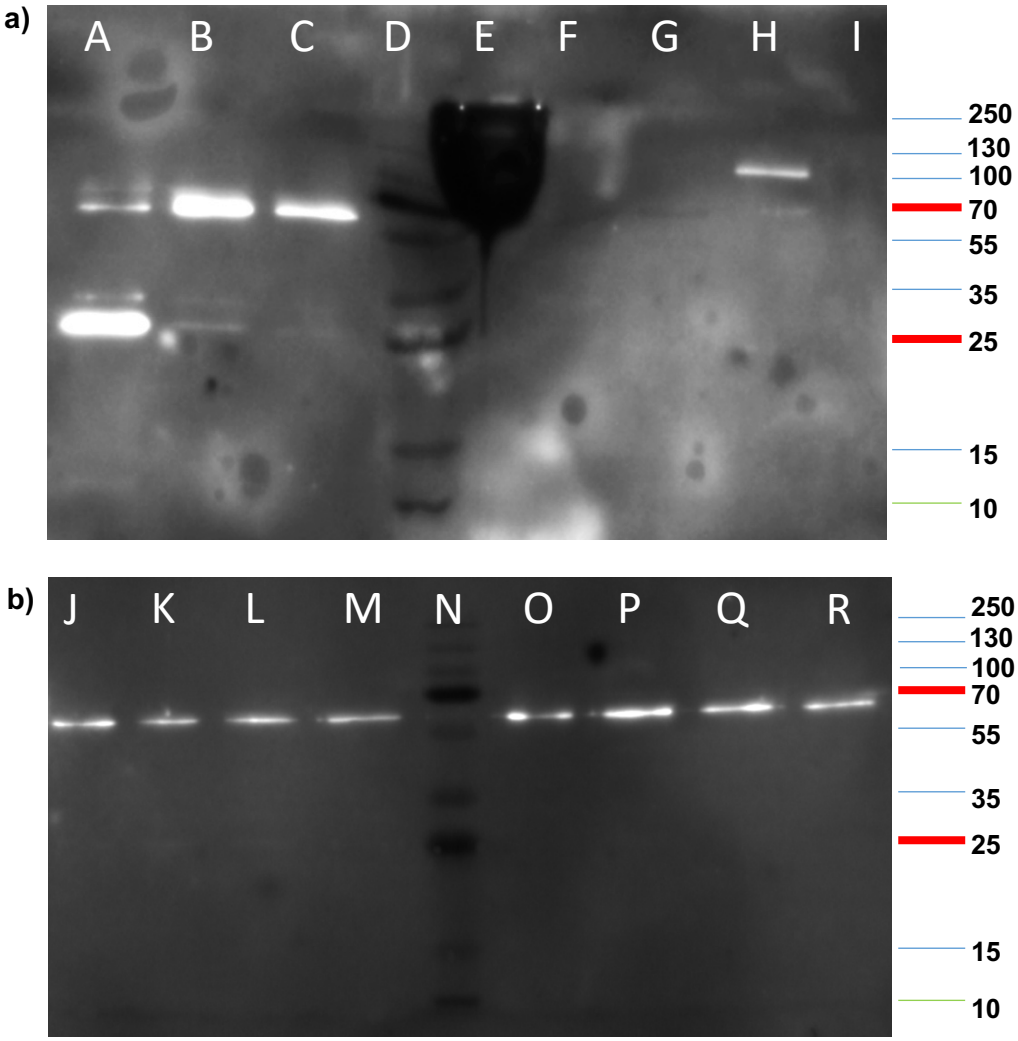

Figure 6.11. Representative Western blots for PADI6 protein in **a)** A) Untransformed E. coli; B) *PADI6*-pET-11a uninduced; C) *PADI6*-pET-11a induced; D) Protein ladder; E) BSA; F) 2102Ep protein; G) NTera-2 protein; H) Recombinant PADI6 (positive control); I) Pooled GV oocytes (x20) and **b)** Induced bacterial lysates at different time points. J-M *PADI6*-pDEST15: J) 3hr time point; K) 2hr time point; L) 1hr time point; M) 0hr time point; N) Protein ladder; O-R *PADI6*-pET-11a: O) 3hr time point; P) 2hr time point; Q) 1hr time point; R) 0hr time point.

6.3.2 Experiment 2: Amino acid profiling following *PADI6* KD during bovine oocyte maturation *in vitro*

AAP was conducted following *PADI6* KD as a functional index of the effect of gene KD during bovine oocyte maturation *in vitro*. To this end, cumulus-enclosed GV oocytes were microinjected with *PADI6* dsiRNA and subject to normal IVM as described in Section 6.2.2. After ~18 hours, oocytes were transferred to drops of AAP-IVM media for approximately 6 hours. The oocytes were removed from media drops and frozen in RNAGEM lysis buffer for real-time PCR analysis of *PADI6* expression. Meanwhile the AA content of the media drops was analysed by HPLC. A total of 91 oocytes (DB: n=28; SCR: n=26; KD: n=37) across 4 repeat cultures were analysed. The real-time PCR and HPLC data were then matched to assess whether the degree of KD of *PADI6* was reflected in AA metabolism.

6.3.2.1 Molecular analysis of *PADI6* KD in AAP-analysed oocytes

Following real-time PCR of MII oocytes from AAP media drops, *PADI6* KD (%) was calculated for each oocyte compared to the mean *PADI6* expression of DB-injected oocytes within the same culture. This was done for oocytes from the first 3 repeat cultures (DB: n=21; SCR: n=19; KD: n=31). The results are shown in Figure 6.12 with each bar corresponding to percentage *PADI6* KD for an individual oocyte. The results show that there was high variability in the KD of *PADI6.* Some oocytes appeared to have an increased expression of *PADI6* compared to DB-injected controls (shown as negative values) and were therefore excluded from the analysis. Increased *PADI6* mRNA levels may have been caused by ineffective KD of *PADI6* gene expression or upregulation of *PADI6* in the oocyte to compensate for gene KD. In consideration of the variability of KD, 2 groups were created: high *PADI6* KD and low *PADI6* KD. High *PADI6* KD was described as >50% KD compared to mean DB *PADI6* expression and low *PADI6* KD was described as <50% compared to mean DB *PADI6* expression (shown by the red line in Figure 6.12). Coincidentally, this resulted in an equal split of samples with 12 samples falling into each group.

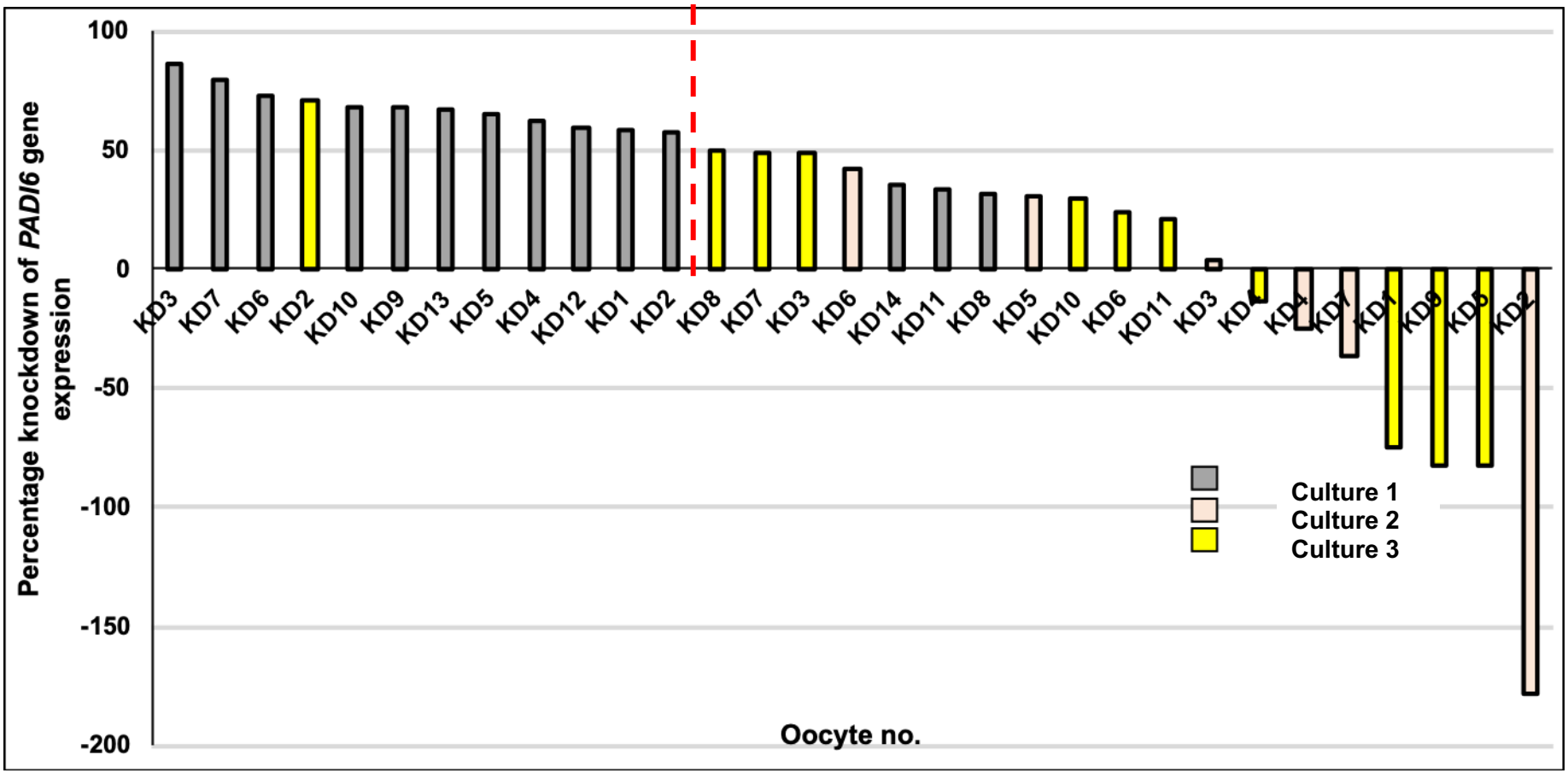

Figure 6.12. Percentage KD of *PADI6* expression calculated using the mean *PADI6* expression in DB-control group for each culture. Each bar represents an individual oocyte while the different colours represent the independent culture cohort. The oocytes with negative values had increased *PADI6* abundance compared to DB group and were excluded from analysis. The red line represents the cut off between low and high *PADI6* KD at 50% *PADI6* KD.

6.3.2.2 Evaluation of overall amino acid turnover, release and consumption from oocytes following *PADI6* KD

The consumption, release, net turnover and total turnover of AAs was calculated for each injection group (DB, SCR and KD) (Figure 6.13a) as well as the high and low PADI6 KD groups defined in Section 6.3.2.1 (Figure 6.13b). Total turnover described the sum of consumed and released AAs. There were no significant differences in total AA turnover between oocytes from different injection groups ($p>0.05$). Similarly, release and consumption of AAs were not significantly different between oocytes after injection with different species ($p>0.05$). DB-injected oocytes appeared to release more AAs than the other 2 groups but this was not statistically significant ($p>0.05$). Net consumption and release of AAs was calculated by deducting the consumed AA from the released AAs. Oocytes in the total KD injection group consumed more AAs than they released while oocytes in the SCR group released more AAs than they consumed ($p>0.05$) (Figure 6.13a). However, net turnover of AAs was different after separating oocytes in the KD group according to *PADI6* expression: oocytes in the high *PADI6* KD group had an overall consumption of AAs whereas oocytes in the low *PADI6* KD group had an overall release of AAs, although this was not significant ($p>0.05$) (Figure 6.13b). Oocytes in the DB group consumed and released AAs in equal amounts, giving a net turnover of ~ 0 ($p>0.05$).

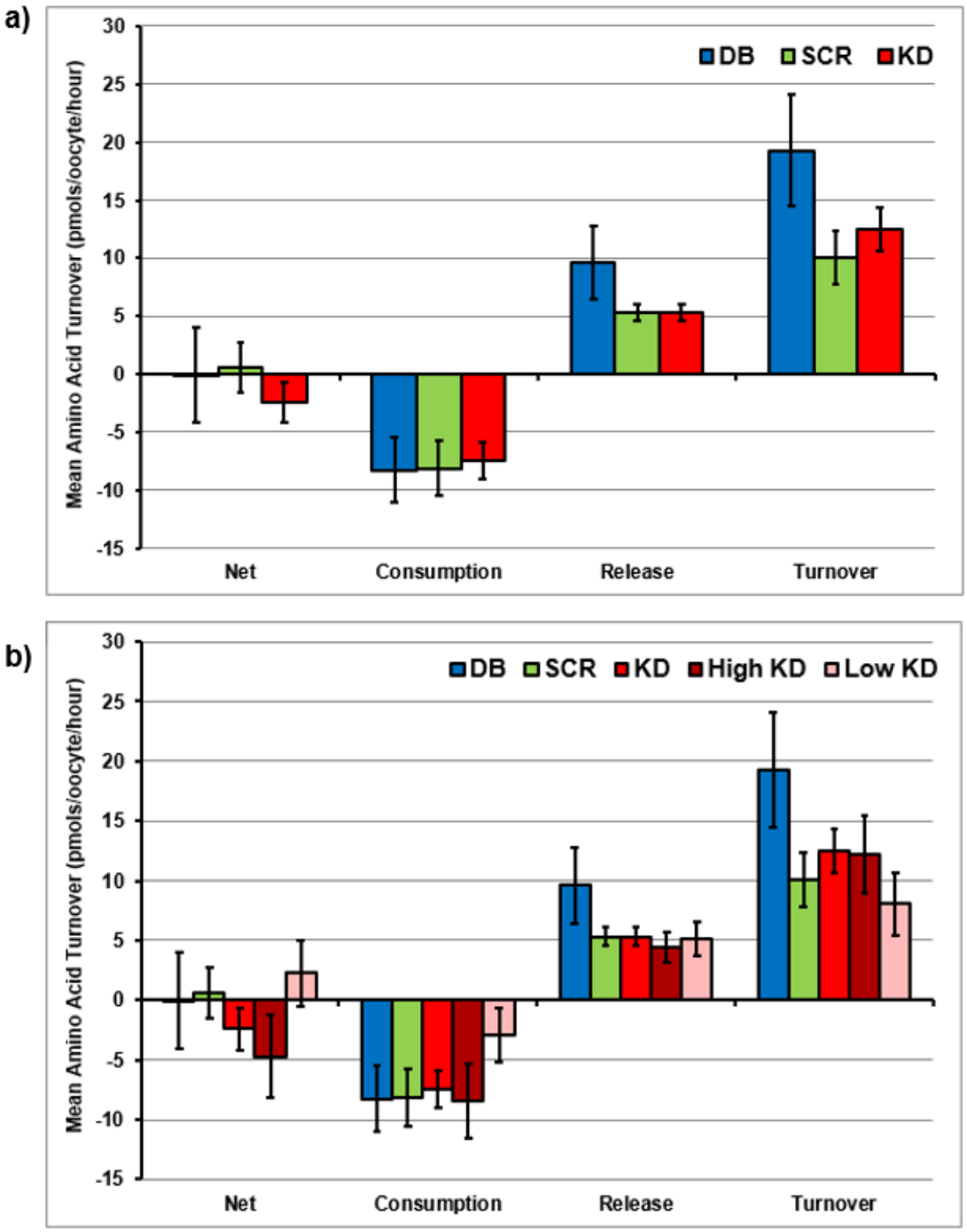

Figure 6.13. AA turnover (pmol/oocyte/hr) in **a)** injection groups DB, SCR and KD and **b)** injection groups DB, SCR and KD as well as high (dark red) and low (pink) *PADI6* KD groups according to Section 6.3.2.1. AA release, consumption, turnover and net turnover are displayed. Individual bars show the mean ±SEM ($p>0.05$).

6.3.2.3 Evaluation of release/consumption of individual amino acids from oocytes following *PADI6* KD

Firstly, the data for each AA for each drop and injection group was assessed to identify significant differences from zero change in concentration using the Wilcoxon signed rank test. This was performed to validate whether there was significant consumption or release of each AA. While no significant differences between groups were identified by ANOVA, results showed that the AAs that were significantly consumed and released according to the Wilcoxon signed rank test (significantly different from 0) varied between injection groups (Table 6.16). Aspartic acid was significantly consumed by all 3 injection groups ($p<0.05$) (Table 6.16a). This was the only AA that was significantly consumed in oocytes from DB and SCR injection groups. In *PADI6* KD oocytes, tryptophan (Trp) was also significantly consumed ($p<0.05$). On the other hand, a greater number of AAs were released than consumed in all injection groups (Table 6.16b). Alanine (Ala), methionine (Met) and phenylalanine (Phe) were significantly released by oocytes from all 3 injection groups ($p<0.05$). DB injection group was the only group to significantly release lysine (Lys) while *PADI6* KD group was the only group to significantly release glutamine (Glu) ($p<0.05$). Both SCR and *PADI6* KD injection groups significantly released arginine (Arg) ($p<0.05$) but DB injection group did not ($p>0.05$).

Figure 6.14 shows a graphical representation of individual AA turnover for each injection group. Although there were no significant differences in AA release/consumption between injection groups ($p>0.05$), some qualitative differences were observed. Firstly, DB and SCR oocytes appeared to consume glutamine while *PADI6* KD oocytes appeared to release it. This was also observed for histidine (His), threonine (Thr), tyrosine (Tyr) and possibly valine (Val). Conversely, lysine appeared to be consumed in the SCR injection group but released in the DB and KD injection groups ($p>0.05$). The other 12 AAs showed no qualitative changes in release or consumption between the different groups.

Table 6.16 AA **a)** consumption and **b)** release by MII oocytes from each injection group (pmol/oocyte/hr) ($p<0.05$). Data shows the mean ±SEM for each AA that was significantly different from 0 according to the Wilcoxon signed rank test, indicative of significant consumption or release. NS is shown where the data were not significant for a specific injection group.

a)

Amino acid	Significantly consumed AAs in each injection groups (pmol/oocyte/hr)		
	DB	**SCR**	**KD**
Asn	0.8 ± 0.3	1.1 ± 0.3	1.3 ± 0.6
Trp	NS	NS	0.2 ± 0.5

b)

Amino acid	Significantly released AAs in each injection groups (pmol/oocyte/hr)		
	DB	**SCR**	**KD**
Ala	0.4 ± 0.1	0.4 ± 0.1	0.5± 0.1
Arg	NS	0.2± 0.1	0.5 ± 0.3
Glu	NS	NS	0.6 ± 0.3
Lys	0.3 ± 0.1	NS	NS
Met	0.6 ± 0.2	0.6 ± 0.1	0.3± 0.1
Phe	0.4 ± 0.2	0.7 ± 0.1	1.4± 0.2

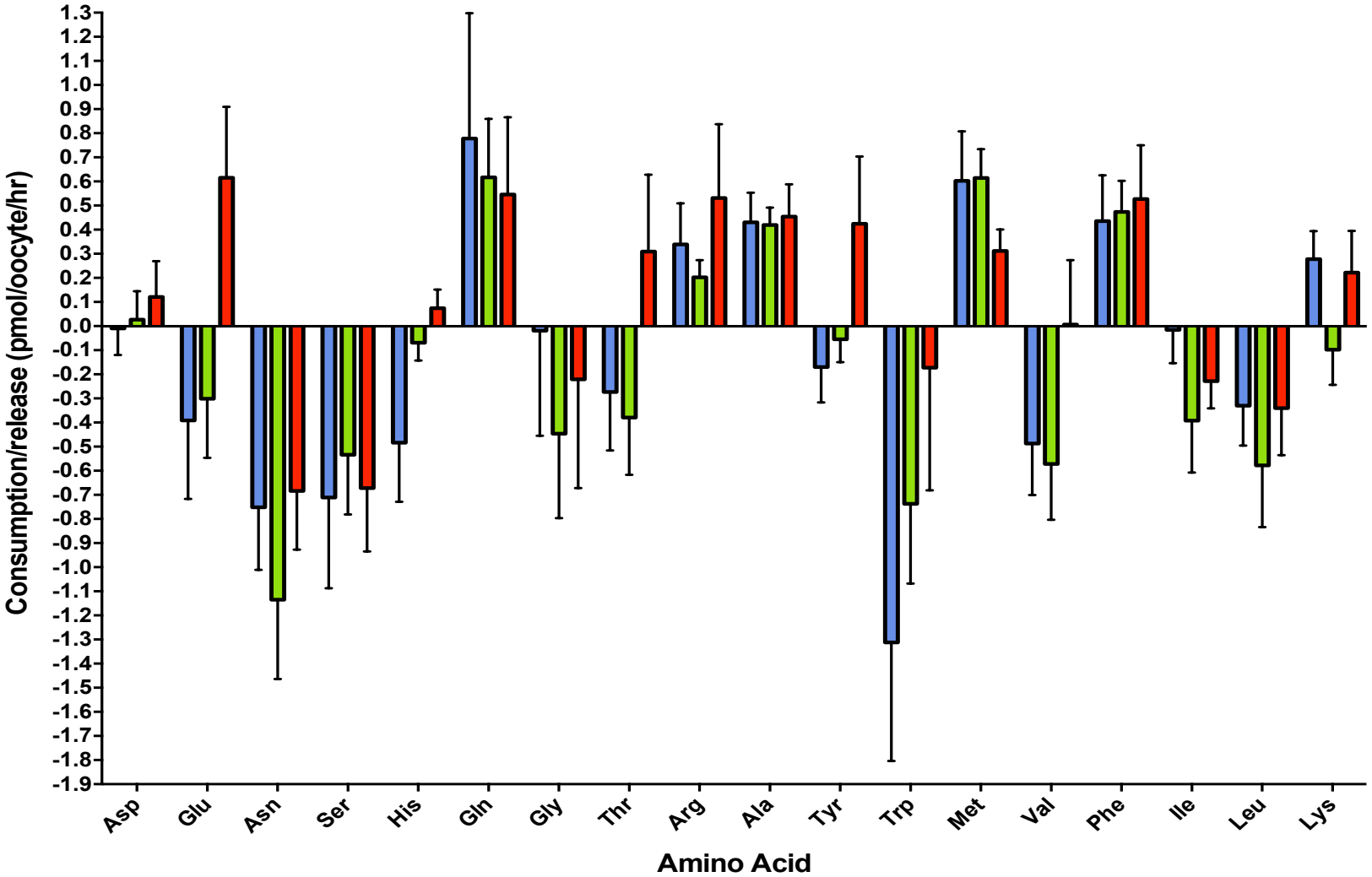

Figure 6.14. AA turnover for each injection group (DB, SCR and KD) ($p>0.05$). Bar height indicates total turnover (sum of release and consumption).

6.3.3 Experiment 3: *In vitro* fertilisation of bovine oocytes following *PADI6* KD during IVM

IVF was performed following KD of *PADI6* in GV oocytes to assess the role of oocyte derived *PADI6* in embryo development. GV oocytes were microinjected with DB, SCR or *PADI6* dsiRNA species during IVM and subsequently fertilised with bovine sperm. A group of GV oocytes that were not injected were cultured through IVM, IVF and embryo culture alongside the microinjected oocyte groups as a non-injected (NI) control to investigate the impact of microinjection of oocytes on embryo development. COCs were photographed prior to injection, after 24-hour IVM and on day 2 of embryo culture following IVF. Figure 6.15 shows representative images of oocytes and embryos from each injection group. Oocytes from all injection groups showed similar levels of cumulus expansion and mucification. Viability and embryo cleavage were assessed for each injection group on Day 1 or 2 of culture (Figure 6.16). This cut-off was chosen to obtain 2-8 cell embryos because *PADI6* expression decreases following EGA in bovine (8-16 cell stage). The results showed that microinjection of GV oocytes with *PADI6* dsiRNA significantly reduced cell viability measured by the number of neutral red dyed zygotes/embryos on Day 1 or 2 of embryo culture compared to NI control ($p<0.05$) (Figure 6.16b). There were no significant differences ($p>0.05$) in cell viability between injected controls (DB and SCR) and NI controls ($p>0.05$). Similarly, there were no significant differences ($p>0.05$) in cell viability between injected groups (DB, SCR and KD). Qualitatively, cell viability appeared to be reduced in DB and SCR-injected groups compared to the NI control, although this was not significant ($p>0.05$). The embryo cleavage rate was significantly lower in the *PADI6* KD group compared to the NI group ($p<0.05$). Again, there were no differences in embryonic cleavage between DB, SCR and KD groups or between injected and NI control groups ($p>0.05$) (Figure 6.16c). Embryonic cleavage appeared to be reduced in DB and SCR-injected groups compared to the NI control, but this was not significant ($p>0.05$). Overall, it is likely that the microinjection procedure *per se* plays a role in reducing cell viability and risks the introduction of polyspermic fertilisation which may reduce developmental competence but that *PADI6* dsiRNA augments the effect to create a significant difference between KD and NI groups.

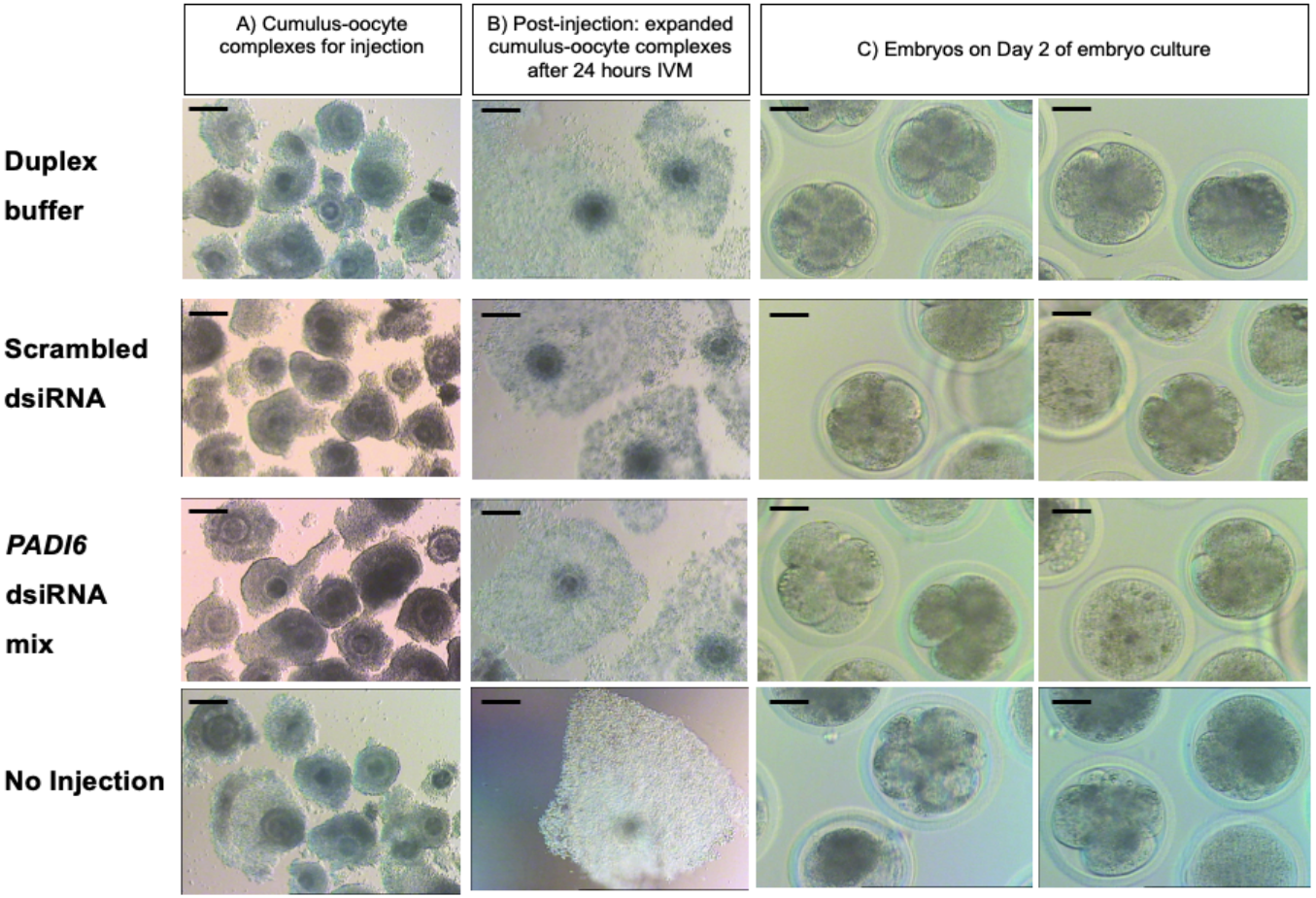

Figure 6.15. Examples of cumulus-oocyte complexes (COCs) microinjected with duplex buffer, scrambled or *PADI6* dsiRNA and non-injected controls followed by IVM and IVF: **a)** COCs prior to injection; **b)** Injected COCs after IVM showing cumulus expansion and mucification; **c)** Embryos on day 2 of embryo culture. Columns A and B were photographed at 40X, and column C at 200X magnification. Scale bar = 40 µm.

a)

	DB	SCR	KD	NI
No of live zygotes/embryos (%)	46/75 61%	40/71 56%	51/111 46%	60/62 97%
No. of cleaved embryos (%)	33/75 44%	28/71 39%	33/111 30%	51/62 81%

b)

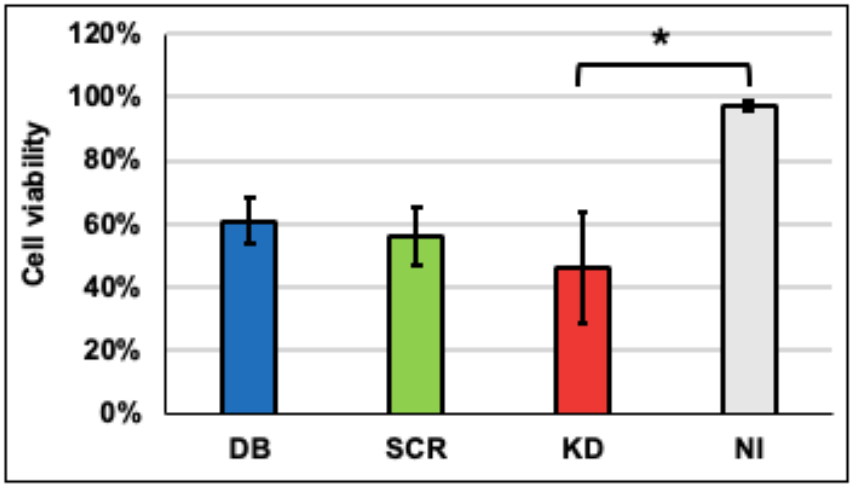

c)

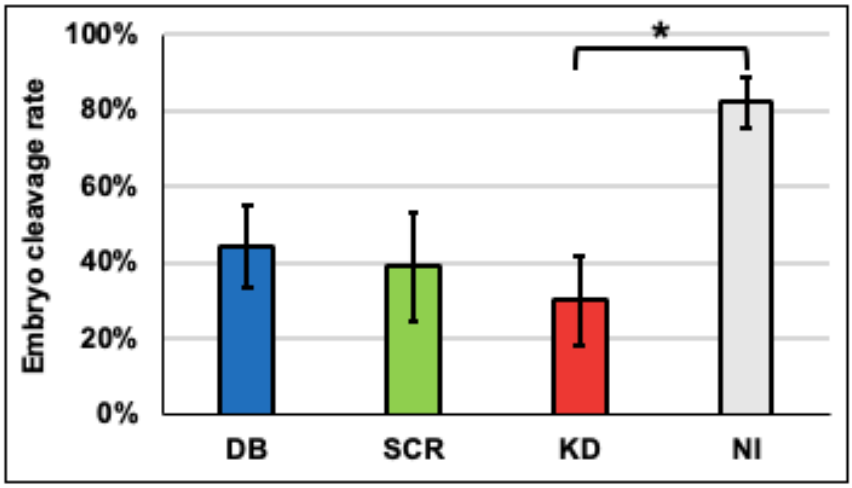

Figure 6.16. Cell viability and embryo cleavage rate on Day 1 or 2 of embryo culture after microinjection of GV oocytes with DB, SCR or *PADI6* KD injection species followed by bovine IVM and IVF: **a)** The number and percentage of live zygotes/embryos and cleaved embryos; **b)** Cell viability; **c)** Embryo cleavage rate for each injection group. Individual bars show the mean ±SEM. Non-injected (NI) oocytes were cultured alongside the microinjected oocytes as a control group. Significance is shown on the graph (*) where $p<0.05$.

Embryos from each injection group were sorted according to their developmental stage and lysed for Smart-seq2 cDNA synthesis. 0a shows the number of embryos that were retrieved on day 1 or 2 at each developmental stage for each injection group (DB, SCR and KD). Qualitatively, the number of embryos at each embryonic stage did not appear to differ between DB and KD injection groups. However, the number of 2-cell embryos in the SCR group appeared to be lower than the other groups and the number of 4-cell embryos appeared to be higher. It may be that early embryo development was accelerated in the SCR group but without thorough statistical analysis and further repeats, interpretation should be made with caution. Next, real-time PCR was used to investigate the transcript abundance of *PADI6* in embryos following microinjection (0b). The results showed that there were no significant differences in *PADI6* expression between the different injection groups (DB, SCR and KD) at all embryonic stages that were analysed ($p>0.05$). This suggests that there may be transcription of *PADI6* after the MII oocyte stage in the bovine as *PADI6* expression appears to have recovered in the embryos that were analysed here.

a)

Embryonic stage	No. of embryos			
	DB	SCR	KD	NI
2-cell	7	3	13	10
4-cell	5	9	11	15
6-cell	5	7	7	12
8-cell	3	1	1	0
Total	20	20	32	37

b)

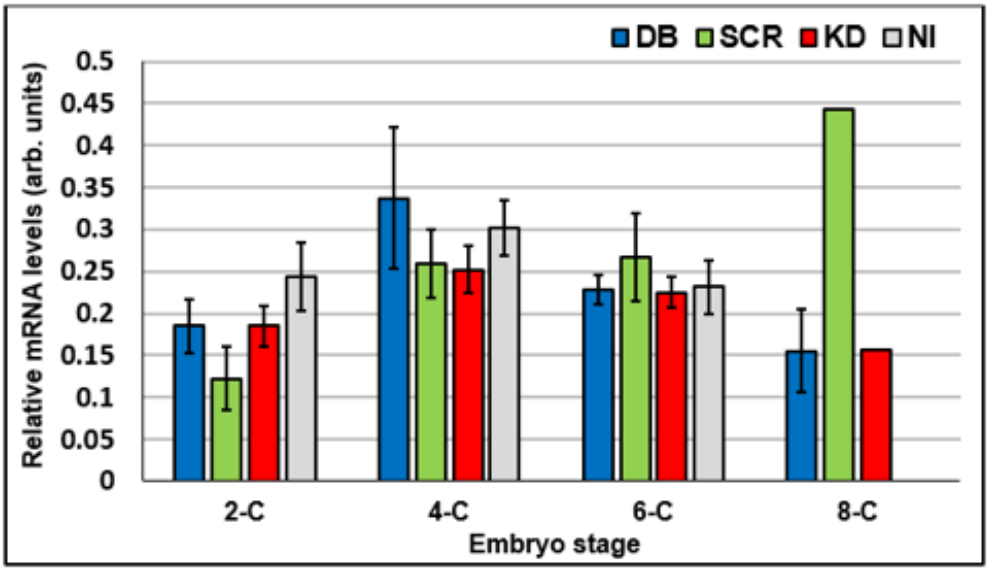

Figure 6.17. **a)** The number of bovine embryos that were retrieved on day 1 or 2 at each developmental stage (from 2-cell to 8-cell) for each injection group (DB, SCR and KD). **b)** Expression of bovine *PADI6* across early embryo development after microinjection with DB, SCR or KD injection species ($p>0.05$). Individual bars show the mean ±SEM. The 'n' values for each embryonic stage and injection group are as detailed in **a).**

6.4 Discussion

There were many potential approaches to investigate the functional analysis of *PADI6* gene KD. Here, 3 approaches were explored: PADI6 protein analysis, oocyte metabolic profiling and embryo culture following KD of *PADI6*. Firstly, investigation of PADI6 protein in bovine oocytes was hindered by the unavailability of a bovine antibody. Furthermore, attempts to produce a recombinant human PADI6 in a bacterial expression system were unsuccessful due to the strain of bacteria that were used. Secondly, metabolic profiling showed that KD of *PADI6* might have a functional effect on the AA metabolism of bovine MII oocytes at the time points studied. Finally, KD of *PADI6* in GV oocytes appeared to recover by the 2-cell embryo stage, suggesting that either there is transcription of *PADI6* after the MII oocyte stage in the bovine or that sufficient stored protein was still available to negate any effects of KD.

6.4.1 Experiment 1: Cloning of human *PADI6* ORF into bacterial expression vectors

2 different methods of cloning were explored to produce *PADI6* clones with different properties that could be used in multiple expression systems. pET vector cloning relies on the presence of unique restriction sites to cleave the DNA or vector only once. As a result, it can be tailored for directional cloning through the use of 2 different restriction enzymes and is fairly inexpensive. However, as a unique site did not exist here, pET vector cloning became arduous (Rohweder et al., 2018). Site-directed mutagenesis was necessary to create a suitable restriction site (Castorena-Torres et al., 2016). In addition to this, creating a pET vector did not produce a versatile system for future cloning. The technique must be performed again in order to create another vector. On the other hand, there were a wide range of pET vectors available containing various tags and selective markers. pET-11a was chosen as it had no tag, which is beneficial in this study as the *PADI6* ORF clone possessed a C terminus histidine tag.

At the same time, gateway cloning was executed to clone *PADI6* for protein expression (Hartley et al., 2000). This method negated the use of restriction enzymes, which can be problematic due to multiple cutting sites, inefficient digestion and incompatible ends (Liu et al., 1998a). It also produced a versatile system that could input a gene of interest into a range of destination vectors. This can facilitate protein expression in a variety of organisms and allow the incorporation of different protein tags depending upon downstream processes (Reece-Hoyes and Walhout, 2018). Conversely, the proprietary

gateway enzymes and vectors were expensive to buy. The *E. coli* destination vectors that were available in this research contained high molecular weight tags such as glutathione S-transferase (GST). Large tags such as this may alter the native protein folding and enzymatic function thereby hindering PADI6 activity (Kimple et al., 2013).

Overall, the 2 cloning methods that were executed counteract each other's limitations. pET-11a cloning produced a vector that would express PADI6 with a small C terminus histidine tag that is unlikely to affect its native protein structure or enzymatic function. Contrastingly, gateway cloning produced a versatile expression system that may not be suitable initially for PADI6 production in *E. coli* but which may be useful for future experiments looking at PADI6 protein expression in mammalian cells.

6.4.1.1 Human PADI6 protein production using a bacterial expression system

Cloning of human *PADI6* ORF into both expression vectors was verified by sequencing. Despite this authentication, bacterial PADI6 production was unsuccessful. There are many reasons why recombinant protein induction fails but unfortunately there was no time to investigate and troubleshoot the issues. The most likely reason for the failure reported here is that the bacterial strain that was available for use, DH5α chemically competent *E. coli,* are not suitable for protein expression. Although DH5α have been used in other studies for protein production (Dracheva et al., 1995), the main use for these cells is for sub cloning meaning that they efficiently uptake and propagate plasmids (Taylor et al., 1993). In hindsight, bacterial strains such as BL21AI or BL21(DE3) *E. coli* should have been used. BL21AI and BL21(DE3) are capable of strongly expressing proteins upon induction with L-arabinose and IPTG, respectively (Sorensen and Mortensen, 2005). The observed banding in bacterial lysates in Figure 6.11 and Appendix IV.C is likely to be due to unspecific labelling of bacterial proteins as it was seen in untransformed and uninduced, as well as induced, *E. coli* samples. Other reasons for failed protein production include disruption to initiation start site upon insertion into the vector, RNA or protein degradation and protein toxicity to bacteria (Rosano and Ceccarelli, 2014). With more time, the correct bacterial strains could have been transformed with *PADI6*-vectors and protein production attempted again. General antibodies for GST or histidine could have been used to verify the presence of PADI6 from each vector. This would also confirm the specificity of the PADI6 antibody (PA5-45758, Invitrogen). However, once successfully produced, there would be no guarantee

that the PADI6 protein would be biologically active and any protein produced would need to be thoroughly evaluated before use to counteract oocyte loss of PADI6 following siRNAi KD experiments.

6.4.1.2 Use of human PADI6 antibody to detect PADI6 in embryo carcinoma cell lines and bovine PADI6 protein in GV oocytes

The human PADI6 antibody that was chosen for protein analysis was tested by Invitrogen in RPMI 8226 cell lysates originating from myeloma from peripheral blood and had not been cited in any publications so a recombinant human PADI6 protein was purchased as a positive control. The expected molecular weight of the purchased human PADI6 protein was approximately 100 kDa as it was tagged with a GST tag. Figure 6.11a shows the identification of a single band between 100 and 130 kDa that is expected to be that of the purchased PADI6. If this is true, the human PADI6 antibody effectively detects human PADI6 protein. Considering this, PADI6 protein was not detected in human ECC lines, 2102Ep and NTera-2 (Figure 6.11a). Although these cells express pluripotency genes such as *OCT4* and *NANOG*, expression of *PADI6* appears to be more restricted (Josephson et al., 2007). Neither embryonic stem cells (ESCs) nor induced pluripotent stem cells (iPSCs) express *PADI6* suggesting that it is tightly regulated by temporal and spatial factors in the oocyte (Christophorou et al., 2014). This also leads us to question the applicability of ECCs, ESCs and iPSCs in studying early embryo development.

Finally, the human PADI6 antibody could not detect bovine PADI6 in bovine GV oocytes. GV oocytes were chosen for protein analysis as bovine *PADI6* gene expression is at its highest at this stage compared to other stages of preimplantation development (Figure 3.6). The human PADI6 peptide (Table 6.11) used to raise the antibody was approximately 59% similar to bovine PADI6. According to the company, a similarity of 85% or above is necessary for cross reactivity therefore it was unable to detect the bovine protein. Another use for the PADI6 antibody and recombinant protein was to KD PADI6 protein expression and rescue it to reverse the KD phenotype. For the same reason, neither the human PADI6 antibody nor human recombinant protein would have been likely to be biologically active and effective to do this in bovine oocytes.

To overcome these limitations and investigate bovine PADI6 expression in oocytes, a specific bovine antibody would need to be purchased or generated. This would be costly and time-consuming as bovine PADI6 antibodies are not commercially available and would therefore have to be custom made by injecting a host species with a recombinant

bovine PADI6 peptide or full-length protein. Similarly, cloning of bovine *PADI6* gene into a bacterial expression system could be performed although this method has proved unsuccessful (Section 6.3.1) and was shown to be laborious and would require significant troubleshooting before it could be used for the desired application. Overall, analysis of bovine PADI6 protein expression is necessary to understand the function of PADI6 in the bovine oocyte and preimplantation embryo and should be the aim of continuing this research.

6.4.2 Experiment 2: The impact of *PADI6* KD on bovine oocyte metabolism

Metabolic profiling of *PADI6*^{KD} oocytes was chosen as a relevant functional index of *PADI6* KD. RNA-seq analysis in Chapter 5 suggested that amino acid metabolism was affected following *PADI6* KD. Changes to the metabolism of the MII oocyte as a result of *PADI6* KD could reflect dysregulation of related metabolic processes and disruption to oocyte health (Section 6.1.2). For example, glutamine, aspartate and glycine serve as substrates for the synthesis of purine and pyrimidine nucleotides for mRNA (Collado-Fernandez et al., 2012). If KD of *PADI6* directly or indirectly impacts transcription in the oocyte, changes to AA metabolism would be expected. Moreover, methionine acts as a donor of methyl groups therefore dysregulation of epigenetic pathways following *PADI6* KD might influence methionine metabolism (Niculescu and Zeisel, 2002). Overall, the results showed that there were no significant differences in AA consumption, release, net turnover and total turnover between the different injection species ($p>0.05$) (Figure 6.13). However, after matching the *PADI6* expression and HPLC data, differences were observed in net turnover between high and low *PADI6* KD groups. An overall consumption of AAs was observed in high *PADI6* KD oocytes while an overall release of AAs was observed in low *PADI6* KD oocytes ($p>0.05$). A greater number of replicates would be necessary to show significance as there was high variability between oocytes and the degree of dsiRNA knockdown. Together, these data suggest that there may be some functional effect of *PADI6* KD on AA turnover in MII oocytes. Given the relationship between AA profiles and oocyte health, changes to AA turnover may be an indirect effect of other perturbations in the *PADI6*^{KD} oocyte.

Oocytes from all injection groups significantly consumed aspartic acid ($p<0.05$). Studies in rats and humans suggest that aspartic acid in the follicular fluid might increase LH levels and therefore promote oocyte maturation and follicle luteinisation (D'Aniello et al., 1996; D'Aniello et al., 2007). Furthermore, aspartic acid is necessary for the formation of

intermediates in the tricarboxylic acid (TCA) cycle for mitochondrial oxidative metabolism (Cetica et al., 2003). Meiotic and cytoplasmic maturation have high energy requirements so this would support the observed consumption of aspartic acid during oocyte maturation in all injection groups. Oocytes from all injection groups significantly released alanine, methionine and phenylalanine ($p<0.05$). The *PADI6* KD group was the only group to significantly release glutamine and consume tryptophan ($p<0.05$). Glutamine is required for mRNA synthesis and oxidative metabolism through the TCA cycle which suggests that KD of *PADI6* might impact oocyte maturation and consequently, developmental competence. Likewise, the *PADI6* KD group appeared to release valine while DB and SCR groups consumed valine ($p>0.05$). This is interesting given the observed downregulation of *BCKDHA* in *PADI6*^{KD} oocytes following RNA-seq (Figure 5.13). As described previously, *BCKDHA* is responsible for the breakdown of 3 AAs including valine (Pan et al., 2018). Downregulation of *BCKDHA* might result in reduced breakdown of valine and increased excretion into the media. Both SCR and KD groups significantly increased the release of arginine ($p<0.05$) but DB injection group did not ($p>0.05$). This suggests a potential impact of *PADI6* KD may be evident later on in embryo cleavage development than was investigated in the present study, as such this observation should be followed-up in future studies. In the literature, release/consumption of alanine, arginine, glutamine, leucine and tryptophan is strongly associated with developmental competence of the bovine MII oocyte (Hemmings et al., 2012). Similar associations have also been made in human oocytes and embryos (Hemmings et al., 2013; Houghton et al., 2002; Stokes et al., 2007). Excessive release of alanine is associated with a reduction in embryonic cleavage in bovine and humans (Hemmings et al., 2012; Houghton et al., 2002). Alanine release is thought to be associated with increased AA turnover and disposal of ammonia from embryos (Donnay et al., 1999; Houghton et al., 2002). Ammonia is a product of amino acid metabolism and a by-product of conversion of peptidylarginine to peptidylcitrulline by PADI enzymes (Bicker and Thompson, 2013). Dysregulation of PADI enzyme activity might therefore result in altered ammonia disposal and amino acid metabolism. Research into the effects of ammonia on bovine blastocysts suggest that ammonia is released as free ions or fixed with alanine and possibly glutamine and arginine (Orsi and Leese, 2004). Here, *PADI6*^{KD} oocytes significantly released alanine, glutamine and arginine, indicating a potential increase in ammonia disposal in PADI6 KD oocytes. On the other hand, release of alanine by oocytes from all injection groups in this study may therefore indicate that the microinjection procedure decreases developmental competence of the oocyte. Decreased developmental competence is also associated with increased consumption of arginine and glutamine and increased release of tryptophan in bovine (Hemmings et

al., 2012). Here, the inverse of this is seen in the *PADI6* KD group which suggests that microinjection of *PADI6* does not affect developmental competence by disrupting AA oocyte metabolism. Overall further investigation of late preimplantation embryos is necessary to confirm the impact of *PADI6* KD on oocyte and embryo developmental competence. This study shows that AAP could be used as a non-invasive assessment of viability and oocyte quality after microinjection.

Our current AA assay system could not be used to detect citrulline, but other researchers have reported using HPLC to detect L-citrulline (Jayaprakasha et al., 2011; Shafaei et al., 2015). However, citrullination by PADI proteins is not accompanied by the removal of free citrulline from the cell or media, but instead involves the conversion of arginine to citrulline which releases ammonia as a by-product (Bicker and Thompson, 2013). Additionally, these published methods used much higher sample volumes than those used for individual oocyte cultures, which would likely mask any oocyte-induced changes in citrulline concentration. Therefore, using HPLC to measure citrulline is unlikely to detect citrullination by PADI6. A more promising approach may be to measure the release of ammonia between control and KD oocytes as a possible indicator of citrullination. A metabolomics approached using liquid chromatography mass spectrometry could potentially identify putative changes in citrulline as well as other metabolites, though again the oocyte sample volumes available for analysis are very limited which may restrict assay utility. Recent advances in chemical labelling of citrullinated proteins have aided identification of novel PADI substrates and citrullination sites by mass spectrometry (Clancy et al., 2016). However, a method of extracting the high protein content from very small volumes of maturation media is not widely available. For example, acetonitrile precipitation approach would require a 1 in 1000 dilution of the original sample (Demacker et al., 2009). Unfortunately, pathway analysis of citrulline biosynthesis, protein citrullination, arginine biosynthesis, citrulline-nitric oxide cycle and arginine degradation produced no results following *PADI6* KD. This suggests that *PADI6* might have lost its citrullinating ability, as described by Raijmakers et al. (2007) previously.

6.4.3 Experiment 3: Recovery of *PADI6* expression in bovine embryos following KD in GV oocytes

After achieving successful KD of *PADI6* in bovine oocytes, it was necessary to explore the impact of gene KD on embryo developmental competence. There was a significant reduction in zygote/embryo viability and embryonic cleavage in the *PADI6* KD group compared to NI controls, however, this was not observed between the KD and control-injected groups. This suggests that there might have been a synergistic effect of the microinjection procedure and *PADI6* dsiRNA that caused a significant change compared to NI control oocytes. With no significant differences observed between DB, SCR and KD microinjection groups, further investigations and repeat cultures are necessary to investigate whether this is a true effect of PADI6 dsiRNA.

DsiRNA KD is often favourable for its transient ability to KD genes of interest, therefore it was interesting to evaluate the transcript abundance of *PADI6* in the embryo after dsiRNA microinjection (Podolska and Svoboda, 2011). The results showed that *PADI6* transcript abundance in the KD group was similar to control-injected oocytes in all of the developmental stages that were analysed (2-8 cell embryos). This suggests that there may be transcription of *PADI6* after the MII oocyte stage in the bovine, or that *PADI6* may be upregulated to compensate for its reduction. Wang et al. (2012b) microinjected bovine oocytes with dsiRNA to achieve KD of *IGF-IR*, however, in order to achieve KD in 2-cell embryos, 1-cell zygotes were microinjected with dsiRNA. This suggests that recovery of gene expression following RNAi in oocytes may be a common occurrence and that by using zygotes, the effects of RNAi can be observed in the early embryo. Furthermore, storage of *PADI6* transcripts during oocyte maturation might prevent accessibility and degradation of *PADI6* mRNA by dsiRNA. After fertilisation, activation of the oocyte might stimulate polyadenylation and translation of *PADI6* mRNA, therefore appearing to rescue KD of *PADI6*. Indeed, Figure 3.6 showed that *PADI6* transcript abundance significantly increased from MII oocyte to 6-cell embryo stage, supporting the view that KD of *PADI6* is rescued in the embryo. To this end, a time course of detection of *PADI6* mRNA and protein expression in oocytes and embryos following siRNA injection is necessary to assess *PADI6* KD longevity by real-time PCR and Western blotting and/or immunohistochemistry.

On the other hand, with the variable nature of dsiRNA KD, it could be that *PADI6* expression was not significantly ablated during microinjection of GV oocytes. This would explain why *PADI6* expression was unchanged in the early embryo. This limitation was

a consideration throughout the experiment. As the expression of *PADI6* could not be measured in live oocytes after KD, a solution was to take a subset of MII oocytes after microinjection with dsiRNA and assess *PADI6* expression using real-time PCR. The problem with this was that the numbers of oocytes, considering the percentage of cell death, were too low to allow removal of oocytes for analysis prior to IVF. As a result, the expression of *PADI6* was evaluated during the first few cleavage divisions instead of allowing embryos to reach the blastocyst stage where *PADI6* is no longer expressed. Due to time constraints, further investigation into the development of *PADI6*^{KD} embryo was not conducted. It remains necessary to assess the ability of *PADI6* KD oocytes to reach the blastocyst stage. This would require activation of the embryonic genome and provide a better index of developmental competence.

Finally, although *PADI6* gene expression was unchanged in the embryo, the effect of *PADI6* KD on the expression of other genes may have been longer lasting. In Chapter 5 the results showed that there were changes to key epigenetic regulators in the oocyte after *PADI6* KD. There was also dysregulation of an imprinted gene, *PLAGL1*. Fertilisation encompasses an important reprogramming event whereby gamete-specific epigenetic marks are erased in preparation for a new somatic epigenome (Morgan et al., 2005). Dysregulation to epigenetic regulators at this crucial time point may have a detrimental effect on the embryo, specifically on EGA. Considering this, it would be interesting to perform targeted real-time PCR analysis and RNA-seq of *PADI6*^{KD} embryos across the whole preimplantation embryo developmental time course to the blastocyst stage to investigate the long-term impact of *PADI6* KD in GV oocytes.

6.4.4 Conclusion

This work successfully created 2 sequence-verified *PADI6* vectors by exploring different cloning methods, pET vector cloning and gateway cloning that may be useful tools for future research. Western blot analysis using a human PADI6 antibody highlighted the species differences in PADI6 protein and the necessity for a bovine PADI6 antibody. Moreover, metabolic profiling of MII oocytes suggested that there may be some functional effect of *PADI6* KD on AA turnover compared to control-injected and non-injected oocytes and that this may be linked to alterations in gene expression observed in Chapter 5, however changes in AAP of oocytes may also reflect the impact of *PADI6* KD on oocyte health. Furthermore, investigation into citrullination pathways following *PADI6* KD suggests that PADI6 might have lost its deiminase activity. Finally, IVF of *PADI6*^{KD} oocytes indicated that *PADI6* transcript abundance recovers in the bovine embryo. Further functional analyses of *PADI6*^{KD} oocytes are necessary to provide a greater understanding of *PADI6* function in the bovine oocyte.

Chapter 7 General Discussion

The results presented in this thesis have extended our understanding of the biology of *PADI6* during bovine oocyte maturation. The data presented has mapped the expression of *PADI6* and other MEG transcripts across oocyte and embryo development. Furthermore, KD of *PADI6* using dsiRNA has provided preliminary insights into the roles played by PADI6 during the GV to MII transition in bovine oocytes *in vitro*. Overall, the data suggest that *PADI6* is involved in transcriptional regulation of a subset of epigenetic regulators, which may impact on oocyte developmental competence and embryonic genome activation in monovulatory species.

7.1 Characterisation of *PADI6* and MEGs in the bovine

The expression of MEGs is often considered to be a good marker of oocyte developmental competence (Conti and Franciosi, 2018). During oocyte maturation, the transcription and storage of mRNA is crucial to enable the synthesis of proteins that function in maturation, fertilisation and early embryo development (Ajduk et al., 2008). Together, MEGs form regulatory mechanisms that are necessary to orchestrate developmental processes at the correct time points. The first step to understanding gene function in the oocyte and embryo is to characterise the gene expression at different time points across preimplantation development. This enables inferences to be made about the origin of transcripts, be it maternal or zygotic, and potential regulatory mechanisms that are controlling gene expression. Furthermore, considering the involvement of *PADI6* and SCMC genes in human pathologies, characterisation of MEGs during “normal” development facilitates the study of developmentally incompetent oocytes and may led to advances in ART such as IVF (Alazami et al., 2015; Docherty et al., 2015; Maddirevula et al., 2017; Meyer et al., 2009; Murdoch et al., 2006; Parry et al., 2011).

There remains a need for deeper understanding of oocyte mechanisms and preimplantation embryo development in larger mammals. For many years the mouse has been used to study preimplantation development due to its small size, short generation interval and ability to create inbred mouse strains; however, with time, the distinction between mouse and human has become more evident (Taft, 2008). Differences in culture conditions and metabolic requirements and follicle selection have meant that the bovine model is now considered to be more physiologically relevant to humans than the mouse (Menezo and Herubel, 2002). Humans and bovine are monoovular species

indicating that only 1 secondary oocyte is ovulated per cycle (Adams and Pierson, 1995). Regulatory mechanisms such as polyadenylation that are present in the oocytes of humans and bovine are not observed in mice (Menezo and Herubel, 2002). Likewise, bovine embryos better reflect the timing of epigenetic reprogramming and EGA in human development than the mouse model (Bettegowda et al., 2008). Still, there is little information in the literature regarding the expression of SCMC members during bovine oogenesis and preimplantation embryogenesis. In light of the similarities between bovine and human oocyte and preimplantation embryo development, it was evident that this knowledge gap needed to be addressed.

The results that were presented in this thesis showed that *PADI6* expression was oocyte and early preimplantation embryo-specific in the bovine (Chapter 3). *PADI6* was expressed in the GV and MII oocyte as well as the early embryo up to the 16-cell stage but it was not expressed after EGA in the morula, blastocyst and expanded blastocyst embryos. To our knowledge, this is the first characterisation of *PADI6* during bovine oocyte maturation and preimplantation embryo development. *PADI6* expression was absent from somatic tissues of the ovary, except for the OC sample. The low detection of *PADI6* in this sample is likely to originate from early stage follicles that reside in this region of the ovary (Newton, 1998). Furthermore, *PADI6* was not expressed in non-ovarian somatic tissue, further confirming its specificity as oocyte and embryo specific. Studies in mice were consistent with our observations showing that *PADI6* expression is restricted to oocytes and preimplantation embryos (Choi et al., 2010; Wright et al., 2003). However, Zhang et al. (2004) showed that *PADI6* was highly expressed in peripheral blood leukocytes and ovary, and weakly expressed in liver, lung, testis, spleen, thymus and pancreas in humans. In this study, there was only 1 RNA sample available for the majority of bovine somatic tissues that were analysed therefore the results may not reflect the actual expression of *PADI6* in bovine somatic tissues. Despite this, research in other species including humans suggests that *PADI6* is predominantly expressed in the oocyte and early embryo.

The expression patterns of SCMC and *NLRP* genes in bovine preimplantation development were characteristic of MEGs with gene expression highest in the oocyte and early embryo, followed by a sharp decline after EGA. The data presented here is consistent with that in the literature. RNA-seq by Reyes et al. (2015) supported microarray data (Mamo et al., 2011) showing that *NLRP5* sharply decreased from the GV to MII stage in the bovine, as observed here in Figure 3.9. Consistent with our reports in bovine, SCMC members, *Mater/NLRP5, Floped/OOEP* and *Tle6/TLE6* were

expressed in the maturing mouse and ovine oocyte and embryo prior to EGA (2-cell and 8-16-cell stage in mice and ovine, respectively (Bebbere et al., 2014; Li et al., 2008a). In this thesis, *DNMT1* expression was constant during oocyte maturation and preimplantation embryo development to the 8-cell stage; however, Misirlioglu et al. (2006) detected higher *DNMT1* expression in MII oocytes compared to 8-cell bovine embryos. This might be due to sampling of different sized follicles as *DNMT1* expression was detected at higher levels in oocytes from larger bovine follicles by Racedo et al. (2009). Conversely, expression of *DNMT3A/B* and *ZFP57* was lower in the early stages of preimplantation development and began to increase after EGA, indicative of zygotic transcription. RNA-seq results by Graf et al. (2014) showed that zygotic *DNMT3B* and *ZFP57* were activated at the 8-cell stage while *DNMT3A* was first expressed at the blastocyst stage in bovine. Interestingly, this dataset of zygotic transcripts did not contain any SCMC or *NLRP* genes, indicating that they are transcribed from the maternal genome (Graf et al., 2014). *DPPA3* was highly expressed throughout early preimplantation embryo development, but there was a reduction in transcript abundance that correlated with EGA. In the study by Graf et al. (2014), transcription of zygotic *DPPA3* was recognised from the paternal allele around the 16-cell stage therefore it is likely that maternal *DPPA3* was translated or degraded around the time of EGA. Expression of *TRIM28* was fairly consistent across bovine oocyte and embryo stages, only increasing in the morula embryo.

The advent of RNA-seq has allowed the transcriptomes of individual oocytes and embryos to be comprehensively characterised (Tang et al., 2009). Many studies have performed widespread transcriptome analyses in different stages of bovine preimplantation development by RNA-seq (Chitwood et al., 2013; Driver et al., 2012; Graf et al., 2014; Huang and Khatib, 2010; Mamo et al., 2011; Reyes et al., 2015; Robert et al., 2011). By analysing the impact of polyadenylation during oocyte maturation, Reyes et al. (2015) found that, for many mRNAs, transcript abundance did not change from GV to MII stage. Instead, the length of polyA tail was altered, which indicates that there is mRNA storage in the oocyte. This is significant for our findings as the observed fluctuations in transcript abundance from qPCR experiments may actually signify changes in polyA tail length or storage of mRNAs, which might be regulated in the oocyte by PADI6 (Section 7.6.3).

7.2 Validation and experimental design for the targeted KD of *PADI6* during the IVM of bovine oocytes using dsiRNA species

The innate cellular process of RNAi has been harnessed by researchers as a tool to investigate the function of novel genes. In summary, exogenous dsiRNA becomes incorporated into the RISC and the passenger strand is degraded. The RISC is targeted to the homologous mRNA by the guide strand. RISC-member and endonuclease, AGO2, cleaves the target mRNA and it is subsequently degraded in cytoplasmic P-bodies. AGO2 is an essential component of the RISC. Lykke-Andersen and colleagues used RNAi to ablate maternal Ago2 from mouse zygotes (Lykke-Andersen et al., 2008). This resulted in embryonic arrest, with 76% of embryos arresting at the 2-cell stage (EGA in mice). They also demonstrated that a subset of maternal mRNAs, including *Mosg, Gbx2, Fgfr2* and *Lepr-2*, were stabilised in AGO2 KD zygotes, compared to controls. Microarray screens identified endogenous miRNAs that could potentially target such genes for degradation via AGO2/RISC. This work suggested that AGO2 was necessary to degrade a subset of maternal mRNAs prior to EGA in the mouse, and that the mechanism through which this occurs may involve endogenously expressed miRNAs.

It was hoped that targeted gene KD during IVM of bovine oocytes by microinjection of dsiRNA species would support investigation of the function of genes such as *PADI6*. With different means of administering dsiRNAs to a cell including transfection and electroporation, microinjection was chosen due to its repeatability between cells and across different culture weeks (Zhang and Yu, 2008). Microinjection was easily incorporated into the current IVM culture system (Figure 2.1 and Figure 4.4), which enabled oocytes to resume meiosis and complete oocyte maturation as described for non-injected oocytes in Chapter 2. Previously, Cotterill (2008) used a 2-day culture system to achieve gene KD during IVM of ovine oocytes. To this end, oocytes were retrieved from abattoir-derived ovaries, subject to denudation and subsequently, microinjected with dsiRNA. Oocytes were then incubated with cilostamide, a PDE3 inhibitor, for 24 hours to delay maturation. On day 2, oocytes were co-cultured with cumulus shells from oocytectomised COCs from fresh abattoir-derived ovaries for 24 hours. Finally, on day 3, oocytes were assessed for maturation and collected for downstream analyses. Clearly this system for dsiRNA KD during IVM is a longer process. It requires travelling to the abattoir on 2 consecutive days and necessitates more work than the system that is described in this thesis; however, the advantage lies in the

injection of denuded oocytes. In the current system, microinjection of COCs was technically challenging as cumulus cells mask the oocyte making it difficult to visualise and handle. As a result, the injection pipette might miss the oocyte and KD would not be achieved. Care was taken to ensure that the oocyte was injected with dsiRNA by observing a small movement of oocyte cytoplasm, but this was not always possible. In part, this may explain the variability that was detected in the KD of *PADI6* gene expression. In the 2-day system, microinjection of denuded oocytes may produce a greater number of successful KDs but lower oocyte survival rates as a result of denudation and longer culture time.

There are slight variations between published methodologies for microinjection of siRNA. Lee et al. (2014a) microinjected bovine cumulus-enclosed GV oocytes with siRNA and delayed meiotic maturation for 48 hours by incubation with cyclin-dependent kinase (CDK) inhibitor roscovitine. The delay, often called a pre-maturation stage, was included to allow more time for siRNAs to deplete endogenous transcripts with the hope of achieving a better gene KD. Maturation inhibitors have also been shown to enhance oocyte growth and developmental competence (Lee et al., 2017; Vanhoutte et al., 2008). On the other hand, some evidence suggests that delaying fertilisation by extended *in vitro* culture of mouse oocytes decreases developmental competence of the oocyte (Jee et al., 2009). Culturing bovine oocytes in PDE inhibitors for 9 hours caused complete loss of gap junctions between the oocyte and cumulus cells (Thomas et al., 2004). However, culture in PDE inhibitors for 6 hours did not affect embryonic cleavage, blastocyst rate or blastocyst cell number (Li et al., 2016). Thus it appears that the pre-maturation culture time must be optimised in order for it to be advantageous for subsequent embryo development. Following optimisation, the system described in this thesis could be improved by the incorporation of a pre-maturation stage after dsiRNA microinjection of GV oocytes.

In Chapter 4.2, the parameters for microinjection of bovine COCs were optimised. The injection volume was estimated experimentally by counting the number of injections that were taken to deplete a known starting volume. This estimate was comparable to estimated volumes in the literature (Bettegowda et al., 2007); however, measuring small volumes such as these is likely to be inaccurate. The main aim of the injection parameters was to maintain cell viability and competence. This was successfully achieved as an average of 81% of oocytes matured following microinjection with PBS (Table 4.7), which was comparable to oocyte maturation of non-injected oocytes (Figure 3.4).

Next, validation of dsiRNAs and primers was performed to evaluate the most effective reagents for KD and detection of *PADI6* transcript abundance. As discussed in Chapter 4, dsiRNA and primer design are mutually dependent. Primers must be designed according to the dsiRNA target region to detect cleavage of the gene of interest. Primers that bind outside of these regions may result in amplification of a fragment of the cleaved transcript, producing a false positive result (Holmes et al., 2010; Mainland et al., 2017). Likewise, dsiRNAs should be designed to target highly expressed exonic regions to achieve an effective gene KD. RNA-seq data from ovine species suggested that exons 9 and 13 of bovine *PADI6* would be effective targets for dsiRNA. After the design process, both primers and dsiRNAs were tested experimentally as there may be unknown properties of the transcript that preclude binding to the homologous sequence. 5 dsiRNAs were tested and oocyte-specific *PADI6* KDs were created using the microinjection and IVM system described in Chapter 4.

The preliminary data for targeted KD of oocyte *PADI6* showed that dsiRNAs in exon 9 and primer set 9B gave the most consistent reduction in *PADI6* gene expression compared to the other dsiRNA and primer combinations. These experiments were performed alongside microinjection training so the number of oocytes per microinjection group was low (n = 2-5 individual oocytes) and the appropriate experimental repeats were not performed. Nevertheless, the subsequent experimental design to determine the best dsiRNA species to KD *PADI6* contained an adequate number of oocytes and experimental repeats. It showed that a combination of 3 dsiRNAs targeting exon 9 was effective at reducing P*ADI6* transcript abundance (0.047 ± 0.05 arb. units, n = 17) in comparison to SCR-injected controls (0.14 ± 0.02 arb. units, n = 19) and DB-injected controls (0.13 ± 0.02 arb. units, n = 22) (Figure 4.8). RNAi is known to produce variable results due to differences in the amount of dsiRNA entering a cell or in the starting amount of mRNA in a cell (O'Meara et al., 2011). Further, the technical challenges of microinjection of COCs also cause variability in gene KD. As a result, oocytes with the greatest reduction in *PADI6* transcript abundance compared to control-injected oocytes were chosen for further analysis (Figure 4.9). The average reduction in *PADI6* gene expression was 74±3.6% following dsiRNA injection (0.03 ± 0.09 arb. units, n = 20) in comparison to SCR-injected oocytes (0.11 ± 0.02 arb. units, n = 10) and DB-injected oocytes (0.11 ± 0.02 arb. units, n = 11). The success of *PADI6* KD was verified by RNA-seq (Chapter 5).

7.3 Evaluation of MII oocytes following *PADI6* KD

KD of *PADI6* did not significantly affect oocyte meiotic progression and cumulus expansion ($p>0.05$). The KD experiments showed that there were no significant differences in oocyte viability or maturation between control-injected oocytes and *PADI6*^{KD} oocytes ($p>0.05$). In particular, maturation rates of viable oocytes after *PADI6* KD in Chapter 4 (64% ± 20%, n = 27, Figure 4.10) were not significantly different to non-injected oocytes from Chapter 3 (83% ± 3.6%, n = 242, Figure 3.6). Similarly, there were no differences in COC morphology, cumulus mass or cumulus expansion between control-injected oocytes and *PADI6*^{KD} oocytes. The results suggest that KD of *PADI6* did not affect the capacity of GV oocytes to complete meiotic progression over 24 hours IVM; however, it could still have functional importance for oocyte developmental competence. This is consistent with the mouse literature where *Padi6* knockout oocytes progress to MII without disruption (Esposito et al., 2007). Furthermore, when the AAP was matched with the *PADI6* KD results reduction of *PADI6* expression appeared to have some effect on AA metabolism compared to control-injected oocytes. This may be a direct effect of *PADI6* KD on oocyte metabolism or a general impact of *PADI6* KD on oocyte health. Aside from post-translational citrullination, there are no proposed roles for PADI6 in oocyte metabolism in the literature therefore it is unlikely that PADI6 functions in oocyte metabolism and the transition from GV to MII in bovine. The AA profiles of microinjected MII oocytes were not compared to non-injected MII oocytes. It may be that the microinjection technique *per se* affects AA metabolism, but this would be the same for all of the groups that were analysed here. Finally, AAP could be a useful tool for assessing oocyte quality after microinjection as it has been shown to be a reliable indicator of developmental competence in humans and bovine (Hemmings et al., 2012; Hemmings et al., 2013; Houghton et al., 2002; Stokes et al., 2007).

Investigation into the expression of *PADI* family genes in Chapter 3 confirmed the wide tissue distribution documented elsewhere (Mechin et al., 2007). However, *PADI3* and *PADI4* were observed at very low levels in the bovine GV oocyte sample. Although the data in Chapter 3 suggests that *PADI1-4* are not abundant genes in the oocyte, studies in polyovulatory mice and pigs have suggested otherwise (Brahmajosyula and Miyake, 2013; Zhang et al., 2016). It is understood that genes within a family can have redundant roles or the ability to compensate for the loss of a related gene (Busca et al., 2016). With the success of *PADI6* KD in the oocyte, it was critical to investigate the transcript abundance of *PADI1-4* in *PADI6*^{KD} oocytes. Preliminary analysis of *PADI1-4* in DB-injected MII oocytes showed that all 4 *PADI* genes were expressed at very low levels

(<0.0025 arb. units, n = 3) compared to *PADI6* (0.11 ±0.016 arb. units, n = 11) (Figure 4.14 and Figure 4.9). Furthermore, expression of *PADI1-4* did not significantly change in *PADI6*^{KD} oocytes (n = 3) compared to DB-injected control oocytes (p>0.05). Although the number of oocytes that were analysed was low and the results should be interpreted with caution, the RNA-seq data confirmed that transcription of *PADI1-4* was absent from bovine MII oocytes (Section 5.3.4.2). Therefore, the collective results from these studies suggested that *PADI6* is the predominant *PADI* family member in the bovine oocyte, which enabled investigation of gene function by dsiRNA KD during the IVM of oocytes from this species. Furthermore, it is likely that the transcriptomic changes that are documented in Chapter 5 are due to *PADI6* KD and not due to changes in *PADI1-4* expression.

With this in mind, Christophorou et al. (2014) investigated the role of PADI4 in pluripotency in mouse embryos. They found that treatment of 2-cell mouse embryos with an unspecific PADI inhibitor, Cl-amidine, resulted in complete developmental arrest at 8-cell stage. When they reduced the concentration of Cl-amidine to prevent embryonic arrest, they found that there was an increase in differentiated trophoblast cells at the blastocyst stage. It is important to note that they did not look to see if other PADI members were inhibited in mouse embryos therefore it may be that the observed effects are actually due to inhibition of PADI6. This is further supported by the observation that the SCMC-related condition FBHM is characterised by hyperproliferation of trophoblast cells. They also used mouse embryonic stem cells (mESCs) to look for substrates of PADI4 activity. They concluded that *Dnmt3b* and *Trim28* were potential substrates for PADI4. They noted that *Padi6* was not detected in mESCs or mouse induced pluripotent stem cells (iPSCs) after reprogramming. This shows that mESCs and iPSCs are not good models for investigation of *Padi6* and suggests that *Padi4* may function redundantly in these cells to regulate *Padi6* substrates, *Dnmt3b* and *Trim28.* This might confirm our findings in Chapter 5 that also identified *DNMT3A* and *TRIM28* as potential downstream targets of *PADI6* in the bovine. Overall, morphological evaluations of oocyte maturation and cumulus cell expansion along with a reduction in *PADI6* transcript abundance have proven that the dsiRNA microinjection approach and IVM culture system can be used for targeted gene KD during IVM of bovine oocytes. The system reported in Chapter 4 therefore formed the basis for the study of *PADI6* function in bovine oocytes in Chapters 5 and 6.

7.4 Transcriptome analysis of the impact of *PADI6* KD in GV oocytes on MII oocytes derived by IVM

Characterisation of gene expression in the bovine species (Chapter 3) showed that *PADI6* is an oocyte-specific gene that is transcribed from the maternal genome and depleted after EGA. Validation experiments following *PADI6* KD suggested that it does not function in meiotic maturation or cumulus expansion. From the literature, it is understood that PADI6 localises to CPL structures in the oocyte (Wright et al., 2003). CPLs form during oogenesis and provide a storage site for ribosomes and RNAs (Bachvarova et al., 1981; Sternlicht and Schultz, 1981). Yurttas et al. (2008) showed that ablation of *Padi6* in mouse oocytes caused an increase in free ribosomes as they were released from CPLs. Reduced levels and aberrant localisation of RNA pol II were also detected in *Padi6*$^{-/-}$ embryos. More recently, other members of the SCMC were identified as necessary for CPL formation (Kim et al., 2010; Tashiro et al., 2010). Ablation of *Mater* or *Padi6* resulted in a reduction in mRNA and protein synthesis in mouse embryos (Tong et al., 2000; Yurttas et al., 2008). The literature suggests that PADI6 functions in transcriptional regulation in the oocyte and early embryo, and that the role of PADI6 is associated with CPLs and the SCMC. To this end, it was important to investigate the transcriptome of *PADI6*^{KD} oocytes.

In an attempt to identify the regulatory networks of bovine *PADI6* function, targeted real-time PCR analysis and RNA-seq were performed following *PADI6* KD in comparison to control-injected MII oocytes. Oocytes with an average reduction in transcript levels for *PADI6* of 74±3.6% (0.03 ±0.004 arb. units, n = 20) following dsiRNA microinjection were generated in Chapter 4 alongside SCR-injected oocytes (0.12 ±0.014 arb. units, n = 10) and DB-injected oocytes (0.11 ±0.016 arb. units, n = 11). Bovine real-time PCR arrays were used to investigate markers of oocyte quality, and imprinted genes and epigenetic regulators in *PADI6*^{KD} oocytes. Genes were labelled as markers of oocyte quality because disruption to their expression negatively impacts the oocyte. Global changes to these genes would suggest a role for *PADI6* in oocyte maturation. On the other hand, changes to the expression of imprinted genes and epigenetic regulators would suggest a role for *PADI6* in imprinting regulation and developmental competence of the embryo.

The results from the oocyte quality marker array showed that of the 23 genes that were analysed, 2 were dysregulated in *PADI6*^{KD} oocytes: *PRDX1* and *ZP1*. The majority of transcripts were not affected by KD of *PADI6* which suggests that PADI6 does not play

a major functional role in the progression of oocyte maturation. *PRDX1* was not significantly changed between DB-injected and *PADI6*^{KD} oocytes. This suggests that the differences that were observed between SCR-injected and *PADI6*^{KD} oocytes might be an artefact of the microinjection methodology as opposed to a direct effect of *PADI6* KD. Alternatively, both *PRDX1* and *ZP1* were downregulated in *PADI6*^{KD} oocytes compared to control-injected oocytes. As discussed previously, this may be an effect of deadenylation of transcripts as an oligo-dT method was used for cDNA synthesis. In support of this, there was no differential expression of *PRDX1* or *ZP1* in the RNA-seq data. In conclusion, it seems that *PADI6* is not involved in oocyte maturation as the majority of genes that were analysed did not change from GV to MII transition following KD of *PADI6*.

On the other hand, analysis of imprinted genes and epigenetic regulators identified a number of significant alterations in gene expression. Initial screening of 35 genes in a subset of samples (n = 6-7 oocytes) identified upregulation of *DNMT3B* and *PRMT5* expression as well as SCMC member, *OOEP* expression in *PADI6*^{KD} oocytes compared to DB-injected oocytes. SCR-injected oocytes were not analysed due to limited amount of cDNA available for each single oocyte sample and the large number of genes that were analysed using the arrays. The samples that were included in this experiment were all generated from the same culture week. After analysing more samples (DB n = 11; SCR n = 10; KD n = 20), *DNMT3B, OOEP* and *PRMT5* were found not to be differentially expressed between *PADI6*^{KD} oocytes compared to control-injected oocytes. This suggests that the result was an effect of the culture conditions as it was not present upon the inclusion of additional samples from different culture weeks.

Finally, in depth real-time PCR analysis of oocytes with the greatest reduction in *PADI6* transcripts resulted in differential expression of 5 genes in *PADI6*^{KD} oocytes (n = 20) compared to control-injected oocytes (DB n = 11; SCR n = 10). *DNMT3A* and *DPPA3* were upregulated while *PLAGL1, TRIM28* and *ZFP57* were downregulated in *PADI6*^{KD} oocytes. These findings were interesting as DNMT3A, DPPA3, TRIM28 and ZFP57 are involved in regulating methylation of the genome, while *PLAGL1* is a maternally methylated gene. As stated in Chapter 5, DNMT3A is a *de novo* methylating enzyme that is essential for establishing methylation of the maternal genome during oocyte growth (Kaneda et al., 2010). DPPA3 is responsible for protecting maternal imprinted loci from active TET-mediated demethylation upon fertilisation (Nakamura et al., 2007). Similarly, TRIM28-ZFP57 protect imprinted loci from demethylation. ZFP57 binds to methylated DNA at a specific motif in differentially methylated regions (Quenneville et al., 2011).

TRIM28 recognises ZFP57 and recruits SETDB1 and DNMT1 to the DNA to promote heterochromatin formation (Denomme and Mann, 2013). Still, the puzzling question remains as to why KD of *PADI6* disrupted the expression of epigenetic regulators, *DNMT3A, DPPA3, TRIM28* and *ZFP57.* Considering the relationship between PADI6, the SCMC, and the documented human imprinting pathologies caused by disruption to SCMC genes, it may be that PADI6 and the SCMC work together to regulate epigenetic factors in the oocyte. Of all of the SCMC genes, *NLRP2* and *NLRP7* were downregulated following KD of *PADI6* (p=0.01 and 0.006, respectively).

Disruption to epigenetic regulators may explain the dysregulation of *PLAGL1* in *PADI6*^{KD} oocytes. *PLAGL1* is an imprinted gene that is maternally methylated during oocyte maturation. Described in mice, it is involved in controlling embryonic growth by regulating genes such as *Igf2/H19* locus (Varrault et al., 2006). Increased expression of *DNMT3A* in *PADI6*^{KD} oocytes may be responsible for methylation of the *PLAGL1* locus, resulting in its downregulation. *Trim28* is also thought to regulate methylation at the *Plagl1* locus in mice so the result may also be an effect of *TRIM28* dysregulation in *PADI6*^{KD} oocytes (Dalgaard et al., 2016). Despite the short period (24 hours) of dsiRNA treatment that was carried out in this thesis, it appears that *PADI6* KD affected the expression of epigenetic regulators which impacted the expression of imprinted gene, *PLAGL1*.

The RNA-seq results confirmed KD of *PADI6* gene expression and validated our experimental system for targeted gene KD by microinjection of siRNA species into bovine GV oocytes undergoing IVM. It also identified differential expression of a number of important oocyte and embryo genes. The FDR was too high to rule out false positive results. This may be due to variability in dsiRNA KD of *PADI6* as described in Section 7.2, or genetic variation between individual oocytes. Sequencing a greater number of oocytes may improve the FDR and produce some significant candidates for further study. Nevertheless, with the published knowledge that NOBOX regulates expression of *PADI6*, the discovery that *NOBOX* is downregulated following KD of *PADI6* presents an interesting finding indicative of a regulatory loop or negative feedback between the 2 genes. Other interesting candidates were *KRT5* and *8* – supposed components of CPLs. It is well understood that ablation of *PADI6* and other SCMC genes disrupts CPL formation therefore it is not surprising that KD of *PADI6* results in downregulation of CPL components (Kim et al., 2010; Tashiro et al., 2010; Wright et al., 2003). Finally, all of the DEGs in *PADI6*^{KD} oocytes had a functionally relevant role in the oocyte or embryo. Specifically, KD of *PADI6* appeared to disrupt a network of regulatory factors involved in translation termed the RNA damage pathway. Both ribosomal and mitochondrial

components were upregulated in response to *PADI6* KD. This supports previous studies that have shown disruption to ribosomes, RNA Pol II and mitochondria following loss of *Padi6* in mouse (Fernandes et al., 2012; Kan et al., 2012; Mehlmann et al., 1995; Yurttas et al., 2008). Mitochondria and the cytoskeleton are interlinked: mitochondrial activity is required for cytoskeletal reorganisation (Zeng, 2009) while redistribution of mitochondria by cytoskeletal components is required for meiotic maturation and embryo development (Kan et al., 2012). Similarly, distribution of ribosomes depends on the formation and maintenance of CPLs, which requires PADI6 (Wright et al., 2003; Yurttas et al., 2008). Further research is necessary to look at the impact of *PADI6* KD in bovine oocytes on CPLs to determine whether dysregulation of the RNA damage pathway occurs as a result of CPL disorganisation.

7.5 Production of recombinant human PADI6 protein using a bacterial expression system

Following the characterisation of *PADI6* gene expression in bovine, it was crucial to investigate changes in PADI6 protein expression. It is well understood that the relationship between mRNA and protein levels is not linear due to variations in stability and regulation of the transcript and protein, respectively (Liu et al., 2016). Similarly, dsiRNA KD of a transcript does not guarantee KD of the protein (Wu et al., 2004). Thus far, our data has shown that *PADI6* is an important MEG that is present during oocyte maturation and early embryo development but not transcribed after EGA. Furthermore, disruption to *PADI6* expression affects the transcript abundance of a variety of key genes in the oocyte. The question remains as to how PADI6 protein regulates the changes that have been observed here.

Attempts were made to create a recombinant human PADI6 protein that could be used as a tool for analysis of PADI6. Without the availability of a bovine antibody, a human PADI6 antibody was purchased instead. Together, it was hoped that these reagents would assist in the characterisation of PADI6 protein in the bovine. Unfortunately, the human antibody could not detect bovine PADI6 and there were issues with the bacterial expression system. The bacterial vector sequences were verified and the *PADI6* gene appeared to be inserted correctly into the open reading frame. Although there are many reasons as to why bacterial PADI6 expression failed, it was most likely caused by the use of an incorrect bacterial strain for protein expression. *E. coli* strains such as BL21 would have been more appropriate host expression systems. In the future, sequence-verified PADI6 expression vectors should be used to transform BL21 *E. coli* cells and the experiments for bacterial induction and protein production repeated to see if this solves the issue. Finally, with the advancement of proteomics, it will become easier to characterise bovine proteins without the use of antibodies. A number of proteomic studies in bovine oocytes have identified changes in MEGs such as PADI6, SCMC members, ZP proteins, DNMT1, TRIM28, and PRDX1 and PRDX2 during oocyte maturation (Chen et al., 2016; Memili et al., 2007; Peddinti et al., 2010). Further, analysis of MII oocytes compared to early stage embryos showed that KHDC3L protein expression significantly decreased after fertilisation, which is consistent with the characterisation of *KHDC3L* gene expression detailed in Chapter 3 (Deutsch et al., 2014). To conclude, such approaches in proteomics will enable vast expansion of our

knowledge of the oocyte proteome, and allow investigation into model organisms such as bovine, whose research was previously restricted by a lack of appropriate reagents.

7.6 Exploring the potential roles of PADI6 in bovine preimplantation development

In the literature, there are many facets to the potential function and regulation of PADI6. Firstly, there is much debate over its enzymatic activity. Esposito et al. (2007) claimed to detect a reduction in citrulline levels following ablation of *Padi6* in mouse oocytes, while Raijmakers et al. (2007) failed to show the catalysis of substrates by PADI6 during *in vitro* enzyme assays. Secondly, PADI family members (1-4) rely on calcium binding for their activation, but comparative analyses of AA sequences concluded that PADI6 cannot bind calcium (Arita et al., 2004; Raijmakers et al., 2007). This led other researchers to discover that PADI6 is phosphorylated during the GV to MII transition, suggesting that phosphorylation could be a novel mechanism for regulating PADI6 function (Rose et al., 2012; Snow et al., 2008). As the fifth member of the SCMC, PADI6 is likely to play a role in at least 1 of the many proposed functions of this multiprotein complex (Bebbere et al., 2016). Finally, with a clear relationship between PADI6, CPLs and the SCMC, further research is necessary to interrogate what PADI6 is really doing in the oocyte (Esposito et al., 2007; Kim et al., 2010; Wright et al., 2003).

7.6.1 Citrullination

Citrullination, and inhibition of citrullination by PAD inhibitor Cl-amidine, has been observed in mouse oocytes and embryos (Kan et al., 2012). PADI1 has been detected in mouse oocytes (Zhang et al., 2016) and PADI4 in oocytes from both mice and pigs (Brahmajosyula and Miyake, 2013). Both PADI1 and PADI4 are believed to function in histone citrullination. In this study, RNA-seq showed that *PADI1-4* were not expressed at the mRNA level in bovine MII oocytes. This could be due to the translation of *PADI* transcripts to protein for functioning in histone citrullination as observed in mice and pigs. However, analysis of additional RNA-seq data from our lab (Picton and Huntriss, unpublished) showed that *PADI1-4* were not present in bovine GV oocytes or early-staged follicles, suggesting that *PADI1-4* are not expressed at the mRNA or protein level in bovine oocytes. This suggests that *PADI6* is the prominent PADI family member and citrullinating enzyme in the bovine oocyte. To our knowledge, citrullination has not been characterised during bovine oocyte maturation and preimplantation embryo development

therefore it is not yet known if histone citrullination is present, as described in mice and pigs. As previously discussed, the citrullinating ability of PADI6 is under debate due to the loss of conserved calcium binding sites that facilitate its activity (Arita et al., 2004; Raijmakers et al., 2007). Snow et al. (2008) argued that this was potentially an advantageous evolutionary divergence away from requiring calcium as a cofactor in order to maintain tight regulation of citrullination in the oocyte and embryo. If PADI6 has citrullinating ability, it may be that it regulates gene expression by citrullinating histones at the promoters of genes, such as epigenetic regulators, in a similar way to PADI4 at the TFF1 promoter in MCF7 cells (Wang et al., 2004). However, investigation into the role of DEGs in citrullination and arginine metabolism revealed no effect on these pathways following KD of *PADI6* (Section 6.4.2). Moreover, PADI6 is unlikely to regulate the diverse number of factors identified by RNA-seq at the protein level by citrullination. In light of this and previous studies, it appears that PADI6 does not function as a deiminase in the bovine oocyte.

7.6.2 SCMC and epigenetics

The SCMC is a prominent complex in the oocyte that is essential for embryonic development (Li et al., 2008a; Zhu et al., 2015). In concordance with other species, SCMC genes are highly expressed in the bovine oocyte and preimplantation embryo prior to EGA. Despite the involvement of SCMC members in human imprinting pathologies, the role of the SCMC in epigenetic regulation of the oocyte and embryo is unclear (Begemann et al., 2018). From the literature and the findings in this thesis, it is likely that PADI6 constitutes a member of the SCMC (Wright et al., 2003) as downregulation of SCMC members *NLRP2* and *NLRP7* was observed following KD of *PADI6*. KD of *PADI6* also caused dysregulation of a subset of epigenetic regulators in the bovine oocyte. Euchromatic histone lysine methyltransferase 2 (*EHMT2*), histone deacetylase (*HDAC*) and lysine histone demethylase 1 A (*KDM1A*) transcripts were not directly affected by KD of *PADI6* (Figure 5.12) however they were identified by IPA as upstream regulators of affected transcripts. This suggest that PADI6, like NLRP2, might regulate the subcellular localisation of epigenetic factors in the oocyte (Bebbere et al., 2016; Mahadevan et al., 2017). Finally, SCMC-related imprinting condition, FBHM, is characterised by hyperproliferation of the trophoblast and extra-embryonic structures (Murdoch et al., 2006; Parry et al., 2011). RNA-seq identified increased levels of trophectoderm lineage regulators *GATA2/3* and *SOX2* in *PADI6*^{KD} oocytes, suggesting a mechanism of action for trophoblast proliferation in FBHM (Bai et al., 2013; Keramari

et al., 2010). Together, it is likely that PADI6 functions with the SCMC in epigenetic regulation and may provide a link between the SCMC and imprinting.

7.6.3 CPLs and storage of maternal components

Finally, it is understood that PADI6 is essential for the formation of CPLs which act as oocyte storage sites for ribosomal components and maternal transcripts (Bachvarova et al., 1981; Sternlicht and Schultz, 1981; Wright et al., 2003). PADI6 also localises RNA-masking protein, MSY2, to CPLs to potentially protect maternal transcripts from degradation (Liu, 2017). It is known that SCMC proteins NLRP5 and OOEP are also required for CPL formation (Kim et al., 2010; Tashiro et al., 2010) and that SCMC members KHDC3L and OOEP can bind to RNA (Pierre et al., 2007; Wang et al., 2012a). The RNA-seq data showing disruption to the RNA damage pathway in *PADI6*^{KD} oocytes further supports the idea that PADI6 is involved in regulation of translation in the oocyte. Increased abundance of ribosomal transcripts may occur as a direct result of loss of storage or as an indirect compensatory mechanism for translational dysregulation in the oocyte. Similarly, mitochondrial components may be upregulated to compensate for mislocalisation of mitochondria or to meet increased energy demands of the oocyte. In light of the large number and diverse nature of transcripts identified by RNA-seq, it is likely that PADI6 functions in translational regulation in the cytoplasm. Overall, this suggests that PADI6 and the SCMC might regulate maternal transcript storage and translation at CPLs in preparation for preimplantation embryo development.

7.7 Future studies

Based on the literature and the results presented in this thesis it is hypothesised that *PADI6* might play a role in the regulation of translation or storage of maternal transcripts in the oocyte in preparation for embryo development and EGA. During the GV to MII transition, it is hypothesised that *PADI6* regulates the storage of maternal transcripts and ribosomes at CPLs and the subcellular localisation of epigenetic factors (Figure 7.1). The actions of PADI6 and the SCMC seem to have an important effect on imprinting and translational regulation. It will be necessary to investigate this hypothesis and further characterise PADI6 using a variety of experimental means.

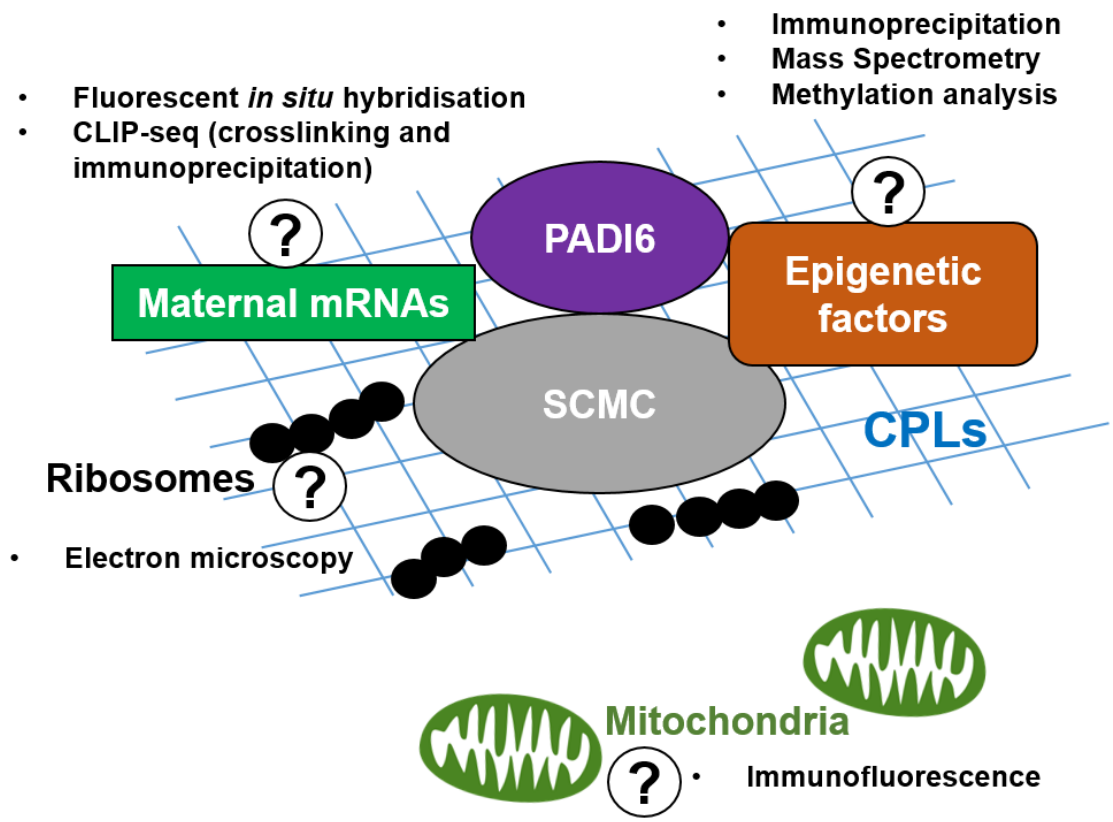

Figure 7.1. Proposed roles for PADI6 and the SCMC in storing maternal transcripts and ribosomes and sequestering epigenetic factors at CPLs. The question marks (?) highlight that further investigations are necessary to determine the relationships and mechanisms through which PADI6 functions and experiments to address such questions are listed.

DsiRNA microinjection proved a useful tool for RNAi of *PADI6* transcripts in bovine oocytes, however variability in knockdown efficiency resulted in insignificant FDR of DEGs following RNA-seq. This also showed that intergenic variation is a limitation of grouping single-cell data in bioinformatic analyses. Although the sample size was smaller, RNA-seq failed to identify the same candidate genes as targeted qPCR analysis, which may highlight the significance of power in a dataset. The bovine oocyte is a good tool for research due to its large size, relative ease of availability and physiological relevance to humans; however, there is a deficit for commercially available bovine-specific reagents. A major limitation to this study was the unavailability of a bovine PADI6 antibody and/or bovine recombinant PADI6 protein. Consequently, the dsiRNA KD of *PADI6* that was achieved could not be verified at the protein level as the human antibody was unable to detect the bovine protein. Not only would a bovine antibody enable the characterisation of PADI6 protein through preimplantation development, it would also open the door to a multitude of other exciting experiments (Figure 7.1). Combined with electron microscopy, a bovine PADI6 antibody could be used to investigate the localisation and movements of PADI6 in relation to CPLs, ribosomes, mitochondria and the meiotic spindle during oocyte maturation and early embryo development. Furthermore, it could be used in immunoprecipitation (IP) experiments to look at the interactions between PADI6 and the SCMC, as well as crosslinking and immunoprecipitation followed by RNA sequencing (CLIP-seq) experiments to investigate potential binding of the SCMC to maternal transcripts such as RNA damage components. Candidate mRNAs could then be visualised using fluorescent *in situ* hybridisation (FISH) to validate localisation with PADI6 and CPLs. In addition, mass spectrometry following IP would reveal both direct and indirect interactors of PADI6 and may shed light on the role of the SCMC in epigenetic regulation in the bovine oocyte. Analysis of the methylation status of genes, including *PLAGL1,* after *PADI6* KD would be necessary to assess the impact of dysregulation of epigenetic factors on the expression of imprinted genes in the oocyte. Moreover, integration of transcriptomic and epigenetic data would facilitate deeper understanding of the role of *PADI6* in oocyte maturation. Further investigation into the expression of other *PADI* family members is also necessary to understand whether there is a compensatory relationship between genes in the bovine oocyte. With this, it would be interesting to analyse changes in citrullination after *PADI6* KD in the bovine oocyte using anti-citrulline antibodies. Finally, this thesis focussed mainly on bovine oocyte maturation, however legacy effects of *PADI6* KD in the oocyte might be expected in the embryo. It would be useful to repeat experiments in the early preimplantation embryo and to look at the impact of *PADI6* KD on EGA.

7.8 Conclusion

Overall, the results of this thesis support the hypothesis that *PADI6* plays a functional role in translational regulation during oocyte maturation in the bovine species. It is unlikely that this function occurs through citrullination given the literature and pathway analysis conducted in Chapter 5. The significant dysregulation of translational machinery and resultant changes in gene expression networks are in accordance with previous studies and the relationship between *PADI6* and CPLs. Moreover, it is possible that *PADI6* supports the SCMC in its role in epigenetic regulation due to the documented associations of SCMC members and imprinting disorders. Further investigations are necessary to determine its mechanism of action. The characterisation of mRNA expression of key MEGs will inform future studies into the role of the SCMC in bovine preimplantation development. The dsiRNA microinjection system that was validated in this thesis offers a suitable tool for the discovery of novel gene functions that might play an important role in preimplantation development. Further, by combining dsiRNA KD of *PADI6* in bovine oocytes and single oocyte RNA-seq, a number of DEGs were identified that will influence investigation into the mechanism of action of *PADI6* and provide potential candidate genes in future studies.

References

AALTONEN, J., LAITINEN, M. P., VUOJOLAINEN, K., JAATINEN, R., HORELLI-KUITUNEN, N., SEPPA, L., LOUHIO, H., TUURI, T., SJOBERG, J., BUTZOW, R., HOVATA, O., DALE, L. & RITVOS, O. 1999. Human growth differentiation factor 9 (GDF-9) and its novel homolog GDF-9B are expressed in oocytes during early folliculogenesis. *J Clin Endocrinol Metab,* 84**,** 2744-50.

ABE, K., YAMAMOTO, R., FRANKE, V., CAO, M., SUZUKI, Y., SUZUKI, M. G., VLAHOVICEK, K., SVOBODA, P., SCHULTZ, R. M. & AOKI, F. 2015. The first murine zygotic transcription is promiscuous and uncoupled from splicing and 3' processing. *EMBO J,* 34**,** 1523-37.

ABE, K. I., FUNAYA, S., TSUKIOKA, D., KAWAMURA, M., SUZUKI, Y., SUZUKI, M. G., SCHULTZ, R. M. & AOKI, F. 2018. Minor zygotic gene activation is essential for mouse preimplantation development. *Proc Natl Acad Sci U S A,* 115**,** E6780-E6788.

ABRAMOWITZ, L. K. & BARTOLOMEI, M. S. 2012. Genomic imprinting: recognition and marking of imprinted loci. *Curr Opin Genet Dev,* 22**,** 72-8.

ADAMS, G. P. & PIERSON, R. A. 1995. Bovine Model for Study of Ovarian Follicular Dynamics in Humans. *Theriogenology,* 43**,** 113-120.

ADAMS, G. P., SINGH, J. & BAERWALD, A. R. 2012. Large animal models for the study of ovarian follicular dynamics in women. *Theriogenology,* 78**,** 1733-48.

ADENOT, P. G., MERCIER, Y., RENARD, J. P. & THOMPSON, E. M. 1997. Differential H4 acetylation of paternal and maternal chromatin precedes DNA replication and differential transcriptional activity in pronuclei of 1-cell mouse embryos. *Development,* 124**,** 4615-25.

AJDUK, A., MALAGOCKI, A. & MALESZEWSKI, M. 2008. Cytoplasmic maturation of mammalian oocytes: development of a mechanism responsible for sperm-induced Ca2+ oscillations. *Reprod Biol,* 8**,** 3-22.

AKINTAYO, A. & STANLEY, P. 2019. Roles for Golgi Glycans in Oogenesis and Spermatogenesis. *Front Cell Dev Biol,* 7**,** 98.

AKOURY, E., ZHANG, L., AO, A. & SLIM, R. 2015. NLRP7 and KHDC3L, the two maternal-effect proteins responsible for recurrent hydatidiform moles, co-localize to the oocyte cytoskeleton. *Hum Reprod,* 30**,** 159-69.

AL-ZUBAIDI, U., LIU, J., CINAR, O., ROBKER, R. L., ADHIKARI, D. & CARROLL, J. 2019. The spatio-temporal dynamics of mitochondrial membrane potential during oocyte maturation. *Mol Hum Reprod,* 25**,** 695-705.

ALAK, B. M., COSKUN, S., FRIEDMAN, C. I., KENNARD, E. A., KIM, M. H. & SEIFER, D. B. 1998. Activin A stimulates meiotic maturation of human oocytes and modulates granulosa cell steroidogenesis in vitro. *Fertil Steril,* 70**,** 1126-30.

ALARCON, C. R., LEE, H., GOODARZI, H., HALBERG, N. & TAVAZOIE, S. F. 2015. N6-methyladenosine marks primary microRNAs for processing. *Nature,* 519**,** 482-5.

ALAZAMI, A. M., AWAD, S. M., COSKUN, S., AL-HASSAN, S., HIJAZI, H., ABDULWAHAB, F. M., POIZAT, C. & ALKURAYA, F. S. 2015. TLE6 mutation causes the earliest known human embryonic lethality. *Genome Biol,* 16**,** 240.

ALBERTINI, D. F. 1992. Cytoplasmic microtubular dynamics and chromatin organization during mammalian oogenesis and oocyte maturation. *Mutat Res,* 296**,** 57-68.

ALEXANDER, K. A., WANG, X., SHIBATA, M., CLARK, A. G. & GARCIA-GARCIA, M. J. 2015. TRIM28 Controls Genomic Imprinting through Distinct Mechanisms during and after Early Genome-wide Reprogramming. *Cell Rep,* 13**,** 1194-1205.

ALLEGRUCCI, C., THURSTON, A., LUCAS, E. & YOUNG, L. 2005. Epigenetics and the germline. *Reproduction,* 129**,** 137-49.

ALLEN, J. J., HERRICK, S. L. & FORTUNE, J. E. 2016. Regulation of steroidogenesis in fetal bovine ovaries: differential effects of LH and FSH. *J Mol Endocrinol,* 57**,** 275-286.

AMDANI, S. N., YESTE, M., JONES, C. & COWARD, K. 2015. Sperm Factors and Oocyte Activation: Current Controversies and Considerations. *Biol Reprod,* 93**,** 50.

AMOUSHAHI, M., SUNDE, L. & LYKKE-HARTMANN, K. 2019. The pivotal roles of the NOD-like receptors with a PYD domain, NLRPs, in oocytes and early embryo development. *Biol Reprod*.

ANCELIN, K., LANGE, U. C., HAJKOVA, P., SCHNEIDER, R., BANNISTER, A. J., KOUZARIDES, T. & SURANI, M. A. 2006. Blimp1 associates with Prmt5 and directs histone arginine methylation in mouse germ cells. *Nat Cell Biol,* 8**,** 623-30.

ANDERSON, E. & ALBERTINI, D. F. 1976. Gap junctions between the oocyte and companion follicle cells in the mammalian ovary. *J Cell Biol,* 71**,** 680-6.

ANDERSON, R. A., BAYNE, R. A., GARDNER, J. & DE SOUSA, P. A. 2010. Brain-derived neurotrophic factor is a regulator of human oocyte maturation and early embryo development. *Fertil Steril,* 93**,** 1394-406.

ANDREWS, P. W., DAMJANOV, I., SIMON, D., BANTING, G. S., CARLIN, C., DRACOPOLI, N. C. & FOGH, J. 1984. Pluripotent embryonal carcinoma clones derived from the human teratocarcinoma cell line Tera-2. Differentiation in vivo and in vitro. *Lab Invest,* 50**,** 147-62.

AOKI, Y. 1997. [Analysis of IL-8 gene transcription in human bronchial epithelial cells by stable transfection of a reporter gene]. *Nihon Kyobu Shikkan Gakkai Zasshi,* 35**,** 602-8.

AOSHIMA, K., INOUE, E., SAWA, H. & OKADA, Y. 2015. Paternal H3K4 methylation is required for minor zygotic gene activation and early mouse embryonic development. *EMBO Rep,* 16**,** 803-12.

ARAMAKI, S., HAYASHI, K., KURIMOTO, K., OHTA, H., YABUTA, Y., IWANARI, H., MOCHIZUKI, Y., HAMAKUBO, T., KATO, Y., SHIRAHIGE, K. & SAITOU, M. 2013. A mesodermal factor, T, specifies mouse germ cell fate by directly activating germline determinants. *Dev Cell,* 27**,** 516-29.

ARDEKANI, A. M. & NAEINI, M. M. 2010. The Role of MicroRNAs in Human Diseases. *Avicenna J Med Biotechnol,* 2**,** 161-79.

ARITA, K., HASHIMOTO, H., SHIMIZU, T., NAKASHIMA, K., YAMADA, M. & SATO, M. 2004. Structural basis for Ca(2+)-induced activation of human PAD4. *Nat Struct Mol Biol,* 11**,** 777-83.

ASAGA, H., NAKASHIMA, K., SENSHU, T., ISHIGAMI, A. & YAMADA, M. 2001. Immunocytochemical localization of peptidylarginine deiminase in human eosinophils and neutrophils. *J Leukoc Biol,* 70**,** 46-51.

AVELLA, M. A., XIONG, B. & DEAN, J. 2013. The molecular basis of gamete recognition in mice and humans. *Mol Hum Reprod,* 19**,** 279-89.

BACHVAROVA, R., DE LEON, V. & SPIEGELMAN, I. 1981. Mouse egg ribosomes: evidence for storage in lattices. *J Embryol Exp Morphol,* 62**,** 153-64.

BAERWALD, A. R., ADAMS, G. P. & PIERSON, R. A. 2003a. Characterization of ovarian follicular wave dynamics in women. *Biology of Reproduction,* 69**,** 1023-1031.

BAERWALD, A. R., ADAMS, G. P. & PIERSON, R. A. 2003b. A new model for ovarian follicular development during the human menstrual cycle. *Fertility and Sterility,* 80**,** 116-122.

BAERWALD, A. R., ADAMS, G. P. & PIERSON, R. A. 2012. Ovarian antral folliculogenesis during the human menstrual cycle: a review. *Hum Reprod Update,* 18**,** 73-91.

BAI, H., SAKURAI, T., GODKIN, J. D. & IMAKAWA, K. 2013. Expression and potential role of GATA factors in trophoblast development. *J Reprod Dev,* 59**,** 1-6.

BAIRD, D. T. & MCNEILLY, A. S. 1981. Gonadotrophic control of follicular development and function during the oestrous cycle of the ewe. *J Reprod Fertil Suppl,* 30**,** 119-33.

BAKER, T. G. & FRANCHI, L. L. 1967. The fine structure of oogonia and oocytes in human ovaries. *J Cell Sci,* 2**,** 213-24.

BAKHTARI, A. & ROSS, P. J. 2014. DPPA3 prevents cytosine hydroxymethylation of the maternal pronucleus and is required for normal development in bovine embryos. *Epigenetics,* 9**,** 1271-9.

BALTUS, A. E., MENKE, D. B., HU, Y. C., GOODHEART, M. L., CARPENTER, A. E., DE ROOIJ, D. G. & PAGE, D. C. 2006. In germ cells of mouse embryonic ovaries, the decision to enter meiosis precedes premeiotic DNA replication. *Nat Genet,* 38**,** 1430-4.

BANNISTER, A. J. & KOUZARIDES, T. 2011. Regulation of chromatin by histone modifications. *Cell Res,* 21**,** 381-95.

BARIBAULT, H., PRICE, J., MIYAI, K. & OSHIMA, R. G. 1993. Mid-gestational lethality in mice lacking keratin 8. *Genes Dev,* 7**,** 1191-202.

BARLOW, D. P., STOGER, R., HERRMANN, B. G., SAITO, K. & SCHWEIFER, N. 1991. The mouse insulin-like growth factor type-2 receptor is imprinted and closely linked to the Tme locus. *Nature,* 349**,** 84-7.

BARRETT, S. L. & ALBERTINI, D. F. 2010. Cumulus cell contact during oocyte maturation in mice regulates meiotic spindle positioning and enhances developmental competence. *J Assist Reprod Genet,* 27**,** 29-39.

BARTOLOMEI, M. S. & FERGUSON-SMITH, A. C. 2011. Mammalian genomic imprinting. *Cold Spring Harb Perspect Biol,* 3.

BARTON, S. C., SURANI, M. A. & NORRIS, M. L. 1984. Role of paternal and maternal genomes in mouse development. *Nature,* 311**,** 374-6.

BASTEPE, M., FROHLICH, L. F., LINGLART, A., ABU-ZAHRA, H. S., TOJO, K., WARD, L. M. & JUPPNER, H. 2005. Deletion of the NESP55 differentially methylated region causes loss of maternal GNAS imprints and pseudohypoparathyroidism type Ib. *Nat Genet,* 37**,** 25-7.

BAULCOMBE, D. C. 1996. RNA as a target and an initiator of post-transcriptional gene silencing in transgenic plants. *Plant Mol Biol,* 32**,** 79-88.

BEBBERE, D., ARIU, F., BOGLIOLO, L., MASALA, L., MURRONE, O., FATTORINI, M., FALCHI, L. & LEDDA, S. 2014. Expression of maternally derived KHDC3, NLRP5, OOEP and TLE6 is associated with oocyte developmental competence in the ovine species. *BMC Dev Biol,* 14**,** 40.

BEBBERE, D., MASALA, L., ALBERTINI, D. F. & LEDDA, S. 2016. The subcortical maternal complex: multiple functions for one biological structure? *Journal of Assisted Reproduction and Genetics,* 33**,** 1431-1438.

BEG, M. A. & GINTHER, O. J. 2006. Follicle selection in cattle and horses: role of intrafollicular factors. *Reproduction,* 132**,** 365-77.

BEGEMANN, M., REZWAN, F. I., BEYGO, J., DOCHERTY, L. E., KOLAROVA, J., SCHROEDER, C., BUITING, K., CHOKKALINGAM, K., DEGENHARDT, F., WAKELING, E. L., KLEINLE, S., GONZALEZ FASSRAINER, D., OEHL-JASCHKOWITZ, B., TURNER, C. L. S., PATALAN, M., GIZEWSKA, M., BINDER, G., BICH NGOC, C. T., CHI DUNG, V., MEHTA, S. G., BAYNAM, G., HAMILTON-SHIELD, J. P., ALJAREH, S., LOKULO-SODIPE, O., HORTON, R., SIEBERT, R., ELBRACHT, M., TEMPLE, I. K., EGGERMANN, T. & MACKAY, D. J. G. 2018. Maternal variants in NLRP and other maternal effect proteins are associated with multilocus imprinting disturbance in offspring. *J Med Genet,* 55**,** 497-504.

BELL, A. C. & FELSENFELD, G. 2000. Methylation of a CTCF-dependent boundary controls imprinted expression of the Igf2 gene. *Nature,* 405**,** 482-5.

BERENYI, E. 2019. *Function of the oocyte specific imprinting regulator OOEP in bovine oocytes and embryos.* PhD, University of Leeds.

BERG, D. K., SMITH, C. S., PEARTON, D. J., WELLS, D. N., BROADHURST, R., DONNISON, M. & PFEFFER, P. L. 2011. Trophectoderm lineage determination in cattle. *Dev Cell,* 20**,** 244-55.

BERNSTEIN, B. W. & BAMBURG, J. R. 2010. ADF/cofilin: a functional node in cell biology. *Trends Cell Biol,* 20**,** 187-95.

BERNSTEIN, E., CAUDY, A. A., HAMMOND, S. M. & HANNON, G. J. 2001. Role for a bidentate ribonuclease in the initiation step of RNA interference. *Nature,* 409**,** 363-6.

BETTEGOWDA, A., LEE, K. B. & SMITH, G. W. 2008. Cytoplasmic and nuclear determinants of the maternal-to-embryonic transition. *Reprod Fertil Dev,* 20**,** 45-53.

BETTEGOWDA, A., YAO, J., SEN, A., LI, Q., LEE, K. B., KOBAYASHI, Y., PATEL, O. V., COUSSENS, P. M., IRELAND, J. J. & SMITH, G. W. 2007. JY-1, an oocyte-specific gene, regulates granulosa cell function and early embryonic development in cattle. *Proc Natl Acad Sci U S A,* 104**,** 17602-7.

BIAN, C. & YU, X. 2014. PGC7 suppresses TET3 for protecting DNA methylation. *Nucleic Acids Res,* 42**,** 2893-905.

BIANCHI, E., DOE, B., GOULDING, D. & WRIGHT, G. J. 2014. Juno is the egg Izumo receptor and is essential for mammalian fertilization. *Nature,* 508**,** 483-7.

BICKER, K. L. & THOMPSON, P. R. 2013. The protein arginine deiminases: Structure, function, inhibition, and disease. *Biopolymers,* 99**,** 155-63.

BIECHELE, S., LIN, C. J., RINAUDO, P. F. & RAMALHO-SANTOS, M. 2015. Unwind and transcribe: chromatin reprogramming in the early mammalian embryo. *Curr Opin Genet Dev,* 34**,** 17-23.

BIERKAMP, C., LUXEY, M., METCHAT, A., AUDOUARD, C., DUMOLLARD, R. & CHRISTIANS, E. 2010. Lack of maternal Heat Shock Factor 1 results in multiple cellular and developmental defects, including mitochondrial damage and altered redox homeostasis, and leads to reduced survival of mammalian oocytes and embryos. *Dev Biol,* 339**,** 338-53.

BINELLI, M. & MURPHY, B. D. 2010. Coordinated regulation of follicle development by germ and somatic cells. *Reprod Fertil Dev,* 22**,** 1-12.

BIRD, A. 2002. DNA methylation patterns and epigenetic memory. *Genes Dev,* 16**,** 6-21.

BLEIL, J. D., BEALL, C. F. & WASSARMAN, P. M. 1981. Mammalian sperm-egg interaction: fertilization of mouse eggs triggers modification of the major zona pellucida glycoprotein, ZP2. *Dev Biol,* 86**,** 189-97.

BOERKE, A., DIELEMAN, S. J. & GADELLA, B. M. 2007. A possible role for sperm RNA in early embryo development. *Theriogenology,* 68 Suppl 1**,** S147-55.

BOGLIOTTI, Y. S., CHUNG, N., PAULSON, E., CHITWOOD, J., HALSTEAD, M., KERN, C., SCHULTZ, R. M. & ROSS, P. J. 2019. Transcript profiling of bovine embryos implicates specific transcription factors in the maternal-to-embryo transition. *Biol Reprod*.

BOGLIOTTI, Y. S. & ROSS, P. J. 2015. Molecular mechanisms of transcriptional and chromatin remodeling around embryonic genome activation. *Animal Reproduction,* 12**,** 52-61.

BONNET, A., DALBIES-TRAN, R. & SIRARD, M. A. 2008. Opportunities and challenges in applying genomics to the study of oogenesis and follicullogenesis in farm animals. *Reproduction,* 135**,** 119-128.

BORENFREUND, E. & BORRERO, O. 1984. In vitro cytotoxicity assays. Potential alternatives to the Draize ocular allergy test. *Cell Biol Toxicol,* 1**,** 55-65.

BORREGAARD, N. 2010. Neutrophils, from marrow to microbes. *Immunity,* 33**,** 657-70.

BOSTICK, M., KIM, J. K., ESTEVE, P. O., CLARK, A., PRADHAN, S. & JACOBSEN, S. E. 2007. UHRF1 plays a role in maintaining DNA methylation in mammalian cells. *Science,* 317**,** 1760-4.

BRAHMAJOSYULA, M. & MIYAKE, M. 2013. Localization and expression of peptidylarginine deiminase 4 (PAD4) in mammalian oocytes and preimplantation embryos. *Zygote,* 21**,** 314-24.
BRAIDOTTI, G., BAUBEC, T., PAULER, F., SEIDL, C., SMRZKA, O., STRICKER, S., YOTOVA, I. & BARLOW, D. P. 2004. The Air noncoding RNA: an imprinted cis-silencing transcript. *Cold Spring Harb Symp Quant Biol,* 69**,** 55-66.
BRANCO, M. R., ODA, M. & REIK, W. 2008. Safeguarding parental identity: Dnmt1 maintains imprints during epigenetic reprogramming in early embryogenesis. *Genes Dev,* 22**,** 1567-71.
BRANKIN, V., QUINN, R. L., WEBB, R. & HUNTER, M. G. 2005. Evidence for a functional bone morphogenetic protein (BMP) system in the porcine ovary. *Domest Anim Endocrinol,* 28**,** 367-79.
BRAUDE, P., BOLTON, V. & MOORE, S. 1988. Human gene expression first occurs between the four- and eight-cell stages of preimplantation development. *Nature,* 332**,** 459-61.
BRUNET, S. & VERLHAC, M. H. 2011. Positioning to get out of meiosis: the asymmetry of division. *Hum Reprod Update,* 17**,** 68-75.
BULTMAN, S. J., GEBUHR, T. C., PAN, H., SVOBODA, P., SCHULTZ, R. M. & MAGNUSON, T. 2006. Maternal BRG1 regulates zygotic genome activation in the mouse. *Genes Dev,* 20**,** 1744-54.
BURKART, A. D., XIONG, B., BAIBAKOV, B., JIMENEZ-MOVILLA, M. & DEAN, J. 2012. Ovastacin, a cortical granule protease, cleaves ZP2 in the zona pellucida to prevent polyspermy. *J Cell Biol,* 197**,** 37-44.
BURKHOLDER, G. D., COMINGS, D. E. & OKADA, T. A. 1971. A storage form of ribosomes in mouse oocytes. *Exp Cell Res,* 69**,** 361-71.
BUSCA, R., POUYSSEGUR, J. & LENORMAND, P. 2016. ERK1 and ERK2 Map Kinases: Specific Roles or Functional Redundancy? *Front Cell Dev Biol,* 4**,** 53.
BYSKOV, A. G., YDING ANDERSEN, C., HOSSAINI, A. & GUOLIANG, X. 1997. Cumulus cells of oocyte-cumulus complexes secrete a meiosis-activating substance when stimulated with FSH. *Mol Reprod Dev,* 46**,** 296-305.
CAGNONE, G. L., DUFORT, I., VIGNEAULT, C. & SIRARD, M. A. 2012. Differential gene expression profile in bovine blastocysts resulting from hyperglycemia exposure during early cleavage stages. *Biol Reprod,* 86**,** 50.
CAMMAS, F., MARK, M., DOLLE, P., DIERICH, A., CHAMBON, P. & LOSSON, R. 2000. Mice lacking the transcriptional corepressor TIF1beta are defective in early postimplantation development. *Development,* 127**,** 2955-63.
CAMPBELL, B. K., SCARAMUZZI, R. J. & WEBB, R. 1995. Control of antral follicle development and selection in sheep and cattle. *J Reprod Fertil Suppl,* 49**,** 335-50.
CAMPBELL, B. K., SCARAMUZZI, R. J. & WEBB, R. 1996. Induction and maintenance of oestradiol and immunoreactive inhibin production with FSH by ovine granulosa cells cultured in serum-free media. *J Reprod Fertil,* 106**,** 7-16.
CANOVAS, S. & ROSS, P. J. 2016. Epigenetics in preimplantation mammalian development. *Theriogenology,* 86**,** 69-79.
CAPCO, D. G., GALLICANO, G. I., MCGAUGHEY, R. W., DOWNING, K. H. & LARABELL, C. A. 1993. Cytoskeletal sheets of mammalian eggs and embryos: a lattice-like network of intermediate filaments. *Cell Motil Cytoskeleton,* 24**,** 85-99.
CAPCO, D. G. & MCGAUGHEY, R. W. 1986. Cytoskeletal reorganization during early mammalian development: analysis using embedment-free sections. *Dev Biol,* 115**,** 446-58.
CARBALLADA, R., DEGEFA, T. & ESPONDA, P. 2000. Transfection of mouse eggs and embryos using DNA combined to cationic liposomes. *Mol Reprod Dev,* 56**,** 360-5.

CARLETTI, M. Z., FIEDLER, S. D. & CHRISTENSON, L. K. 2010. MicroRNA 21 blocks apoptosis in mouse periovulatory granulosa cells. *Biol Reprod,* 83**,** 286-95.

CARLONE, D. L. & SKALNIK, D. G. 2001. CpG binding protein is crucial for early embryonic development. *Mol Cell Biol,* 21**,** 7601-6.

CARLSON, L. L., PAGE, A. W. & BESTOR, T. H. 1992. Properties and localization of DNA methyltransferase in preimplantation mouse embryos: implications for genomic imprinting. *Genes Dev,* 6**,** 2536-41.

CARRINGTON, J. C. & AMBROS, V. 2003. Role of microRNAs in plant and animal development. *Science,* 301**,** 336-8.

CASTORENA-TORRES, F., PENUELAS-URQUIDES, K. & DE LEON, M. B. 2016. Site-Directed Mutagenesis by Polymerase Chain Reaction. *Polymerase Chain Reaction for Biomedical Applications***,** 159-173.

CERMELLI, S., GUO, Y., GROSS, S. P. & WELTE, M. A. 2006. The lipid-droplet proteome reveals that droplets are a protein-storage depot. *Curr Biol,* 16**,** 1783-95.

CETICA, P., PINTOS, L., DALVIT, G. & BECONI, M. 2003. Involvement of enzymes of amino acid metabolism and tricarboxylic acid cycle in bovine oocyte maturation in vitro. *Reproduction,* 126**,** 753-63.

CHALBI, M., BARRAUD-LANGE, V., RAVAUX, B., HOWAN, K., RODRIGUEZ, N., SOULE, P., NDZOUDI, A., BOUCHEIX, C., RUBINSTEIN, E., WOLF, J. P., ZIYYAT, A., PEREZ, E., PINCET, F. & GOURIER, C. 2014. Binding of sperm protein Izumo1 and its egg receptor Juno drives Cd9 accumulation in the intercellular contact area prior to fusion during mammalian fertilization. *Development,* 141**,** 3732-9.

CHAMBERS, E. L., GOSDEN, R. G., YAP, C. & PICTON, H. M. 2010. In situ identification of follicles in ovarian cortex as a tool for quantifying follicle density, viability and developmental potential in strategies to preserve female fertility. *Hum Reprod,* 25**,** 2559-68.

CHANNING, C. P. 1980. Progesterone and estrogen secretion by cultured monkey ovarian cell types: influences of follicular size, serum luteinizing hormone levels, and follicular fluid estrogen levels. *Endocrinology,* 107**,** 342-52.

CHAVANAS, S., MECHIN, M. C., TAKAHARA, H., KAWADA, A., NACHAT, R., SERRE, G. & SIMON, M. 2004. Comparative analysis of the mouse and human peptidylarginine deiminase gene clusters reveals highly conserved non-coding segments and a new human gene, PADI6. *Gene,* 330**,** 19-27.

CHAZAUD, C., YAMANAKA, Y., PAWSON, T. & ROSSANT, J. 2006. Early lineage segregation between epiblast and primitive endoderm in mouse blastocysts through the Grb2-MAPK pathway. *Dev Cell,* 10**,** 615-24.

CHEGINI, N. & FLANDERS, K. C. 1992. Presence of transforming growth factor-beta and their selective cellular localization in human ovarian tissue of various reproductive stages. *Endocrinology,* 130**,** 1707-15.

CHEN, L., RUSSELL, P. T. & LARSEN, W. J. 1993. Functional-Significance of Cumulus Expansion in the Mouse - Roles for the Preovulatory Synthesis of Hyaluronic-Acid within the Cumulus Mass. *Molecular Reproduction and Development,* 34**,** 87-93.

CHEN, L., ZHAI, L., QU, C., ZHANG, C., LI, S., WU, F., QI, Y., LU, F., XU, P., LI, X. & SHI, D. 2016. Comparative Proteomic Analysis of Buffalo Oocytes Matured in vitro Using iTRAQ Technique. *Sci Rep,* 6**,** 31795.

CHENG, H., ZHANG, J., ZHANG, S., ZHAI, Y., JIANG, Y., AN, X., MA, X., ZHANG, X., LI, Z. & TANG, B. 2019. Tet3 is required for normal in vitro fertilization preimplantation embryos development of bovine. *Mol Reprod Dev,* 86**,** 298-307.

CHERRINGTON, B. D., MORENCY, E., STRUBLE, A. M., COONROD, S. A. & WAKSHLAG, J. J. 2010. Potential role for peptidylarginine deiminase 2 (PAD2) in citrullination of canine mammary epithelial cell histones. *PLoS One,* 5**,** e11768.

CHEW, T. G., LORTHONGPANICH, C., ANG, W. X., KNOWLES, B. B. & SOLTER, D. 2012. Symmetric cell division of the mouse zygote requires an actin network. *Cytoskeleton (Hoboken),* 69**,** 1040-6.
CHIQUOINE, A. D. 1954. The identification, origin, and migration of the primordial germ cells in the mouse embryo. *Anat Rec,* 118**,** 135-46.
CHITWOOD, J. L., RINCON, G., KAISER, G. G., MEDRANO, J. F. & ROSS, P. J. 2013. RNA-seq analysis of single bovine blastocysts. *BMC Genomics,* 14**,** 350.
CHOI, M., LEE, O. H., JEON, S., PARK, M., LEE, D. R., KO, J. J., YOON, T. K., RAJKOVIC, A. & CHOI, Y. 2010. The oocyte-specific transcription factor, Nobox, regulates the expression of Pad6, a peptidylarginine deiminase in the oocyte. *Febs Letters,* 584**,** 3629-34.
CHOI, Y., BALLOW, D. J., XIN, Y. & RAJKOVIC, A. 2008a. Lim homeobox gene, lhx8, is essential for mouse oocyte differentiation and survival. *Biol Reprod,* 79**,** 442-9.
CHOI, Y., GEHRING, M., JOHNSON, L., HANNON, M., HARADA, J. J., GOLDBERG, R. B., JACOBSEN, S. E. & FISCHER, R. L. 2002. DEMETER, a DNA glycosylase domain protein, is required for endosperm gene imprinting and seed viability in arabidopsis. *Cell,* 110**,** 33-42.
CHOI, Y., QIN, Y., BERGER, M. F., BALLOW, D. J., BULYK, M. L. & RAJKOVIC, A. 2007. Microarray analyses of newborn mouse ovaries lacking Nobox. *Biol Reprod,* 77**,** 312-9.
CHOI, Y. & RAJKOVIC, A. 2006a. Characterization of NOBOX DNA binding specificity and its regulation of Gdf9 and Pou5f1 promoters. *J Biol Chem,* 281**,** 35747-56.
CHOI, Y. & RAJKOVIC, A. 2006b. Genetics of early mammalian folliculogenesis. *Cell Mol Life Sci,* 63**,** 579-90.
CHOI, Y., YUAN, D. & RAJKOVIC, A. 2008b. Germ cell-specific transcriptional regulator sohlh2 is essential for early mouse folliculogenesis and oocyte-specific gene expression. *Biol Reprod,* 79**,** 1176-82.
CHOTALIA, M., SMALLWOOD, S. A., RUF, N., DAWSON, C., LUCIFERO, D., FRONTERA, M., JAMES, K., DEAN, W. & KELSEY, G. 2009. Transcription is required for establishment of germline methylation marks at imprinted genes. *Genes Dev,* 23**,** 105-17.
CHRISTIANS, E., BOIANI, M., GARAGNA, S., DESSY, C., REDI, C. A., RENARD, J. P. & ZUCCOTTI, M. 1999. Gene expression and chromatin organization during mouse oocyte growth. *Dev Biol,* 207**,** 76-85.
CHRISTIANS, E., CAMPION, E., THOMPSON, E. M. & RENARD, J. P. 1995. Expression of the HSP 70.1 gene, a landmark of early zygotic activity in the mouse embryo, is restricted to the first burst of transcription. *Development,* 121**,** 113-22.
CHRISTOPHOROU, M. A., CASTELO-BRANCO, G., HALLEY-STOTT, R. P., OLIVEIRA, C. S., LOOS, R., RADZISHEUSKAYA, A., MOWEN, K. A., BERTONE, P., SILVA, J. C., ZERNICKA-GOETZ, M., NIELSEN, M. L., GURDON, J. B. & KOUZARIDES, T. 2014. Citrullination regulates pluripotency and histone H1 binding to chromatin. *Nature,* 507**,** 104-8.
CICCONE, D. N., SU, H., HEVI, S., GAY, F., LEI, H., BAJKO, J., XU, G., LI, E. & CHEN, T. 2009. KDM1B is a histone H3K4 demethylase required to establish maternal genomic imprints. *Nature,* 461**,** 415-8.
CIRIO, M. C., MARTEL, J., MANN, M., TOPPINGS, M., BARTOLOMEI, M., TRASLER, J. & CHAILLET, J. R. 2008. DNA methyltransferase 1o functions during preimplantation development to preclude a profound level of epigenetic variation. *Dev Biol,* 324**,** 139-50.
CLANCY, K. W., WEERAPANA, E. & THOMPSON, P. R. 2016. Detection and identification of protein citrullination in complex biological systems. *Curr Opin Chem Biol,* 30**,** 1-6.
CLARKSON, Y. L., MCLAUGHLIN, M., WATERFALL, M., DUNLOP, C. E., SKEHEL, P. A., ANDERSON, R. A. & TELFER, E. E. 2018. Initial characterisation of adult

human ovarian cell populations isolated by DDX4 expression and aldehyde dehydrogenase activity. *Sci Rep,* 8**,** 6953.
CLEGG, K. B. & PIKO, L. 1983. Poly(A) length, cytoplasmic adenylation and synthesis of poly(A)+ RNA in early mouse embryos. *Dev Biol,* 95**,** 331-41.
CLIFT, D. & SCHUH, M. 2013. Restarting life: fertilization and the transition from meiosis to mitosis. *Nat Rev Mol Cell Biol,* 14**,** 549-62.
COLLADO-FERNANDEZ, E., PICTON, H. M. & DUMOLLARD, R. 2012. Metabolism throughout follicle and oocyte development in mammals. *Int J Dev Biol,* 56**,** 799-808.
CONNER, S. J., LEFIEVRE, L., HUGHES, D. C. & BARRATT, C. L. 2005. Cracking the egg: increased complexity in the zona pellucida. *Hum Reprod,* 20**,** 1148-52.
CONOVER, J. C., TEMELES, G. L., ZIMMERMANN, J. W., BURKE, B. & SCHULTZ, R. M. 1991. Stage-specific expression of a family of proteins that are major products of zygotic gene activation in the mouse embryo. *Dev Biol,* 144**,** 392-404.
CONSTANCIA, M., HEMBERGER, M., HUGHES, J., DEAN, W., FERGUSON-SMITH, A., FUNDELE, R., STEWART, F., KELSEY, G., FOWDEN, A., SIBLEY, C. & REIK, W. 2002. Placental-specific IGF-II is a major modulator of placental and fetal growth. *Nature,* 417**,** 945-8.
CONTI, M., ANDERSEN, C. B., RICHARD, F., MEHATS, C., CHUN, S. Y., HORNER, K., JIN, C. & TSAFRIRI, A. 2002. Role of cyclic nucleotide signaling in oocyte maturation. *Mol Cell Endocrinol,* 187**,** 153-9.
CONTI, M. & FRANCIOSI, F. 2018. Acquisition of oocyte competence to develop as an embryo: integrated nuclear and cytoplasmic events. *Hum Reprod Update,* 24**,** 245-266.
CONTI, M., HSIEH, M., ZAMAH, A. M. & OH, J. S. 2012. Novel signaling mechanisms in the ovary during oocyte maturation and ovulation. *Mol Cell Endocrinol,* 356**,** 65-73.
CORTELLINO, S., XU, J., SANNAI, M., MOORE, R., CARETTI, E., CIGLIANO, A., LE COZ, M., DEVARAJAN, K., WESSELS, A., SOPRANO, D., ABRAMOWITZ, L. K., BARTOLOMEI, M. S., RAMBOW, F., BASSI, M. R., BRUNO, T., FANCIULLI, M., RENNER, C., KLEIN-SZANTO, A. J., MATSUMOTO, Y., KOBI, D., DAVIDSON, I., ALBERTI, C., LARUE, L. & BELLACOSA, A. 2011. Thymine DNA glycosylase is essential for active DNA demethylation by linked deamination-base excision repair. *Cell,* 146**,** 67-79.
COTICCHIO, G., DAL-CANTO, M., GUGLIELMO, M. C., MIGNINI-RENZINI, M. & FADINI, R. 2012. Human oocyte maturation in vitro. *Int J Dev Biol,* 56**,** 909-18.
COTICCHIO, G., DAL CANTO, M., MIGNINI RENZINI, M., GUGLIELMO, M. C., BRAMBILLASCA, F., TURCHI, D., NOVARA, P. V. & FADINI, R. 2015. Oocyte maturation: gamete-somatic cells interactions, meiotic resumption, cytoskeletal dynamics and cytoplasmic reorganization. *Hum Reprod Update,* 21**,** 427-54.
COTICCHIO, G., GUGLIELMO, M. C., ALBERTINI, D. F., DAL CANTO, M., MIGNINI RENZINI, M., DE PONTI, E. & FADINI, R. 2014. Contributions of the actin cytoskeleton to the emergence of polarity during maturation in human oocytes. *Mol Hum Reprod,* 20**,** 200-7.
COTTERILL, M. 2008. *Gene function during the development of ovine oocytes and ovarian follicles.*, University of Leeds.
COTTERILL, M., CATT, S. L. & PICTON, H. M. 2012. Characterisation of the cellular and molecular responses of ovine oocytes and their supporting somatic cells to pre-ovulatory levels of LH and FSH during in vitro maturation. *Reproduction,* 144**,** 195-207.
COTTERILL, M., HARRIS, S. E., COLLADO FERNANDEZ, E., LU, J., HUNTRISS, J. D., CAMPBELL, B. K. & PICTON, H. M. 2013. The activity and copy number of mitochondrial DNA in ovine oocytes throughout oogenesis in vivo and during oocyte maturation in vitro. *Mol Hum Reprod,* 19**,** 444-50.

CRAN, D. G. & CHENG, W. T. K. 1985. Changes in Cortical Granules during Porcine Oocyte Maturation. *Gamete Research,* 11**,** 311-319.
CROSBY, I. M., GANDOLFI, F. & MOOR, R. M. 1988. Control of protein synthesis during early cleavage of sheep embryos. *J Reprod Fertil,* 82**,** 769-75.
CULLEN, B. R. 2006. Enhancing and confirming the specificity of RNAi experiments. *Nat Methods,* 3**,** 677-81.
CURTIS, D., LEHMANN, R. & ZAMORE, P. D. 1995. Translational regulation in development. *Cell,* 81**,** 171-8.
D'ANIELLO, A., DI COSMO, A., DI CRISTO, C., ANNUNZIATO, L., PETRUCELLI, L. & FISHER, G. 1996. Involvement of D-aspartic acid in the synthesis of testosterone in rat testes. *Life Sci,* 59**,** 97-104.
D'ANIELLO, G., GRIECO, N., DI FILIPPO, M. A., CAPPIELLO, F., TOPO, E., D'ANIELLO, E. & RONSINI, S. 2007. Reproductive implication of D-aspartic acid in human pre-ovulatory follicular fluid. *Hum Reprod,* 22**,** 3178-83.
DALGAARD, K., LANDGRAF, K., HEYNE, S., LEMPRADL, A., LONGINOTTO, J., GOSSENS, K., RUF, M., ORTHOFER, M., STROGANTSEV, R., SELVARAJ, M., LU, T. T., CASAS, E., TEPERINO, R., SURANI, M. A., ZVETKOVA, I., RIMMINGTON, D., TUNG, Y. C., LAM, B., LARDER, R., YEO, G. S., O'RAHILLY, S., VAVOURI, T., WHITELAW, E., PENNINGER, J. M., JENUWEIN, T., CHEUNG, C. L., FERGUSON-SMITH, A. C., COLL, A. P., KORNER, A. & POSPISILIK, J. A. 2016. Trim28 Haploinsufficiency Triggers Bi-stable Epigenetic Obesity. *Cell,* 164**,** 353-64.
DALTON, C. M. & CARROLL, J. 2013. Biased inheritance of mitochondria during asymmetric cell division in the mouse oocyte. *J Cell Sci,* 126**,** 2955-64.
DANFOUR, M. A. 2001. *Influence of the environment on mammalian oocyte development.* University of Leeds.
DAVID, G. F. X., KUMAR, T. C. A. & BAKER, T. G. 1974. Uptake of Tritiated-Thymidine by Primordial Germinal Cells in Ovaries of Adult Slender Loris. *Journal of Reproduction and Fertility,* 41**,** 447-+.
DAVIDSON, E. H. 1976. *Gene activity in early development,* New York, Academic Press.
DAVIS, W., JR., DE SOUSA, P. A. & SCHULTZ, R. M. 1996. Transient expression of translation initiation factor eIF-4C during the 2-cell stage of the preimplantation mouse embryo: identification by mRNA differential display and the role of DNA replication in zygotic gene activation. *Dev Biol,* 174**,** 190-201.
DE LA FUENTE, R. & EPPIG, J. J. 2001. Transcriptional activity of the mouse oocyte genome: Companion granulosa cells modulate transcription and chromatin remodeling. *Developmental Biology,* 229**,** 224-236.
DE PAEPE, C., KRIVEGA, M., CAUFFMAN, G., GEENS, M. & VAN DE VELDE, H. 2014. Totipotency and lineage segregation in the human embryo. *Mol Hum Reprod,* 20**,** 599-618.
DEB, K., CHATURVEDI, M. M. & JAISWAL, Y. K. 2004. Comprehending the role of LPS in Gram-negative bacterial vaginosis: ogling into the causes of unfulfilled child-wish. *Arch Gynecol Obstet,* 270**,** 133-46.
DELAVAL, K., GOVIN, J., CERQUEIRA, F., ROUSSEAUX, S., KHOCHBIN, S. & FEIL, R. 2007. Differential histone modifications mark mouse imprinting control regions during spermatogenesis. *EMBO J,* 26**,** 720-9.
DEMACKER, P. N., BEIJERS, A. M., VAN DAAL, H., DONNELLY, J. P., BLIJLEVENS, N. M. & VAN DEN OUWELAND, J. M. 2009. Plasma citrulline measurement using UPLC tandem mass-spectrometry to determine small intestinal enterocyte pathology. *J Chromatogr B Analyt Technol Biomed Life Sci,* 877**,** 387-92.
DEMIRAY, S. B., YILMAZ, O., GOKER, E. N. T., TAVMERGEN, E., CALIMLIOGLU, N., SEZERMAN, U., SOYKAM, H. O. & OKTEM, G. 2017. Expression of the Bone Morphogenetic Protein-2 (BMP2) in the Human Cumulus Cells as a Biomarker of Oocytes and Embryo Quality. *J Hum Reprod Sci,* 10**,** 194-200.

DEMOND, H., ANVAR, Z., JAHROMI, B. N., SPARAGO, A., VERMA, A., DAVARI, M., CALZARI, L., RUSSO, S., JAHROMI, M. A., MONK, D., ANDREWS, S., RICCIO, A. & KELSEY, G. 2019. A KHDC3L mutation resulting in recurrent hydatidiform mole causes genome-wide DNA methylation loss in oocytes and persistent imprinting defects post-fertilisation. *Genome Med,* 11**,** 84.

DENG, M., SURANENI, P., SCHULTZ, R. M. & LI, R. 2007. The Ran GTPase mediates chromatin signaling to control cortical polarity during polar body extrusion in mouse oocytes. *Dev Cell,* 12**,** 301-8.

DENOMME, M. M. & MANN, M. R. 2013. Maternal control of genomic imprint maintenance. *Reprod Biomed Online,* 27**,** 629-36.

DEPLUS, R., DENIS, H., PUTMANS, P., CALONNE, E., FOURREZ, M., YAMAMOTO, K., SUZUKI, A. & FUKS, F. 2014. Citrullination of DNMT3A by PADI4 regulates its stability and controls DNA methylation. *Nucleic Acids Res,* 42**,** 8285-96.

DEUTSCH, D. R., FROHLICH, T., OTTE, K. A., BECK, A., HABERMANN, F. A., WOLF, E. & ARNOLD, G. J. 2014. Stage-specific proteome signatures in early bovine embryo development. *J Proteome Res,* 13**,** 4363-76.

DI LORENZO, A. & BEDFORD, M. T. 2011. Histone arginine methylation. *Febs Letters,* 585**,** 2024-2031.

DIETZEL, E., WESSLING, J., FLOEHR, J., SCHAFER, C., ENSSLEN, S., DENECKE, B., ROSING, B., NEULEN, J., VEITINGER, T., SPEHR, M., TROPARTZ, T., TOLBA, R., RENNE, T., EGERT, A., SCHORLE, H., GOTTENBUSCH, Y., HILDEBRAND, A., YIALLOUROS, I., STOCKER, W., WEISKIRCHEN, R. & JAHNEN-DECHENT, W. 2013. Fetuin-B, a liver-derived plasma protein is essential for fertilization. *Dev Cell,* 25**,** 106-12.

DISSEN, G. A., ROMERO, C., HIRSHFIELD, A. N. & OJEDA, S. R. 2001. Nerve growth factor is required for early follicular development in the mammalian ovary. *Endocrinology,* 142**,** 2078-86.

DOCHERTY, L. E., REZWAN, F. I., POOLE, R. L., TURNER, C. L., KIVUVA, E., MAHER, E. R., SMITHSON, S. F., HAMILTON-SHIELD, J. P., PATALAN, M., GIZEWSKA, M., PEREGUD-POGORZELSKI, J., BEYGO, J., BUITING, K., HORSTHEMKE, B., SOELLNER, L., BEGEMANN, M., EGGERMANN, T., BAPLE, E., MANSOUR, S., TEMPLE, I. K. & MACKAY, D. J. 2015. Mutations in NLRP5 are associated with reproductive wastage and multilocus imprinting disorders in humans. *Nat Commun,* 6**,** 8086.

DOHERTY, A. S., BARTOLOMEI, M. S. & SCHULTZ, R. M. 2002. Regulation of stage-specific nuclear translocation of Dnmt1o during preimplantation mouse development. *Dev Biol,* 242**,** 255-66.

DONG, J., ALBERTINI, D. F., NISHIMORI, K., KUMAR, T. R., LU, N. & MATZUK, M. M. 1996. Growth differentiation factor-9 is required during early ovarian folliculogenesis. *Nature,* 383**,** 531-5.

DONNAY, I., PARTRIDGE, R. J. & LEESE, H. J. 1999. Can embryo metabolism be used for selecting bovine embryos before transfer? *Reprod Nutr Dev,* 39**,** 523-33.

DOWNS, S. M., COLEMAN, D. L., WARD-BAILEY, P. F. & EPPIG, J. J. 1985. Hypoxanthine is the principal inhibitor of murine oocyte maturation in a low molecular weight fraction of porcine follicular fluid. *Proc Natl Acad Sci U S A,* 82**,** 454-8.

DOWNS, S. M., DANIEL, S. A. & EPPIG, J. J. 1988. Induction of maturation in cumulus cell-enclosed mouse oocytes by follicle-stimulating hormone and epidermal growth factor: evidence for a positive stimulus of somatic cell origin. *J Exp Zool,* 245**,** 86-96.

DRACHEVA, S., PALERMO, R. E., POWERS, G. D. & WAUGH, D. S. 1995. Expression of soluble human interleukin-2 receptor alpha-chain in Escherichia coli. *Protein Expr Purif,* 6**,** 737-47.

DREYFUSS, G., HENTZE, M. & LAMOND, A. I. 1996. From transcript to protein. *Cell,* 85**,** 963-72.

DRIVER, A. M., PENAGARICANO, F., HUANG, W., AHMAD, K. R., HACKBART, K. S., WILTBANK, M. C. & KHATIB, H. 2012. RNA-Seq analysis uncovers transcriptomic variations between morphologically similar in vivo- and in vitro-derived bovine blastocysts. *BMC Genomics,* 13**,** 118.

DUAN, J. E., JIANG, Z. C., ALQAHTANI, F., MANDOIU, I., DONG, H., ZHENG, X., MARJANI, S. L., CHEN, J. & TIAN, X. C. 2019. Methylome Dynamics of Bovine Gametes and in vivo Early Embryos. *Front Genet,* 10**,** 512.

DUBE, J. L., WANG, P., ELVIN, J., LYONS, K. M., CELESTE, A. J. & MATZUK, M. M. 1998. The bone morphogenetic protein 15 gene is X-linked and expressed in oocytes. *Mol Endocrinol,* 12**,** 1809-17.

DUCIBELLA, T., SCHULTZ, R. M. & OZIL, J. P. 2006. Role of calcium signals in early development. *Semin Cell Dev Biol,* 17**,** 324-32.

DUCKWORTH, B. C., WEAVER, J. S. & RUDERMAN, J. V. 2002. G2 arrest in Xenopus oocytes depends on phosphorylation of cdc25 by protein kinase A. *Proc Natl Acad Sci U S A,* 99**,** 16794-9.

DUENEZ-GUZMAN, E. A. & HAIG, D. 2014. The evolution of reproduction-related NLRP genes. *J Mol Evol,* 78**,** 194-201.

DUKE, K. L. 1967. Ovogenetic activity of the fetal-type in the ovary of the adult slow loris, Nycticebus coucang. *Folia Primatol (Basel),* 7**,** 150-4.

DUMOLLARD, R., MARANGOS, P., FITZHARRIS, G., SWANN, K., DUCHEN, M. & CARROLL, J. 2004. Sperm-triggered [Ca2+] oscillations and Ca2+ homeostasis in the mouse egg have an absolute requirement for mitochondrial ATP production. *Development,* 131**,** 3057-67.

DUMONT, J., UMBHAUER, M., RASSINIER, P., HANAUER, A. & VERLHAC, M. H. 2005. p90Rsk is not involved in cytostatic factor arrest in mouse oocytes. *J Cell Biol,* 169**,** 227-31.

DURLINGER, A. L., GRUIJTERS, M. J., KRAMER, P., KARELS, B., KUMAR, T. R., MATZUK, M. M., ROSE, U. M., DE JONG, F. H., UILENBROEK, J. T., GROOTEGOED, J. A. & THEMMEN, A. P. 2001. Anti-Mullerian hormone attenuates the effects of FSH on follicle development in the mouse ovary. *Endocrinology,* 142**,** 4891-9.

DURLINGER, A. L., KRAMER, P., KARELS, B., DE JONG, F. H., UILENBROEK, J. T., GROOTEGOED, J. A. & THEMMEN, A. P. 1999. Control of primordial follicle recruitment by anti-Mullerian hormone in the mouse ovary. *Endocrinology,* 140**,** 5789-96.

EGGERMANN, T., PEREZ DE NANCLARES, G., MAHER, E. R., TEMPLE, I. K., TUMER, Z., MONK, D., MACKAY, D. J., GRONSKOV, K., RICCIO, A., LINGLART, A. & NETCHINE, I. 2015. Imprinting disorders: a group of congenital disorders with overlapping patterns of molecular changes affecting imprinted loci. *Clin Epigenetics,* 7**,** 123.

ELBASHIR, S. M., HARBORTH, J., LENDECKEL, W., YALCIN, A., WEBER, K. & TUSCHL, T. 2001a. Duplexes of 21-nucleotide RNAs mediate RNA interference in cultured mammalian cells. *Nature,* 411**,** 494-8.

ELBASHIR, S. M., MARTINEZ, J., PATKANIOWSKA, A., LENDECKEL, W. & TUSCHL, T. 2001b. Functional anatomy of siRNAs for mediating efficient RNAi in Drosophila melanogaster embryo lysate. *EMBO J,* 20**,** 6877-88.

ELLEDEROVA, Z., KOVAROVA, H., MELO-STERZA, F., LIVINGSTONE, M., TOMEK, W. & KUBELKA, M. 2006. Suppression of translation during in vitro maturation of pig oocytes despite enhanced formation of cap-binding protein complex eIF4F and 4E-BP1 hyperphosphorylation. *Mol Reprod Dev,* 73**,** 68-76.

EPPIG, J. J. 2001. Oocyte control of ovarian follicular development and function in mammals. *Reproduction,* 122**,** 829-38.

EPPIG, J. J. & DOWNS, S. M. 1987. The effect of hypoxanthine on mouse oocyte growth and development in vitro: maintenance of meiotic arrest and gonadotropin-induced oocyte maturation. *Dev Biol,* 119**,** 313-21.

EPPIG, J. J., WIGGLESWORTH, K. & PENDOLA, F. L. 2002. The mammalian oocyte orchestrates the rate of ovarian follicular development. *Proc Natl Acad Sci U S A,* 99**,** 2890-4.

ERCOLANI, L., FLORENCE, B., DENARO, M. & ALEXANDER, M. 1988. Isolation and complete sequence of a functional human glyceraldehyde-3-phosphate dehydrogenase gene. *J Biol Chem,* 263**,** 15335-41.

ERNST, E. H., GRONDAHL, M. L., GRUND, S., HARDY, K., HEUCK, A., SUNDE, L., FRANKS, S., ANDERSEN, C. Y., VILLESEN, P. & LYKKE-HARTMANN, K. 2017. Dormancy and activation of human oocytes from primordial and primary follicles: molecular clues to oocyte regulation. *Hum Reprod,* 32**,** 1684-1700.

ESPOSITO, G., VITALE, A. M., LEIJTEN, F. P., STRIK, A. M., KOONEN-REEMST, A. M., YURTTAS, P., ROBBEN, T. J., COONROD, S. & GOSSEN, J. A. 2007. Peptidylarginine deiminase (PAD) 6 is essential for oocyte cytoskeletal sheet formation and female fertility. *Mol Cell Endocrinol,* 273**,** 25-31.

FADDY, M. J., GOSDEN, R. G., GOUGEON, A., RICHARDSON, S. J. & NELSON, J. F. 1992. Accelerated disappearance of ovarian follicles in mid-life: implications for forecasting menopause. *Hum Reprod,* 7**,** 1342-6.

FAIR, T., HULSHOF, S. C., HYTTEL, P., GREVE, T. & BOLAND, M. 1997a. Nucleus ultrastructure and transcriptional activity of bovine oocytes in preantral and early antral follicles. *Mol Reprod Dev,* 46**,** 208-15.

FAIR, T., HULSHOF, S. C., HYTTEL, P., GREVE, T. & BOLAND, M. 1997b. Oocyte ultrastructure in bovine primordial to early tertiary follicles. *Anat Embryol (Berl),* 195**,** 327-36.

FAIR, T., HYTTEL, P. & GREVE, T. 1995. Bovine oocyte diameter in relation to maturational competence and transcriptional activity. *Mol Reprod Dev,* 42**,** 437-42.

FAIR, T., HYTTEL, P., LONERGAN, P. & BOLAND, M. P. 2001. Immunolocalization of nucleolar proteins during bovine oocyte growth, meiotic maturation, and fertilization. *Biol Reprod,* 64**,** 1516-25.

FALLAHIAN, M., SEBIRE, N. J., SAVAGE, P. M., SECKL, M. J. & FISHER, R. A. 2013. Mutations in NLRP7 and KHDC3L confer a complete hydatidiform mole phenotype on digynic triploid conceptions. *Hum Mutat,* 34**,** 301-8.

FAMILIARI, G., HEYN, R., RELUCENTI, M. & SATHANANTHAN, H. 2008. Structural changes of the zona pellucida during fertilization and embryo development. *Front Biosci,* 13**,** 6730-51.

FARHADOVA, S., GOMEZ-VELAZQUEZ, M. & FEIL, R. 2019. Stability and Lability of Parental Methylation Imprints in Development and Disease. *Genes (Basel),* 10.

FARINI, D., LA SALA, G., TEDESCO, M. & DE FELICI, M. 2007. Chemoattractant action and molecular signaling pathways of Kit ligand on mouse primordial germ cells. *Dev Biol,* 306**,** 572-83.

FATEHI, A. N., ZEINSTRA, E. C., KOOIJ, R. V., COLENBRANDER, B. & BEVERS, M. M. 2002. Effect of cumulus cell removal of in vitro matured bovine oocytes prior to in vitro fertilization on subsequent cleavage rate. *Theriogenology,* 57**,** 1347-55.

FERNANDES, R., TSUDA, C., PERUMALSAMY, A. L., NARANIAN, T., CHONG, J., ACTON, B. M., TONG, Z. B., NELSON, L. M. & JURISICOVA, A. 2012. NLRP5 mediates mitochondrial function in mouse oocytes and embryos. *Biol Reprod,* 86**,** 138, 1-10.

FERREIRA, E. M., VIREQUE, A. A., ADONA, P. R., MEIRELLES, F. V., FERRIANI, R. A. & NAVARRO, P. A. 2009. Cytoplasmic maturation of bovine oocytes: structural and biochemical modifications and acquisition of developmental competence. *Theriogenology,* 71**,** 836-48.

FINDLAY, J. K. 1993. An update on the roles of inhibin, activin, and follistatin as local regulators of folliculogenesis. *Biol Reprod,* 48**,** 15-23.

FIRE, A., XU, S., MONTGOMERY, M. K., KOSTAS, S. A., DRIVER, S. E. & MELLO, C. C. 1998. Potent and specific genetic interference by double-stranded RNA in Caenorhabditis elegans. *Nature,* 391**,** 806-11.
FITZHARRIS, G. & BALTZ, J. M. 2006. Granulosa cells regulate intracellular pH of the murine growing oocyte via gap junctions: development of independent homeostasis during oocyte growth. *Development,* 133**,** 591-599.
FITZHARRIS, G., MARANGOS, P. & CARROLL, J. 2007. Changes in endoplasmic reticulum structure during mouse oocyte maturation are controlled by the cytoskeleton and cytoplasmic dynein. *Dev Biol,* 305**,** 133-44.
FLEMING, T. P., SHETH, B. & FESENKO, I. 2001. Cell adhesion in the preimplantation mammalian embryo and its role in trophectoderm differentiation and blastocyst morphogenesis. *Front Biosci,* 6**,** D1000-7.
FORBES, K. 2013. IFPA Gabor Than Award lecture: molecular control of placental growth: the emerging role of microRNAs. *Placenta,* 34 Suppl**,** S27-33.
FORDE, N. & LONERGAN, P. 2012. Transcriptomic analysis of the bovine endometrium: What is required to establish uterine receptivity to implantation in cattle? *J Reprod Dev,* 58**,** 189-95.
FOURNIER, C., GOTO, Y., BALLESTAR, E., DELAVAL, K., HEVER, A. M., ESTELLER, M. & FEIL, R. 2002. Allele-specific histone lysine methylation marks regulatory regions at imprinted mouse genes. *EMBO J,* 21**,** 6560-70.
FOYGEL, K., CHOI, B., JUN, S., LEONG, D. E., LEE, A., WONG, C. C., ZUO, E., ECKART, M., REIJO PERA, R. A., WONG, W. H. & YAO, M. W. 2008. A novel and critical role for Oct4 as a regulator of the maternal-embryonic transition. *PLoS One,* 3**,** e4109.
FRASER, R. & LIN, C. J. 2016. Epigenetic reprogramming of the zygote in mice and men: on your marks, get set, go! *Reproduction,* 152**,** R211-R222.
FREITAS-LOPES, M. A., MAFRA, K., DAVID, B. A., CARVALHO-GONTIJO, R. & MENEZES, G. B. 2017. Differential Location and Distribution of Hepatic Immune Cells. *Cells,* 6.
FRIEDMAN, J. R., WEBSTER, B. M., MASTRONARDE, D. N., VERHEY, K. J. & VOELTZ, G. K. 2010. ER sliding dynamics and ER-mitochondrial contacts occur on acetylated microtubules. *J Cell Biol,* 190**,** 363-75.
FROHLICH, L. F., MRAKOVCIC, M., STEINBORN, R., CHUNG, U. I., BASTEPE, M. & JUPPNER, H. 2010. Targeted deletion of the Nesp55 DMR defines another Gnas imprinting control region and provides a mouse model of autosomal dominant PHP-Ib. *Proc Natl Acad Sci U S A,* 107**,** 9275-80.
FU, Y., XU, J. J., SUN, X. L., JIANG, H., HAN, D. X., LIU, C., GAO, Y., YUAN, B. & ZHANG, J. B. 2017. Function of JARID2 in bovines during early embryonic development. *PeerJ,* 5**,** e4189.
FUJIWARA, T., NAKADA, K., SHIRAKAWA, H. & MIYAZAKI, S. 1993. Development of inositol trisphosphate-induced calcium release mechanism during maturation of hamster oocytes. *Dev Biol,* 156**,** 69-79.
GABORY, A., RIPOCHE, M. A., LE DIGARCHER, A., WATRIN, F., ZIYYAT, A., FORNE, T., JAMMES, H., AINSCOUGH, J. F., SURANI, M. A., JOURNOT, L. & DANDOLO, L. 2009. H19 acts as a trans regulator of the imprinted gene network controlling growth in mice. *Development,* 136**,** 3413-21.
GAHLAY, G., GAUTHIER, L., BAIBAKOV, B., EPIFANO, O. & DEAN, J. 2010. Gamete recognition in mice depends on the cleavage status of an egg's zona pellucida protein. *Science,* 329**,** 216-9.
GALLICANO, G. I., MCGAUGHEY, R. W. & CAPCO, D. G. 1992. Cytoskeletal sheets appear as universal components of mammalian eggs. *J Exp Zool,* 263**,** 194-203.
GAO, Z., ZHANG, X., YU, X., QIN, D., XIAO, Y., YU, Y., XIANG, Y., NIE, X., LU, X., LIU, W., YI, Z. & LI, L. 2018. Zbed3 participates in the subcortical maternal complex and regulates the distribution of organelles. *J Mol Cell Biol,* 10**,** 74-88.

GARCIA, R. B., PEREYRA-ALFONSO, S. & SOTELO, J. R. 1979. Protein-synthesizing machinery in the growing oocyte of the cyclic mouse. A quantitative electron microscopic study. *Differentiation,* 14**,** 101-6.

GASPEROWICZ, M. & NATALE, D. R. 2011. Establishing three blastocyst lineages--then what? *Biol Reprod,* 84**,** 621-30.

GAY, G., WAGNER, D. T., KEATINGE-CLAY, A. T. & GAY, D. C. 2014. Rapid modification of the pET-28 expression vector for ligation independent cloning using homologous recombination in Saccharomyces cerevisiae. *Plasmid,* 76**,** 66-71.

GEHRING, M., HUH, J. H., HSIEH, T. F., PENTERMAN, J., CHOI, Y., HARADA, J. J., GOLDBERG, R. B. & FISCHER, R. L. 2006. DEMETER DNA glycosylase establishes MEDEA polycomb gene self-imprinting by allele-specific demethylation. *Cell,* 124**,** 495-506.

GEORGES, A., AUGUSTE, A., BESSIERE, L., VANET, A., TODESCHINI, A. L. & VEITIA, R. A. 2014. FOXL2: a central transcription factor of the ovary. *J Mol Endocrinol,* 52**,** R17-33.

GIGLI, I., CUSHMAN, R. A., WAHL, C. M. & FORTUNE, J. E. 2005. Evidence for a role for anti-Mullerian hormone in the suppression of follicle activation in mouse ovaries and bovine ovarian cortex grafted beneath the chick chorioallantoic membrane. *Mol Reprod Dev,* 71**,** 480-8.

GILCHRIST, R. B., RITTER, L. J., MYLLYMAA, S., KAIVO-OJA, N., DRAGOVIC, R. A., HICKEY, T. E., RITVOS, O. & MOTTERSHEAD, D. G. 2006. Molecular basis of oocyte-paracrine signalling that promotes granulosa cell proliferation. *J Cell Sci,* 119**,** 3811-21.

GINNO, P. A., LOTT, P. L., CHRISTENSEN, H. C., KORF, I. & CHEDIN, F. 2012. R-loop formation is a distinctive characteristic of unmethylated human CpG island promoters. *Mol Cell,* 45**,** 814-25.

GINSBURG, M., SNOW, M. H. & MCLAREN, A. 1990. Primordial germ cells in the mouse embryo during gastrulation. *Development,* 110**,** 521-8.

GINTHER, O. J., BEG, M. A., BERGFELT, D. R., DONADEU, F. X. & KOT, K. 2001. Follicle selection in monovular species. *Biol Reprod,* 65**,** 638-47.

GINTHER, O. J., BEG, M. A., DONADEU, F. X. & BERGFELT, D. R. 2003. Mechanism of follicle deviation in monovular farm species. *Anim Reprod Sci,* 78**,** 239-57.

GINTHER, O. J., KOT, K., KULICK, L. J., MARTIN, S. & WILTBANK, M. C. 1996. Relationships between FSH and ovarian follicular waves during the last six months of pregnancy in cattle. *J Reprod Fertil,* 108**,** 271-9.

GIRALDEZ, A. J. 2010. microRNAs, the cell's Nepenthe: clearing the past during the maternal-to-zygotic transition and cellular reprogramming. *Curr Opin Genet Dev,* 20**,** 369-75.

GLASER, R. L., RAMSAY, J. P. & MORISON, I. M. 2006. The imprinted gene and parent-of-origin effect database now includes parental origin of de novo mutations. *Nucleic Acids Res,* 34**,** D29-31.

GLISTER, C., RICHARDS, S. L. & KNIGHT, P. G. 2005. Bone morphogenetic proteins (BMP) -4, -6, and -7 potently suppress basal and luteinizing hormone-induced androgen production by bovine theca interna cells in primary culture: could ovarian hyperandrogenic dysfunction be caused by a defect in thecal BMP signaling? *Endocrinology,* 146**,** 1883-92.

GODDARD, M. J. & PRATT, H. P. 1983. Control of events during early cleavage of the mouse embryo: an analysis of the '2-cell block'. *J Embryol Exp Morphol,* 73**,** 111-33.

GOISSIS, M. D. & CIBELLI, J. B. 2014. Functional characterization of SOX2 in bovine preimplantation embryos. *Biol Reprod,* 90**,** 30.

GOLBUS, M. S., CALARCO, P. G. & EPSTEIN, C. J. 1973. The effects of inhibitors of RNA synthesis (alpha-amanitin and actinomycin D) on preimplantation mouse embryogenesis. *J Exp Zool,* 186**,** 207-16.

GOLDING, M. C. & WESTHUSIN, M. E. 2003. Analysis of DNA (cytosine 5) methyltransferase mRNA sequence and expression in bovine preimplantation embryos, fetal and adult tissues. *Gene Expr Patterns,* 3**,** 551-8.

GOLL, M. G. & BESTOR, T. H. 2005. Eukaryotic cytosine methyltransferases. *Annu Rev Biochem,* 74**,** 481-514.

GONG, Z., MORALES-RUIZ, T., ARIZA, R. R., ROLDAN-ARJONA, T., DAVID, L. & ZHU, J. K. 2002. ROS1, a repressor of transcriptional gene silencing in Arabidopsis, encodes a DNA glycosylase/lyase. *Cell,* 111**,** 803-14.

GOOSSENS, K., VAN POUCKE, M., VAN SOOM, A., VANDESOMPELE, J., VAN ZEVEREN, A. & PEELMAN, L. J. 2005. Selection of reference genes for quantitative real-time PCR in bovine preimplantation embryos. *BMC Dev Biol,* 5**,** 27.

GRAF, A., KREBS, S., ZAKHARTCHENKO, V., SCHWALB, B., BLUM, H. & WOLF, E. 2014. Fine mapping of genome activation in bovine embryos by RNA sequencing. *Proc Natl Acad Sci U S A,* 111**,** 4139-44.

GREEN, S. J., VENKATRAMANAN, R. & NAQIB, A. 2015. Deconstructing the polymerase chain reaction: understanding and correcting bias associated with primer degeneracies and primer-template mismatches. *PLoS One,* 10**,** e0128122.

GRUIJTERS, M. J., VISSER, J. A., DURLINGER, A. L. & THEMMEN, A. P. 2003. Anti-Mullerian hormone and its role in ovarian function. *Mol Cell Endocrinol,* 211**,** 85-90.

GU, T. P., GUO, F., YANG, H., WU, H. P., XU, G. F., LIU, W., XIE, Z. G., SHI, L., HE, X., JIN, S. G., IQBAL, K., SHI, Y. G., DENG, Z., SZABO, P. E., PFEIFER, G. P., LI, J. & XU, G. L. 2011. The role of Tet3 DNA dioxygenase in epigenetic reprogramming by oocytes. *Nature,* 477**,** 606-10.

GU, Y., RUNYAN, C., SHOEMAKER, A., SURANI, A. & WYLIE, C. 2009. Steel factor controls primordial germ cell survival and motility from the time of their specification in the allantois, and provides a continuous niche throughout their migration. *Development,* 136**,** 1295-303.

GUO, D., WU, W., TANG, Q., QIAO, S., CHEN, Y., CHEN, M., TENG, M., LU, C., DING, H., XIA, Y., HU, L., CHEN, D., SHA, J. & WANG, X. 2017. The impact of BMI on sperm parameters and the metabolite changes of seminal plasma concomitantly. *Oncotarget,* 8**,** 48619-48634.

GUO, F., LI, X., LIANG, D., LI, T., ZHU, P., GUO, H., WU, X., WEN, L., GU, T. P., HU, B., WALSH, C. P., LI, J., TANG, F. & XU, G. L. 2014. Active and passive demethylation of male and female pronuclear DNA in the mammalian zygote. *Cell Stem Cell,* 15**,** 447-459.

GYORGY, B., TOTH, E., TARCSA, E., FALUS, A. & BUZAS, E. I. 2006. Citrullination: a posttranslational modification in health and disease. *Int J Biochem Cell Biol,* 38**,** 1662-77.

HACKETT, J. A., SENGUPTA, R., ZYLICZ, J. J., MURAKAMI, K., LEE, C., DOWN, T. A. & SURANI, M. A. 2013. Germline DNA demethylation dynamics and imprint erasure through 5-hydroxymethylcytosine. *Science,* 339**,** 448-52.

HACKETT, J. A., ZYLICZ, J. J. & SURANI, M. A. 2012. Parallel mechanisms of epigenetic reprogramming in the germline. *Trends Genet,* 28**,** 164-74.

HAJKOVA, P., ANCELIN, K., WALDMANN, T., LACOSTE, N., LANGE, U. C., CESARI, F., LEE, C., ALMOUZNI, G., SCHNEIDER, R. & SURANI, M. A. 2008. Chromatin dynamics during epigenetic reprogramming in the mouse germ line. *Nature,* 452**,** 877-81.

HAJKOVA, P., ERHARDT, S., LANE, N., HAAF, T., EL-MAARRI, O., REIK, W., WALTER, J. & SURANI, M. A. 2002. Epigenetic reprogramming in mouse primordial germ cells. *Mech Dev,* 117**,** 15-23.

HALL, B., LIMAYE, A. & KULKARNI, A. B. 2009. Overview: generation of gene knockout mice. *Curr Protoc Cell Biol,* Chapter 19**,** Unit 19 12 19 12 1-17.

HAMATANI, T., CARTER, M. G., SHAROV, A. A. & KO, M. S. 2004. Dynamics of global gene expression changes during mouse preimplantation development. *Dev Cell,* 6**,** 117-31.

HAMMOND, S. M., BERNSTEIN, E., BEACH, D. & HANNON, G. J. 2000. An RNA-directed nuclease mediates post-transcriptional gene silencing in Drosophila cells. *Nature,* 404**,** 293-6.

HANDY, D. E., CASTRO, R. & LOSCALZO, J. 2011. Epigenetic modifications: basic mechanisms and role in cardiovascular disease. *Circulation,* 123**,** 2145-56.

HANEY, A. F. & SCHOMBERG, D. W. 1981. Estrogen and progesterone production by developing porcine follicles in vitro: evidence for estrogen formation by theca. *Endocrinology,* 109**,** 971-7.

HANRAHAN, J. P., GREGAN, S. M., MULSANT, P., MULLEN, M., DAVIS, G. H., POWELL, R. & GALLOWAY, S. M. 2004. Mutations in the genes for oocyte-derived growth factors GDF9 and BMP15 are associated with both increased ovulation rate and sterility in Cambridge and Belclare sheep (Ovis aries). *Biol Reprod,* 70**,** 900-9.

HARA, S., TAKANO, T., FUJIKAWA, T., YAMADA, M., WAKAI, T., KONO, T. & OBATA, Y. 2014. Forced expression of DNA methyltransferases during oocyte growth accelerates the establishment of methylation imprints but not functional genomic imprinting. *Hum Mol Genet,* 23**,** 3853-64.

HARRIS, S. E., ADRIAENS, I., LEESE, H. J., GOSDEN, R. G. & PICTON, H. M. 2007. Carbohydrate metabolism by murine ovarian follicles and oocytes grown in vitro. *Reproduction,* 134**,** 415-24.

HARRIS, S. E., LEESE, H. J., GOSDEN, R. G. & PICTON, H. M. 2009. Pyruvate and oxygen consumption throughout the growth and development of murine oocytes. *Mol Reprod Dev,* 76**,** 231-8.

HARTLEY, J. L., TEMPLE, G. F. & BRASCH, M. A. 2000. DNA cloning using in vitro site-specific recombination. *Genome Res,* 10**,** 1788-95.

HASHIMOTO, S., YAMANAKA, M., YAMOCHI, T., IWATA, H., KAWAHARA-MIKI, R., INOUE, M. & MORIMOTO, Y. 2019. Mitochondrial function in immature bovine oocytes is improved by an increase of cellular cyclic AMP. *Sci Rep,* 9**,** 5167.

HATADA, I. & MUKAI, T. 1995. Genomic imprinting of p57KIP2, a cyclin-dependent kinase inhibitor, in mouse. *Nat Genet,* 11**,** 204-6.

HATTORI, H., HIURA, H., KITAMURA, A., MIYAUCHI, N., KOBAYASHI, N., TAKAHASHI, S., OKAE, H., KYONO, K., KAGAMI, M., OGATA, T. & ARIMA, T. 2019. Association of four imprinting disorders and ART. *Clin Epigenetics,* 11**,** 21.

HAYASHI, K., KOBAYASHI, T., UMINO, T., GOITSUKA, R., MATSUI, Y. & KITAMURA, D. 2002. SMAD1 signaling is critical for initial commitment of germ cell lineage from mouse epiblast. *Mech Dev,* 118**,** 99-109.

HAYDER, H., O'BRIEN, J., NADEEM, U. & PENG, C. 2018. MicroRNAs: crucial regulators of placental development. *Reproduction,* 155**,** R259-R271.

HAYWARD, B. E., DE VOS, M., TALATI, N., ABDOLLAHI, M. R., TAYLOR, G. R., MEYER, E., WILLIAMS, D., MAHER, E. R., SETNA, F., NAZIR, K., HUSSAINI, S., JAFRI, H., RASHID, Y., SHERIDAN, E. & BONTHRON, D. T. 2009. Genetic and epigenetic analysis of recurrent hydatidiform mole. *Hum Mutat,* 30**,** E629-39.

HE, Y. F., LI, B. Z., LI, Z., LIU, P., WANG, Y., TANG, Q., DING, J., JIA, Y., CHEN, Z., LI, L., SUN, Y., LI, X., DAI, Q., SONG, C. X., ZHANG, K., HE, C. & XU, G. L. 2011. Tet-mediated formation of 5-carboxylcytosine and its excision by TDG in mammalian DNA. *Science,* 333**,** 1303-7.

HEDRICK, J. L., URCH, U. A. & HARDY, D. M. 1989. Structure-Function Properties of the Sperm Enzyme Acrosin. *Acs Symposium Series,* 389**,** 215-229.

HEID, C. A., STEVENS, J., LIVAK, K. J. & WILLIAMS, P. M. 1996. Real time quantitative PCR. *Genome Res,* 6**,** 986-94.

HEMMINGS, K. E., LEESE, H. J. & PICTON, H. M. 2012. Amino acid turnover by bovine oocytes provides an index of oocyte developmental competence in vitro. *Biol Reprod,* 86**,** 165, 1-12.

HEMMINGS, K. E., MARUTHINI, D., VYJAYANTHI, S., HOGG, J. E., BALEN, A. H., CAMPBELL, B. K., LEESE, H. J. & PICTON, H. M. 2013. Amino acid turnover by human oocytes is influenced by gamete developmental competence, patient characteristics and gonadotrophin treatment. *Hum Reprod,* 28**,** 1031-44.

HILL, P. W., AMOUROUX, R. & HAJKOVA, P. 2014. DNA demethylation, Tet proteins and 5-hydroxymethylcytosine in epigenetic reprogramming: an emerging complex story. *Genomics,* 104**,** 324-33.

HILL, P. W. S., LEITCH, H. G., REQUENA, C. E., SUN, Z., AMOUROUX, R., ROMAN-TRUFERO, M., BORKOWSKA, M., TERRAGNI, J., VAISVILA, R., LINNETT, S., BAGCI, H., DHARMALINGHAM, G., HABERLE, V., LENHARD, B., ZHENG, Y., PRADHAN, S. & HAJKOVA, P. 2018. Epigenetic reprogramming enables the transition from primordial germ cell to gonocyte. *Nature,* 555**,** 392-396.

HIRASAWA, R., CHIBA, H., KANEDA, M., TAJIMA, S., LI, E., JAENISCH, R. & SASAKI, H. 2008. Maternal and zygotic Dnmt1 are necessary and sufficient for the maintenance of DNA methylation imprints during preimplantation development. *Genes Dev,* 22**,** 1607-16.

HIROKAWA, N., NODA, Y. & OKADA, Y. 1998. Kinesin and dynein superfamily proteins in organelle transport and cell division. *Curr Opin Cell Biol,* 10**,** 60-73.

HO, H. C. & SUAREZ, S. S. 2001. Hyperactivation of mammalian spermatozoa: function and regulation. *Reproduction,* 122**,** 519-26.

HOLLIDAY, R. & PUGH, J. E. 1975. DNA modification mechanisms and gene activity during development. *Science,* 187**,** 226-32.

HOLMES, K., WILLIAMS, C. M., CHAPMAN, E. A. & CROSS, M. J. 2010. Detection of siRNA induced mRNA silencing by RT-qPCR: considerations for experimental design. *BMC Res Notes,* 3**,** 53.

HOLOCH, D. & MOAZED, D. 2015. RNA-mediated epigenetic regulation of gene expression. *Nat Rev Genet,* 16**,** 71-84.

HORIE, K., FUJITA, J., TAKAKURA, K., KANZAKI, H., SUGINAMI, H., IWAI, M., NAKAYAMA, H. & MORI, T. 1993. The expression of c-kit protein in human adult and fetal tissues. *Hum Reprod,* 8**,** 1955-62.

HORIE, K., TAKAKURA, K., TAII, S., NARIMOTO, K., NODA, Y., NISHIKAWA, S., NAKAYAMA, H., FUJITA, J. & MORI, T. 1991. The expression of c-kit protein during oogenesis and early embryonic development. *Biol Reprod,* 45**,** 547-52.

HORNER, V. L. & WOLFNER, M. F. 2008. Transitioning from egg to embryo: triggers and mechanisms of egg activation. *Dev Dyn,* 237**,** 527-44.

HOUGHTON, F. D., HAWKHEAD, J. A., HUMPHERSON, P. G., HOGG, J. E., BALEN, A. H., RUTHERFORD, A. J. & LEESE, H. J. 2002. Non-invasive amino acid turnover predicts human embryo developmental capacity. *Hum Reprod,* 17**,** 999-1005.

HOWELL, C. Y., BESTOR, T. H., DING, F., LATHAM, K. E., MERTINEIT, C., TRASLER, J. M. & CHAILLET, J. R. 2001. Genomic imprinting disrupted by a maternal effect mutation in the Dnmt1 gene. *Cell,* 104**,** 829-38.

HSUEH, A. J., BILLIG, H. & TSAFRIRI, A. 1994. Ovarian follicle atresia: a hormonally controlled apoptotic process. *Endocr Rev,* 15**,** 707-24.

HU, X., HIPOLITO, S., LYNN, R., ABRAHAM, V., RAMOS, S. & WONG-STAAL, F. 2004. Relative gene-silencing efficiencies of small interfering RNAs targeting sense and antisense transcripts from the same genetic locus. *Nucleic Acids Res,* 32**,** 4609-17.

HUAN, Y., XIE, B., LIU, S., KONG, Q. & LIU, Z. 2015. A novel role for DNA methyltransferase 1 in regulating oocyte cytoplasmic maturation in pigs. *PLoS One,* 10**,** e0127512.

HUANG, E. J., NOCKA, K. H., BUCK, J. & BESMER, P. 1992. Differential expression and processing of two cell associated forms of the kit-ligand: KL-1 and KL-2. *Mol Biol Cell,* 3**,** 349-62.

HUANG, H. L., LV, C., ZHAO, Y. C., LI, W., HE, X. M., LI, P., SHA, A. G., TIAN, X., PAPASIAN, C. J., DENG, H. W., LU, G. X. & XIAO, H. M. 2014. Mutant ZP1 in familial infertility. *N Engl J Med,* 370**,** 1220-6.

HUANG, S. & WANG, Y. 2017. Golgi structure formation, function, and post-translational modifications in mammalian cells. *F1000Res,* 6**,** 2050.

HUANG, W. & KHATIB, H. 2010. Comparison of transcriptomic landscapes of bovine embryos using RNA-Seq. *BMC Genomics,* 11**,** 711.

HUNTRISS, J., BALEN, A. H., SINCLAIR, K. D., BRISON, D. R., PICTON, H. M. & ROYAL COLLEGE OF OBSTETRICIANS, G. 2018. Epigenetics and Reproductive Medicine: Scientific Impact Paper No. 57. *BJOG,* 125**,** e43-e54.

HUNTRISS, J., GOSDEN, R., HINKINS, M., OLIVER, B., MILLER, D., RUTHERFORD, A. J. & PICTON, H. M. 2002. Isolation, characterization and expression of the human Factor In the Germline alpha (FIGLA) gene in ovarian follicles and oocytes. *Mol Hum Reprod,* 8**,** 1087-95.

HUNTRISS, J., HINKINS, M., OLIVER, B., HARRIS, S. E., BEAZLEY, J. C., RUTHERFORD, A. J., GOSDEN, R. G., LANZENDORF, S. E. & PICTON, H. M. 2004. Expression of mRNAs for DNA methyltransferases and methyl-CpG-binding proteins in the human female germ line, preimplantation embryos, and embryonic stem cells. *Mol Reprod Dev,* 67**,** 323-36.

HUNTRISS, J., HINKINS, M. & PICTON, H. M. 2006. cDNA cloning and expression of the human NOBOX gene in oocytes and ovarian follicles. *Mol Hum Reprod,* 12**,** 283-9.

HUNTRISS, J., LU, J., HEMMINGS, K., BAYNE, R., ANDERSON, R., RUTHERFORD, A., BALEN, A., ELDER, K. & PICTON, H. M. 2017. Isolation and expression of the human gametocyte-specific factor 1 gene (GTSF1) in fetal ovary, oocytes, and preimplantation embryos. *J Assist Reprod Genet,* 34**,** 23-31.

HUSSEIN, T. S., FROILAND, D. A., AMATO, F., THOMPSON, J. G. & GILCHRIST, R. B. 2005. Oocytes prevent cumulus cell apoptosis by maintaining a morphogenic paracrine gradient of bone morphogenetic proteins. *J Cell Sci,* 118**,** 5257-68.

HUTT, K. J. & ALBERTINI, D. F. 2007. An oocentric view of folliculogenesis and embryogenesis. *Reprod Biomed Online,* 14**,** 758-64.

HUTT, K. J., MCLAUGHLIN, E. A. & HOLLAND, M. K. 2006. Kit ligand and c-Kit have diverse roles during mammalian oogenesis and folliculogenesis. *Mol Hum Reprod,* 12**,** 61-9.

HYTTEL, P., CALLESEN, H. & GREVE, T. 1986. Ultrastructural features of preovulatory oocyte maturation in superovulated cattle. *J Reprod Fertil,* 76**,** 645-56.

HYTTEL, P., FAIR, T., CALLESEN, H. & GREVE, T. 1997. Oocyte growth, capacitation and final maturation in cattle. *Theriogenology,* 47**,** 23-32.

ICKOWICZ, D., FINKELSTEIN, M. & BREITBART, H. 2012. Mechanism of sperm capacitation and the acrosome reaction: role of protein kinases. *Asian J Androl,* 14**,** 816-21.

IGLESIAS-PLATAS, I., MARTIN-TRUJILLO, A., PETAZZI, P., GUILLAUMET-ADKINS, A., ESTELLER, M. & MONK, D. 2014. Altered expression of the imprinted transcription factor PLAGL1 deregulates a network of genes in the human IUGR placenta. *Hum Mol Genet,* 23**,** 6275-85.

IMSCHENETZKY, M., PUCHI, M., MORIN, V., MEDINA, R. & MONTECINO, M. 2003. Chromatin remodeling during sea urchin early development: molecular determinants for pronuclei formation and transcriptional activation. *Gene,* 322**,** 33-46.

INOUE, A., OGUSHI, S., SAITOU, M., SUZUKI, M. G. & AOKI, F. 2011a. Involvement of mouse nucleoplasmin 2 in the decondensation of sperm chromatin after fertilization. *Biol Reprod,* 85**,** 70-7.

INOUE, A., SHEN, L., DAI, Q., HE, C. & ZHANG, Y. 2011b. Generation and replication-dependent dilution of 5fC and 5caC during mouse preimplantation development. *Cell Res,* 21**,** 1670-6.

INOUE, A. & ZHANG, Y. 2011. Replication-dependent loss of 5-hydroxymethylcytosine in mouse preimplantation embryos. *Science,* 334**,** 194.

INOUE, N., IKAWA, M., ISOTANI, A. & OKABE, M. 2005. The immunoglobulin superfamily protein Izumo is required for sperm to fuse with eggs. *Nature,* 434**,** 234-8.

INOUE, N., IKAWA, M. & OKABE, M. 2011c. The mechanism of sperm-egg interaction and the involvement of IZUMO1 in fusion. *Asian J Androl,* 13**,** 81-7.

IQBAL, K., JIN, S. G., PFEIFER, G. P. & SZABO, P. E. 2011. Reprogramming of the paternal genome upon fertilization involves genome-wide oxidation of 5-methylcytosine. *Proc Natl Acad Sci U S A,* 108**,** 3642-7.

ISHIGAMI, A. & MARUYAMA, N. 2010. Importance of research on peptidylarginine deiminase and citrullinated proteins in age-related disease. *Geriatr Gerontol Int,* 10 Suppl 1**,** S53-8.

ISHIHARA, K., OSHIMURA, M. & NAKAO, M. 2006. CTCF-dependent chromatin insulator is linked to epigenetic remodeling. *Mol Cell,* 23**,** 733-42.

ITO, S., SHEN, L., DAI, Q., WU, S. C., COLLINS, L. B., SWENBERG, J. A., HE, C. & ZHANG, Y. 2011. Tet proteins can convert 5-methylcytosine to 5-formylcytosine and 5-carboxylcytosine. *Science,* 333**,** 1300-3.

IVANOVA, I., MUCH, C., DI GIACOMO, M., AZZI, C., MORGAN, M., MOREIRA, P. N., MONAHAN, J., CARRIERI, C., ENRIGHT, A. J. & O'CARROLL, D. 2017. The RNA m(6)A Reader YTHDF2 Is Essential for the Post-transcriptional Regulation of the Maternal Transcriptome and Oocyte Competence. *Mol Cell,* 67**,** 1059-1067 e4.

JACKSON, A. L., BARTZ, S. R., SCHELTER, J., KOBAYASHI, S. V., BURCHARD, J., MAO, M., LI, B., CAVET, G. & LINSLEY, P. S. 2003. Expression profiling reveals off-target gene regulation by RNAi. *Nat Biotechnol,* 21**,** 635-7.

JACKSON, B. W., GRUND, C., SCHMID, E., BURKI, K., FRANKE, W. W. & ILLMENSEE, K. 1980. Formation of cytoskeletal elements during mouse embryogenesis. Intermediate filaments of the cytokeratin type and desmosomes in preimplantation embryos. *Differentiation,* 17**,** 161-79.

JAMNONGJIT, M. & HAMMES, S. R. 2005. Oocyte maturation: the coming of age of a germ cell. *Semin Reprod Med,* 23**,** 234-41.

JANSOVA, D., TETKOVA, A., KONCICKA, M., KUBELKA, M. & SUSOR, A. 2018. Localization of RNA and translation in the mammalian oocyte and embryo. *PLoS One,* 13**,** e0192544.

JAQUEMAR, D., KUPRIYANOV, S., WANKELL, M., AVIS, J., BENIRSCHKE, K., BARIBAULT, H. & OSHIMA, R. G. 2003. Keratin 8 protection of placental barrier function. *J Cell Biol,* 161**,** 749-56.

JAYAPRAKASHA, G. K., MURTHY, K. N. C. & PATIL, B. S. 2011. Rapid HPLC-UV method for quantification of L-citrulline in watermelon and its potential role on smooth muscle relaxation markers. *Food Chemistry,* 127**,** 240-248.

JEDRUSIK, A., PARFITT, D. E., GUO, G., SKAMAGKI, M., GRABAREK, J. B., JOHNSON, M. H., ROBSON, P. & ZERNICKA-GOETZ, M. 2008. Role of Cdx2 and cell polarity in cell allocation and specification of trophectoderm and inner cell mass in the mouse embryo. *Genes Dev,* 22**,** 2692-706.

JEE, B. C., CHEN, H. Y. & CHIAN, R. C. 2009. Effect of a phosphodiesterase type 3 inhibitor in oocyte maturation medium on subsequent mouse embryo development. *Fertil Steril,* 91**,** 2037-42.

JEON, H. J., PARK, Y. S., CHO, D. H., KIM, J. S., KIM, E., CHAE, H. Z., CHUN, S. Y. & OH, J. S. 2017. Peroxiredoxins are required for spindle assembly, chromosome organization, and polarization in mouse oocytes. *Biochem Biophys Res Commun,* 489**,** 193-199.

JEONG, Y. J., CHOI, H. W., SHIN, H. S., CUI, X. S., KIM, N. H., GERTON, G. L. & JUN, J. H. 2005. Optimization of real time RT-PCR methods for the analysis of gene expression in mouse eggs and preimplantation embryos. *Mol Reprod Dev,* 71**,** 284-9.

JIA, D., JURKOWSKA, R. Z., ZHANG, X., JELTSCH, A. & CHENG, X. 2007. Structure of Dnmt3a bound to Dnmt3L suggests a model for de novo DNA methylation. *Nature,* 449**,** 248-51.

JIANG, Z., LIN, J., DONG, H., ZHENG, X., MARJANI, S. L., DUAN, J., OUYANG, Z., CHEN, J. & TIAN, X. C. 2018. DNA methylomes of bovine gametes and in vivo produced preimplantation embryos. *Biol Reprod,* 99**,** 949-959.

JIANG, Z., SUN, J., DONG, H., LUO, O., ZHENG, X., OBERGFELL, C., TANG, Y., BI, J., O'NEILL, R., RUAN, Y., CHEN, J. & TIAN, X. C. 2014. Transcriptional profiles of bovine in vivo pre-implantation development. *BMC Genomics,* 15**,** 756.

JIN, M., FUJIWARA, E., KAKIUCHI, Y., OKABE, M., SATOUH, Y., BABA, S. A., CHIBA, K. & HIROHASHI, N. 2011. Most fertilizing mouse spermatozoa begin their acrosome reaction before contact with the zona pellucida during in vitro fertilization. *Proc Natl Acad Sci U S A,* 108**,** 4892-6.

JIN, Z., LI, R., ZHOU, C., SHI, L., ZHANG, X., YANG, Z. & ZHANG, D. 2016. Efficient Gene Knockdown in Mouse Oocytes through Peptide Nanoparticle-Mediated SiRNA Transfection. *PLoS One,* 11**,** e0150462.

JODAR, M. 2019. Sperm and seminal plasma RNAs: What roles do they play beyond fertilization? *Reproduction*.

JODAR, M., SENDLER, E., MOSKOVTSEV, S. I., LIBRACH, C. L., GOODRICH, R., SWANSON, S., HAUSER, R., DIAMOND, M. P. & KRAWETZ, S. A. 2015. Absence of sperm RNA elements correlates with idiopathic male infertility. *Sci Transl Med,* 7**,** 295re6.

JOHNSON, J., CANNING, J., KANEKO, T., PRU, J. K. & TILLY, J. L. 2004. Germline stem cells and follicular renewal in the postnatal mammalian ovary. *Nature,* 428**,** 145-50.

JOHNSON, J., SKAZNIK-WIKIEL, M., LEE, H. J., NIIKURA, Y., TILLY, J. C. & TILLY, J. L. 2005. Setting the record straight on data supporting postnatal oogenesis in female mammals. *Cell Cycle,* 4**,** 1471-7.

JOHNSON, M. H. & MCCONNELL, J. M. 2004. Lineage allocation and cell polarity during mouse embryogenesis. *Semin Cell Dev Biol,* 15**,** 583-97.

JOHNSON, M. H. & ZIOMEK, C. A. 1981. The foundation of two distinct cell lineages within the mouse morula. *Cell,* 24**,** 71-80.

JOHNSON, W. H., LOSKUTOFF, N. M., PLANTE, Y. & BETTERIDGE, K. J. 1995. Production of four identical calves by the separation of blastomeres from an in vitro derived four-cell embryo. *Vet Rec,* 137**,** 15-6.

JOSEPHSON, R., ORDING, C. J., LIU, Y., SHIN, S., LAKSHMIPATHY, U., TOUMADJE, A., LOVE, B., CHESNUT, J. D., ANDREWS, P. W., RAO, M. S. & AUERBACH, J. M. 2007. Qualification of embryonal carcinoma 2102Ep as a reference for human embryonic stem cell research. *Stem Cells,* 25**,** 437-46.

JOSHI, S., DAVIES, H., SIMS, L. P., LEVY, S. E. & DEAN, J. 2007. Ovarian gene expression in the absence of FIGLA, an oocyte-specific transcription factor. *BMC Dev Biol,* 7**,** 67.

JUDSON, H., HAYWARD, B. E., SHERIDAN, E. & BONTHRON, D. T. 2002. A global disorder of imprinting in the human female germ line. *Nature,* 416**,** 539-42.

JUENGEL, J. L., HUDSON, N. L., BERG, M., HAMEL, K., SMITH, P., LAWRENCE, S. B., WHITING, L. & MCNATTY, K. P. 2009. Effects of active immunization against growth differentiation factor 9 and/or bone morphogenetic protein 15 on ovarian function in cattle. *Reproduction,* 138**,** 107-14.

JUKAM, D., SHARIATI, S. A. M. & SKOTHEIM, J. M. 2017. Zygotic Genome Activation in Vertebrates. *Dev Cell,* 42**,** 316-332.

KAN, R., JIN, M., SUBRAMANIAN, V., CAUSEY, C. P., THOMPSON, P. R. & COONROD, S. A. 2012. Potential role for PADI-mediated histone citrullination in preimplantation development. *BMC Dev Biol,* 12**,** 19.

KAN, R., YURTTAS, P., KIM, B., JIN, M., WO, L., LEE, B., GOSDEN, R. & COONROD, S. A. 2011. Regulation of mouse oocyte microtubule and organelle dynamics by PADI6 and the cytoplasmic lattices. *Dev Biol,* 350**,** 311-22.

KANEDA, M., HIRASAWA, R., CHIBA, H., OKANO, M., LI, E. & SASAKI, H. 2010. Genetic evidence for Dnmt3a-dependent imprinting during oocyte growth obtained by conditional knockout with Zp3-Cre and complete exclusion of Dnmt3b by chimera formation. *Genes Cells,* 15**,** 169-79.

KANEDA, M., OKANO, M., HATA, K., SADO, T., TSUJIMOTO, N., LI, E. & SASAKI, H. 2004. Essential role for de novo DNA methyltransferase Dnmt3a in paternal and maternal imprinting. *Nature,* 429**,** 900-3.

KANEMITSU, M. Y. & LAU, A. F. 1993. Epidermal growth factor stimulates the disruption of gap junctional communication and connexin43 phosphorylation independent of 12-0-tetradecanoylphorbol 13-acetate-sensitive protein kinase C: the possible involvement of mitogen-activated protein kinase. *Mol Biol Cell,* 4**,** 837-48.

KARMAKAR, S. & DAS, C. 2002. Regulation of trophoblast invasion by IL-1beta and TGF-beta1. *Am J Reprod Immunol,* 48**,** 210-9.

KE, S., ALEMU, E. A., MERTENS, C., GANTMAN, E. C., FAK, J. J., MELE, A., HARIPAL, B., ZUCKER-SCHARFF, I., MOORE, M. J., PARK, C. Y., VAGBO, C. B., KUSSNIERCZYK, A., KLUNGLAND, A., DARNELL, J. E., JR. & DARNELL, R. B. 2015. A majority of m6A residues are in the last exons, allowing the potential for 3' UTR regulation. *Genes Dev,* 29**,** 2037-53.

KENIRY, A., OXLEY, D., MONNIER, P., KYBA, M., DANDOLO, L., SMITS, G. & REIK, W. 2012. The H19 lincRNA is a developmental reservoir of miR-675 that suppresses growth and Igf1r. *Nat Cell Biol,* 14**,** 659-65.

KERAMARI, M., RAZAVI, J., INGMAN, K. A., PATSCH, C., EDENHOFER, F., WARD, C. M. & KIMBER, S. J. 2010. Sox2 is essential for formation of trophectoderm in the preimplantation embryo. *PLoS One,* 5**,** e13952.

KESHET, I., LIEMAN-HURWITZ, J. & CEDAR, H. 1986. DNA methylation affects the formation of active chromatin. *Cell,* 44**,** 535-43.

KETTING, R. F. 2011. The many faces of RNAi. *Dev Cell,* 20**,** 148-61.

KETTING, R. F., HAVERKAMP, T. H., VAN LUENEN, H. G. & PLASTERK, R. H. 1999. Mut-7 of C. elegans, required for transposon silencing and RNA interference, is a homolog of Werner syndrome helicase and RNaseD. *Cell,* 99**,** 133-41.

KEZELE, P. & SKINNER, M. K. 2003. Regulation of ovarian primordial follicle assembly and development by estrogen and progesterone: endocrine model of follicle assembly. *Endocrinology,* 144**,** 3329-37.

KEZELE, P. R., NILSSON, E. E. & SKINNER, M. K. 2002a. Insulin but not insulin-like growth factor-1 promotes the primordial to primary follicle transition. *Mol Cell Endocrinol,* 192**,** 37-43.

KEZELE, P. R., NILSSON, E. E. & SKINNER, M. K. 2002b. Insulin but not insulin-like growth factor-1 promotes the primordial to primary follicle transition. *Molecular and Cellular Endocrinology,* 192**,** 37-43.

KIM, B., KAN, R., ANGUISH, L., NELSON, L. M. & COONROD, S. A. 2010. Potential role for MATER in cytoplasmic lattice formation in murine oocytes. *PLoS One,* 5**,** e12587.

KIM, B., ZHANG, X., KAN, R., COHEN, R., MUKAI, C., TRAVIS, A. J. & COONROD, S. A. 2014. The role of MATER in endoplasmic reticulum distribution and calcium homeostasis in mouse oocytes. *Dev Biol,* 386**,** 331-9.

KIM, D., LANGMEAD, B. & SALZBERG, S. L. 2015a. HISAT: a fast spliced aligner with low memory requirements. *Nat Methods,* 12**,** 357-60.

KIM, J. 2008. Multiple YY1 and CTCF binding sites in imprinting control regions. *Epigenetics,* 3**,** 115-8.

KIM, J., KIM, J. S., JEON, Y. J., KIM, D. W., YANG, T. H., SOH, Y., LEE, H. K., CHOI, N. J., PARK, S. B., SEO, K. S., CHUNG, H. M., LEE, D. S. & CHAE, J. I. 2011. Identification of maturation and protein synthesis related proteins from porcine oocytes during in vitro maturation. *Proteome Sci,* 9**,** 28.

KIM, J. H. & RICHTER, J. D. 2006. Opposing polymerase-deadenylase activities regulate cytoplasmic polyadenylation. *Molecular Cell,* 24**,** 173-183.

KIM, S., YU, N. K. & KAANG, B. K. 2015b. CTCF as a multifunctional protein in genome regulation and gene expression. *Exp Mol Med,* 47**,** e166.

KIMBLE, K. M., DICKINSON, S. E. & BIASE, F. H. 2018. Extraction of total RNA from single-oocytes and single-cell mRNA sequencing of swine oocytes. *BMC Res Notes,* 11**,** 155.

KIMPLE, M. E., BRILL, A. L. & PASKER, R. L. 2013. Overview of affinity tags for protein purification. *Curr Protoc Protein Sci,* 73**,** 9 9 1-9 9 23.

KIMURA, M., KIM, E., KANG, W., YAMASHITA, M., SAIGO, M., YAMAZAKI, T., NAKANISHI, T., KASHIWABARA, S. & BABA, T. 2009. Functional roles of mouse sperm hyaluronidases, HYAL5 and SPAM1, in fertilization. *Biol Reprod,* 81**,** 939-47.

KITASAKA, H., KAWAI, T., HOQUE, S. A. M., UMEHARA, T., FUJITA, Y. & SHIMADA, M. 2018. Inductions of granulosa cell luteinization and cumulus expansion are dependent on the fibronectin-integrin pathway during ovulation process in mice. *PLoS One,* 13**,** e0192458.

KNIGHT, P. G. & GLISTER, C. 2006. TGF-beta superfamily members and ovarian follicle development. *Reproduction,* 132**,** 191-206.

KOHL, A. & GRUTTER, M. G. 2004. Fire and death: the pyrin domain joins the death-domain superfamily. *C R Biol,* 327**,** 1077-86.

KOHLI, R. M. & ZHANG, Y. 2013. TET enzymes, TDG and the dynamics of DNA demethylation. *Nature,* 502**,** 472-9.

KOROTKEVICH, E., NIWAYAMA, R., COURTOIS, A., FRIESE, S., BERGER, N., BUCHHOLZ, F. & HIIRAGI, T. 2017. The Apical Domain Is Required and Sufficient for the First Lineage Segregation in the Mouse Embryo. *Dev Cell,* 40**,** 235-247 e7.

KOU, Y. C., SHAO, L., PENG, H. H., ROSETTA, R., DEL GAUDIO, D., WAGNER, A. F., AL-HUSSAINI, T. K. & VAN DEN VEYVER, I. B. 2008. A recurrent intragenic genomic duplication, other novel mutations in NLRP7 and imprinting defects in recurrent biparental hydatidiform moles. *Mol Hum Reprod,* 14**,** 33-40.

KOUZARIDES, T. 2007. Chromatin modifications and their function. *Cell,* 128**,** 693-705.

KROL, J., LOEDIGE, I. & FILIPOWICZ, W. 2010. The widespread regulation of microRNA biogenesis, function and decay. *Nat Rev Genet,* 11**,** 597-610.

KUNG, J. T., COLOGNORI, D. & LEE, J. T. 2013. Long noncoding RNAs: past, present, and future. *Genetics,* 193**,** 651-69.

KUO, M. H. & ALLIS, C. D. 1998. Roles of histone acetyltransferases and deacetylases in gene regulation. *Bioessays,* 20**,** 615-26.

KURIHARA, Y., KAWAMURA, Y., UCHIJIMA, Y., AMAMO, T., KOBAYASHI, H., ASANO, T. & KURIHARA, H. 2008. Maintenance of genomic methylation patterns during preimplantation development requires the somatic form of DNA methyltransferase 1. *Dev Biol,* 313**,** 335-46.

KURIMOTO, K., YABUTA, Y., OHINATA, Y., SHIGETA, M., YAMANAKA, K. & SAITOU, M. 2008a. Complex genome-wide transcription dynamics orchestrated by Blimp1 for the specification of the germ cell lineage in mice. *Genes Dev,* 22**,** 1617-35.

KURIMOTO, K., YAMAJI, M., SEKI, Y. & SAITOU, M. 2008b. Specification of the germ cell lineage in mice: a process orchestrated by the PR-domain proteins, Blimp1 and Prdm14. *Cell Cycle,* 7**,** 3514-8.

KWINTKIEWICZ, J. & GIUDICE, L. C. 2009. The interplay of insulin-like growth factors, gonadotropins, and endocrine disruptors in ovarian follicular development and function. *Semin Reprod Med,* 27**,** 43-51.

LAEMMLI, U. K. 1970. Cleavage of structural proteins during the assembly of the head of bacteriophage T4. *Nature,* 227**,** 680-5.
LANGE, S., GALLAGHER, M., KHOLIA, S., KOSGODAGE, U. S., HRISTOVA, M., HARDY, J. & INAL, J. M. 2017. Peptidylarginine Deiminases-Roles in Cancer and Neurodegeneration and Possible Avenues for Therapeutic Intervention via Modulation of Exosome and Microvesicle (EMV) Release? *Int J Mol Sci,* 18.
LATHAM, K. E. & SCHULTZ, R. M. 2001. Embryonic genome activation. *Front Biosci,* 6**,** D748-59.
LAVAGI, I., KREBS, S., SIMMET, K., BECK, A., ZAKHARTCHENKO, V., WOLF, E. & BLUM, H. 2018. Single-cell RNA sequencing reveals developmental heterogeneity of blastomeres during major genome activation in bovine embryos. *Sci Rep,* 8**,** 4071.
LAWSON, K. A., DUNN, N. R., ROELEN, B. A., ZEINSTRA, L. M., DAVIS, A. M., WRIGHT, C. V., KORVING, J. P. & HOGAN, B. L. 1999. Bmp4 is required for the generation of primordial germ cells in the mouse embryo. *Genes Dev,* 13**,** 424-36.
LAWSON, K. A. & HAGE, W. J. 1994. Clonal analysis of the origin of primordial germ cells in the mouse. *Ciba Found Symp,* 182**,** 68-84; discussion 84-91.
LAZARAVICIUTE, G., KAUSER, M., BHATTACHARYA, S., HAGGARTY, P. & BHATTACHARYA, S. 2014. A systematic review and meta-analysis of DNA methylation levels and imprinting disorders in children conceived by IVF/ICSI compared with children conceived spontaneously. *Hum Reprod Update,* 20**,** 840-52.
LEE, H., ELAHI, F., LEE, J., LEE, S. T., HYUN, S. H. & LEE, E. 2017. Supplement of cilostamide in growth medium improves oocyte maturation and developmental competence of embryos derived from small antral follicles in pigs. *Theriogenology,* 91**,** 1-8.
LEE, K. B., WEE, G., ZHANG, K., FOLGER, J. K., KNOTT, J. G. & SMITH, G. W. 2014a. Functional role of the bovine oocyte-specific protein JY-1 in meiotic maturation, cumulus expansion, and subsequent embryonic development. *Biol Reprod,* 90**,** 69.
LEE, M., CHOI, Y., KIM, K., JIN, H., LIM, J., NGUYEN, T. A., YANG, J., JEONG, M., GIRALDEZ, A. J., YANG, H., PATEL, D. J. & KIM, V. N. 2014b. Adenylation of maternally inherited microRNAs by Wispy. *Mol Cell,* 56**,** 696-707.
LEE, R. C., FEINBAUM, R. L. & AMBROS, V. 1993. The C. elegans heterochronic gene lin-4 encodes small RNAs with antisense complementarity to lin-14. *Cell,* 75**,** 843-54.
LEE, W. S., OTSUKA, F., MOORE, R. K. & SHIMASAKI, S. 2001. Effect of bone morphogenetic protein-7 on folliculogenesis and ovulation in the rat. *Biol Reprod,* 65**,** 994-9.
LEFIEVRE, L., CONNER, S. J., SALPEKAR, A., OLUFOWOBI, O., ASHTON, P., PAVLOVIC, B., LENTON, W., AFNAN, M., BREWIS, I. A., MONK, M., HUGHES, D. C. & BARRATT, C. L. 2004. Four zona pellucida glycoproteins are expressed in the human. *Hum Reprod,* 19**,** 1580-6.
LI, E., BESTOR, T. H. & JAENISCH, R. 1992. Targeted mutation of the DNA methyltransferase gene results in embryonic lethality. *Cell,* 69**,** 915-26.
LI, G. P., LIU, Y., BUNCH, T. D., WHITE, K. L. & ASTON, K. I. 2005. Asymmetric division of spindle microtubules and microfilaments during bovine meiosis from metaphase I to metaphase III. *Mol Reprod Dev,* 71**,** 220-6.
LI, H., HANDSAKER, B., WYSOKER, A., FENNELL, T., RUAN, J., HOMER, N., MARTH, G., ABECASIS, G., DURBIN, R. & GENOME PROJECT DATA PROCESSING, S. 2009. The Sequence Alignment/Map format and SAMtools. *Bioinformatics,* 25**,** 2078-9.

LI, J. Y., LEES-MURDOCK, D. J., XU, G. L. & WALSH, C. P. 2004. Timing of establishment of paternal methylation imprints in the mouse. *Genomics,* 84**,** 952-60.
LI, L., BAIBAKOV, B. & DEAN, J. 2008a. A subcortical maternal complex essential for preimplantation mouse embryogenesis. *Dev Cell,* 15**,** 416-25.
LI, L., LU, X. & DEAN, J. 2013. The maternal to zygotic transition in mammals. *Mol Aspects Med,* 34**,** 919-38.
LI, L., ZHENG, P. & DEAN, J. 2010a. Maternal control of early mouse development. *Development,* 137**,** 859-70.
LI, P., LI, M., LINDBERG, M. R., KENNETT, M. J., XIONG, N. & WANG, Y. 2010b. PAD4 is essential for antibacterial innate immunity mediated by neutrophil extracellular traps. *J Exp Med,* 207**,** 1853-62.
LI, P., YAO, H., ZHANG, Z., LI, M., LUO, Y., THOMPSON, P. R., GILMOUR, D. S. & WANG, Y. 2008b. Regulation of p53 target gene expression by peptidylarginine deiminase 4. *Mol Cell Biol,* 28**,** 4745-58.
LI, Q. Y., LOU, J., YANG, X. G., LU, Y. Q., LU, S. S. & LU, K. H. 2016. Effect of the meiotic inhibitor cilostamide on resumption of meiosis and cytoskeletal distribution in buffalo oocytes. *Anim Reprod Sci,* 174**,** 37-44.
LI, X., ITO, M., ZHOU, F., YOUNGSON, N., ZUO, X., LEDER, P. & FERGUSON-SMITH, A. C. 2008c. A maternal-zygotic effect gene, Zfp57, maintains both maternal and paternal imprints. *Dev Cell,* 15**,** 547-57.
LI, Y., ZHANG, Z., CHEN, J., LIU, W., LAI, W., LIU, B., LI, X., LIU, L., XU, S., DONG, Q., WANG, M., DUAN, X., TAN, J., ZHENG, Y., ZHANG, P., FAN, G., WONG, J., XU, G. L., WANG, Z., WANG, H., GAO, S. & ZHU, B. 2018. Stella safeguards the oocyte methylome by preventing de novo methylation mediated by DNMT1. *Nature,* 564**,** 136-140.
LIANG, L., SOYAL, S. M. & DEAN, J. 1997. FIGalpha, a germ cell specific transcription factor involved in the coordinate expression of the zona pellucida genes. *Development,* 124**,** 4939-47.
LIAO, Y., SMYTH, G. K. & SHI, W. 2014. featureCounts: an efficient general purpose program for assigning sequence reads to genomic features. *Bioinformatics,* 30**,** 923-30.
LIM, E. J. & CHOI, Y. 2012. Transcription factors in the maintenance and survival of primordial follicles. *Clin Exp Reprod Med,* 39**,** 127-31.
LINTERN-MOORE, S. & MOORE, G. P. 1979. The initiation of follicle and oocyte growth in the mouse ovary. *Biol Reprod,* 20**,** 773-8.
LIPERIS, G. 2013. *The function of gametocyte specific factor 1 (GTSF1) in mammalian oocyte and ovarian follicle development.*, University of Leeds.
LISHKO, P. V., BOTCHKINA, I. L. & KIRICHOK, Y. 2011. Progesterone activates the principal Ca2+ channel of human sperm. *Nature,* 471**,** 387-91.
LIU, H. & AOKI, F. 2002. Transcriptional activity associated with meiotic competence in fully grown mouse GV oocytes. *Zygote,* 10**,** 327-32.
LIU, L., KONG, N. N., XIA, G. L. & ZHANG, M. J. 2013. Molecular control of oocyte meiotic arrest and resumption. *Reproduction Fertility and Development,* 25**,** 463-471.
LIU, M. 2011. The biology and dynamics of mammalian cortical granules. *Reprod Biol Endocrinol,* 9**,** 149.
LIU, Q., LI, M. Z., LEIBHAM, D., CORTEZ, D. & ELLEDGE, S. J. 1998a. The univector plasmid-fusion system, a method for rapid construction of recombinant DNA without restriction enzymes. *Curr Biol,* 8**,** 1300-9.
LIU, X., ANDOH, K., YOKOTA, H., KOBAYASHI, J., ABE, Y., YAMADA, K., MIZUNUMA, H. & IBUKI, Y. 1998b. Effects of growth hormone, activin, and follistatin on the development of preantral follicle from immature female mice. *Endocrinology,* 139**,** 2342-7.

LIU, X., MORENCY, E., LI, T., QIN, H., ZHANG, X., ZHANG, X. & COONROD, S. 2017. Role for PADI6 in securing the mRNA-MSY2 complex to the oocyte cytoplasmic lattices. *Cell Cycle,* 16**,** 360-366.

LIU, Y., BEYER, A. & AEBERSOLD, R. 2016. On the Dependency of Cellular Protein Levels on mRNA Abundance. *Cell,* 165**,** 535-50.

LIVAK, K. J. & SCHMITTGEN, T. D. 2001. Analysis of relative gene expression data using real-time quantitative PCR and the 2(-Delta Delta C(T)) Method. *Methods,* 25**,** 402-8.

LODDE, V., LUCIANO, A. M., FRANCIOSI, F., LABRECQUE, R. & SIRARD, M. A. 2017. Accumulation of Chromatin Remodelling Enzyme and Histone Transcripts in Bovine Oocytes. *Results Probl Cell Differ,* 63**,** 223-255.

LODDE, V., MODINA, S., GALBUSERA, C., FRANCIOSI, F. & LUCIANO, A. M. 2007. Large-scale chromatin remodeling in germinal vesicle bovine oocytes: interplay with gap junction functionality and developmental competence. *Mol Reprod Dev,* 74**,** 740-9.

LONERGAN, P., KHATIR, H., CAROLAN, C. & MERMILLOD, P. 1997. Bovine blastocyst production in vitro after inhibition of oocyte meiotic resumption for 24 h. *J Reprod Fertil,* 109**,** 355-65.

LORAINE, A. E., BLAKLEY, I. C., JAGADEESAN, S., HARPER, J., MILLER, G. & FIRON, N. 2015. Analysis and visualization of RNA-Seq expression data using RStudio, Bioconductor, and Integrated Genome Browser. *Methods Mol Biol,* 1284**,** 481-501.

LORCA, T., CRUZALEGUI, F. H., FESQUET, D., CAVADORE, J. C., MERY, J., MEANS, A. & DOREE, M. 1993. Calmodulin-dependent protein kinase II mediates inactivation of MPF and CSF upon fertilization of Xenopus eggs. *Nature,* 366**,** 270-3.

LORCA, T., GALAS, S., FESQUET, D., DEVAULT, A., CAVADORE, J. C. & DOREE, M. 1991. Degradation of the proto-oncogene product p39mos is not necessary for cyclin proteolysis and exit from meiotic metaphase: requirement for a Ca(2+)-calmodulin dependent event. *EMBO J,* 10**,** 2087-93.

LU, X., GAO, Z., QIN, D. & LI, L. 2017. A Maternal Functional Module in the Mammalian Oocyte-To-Embryo Transition. *Trends Mol Med,* 23**,** 1014-1023.

LUCIANO, A. M., FRANCIOSI, F., MODINA, S. C. & LODDE, V. 2011. Gap junction-mediated communications regulate chromatin remodeling during bovine oocyte growth and differentiation through cAMP-dependent mechanism(s). *Biol Reprod,* 85**,** 1252-9.

LUCIANO, A. M. & SIRARD, M. A. 2018. Successful in vitro maturation of oocytes: a matter of follicular differentiation. *Biol Reprod,* 98**,** 162-169.

LUCIFERO, D., MERTINEIT, C., CLARKE, H. J., BESTOR, T. H. & TRASLER, J. M. 2002. Methylation dynamics of imprinted genes in mouse germ cells. *Genomics,* 79**,** 530-8.

LYKKE-ANDERSEN, K., GILCHRIST, M. J., GRABAREK, J. B., DAS, P., MISKA, E. & ZERNICKA-GOETZ, M. 2008. Maternal Argonaute 2 is essential for early mouse development at the maternal-zygotic transition. *Mol Biol Cell,* 19**,** 4383-92.

LYLE, R., WATANABE, D., TE VRUCHTE, D., LERCHNER, W., SMRZKA, O. W., WUTZ, A., SCHAGEMAN, J., HAHNER, L., DAVIES, C. & BARLOW, D. P. 2000. The imprinted antisense RNA at the Igf2r locus overlaps but does not imprint Mas1. *Nat Genet,* 25**,** 19-21.

LYON, M. F. 1999. Imprinting and X-chromosome inactivation. *Results Probl Cell Differ,* 25**,** 73-90.

MA, M., ZHOU, L., GUO, X., LV, Z., YU, Y., DING, C., ZHANG, P., BI, Y., XIE, J., WANG, L., LIN, M., ZHOU, Z., HUO, R., SHA, J. & ZHOU, Q. 2009. Decreased cofilin1 expression is important for compaction during early mouse embryo development. *Biochim Biophys Acta,* 1793**,** 1804-10.

MACKAY, D. J., CALLAWAY, J. L., MARKS, S. M., WHITE, H. E., ACERINI, C. L., BOONEN, S. E., DAYANIKLI, P., FIRTH, H. V., GOODSHIP, J. A., HAEMERS, A. P., HAHNEMANN, J. M., KORDONOURI, O., MASOUD, A. F., OESTERGAARD, E., STORR, J., ELLARD, S., HATTERSLEY, A. T., ROBINSON, D. O. & TEMPLE, I. K. 2008. Hypomethylation of multiple imprinted loci in individuals with transient neonatal diabetes is associated with mutations in ZFP57. *Nat Genet,* 40**,** 949-51.

MADAN, P., ROSE, K. & WATSON, A. J. 2007. Na/K-ATPase beta1 subunit expression is required for blastocyst formation and normal assembly of trophectoderm tight junction-associated proteins. *J Biol Chem,* 282**,** 12127-34.

MADDIREVULA, S., COSKUN, S., AWARTANI, K., ALSAIF, H., ABDULWAHAB, F. M. & ALKURAYA, F. S. 2017. The human knockout phenotype of PADI6 is female sterility caused by cleavage failure of their fertilized eggs. *Clin Genet,* 91**,** 344-345.

MADGWICK, S. & JONES, K. T. 2007. How eggs arrest at metaphase II: MPF stabilisation plus APC/C inhibition equals Cytostatic Factor. *Cell Div,* 2**,** 4.

MAGARAKI, A., VAN DER HEIJDEN, G., SLEDDENS-LINKELS, E., MAGARAKIS, L., VAN CAPPELLEN, W. A., PETERS, A., GRIBNAU, J., BAARENDS, W. M. & EIJPE, M. 2017. Silencing markers are retained on pericentric heterochromatin during murine primordial germ cell development. *Epigenetics Chromatin,* 10**,** 11.

MAHADEVAN, S., SATHAPPAN, V., UTAMA, B., LORENZO, I., KASKAR, K. & VAN DEN VEYVER, I. B. 2017. Maternally expressed NLRP2 links the subcortical maternal complex (SCMC) to fertility, embryogenesis and epigenetic reprogramming. *Sci Rep,* 7**,** 44667.

MAHADEVAN, S., WEN, S., WAN, Y. W., PENG, H. H., OTTA, S., LIU, Z., IACOVINO, M., MAHEN, E. M., KYBA, M., SADIKOVIC, B. & VAN DEN VEYVER, I. B. 2014. NLRP7 affects trophoblast lineage differentiation, binds to overexpressed YY1 and alters CpG methylation. *Hum Mol Genet,* 23**,** 706-16.

MAINLAND, R. L., LYONS, T. A., RUTH, M. M. & KRAMER, J. M. 2017. Optimal RNA isolation method and primer design to detect gene knockdown by qPCR when validating Drosophila transgenic RNAi lines. *BMC Res Notes,* 10**,** 647.

MAITI, A. & DROHAT, A. C. 2011. Thymine DNA glycosylase can rapidly excise 5-formylcytosine and 5-carboxylcytosine: potential implications for active demethylation of CpG sites. *J Biol Chem,* 286**,** 35334-8.

MALHI, P. S., ADAMS, G. P., MAPLETOFT, R. J. & SINGH, J. 2007. Oocyte developmental competence in a bovine model of reproductive aging. *Reproduction,* 134**,** 233-9.

MAMO, S., CARTER, F., LONERGAN, P., LEAL, C. L., AL NAIB, A., MCGETTIGAN, P., MEHTA, J. P., EVANS, A. C. & FAIR, T. 2011. Sequential analysis of global gene expression profiles in immature and in vitro matured bovine oocytes: potential molecular markers of oocyte maturation. *BMC Genomics,* 12**,** 151.

MAMO, S., GAL, A. B., BODO, S. & DINNYES, A. 2007. Quantitative evaluation and selection of reference genes in mouse oocytes and embryos cultured in vivo and in vitro. *BMC Dev Biol,* 7**,** 14.

MANOVA, K., HUANG, E. J., ANGELES, M., DE LEON, V., SANCHEZ, S., PRONOVOST, S. M., BESMER, P. & BACHVAROVA, R. F. 1993. The expression pattern of the c-kit ligand in gonads of mice supports a role for the c-kit receptor in oocyte growth and in proliferation of spermatogonia. *Dev Biol,* 157**,** 85-99.

MAO, L., LOU, H., LOU, Y., WANG, N. & JIN, F. 2014. Behaviour of cytoplasmic organelles and cytoskeleton during oocyte maturation. *Reprod Biomed Online,* 28**,** 284-99.

MARCEL, M. 2011. Cutadapt removes adapter sequences from high-throughput sequencing reads. *EMBnet.journal,* 17**,** 10-12.

MARCHO, C., BEVILACQUA, A., TREMBLAY, K. D. & MAGER, J. 2015. Tissue-specific regulation of Igf2r/Airn imprinting during gastrulation. *Epigenetics Chromatin,* 8**,** 10.

MARCINKIEWICZ, J. L., BALCHAK, S. K. & MORRISON, L. J. 2002. The involvement of tumor necrosis factor-alpha (TNF) as an intraovarian regulator of oocyte apoptosis in the neonatal rat. *Front Biosci,* 7**,** d1997-2005.

MARLOW, F. L. 2010. *Maternal Control of Development in Vertebrates: My Mother Made Me Do It!* San Rafael (CA).

MARLOW, F. L. 2018. Recent advances in understanding oogenesis: interactions with the cytoskeleton, microtubule organization, and meiotic spindle assembly in oocytes. *F1000Res,* 7.

MARO, B., JOHNSON, M. H., WEBB, M. & FLACH, G. 1986. Mechanism of polar body formation in the mouse oocyte: an interaction between the chromosomes, the cytoskeleton and the plasma membrane. *J Embryol Exp Morphol,* 92**,** 11-32.

MARSCHALL, A. L., DUBEL, S. & BOLDICKE, T. 2015. Specific in vivo knockdown of protein function by intrabodies. *MAbs,* 7**,** 1010-35.

MARSISCHKY, G. & LABAER, J. 2004. Many paths to many clones: a comparative look at high-throughput cloning methods. *Genome Res,* 14**,** 2020-8.

MARTIN, J. J., WOODS, D. C. & TILLY, J. L. 2019. Implications and Current Limitations of Oogenesis from Female Germline or Oogonial Stem Cells in Adult Mammalian Ovaries. *Cells,* 8.

MARTINON, F., GAIDE, O., PETRILLI, V., MAYOR, A. & TSCHOPP, J. 2007. NALP inflammasomes: a central role in innate immunity. *Semin Immunopathol,* 29**,** 213-29.

MARTINS DA SILVA, S. J., BAYNE, R. A., CAMBRAY, N., HARTLEY, P. S., MCNEILLY, A. S. & ANDERSON, R. A. 2004. Expression of activin subunits and receptors in the developing human ovary: activin A promotes germ cell survival and proliferation before primordial follicle formation. *Dev Biol,* 266**,** 334-45.

MARTINS DA SILVA, S. J., GARDNER, J. O., TAYLOR, J. E., SPRINGBETT, A., DE SOUSA, P. A. & ANDERSON, R. A. 2005. Brain-derived neurotrophic factor promotes bovine oocyte cytoplasmic competence for embryo development. *Reproduction,* 129**,** 423-34.

MASCIARELLI, S., HORNER, K., LIU, C., PARK, S. H., HINCKLEY, M., HOCKMAN, S., NEDACHI, T., JIN, C., CONTI, M. & MANGANIELLO, V. 2004. Cyclic nucleotide phosphodiesterase 3A-deficient mice as a model of female infertility. *J Clin Invest,* 114**,** 196-205.

MASTRONARDI, F. G., WOOD, D. D., MEI, J., RAIJMAKERS, R., TSEVELEKI, V., DOSCH, H. M., PROBERT, L., CASACCIA-BONNEFIL, P. & MOSCARELLO, M. A. 2006. Increased citrullination of histone H3 in multiple sclerosis brain and animal models of demyelination: a role for tumor necrosis factor-induced peptidylarginine deiminase 4 translocation. *J Neurosci,* 26**,** 11387-96.

MASUI, Y. & MARKERT, C. L. 1971. Cytoplasmic control of nuclear behavior during meiotic maturation of frog oocytes. *J Exp Zool,* 177**,** 129-45.

MATSUDAIRA, P. 1987. Sequence from picomole quantities of proteins electroblotted onto polyvinylidene difluoride membranes. *J Biol Chem,* 262**,** 10035-8.

MATTSON, B. A. & ALBERTINI, D. F. 1990. Oogenesis: chromatin and microtubule dynamics during meiotic prophase. *Mol Reprod Dev,* 25**,** 374-83.

MATZUK, M. M., KUMAR, T. R., SHOU, W., COERVER, K. A., LAU, A. L., BEHRINGER, R. R. & FINEGOLD, M. J. 1996. Transgenic models to study the roles of inhibins and activins in reproduction, oncogenesis, and development. *Recent Prog Horm Res,* 51**,** 123-54; discussion 155-7.

MATZUK, M. M., KUMAR, T. R., VASSALLI, A., BICKENBACH, J. R., ROOP, D. R., JAENISCH, R. & BRADLEY, A. 1995. Functional analysis of activins during mammalian development. *Nature,* 374**,** 354-6.

MAY-PANLOUP, P., VIGNON, X., CHRETIEN, M. F., HEYMAN, Y., TAMASSIA, M., MALTHIERY, Y. & REYNIER, P. 2005. Increase of mitochondrial DNA content and transcripts in early bovine embryogenesis associated with upregulation of mtTFA and NRF1 transcription factors. *Reprod Biol Endocrinol,* 3**,** 65.

MCGRATH, J. & SOLTER, D. 1984. Completion of mouse embryogenesis requires both the maternal and paternal genomes. *Cell,* 37**,** 179-83.

MCGRATH, S. A., ESQUELA, A. F. & LEE, S. J. 1995. Oocyte-specific expression of growth/differentiation factor-9. *Mol Endocrinol,* 9**,** 131-6.

MCGRAW, S., VIGNEAULT, C., TREMBLAY, K. & SIRARD, M. A. 2006. Characterization of linker histone H1FOO during bovine in vitro embryo development. *Mol Reprod Dev,* 73**,** 692-9.

MCLAUGHLIN, E. A. & MCIVER, S. C. 2009. Awakening the oocyte: controlling primordial follicle development. *Reproduction,* 137**,** 1-11.

MCLAY, D. W. & CLARKE, H. J. 2003. Remodelling the paternal chromatin at fertilization in mammals. *Reproduction,* 125**,** 625-33.

MCNATTY, K. P., FIDLER, A. E., JUENGEL, J. L., QUIRKE, L. D., SMITH, P. R., HEATH, D. A., LUNDY, T., O'CONNELL, A. & TISDALL, D. J. 2000. Growth and paracrine factors regulating follicular formation and cellular function. *Mol Cell Endocrinol,* 163**,** 11-20.

MCNATTY, K. P., MAKRIS, A., DEGRAZIA, C., OSATHANONDH, R. & RYAN, K. J. 1979. The production of progesterone, androgens, and estrogens by granulosa cells, thecal tissue, and stromal tissue from human ovaries in vitro. *J Clin Endocrinol Metab,* 49**,** 687-99.

MCNATTY, K. P., MOORE, L. G., HUDSON, N. L., QUIRKE, L. D., LAWRENCE, S. B., READER, K., HANRAHAN, J. P., SMITH, P., GROOME, N. P., LAITINEN, M., RITVOS, O. & JUENGEL, J. L. 2004. The oocyte and its role in regulating ovulation rate: a new paradigm in reproductive biology. *Reproduction,* 128**,** 379-86.

MCNATTY, K. P., SMITH, P., MOORE, L. G., READER, K., LUN, S., HANRAHAN, J. P., GROOME, N. P., LAITINEN, M., RITVOS, O. & JUENGEL, J. L. 2005. Oocyte-expressed genes affecting ovulation rate. *Mol Cell Endocrinol,* 234**,** 57-66.

MECHIN, M. C., SEBBAG, M., ARNAUD, J., NACHAT, R., FOULQUIER, C., ADOUE, V., COUDANE, F., DUPLAN, H., SCHMITT, A. M., CHAVANAS, S., GUERRIN, M., SERRE, G. & SIMON, M. 2007. Update on peptidylarginine deiminases and deimination in skin physiology and severe human diseases. *Int J Cosmet Sci,* 29**,** 147-68.

MEHLMANN, L. M. 2005. Stops and starts in mammalian oocytes: recent advances in understanding the regulation of meiotic arrest and oocyte maturation. *Reproduction,* 130**,** 791-9.

MEHLMANN, L. M., JONES, T. L. & JAFFE, L. A. 2002. Meiotic arrest in the mouse follicle maintained by a Gs protein in the oocyte. *Science,* 297**,** 1343-5.

MEHLMANN, L. M., MIKOSHIBA, K. & KLINE, D. 1996. Redistribution and increase in cortical inositol 1,4,5-trisphosphate receptors after meiotic maturation of the mouse oocyte. *Dev Biol,* 180**,** 489-98.

MEHLMANN, L. M., TERASAKI, M., JAFFE, L. A. & KLINE, D. 1995. Reorganization of the endoplasmic reticulum during meiotic maturation of the mouse oocyte. *Dev Biol,* 170**,** 607-15.

MEHTA, J., DINERMAN, J., MEHTA, P., SALDEEN, T. G., LAWSON, D., DONNELLY, W. H. & WALLIN, R. 1989. Neutrophil function in ischemic heart disease. *Circulation,* 79**,** 549-56.

MEISTER, G. & TUSCHL, T. 2004. Mechanisms of gene silencing by double-stranded RNA. *Nature,* 431**,** 343-9.

MEMILI, E., PEDDINTI, D., SHACK, L. A., NANDURI, B., MCCARTHY, F., SAGIRKAYA, H. & BURGESS, S. C. 2007. Bovine germinal vesicle oocyte and cumulus cell proteomics. *Reproduction,* 133**,** 1107-20.

MENEZO, Y. J. & HERUBEL, F. 2002. Mouse and bovine models for human IVF. *Reprod Biomed Online,* 4**,** 170-5.
MESSAED, C., AKOURY, E., DJURIC, U., ZENG, J., SALEH, M., GILBERT, L., SEOUD, M., QURESHI, S. & SLIM, R. 2011. NLRP7, a nucleotide oligomerization domain-like receptor protein, is required for normal cytokine secretion and co-localizes with Golgi and the microtubule-organizing center. *J Biol Chem,* 286**,** 43313-23.
MESSERSCHMIDT, D. M. 2012. Should I stay or should I go: protection and maintenance of DNA methylation at imprinted genes. *Epigenetics,* 7**,** 969-75.
MESSERSCHMIDT, D. M., DE VRIES, W., ITO, M., SOLTER, D., FERGUSON-SMITH, A. & KNOWLES, B. B. 2012. Trim28 is required for epigenetic stability during mouse oocyte to embryo transition. *Science,* 335**,** 1499-502.
MESSERSCHMIDT, D. M., KNOWLES, B. B. & SOLTER, D. 2014. DNA methylation dynamics during epigenetic reprogramming in the germline and preimplantation embryos. *Genes Dev,* 28**,** 812-28.
METCHAT, A., AKERFELT, M., BIERKAMP, C., DELSINNE, V., SISTONEN, L., ALEXANDRE, H. & CHRISTIANS, E. S. 2009. Mammalian heat shock factor 1 is essential for oocyte meiosis and directly regulates Hsp90alpha expression. *J Biol Chem,* 284**,** 9521-8.
MEYER, E., LIM, D., PASHA, S., TEE, L. J., RAHMAN, F., YATES, J. R., WOODS, C. G., REIK, W. & MAHER, E. R. 2009. Germline mutation in NLRP2 (NALP2) in a familial imprinting disorder (Beckwith-Wiedemann Syndrome). *PLoS Genet,* 5**,** e1000423.
MEYER, K. D., SALETORE, Y., ZUMBO, P., ELEMENTO, O., MASON, C. E. & JAFFREY, S. R. 2012. Comprehensive analysis of mRNA methylation reveals enrichment in 3' UTRs and near stop codons. *Cell,* 149**,** 1635-46.
MILLER, D. 2015. Confrontation, Consolidation, and Recognition: The Oocyte's Perspective on the Incoming Sperm. *Cold Spring Harb Perspect Med,* 5**,** a023408.
MINAMI, N., SUZUKI, T. & TSUKAMOTO, S. 2007. Zygotic gene activation and maternal factors in mammals. *J Reprod Dev,* 53**,** 707-15.
MINSHULL, J., SUN, H., TONKS, N. K. & MURRAY, A. W. 1994. A MAP kinase-dependent spindle assembly checkpoint in Xenopus egg extracts. *Cell,* 79**,** 475-86.
MISIRLIOGLU, M., PAGE, G. P., SAGIRKAYA, H., KAYA, A., PARRISH, J. J., FIRST, N. L. & MEMILI, E. 2006. Dynamics of global transcriptome in bovine matured oocytes and preimplantation embryos. *Proc Natl Acad Sci U S A,* 103**,** 18905-10.
MIYAZAKI, S., SHIRAKAWA, H., NAKADA, K. & HONDA, Y. 1993. Essential role of the inositol 1,4,5-trisphosphate receptor/Ca2+ release channel in Ca2+ waves and Ca2+ oscillations at fertilization of mammalian eggs. *Dev Biol,* 158**,** 62-78.
MLOTSHWA, S., VOINNET, O., METTE, M. F., MATZKE, M., VAUCHERET, H., DING, S. W., PRUSS, G. & VANCE, V. B. 2002. RNA silencing and the mobile silencing signal. *Plant Cell,* 14 Suppl**,** S289-301.
MOGESSIE, B. & SCHUH, M. 2017. Actin protects mammalian eggs against chromosome segregation errors. *Science,* 357.
MOGLABEY, Y. B., KIRCHEISEN, R., SEOUD, M., EL MOGHARBEL, N., VAN DEN VEYVER, I. & SLIM, R. 1999. Genetic mapping of a maternal locus responsible for familial hydatidiform moles. *Hum Mol Genet,* 8**,** 667-71.
MOLYNEAUX, K. A., ZINSZNER, H., KUNWAR, P. S., SCHAIBLE, K., STEBLER, J., SUNSHINE, M. J., O'BRIEN, W., RAZ, E., LITTMAN, D., WYLIE, C. & LEHMANN, R. 2003. The chemokine SDF1/CXCL12 and its receptor CXCR4 regulate mouse germ cell migration and survival. *Development,* 130**,** 4279-86.
MONK, D., MACKAY, D. J. G., EGGERMANN, T., MAHER, E. R. & RICCIO, A. 2019. Genomic imprinting disorders: lessons on how genome, epigenome and environment interact. *Nat Rev Genet,* 20**,** 235-248.

MONK, D., SANCHEZ-DELGADO, M. & FISHER, R. 2017. NLRPs, the subcortical maternal complex and genomic imprinting. *Reproduction,* 154**,** R161-R170.
MONK, M., BOUBELIK, M. & LEHNERT, S. 1987. Temporal and regional changes in DNA methylation in the embryonic, extraembryonic and germ cell lineages during mouse embryo development. *Development,* 99**,** 371-82.
MONNIAUX, D. 2016. Driving folliculogenesis by the oocyte-somatic cell dialog: Lessons from genetic models. *Theriogenology,* 86**,** 41-53.
MOORE, R. K., ERICKSON, G. F. & SHIMASAKI, S. 2004. Are BMP-15 and GDF-9 primary determinants of ovulation quota in mammals? *Trends Endocrinol Metab,* 15**,** 356-61.
MORENO, R. D., SCHATTEN, G. & RAMALHO-SANTOS, J. 2002. Golgi apparatus dynamics during mouse oocyte in vitro maturation: effect of the membrane trafficking inhibitor brefeldin A. *Biol Reprod,* 66**,** 1259-66.
MORGAN, H. D., SANTOS, F., GREEN, K., DEAN, W. & REIK, W. 2005. Epigenetic reprogramming in mammals. *Hum Mol Genet,* 14 Spec No 1**,** R47-58.
MORRISON, D. K. 2009. The 14-3-3 proteins: integrators of diverse signaling cues that impact cell fate and cancer development. *Trends Cell Biol,* 19**,** 16-23.
MURDOCH, S., DJURIC, U., MAZHAR, B., SEOUD, M., KHAN, R., KUICK, R., BAGGA, R., KIRCHEISEN, R., AO, A., RATTI, B., HANASH, S., ROULEAU, G. A. & SLIM, R. 2006. Mutations in NALP7 cause recurrent hydatidiform moles and reproductive wastage in humans. *Nat Genet,* 38**,** 300-2.
MUSSE, A. A., LI, Z., ACKERLEY, C. A., BIENZLE, D., LEI, H., POMA, R., HARAUZ, G., MOSCARELLO, M. A. & MASTRONARDI, F. G. 2008. Peptidylarginine deiminase 2 (PAD2) overexpression in transgenic mice leads to myelin loss in the central nervous system. *Dis Model Mech,* 1**,** 229-40.
NAGANO, T., MITCHELL, J. A., SANZ, L. A., PAULER, F. M., FERGUSON-SMITH, A. C., FEIL, R. & FRASER, P. 2008. The Air noncoding RNA epigenetically silences transcription by targeting G9a to chromatin. *Science,* 322**,** 1717-20.
NAKAMURA, N. 2010. Emerging new roles of GM130, a cis-Golgi matrix protein, in higher order cell functions. *J Pharmacol Sci,* 112**,** 255-64.
NAKAMURA, T., ARAI, Y., UMEHARA, H., MASUHARA, M., KIMURA, T., TANIGUCHI, H., SEKIMOTO, T., IKAWA, M., YONEDA, Y., OKABE, M., TANAKA, S., SHIOTA, K. & NAKANO, T. 2007. PGC7/Stella protects against DNA demethylation in early embryogenesis. *Nat Cell Biol,* 9**,** 64-71.
NAKAMURA, T., LIU, Y. J., NAKASHIMA, H., UMEHARA, H., INOUE, K., MATOBA, S., TACHIBANA, M., OGURA, A., SHINKAI, Y. & NAKANO, T. 2012. PGC7 binds histone H3K9me2 to protect against conversion of 5mC to 5hmC in early embryos. *Nature,* 486**,** 415-9.
NAKASHIMA, K., HAGIWARA, T. & YAMADA, M. 2002. Nuclear localization of peptidylarginine deiminase V and histone deimination in granulocytes. *Journal of Biological Chemistry,* 277**,** 49562-49568.
NAMGOONG, S. & KIM, N. H. 2016. Roles of actin binding proteins in mammalian oocyte maturation and beyond. *Cell Cycle,* 15**,** 1830-43.
NEELI, I., KHAN, S. N. & RADIC, M. 2008. Histone deimination as a response to inflammatory stimuli in neutrophils. *J Immunol,* 180**,** 1895-902.
NEWTON, H. 1998. The cryopreservation of ovarian tissue as a strategy for preserving the fertility of cancer patients. *Hum Reprod Update,* 4**,** 237-47.
NGANVONGPANIT, K., MULLER, H., RINGS, F., GILLES, M., JENNEN, D., HOLKER, M., THOLEN, E., SCHELLANDER, K. & TESFAYE, D. 2006. Targeted suppression of E-cadherin gene expression in bovine preimplantation embryo by RNA interference technology using double-stranded RNA. *Mol Reprod Dev,* 73**,** 153-63.
NGUYEN, N. M., ZHANG, L., REDDY, R., DERY, C., ARSENEAU, J., CHEUNG, A., SURTI, U., HOFFNER, L., SEOUD, M., ZAATARI, G., BAGGA, R., SRINIVASAN, R., COULLIN, P., AO, A. & SLIM, R. 2014. Comprehensive genotype-phenotype

correlations between NLRP7 mutations and the balance between embryonic tissue differentiation and trophoblastic proliferation. *J Med Genet,* 51**,** 623-34.
NICULESCU, M. D. & ZEISEL, S. H. 2002. Diet, methyl donors and DNA methylation: interactions between dietary folate, methionine and choline. *J Nutr,* 132**,** 2333S-2335S.
NIKAS, G., AO, A., WINSTON, R. M. & HANDYSIDE, A. H. 1996. Compaction and surface polarity in the human embryo in vitro. *Biol Reprod,* 55**,** 32-7.
NIKOLIC, A., VOLAREVIC, V., ARMSTRONG, L., LAKO, M. & STOJKOVIC, M. 2016. Primordial Germ Cells: Current Knowledge and Perspectives. *Stem Cells Int,* 2016**,** 1741072.
NILSSON, E., PARROTT, J. A. & SKINNER, M. K. 2001. Basic fibroblast growth factor induces primordial follicle development and initiates folliculogenesis. *Mol Cell Endocrinol,* 175**,** 123-30.
NILSSON, E. E., KEZELE, P. & SKINNER, M. K. 2002. Leukemia inhibitory factor (LIF) promotes the primordial to primary follicle transition in rat ovaries. *Mol Cell Endocrinol,* 188**,** 65-73.
NILSSON, E. E., SCHINDLER, R., SAVENKOVA, M. I. & SKINNER, M. K. 2011. Inhibitory actions of Anti-Mullerian Hormone (AMH) on ovarian primordial follicle assembly. *PLoS One,* 6**,** e20087.
NILSSON, E. E. & SKINNER, M. K. 2004. Kit ligand and basic fibroblast growth factor interactions in the induction of ovarian primordial to primary follicle transition. *Mol Cell Endocrinol,* 214**,** 19-25.
NILSSON, E. E. & SKINNER, M. K. 2009. Progesterone regulation of primordial follicle assembly in bovine fetal ovaries. *Mol Cell Endocrinol,* 313**,** 9-16.
NISHIKIMI, A., MUKAI, J. & YAMADA, M. 1999. Nuclear translocation of nuclear factor kappa B in early 1-cell mouse embryos. *Biol Reprod,* 60**,** 1536-41.
NORDIN, M., BERGMAN, D., HALJE, M., ENGSTROM, W. & WARD, A. 2014. Epigenetic regulation of the Igf2/H19 gene cluster. *Cell Prolif,* 47**,** 189-99.
NORRIS, R. P., FREUDZON, M., MEHLMANN, L. M., COWAN, A. E., SIMON, A. M., PAUL, D. L., LAMPE, P. D. & JAFFE, L. A. 2008. Luteinizing hormone causes MAP kinase-dependent phosphorylation and closure of connexin 43 gap junctions in mouse ovarian follicles: one of two paths to meiotic resumption. *Development,* 135**,** 3229-38.
NORRIS, R. P., RATZAN, W. J., FREUDZON, M., MEHLMANN, L. M., KRALL, J., MOVSESIAN, M. A., WANG, H., KE, H., NIKOLAEV, V. O. & JAFFE, L. A. 2009. Cyclic GMP from the surrounding somatic cells regulates cyclic AMP and meiosis in the mouse oocyte. *Development,* 136**,** 1869-78.
NTOSTIS, P., CARTER, D., ILES, D., HUNTRISS, J., TZETIS, M. & MILLER, D. 2017. Potential sperm contributions to the murine zygote predicted by in silico analysis. *Reproduction,* 154**,** 777-788.
O'DOHERTY, A. M., O'SHEA, L. C. & FAIR, T. 2012. Bovine DNA methylation imprints are established in an oocyte size-specific manner, which are coordinated with the expression of the DNMT3 family proteins. *Biol Reprod,* 86**,** 67.
O'MEARA, C. M., MURRAY, J. D., MAMO, S., GALLAGHER, E., ROCHE, J. & LONERGAN, P. 2011. Gene silencing in bovine zygotes: siRNA transfection versus microinjection. *Reprod Fertil Dev,* 23**,** 534-43.
OBATA, Y. & KONO, T. 2002. Maternal primary imprinting is established at a specific time for each gene throughout oocyte growth. *J Biol Chem,* 277**,** 5285-9.
OHINATA, Y., OHTA, H., SHIGETA, M., YAMANAKA, K., WAKAYAMA, T. & SAITOU, M. 2009. A signaling principle for the specification of the germ cell lineage in mice. *Cell,* 137**,** 571-84.
OHINATA, Y., PAYER, B., O'CARROLL, D., ANCELIN, K., ONO, Y., SANO, M., BARTON, S. C., OBUKHANYCH, T., NUSSENZWEIG, M., TARAKHOVSKY, A., SAITOU, M. & SURANI, M. A. 2005. Blimp1 is a critical determinant of the germ cell lineage in mice. *Nature,* 436**,** 207-213.

OHNO, R., NAKAYAMA, M., NARUSE, C., OKASHITA, N., TAKANO, O., TACHIBANA, M., ASANO, M., SAITOU, M. & SEKI, Y. 2013. A replication-dependent passive mechanism modulates DNA demethylation in mouse primordial germ cells. *Development,* 140**,** 2892-903.

OHSUGI, M., ZHENG, P., BAIBAKOV, B., LI, L. & DEAN, J. 2008. Maternally derived FILIA-MATER complex localizes asymmetrically in cleavage-stage mouse embryos. *Development,* 135**,** 259-69.

OHSUMI, K., KOYANAGI, A., YAMAMOTO, T. M., GOTOH, T. & KISHIMOTO, T. 2004. Emi1-mediated M-phase arrest in Xenopus eggs is distinct from cytostatic factor arrest. *Proc Natl Acad Sci U S A,* 101**,** 12531-6.

OKADA, Y. & YAMAGUCHI, K. 2017. Epigenetic modifications and reprogramming in paternal pronucleus: sperm, preimplantation embryo, and beyond. *Cell Mol Life Sci,* 74**,** 1957-1967.

OKANO, M., BELL, D. W., HABER, D. A. & LI, E. 1999. DNA methyltransferases Dnmt3a and Dnmt3b are essential for de novo methylation and mammalian development. *Cell,* 99**,** 247-57.

OKTEM, O. & URMAN, B. 2010. Understanding follicle growth in vivo. *Hum Reprod,* 25**,** 2944-54.

OOI, S. K., QIU, C., BERNSTEIN, E., LI, K., JIA, D., YANG, Z., ERDJUMENT-BROMAGE, H., TEMPST, P., LIN, S. P., ALLIS, C. D., CHENG, X. & BESTOR, T. H. 2007. DNMT3L connects unmethylated lysine 4 of histone H3 to de novo methylation of DNA. *Nature,* 448**,** 714-7.

OREN-BENAROYA, R., ORVIETO, R., GAKAMSKY, A., PINCHASOV, M. & EISENBACH, M. 2008. The sperm chemoattractant secreted from human cumulus cells is progesterone. *Hum Reprod,* 23**,** 2339-45.

ORSI, N. M. & LEESE, H. J. 2004. Ammonium exposure and pyruvate affect the amino acid metabolism of bovine blastocysts in vitro. *Reproduction,* 127**,** 131-40.

OTSUKA, F., MOORE, R. K., IEMURA, S., UENO, N. & SHIMASAKI, S. 2001. Follistatin inhibits the function of the oocyte-derived factor BMP-15. *Biochem Biophys Res Commun,* 289**,** 961-6.

OTSUKA, F. & SHIMASAKI, S. 2002. A negative feedback system between oocyte bone morphogenetic protein 15 and granulosa cell kit ligand: its role in regulating granulosa cell mitosis. *Proc Natl Acad Sci U S A,* 99**,** 8060-5.

OTSUKA, F., YAO, Z. X., LEE, T. H., YAMAMOTO, S., ERICKSON, G. F. & SHIMASAKI, S. 2000. Bone morphogenetic protein-15 - Identification of target cells and biological functions. *Journal of Biological Chemistry,* 275**,** 39523-39528.

PALAUQUI, J. C., ELMAYAN, T., POLLIEN, J. M. & VAUCHERET, H. 1997. Systemic acquired silencing: transgene-specific post-transcriptional silencing is transmitted by grafting from silenced stocks to non-silenced scions. *EMBO J,* 16**,** 4738-45.

PAN, B. & LI, J. 2019. The art of oocyte meiotic arrest regulation. *Reprod Biol Endocrinol,* 17**,** 8.

PAN, H., O'BRIEN M, J., WIGGLESWORTH, K., EPPIG, J. J. & SCHULTZ, R. M. 2005. Transcript profiling during mouse oocyte development and the effect of gonadotropin priming and development in vitro. *Dev Biol,* 286**,** 493-506.

PAN, Y., JING, J., QIAO, L., LIU, J., ZHAO, J., AN, L., LI, B., WANG, W., LIANG, C. & LIU, W. 2018. miR-124-3p affects the formation of intramuscular fat through alterations in branched chain amino acid consumption in sheep. *Biochem Biophys Res Commun,* 495**,** 1769-1774.

PAN, Z., ZHANG, J., LI, Q., LI, Y., SHI, F., XIE, Z. & LIU, H. 2012. Current advances in epigenetic modification and alteration during mammalian ovarian folliculogenesis. *J Genet Genomics,* 39**,** 111-23.

PANGAS, S. A., CHOI, Y., BALLOW, D. J., ZHAO, Y., WESTPHAL, H., MATZUK, M. M. & RAJKOVIC, A. 2006. Oogenesis requires germ cell-specific transcriptional regulators Sohlh1 and Lhx8. *Proc Natl Acad Sci U S A,* 103**,** 8090-5.

PANIGONE, S., HSIEH, M., FU, M., PERSANI, L. & CONTI, M. 2008. Luteinizing hormone signaling in preovulatory follicles involves early activation of the epidermal growth factor receptor pathway. *Mol Endocrinol,* 22**,** 924-36.

PANKHURST, M. W. 2017. A putative role for anti-Mullerian hormone (AMH) in optimising ovarian reserve expenditure. *J Endocrinol,* 233**,** R1-R13.

PANSKY, B. & MOSSMAN, H. W. 1953. The regenerative capacity of the rabbit ovary. *Anat Rec,* 116**,** 19-51.

PARIS, J. & RICHTER, J. D. 1990. Maturation-specific polyadenylation and translational control: diversity of cytoplasmic polyadenylation elements, influence of poly(A) tail size, and formation of stable polyadenylation complexes. *Mol Cell Biol,* 10**,** 5634-45.

PARK, C. Y., CHOI, Y. S. & MCMANUS, M. T. 2010. Analysis of microRNA knockouts in mice. *Hum Mol Genet,* 19**,** R169-75.

PARK, J. Y., SU, Y. Q., ARIGA, M., LAW, E., JIN, S. L. & CONTI, M. 2004. EGF-like growth factors as mediators of LH action in the ovulatory follicle. *Science,* 303**,** 682-4.

PARRISH, J. J., KROGENAES, A. & SUSKO-PARRISH, J. L. 1995. Effect of bovine sperm separation by either swim-up or Percoll method on success of in vitro fertilization and early embryonic development. *Theriogenology,* 44**,** 859-69.

PARROTT, J. A. & SKINNER, M. K. 1999. Kit-ligand/stem cell factor induces primordial follicle development and initiates folliculogenesis. *Endocrinology,* 140**,** 4262-71.

PARRY, D. A., LOGAN, C. V., HAYWARD, B. E., SHIRES, M., LANDOLSI, H., DIGGLE, C., CARR, I., RITTORE, C., TOUITOU, I., PHILIBERT, L., FISHER, R. A., FALLAHIAN, M., HUNTRISS, J. D., PICTON, H. M., MALIK, S., TAYLOR, G. R., JOHNSON, C. A., BONTHRON, D. T. & SHERIDAN, E. G. 2011. Mutations causing familial biparental hydatidiform mole implicate c6orf221 as a possible regulator of genomic imprinting in the human oocyte. *Am J Hum Genet,* 89**,** 451-8.

PARTE, S., BHARTIYA, D., TELANG, J., DAITHANKAR, V., SALVI, V., ZAVERI, K. & HINDUJA, I. 2011. Detection, characterization, and spontaneous differentiation in vitro of very small embryonic-like putative stem cells in adult mammalian ovary. *Stem Cells Dev,* 20**,** 1451-64.

PAYER, B., SAITOU, M., BARTON, S. C., THRESHER, R., DIXON, J. P., ZAHN, D., COLLEDGE, W. H., CARLTON, M. B., NAKANO, T. & SURANI, M. A. 2003. Stella is a maternal effect gene required for normal early development in mice. *Curr Biol,* 13**,** 2110-7.

PAYNE, C. & SCHATTEN, G. 2003. Golgi dynamics during meiosis are distinct from mitosis and are coupled to endoplasmic reticulum dynamics until fertilization. *Dev Biol,* 264**,** 50-63.

PAYNTON, B. V., REMPEL, R. & BACHVAROVA, R. 1988. Changes in state of adenylation and time course of degradation of maternal mRNAs during oocyte maturation and early embryonic development in the mouse. *Dev Biol,* 129**,** 304-14.

PEDDINTI, D., MEMILI, E. & BURGESS, S. C. 2010. Proteomics-based systems biology modeling of bovine germinal vesicle stage oocyte and cumulus cell interaction. *PLoS One,* 5**,** e11240.

PENG, H., CHANG, B., LU, C., SU, J., WU, Y., LV, P., WANG, Y., LIU, J., ZHANG, B., QUAN, F., GUO, Z. & ZHANG, Y. 2012. Nlrp2, a maternal effect gene required for early embryonic development in the mouse. *PLoS One,* 7**,** e30344.

PENG, X. R., HSUEH, A. J., LAPOLT, P. S., BJERSING, L. & NY, T. 1991. Localization of luteinizing hormone receptor messenger ribonucleic acid expression in ovarian cell types during follicle development and ovulation. *Endocrinology,* 129**,** 3200-7.

PENNETIER, S., UZBEKOVA, S., PERREAU, C., PAPILLIER, P., MERMILLOD, P. & DALBIES-TRAN, R. 2004. Spatio-temporal expression of the germ cell marker

genes MATER, ZAR1, GDF9, BMP15,andVASA in adult bovine tissues, oocytes, and preimplantation embryos. *Biol Reprod,* 71**,** 1359-66.
PEPLING, M. E. 2006. From primordial germ cell to primordial follicle: mammalian female germ cell development. *Genesis,* 44**,** 622-32.
PEPLING, M. E. & SPRADLING, A. C. 1998. Female mouse germ cells form synchronously dividing cysts. *Development,* 125**,** 3323-8.
PEPLING, M. E. & SPRADLING, A. C. 2001. Mouse ovarian germ cell cysts undergo programmed breakdown to form primordial follicles. *Dev Biol,* 234**,** 339-51.
PERSENGIEV, S. P., ZHU, X. & GREEN, M. R. 2004. Nonspecific, concentration-dependent stimulation and repression of mammalian gene expression by small interfering RNAs (siRNAs). *RNA,* 10**,** 12-8.
PETRUSSA, L., VAN DE VELDE, H. & DE RYCKE, M. 2014. Dynamic regulation of DNA methyltransferases in human oocytes and preimplantation embryos after assisted reproductive technologies. *Mol Hum Reprod,* 20**,** 861-74.
PICELLI, S., FARIDANI, O. R., BJORKLUND, A. K., WINBERG, G., SAGASSER, S. & SANDBERG, R. 2014. Full-length RNA-seq from single cells using Smart-seq2. *Nat Protoc,* 9**,** 171-81.
PICTON, H., BRIGGS, D. & GOSDEN, R. 1998. The molecular basis of oocyte growth and development. *Mol Cell Endocrinol,* 145**,** 27-37.
PICTON, H. M. 2001. Activation of follicle development: the primordial follicle. *Theriogenology,* 55**,** 1193-210.
PICTON, H. M. & MCNEILLY, A. S. 1991. Evidence to support a follicle-stimulating hormone threshold theory for follicle selection in ewes chronically treated with gonadotrophin-releasing hormone agonist. *J Reprod Fertil,* 93**,** 43-51.
PIERRE, A., GAUTIER, M., CALLEBAUT, I., BONTOUX, M., JEANPIERRE, E., PONTAROTTI, P. & MONGET, P. 2007. Atypical structure and phylogenomic evolution of the new eutherian oocyte- and embryo-expressed KHDC1/DPPA5/ECAT1/OOEP gene family. *Genomics,* 90**,** 583-94.
PLASTERK, R. H. 2002. RNA silencing: the genome's immune system. *Science,* 296**,** 1263-5.
PODOLSKA, K. & SVOBODA, P. 2011. Targeting genes in living mammals by RNA interference. *Brief Funct Genomics,* 10**,** 238-47.
POLI, M., ORI, A., CHILD, T., JAROUDI, S., SPATH, K., BECK, M. & WELLS, D. 2015. Characterization and quantification of proteins secreted by single human embryos prior to implantation. *EMBO Mol Med,* 7**,** 1465-79.
PORRAS-GOMEZ, T. J. & MORENO-MENDOZA, N. 2017. Neo-oogenesis in mammals. *Zygote,* 25**,** 404-422.
POSADA, J., YEW, N., AHN, N. G., VANDE WOUDE, G. F. & COOPER, J. A. 1993. Mos stimulates MAP kinase in Xenopus oocytes and activates a MAP kinase kinase in vitro. *Mol Cell Biol,* 13**,** 2546-53.
POYNTON, R. A. & HAMPTON, M. B. 2014. Peroxiredoxins as biomarkers of oxidative stress. *Biochim Biophys Acta,* 1840**,** 906-12.
PUGA MOLINA, L. C., LUQUE, G. M., BALESTRINI, P. A., MARIN-BRIGGILER, C. I., ROMAROWSKI, A. & BUFFONE, M. G. 2018. Molecular Basis of Human Sperm Capacitation. *Front Cell Dev Biol,* 6**,** 72.
QI, S. T., MA, J. Y., WANG, Z. B., GUO, L., HOU, Y. & SUN, Q. Y. 2016. N6-Methyladenosine Sequencing Highlights the Involvement of mRNA Methylation in Oocyte Meiotic Maturation and Embryo Development by Regulating Translation in Xenopus laevis. *J Biol Chem,* 291**,** 23020-23026.
QIAN, J., NGUYEN, N. M. P., REZAEI, M., HUANG, B., TAO, Y., ZHANG, X., CHENG, Q., YANG, H., ASANGLA, A., MAJEWSKI, J. & SLIM, R. 2018. Biallelic PADI6 variants linking infertility, miscarriages, and hydatidiform moles. *Eur J Hum Genet,* 26**,** 1007-1013.
QIN, Y., TANG, T., LI, W., LIU, Z., YANG, X., SHI, X., SUN, G., LIU, X., WANG, M., LIANG, X., CONG, P., MO, D., LIU, X., CHEN, Y. & HE, Z. 2019. Bone

Morphogenetic Protein 15 Knockdown Inhibits Porcine Ovarian Follicular Development and Ovulation. *Front Cell Dev Biol,* 7**,** 286.
QUENNEVILLE, S., VERDE, G., CORSINOTTI, A., KAPOPOULOU, A., JAKOBSSON, J., OFFNER, S., BAGLIVO, I., PEDONE, P. V., GRIMALDI, G., RICCIO, A. & TRONO, D. 2011. In embryonic stem cells, ZFP57/KAP1 recognize a methylated hexanucleotide to affect chromatin and DNA methylation of imprinting control regions. *Mol Cell,* 44**,** 361-72.
QUINLAN, A. R. 2014. BEDTools: The Swiss-Army Tool for Genome Feature Analysis. *Curr Protoc Bioinformatics,* 47**,** 11 12 1-34.
QUINN, P. & HORSTMAN, F. C. 1998. Is the mouse a good model for the human with respect to the development of the preimplantation embryo in vitro? *Hum Reprod,* 13 Suppl 4**,** 173-83.
RACEDO, S. E., RAWE, V. Y. & NIEMANN, H. 2012. Dynamic changes of the Golgi apparatus during bovine in vitro oocyte maturation. *Reproduction,* 143**,** 439-47.
RACEDO, S. E., WRENZYCKI, C., LEPIKHOV, K., SALAMONE, D., WALTER, J. & NIEMANN, H. 2009. Epigenetic modifications and related mRNA expression during bovine oocyte in vitro maturation. *Reprod Fertil Dev,* 21**,** 738-48.
RAHMAN, M. S., KWON, W. S. & PANG, M. G. 2017. Prediction of male fertility using capacitation-associated proteins in spermatozoa. *Mol Reprod Dev,* 84**,** 749-759.
RAIJMAKERS, R., ZENDMAN, A. J., EGBERTS, W. V., VOSSENAAR, E. R., RAATS, J., SOEDE-HUIJBREGTS, C., RUTJES, F. P., VAN VEELEN, P. A., DRIJFHOUT, J. W. & PRUIJN, G. J. 2007. Methylation of arginine residues interferes with citrullination by peptidylarginine deiminases in vitro. *J Mol Biol,* 367**,** 1118-29.
RAJKOVIC, A., PANGAS, S. A., BALLOW, D., SUZUMORI, N. & MATZUK, M. M. 2004. NOBOX deficiency disrupts early folliculogenesis and oocyte-specific gene expression. *Science,* 305**,** 1157-9.
RAKYAN, V. K., DOWN, T. A., THORNE, N. P., FLICEK, P., KULESHA, E., GRAF, S., TOMAZOU, E. M., BACKDAHL, L., JOHNSON, N., HERBERTH, M., HOWE, K. L., JACKSON, D. K., MIRETTI, M. M., FIEGLER, H., MARIONI, J. C., BIRNEY, E., HUBBARD, T. J., CARTER, N. P., TAVARE, S. & BECK, S. 2008. An integrated resource for genome-wide identification and analysis of human tissue-specific differentially methylated regions (tDMRs). *Genome Res,* 18**,** 1518-29.
RAMBAGS, B. P., VAN BOXTEL, D. C., THARASANIT, T., LENSTRA, J. A., COLENBRANDER, B. & STOUT, T. A. 2014. Advancing maternal age predisposes to mitochondrial damage and loss during maturation of equine oocytes in vitro. *Theriogenology,* 81**,** 959-65.
RAMOS, S. B., STUMPO, D. J., KENNINGTON, E. A., PHILLIPS, R. S., BOCK, C. B., RIBEIRO-NETO, F. & BLACKSHEAR, P. J. 2004. The CCCH tandem zinc-finger protein Zfp36l2 is crucial for female fertility and early embryonic development. *Development,* 131**,** 4883-93.
RANKIN, T., TALBOT, P., LEE, E. & DEAN, J. 1999. Abnormal zonae pellucidae in mice lacking ZP1 result in early embryonic loss. *Development,* 126**,** 3847-55.
RASMUSSEN, K. D. & HELIN, K. 2016. Role of TET enzymes in DNA methylation, development, and cancer. *Genes Dev,* 30**,** 733-50.
REBOLLEDO-JARAMILLO, B., SU, M. S., STOLER, N., MCELHOE, J. A., DICKINS, B., BLANKENBERG, D., KORNELIUSSEN, T. S., CHIAROMONTE, F., NIELSEN, R., HOLLAND, M. M., PAUL, I. M., NEKRUTENKO, A. & MAKOVA, K. D. 2014. Maternal age effect and severe germ-line bottleneck in the inheritance of human mitochondrial DNA. *Proc Natl Acad Sci U S A,* 111**,** 15474-9.
REDDY, P., SHEN, L., REN, C., BOMAN, K., LUNDIN, E., OTTANDER, U., LINDGREN, P., LIU, Y. X., SUN, Q. Y. & LIU, K. 2005. Activation of Akt (PKB) and suppression of FKHRL1 in mouse and rat oocytes by stem cell factor during follicular activation and development. *Dev Biol,* 281**,** 160-70.

REDDY, R., AKOURY, E., PHUONG NGUYEN, N. M., ABDUL-RAHMAN, O. A., DERY, C., GUPTA, N., DALEY, W. P., AO, A., LANDOLSI, H., ANN FISHER, R., TOUITOU, I. & SLIM, R. 2013. Report of four new patients with protein-truncating mutations in C6orf221/KHDC3L and colocalization with NLRP7. *Eur J Hum Genet,* 21**,** 957-64.

REDDY, R., NGUYEN, N. M., SARRABAY, G., REZAEI, M., RIVAS, M. C., KAVASOGLU, A., BERKIL, H., ELSHAFEY, A., ABDALLA, E., NUNEZ, K. P., DREYFUS, H., PHILIPPE, M., HADIPOUR, Z., DURMAZ, A., EATON, E. E., SCHUBERT, B., ULKER, V., HADIPOUR, F., TOUITOU, I., FARDAEI, M. & SLIM, R. 2016. The genomic architecture of NLRP7 is Alu rich and predisposes to disease-associated large deletions. *Eur J Hum Genet,* 24**,** 1516.

REECE-HOYES, J. S. & WALHOUT, A. J. M. 2018. Gateway Recombinational Cloning. *Cold Spring Harb Protoc,* 2018.

REIK, W., DEAN, W. & WALTER, J. 2001. Epigenetic reprogramming in mammalian development. *Science,* 293**,** 1089-93.

REIK, W. & WALTER, J. 2001a. Evolution of imprinting mechanisms: the battle of the sexes begins in the zygote. *Nat Genet,* 27**,** 255-6.

REIK, W. & WALTER, J. 2001b. Genomic imprinting: parental influence on the genome. *Nat Rev Genet,* 2**,** 21-32.

REIMANN, J. D., FREED, E., HSU, J. Y., KRAMER, E. R., PETERS, J. M. & JACKSON, P. K. 2001. Emi1 is a mitotic regulator that interacts with Cdc20 and inhibits the anaphase promoting complex. *Cell,* 105**,** 645-55.

REPETTO, G., DEL PESO, A. & ZURITA, J. L. 2008. Neutral red uptake assay for the estimation of cell viability/cytotoxicity. *Nat Protoc,* 3**,** 1125-31.

REYES, J. M., CHITWOOD, J. L. & ROSS, P. J. 2015. RNA-Seq profiling of single bovine oocyte transcript abundance and its modulation by cytoplasmic polyadenylation. *Mol Reprod Dev,* 82**,** 103-14.

REYES, J. M. & ROSS, P. J. 2016. Cytoplasmic polyadenylation in mammalian oocyte maturation. *Wiley Interdiscip Rev RNA,* 7**,** 71-89.

REZAEI, M., NGUYEN, N. M., FOROUGHINIA, L., DASH, P., AHMADPOUR, F., VERMA, I. C., SLIM, R. & FARDAEI, M. 2016. Two novel mutations in the KHDC3L gene in Asian patients with recurrent hydatidiform mole. *Hum Genome Var,* 3**,** 16027.

RICHARDS, A. J., ENDERS, G. C. & RESNICK, J. L. 1999. Activin and TGFbeta limit murine primordial germ cell proliferation. *Dev Biol,* 207**,** 470-5.

RIGGS, A. D. 1975. X inactivation, differentiation, and DNA methylation. *Cytogenet Cell Genet,* 14**,** 9-25.

RIMON-DAHARI, N., YERUSHALMI-HEINEMANN, L., ALYAGOR, L. & DEKEL, N. 2016. Ovarian Folliculogenesis. *Results Probl Cell Differ,* 58**,** 167-90.

RISO, V., CAMMISA, M., KUKREJA, H., ANVAR, Z., VERDE, G., SPARAGO, A., ACURZIO, B., LAD, S., LONARDO, E., SANKAR, A., HELIN, K., FEIL, R., FICO, A., ANGELINI, C., GRIMALDI, G. & RICCIO, A. 2016. ZFP57 maintains the parent-of-origin-specific expression of the imprinted genes and differentially affects non-imprinted targets in mouse embryonic stem cells. *Nucleic Acids Res,* 44**,** 8165-78.

ROBERT, C., MCGRAW, S., MASSICOTTE, L., PRAVETONI, M., GANDOLFI, F. & SIRARD, M. A. 2002. Quantification of housekeeping transcript levels during the development of bovine preimplantation embryos. *Biol Reprod,* 67**,** 1465-72.

ROBERT, C., NIEMINEN, J., DUFORT, I., GAGNE, D., GRANT, J. R., CAGNONE, G., PLOURDE, D., NIVET, A. L., FOURNIER, E., PAQUET, E., BLAZEJCZYK, M., RIGAULT, P., JUGE, N. & SIRARD, M. A. 2011. Combining resources to obtain a comprehensive survey of the bovine embryo transcriptome through deep sequencing and microarrays. *Mol Reprod Dev,* 78**,** 651-64.

ROBINSON, M. D., MCCARTHY, D. J. & SMYTH, G. K. 2010. edgeR: a Bioconductor package for differential expression analysis of digital gene expression data. *Bioinformatics,* 26**,** 139-40.
RODDA, D. J., CHEW, J. L., LIM, L. H., LOH, Y. H., WANG, B., NG, H. H. & ROBSON, P. 2005. Transcriptional regulation of nanog by OCT4 and SOX2. *J Biol Chem,* 280**,** 24731-7.
RODGERS, R. J. & IRVING-RODGERS, H. F. 2010. Formation of the ovarian follicular antrum and follicular fluid. *Biol Reprod,* 82**,** 1021-9.
ROELES, J. & TSIAVALIARIS, G. 2019. Actin-microtubule interplay coordinates spindle assembly in human oocytes. *Nat Commun,* 10**,** 4651.
ROGERS, G. E., HARDING, H. W. & LLEWELLYN-SMITH, I. J. 1977. The origin of citrulline-containing proteins in the hair follicle and the chemical nature of trichohyalin, an intracellular precursor. *Biochim Biophys Acta,* 495**,** 159-75.
ROHWEDER, B., SEMMELMANN, F., ENDRES, C. & STERNER, R. 2018. Standardized cloning vectors for protein production and generation of large gene libraries in Escherichia coli. *Biotechniques,* 64**,** 24-26.
ROMAR, R., DE SANTIS, T., PAPILLIER, P., PERREAU, C., THELIE, A., DELL'AQUILA, M. E., MERMILLOD, P. & DALBIES-TRAN, R. 2011. Expression of maternal transcripts during bovine oocyte in vitro maturation is affected by donor age. *Reprod Domest Anim,* 46**,** e23-30.
RONG, Y., JI, S. Y., ZHU, Y. Z., WU, Y. W., SHEN, L. & FAN, H. Y. 2019. ZAR1 and ZAR2 are required for oocyte meiotic maturation by regulating the maternal transcriptome and mRNA translational activation. *Nucleic Acids Res,* 47**,** 11387-11402.
ROOVERS, E. F., ROSENKRANZ, D., MAHDIPOUR, M., HAN, C. T., HE, N., CHUVA DE SOUSA LOPES, S. M., VAN DER WESTERLAKEN, L. A., ZISCHLER, H., BUTTER, F., ROELEN, B. A. & KETTING, R. F. 2015. Piwi proteins and piRNAs in mammalian oocytes and early embryos. *Cell Rep,* 10**,** 2069-82.
ROSANO, G. L. & CECCARELLI, E. A. 2014. Recombinant protein expression in Escherichia coli: advances and challenges. *Front Microbiol,* 5**,** 172.
ROSE, R., ROSE, M. & OTTMANN, C. 2012. Identification and structural characterization of two 14-3-3 binding sites in the human peptidylarginine deiminase type VI. *J Struct Biol,* 180**,** 65-72.
ROSSANT, J. & TAM, P. P. 2009. Blastocyst lineage formation, early embryonic asymmetries and axis patterning in the mouse. *Development,* 136**,** 701-13.
ROTH, B. M., PRUSS, G. J. & VANCE, V. B. 2004. Plant viral suppressors of RNA silencing. *Virus Res,* 102**,** 97-108.
ROVANI, M. T., GASPERIN, B. G., FERREIRA, R., DUGGAVATHI, R., BORDIGNON, V. & GONCALVES, P. B. D. 2017. Methods to study ovarian function in monovulatory species using the cow as a model. *Animal Reproduction,* 14**,** 383-391.
RUGG-GUNN, P. J., FERGUSON-SMITH, A. C. & PEDERSEN, R. A. 2007. Status of genomic imprinting in human embryonic stem cells as revealed by a large cohort of independently derived and maintained lines. *Hum Mol Genet,* 16 Spec No. 2**,** R243-51.
RUSSELL, D. L., GILCHRIST, R. B., BROWN, H. M. & THOMPSON, J. G. 2016. Bidirectional communication between cumulus cells and the oocyte: Old hands and new players? *Theriogenology,* 86**,** 62-8.
SAADEH, H. & SCHULZ, R. 2014. Protection of CpG islands against de novo DNA methylation during oogenesis is associated with the recognition site of E2f1 and E2f2. *Epigenetics Chromatin,* 7**,** 26.
SAGAN, S. M. & SARNOW, P. 2013. Molecular biology. RNAi, Antiviral after all. *Science,* 342**,** 207-8.
SAGATA, N. 1996. Meiotic metaphase arrest in animal oocytes: its mechanisms and biological significance. *Trends Cell Biol,* 6**,** 22-8.

SAITO, K. & SIOMI, M. C. 2010. Small RNA-mediated quiescence of transposable elements in animals. *Dev Cell,* 19**,** 687-97.
SAITOU, M., PAYER, B., O'CARROLL, D., OHINATA, Y. & SURANI, M. A. 2005. Blimp1 and the emergence of the germ line during development in the mouse. *Cell Cycle,* 4**,** 1736-40.
SAKASHITA, A., KOBAYASHI, H., WAKAI, T., SOTOMARU, Y., HATA, K. & KONO, T. 2014. Dynamics of genomic 5-hydroxymethylcytosine during mouse oocyte growth. *Genes Cells,* 19**,** 629-36.
SALHA, O., ABUSHEIKHA, N. & SHARMA, V. 1998. Dynamics of human follicular growth and in-vitro oocyte maturation. *Hum Reprod Update,* 4**,** 816-32.
SALILEW-WONDIM, D., SAEED-ZIDANE, M., HOELKER, M., GEBREMEDHN, S., POIRIER, M., PANDEY, H. O., THOLEN, E., NEUHOFF, C., HELD, E., BESENFELDER, U., HAVLICEK, V., RINGS, F., FOURNIER, E., GAGNE, D., SIRARD, M. A., ROBERT, C., GAD, A., SCHELLANDER, K. & TESFAYE, D. 2018. Genome-wide DNA methylation patterns of bovine blastocysts derived from in vivo embryos subjected to in vitro culture before, during or after embryonic genome activation. *BMC Genomics,* 19**,** 424.
SAMWER, M., DEHNE, H. J., SPIRA, F., KOLLMAR, M., GERLICH, D. W., URLAUB, H. & GORLICH, D. 2013. The nuclear F-actin interactome of Xenopus oocytes reveals an actin-bundling kinesin that is essential for meiotic cytokinesis. *EMBO J,* 32**,** 1886-902.
SANCHEZ-DELGADO, M., MARTIN-TRUJILLO, A., TAYAMA, C., VIDAL, E., ESTELLER, M., IGLESIAS-PLATAS, I., DEO, N., BARNEY, O., MACLEAN, K., HATA, K., NAKABAYASHI, K., FISHER, R. & MONK, D. 2015. Absence of Maternal Methylation in Biparental Hydatidiform Moles from Women with NLRP7 Maternal-Effect Mutations Reveals Widespread Placenta-Specific Imprinting. *PLoS Genet,* 11**,** e1005644.
SANCHEZ, F. & SMITZ, J. 2012. Molecular control of oogenesis. *Biochim Biophys Acta,* 1822**,** 1896-912.
SANDERS, J. R. & SWANN, K. 2016. Molecular triggers of egg activation at fertilization in mammals. *Reproduction,* 152**,** R41-50.
SANFINS, A., RODRIGUES, P. & ALBERTINI, D. F. 2018. GDF-9 and BMP-15 direct the follicle symphony. *J Assist Reprod Genet,* 35**,** 1741-1750.
SANTOS, F., HENDRICH, B., REIK, W. & DEAN, W. 2002. Dynamic reprogramming of DNA methylation in the early mouse embryo. *Dev Biol,* 241**,** 172-82.
SANTOS, F., PETERS, A. H., OTTE, A. P., REIK, W. & DEAN, W. 2005. Dynamic chromatin modifications characterise the first cell cycle in mouse embryos. *Dev Biol,* 280**,** 225-36.
SANTOS, R. R., SCHOEVERS, E. J. & ROELEN, B. A. 2014. Usefulness of bovine and porcine IVM/IVF models for reproductive toxicology. *Reprod Biol Endocrinol,* 12**,** 117.
SASAKI, H. & MATSUI, Y. 2008. Epigenetic events in mammalian germ-cell development: reprogramming and beyond. *Nat Rev Genet,* 9**,** 129-40.
SASKOVA, A., SOLC, P., BARAN, V., KUBELKA, M., SCHULTZ, R. M. & MOTLIK, J. 2008. Aurora kinase A controls meiosis I progression in mouse oocytes. *Cell Cycle,* 7**,** 2368-76.
SATHANANTHAN, A. H. 1997. Mitosis in the human embryo: the vital role of the sperm centrosome (centriole). *Histol Histopathol,* 12**,** 827-56.
SATO, M., KIMURA, T., KUROKAWA, K., FUJITA, Y., ABE, K., MASUHARA, M., YASUNAGA, T., RYO, A., YAMAMOTO, M. & NAKANO, T. 2002. Identification of PGC7, a new gene expressed specifically in preimplantation embryos and germ cells. *Mech Dev,* 113**,** 91-4.
SCHATTEN, G. 1994. The centrosome and its mode of inheritance: the reduction of the centrosome during gametogenesis and its restoration during fertilization. *Dev Biol,* 165**,** 299-335.

SCHIER, A. F. 2007. The maternal-zygotic transition: death and birth of RNAs. *Science,* 316**,** 406-7.
SCHLAFKE, S. & ENDERS, A. C. 1967. Cytological changes during cleavage and blastocyst formation in the rat. *J Anat,* 102**,** 13-32.
SCHMIDT, D., OVITT, C. E., ANLAG, K., FEHSENFELD, S., GREDSTED, L., TREIER, A. C. & TREIER, M. 2004. The murine winged-helix transcription factor Foxl2 is required for granulosa cell differentiation and ovary maintenance. *Development,* 131**,** 933-42.
SCHUH, M. & ELLENBERG, J. 2008. A new model for asymmetric spindle positioning in mouse oocytes. *Curr Biol,* 18**,** 1986-92.
SCHULTZ, R. M. 2002. The molecular foundations of the maternal to zygotic transition in the preimplantation embryo. *Hum Reprod Update,* 8**,** 323-31.
SCHULZ, L. C., EZASHI, T., DAS, P., WESTFALL, S. D., LIVINGSTON, K. A. & ROBERTS, R. M. 2008. Human embryonic stem cells as models for trophoblast differentiation. *Placenta,* 29 Suppl A**,** S10-6.
SEKI, Y., YAMAJI, M., YABUTA, Y., SANO, M., SHIGETA, M., MATSUI, Y., SAGA, Y., TACHIBANA, M., SHINKAI, Y. & SAITOU, M. 2007. Cellular dynamics associated with the genome-wide epigenetic reprogramming in migrating primordial germ cells in mice. *Development,* 134**,** 2627-38.
SELA-ABRAMOVICH, S., EDRY, I., GALIANI, D., NEVO, N. & DEKEL, N. 2006. Disruption of gap junctional communication within the ovarian follicle induces oocyte maturation. *Endocrinology,* 147**,** 2280-6.
SEN, G. L. & BLAU, H. M. 2005. Argonaute 2/RISC resides in sites of mammalian mRNA decay known as cytoplasmic bodies. *Nat Cell Biol,* 7**,** 633-6.
SENFT, A. D., BIKOFF, E. K., ROBERTSON, E. J. & COSTELLO, I. 2019. Genetic dissection of Nodal and Bmp signalling requirements during primordial germ cell development in mouse. *Nat Commun,* 10**,** 1089.
SENSHU, T., AKIYAMA, K., ISHIGAMI, A. & NOMURA, K. 1999. Studies on specificity of peptidylarginine deiminase reactions using an immunochemical probe that recognizes an enzymatically deiminated partial sequence of mouse keratin K1. *J Dermatol Sci,* 21**,** 113-26.
SEPULVEDA-RINCON, L. P., DUBE, D., ADENOT, P., LAFFONT, L., RUFFINI, S., GALL, L., CAMPBELL, B. K., DURANTHON, V., BEAUJEAN, N. & MAALOUF, W. E. 2016. Random Allocation of Blastomere Descendants to the Trophectoderm and ICM of the Bovine Blastocyst. *Biol Reprod,* 95**,** 123.
SHAFAEI, A., AISHA, A. F., SIDDIQUI, M. J. & ISMAIL, Z. 2015. Analysis of L-citrulline and L-arginine in Ficus deltoidea leaf extracts by reverse phase high performance liquid chromatography. *Pharmacognosy Res,* 7**,** 32-7.
SHARMA, P., LIOUTAS, A., FERNANDEZ-FUENTES, N., QUILEZ, J., CARBONELL-CABALLERO, J., WRIGHT, R. H. G., DI VONA, C., LE DILY, F., SCHULLER, R., EICK, D., OLIVA, B. & BEATO, M. 2019. Arginine Citrullination at the C-Terminal Domain Controls RNA Polymerase II Transcription. *Mol Cell,* 73**,** 84-96 e7.
SHEN, L., INOUE, A., HE, J., LIU, Y., LU, F. & ZHANG, Y. 2014. Tet3 and DNA replication mediate demethylation of both the maternal and paternal genomes in mouse zygotes. *Cell Stem Cell,* 15**,** 459-471.
SHI, Y. & MASSAGUE, J. 2003. Mechanisms of TGF-beta signaling from cell membrane to the nucleus. *Cell,* 113**,** 685-700.
SHIMADA, M., YANAI, Y., OKAZAKI, T., NOMA, N., KAWASHIMA, I., MORI, T. & RICHARDS, J. S. 2008. Hyaluronan fragments generated by sperm-secreted hyaluronidase stimulate cytokine/chemokine production via the TLR2 and TLR4 pathway in cumulus cells of ovulated COCs, which may enhance fertilization. *Development,* 135**,** 2001-11.
SHIRAISHI, K., OKADA, A., SHIRAKAWA, H., NAKANISHI, S., MIKOSHIBA, K. & MIYAZAKI, S. 1995. Developmental changes in the distribution of the endoplasmic reticulum and inositol 1,4,5-trisphosphate receptors and the spatial

pattern of Ca2+ release during maturation of hamster oocytes. *Dev Biol,* 170**,** 594-606.
SILVA, C. C., GROOME, N. P. & KNIGHT, P. G. 1999. Demonstration of a suppressive effect of inhibin alpha-subunit on the developmental competence of in vitro matured bovine oocytes. *J Reprod Fertil,* 115**,** 381-8.
SILVA, C. C. & KNIGHT, P. G. 1998. Modulatory actions of activin-A and follistatin on the developmental competence of in vitro-matured bovine oocytes. *Biol Reprod,* 58**,** 558-65.
SIMSEK-DURAN, F., LI, F., FORD, W., SWANSON, R. J., JONES, H. W., JR. & CASTORA, F. J. 2013. Age-associated metabolic and morphologic changes in mitochondria of individual mouse and hamster oocytes. *PLoS One,* 8**,** e64955.
SIOMI, H. & SIOMI, M. C. 2009. On the road to reading the RNA-interference code. *Nature,* 457**,** 396-404.
SIRARD, M. A. 2018. 40 years of bovine IVF in the new genomic selection context. *Reproduction,* 156**,** R1-R7.
SIRARD, M. A. & BILODEAU, S. 1990. Granulosa cells inhibit the resumption of meiosis in bovine oocytes in vitro. *Biol Reprod,* 43**,** 777-83.
SIRARD, M. A., PARRISH, J. J., WARE, C. B., LEIBFRIED-RUTLEDGE, M. L. & FIRST, N. L. 1988. The culture of bovine oocytes to obtain developmentally competent embryos. *Biol Reprod,* 39**,** 546-52.
SKINNER, M. K. 2005. Regulation of primordial follicle assembly and development. *Hum Reprod Update,* 11**,** 461-71.
SKOTHEIM, R. I., LIND, G. E., MONNI, O., NESLAND, J. M., ABELER, V. M., FOSSA, S. D., DUALE, N., BRUNBORG, G., KALLIONIEMI, O., ANDREWS, P. W. & LOTHE, R. A. 2005. Differentiation of human embryonal carcinomas in vitro and in vivo reveals expression profiles relevant to normal development. *Cancer Res,* 65**,** 5588-98.
SLEDZ, C. A., HOLKO, M., DE VEER, M. J., SILVERMAN, R. H. & WILLIAMS, B. R. 2003. Activation of the interferon system by short-interfering RNAs. *Nat Cell Biol,* 5**,** 834-9.
SLIM, R. & MEHIO, A. 2007. The genetics of hydatidiform moles: new lights on an ancient disease. *Clinical Genetics,* 71**,** 25-34.
SMITZ, J., PICTON, H. M., PLATTEAU, P., RUTHERFORD, A., CORTVRINDT, R., CLYDE, J., NOGUEIRA, D., DEVROEY, P., LYBY, K. & GRONDAHL, C. 2007. Principal findings from a multicenter trial investigating the safety of follicular-fluid meiosis-activating sterol for in vitro maturation of human cumulus-enclosed oocytes. *Fertil Steril,* 87**,** 949-64.
SNOOK, R. R., HOSKEN, D. J. & KARR, T. L. 2011. The biology and evolution of polyspermy: insights from cellular and functional studies of sperm and centrosomal behavior in the fertilized egg. *Reproduction,* 142**,** 779-92.
SNOW, A. J., PURI, P., ACKER-PALMER, A., BOUWMEESTER, T., VIJAYARAGHAVAN, S. & KLINE, D. 2008. Phosphorylation-dependent interaction of tyrosine 3-monooxygenase/tryptophan 5-monooxygenase activation protein (YWHA) with PADI6 following oocyte maturation in mice. *Biol Reprod,* 79**,** 337-47.
SOELLNER, L., BEGEMANN, M., DEGENHARDT, F., GEIPEL, A., EGGERMANN, T. & MANGOLD, E. 2017. Maternal heterozygous NLRP7 variant results in recurrent reproductive failure and imprinting disturbances in the offspring. *Eur J Hum Genet*.
SORENSEN, H. P. & MORTENSEN, K. K. 2005. Advanced genetic strategies for recombinant protein expression in Escherichia coli. *J Biotechnol,* 115**,** 113-28.
SOYAL, S. M., AMLEH, A. & DEAN, J. 2000. FIGalpha, a germ cell-specific transcription factor required for ovarian follicle formation. *Development,* 127**,** 4645-54.
SPICER, L. J., AAD, P. Y., ALLEN, D. T., MAZERBOURG, S., PAYNE, A. H. & HSUEH, A. J. 2008. Growth differentiation factor 9 (GDF9) stimulates proliferation and

inhibits steroidogenesis by bovine theca cells: influence of follicle size on responses to GDF9. *Biol Reprod,* 78**,** 243-53.
SPIKINGS, E. C., ALDERSON, J. & ST JOHN, J. C. 2007. Regulated mitochondrial DNA replication during oocyte maturation is essential for successful porcine embryonic development. *Biol Reprod,* 76**,** 327-35.
SPUNGIN, B., MARGALIT, I. & BREITBART, H. 1995. Sperm exocytosis reconstructed in a cell-free system: evidence for the involvement of phospholipase C and actin filaments in membrane fusion. *J Cell Sci,* 108 (Pt 6)**,** 2525-35.
ST JOHN, J. C. 2012. Transmission, inheritance and replication of mitochondrial DNA in mammals: implications for reproductive processes and infertility. *Cell Tissue Res,* 349**,** 795-808.
ST JOHN, J. C., FACUCHO-OLIVEIRA, J., JIANG, Y., KELLY, R. & SALAH, R. 2010. Mitochondrial DNA transmission, replication and inheritance: a journey from the gamete through the embryo and into offspring and embryonic stem cells. *Hum Reprod Update,* 16**,** 488-509.
ST JOHN, J. C., SRIRATTANA, K., TSAI, T. S. & SUN, X. 2017. The mitochondrial genome: how it drives fertility. *Reprod Fertil Dev,* 30**,** 118-139.
STEBBINS-BOAZ, B., CAO, Q., DE MOOR, C. H., MENDEZ, R. & RICHTER, J. D. 1999. Maskin is a CPEB-associated factor that transiently interacts with eIF-4E. *Mol Cell,* 4**,** 1017-27.
STECKLER, T., WANG, J., BARTOL, F. F., ROY, S. K. & PADMANABHAN, V. 2005. Fetal programming: prenatal testosterone treatment causes intrauterine growth retardation, reduces ovarian reserve and increases ovarian follicular recruitment. *Endocrinology,* 146**,** 3185-93.
STEIN, P., ZENG, F., PAN, H. & SCHULTZ, R. M. 2005. Absence of non-specific effects of RNA interference triggered by long double-stranded RNA in mouse oocytes. *Dev Biol,* 286**,** 464-71.
STERNLICHT, A. L. & SCHULTZ, R. M. 1981. Biochemical studies of mammalian oogenesis: kinetics of accumulation of total and poly(A)-containing RNA during growth of the mouse oocyte. *J Exp Zool,* 215**,** 191-200.
STOGER, R., KUBICKA, P., LIU, C. G., KAFRI, T., RAZIN, A., CEDAR, H. & BARLOW, D. P. 1993. Maternal-specific methylation of the imprinted mouse Igf2r locus identifies the expressed locus as carrying the imprinting signal. *Cell,* 73**,** 61-71.
STOJKOVIC, M., MACHADO, S. A., STOJKOVIC, P., ZAKHARTCHENKO, V., HUTZLER, P., GONCALVES, P. B. & WOLF, E. 2001. Mitochondrial distribution and adenosine triphosphate content of bovine oocytes before and after in vitro maturation: correlation with morphological criteria and developmental capacity after in vitro fertilization and culture. *Biol Reprod,* 64**,** 904-9.
STOKES, P. J., HAWKHEAD, J. A., FAWTHROP, R. K., PICTON, H. M., SHARMA, V., LEESE, H. J. & HOUGHTON, F. D. 2007. Metabolism of human embryos following cryopreservation: implications for the safety and selection of embryos for transfer in clinical IVF. *Hum Reprod,* 22**,** 829-35.
STRICKER, S. A. 2006. Structural reorganizations of the endoplasmic reticulum during egg maturation and fertilization. *Semin Cell Dev Biol,* 17**,** 303-13.
STRUMPF, D., MAO, C. A., YAMANAKA, Y., RALSTON, A., CHAWENGSAKSOPHAK, K., BECK, F. & ROSSANT, J. 2005. Cdx2 is required for correct cell fate specification and differentiation of trophectoderm in the mouse blastocyst. *Development,* 132**,** 2093-102.
STURMEY, R. G., BERMEJO-ALVAREZ, P., GUTIERREZ-ADAN, A., RIZOS, D., LEESE, H. J. & LONERGAN, P. 2010. Amino acid metabolism of bovine blastocysts: a biomarker of sex and viability. *Mol Reprod Dev,* 77**,** 285-96.
STURMEY, R. G., BRISON, D. R. & LEESE, H. J. 2008. Symposium: innovative techniques in human embryo viability assessment. Assessing embryo viability by measurement of amino acid turnover. *Reprod Biomed Online,* 17**,** 486-96.

STURMEY, R. G., HAWKHEAD, J. A., BARKER, E. A. & LEESE, H. J. 2009. DNA damage and metabolic activity in the preimplantation embryo. *Hum Reprod,* 24**,** 81-91.

SU, Y. Q., SUGIURA, K., WOO, Y., WIGGLESWORTH, K., KAMDAR, S., AFFOURTIT, J. & EPPIG, J. J. 2007. Selective degradation of transcripts during meiotic maturation of mouse oocytes. *Dev Biol,* 302**,** 104-17.

SU, Y. Q., WU, X., O'BRIEN, M. J., PENDOLA, F. L., DENEGRE, J. N., MATZUK, M. M. & EPPIG, J. J. 2004. Synergistic roles of BMP15 and GDF9 in the development and function of the oocyte-cumulus cell complex in mice: genetic evidence for an oocyte-granulosa cell regulatory loop. *Dev Biol,* 276**,** 64-73.

SUGIURA, K., SU, Y. Q., DIAZ, F. J., PANGAS, S. A., SHARMA, S., WIGGLESWORTH, K., O'BRIEN, M. J., MATZUK, M. M., SHIMASAKI, S. & EPPIG, J. J. 2007. Oocyte-derived BMP15 and FGFs cooperate to promote glycolysis in cumulus cells. *Development,* 134**,** 2593-603.

SUN, Q. Y. 2003. Cellular and molecular mechanisms leading to cortical reaction and polyspermy block in mammalian eggs. *Microsc Res Tech,* 61**,** 342-8.

SUN, Q. Y. & SCHATTEN, H. 2006. Regulation of dynamic events by microfilaments during oocyte maturation and fertilization. *Reproduction,* 131**,** 193-205.

SUN, S. C. & KIM, N. H. 2013. Molecular mechanisms of asymmetric division in oocytes. *Microsc Microanal,* 19**,** 883-97.

SURANI, M. A. & BARTON, S. C. 1983. Development of gynogenetic eggs in the mouse: implications for parthenogenetic embryos. *Science,* 222**,** 1034-6.

SUSOR, A. & KUBELKA, M. 2017. Translational Regulation in the Mammalian Oocyte. *Results Probl Cell Differ,* 63**,** 257-295.

SUTTON, M. L., GILCHRIST, R. B. & THOMPSON, J. G. 2003. Effects of in-vivo and in-vitro environments on the metabolism of the cumulus-oocyte complex and its influence on oocyte developmental capacity. *Human Reproduction Update,* 9**,** 35-48.

SUZUKI, T., HIGGINS, P. J. & CRAWFORD, D. R. 2000. Control selection for RNA quantitation. *Biotechniques,* 29**,** 332-7.

SVOBODA, P., STEIN, P., HAYASHI, H. & SCHULTZ, R. M. 2000. Selective reduction of dormant maternal mRNAs in mouse oocytes by RNA interference. *Development,* 127**,** 4147-56.

SWANN, K. & LAI, F. A. 2016. Egg Activation at Fertilization by a Soluble Sperm Protein. *Physiol Rev,* 96**,** 127-49.

SYBIRNA, A., WONG, F. C. K. & SURANI, M. A. 2019. Genetic basis for primordial germ cells specification in mouse and human: Conserved and divergent roles of PRDM and SOX transcription factors. *Immortal Germline,* 135**,** 35-89.

SZOLLOSI, D., CALARCO, P. & DONAHUE, R. P. 1972. Absence of centrioles in the first and second meiotic spindles of mouse oocytes. *J Cell Sci,* 11**,** 521-41.

TAFT, R. A. 2008. Virtues and limitations of the preimplantation mouse embryo as a model system. *Theriogenology,* 69**,** 10-6.

TANG, F., BARBACIORU, C., WANG, Y., NORDMAN, E., LEE, C., XU, N., WANG, X., BODEAU, J., TUCH, B. B., SIDDIQUI, A., LAO, K. & SURANI, M. A. 2009. mRNA-Seq whole-transcriptome analysis of a single cell. *Nat Methods,* 6**,** 377-82.

TARKOWSKI, A. K. & WROBLEWSKA, J. 1967. Development of blastomeres of mouse eggs isolated at the 4- and 8-cell stage. *J Embryol Exp Morphol,* 18**,** 155-80.

TASHIRO, F., KANAI-AZUMA, M., MIYAZAKI, S., KATO, M., TANAKA, T., TOYODA, S., YAMATO, E., KAWAKAMI, H., MIYAZAKI, T. & MIYAZAKI, J. 2010. Maternal-effect gene Ces5/Ooep/Moep19/Floped is essential for oocyte cytoplasmic lattice formation and embryonic development at the maternal-zygotic stage transition. *Genes Cells,* 15**,** 813-28.

TAYLOR, R. G., WALKER, D. C. & MCINNES, R. R. 1993. E. coli host strains significantly affect the quality of small scale plasmid DNA preparations used for sequencing. *Nucleic Acids Res,* 21**,** 1677-8.

TELFER, E. E., GOSDEN, R. G., BYSKOV, A. G., SPEARS, N., ALBERTINI, D., ANDERSEN, C. Y., ANDERSON, R., BRAW-TAL, R., CLARKE, H., GOUGEON, A., MCLAUGHLIN, E., MCLAREN, A., MCNATTY, K., SCHATTEN, G., SILBER, S. & TSAFRIRI, A. 2005. On regenerating the ovary and generating controversy. *Cell,* 122**,** 821-2.

TELFORD, N. A., WATSON, A. J. & SCHULTZ, G. A. 1990. Transition from maternal to embryonic control in early mammalian development: a comparison of several species. *Mol Reprod Dev,* 26**,** 90-100.

TESFAYE, D., GEBREMEDHN, S., SALILEW-WONDIM, D., HAILAY, T., HOELKER, M., GROSSE-BRINKHAUS, C. & SCHELLANDER, K. 2018. MicroRNAs: tiny molecules with a significant role in mammalian follicular and oocyte development. *Reproduction,* 155**,** R121-R135.

THELIE, A., PAPILLIER, P., PENNETIER, S., PERREAU, C., TRAVERSO, J. M., UZBEKOVA, S., MERMILLOD, P., JOLY, C., HUMBLOT, P. & DALBIES-TRAN, R. 2007. Differential regulation of abundance and deadenylation of maternal transcripts during bovine oocyte maturation in vitro and in vivo. *BMC Dev Biol,* 7**,** 125.

THOMAS, R. E., THOMPSON, J. G., ARMSTRONG, D. T. & GILCHRIST, R. B. 2004. Effect of specific phosphodiesterase isoenzyme inhibitors during in vitro maturation of bovine oocytes on meiotic and developmental capacity. *Biol Reprod,* 71**,** 1142-9.

THOMAS, W. K. & SEIDEL, G. E., JR. 1993. Effects of cumulus cells on culture of bovine embryos derived from oocytes matured and fertilized in vitro. *J Anim Sci,* 71**,** 2506-10.

TIAN, X., PASCAL, G., FOUCHECOURT, S., PONTAROTTI, P. & MONGET, P. 2009a. Gene birth, death, and divergence: the different scenarios of reproduction-related gene evolution. *Biol Reprod,* 80**,** 616-21.

TIAN, X., PASCAL, G. & MONGET, P. 2009b. Evolution and functional divergence of NLRP genes in mammalian reproductive systems. *BMC Evol Biol,* 9**,** 202.

TILBURGS, T., MEISSNER, T. B., FERREIRA, L. M. R., MULDER, A., MUSUNURU, K., YE, J. & STROMINGER, J. L. 2017. NLRP2 is a suppressor of NF-kB signaling and HLA-C expression in human trophoblasts. *Biol Reprod,* 96**,** 831-842.

TILGNER, K., ATKINSON, S. P., GOLEBIEWSKA, A., STOJKOVIC, M., LAKO, M. & ARMSTRONG, L. 2008. Isolation of primordial germ cells from differentiating human embryonic stem cells. *Stem Cells,* 26**,** 3075-85.

TINI, M., BENECKE, A., UM, S. J., TORCHIA, J., EVANS, R. M. & CHAMBON, P. 2002. Association of CBP/p300 acetylase and thymine DNA glycosylase links DNA repair and transcription. *Mol Cell,* 9**,** 265-77.

TIWARI, M. & CHAUBE, S. K. 2017. Maturation promoting factor destabilization mediates human chorionic gonadotropin induced meiotic resumption in rat oocytes. *Dev Growth Differ,* 59**,** 603-614.

TOMBES, R. M., SIMERLY, C., BORISY, G. G. & SCHATTEN, G. 1992. Meiosis, egg activation, and nuclear envelope breakdown are differentially reliant on Ca2+, whereas germinal vesicle breakdown is Ca2+ independent in the mouse oocyte. *J Cell Biol,* 117**,** 799-811.

TOMEK, W., MELO STERZA, F. A., KUBELKA, M., WOLLENHAUPT, K., TORNER, H., ANGER, M. & KANITZ, W. 2002a. Regulation of translation during in vitro maturation of bovine oocytes: the role of MAP kinase, eIF4E (cap binding protein) phosphorylation, and eIF4E-BP1. *Biol Reprod,* 66**,** 1274-82.

TOMEK, W., TORNER, H. & KANITZ, W. 2002b. Comparative analysis of protein synthesis, transcription and cytoplasmic polyadenylation of mRNA during maturation of bovine oocytes in vitro. *Reprod Domest Anim,* 37**,** 86-91.

TOMIZAWA, S., KOBAYASHI, H., WATANABE, T., ANDREWS, S., HATA, K., KELSEY, G. & SASAKI, H. 2011. Dynamic stage-specific changes in imprinted differentially methylated regions during early mammalian development and prevalence of non-CpG methylation in oocytes. *Development,* 138**,** 811-20.

TOMIZAWA, S., NOWACKA-WOSZUK, J. & KELSEY, G. 2012. DNA methylation establishment during oocyte growth: mechanisms and significance. *Int J Dev Biol,* 56**,** 867-75.

TONG, Z. B., GOLD, L., DE POL, A., VANEVSKI, K., DORWARD, H., SENA, P., PALUMBO, C., BONDY, C. A. & NELSON, L. M. 2004. Developmental expression and subcellular localization of mouse MATER, an oocyte-specific protein essential for early development. *Endocrinology,* 145**,** 1427-34.

TONG, Z. B., GOLD, L., PFEIFER, K. E., DORWARD, H., LEE, E., BONDY, C. A., DEAN, J. & NELSON, L. M. 2000. Mater, a maternal effect gene required for early embryonic development in mice. *Nat Genet,* 26**,** 267-8.

TONG, Z. B. & NELSON, L. M. 1999. A mouse gene encoding an oocyte antigen associated with autoimmune premature ovarian failure. *Endocrinology,* 140**,** 3720-6.

TORRES-PADILLA, M. E., PARFITT, D. E., KOUZARIDES, T. & ZERNICKA-GOETZ, M. 2007. Histone arginine methylation regulates pluripotency in the early mouse embryo. *Nature,* 445**,** 214-8.

TORRES-PADILLA, M. E. & ZERNICKA-GOETZ, M. 2006. Role of TIF1alpha as a modulator of embryonic transcription in the mouse zygote. *J Cell Biol,* 174**,** 329-38.

TOWBIN, H., STAEHELIN, T. & GORDON, J. 1979. Electrophoretic transfer of proteins from polyacrylamide gels to nitrocellulose sheets: procedure and some applications. *Proc Natl Acad Sci U S A,* 76**,** 4350-4.

TRAPPHOFF, T., HEILIGENTAG, M., DANKERT, D., DEMOND, H., DEUTSCH, D., FROHLICH, T., ARNOLD, G. J., GRUMMER, R., HORSTHEMKE, B. & EICHENLAUB-RITTER, U. 2016. Postovulatory aging affects dynamics of mRNA, expression and localization of maternal effect proteins, spindle integrity and pericentromeric proteins in mouse oocytes. *Hum Reprod,* 31**,** 133-49.

TRAVERSO, J. M., DONNAY, I. & LEQUARRE, A. S. 2005. Effects of polyadenylation inhibition on meiosis progression in relation to the polyadenylation status of cyclins A2 and B1 during in vitro maturation of bovine oocytes. *Mol Reprod Dev,* 71**,** 107-14.

TREMBLAY, K. D., DURAN, K. L. & BARTOLOMEI, M. S. 1997. A 5' 2-kilobase-pair region of the imprinted mouse H19 gene exhibits exclusive paternal methylation throughout development. *Mol Cell Biol,* 17**,** 4322-9.

TRIGLIA, D., BRAA, S. S., YONAN, C. & NAUGHTON, G. K. 1991. In vitro toxicity of various classes of test agents using the neutral red assay on a human three-dimensional physiologic skin model. *In Vitro Cell Dev Biol,* 27A**,** 239-44.

TRIPURANI, S. K., WEE, G., LEE, K. B., SMITH, G. W., WANG, L. & JIANBOYAO 2013. MicroRNA-212 post-transcriptionally regulates oocyte-specific basic-helix-loop-helix transcription factor, factor in the germline alpha (FIGLA), during bovine early embryogenesis. *PLoS One,* 8**,** e76114.

TSAI, P. S., VAN HAEFTEN, T. & GADELLA, B. M. 2011. Preparation of the cortical reaction: maturation-dependent migration of SNARE proteins, clathrin, and complexin to the porcine oocyte's surface blocks membrane traffic until fertilization. *Biol Reprod,* 84**,** 327-35.

TSENG, H. 1999. DNA cloning without restriction enzyme and ligase. *Biotechniques,* 27**,** 1240-4.

TSUKAMOTO, S. & TATSUMI, T. 2018. Degradation of maternal factors during preimplantation embryonic development. *J Reprod Dev,* 64**,** 217-222.

TUCK, A. R., ROBKER, R. L., NORMAN, R. J., TILLEY, W. D. & HICKEY, T. E. 2015. Expression and localisation of c-kit and KITL in the adult human ovary. *J Ovarian Res,* 8**,** 31.

TUNG, J. J., HANSEN, D. V., BAN, K. H., LOKTEV, A. V., SUMMERS, M. K., ADLER, J. R., 3RD & JACKSON, P. K. 2005. A role for the anaphase-promoting complex inhibitor Emi2/XErp1, a homolog of early mitotic inhibitor 1, in cytostatic factor arrest of Xenopus eggs. *Proc Natl Acad Sci U S A,* 102**,** 4318-23.

TUNQUIST, B. J. & MALLER, J. L. 2003. Under arrest: cytostatic factor (CSF)-mediated metaphase arrest in vertebrate eggs. *Genes Dev,* 17**,** 683-710.

UDA, M., OTTOLENGHI, C., CRISPONI, L., GARCIA, J. E., DEIANA, M., KIMBER, W., FORABOSCO, A., CAO, A., SCHLESSINGER, D. & PILIA, G. 2004. Foxl2 disruption causes mouse ovarian failure by pervasive blockage of follicle development. *Hum Mol Genet,* 13**,** 1171-81.

UYSAL, F., AKKOYUNLU, G. & OZTURK, S. 2015. Dynamic expression of DNA methyltransferases (DNMTs) in oocytes and early embryos. *Biochimie,* 116**,** 103-13.

UYSAL, F., OZTURK, S. & AKKOYUNLU, G. 2017. DNMT1, DNMT3A and DNMT3B proteins are differently expressed in mouse oocytes and early embryos. *J Mol Histol,* 48**,** 417-426.

VACCARI, S., HORNER, K., MEHLMANN, L. M. & CONTI, M. 2008. Generation of mouse oocytes defective in cAMP synthesis and degradation: endogenous cyclic AMP is essential for meiotic arrest. *Dev Biol,* 316**,** 124-34.

VACCARI, S., WEEKS, J. L., 2ND, HSIEH, M., MENNITI, F. S. & CONTI, M. 2009. Cyclic GMP signaling is involved in the luteinizing hormone-dependent meiotic maturation of mouse oocytes. *Biol Reprod,* 81**,** 595-604.

VALLEE, M., GRAVEL, C., PALIN, M. F., REGHENAS, H., STOTHARD, P., WISHART, D. S. & SIRARD, M. A. 2005. Identification of novel and known oocyte-specific genes using complementary DNA subtraction and microarray analysis in three different species. *Biol Reprod,* 73**,** 63-71.

VAN BLERKOM, J. 2004. Mitochondria in human oogenesis and preimplantation embryogenesis: engines of metabolism, ionic regulation and developmental competence. *Reproduction,* 128**,** 269-80.

VAN BLERKOM, J., DAVIS, P. & ALEXANDER, S. 2000. Differential mitochondrial distribution in human pronuclear embryos leads to disproportionate inheritance between blastomeres: relationship to microtubular organization, ATP content and competence. *Hum Reprod,* 15**,** 2621-33.

VAN BLERKOM, J., DAVIS, P., MATHWIG, V. & ALEXANDER, S. 2002. Domains of high-polarized and low-polarized mitochondria may occur in mouse and human oocytes and early embryos. *Hum Reprod,* 17**,** 393-406.

VAN DE LAGEMAAT, L. N., FLENLEY, M., LYNCH, M. D., GARRICK, D., TOMLINSON, S. R., KRANC, K. R. & VERNIMMEN, D. 2018. CpG binding protein (CFP1) occupies open chromatin regions of active genes, including enhancers and non-CpG islands. *Epigenetics Chromatin,* 11**,** 59.

VAN WEZEL, I. L., UMAPATHYSIVAM, K., TILLEY, W. D. & RODGERS, R. J. 1995. Immunohistochemical localization of basic fibroblast growth factor in bovine ovarian follicles. *Mol Cell Endocrinol,* 115**,** 133-40.

VANHOUTTE, L., NOGUEIRA, D., GERRIS, J., DHONT, M. & DE SUTTER, P. 2008. Effect of temporary nuclear arrest by phosphodiesterase 3-inhibitor on morphological and functional aspects of in vitro matured mouse oocytes. *Mol Reprod Dev,* 75**,** 1021-30.

VARRAULT, A., GUEYDAN, C., DELALBRE, A., BELLMANN, A., HOUSSAMI, S., AKNIN, C., SEVERAC, D., CHOTARD, L., KAHLI, M., LE DIGARCHER, A., PAVLIDIS, P. & JOURNOT, L. 2006. Zac1 regulates an imprinted gene network critically involved in the control of embryonic growth. *Dev Cell,* 11**,** 711-22.

VASSENA, R., BOUE, S., GONZALEZ-ROCA, E., ARAN, B., AUER, H., VEIGA, A. & IZPISUA BELMONTE, J. C. 2011. Waves of early transcriptional activation and pluripotency program initiation during human preimplantation development. *Development,* 138**,** 3699-709.

VENDOLA, K. A., ZHOU, J., ADESANYA, O. O., WEIL, S. J. & BONDY, C. A. 1998. Androgens stimulate early stages of follicular growth in the primate ovary. *J Clin Invest,* 101**,** 2622-9.

VERLHAC, M. H., LEFEBVRE, C., GUILLAUD, P., RASSINIER, P. & MARO, B. 2000. Asymmetric division in mouse oocytes: with or without Mos. *Curr Biol,* 10**,** 1303-6.

VERMANDE-VAN ECK, G. J. 1956. Neo-ovogenesis in the adult monkey; consequences of atresia of ovocytes. *Anat Rec,* 125**,** 207-24.

VERMEULEN, A., BEHLEN, L., REYNOLDS, A., WOLFSON, A., MARSHALL, W. S., KARPILOW, J. & KHVOROVA, A. 2005. The contributions of dsRNA structure to Dicer specificity and efficiency. *RNA,* 11**,** 674-82.

VIRANT-KLUN, I. 2015. Postnatal oogenesis in humans: a review of recent findings. *Stem Cells Cloning,* 8**,** 49-60.

VIRANT-KLUN, I., ZECH, N., ROZMAN, P., VOGLER, A., CVJETICANIN, B., KLEMENC, P., MALICEV, E. & MEDEN-VRTOVEC, H. 2008. Putative stem cells with an embryonic character isolated from the ovarian surface epithelium of women with no naturally present follicles and oocytes. *Differentiation,* 76**,** 843-56.

VISCONTI, P. E., MOORE, G. D., BAILEY, J. L., LECLERC, P., CONNORS, S. A., PAN, D., OLDS-CLARKE, P. & KOPF, G. S. 1995. Capacitation of mouse spermatozoa. II. Protein tyrosine phosphorylation and capacitation are regulated by a cAMP-dependent pathway. *Development,* 121**,** 1139-50.

VISCONTI, P. E., NING, X., FORNES, M. W., ALVAREZ, J. G., STEIN, P., CONNORS, S. A. & KOPF, G. S. 1999. Cholesterol efflux-mediated signal transduction in mammalian sperm: cholesterol release signals an increase in protein tyrosine phosphorylation during mouse sperm capacitation. *Dev Biol,* 214**,** 429-43.

VISSER, J. A. & THEMMEN, A. P. 2005. Anti-Mullerian hormone and folliculogenesis. *Mol Cell Endocrinol,* 234**,** 81-6.

VITT, U. A., MCGEE, E. A., HAYASHI, M. & HSUEH, A. J. 2000. In vivo treatment with GDF-9 stimulates primordial and primary follicle progression and theca cell marker CYP17 in ovaries of immature rats. *Endocrinology,* 141**,** 3814-20.

VOLPE, T. A., KIDNER, C., HALL, I. M., TENG, G., GREWAL, S. I. & MARTIENSSEN, R. A. 2002. Regulation of heterochromatic silencing and histone H3 lysine-9 methylation by RNAi. *Science,* 297**,** 1833-7.

VOSSENAAR, E. R., ZENDMAN, A. J., VAN VENROOIJ, W. J. & PRUIJN, G. J. 2003. PAD, a growing family of citrullinating enzymes: genes, features and involvement in disease. *Bioessays,* 25**,** 1106-18.

VU, T. H., LI, T. & HOFFMAN, A. R. 2004. Promoter-restricted histone code, not the differentially methylated DNA regions or antisense transcripts, marks the imprinting status of IGF2R in human and mouse. *Hum Mol Genet,* 13**,** 2233-45.

WAEHNELDT, T. V. 1975. Sodium dodecyl sulfate in protein chemistry. *Biosystems,* 6**,** 176-87.

WAN, L. B., PAN, H., HANNENHALLI, S., CHENG, Y., MA, J., FEDORIW, A., LOBANENKOV, V., LATHAM, K. E., SCHULTZ, R. M. & BARTOLOMEI, M. S. 2008. Maternal depletion of CTCF reveals multiple functions during oocyte and preimplantation embryo development. *Development,* 135**,** 2729-38.

WANG, F., AN, G. Y., ZHANG, Y., LIU, H. L., CUI, X. S., KIM, N. H. & SUN, S. C. 2014a. Arp2/3 complex inhibition prevents meiotic maturation in porcine oocytes. *PLoS One,* 9**,** e87700.

WANG, F., TIAN, X., ZHOU, Y., TAN, D., ZHU, S., DAI, Y. & LIU, G. 2014b. Melatonin improves the quality of in vitro produced (IVP) bovine embryos: implications for

blastocyst development, cryotolerance, and modifications of relevant gene expression. *PLoS One,* 9**,** e93641.
WANG, H. & DEY, S. K. 2006. Roadmap to embryo implantation: clues from mouse models. *Nat Rev Genet,* 7**,** 185-99.
WANG, J., XU, M., ZHU, K., LI, L. & LIU, X. 2012a. The N-terminus of FILIA forms an atypical KH domain with a unique extension involved in interaction with RNA. *PLoS One,* 7**,** e30209.
WANG, L. M., WEN, J. X., YUAN, J. L., CANG, M. & LIU, D. J. 2012b. Knockdown of IGF-IR by siRNA injection during bovine preimplantation embryonic development. *Cytotechnology,* 64**,** 165-72.
WANG, Q. & LATHAM, K. E. 1997. Requirement for protein synthesis during embryonic genome activation in mice. *Mol Reprod Dev,* 47**,** 265-70.
WANG, X., SONG, D., MYKYTENKO, D., KUANG, Y., LV, Q., LI, B., CHEN, B., MAO, X., XU, Y., ZUKIN, V., MAZUR, P., MU, J., YAN, Z., ZHOU, Z., LI, Q., LIU, S., JIN, L., HE, L., SANG, Q., SUN, Z., DONG, X. & WANG, L. 2018a. Novel mutations in genes encoding subcortical maternal complex proteins may cause human embryonic developmental arrest. *Reprod Biomed Online,* 36**,** 698-704.
WANG, X., ZHAO, Q., WANG, L., LIU, J., PU, H., XIE, S., RU, C. & SUN, Y. 2018b. Effect of Cell Inner Pressure on Deposition Volume in Microinjection. *Langmuir,* 34**,** 10287-10292.
WANG, X. H., ALIYARI, R., LI, W. X., LI, H. W., KIM, K., CARTHEW, R., ATKINSON, P. & DING, S. W. 2006. RNA interference directs innate immunity against viruses in adult Drosophila. *Science,* 312**,** 452-4.
WANG, Y., LI, M., STADLER, S., CORRELL, S., LI, P., WANG, D., HAYAMA, R., LEONELLI, L., HAN, H., GRIGORYEV, S. A., ALLIS, C. D. & COONROD, S. A. 2009. Histone hypercitrullination mediates chromatin decondensation and neutrophil extracellular trap formation. *J Cell Biol,* 184**,** 205-13.
WANG, Y., WYSOCKA, J., SAYEGH, J., LEE, Y. H., PERLIN, J. R., LEONELLI, L., SONBUCHNER, L. S., MCDONALD, C. H., COOK, R. G., DOU, Y., ROEDER, R. G., CLARKE, S., STALLCUP, M. R., ALLIS, C. D. & COONROD, S. A. 2004. Human PAD4 regulates histone arginine methylation levels via demethylimination. *Science,* 306**,** 279-83.
WATSON, A. J., NATALE, D. R. & BARCROFT, L. C. 2004. Molecular regulation of blastocyst formation. *Anim Reprod Sci,* 82-83**,** 583-92.
WATSON, R. J., SCHILDRAUT, I., QIANG, B. Q., MARTIN, S. M. & VISENTIN, L. P. 1982. NdeI: a restriction endonuclease from Neisseria denitrificans which cleaves DNA at 5'-CATATG-3' sequences. *FEBS Lett,* 150**,** 114-6.
WEBER, A. R., KRAWCZYK, C., ROBERTSON, A. B., KUSNIERCZYK, A., VAGBO, C. B., SCHUERMANN, D., KLUNGLAND, A. & SCHAR, P. 2016. Biochemical reconstitution of TET1-TDG-BER-dependent active DNA demethylation reveals a highly coordinated mechanism. *Nat Commun,* 7**,** 10806.
WEI, Q., ZHONG, L., ZHANG, S., MU, H., XIANG, J., YUE, L., DAI, Y. & HAN, J. 2017. Bovine lineage specification revealed by single-cell gene expression analysis from zygote to blastocyst. *Biol Reprod,* 97**,** 5-17.
WEI, Y., HUAN, Y., SHI, Y., LIU, Z., BOU, G., LUO, Y., ZHANG, L., YANG, C., KONG, Q., TIAN, J., XIA, P., SUN, Q. Y. & LIU, Z. 2011. Unfaithful maintenance of methylation imprints due to loss of maternal nuclear Dnmt1 during somatic cell nuclear transfer. *PLoS One,* 6**,** e20154.
WESSEL, G. M., CONNER, S. D. & BERG, L. 2002. Cortical granule translocation is microfilament mediated and linked to meiotic maturation in the sea urchin oocyte. *Development,* 129**,** 4315-25.
WHITAKER, M. 2006. Calcium at fertilization and in early development. *Physiological Reviews,* 86**,** 25-88.

WHITE, Y. A., WOODS, D. C., TAKAI, Y., ISHIHARA, O., SEKI, H. & TILLY, J. L. 2012. Oocyte formation by mitotically active germ cells purified from ovaries of reproductive-age women. *Nat Med,* 18**,** 413-21.

WIANNY, F. & ZERNICKA-GOETZ, M. 2000. Specific interference with gene function by double-stranded RNA in early mouse development. *Nat Cell Biol,* 2**,** 70-5.

WIEKOWSKI, M., MIRANDA, M. & DEPAMPHILIS, M. L. 1991. Regulation of gene expression in preimplantation mouse embryos: effects of the zygotic clock and the first mitosis on promoter and enhancer activities. *Dev Biol,* 147**,** 403-14.

WIJAYARATHNA, R. & DE KRETSER, D. M. 2016. Activins in reproductive biology and beyond. *Hum Reprod Update,* 22**,** 342-57.

WILKINS, C., DISHONGH, R., MOORE, S. C., WHITT, M. A., CHOW, M. & MACHACA, K. 2005. RNA interference is an antiviral defence mechanism in Caenorhabditis elegans. *Nature,* 436**,** 1044-7.

WILKINS, J. F., UBEDA, F. & VAN CLEVE, J. 2016. The evolving landscape of imprinted genes in humans and mice: Conflict among alleles, genes, tissues, and kin. *Bioessays,* 38**,** 482-9.

WINATA, C. L. & KORZH, V. 2018. The translational regulation of maternal mRNAs in time and space. *FEBS Lett,* 592**,** 3007-3023.

WOSSIDLO, M., NAKAMURA, T., LEPIKHOV, K., MARQUES, C. J., ZAKHARTCHENKO, V., BOIANI, M., ARAND, J., NAKANO, T., REIK, W. & WALTER, J. 2011. 5-Hydroxymethylcytosine in the mammalian zygote is linked with epigenetic reprogramming. *Nat Commun,* 2**,** 241.

WRIGHT, E. C., HALE, B. J., YANG, C. X., NJOKA, J. G. & ROSS, J. W. 2016. MicroRNA-21 and PDCD4 expression during in vitro oocyte maturation in pigs. *Reprod Biol Endocrinol,* 14**,** 21.

WRIGHT, P. W., BOLLING, L. C., CALVERT, M. E., SARMENTO, O. F., BERKELEY, E. V., SHEA, M. C., HAO, Z., JAYES, F. C., BUSH, L. A., SHETTY, J., SHORE, A. N., REDDI, P. P., TUNG, K. S., SAMY, E., ALLIETTA, M. M., SHERMAN, N. E., HERR, J. C. & COONROD, S. A. 2003. ePAD, an oocyte and early embryo-abundant peptidylarginine deiminase-like protein that localizes to egg cytoplasmic sheets. *Dev Biol,* 256**,** 73-88.

WU, G. & SCHOLER, H. R. 2014. Role of Oct4 in the early embryo development. *Cell Regen (Lond),* 3**,** 7.

WU, J., ZHANG, L. & WANG, X. 2000. Maturation and apoptosis of human oocytes in vitro are age-related. *Fertil Steril,* 74**,** 1137-41.

WU, W., HODGES, E., REDELIUS, J. & HOOG, C. 2004. A novel approach for evaluating the efficiency of siRNAs on protein levels in cultured cells. *Nucleic Acids Res,* 32**,** e17.

WU, X., VIVEIROS, M. M., EPPIG, J. J., BAI, Y., FITZPATRICK, S. L. & MATZUK, M. M. 2003. Zygote arrest 1 (Zar1) is a novel maternal-effect gene critical for the oocyte-to-embryo transition. *Nat Genet,* 33**,** 187-91.

WUTZ, A., SMRZKA, O. W., SCHWEIFER, N., SCHELLANDER, K., WAGNER, E. F. & BARLOW, D. P. 1997. Imprinted expression of the Igf2r gene depends on an intronic CpG island. *Nature,* 389**,** 745-9.

WYNN, P., PICTON, H. M., KRAPEZ, J. A., RUTHERFORD, A. J., BALEN, A. H. & GOSDEN, R. G. 1998. Pretreatment with follicle stimulating hormone promotes the numbers of human oocytes reaching metaphase II by in-vitro maturation. *Hum Reprod,* 13**,** 3132-8.

XIA, X., YAN, C., WU, W., ZHOU, Y., HOU, L., ZUO, B., XU, D., REN, Z. & XIONG, Y. 2016. Characterization of the porcine peptidylarginine deiminase type VI gene (PADI6) promoter: Sp1 regulates basal transcription of the porcine PADI6. *Gene,* 575**,** 551-558.

XIONG, J., WU, M., ZHANG, Q., ZHANG, C., XIONG, G., MA, L., LU, Z. & WANG, S. 2019. Proteomic analysis of mouse ovaries during the prepubertal stages. *Exp Cell Res,* 377**,** 36-46.

XU, Y., SHI, Y., FU, J., YU, M., FENG, R., SANG, Q., LIANG, B., CHEN, B., QU, R., LI, B., YAN, Z., MAO, X., KUANG, Y., JIN, L., HE, L., SUN, X. & WANG, L. 2016. Mutations in PADI6 Cause Female Infertility Characterized by Early Embryonic Arrest. *Am J Hum Genet,* 99**,** 744-52.

YAMAGUCHI, S., HONG, K., LIU, R., INOUE, A., SHEN, L., ZHANG, K. & ZHANG, Y. 2013. Dynamics of 5-methylcytosine and 5-hydroxymethylcytosine during germ cell reprogramming. *Cell Res,* 23**,** 329-39.

YAMAGUCHI, S., HONG, K., LIU, R., SHEN, L., INOUE, A., DIEP, D., ZHANG, K. & ZHANG, Y. 2012. Tet1 controls meiosis by regulating meiotic gene expression. *Nature,* 492**,** 443-7.

YAMAJI, M., SEKI, Y., KURIMOTO, K., YABUTA, Y., YUASA, M., SHIGETA, M., YAMANAKA, K., OHINATA, Y. & SAITOU, M. 2008. Critical function of Prdm14 for the establishment of the germ cell lineage in mice. *Nat Genet,* 40**,** 1016-22.

YAMANAKA, K., SAKATANI, M., KUBOTA, K., BALBOULA, A. Z., SAWAI, K. & TAKAHASHI, M. 2011. Effects of downregulating DNA methyltransferase 1 transcript by RNA interference on DNA methylation status of the satellite I region and in vitro development of bovine somatic cell nuclear transfer embryos. *J Reprod Dev,* 57**,** 393-402.

YAMOTO, M., MINAMI, S., NAKANO, R. & KOBAYASHI, M. 1992. Immunohistochemical localization of inhibin/activin subunits in human ovarian follicles during the menstrual cycle. *J Clin Endocrinol Metab,* 74**,** 989-93.

YAN, C., WANG, P., DEMAYO, J., DEMAYO, F. J., ELVIN, J. A., CARINO, C., PRASAD, S. V., SKINNER, S. S., DUNBAR, B. S., DUBE, J. L., CELESTE, A. J. & MATZUK, M. M. 2001. Synergistic roles of bone morphogenetic protein 15 and growth differentiation factor 9 in ovarian function. *Mol Endocrinol,* 15**,** 854-66.

YAN, L., YANG, M., GUO, H., YANG, L., WU, J., LI, R., LIU, P., LIAN, Y., ZHENG, X., YAN, J., HUANG, J., LI, M., WU, X., WEN, L., LAO, K., LI, R., QIAO, J. & TANG, F. 2013. Single-cell RNA-Seq profiling of human preimplantation embryos and embryonic stem cells. *Nat Struct Mol Biol,* 20**,** 1131-9.

YAN, X., DONG, X., ZHANG, W., YIN, H., XIAO, H., CHEN, P. & MA, X. F. 2014. Reference gene selection for quantitative real-time PCR normalization in Reaumuria soongorica. *PLoS One,* 9**,** e104124.

YANG, M. Y. & FORTUNE, J. E. 2006. Testosterone stimulates the primary to secondary follicle transition in bovine follicles in vitro. *Biol Reprod,* 75**,** 924-32.

YANG, Y., WANG, L., HAN, X., YANG, W. L., ZHANG, M., MA, H. L., SUN, B. F., LI, A., XIA, J., CHEN, J., HENG, J., WU, B., CHEN, Y. S., XU, J. W., YANG, X., YAO, H., SUN, J., LYU, C., WANG, H. L., HUANG, Y., SUN, Y. P., ZHAO, Y. L., MENG, A., MA, J., LIU, F. & YANG, Y. G. 2019. RNA 5-Methylcytosine Facilitates the Maternal-to-Zygotic Transition by Preventing Maternal mRNA Decay. *Mol Cell,* 75**,** 1188-1202 e11.

YI, K., RUBINSTEIN, B., UNRUH, J. R., GUO, F., SLAUGHTER, B. D. & LI, R. 2013. Sequential actin-based pushing forces drive meiosis I chromosome migration and symmetry breaking in oocytes. *J Cell Biol,* 200**,** 567-76.

YI, K., UNRUH, J. R., DENG, M., SLAUGHTER, B. D., RUBINSTEIN, B. & LI, R. 2011. Dynamic maintenance of asymmetric meiotic spindle position through Arp2/3-complex-driven cytoplasmic streaming in mouse oocytes. *Nat Cell Biol,* 13**,** 1252-8.

YING, Y., LIU, X. M., MARBLE, A., LAWSON, K. A. & ZHAO, G. Q. 2000. Requirement of Bmp8b for the generation of primordial germ cells in the mouse. *Mol Endocrinol,* 14**,** 1053-63.

YING, Y., QI, X. & ZHAO, G. Q. 2001. Induction of primordial germ cells from murine epiblasts by synergistic action of BMP4 and BMP8B signaling pathways. *Proc Natl Acad Sci U S A,* 98**,** 7858-62.

YING, Y. & ZHAO, G. Q. 2001. Cooperation of endoderm-derived BMP2 and extraembryonic ectoderm-derived BMP4 in primordial germ cell generation in the mouse. *Dev Biol,* 232**,** 484-92.

YOON, S. Y. 2019. Role of Type 1 Inositol 1,4,5-triphosphate Receptors in Mammalian Oocytes. *Dev Reprod,* 23**,** 1-9.

YOSHIDA, H., TAKAKURA, N., KATAOKA, H., KUNISADA, T., OKAMURA, H. & NISHIKAWA, S. I. 1997. Stepwise requirement of c-kit tyrosine kinase in mouse ovarian follicle development. *Dev Biol,* 184**,** 122-37.

YU, J., HECHT, N. B. & SCHULTZ, R. M. 2001. Expression of MSY2 in mouse oocytes and preimplantation embryos. *Biol Reprod,* 65**,** 1260-70.

YU, R., JIH, G., IGLESIAS, N. & MOAZED, D. 2014a. Determinants of heterochromatic siRNA biogenesis and function. *Mol Cell,* 53**,** 262-76.

YU, X. J., YI, Z., GAO, Z., QIN, D., ZHAI, Y., CHEN, X., OU-YANG, Y., WANG, Z. B., ZHENG, P., ZHU, M. S., WANG, H., SUN, Q. Y., DEAN, J. & LI, L. 2014b. The subcortical maternal complex controls symmetric division of mouse zygotes by regulating F-actin dynamics. *Nat Commun,* 5**,** 4887.

YU, Y., DUMOLLARD, R., ROSSBACH, A., LAI, F. A. & SWANN, K. 2010. Redistribution of mitochondria leads to bursts of ATP production during spontaneous mouse oocyte maturation. *J Cell Physiol,* 224**,** 672-80.

YUAN, S., SCHUSTER, A., TANG, C., YU, T., ORTOGERO, N., BAO, J., ZHENG, H. & YAN, W. 2016. Sperm-borne miRNAs and endo-siRNAs are important for fertilization and preimplantation embryonic development. *Development,* 143**,** 635-47.

YUN, Y., AN, P., NING, J., ZHAO, G. M., YANG, W. L. & LEI, A. M. 2015. H1foo is essential for in vitro meiotic maturation of bovine oocytes. *Zygote,* 23**,** 416-25.

YURTTAS, P., VITALE, A. M., FITZHENRY, R. J., COHEN-GOULD, L., WU, W., GOSSEN, J. A. & COONROD, S. A. 2008. Role for PADI6 and the cytoplasmic lattices in ribosomal storage in oocytes and translational control in the early mouse embryo. *Development,* 135**,** 2627-36.

ZAMORE, P. D., TUSCHL, T., SHARP, P. A. & BARTEL, D. P. 2000. RNAi: double-stranded RNA directs the ATP-dependent cleavage of mRNA at 21 to 23 nucleotide intervals. *Cell,* 101**,** 25-33.

ZENG, H. T., YEUNG, W. S., CHEUNG, M. P., HO, P. C., LEE, C. K., ZHUANG, G. L., LIANG, X. Y. & O, W. S. 2009. In vitro-matured rat oocytes have low mitochondrial deoxyribonucleic acid and adenosine triphosphate contents and have abnormal mitochondrial redistribution. *Fertil Steril,* 91**,** 900-7.

ZHAI, Q., WANG, L., ZHAO, P. & LI, T. 2017. Role of citrullination modification catalyzed by peptidylarginine deiminase 4 in gene transcriptional regulation. *Acta Biochim Biophys Sin (Shanghai),* 49**,** 567-572.

ZHAI, Y., YAO, G., RAO, F., WANG, Y., SONG, X. & SUN, F. 2018. Excessive nerve growth factor impairs bidirectional communication between the oocyte and cumulus cells resulting in reduced oocyte competence. *Reprod Biol Endocrinol,* 16**,** 28.

ZHANG, C. H., WANG, Z. B., QUAN, S., HUANG, X., TONG, J. S., MA, J. Y., GUO, L., WEI, Y. C., OUYANG, Y. C., HOU, Y., XING, F. Q. & SUN, Q. Y. 2011. GM130, a cis-Golgi protein, regulates meiotic spindle assembly and asymmetric division in mouse oocyte. *Cell Cycle,* 10**,** 1861-70.

ZHANG, J., DAI, J., ZHAO, E., LIN, Y., ZENG, L., CHEN, J., ZHENG, H., WANG, Y., LI, X., YING, K., XIE, Y. & MAO, Y. 2004. cDNA cloning, gene organization and expression analysis of human peptidylarginine deiminase type VI. *Acta Biochim Pol,* 51**,** 1051-8.

ZHANG, J. & LIU, H. 2015. Cytoplasm replacement following germinal vesicle transfer restores meiotic maturation and spindle assembly in meiotically arrested oocytes. *Reprod Biomed Online,* 31**,** 71-8.

ZHANG, K. & SMITH, G. W. 2015. Maternal control of early embryogenesis in mammals. *Reprod Fertil Dev,* 27**,** 880-96.
ZHANG, M., SU, Y. Q., SUGIURA, K., XIA, G. & EPPIG, J. J. 2010. Granulosa cell ligand NPPC and its receptor NPR2 maintain meiotic arrest in mouse oocytes. *Science,* 330**,** 366-9.
ZHANG, P., DIXON, M., ZUCCHELLI, M., HAMBILIKI, F., LEVKOV, L., HOVATTA, O. & KERE, J. 2008. Expression analysis of the NLRP gene family suggests a role in human preimplantation development. *PLoS One,* 3**,** e2755.
ZHANG, X., BOLT, M., GUERTIN, M. J., CHEN, W., ZHANG, S., CHERRINGTON, B. D., SLADE, D. J., DREYTON, C. J., SUBRAMANIAN, V., BICKER, K. L., THOMPSON, P. R., MANCINI, M. A., LIS, J. T. & COONROD, S. A. 2012. Peptidylarginine deiminase 2-catalyzed histone H3 arginine 26 citrullination facilitates estrogen receptor alpha target gene activation. *Proc Natl Acad Sci U S A,* 109**,** 13331-6.
ZHANG, X., LIU, X., ZHANG, M., LI, T., MUTH, A., THOMPSON, P. R., COONROD, S. A. & ZHANG, X. 2016. Peptidylarginine deiminase 1-catalyzed histone citrullination is essential for early embryo development. *Sci Rep,* 6**,** 38727.
ZHANG, Y. & YU, L. C. 2008. Single-cell microinjection technology in cell biology. *Bioessays,* 30**,** 606-10.
ZHAO, B. S., WANG, X., BEADELL, A. V., LU, Z., SHI, H., KUUSPALU, A., HO, R. K. & HE, C. 2017. m(6)A-dependent maternal mRNA clearance facilitates zebrafish maternal-to-zygotic transition. *Nature,* 542**,** 475-478.
ZHENG, P. & DEAN, J. 2009. Role of Filia, a maternal effect gene, in maintaining euploidy during cleavage-stage mouse embryogenesis. *Proc Natl Acad Sci U S A,* 106**,** 7473-8.
ZHENG, W., CHEN, L., DAI, J., DAI, C., GUO, J., LU, C., GONG, F., LU, G. & LIN, G. 2019. New biallelic mutations in PADI6 cause recurrent preimplantation embryonic arrest characterized by direct cleavage. *J Assist Reprod Genet*.
ZHOU, L. Q. & DEAN, J. 2015. Reprogramming the genome to totipotency in mouse embryos. *Trends Cell Biol,* 25**,** 82-91.
ZHOU, Z., NI, C., WU, L., CHEN, B., XU, Y., ZHANG, Z., MU, J., LI, B., YAN, Z., FU, J., WANG, W., ZHAO, L., DONG, J., SUN, X., KUANG, Y., SANG, Q. & WANG, L. 2019. Novel mutations in ZP1, ZP2, and ZP3 cause female infertility due to abnormal zona pellucida formation. *Hum Genet*.
ZHU, K., YAN, L., ZHANG, X., LU, X., WANG, T., YAN, J., LIU, X., QIAO, J. & LI, L. 2015. Identification of a human subcortical maternal complex. *Mol Hum Reprod,* 21**,** 320-9.
ZIPPER, H., BRUNNER, H., BERNHAGEN, J. & VITZTHUM, F. 2004. Investigations on DNA intercalation and surface binding by SYBR Green I, its structure determination and methodological implications. *Nucleic Acids Res,* 32**,** e103.
ZOU, K., YUAN, Z., YANG, Z., LUO, H., SUN, K., ZHOU, L., XIANG, J., SHI, L., YU, Q., ZHANG, Y., HOU, R. & WU, J. 2009. Production of offspring from a germline stem cell line derived from neonatal ovaries. *Nat Cell Biol,* 11**,** 631-6.
ZUCKERMAN, S. 1951. The Number of Oocytes in the Mature Ovary. *Recent Progress in Hormone Research,* 6**,** 63-109.
ZUO, X., SHENG, J., LAU, H. T., MCDONALD, C. M., ANDRADE, M., CULLEN, D. E., BELL, F. T., IACOVINO, M., KYBA, M., XU, G. & LI, X. 2012. Zinc finger protein ZFP57 requires its co-factor to recruit DNA methyltransferases and maintains DNA methylation imprint in embryonic stem cells via its transcriptional repression domain. *J Biol Chem,* 287**,** 2107-18.
ZWART, R., SLEUTELS, F., WUTZ, A., SCHINKEL, A. H. & BARLOW, D. P. 2001. Bidirectional action of the Igf2r imprint control element on upstream and downstream imprinted genes. *Genes Dev,* 15**,** 2361-6.

Appendices

Appendix I - Embryo culture stock solutions

Table I.I Composition of a) stock A. Once made, stock was sterile filtered and stored for up to 6 weeks at 4°C and b) bicarbonate stock. Once made, stock was sterile filtered and stored for up to 2 weeks at 4°C.

a)

Compound	Quantity	Final Concentration
NaCl SIGMA S5886	6.36 g	1.07×10^3mM
KCl SIGMA P5405	0.534 g	71.6 mM
KH_2PO_4 BDH	0.612 g	11.9 mM
$MgSO_4 \cdot 7H_2O$ SIGMA M1880	0.182 g	7.4 mM
Na-lactate SIGMA L4263	0.991 ml	70 mM
ET water	90.9 ml	

b)

Compound	Quantity	Final Concentration
$NaHCO_3$ SIGMA S6297	1.05 g	250 mM
ET water	50 ml	
Phenol Red SIGMA PO290	15 µl	

Table I.II Composition of a) 32.7 mM pyruvate stock. Once made, stock was sterile filtered and stored for up to 2 weeks at 4°C and b) calcium chloride stock. Once made, stock was sterile filtered and stored for up to 6 weeks at 4°C.

a)

Compounds	Quantity	Final Concentration
Na-Pyruvate SIGMA P4562	0.036 g	32.7 mM
ET water	10ml	

b)

Compounds	Quantity	Final Concentration
$CaCl_2 \cdot 2H_2O$ SIGMA C7902	0.252 g	170 mM
ET water	10ml	

Table I.III Composition of a) glucose stock. Once made, stock was sterile filtered and stored for up to 6 weeks at 4°C and b) glutamine (Gln) stock. Once made, stock was sterile filtered and stored for up to 2 weeks at 4ºC.

a)

Compound	Quantity	Final Concentration
D+Glucose SIGMA G5400	0.108 g	60 mM
ET water	10 ml	

b)

Compound	Quantity	Final Concentration
L-glutamine SIGMA G7513	0.292 g	**200 mM**
ET water	10ml	

Table I.IV Composition of a) HEPES stock and b) lactate stock. Once made, stock was sterile filtered and stored for up to 6 weeks at 4°C.

a)

Compounds	Quantity	Final Concentration
Hepes SIGMA H6147	1.5 g	126 mM
Hepes Sodium salt SIGMA H3784	1.625 g	125 mM
ET water	50 ml	

b)

Compounds	Quantity	Final Concentration
Na-Lactate syrup SIGMA L4263	0.47 ml	332.06 mM
ET water	9.53 ml	

Table I.V Composition of a) magnesium chloride stock and b) S2 stock. Once made, stock was sterile filtered and stored for up to 6 weeks at 4°C.

a)

Compounds	Quantity	Final Concentration
$MgCl_2.6H_2O$ SIGMA M2393	0.1 g	49.19 mM
ET water	10 ml	

b)

Compounds	Quantity	Final Concentration
NaCl SIGMA S5886	3.147 g	1.08 M
KCl SIGMA P5405	0.267 g	71.62 mM
KH_2PO_4 SUPELCO 104873	0.081 g	11.9 mM
ET water	50 ml	

Table I.VI Composition of a) stock TL (10x). Once made, stock was sterile filtered and stored for up to 6 weeks at 4°C and b) 47 mM pyruvate stock. Stock was freshly prepared and sterile filtered before every use.

a)

Compounds	Quantity	Final Concentration
NaCl SIGMA S5886	1.6665 g	1.07×10^3 mM
KCl SIGMA P5405	0.0595 g	71.6 mM
NaH_2PO_4 SIGMA 331988	0.0155 g	5 mM
Gentamycin SIGMA G1272 10mg/ml	1.25 ml	
ET water	24.75 ml	

b)

Compounds	Quantity	Final Concentration
Na-pyruvate SIGMA P4562	0.0517 g	47 mM
ET water	10ml	

Table I.VII Composition of a) penicillamine stock and b) hypotaurine stock. Once made, the two stocks were sterile filtered and mixed in a ratio of 1:1. Mixture was stored at -20°C.

a)

Compounds	Quantity	Final Concentration
Penicillamine SIGMA P4875	0.003g	200 µM
ET water	5 ml	

b)

Compounds	Quantity	Final Concentration
Hypotaurine SIGMA H1384	0.0022 g	100 µM
ET water	10 ml	

Table I.VIII Composition of stock a) fatty acid free bovine serum albumin (BSA FAF) and b) stock bovine serum albumin, fraction V (BSA FrV). Once made, stock was sterile filtered and stored for up to 2 weeks at 4°C.

a)

Compounds	Quantity	Final Concentration
BSA FAF SIGMA A6003	2 g	0.2 g/ml
ET water	10 ml	

b)

Compounds	Quantity	Final Concentration
BSA FrV SIGMA 85040C	2 g	0.2 mg/ml
ET water	10 ml	

Appendix II - Molecular buffers and solutions

Table II.I Composition of 10 x tris-borate ethylenediaminetetraacetic acid (TBE) buffer. For 1 x TBE, dilute 100 ml of 10 x TBE in 900 ml dH_2O.

Compounds	Quantity	Final Concentration
Trizma base SIGMA T1503	121.1 g	1 M
Boric acid SIGMA B0394	61.8 g	1 M
EDTA, disodium salt MILLIPORE 4010-OP	7.4 g	0.02 M
dH_2O	1 L	-

Table II.II Composition of a) 4% stacking and b) 12% separating SDS-PAGE gel

a)

Components	Volume
Distilled water	3 ml
4 x stacking buffer 0.5 M Tris pH 6.8 0.4% Sodium dodecyl sulfate (SDS)	1.3 ml
40% acrylamide BIO-RAD 1610146	0.49 ml
10% APS SIGMA A3678	50 µl
TEMED BIO-RAD 1610800	10 µl

b)

Components	Volume
Distilled water	4.4 ml
4 x resolving buffer 1.5 M Tris pH 8.8 0.4% Sodium dodecyl sulfate (SDS)	2.6 ml
40% acrylamide BIO-RAD 1610146	3 ml
10% APS SIGMA A3678	50 µl
TEMED BIO-RAD 1610800	15 µl

Table II.III Composition of a) 10 x running buffer. For 1 x running buffer, dilute 100 ml of 10 x running buffer in 900 ml dH_2O and b) 10 x transfer buffer. For 1 x transfer buffer, dilute 100 ml of 10 x transfer buffer in 700 ml of dH_2O and 200 ml of methanol (10499560, Fisher chemical).

a)

Components
0.25 M Trizma base SIGMA T1503
1.92 M Glycine SIGMA G8898
1% Sodium dodecyl sulfate (SDS) SIGMA 436143

b)

Components
0.25 M Trizma base SIGMA T1503
1.92 M Glycine SIGMA G8898

Table II.IV Composition of a) Luria-Bertani (LB) broth and b) Luria-Bertani (LB) agar.

a)

Components	Amount
Tryptone MILLIPORE 93657	10 g
Yeast Extract MILLIPORE 01497	5 g
NaCl SIGMA S5886	10 g
dH_20	1000 ml

b)

Components	Amount
Tryptone MILLIPORE 93657	4 g
Yeast Extract MILLIPORE 01497	2 g
NaCl SIGMA S5886	4 g
Agar SIGMA A1296	6 g
dH_20	400 ml

Table II.V Composition of a) 10 x TBS-T. Once made, pH was adjusted to 7.6 and b) RIPA buffer.

a)

Components
0.2 M Trizma base SIGMA T1503
1.5 M NaCl SIGMA S5886
1% Tween-20 SIGMA P1379

b)

Components
50 mM Trizma base, pH 8.0 SIGMA T1503
150 mM NaCl SIGMA S5886
0.5% Sodium deoxycholate SIGMA D6750
0.1% Sodium dodecyl sulfate (SDS) SIGMA 436143
0.1% Triton X-100 SIGMA T8787
1 x Protease inhibitor cocktail PROMEGA G6521

Appendix III - Primer sequences

Table III.I Unsuccessful bovine *PADI* family primer sequences

Gene	Primer sequences (5'→3')	Product size	Reference
PADI1	F: CATAGGCAAATCAGGACAAGGA R: GATGGAGGCAGGCATTAACA	91 bp	ENSBTAT00000015977.6
PADI1	F: GAGATGATTCCCTCCGTGTTT R: CAGGAGACAGTAGCTGGTAAAG	139 bp	
PADI2	F: GCTCTTCAGAGAGAAGCAGAAG R: GAGGCTCTCATTGGACAGAATC	115 bp	ENSBTAT00000004411.6
PADI2	F: GTGAAGAACCTGGTGGAGAAA R: GCCTCGATGTAGCCAAACT	110 bp	
PADI3	F: AGAGGATTGTGCGCGTATC R: CTCGGGAACTGACCCATAAAT	95 bp	ENSBTAT00000015978.6
PADI3	F: GTCACGTTCAGATTTCCTACCA R: TTCACAGTTCAGGTCACAGTC	110 bp	
PADI4	F: GGATGAGATGGAGATTGGCTAC R: ACCCAGCATGCACTTGAT	112 bp	ENSBTAT00000015991.6
PADI4	F: GGACCAGCAGGTTCAGATT R: GTCTGCACTCAGGGAGATTT	97 bp	

Table III.II Bovine MEG primer sequences

Gene	Primer sequences (5'→3')	Product size	Reference
DNMT1	F: ACCGTATTGGCCGCATAAA R: GGGTAGACTTGTGTGTGTTCTC	123 bp	NM_182651.2
DNMT3 A	F: CGAGGTAGTGACACAAGGTTAAA R: CTTCTGGGTGCTGATACTTCTC	98 bp	NM_001206502.2
DNMT3 B	F: CTCCGAGATTCCAGCAGATAAG R: GTACATGGCCTTCCTGTAAGAG	103 bp	NM_181813.2
DPPA3	F: GAGCCTACAGCATCACCTTC R: GGTCCAGGTTGGGTTATCTTC	104 bp	NM_001111108.2
FIGLA	F: ACGAGACCCCGATCATCAGA R: GGGGAATCTATCCACTGCCA	161 bp	NM_001281920.1
GNAS	F: GAGTGCCCAGACTACCAGGA R: AGACGCTCGGTGAGAGACTG	172 bp	NM_001271771.1
HAT1	F: GCAACATGCTAGACGGGTTT	218 bp	NM_001034347.1

	R: GCTGTTCATGTTGCATGCTT		
KDM1A	F: AAGGAACTCCATCAGCAATACA R: ATTCCTTACACAGGGCAGTTAG	115 bp	XM_005203319.2
KHDC3L	F: GACTACAGCATGGCCTCTCCC R: GATGAACGTGAAGCAGGGTC	241 bp	ENSBTAT00000081682.1
MEST	F: TGTTCCCTTATCTGTCGTGTAATC R: GTGTGAGTCAGGTGGACTTTAG	100 bp	NM_001083368.1
MTHFR	F: GTTCTTCGTTTCTCCCCAGC R: CACCAGAGCACAGACTCTCA	150 bp	NM_001011685.1
NLRP2	F: GTGCGAGGCTTTGAAGAAAC R: TTACTCCACTGGACCCCAAG	164 bp	ENSBTAT00000074039.1
NLRP5	F: AAATAAGGTGGCGGACCAGG R: GTCCTCGCACAGAAGGTTCA	385 bp	NM_001007814.2
NLRP7	F: GATCTCACTGCAGGTAGGAAAG R: CCCAGAGTTGGAGAGAATGATG	110 bp	ENSBTAT00000062990.2
OOEP	F: GTCGAAGTCACCGTTTTCGC R: CTCACGCTCCTGACAACACT	196 bp	ENSBTAT00000077348.1
PADI6	F: TGCTCTTTGAAGGGCTTAGG R: TCATTCTGCTTCCTCATCTTCTC	103 bp	XM_002685797.5
PHLDA2	F: GCTCCAGGTGTGGAAGAAGA R: GACGCGTTCCAGTAGCTCTC	219 bp	NM_001076521.2
PLAGL1	F: GGTGGAAATGAGGCAGGATAG R: CACTAGCCATGAGCACTATGAG	102 bp	XM_015472892.2
PRMT5	F: AAGCAGGGGTTTGATTTCCT R: TATGCCCCAAAATTCAGCTC	245 bp	NM_001105374.1
SETDB1	F: GCTGAGACACCAAACGTCAAAA R:ACATAGGAAGCATAGCCATCATCA	71 bp	XM_005203829.4
STAT3	F: CAACCTTGCTAACGTCCAGATA R: CAGAGGAAGCTATGCCAATACA	119 bp	NM_001012671.2
TET1	F: CCTTCATCACTGTCCGTCTTT R: GTGAGCTGTTGTGTGACTTAGA	95 bp	XM_024986940.1
TET2	F: AGGTTTGGACAGAAGGGTAAAG R: GCAATAGGACATCCCTGAGAAC	89 bp	XM_005207682.4
TET3	F: GTCCCAGCATAAGGAGAAGAAG R: GTGACCTTCGTGTAGGCATAG	105 BP	XM_024999365.1
TLE6	F: ATCCTCTGTCATGTGCTGTG R: CTCAGTATGTGAGCTGGTACAC	95 bp	XM_010807029.3
TRIM28	F: GCTCTCCAAGAAGCTGATCTAC R: CGTTGAGGTCCCACTGAAAT	104 bp	ENSBTAT00000008424.6
ZFP57	F: CTCAGTTGCTGGAAGGTAGATAG R: CTTCTCTTCCATGCTGTCTCTT	102 bp	XM_010818393.3

Table III.III Primer sequences for oocyte quality marker genes in the bovine real-time PCR array purchased from RealTimePrimers.com

Gene		**Primer sequences (5'→3')**
AURKA	Aurora kinase A	F: GGAGGGAGGTCCCTAGTCTG R: TCTCAGTGCTAAGGGGTGCT
BDNF	Brain-derived neurotrophic factor	F: CATGACCAGAAGGGAAACAG R: GCAACAAACCACAACATTGA
BMP15	Bone morphogenetic protein 15	F: CCTTTTCAAGTCAGCTTCCA R: GCATGATTGGGAGAATTGAG
BMP2	Bone morphogenetic protein 2	F: TGTGGACTTCAGTGATGTGG R: GACCAGAGTTTGGACAATGG
FIGLA	Factor in the germline alpha	F: CCTCAGAGGTGCAACTGAAT R: TCATTCTTCAAGCCCATAGC

GAPDH	Glyceraldehyde 3-phosphate dehydrogenase	F: GAAACCTGCCAAGTATGATGAG R: CAGCATCGAAGGTAGAAGAGTG
GDF9	Growth differentiation factor 9	F: TGAATTGAAGAAGCCTCTGG R: CAATCCAGTTGTCCCACTTC
GTSF1	Gametocyte specific factor 1	F: TGCCCCTATGATAAAAACCA R: ACGTGCTCTCAGCCATAGTC
H1FOO	H1 histone family, member o, oocyte-specific	F: ACACAGCCTGGAAGTCAGAG R: CGCTTTGGACACTGAAGACT
H2A	Histone H2A	F: ATGTCTGGACGTGGAAAAGG R: ATCACAGCCGCCAAATAAAC
HSF1	Heat shock factor 1	F: GGAAAGTGACCAGTGTGTCC R: GGATGAGCTTGTTGACGACT
IZUMO1R	IZUMO1 receptor	F: CAACTTCAGCCTGGTTCACT R: GGAGCACTGGTAGAAGCAGA
LHX8	LIM homeobox 8	F: TCCAAAACCAGCAAAAAGAG R: GTGGCGTGCTCTACAGTTCT
NOBOX	Newborn ovary homeobox	F: CTGTCCATGGAATTCTCCAG R: GACTCAGCACAGGAGAAGGA
OCT4	POU class 5 homeobox 1	F: GTTTTGAGGCTTTGCAGCTC R: CTCCAGGTTGCCTCTCACTC
PRDX1	Peroxiredoxin 1	F: GCTTTCAGTGATAGGGCAGA R: TCCTTGTTTCTTGGGTGTGT
PRDX2	Peroxiredoxin 2	F: GGTCCAGGCTTTCCAGTACA R: TGGAGTCTGAAGGAGCAGGT
SOHLH2	Spermatogenesis and oogenesis specific basic helix-loop-helix 2	F: CACGGAGCTGATATTGCTTT R: TCAGGTTCTTCAGGCTTCAC
YWHAZ	Tyrosine 3-monooxygenase /tryptophan 5-monoxygenase activation protein, zeta	F: AGACGGAAGGTGCTGAGAAA R: CCTCAGCCAAGTAGCGGTAG
ZAR1	Zygote arrest 1	F: TCACTGCAAGGACTGCAATA R: CAGGTGATATCCTCCACTCG
ZP1	Zona pellucida glycoprotein 1	F: ACCCAGAAAAGCTCACACTG R: GCTGATCATGTCTTCCTGCT
ZP2	Zona pellucida glycoprotein 2	F: TCCTCCAGTTCACAGTGGAT R: GAGGACTTGCTGAAGGAACA
ZP3	Zona pellucida glycoprotein 3	F: TCTTAATCGTTGGAGCCTTG R: GCTGAGCAACTCATCTCCAT

Table III.IV Primer sequences for imprinted genes and epigenetic regulators in the bovine qPCR array purchased from RealTimePrimers.com.

Gene		**Primer sequences (5'→3')**
ASCL2	Achaete-scute family bHLH transcription factor	F: ACCCAAGGCTAGTGTGCAAG R: CATAAAGCCCTCTCCCCTTC
DNMT1	DNA methyltransferase 1	F: AGTGGGGGACTGTGTTTCTG R: TGCTGTGGATGTACGAGAGC
DNMT3A	DNA methyltransferase 3 alpha	F: AGCACAACGGAGAAGCCTAA R: CAGCAGATGGTGCAGTAGGA
DNMT3B	DNA methyltransferase 3 beta	F: TCAGGATGGGAAGGAGTTTG R: CTGCTGGAATCTCGGAGAAC
DNMT3L	DNA methyltransferase 3-like	F: CTGCTGGAATCTCGGAGAAC R: GGCTCTCTCTTCCACACAGG
EHMT2	Euchromatic histone-lysine N-methyltransferase 2	F: ACCTCAGATGTGGCCAAAAG R: GTTCAGCCAGAGCTTCAACC
ELP3	Elongator acetyltransferase complex subunit 3	F: AGGGCTCTATGAGCTGTGGA R: TGAGCTGACTAACGGCATTG

GAPDH	Glyceraldehyde 3-phosphate dehydrogenase	F: GAAACCTGCCAAGTATGATGAG R: CAGCATCGAAGGTAGAAGAGTG
H19	H19 (imprinted; maternally expressed transcript)	F: GACACCCAGAACCCTCAAGA R: CCTTCCAGAGCTGATTCCTG
H2A	Histone H2A	F: ATGTCTGGACGTGGAAAAGG R: ATCACAGCCGCCAAATAAAC
HAT1	Histone acetyltransferase 1	F: GCAACATGCTAGACGGGTTT R: GCTGTTCATGTTGCATGCTT
IGF2	Insulin-like growth factor 2	F: GCCCTGCTGGAGACTTACTG R: GGTGACTCTTGGCCTCTCTG
IGF2R	Insulin-like growth factor 2 receptor	F: GTCGTGCAGATCAGTCCTCA R: TCGTTCTGGAGCTGAAAGGT
KAT5	Lysine acetyltransferase 5	F: TCGACTCCAAGTGTCTGCAC R: CTTCTGGAGTGGTCCTCAGC
KDM1B	Lysine demethylase 1B	F: AGTGTCAGAAGTGCCCAACC R: TCGTTGGGTTGGTAGAAAGG
KHDC3L	KH domain containing 3-like	F: GACTACAGCATGGCCTCTCC R: CCTCCAGATGAACTGCCTTC
MEG3	Maternally expressed gene 3	F: ACCTGTCTCACGCTTCTCGT R: TCCTGAGAGCTGGTGGAGTT
MEG9	Maternally expressed 9	F: GCCTGCCACACTTTATGGTT R: CAGAGACAGCTTTGCCAACA
MEST	Mesoderm specific transcript	F: AAGGGACTGCGCATCTTCTA R: TGAAGCCAAAGCCTAGGAAA
MIMT1	MER1 repeat containing imprinted transcript 1	F: GCTCTTAAAAGGGCATGCTG R: CCATCATCCTTCCTGGAGAA
MSK2	Ribosomal protein S6 kinase, 90kDa, polypeptide 4	F: CGAAATGTTCACCCACCTCT R: GACAATGTGACCCTCGGAGT
NAP1L5	Nucleosome assembly protein 1-like 5	F: TTCCAGGCTCTGGAGAAAAA R: CTCTGCTGCAGGCTCTTCTT
NLRP2	NLR family, pyrin domain containing 2	F: GTGCGAGGCTTTGAAGAAAC R: TTACTCCACTGGACCCCAAG
NLRP5	NLR family, pyrin domain containing 5	F: CGGAGGCTCCTACTGTTCTG R: CCTGGTCTCTGAAGGTGAGC
NNAT	Neuronatin	F: CGACAACTCTGTGCCTGTGT R: AGATGGGATTCGTTTTCGTG
OOEP	Oocyte expressed protein	F: TTGACGCTGGGAACCTAGTC R: TCTCACGCTCCTGACAACAC
PADI6	Peptidylarginine deiminase 6	F: TCGGAGACTTCTGCTCCTGT R: CTGGAGACGCATAGGGAGAG
PEG10	Paternally expressed gene 10	F: ATTGTTCATTGGCTGGAAGG R: GCTTTGGGTTGCTTTCTGAG
PEG3	Paternally expressed gene 3	F: CTGTACGTGGATTGGCCTTT R: TAGGCACGCGTGATCTAGTG
PGK1	Phosphoglycerate kinase 1	F: CTGCTGTTCCAAGCATCAAA R: GCACAAGCCTTCTCCACTTC
PHLDA2	Pleckstrin homology domain, family A, member 2	F: CCAGGTGTGGAAGAAGAAGC R: GACGCGTTCCAGTAGCTCTC
PLAGL1	Pleiomorphic adenoma gene-like 1	F: GGACCCCAAGCTTAGAAAGG R: TTTGGAGGTGGTTCTTCAGG
PRMT5	Protein arginine methyltransferase 5	F: AAGCAGGGGTTTGATTTCCT R: TATGCCCCAAAATTCAGCTC
SETD7	SET domain containing lysine methyltransferase 7	F: GCCCCGTGATGTTCTACACT R: TGGTGGTAACGGAAAAGGAG
SNRPN	Small nuclear ribonucleoprotein polypeptide N	F: GTTCCAGCTGGTGTTCCAAT R: TGGAGGAGCCATAATTCCTG
TET1	Tet methylcytosine dioxygenase 1	F: CCTCTCCAACCAACCAGTGT R: GAATTTGTGCTGGGTCTGGT
TET2	Tet methylcytosine dioxygenase 2	F: GTAAGGCCGGTGACAGTGAT

		R: TTTCTCGCCAGAGGTTCTGT
TET3	Tet methylcytosine dioxygenase 3	F: GAAAGGCCAGAAGCACTCAC R: TGAAGGGAAGGGTGTCTGTC
TLE6	Transducer like enhancer of split 6	F: TGACCTCTTGGGGTCATCTC R: GGAAGTTTTCTGCCTGCTTG
TRIM28	Tripartite motif containing 28	F: ACTCCACCTTCTCCCCAGAT R: TCCGTCAGCTTGTTGAACTG
TSSC4	Tumour suppressing subtransferable candidate 4	F: CGACAGGAAGAGGGTATCCA R: AAACCCACTGTCTCCACCAG
USP29	Ubiquitin specific peptidase 29	F: ACACACCTCCTGGTGACTCC R: TGACCCTTCAGCGATCTTCT
XIST	X (inactive)-specific transcript	F: TTGAATGGGATTTGGGGTAA R: AGTAGTGTGGCCTTGGGATG
YWHAZ	Tyrosine 3-monooxygenase /tryptophan 5-monoxygenase activation protein, zeta	F: AGACGGAAGGTGCTGAGAAA R: CCTCAGCCAAGTAGCGGTAG
ZFP57	Zinc finger protein 57	F: TTAACCCACCTCAAGATCCA R: TGAGTGTGTTGGATGAGTGG

Appendix IV - Supplementary Results

IV.A Chapter 5 – Gene expression analysis of *Padi6*^{KD} MII oocytes

Of the 26 genes subject to thorough qPCR testing for changes in gene expression between control and *PADI6*^{KD} MII oocytes, only 4 genes were significantly altered. The remaining 22 genes were unchanged between different microinjection groups. Figures IV.I, IV.II and IV.III show expression of *DNMT1, GNAS, HAT1, KDM1, KHDC3L, MEST, MTHFR, NLRP2, NLRP5, NLRP7, PHLDA2, SETDB1, STAT3, TET1, 2, 3* and *TLE6.*

IV.B Oocyte quality marker array results from a single culture week (as discussed in Section 5.4.2)

The data from the oocyte quality marker array was re-analysed to specifically look at the data points that were analysed using the imprinted gene and epigenetic regulator array. These samples included 6 DB-injected oocytes and 7 *PADI6*^{KD} oocytes that were produced from the same culture week. This was done to see if the culture conditions of this week had caused a global alteration in gene expression as discussed in Section 5.4.2. Figure IV.IV shows the results. 2 out of 20 genes that were analysed were upregulated in these samples. The genes, GTSF1 and LHX8, were not upregulated when all samples were analysed (see Figure 5.2).

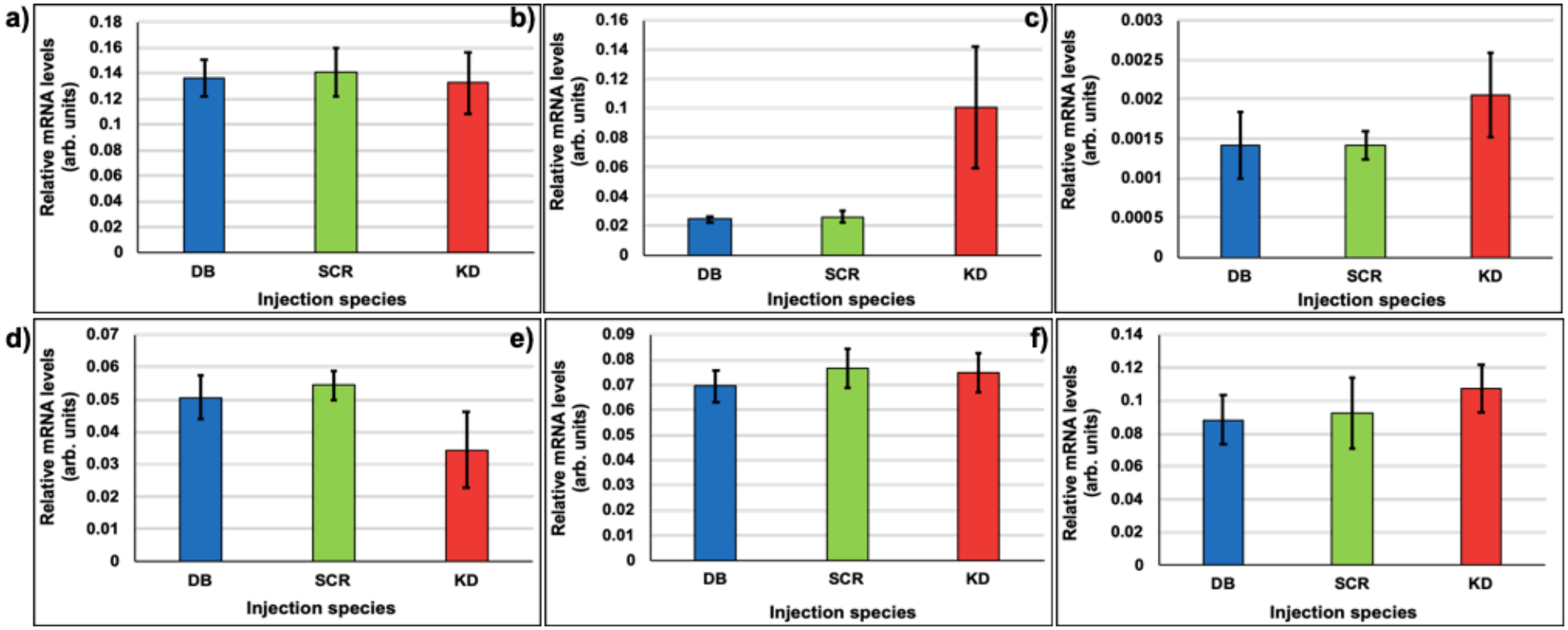

Figure IV.I Relative transcript abundance of a) *DNMT1,* b) *FIGLA,* c) *GNAS,* d) *HAT1,* e) *KDM1A* and f) *KHDC3L* after microinjection with DB (n = 11), SCR (n = 10) or *PADI6* dsiRNA (n = 20) (p>0.05).

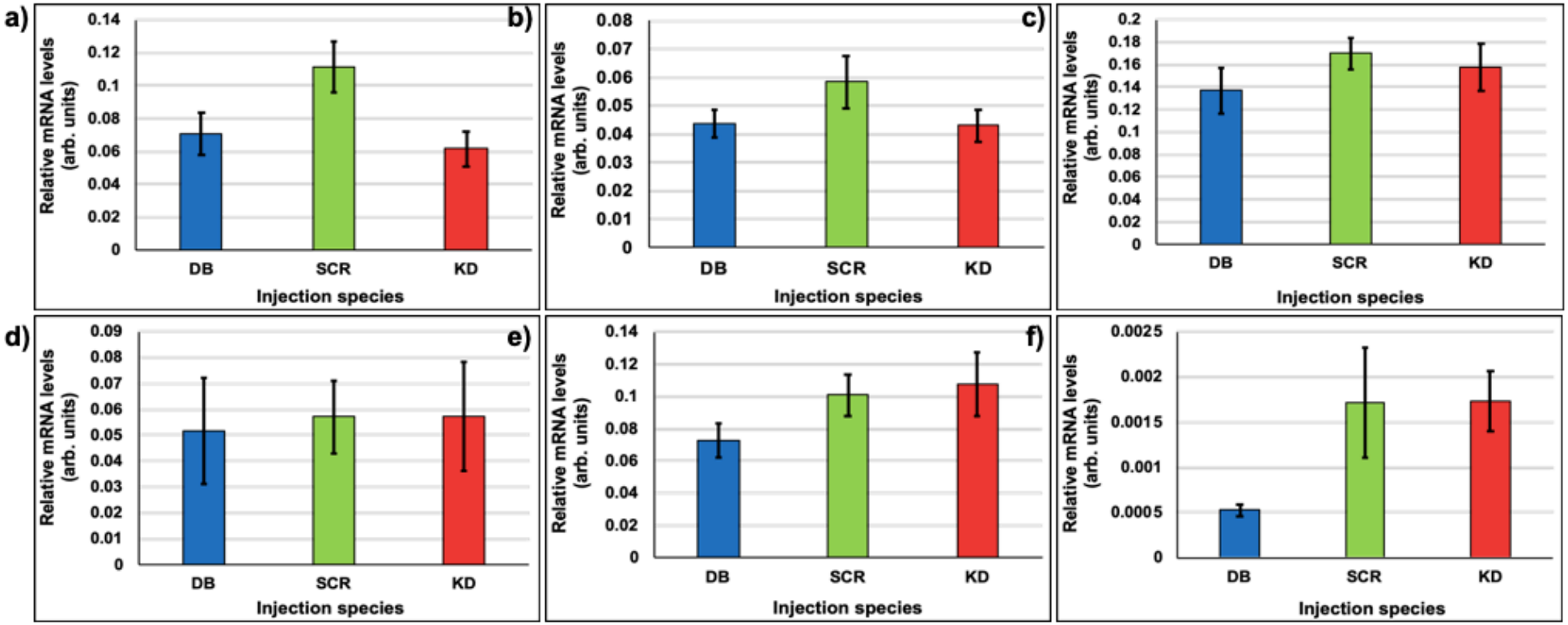

Figure IV.II Relative transcript abundance of a) *MEST,* b) *MTHFR,* c) *NLRP2,* d) *NLRP5,* e) *NLRP7* and f) *PHLDA2* after microinjection with DB (n = 11), SCR (n = 10) or *PADI6* dsiRNA (n = 20) ($p>0.05$).

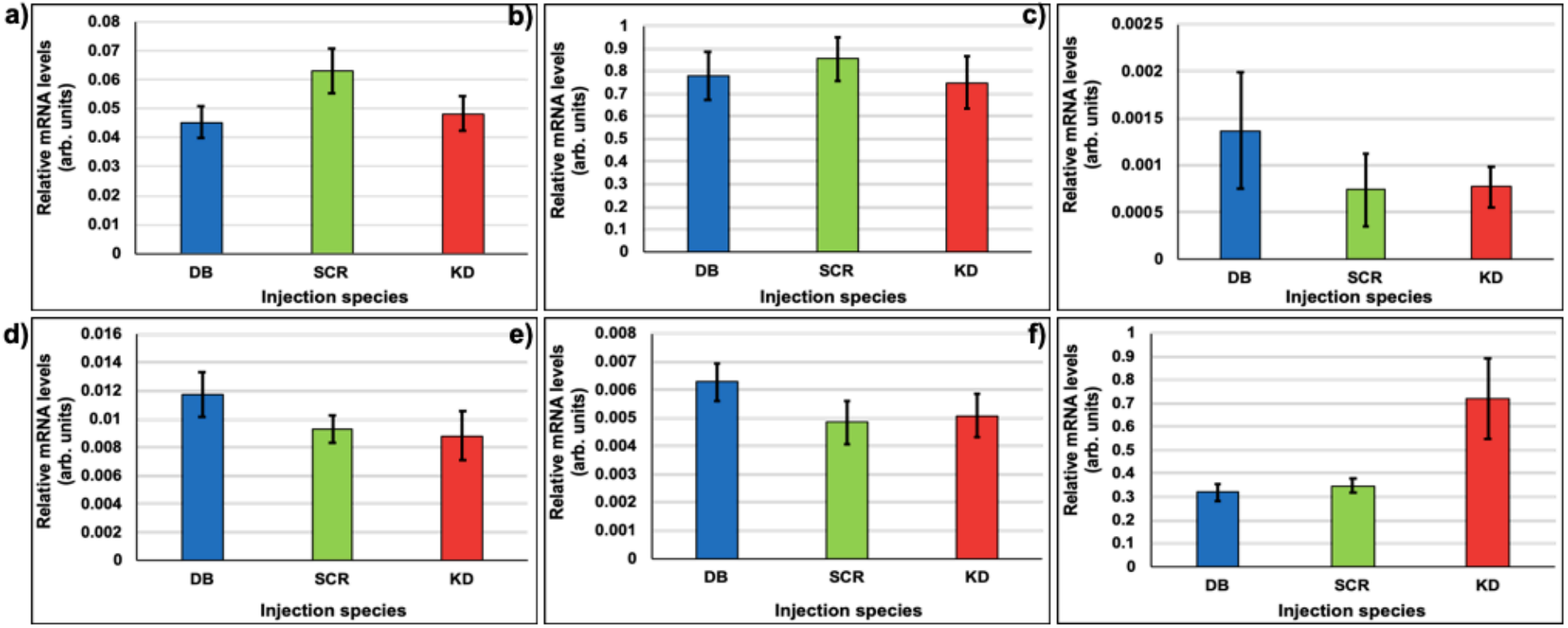

Figure IV.III Relative transcript abundance of a) *SETDB1,* b) *STAT3,* c) *TET1,* d) *TET2,* e) *TET3* and f) *TLE6* after microinjection with DB (n = 11), SCR (n = 10) or *PADI6* dsiRNA (n = 20) (p>0.05).

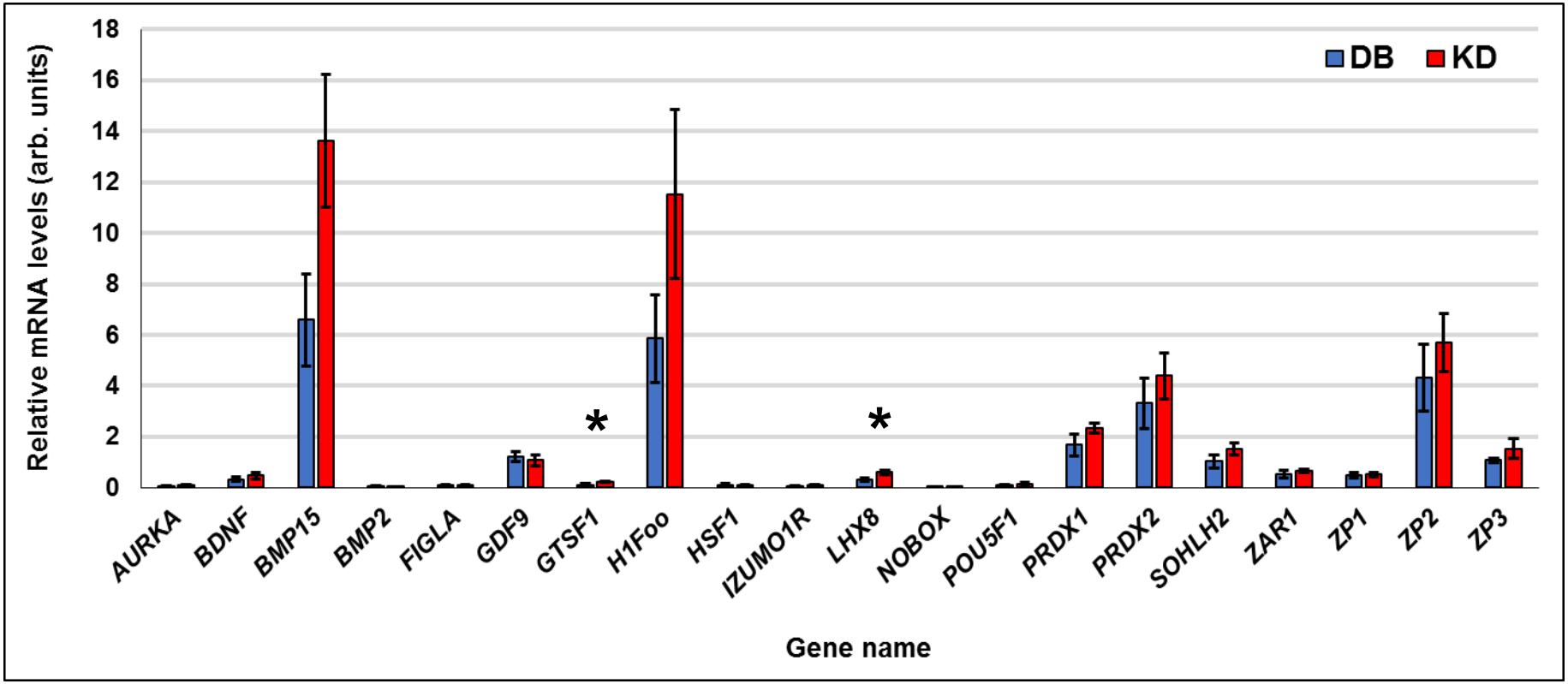

Figure IV.IV Real-time PCR quantification of the effect of *PADI6* KD on the expression of oocyte quality markers in high *PADI6* KD oocytes (n = 7) compared to DB control oocytes (n = 6) from the one discrete culture week. The data were standardised against *GAPDH, H2A* and *YWHAZ* housekeeping mRNA levels. Individual bars show the mean ±SEM. Due to the number of genes screened triplicate repeats were not performed. *PADI6* KD oocytes exhibited a statistically significant difference for *GTSF1* and *LHX8* mRNA levels (* = $p<0.05$) compared to control-injected oocytes. No other significant differences were observed ($p>0.05$).

IV.C Chapter 6 – Western blotting for PADI6

The Western blot from Chapter 6 was repeated 3 times and the same result was obtained each time. The other 2 repeats are shown in Figure IV.V. The upper band in the untransformed *E. coli* sample (lane A) is missing from both of these repeats. This is probably due to the poor quality of the sample as the lower band is also much less prominent than in Figure 6.10. Similarly, the lower band in lanes B and C is barely detected, although faint bands can be seen in Figure IV.Vb.

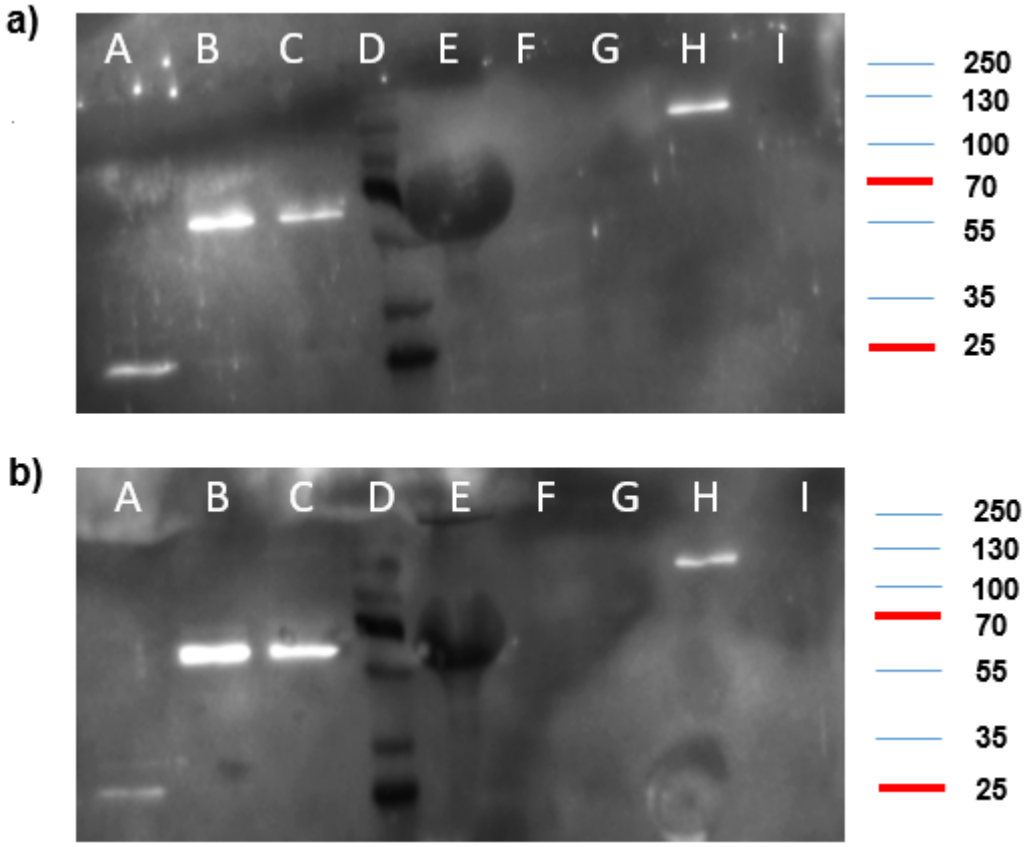

Figure IV.V Repeat no. 2 **(a)** and 3 **(b)** of Western blot for PADI6 protein in: A) Untransformed *E. coli*; B) *PADI6*-pET-11a uninduced; C) *PADI6*-pET-11a induced; D) Protein ladder; E) BSA; F) 2102Ep protein; G) NTera-2 protein; H) Recombinant PADI6; I) **(a)** Pooled GV oocytes (x20) and **(b)** Pooled GV oocytes (x50). The protein ladder molecular weights (kDa) are shown on the right.